

Arthritis & Rheumatology

An Official Journal of the American College of Rheumatology
www.arthritisrheum.org and wileyonlinelibrary.com

GENERAL INFORMATION

TO SUBSCRIBE

Institutions and Non-Members

Email: wileyonlinelibrary.com
Phone: (201) 748-6645
Write: Wiley Periodicals LLC
Attn: Journals Admin Dept
UK
111 River Street
Hoboken, NJ 07030

Volumes 74, 2022:
Institutional Print Only:

Institutional Online Only:
Institutional Print and
Online Only:

Arthritis & Rheumatology and Arthritis Care & Research:
\$2,603 in US, Canada, and Mexico
\$2,603 outside North America

\$2,495 in US, Canada, Mexico, and outside North America
\$2,802 in US, Canada, and Mexico; \$2,802 outside
North America

For submission instructions, subscription, and all other information visit: wileyonlinelibrary.com.

Arthritis & Rheumatology accepts articles for Open Access publication. Please visit <https://authorservices.wiley.com/author-resources/Journal-Authors/open-access/hybrid-open-access.html> for further information about OnlineOpen.

Wiley's Corporate Citizenship initiative seeks to address the environmental, social, economic, and ethical challenges faced in our business and which are important to our diverse stakeholder groups. Since launching the initiative, we have focused on sharing our content with those in need, enhancing community philanthropy, reducing our carbon impact, creating global guidelines and best practices for paper use, establishing a vendor code of ethics, and engaging our colleagues and other stakeholders in our efforts.

Follow our progress at www.wiley.com/go/citizenship.

Access to this journal is available free online within institutions in the developing world through the HINARI initiative with the WHO. For information, visit www.healthinternetwork.org.

Disclaimer

The Publisher, the American College of Rheumatology, and Editors cannot be held responsible for errors or any consequences arising from the use of information contained in this journal; the views and opinions expressed do not necessarily reflect those of the Publisher, the American College of Rheumatology and Editors, neither does the publication of advertisements constitute any endorsement by the Publisher, the American College of Rheumatology and Editors of the products advertised.

Members:

American College of Rheumatology/Association of Rheumatology Professionals

For membership rates, journal subscription information, and change of address, please write:

American College of Rheumatology
2200 Lake Boulevard
Atlanta, GA 30319-5312
(404) 633-3777

ADVERTISING SALES AND COMMERCIAL REPRINTS

Sales: Kathleen Malseed, National Account Manager
E-mail: kmalseed@pminy.com
Phone: (215) 852-9824
Pharmaceutical Media, Inc.
30 East 33rd Street, New York, NY 10016

Production: Patti McCormack
E-mail: pmccormack@pminy.com
Phone: (212) 904-0376
Pharmaceutical Media, Inc.
30 East 33rd Street, New York, NY 10016

Publisher: Arthritis & Rheumatology is published by Wiley Periodicals LLC, 101 Station Landing, Suite 300, Medford, MA 02155

Production Editor: Ramona Talantor, artprod@wiley.com

ARTHRITIS & RHEUMATOLOGY (Print ISSN 2326-5191; Online ISSN 2326-5205 at Wiley Online Library, wileyonlinelibrary.com) is published monthly on behalf of the American College of Rheumatology by Wiley Periodicals LLC, a Wiley Company, 111 River Street, Hoboken, NJ 07030-5774. Periodicals postage paid at Hoboken, NJ and additional offices. POSTMASTER: Send all address changes to Arthritis & Rheumatology, Wiley Periodicals LLC, c/o The Sheridan Press, PO Box 465, Hanover, PA 17331. **Send subscription inquiries care of** Wiley Periodicals LLC, Attn: Journals Admin Dept UK, 111 River Street, Hoboken, NJ 07030, (201) 748-6645 (nonmember subscribers only; American College of Rheumatology/Association of Rheumatology Health Professionals members should contact the American College of Rheumatology). **Subscription Price:** (Volumes 74, 2022: Arthritis & Rheumatology and Arthritis Care & Research) Print only: \$2,603.00 in U.S., Canada and Mexico, \$2,603.00 rest of world. For all other prices please consult the journal's website at wileyonlinelibrary.com. All subscriptions containing a print element, shipped outside U.S., will be sent by air. Payment must be made in U.S. dollars drawn on U.S. bank. Prices are exclusive of tax. Asia-Pacific GST, Canadian GST and European VAT will be applied at the appropriate rates. For more information on current tax rates, please go to www.wileyonlinelibrary.com/tax-vat. The price includes online access to the current and all online backfiles to January 1st 2018, where available. For other pricing options including access information and terms and conditions, please visit <https://onlinelibrary.wiley.com/library-info/products/price-lists>. Terms of use can be found here: <https://onlinelibrary.wiley.com/terms-and-conditions>. **Delivery Terms and Legal Title:** Where the subscription price includes print issues and delivery is to the recipient's address, delivery terms are Delivered at Place (DAP); the recipient is responsible for paying any import duty or taxes. Title to all issues transfers Free of Board (FOB) our shipping point, freight prepaid. We will endeavor to fulfill claims for missing or damaged copies within six months of publication, within our reasonable discretion and subject to availability. **Change of Address:** Please forward to the subscriptions address listed above 6 weeks prior to move; enclose present mailing label with change of address. **Claims** for undelivered copies will be accepted only after the following issue has been received. Please enclose a copy of the mailing label or cite your subscriber reference number in order to expedite handling. Missing copies will be supplied when losses have been sustained in transit and where reserve stock permits. Send claims care of Wiley Periodicals LLC, Attn: Journals Admin Dept UK, 111 River Street, Hoboken, NJ 07030. If claims are not resolved satisfactorily, please write to Subscription Distribution c/o Wiley Periodicals LLC, 111 River Street, Hoboken, NJ 07030. **Cancellations:** Subscription cancellations will not be accepted after the first issue has been mailed. **Journal Customer Services:** For ordering information, claims and any enquiry concerning your journal subscription please go to <https://wolsupport.wiley.com/s/contactsupport?tabset-a7d10=2> or contact your nearest office. **Americas:** Email: cs-journals@wiley.com; Tel: +1 877 762 2974. **Europe, Middle East and Africa:** Email: cs-journals@wiley.com; Tel: +44 (0) 1865 778315; 0800 1800 536 (Germany). **Asia Pacific:** Email: cs-journals@wiley.com; Tel: +65 6511 8000. **Japan:** For Japanese speaking support, Email: cs-japan@wiley.com. **Visit our Online Customer Help** at <https://wolsupport.wiley.com/s/contactsupport?tabset-a7d10=2>. **Back Issues:** Single issues from current and prior year volumes are available at the current single issue price from csjournals@wiley.com. Earlier issues may be obtained from Periodicals Service Company, 351 Fairview Avenue-Ste 300, Hudson, NY 12534, USA. Tel: +1 518 822-9300, Fax: +1 518 822-9305, Email: psc@periodicals.com. Printed in the USA by The Sheridan Group.

Arthritis & Rheumatology

An Official Journal of the American College of Rheumatology
www.arthritisrheum.org and wileyonlinelibrary.com

Editor

Daniel H. Solomon, MD, MPH, *Boston*

Deputy Editors

Richard J. Bucala, MD, PhD, *New Haven*

Mariana J. Kaplan, MD, *Bethesda*

Peter A. Nigrovic, MD, *Boston*

Co-Editors

Karen H. Costenbader, MD, MPH, *Boston*

David T. Felson, MD, MPH, *Boston*

Richard F. Loeser Jr., MD, *Chapel Hill*

Social Media Editor

Paul H. Sufka, MD, *St. Paul*

Journal Publications Committee

Amr Sawalha, MD, *Chair, Pittsburgh*

Susan Boackle, MD, *Denver*

Aileen Davis, PhD, *Toronto*

Deborah Feldman, PhD, *Montreal*

Donnamarie Krause, PhD, OTR/L, *Las Vegas*

Wilson Kuswanto, MD, PhD, *Stanford*

Michelle Ormseth, MD, *Nashville*

R. Hal Scofield, MD, *Oklahoma City*

Editorial Staff

Kimberly M. Murphy, *Managing Editor, Atlanta*

Lesley W. Allen, *Assistant Managing Editor, Atlanta*

Ilani S. Lorber, MA, *Assistant Managing Editor, Atlanta*

Rasa G. Hamilton, *Manuscript Editor, Atlanta*

Stefanie L. McKain, *Manuscript Editor, Atlanta*

Scott C. O'Brien, MPH, MA, *Manuscript Editor, Atlanta*

Sara Omer, *Manuscript Editor, Atlanta*

Christopher Reynolds, MA, *Editorial Coordinator, Atlanta*

Brittany Swett, MPH, *Assistant Editor, Boston*

Associate Editors

Marta Alarcón-Riquelme, MD, PhD, *Granada*

Heather G. Allore, PhD, *New Haven*

Neal Basu, MD, PhD, *Glasgow*

Edward M. Behrens, MD, *Philadelphia*

Bryce Binstadt, MD, PhD, *Minneapolis*

Nunzio Bottini, MD, PhD, *San Diego*

John Carrino, MD, MPH, *New York*

Lisa Christopher-Stine, MD, MPH,

Baltimore

Andrew Cope, MD, PhD, *London*

Adam P. Croft, MBChB, PhD, MRCP,

Birmingham

Nicola Dalbeth, MD, FRACP, *Auckland*

Brian M. Feldman, MD, FRCPC, MSc, *Toronto*

Richard A. Furie, MD, *Great Neck*

J. Michelle Kahlenberg, MD, PhD,

Ann Arbor

Benjamin Leder, MD, *Boston*

Yvonne Lee, MD, MMSc, *Chicago*

Katherine Liao, MD, MPH, *Boston*

Bing Lu, MD, DrPH, *Boston*

Stephen P. Messier, PhD,

Winston-Salem

Rachel E. Miller, PhD, *Chicago*

Janet E. Pope, MD, MPH, *FRCPC,*

London, Ontario

Christopher T. Ritchlin, MD, MPH,

Rochester

William Robinson, MD, PhD, *Stanford*

Carla R. Scanzello, MD, PhD, *Philadelphia*

Georg Schett, MD, *Erlangen*

Sakae Tanaka, MD, PhD, *Tokyo*

Maria Trojanowska, PhD, *Boston*

Betty P. Tsao, PhD, *Charleston*

Fredrick M. Wigley, MD, *Baltimore*

Edith M. Williams, PhD, MS, *Charleston*

Advisory Editors

Ayaz Aghayev, MD, *Boston*

Joshua F. Baker, MD, MSCE,

Philadelphia

Bonnie Bermas, MD, *Dallas*

Jamie Collins, PhD, *Boston*

Kristen Demoruelle, MD, PhD, *Denver*

Christopher Denton, PhD, FRCP, *London*

Anisha Dua, MD, MPH, *Chicago*

John FitzGerald, MD, *Los Angeles*

Lauren Henderson, MD, MMSc, *Boston*

Monique Hinchcliff, MD, MS, *New Haven*

Hui-Chen Hsu, PhD, *Birmingham*

Mohit Kapoor, PhD, *Toronto*

Seoyoung Kim, MD, ScD, MSCE, *Boston*

Vasileios Kytтарыs, MD, *Boston*

Carl D. Langefeld, PhD,

Winston-Salem

Dennis McGonagle, FRCPI, PhD, *Leeds*

Julie Paik, MD, MHS, *Baltimore*

Amr Sawalha, MD, *Pittsburgh*

Julie Zikherman, MD, *San Francisco*

AMERICAN COLLEGE OF RHEUMATOLOGY

Kenneth G. Saag, MD, MSc, *Birmingham*, **President**

Douglas White, MD, PhD, *La Crosse*, **President-Elect**

Carol Langford, MD, MHS, *Cleveland*, **Treasurer**

Deborah Desir, MD, *New Haven*, **Secretary**

Steven Echard, IOM, CAE, *Atlanta*, **Executive Vice-President**

© 2022 American College of Rheumatology. All rights reserved. No part of this publication may be reproduced, stored or transmitted in any form or by any means without the prior permission in writing from the copyright holder. Authorization to copy items for internal and personal use is granted by the copyright holder for libraries and other users registered with their local Reproduction Rights Organization (RRO), e.g. Copyright Clearance Center (CCC), 222 Rosewood Drive, Danvers, MA 01923, USA (www.copyright.com), provided the appropriate fee is paid directly to the RRO. This consent does not extend to other kinds of copying such as copying for general distribution, for advertising or promotional purposes, for creating new collective works or for resale. Special requests should be addressed to: permissions@wiley.com.

Access Policy: Subject to restrictions on certain backfiles, access to the online version of this issue is available to all registered Wiley Online Library users 12 months after publication. Subscribers and eligible users at subscribing institutions have immediate access in accordance with the relevant subscription type. Please go to onlinelibrary.wiley.com for details.

The views and recommendations expressed in articles, letters, and other communications published in *Arthritis & Rheumatology* are those of the authors and do not necessarily reflect the opinions of the editors, publisher, or American College of Rheumatology. The publisher and the American College of Rheumatology do not investigate the information contained in the classified advertisements in this journal and assume no responsibility concerning them. Further, the publisher and the American College of Rheumatology do not guarantee, warrant, or endorse any product or service advertised in this journal.

Cover design: Todd Machen

© This journal is printed on acid-free paper.

Arthritis & Rheumatology

An Official Journal of the American College of Rheumatology
www.arthritisrheum.org and wileyonlinelibrary.com

VOLUME 74 • July 2022 • NO. 7

In This Issue	AXXX
Journal Club	AXXX
Clinical Connections	AXXX
Editorial	
Arthritis & Rheumatology: "Mid-Term" Report <i>Daniel H. Solomon, Richard Bucala, Mariana J. Kaplan, and Peter A. Nigrovic</i>	1099
Special	
The 2021 EULAR/American College of Rheumatology Points to Consider for Diagnosis, Management and Monitoring of the Interleukin-1 Mediated Autoinflammatory Diseases: Cryopyrin-Associated Periodic Syndromes, Tumour Necrosis Factor Receptor-Associated Periodic Syndrome, Mevalonate Kinase Deficiency, and Deficiency of the Interleukin-1 Receptor Antagonist <i>Micol Romano, Z. Serap Arici, David Piskin, Sara Alehashemi, Daniel Aletaha, Karyl Barron, Susanne Benseler, Roberta A. Berard, Lori Broderick, Fatma Dedeoglu, Michelle Diebold, Karen Durrant, Polly Ferguson, Dirk Foell, Jonathan S. Hausmann, Olcay Y. Jones, Daniel Kastner, Helen J. Lachmann, Ronald M. Laxer, Dorelia Rivera, Nicola Ruperto, Anna Simon, Marinka Twilt, Joost Frenkel, Hal M. Hoffman, Adriana A. de Jesus, Jasmin B. Kuemmerle-Deschner, Seza Ozen, Marco Gattorno, Raphaela Goldbach-Mansky, and Erkan Demirkaya</i>	1102
Review	
The Conundrum of Lung Disease and Drug Hypersensitivity-like Reactions in Systemic Juvenile Idiopathic Arthritis <i>Bryce A. Binstadt and Peter A. Nigrovic</i>	1122
COVID-19	
Endothelial Cell-Activating Antibodies in COVID-19 <i>Hui Shi, Yu Zuo, Sherwin Navaz, Alyssa Harbaugh, Claire K. Hoy, Alex A. Gandhi, Gautam Sule, Srilakshmi Yalavarthi, Kelsey Gockman, Jacqueline A. Madison, Jintao Wang, Melanie Zuo, Yue Shi, Michael D. Maile, Jason S. Knight, and Yogendra Kanthi</i>	1132
Clinical Images	
Clinical Images: Motor Deficiency and Radicular Pain Secondary to Sarcoidosis <i>Coralie Humann, Caroline Raymond, Daniel Wendling, and Frank Verhoeven</i>	1138
Rheumatoid Arthritis	
Brief Report: The Prominent Role of Hematopoietic Peptidyl Arginine Deiminase 4 in Arthritis: Collagen- and Granulocyte Colony-Stimulating Factor-Induced Arthritis Model in C57BL/6 Mice <i>Shoichi Fukui, Sarah Gutch, Saeko Fukui, Deya Cherpokova, Karen Aymonnier, Casey E. Sheehy, Long Chu, and Denisa D. Wagner</i>	1139
IgG Anti-Citrullinated Protein Antibody Variable Domain Glycosylation Increases Before the Onset of Rheumatoid Arthritis and Stabilizes Thereafter: A Cross-Sectional Study Encompassing ~1,500 Samples <i>Theresa Kissel, Lise Hafkenscheid, Tineke J. Wesemael, Mami Tamai, Shin-ya Kawashiri, Atsushi Kawakami, Hani S. El-Gabalawy, Dirkjan van Schaardenburg, Solbritt Rantapää-Dahlqvist, Manfred Wuhler, Annette H. M. van der Helm-van Mil, Cornelia F. Allaart, Diane van der Woude, Hans U. Scherer, Rene E. M. Toes, and Tom W. J. Huizinga</i>	1147
Epigenetic Regulation of Nutrient Transporters in Rheumatoid Arthritis Fibroblast-like Synoviocytes <i>Alyssa Torres, Brian Pedersen, Isidoro Cobo, Rizi Ai, Roxana Coras, Jessica Murillo-Saich, Gyrid Nygaard, Elsa Sanchez-Lopez, Anne Murphy, Wei Wang, Gary S. Firestein, and Monica Guma</i>	1159
Osteoarthritis	
Prevalence Trends of Site-Specific Osteoarthritis From 1990 to 2019: Findings From the Global Burden of Disease Study 2019 <i>Huibin Long, Qiang Liu, Heyong Yin, Kai Wang, Naicheng Diao, Yuqing Zhang, Jianhao Lin, and Ai Guo</i>	1172
Clinical Images	
Clinical Images: Voriconazole-Induced Synovitis, Enthesitis, and Periostitis <i>Larissa Valor-Méndez, Jochen Wacker, Georg Schett, Bernhard Manger, Julia Fürst, Richard Strauß, and Arnd Kleyer</i>	1183
Psoriatic Arthritis	
Association of Cardiac Biomarkers With Cardiovascular Outcomes in Patients With Psoriatic Arthritis and Psoriasis: A Longitudinal Cohort Study <i>Keith Colaco, Ker-Ai Lee, Shadi Akhtari, Raz Winer, Paul Welsh, Naveed Sattar, Iain B. McInnes, Vinod Chandran, Paula Harvey, Richard J. Cook, Dafna D. Gladman, Vincent Pigué, and Lih Eder</i>	1184
Systemic Lupus Erythematosus	
Identification of Mitofusin 1 and Complement Component 1q Subcomponent Binding Protein as Mitochondrial Targets in Systemic Lupus Erythematosus <i>Yann L. C. Becker, Jean-Philippe Gagné, Anne-Sophie Julien, Tania Lévesque, Isabelle Allaëys, Nadine Gougeard, Vicente Rubio, François-Michel Boisvert, Dominique Jean, Eric Wagner, Guy G. Poirier, Paul R. Fortin, and Eric Boillard</i>	1193

Brief Report: Role of Glutaminase 2 in Promoting CD4+ T Cell Production of Interleukin-2 by Supporting Antioxidant Defense in Systemic Lupus Erythematosus <i>Ryo Hisada, Nobuya Yoshida, Seo Yeon K. Orite, Masataka Umeda, Catalina Burbano, Marc Scherlinger, Michihito Kono, Suzanne Krishfield, and George C. Tsokos</i>	1204
B Cell–Specific Deletion of CR6-Interacting Factor 1 Drives Lupus-like Autoimmunity by Activation of Interleukin-17, Interleukin-6, and Pathogenic Follicular Helper T Cells in a Mouse Model <i>Jin-Sil Park, SeungCheon Yang, Sun-Hee Hwang, JeongWon Choi, Seung-Ki Kwok, Young-Yun Kong, Jeehee Youn, Mi-La Cho, and Sung-Hwan Park</i>	1211
Aptamer-Based Screen of Neuropsychiatric Lupus Cerebrospinal Fluid Reveals Potential Biomarkers That Overlap With the Choroid Plexus Transcriptome <i>Kamala Vanarsa, Prashanth Sasidharan, Valeria Duran, Sirisha Gokaraju, Malavika Nidhi, Anto Sam Crosslee Louis Sam Titus, Sanam Soomro, Ariel D. Stock, Evan Der, Chaim Putterman, Benjamin Greenberg, Chi Chiu Mok, John G. Hanly, and Chandra Mohan</i>	1223
Vasculitis	
Critical Role of Notch-1 in Mechanistic Target of Rapamycin Hyperactivity and Vascular Inflammation in Patients With Takayasu Arteritis <i>Wanwan Jiang, Mengyao Sun, Ying Wang, Ming Zheng, Zixin Yuan, Shixiong Mai, Xin Zhang, Longhai Tang, Xiyu Liu, Chunhong Wang, and Zhenke Wen</i>	1235
Systemic Sclerosis	
Self-Assembled Human Skin Equivalents Model Macrophage Activation of Cutaneous Fibrogenesis in Systemic Sclerosis <i>Mengqi Huang, Avi Smith, Matthew Watson, Rajan Bhandari, Lauren M. Baugh, Irena Ivanovska, Trishawna Watkins, Irene Lang, Maria Trojanowska, Lauren D. Black III, Patricia A. Pioli, Jonathan Garlick, and Michael L. Whitfield</i>	1245
Pediatric Rheumatology	
Role for Granulocyte Colony-Stimulating Factor in Neutrophilic Extramedullary Myelopoiesis in a Murine Model of Systemic Juvenile Idiopathic Arthritis <i>Bert Malengier-Devlies, Eline Bernaerts, Kouros Ahmadzadeh, Jessica Filtjens, Jessica Vandenhaute, Bram Boeckx, Oliver Burton, Amber De Visscher, Tania Mitera, Nele Berghmans, Geert Verbeke, Adrian Liston, Diether Lambrechts, Paul Proost, Carine Wouters, and Patrick Matthys</i>	1257
Identification of Distinct Inflammatory Programs and Biomarkers in Systemic Juvenile Idiopathic Arthritis and Related Lung Disease by Serum Proteome Analysis <i>Guangbo Chen, Gail H. Deutsch, Grant S. Schulert, Hong Zheng, SoRi Jang, Bruce Trapnell, Pui Y. Lee, Claudia Macaubas, Katherine Ho, Corinne Schneider, Vivian E. Saper, Adriana Almeida de Jesus, Mark A. Krasnow, Alexei Grom, Raphaela Goldbach-Mansky, Purvesh Khatri, Elizabeth D. Mellins, and Scott W. Canna</i>	1271
Brain Structural Changes During Juvenile Fibromyalgia: Relationships With Pain, Fatigue, and Functional Disability <i>Maria Suñol, Michael F. Payne, Han Tong, Thomas C. Maloney, Tracy V. Ting, Susmita Kashikar-Zuck, Robert C. Coghill, and Marina López-Solà</i>	1284
Letters	
Vascular Deposition of Monosodium Urate Crystals in Gout: Analysis of Cadaveric Tissue by Dual-Energy Computed tomography and Compensated Polarizing Light Microscopy <i>Nicola Dalbeth, Mariam Alhilali, Peter Riordan, Ravi Narang, Ashika Chhana, Sue McGlashan, Anthony Doyle, and Mariano Andres</i>	1295
Sequencing of the 16S Ribosomal DNA Gene and Virulence of the Oral Microbiome in Patients With Rheumatoid Arthritis: Comment on the Article by Kroese et al <i>Yu-Ze Luan, Brian Shiian Chen, and Kevin Sheng-Kai Ma</i>	1296
Reply <i>Johanna M. Kroese, Bernd W. Brandt, Mark J. Buijs, Wim Crielaard, Frank Lobbezoo, Bruno G. Loos, Egija Zaura, Laurette van Boheemen, Dirkjan van Schaardenburg, and Catherine M. C. Volgenant</i>	1297
Increased Cadmium Inhalation as a Possible Explanation for an Increased Risk of Rheumatoid Arthritis Development: Comment on the Article by Okamoto et al <i>David G. Hutchinson</i>	1299
Reply <i>Yuko Okamoto and M. Kristen Demoruelle</i>	1299
Suggested Additions to Future Directions: Comment on the ACR White Paper on Antimalarials and Cardiac Toxicity by Desmarais et al <i>Daniel J. Wallace</i>	1300
Reply <i>Julianna Desmarais, Nicole Fett, James T. Rosenbaum, Karen H. Costenbader, Ellen M. Ginzler, Susan Goodman, James O'Dell, Christian A. Pineau, Gabriela Schmajuk, Victoria P. Werth, Mark S. Link, and Richard Kovacs</i>	1301
Successful Use of Cyclosporin A and Interleukin-1 Blocker Combination Therapy in VEXAS Syndrome: A Single-Center Case Series <i>Corrado Campochiaro, Alessandro Tomelleri, Giulio Cavalli, Giacomo De Luca, Greta Grassini, Maria G. Cangi, and Lorenzo Dagna</i>	1302

Cover image: Immunofluorescence image (from Chen et al., pages 1271–1283) from a lung biopsy section in a patient with systemic juvenile idiopathic arthritis-associated lung disease (SJIA-LD) showing ICAM5 (green) staining largely restricted to interstitial fibroblasts. DAPI-stained nuclei appear in blue, whereas cytokeratin 7 (red) stains alveolar epithelial cells. Histopathology demonstrated the typical pattern of pulmonary alveolar proteinosis and endogenous lipid pneumonia. In this serum proteomics study, peripheral blood soluble ICAM5 levels arose as a promising biomarker of lung disease in SJIA-LD.

In this Issue

Highlights from this issue of *A&R* | By Lara C. Pullen, PhD

First Documentation of Brain Structural Changes During Juvenile Fibromyalgia

Juvenile fibromyalgia (FM), which primarily affects girls, occurs during a critical period of brain development. Typically, synaptic pruning in healthy girls results in a decrease

p. 1284

in frontal gray matter volume (GMV) after age 11. In this issue, Suñol et al (p. 1284) report the results of the first study to assess brain structural alterations in juvenile FM and provide the first evidence of structural alterations in adolescents with juvenile FM. The all-female study reveals that pain-related reductions in the midcingulate cortex (MCC) region may be a structural hallmark of juvenile FM. The investigators also found evidence to suggest that alterations in the regions associated with emotional, self-referential, and

language-related processes may predict disease impact on patients' well-being.

The MCC is not selective for pain, and research has linked activity in this area to multiple functions, including attention, cognitive control, and reward-based learning. Meta-analyses have also previously reported that adult FM patients have GMV reductions in cingulate regions including the MCC. In the current study, investigators found that GMV reductions in the anterior/posterior cingulate cortices of patients with juvenile FM showed partial overlap with findings in adult FM.

Specifically, when the researchers compared juvenile FM patients to controls, they found GMV reductions in the anterior cingulate cortex and the posterior cingulate

cortex. When the researchers examined the juvenile FM group, they found that patients who reported higher functional disability had larger GMV in inferior frontal regions linked to affective, self-referential, and language-related processes. The researchers also found a significant association between functional disability and the left ventrolateral prefrontal cortex. Lastly, the patients' symptom duration was associated with reduced GMV in temporo-parietal areas, including theory of mind- and language-related areas. The authors conclude by noting that the partial overlap between juvenile and adult FM findings reinforces the importance of early symptom identification and intervention to prevent the transition to adult forms of disease.

Self-Assembled Human Skin Equivalent Models for SSc

The research community requires *in vitro* model systems that can represent the interpatient genetic and molecular variability that contributes to the complexity and heterogeneity of systemic sclerosis (SSc). Since *ex vivo*

p. 1245

human tissue preserves the integrity of tissue architecture and the interplay of multiple resident cells within a naive tissue environment, it may represent one solution to this problem. To be effective, such bioengineered *in vitro* models of SSc skin must recapitulate ≥ 1 of the 3 clinical hallmarks of cutaneous fibrosis: altered matrix deposition, inflammatory cell infiltration, and increased dermal rigidity. In addition, the *in vitro* model must overcome the challenge of incorporating myeloid cells to mimic infiltration of inflammatory cells into SSc skin.

In this issue, Huang et al (p. 1245) report the development of *in vitro* skin

models in which the fibroblasts produce their own extracellular matrix to produce a dermal-like tissue. The investigators used stroma synthesized *de novo* from normal dermal fibroblasts (NDFs) and SScDFs to support a fully stratified epithelium to form a self-assembled skin equivalent (saSE) model. The investigators report that SSc saSE constructed with patient-derived fibroblasts and CD14+ peripheral blood monocytes result in macrophages with increased expression of CD206 and CD163 relative to control saSE constructed with healthy control cells. Their data from a saSE suggest that reciprocal activation between macrophages and fibroblasts that is dependent in part on transforming growth factor β activation increases tissue thickness and stiffness. The researchers propose that their saSE system recapitulates the interactions between macrophages and

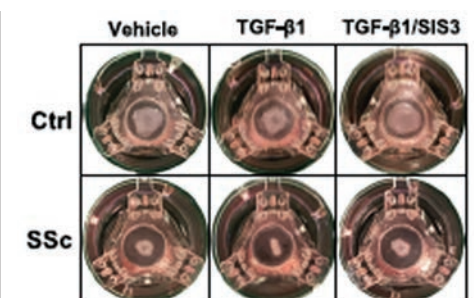


Figure 1. Overhead pictures of control and SSc saSE on day 35.

fibroblasts and thus may serve as a platform for preclinical therapeutic testing and for molecular characterization of SSc skin pathology. The authors conclude their article by stating that saSE provides an opportunity to achieve greater precision in testing personalized responses of potential candidate drugs for SSc.

IgG ACPA Variable Domain Glycosylation Increases Before the Onset of RA and Stabilizes Thereafter

Patients with rheumatoid arthritis (RA) have IgG autoantibodies that are characterized by the abundant presence of bisected and disialylated glycans in the variable domain. Previous studies have demonstrated that N-linked glycan sites are selectively introduced into anti-citrullinated protein antibody (ACPA) B cell receptor sequences upon somatic hypermutation and that variable domain glycan (VDG) levels are significantly elevated in ACPA-positive individuals who subsequently develop RA.

p. 1147

In this issue, Kissel et al (p. 1147) report their comprehensive overview of the expression of VDGs on IgG ACPA over various clinical disease states in RA. They found that the abundance of VDGs on IgG ACPA increases around the time of RA onset and correlates with maturation of the ACPA response. Moreover, while IgG ACPA VDG levels are stable in patients with established disease, a lower degree of VDGs at RA onset correlates with the achievement of drug-free remissions.

The investigators were only able to detect VDG profiles in 70% of the samples analyzed,

but from this data they determined that patients with established RA had constant high expression of glycans on the variable domain of IgG ACPA. Reduced IgG ACPA levels were not, however, the cause of lower VDGs, leading the researchers to hypothesize that VDGs serve as an additional “hit” in determining the fate of the autoreactive B cell response. The authors conclude that, although the underlying biologic mechanisms remain elusive, their data support the concept that variable domain glycosylation relates to an expansion of the ACPA response and contributes to disease development.

Journal Club

A monthly feature designed to facilitate discussion on research methods in rheumatology.

Association of Cardiac Biomarkers with Cardiovascular Outcomes in Patients with PsA and Psoriasis: A Longitudinal Cohort Study

Colaco et al, *Arthritis Rheumatol* 2022; 74:1184–1192.

Conventional cardiovascular (CV) risk scores, such as the Framingham Risk Score (FRS), guide the management of CV risk in the general population and in rheumatic patients. However, these scores tend to underestimate CV risk in patients with psoriatic disease (PsD), because most rely only on traditional CV risk factors and fail to consider the independent risk conferred by immune disease. This study assessed whether 2 cardiac biomarkers, cardiac troponin I (cTnI) and N-terminal pro-brain natriuretic peptide (NT-proBNP), could improve prediction of CV events in patients with PsD, beyond the FRS.

Clinical and laboratory data from 1,000 PsD patients who participated in a longitudinal cohort study were analyzed. The association between cardiac biomarkers and carotid atherosclerosis was assessed in 358 patients by multivariable regression after adjusting for CV risk factors. The authors found that cTnI, but not NT-proBNP, was significantly associated with the extent of carotid atherosclerosis at baseline, and none of the biomarkers predicted progression of atherosclerosis. Next, the association between cardiac biomarkers and incident CV events was assessed using Cox regression models. Both cTnI and NT-proBNP were significantly associated with CV events independently of FRS. Nonlinear relationships were observed for both biomarkers and CV events. Finally, the improvement in prediction of CV events beyond the FRS was tested using measures of risk discrimination and reclassification. The addition of cTnI and NT-proBNP to the FRS did not

demonstrate improvements in any measure of risk discrimination or reclassification.

The study established the association among elevated cardiac biomarkers, atherosclerosis, and clinical CV events in PsD patients. cTnI may be as effective as established measures of carotid atherosclerosis for identifying subclinical atherosclerosis long before clinical events occur. Both cTnI and NT-proBNP are associated with incident CV events independent of traditional CV risk factors and may reflect excess risk in PsD patients. However, the lack of improvement in prediction metrics beyond the FRS does not support the routine use of these cardiac biomarkers for CV risk stratification in asymptomatic PsD patients.

Questions

1. What are the risk factors for CV disease in PsD patients, what is the approach to CV risk stratification in this patient population, and what are the limitations of existing methods?
2. Discuss the statistical approaches and metrics used in this study to assess causal relationships (regression coefficients) versus the approaches used to assess prediction (areas under the curve, reclassification metrics). Were these methods appropriate?
3. How do the results from this study compare to other studies in rheumatoid arthritis, and how can the results inform clinical practice?

In this Issue

Highlights from this issue of *A&R* | By Lara C. Pullen, PhD

First Documentation of Brain Structural Changes During Juvenile Fibromyalgia

Juvenile fibromyalgia (FM), which primarily affects girls, occurs during a critical period of brain development. Typically, synaptic pruning in healthy girls results in a decrease

p. 1284

in frontal gray matter volume (GMV) after age 11. In this issue, Suñol et al (p. 1284) report the results of the first study to assess brain structural alterations in juvenile FM and provide the first evidence of structural alterations in adolescents with juvenile FM. The all-female study reveals that pain-related reductions in the midcingulate cortex (MCC) region may be a structural hallmark of juvenile FM. The investigators also found evidence to suggest that alterations in the regions associated with emotional, self-referential, and

language-related processes may predict disease impact on patients' well-being.

The MCC is not selective for pain, and research has linked activity in this area to multiple functions, including attention, cognitive control, and reward-based learning. Meta-analyses have also previously reported that adult FM patients have GMV reductions in cingulate regions including the MCC. In the current study, investigators found that GMV reductions in the anterior/posterior cingulate cortices of patients with juvenile FM showed partial overlap with findings in adult FM.

Specifically, when the researchers compared juvenile FM patients to controls, they found GMV reductions in the anterior cingulate cortex and the posterior cingulate

cortex. When the researchers examined the juvenile FM group, they found that patients who reported higher functional disability had larger GMV in inferior frontal regions linked to affective, self-referential, and language-related processes. The researchers also found a significant association between functional disability and the left ventrolateral prefrontal cortex. Lastly, the patients' symptom duration was associated with reduced GMV in temporoparietal areas, including theory of mind- and language-related areas. The authors conclude by noting that the partial overlap between juvenile and adult FM findings reinforces the importance of early symptom identification and intervention to prevent the transition to adult forms of disease.

Self-Assembled Human Skin Equivalent Models for SSc

The research community requires *in vitro* model systems that can represent the interpatient genetic and molecular variability that contributes to the complexity and heterogeneity of systemic sclerosis (SSc). Since *ex vivo*

p. 1245

human tissue preserves the integrity of tissue architecture and the interplay of multiple resident cells within a naive tissue environment, it may represent one solution to this problem. To be effective, such bioengineered *in vitro* models of SSc skin must recapitulate ≥ 1 of the 3 clinical hallmarks of cutaneous fibrosis: altered matrix deposition, inflammatory cell infiltration, and increased dermal rigidity. In addition, the *in vitro* model must overcome the challenge of incorporating myeloid cells to mimic infiltration of inflammatory cells into SSc skin.

In this issue, Huang et al (p. 1245) report the development of *in vitro* skin

models in which the fibroblasts produce their own extracellular matrix to produce a dermal-like tissue. The investigators used stroma synthesized *de novo* from normal dermal fibroblasts (NDFs) and SScDFs to support a fully stratified epithelium to form a self-assembled skin equivalent (saSE) model. The investigators report that SSc saSE constructed with patient-derived fibroblasts and CD14+ peripheral blood monocytes result in macrophages with increased expression of CD206 and CD163 relative to control saSE constructed with healthy control cells. Their data from a saSE suggest that reciprocal activation between macrophages and fibroblasts that is dependent in part on transforming growth factor β activation increases tissue thickness and stiffness. The researchers propose that their saSE system recapitulates the interactions between macrophages and

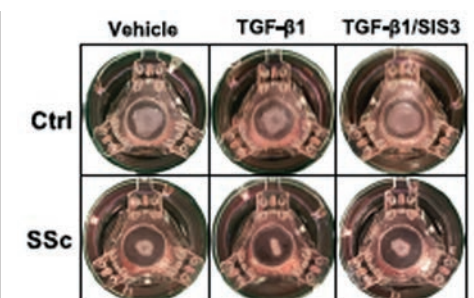


Figure 1. Overhead pictures of control and SSc saSE on day 35.

fibroblasts and thus may serve as a platform for preclinical therapeutic testing and for molecular characterization of SSc skin pathology. The authors conclude their article by stating that saSE provides an opportunity to achieve greater precision in testing personalized responses of potential candidate drugs for SSc.

IgG ACPA Variable Domain Glycosylation Increases Before the Onset of RA and Stabilizes Thereafter

Patients with rheumatoid arthritis (RA) have IgG autoantibodies that are characterized by the abundant presence of bisected and disialylated glycans in the variable

p. 1147

domain. Previous studies have demonstrated that N-linked glycan sites are selectively introduced into anti-citrullinated protein antibody (ACPA) B cell receptor sequences upon somatic hypermutation and that variable domain glycan (VDG) levels are significantly elevated in ACPA-positive individuals who subsequently develop RA.

In this issue, Kissel et al (p. 1147) report their comprehensive overview of the expression of VDGs on IgG ACPA over various clinical disease states in RA. They found that the abundance of VDGs on IgG ACPA increases around the time of RA onset and correlates with maturation of the ACPA response. Moreover, while IgG ACPA VDG levels are stable in patients with established disease, a lower degree of VDGs at RA onset correlates with the achievement of drug-free remissions.

The investigators were only able to detect VDG profiles in 70% of the samples analyzed,

but from this data they determined that patients with established RA had constant high expression of glycans on the variable domain of IgG ACPA. Reduced IgG ACPA levels were not, however, the cause of lower VDGs, leading the researchers to hypothesize that VDGs serve as an additional “hit” in determining the fate of the autoreactive B cell response. The authors conclude that, although the underlying biologic mechanisms remain elusive, their data support the concept that variable domain glycosylation relates to an expansion of the ACPA response and contributes to disease development.

Journal Club

A monthly feature designed to facilitate discussion on research methods in rheumatology.

Association of Cardiac Biomarkers with Cardiovascular Outcomes in Patients with PsA and Psoriasis: A Longitudinal Cohort Study

Colaco et al, *Arthritis Rheumatol* 2022; 74:1184–1192.

Conventional cardiovascular (CV) risk scores, such as the Framingham Risk Score (FRS), guide the management of CV risk in the general population and in rheumatic patients. However, these scores tend to underestimate CV risk in patients with psoriatic disease (PsD), because most rely only on traditional CV risk factors and fail to consider the independent risk conferred by immune disease. This study assessed whether 2 cardiac biomarkers, cardiac troponin I (cTnI) and N-terminal pro-brain natriuretic peptide (NT-proBNP), could improve prediction of CV events in patients with PsD, beyond the FRS.

Clinical and laboratory data from 1,000 PsD patients who participated in a longitudinal cohort study were analyzed. The association between cardiac biomarkers and carotid atherosclerosis was assessed in 358 patients by multivariable regression after adjusting for CV risk factors. The authors found that cTnI, but not NT-proBNP, was significantly associated with the extent of carotid atherosclerosis at baseline, and none of the biomarkers predicted progression of atherosclerosis. Next, the association between cardiac biomarkers and incident CV events was assessed using Cox regression models. Both cTnI and NT-proBNP were significantly associated with CV events independently of FRS. Nonlinear relationships were observed for both biomarkers and CV events. Finally, the improvement in prediction of CV events beyond the FRS was tested using measures of risk discrimination and reclassification. The addition of cTnI and NT-proBNP to the FRS did not

demonstrate improvements in any measure of risk discrimination or reclassification.

The study established the association among elevated cardiac biomarkers, atherosclerosis, and clinical CV events in PsD patients. cTnI may be as effective as established measures of carotid atherosclerosis for identifying subclinical atherosclerosis long before clinical events occur. Both cTnI and NT-proBNP are associated with incident CV events independent of traditional CV risk factors and may reflect excess risk in PsD patients. However, the lack of improvement in prediction metrics beyond the FRS does not support the routine use of these cardiac biomarkers for CV risk stratification in asymptomatic PsD patients.

Questions

1. What are the risk factors for CV disease in PsD patients, what is the approach to CV risk stratification in this patient population, and what are the limitations of existing methods?
2. Discuss the statistical approaches and metrics used in this study to assess causal relationships (regression coefficients) versus the approaches used to assess prediction (areas under the curve, reclassification metrics). Were these methods appropriate?
3. How do the results from this study compare to other studies in rheumatoid arthritis, and how can the results inform clinical practice?

Clinical Connections

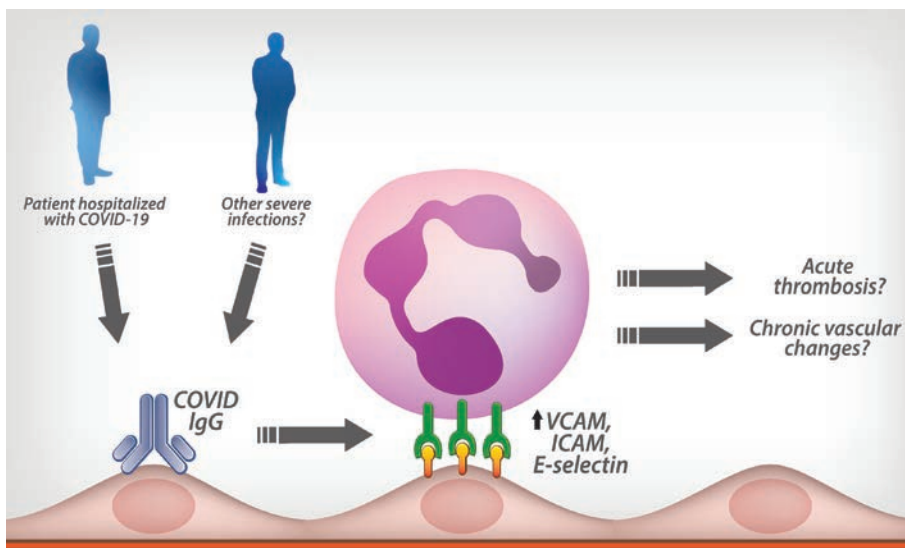
Endothelial Cell–Activating Antibodies in COVID-19

Shi et al, *Arthritis Rheumatol* 2022;74:1132–1138

CORRESPONDENCE

Jason S. Knight, MD, PhD: jsknight@umich.edu

Yogendra Kanthi, MD: yogen.kanthi@nih.gov



KEY POINTS

- At least 1 type of aPL was detected in half of patients hospitalized with COVID-19 during the early months of the pandemic.
- COVID-19 serum activated endothelial cells to express cell adhesion molecules that could potentially serve as a nidus for thrombosis and inflammation.
- Positive testing for aPLs identified COVID-19 serum that was more likely to activate endothelial cells.
- Depletion of total IgG from COVID-19 serum reduced endothelial activation.

SUMMARY

COVID-19–associated coagulopathy predisposes to inflammation and thrombosis in arterial, venous, and microscopic vascular beds. Recently, there have been numerous descriptions of what appears to be de novo autoantibody formation in individuals with severe COVID-19. Furthermore, there is evidence that the circulating B cell compartment of COVID-19 resembles that found in lupus, where naive B cells take an extrafollicular route to becoming antibody-producing cells and thereby bypass the normal tolerance checkpoints provided by the germinal center. While potentially prothrombotic antiphospholipid antibodies (aPLs) have regularly been detected in association with severe COVID-19, the extent to which these antibodies contribute to vascular inflammation in COVID-19 remains to be fully elucidated.

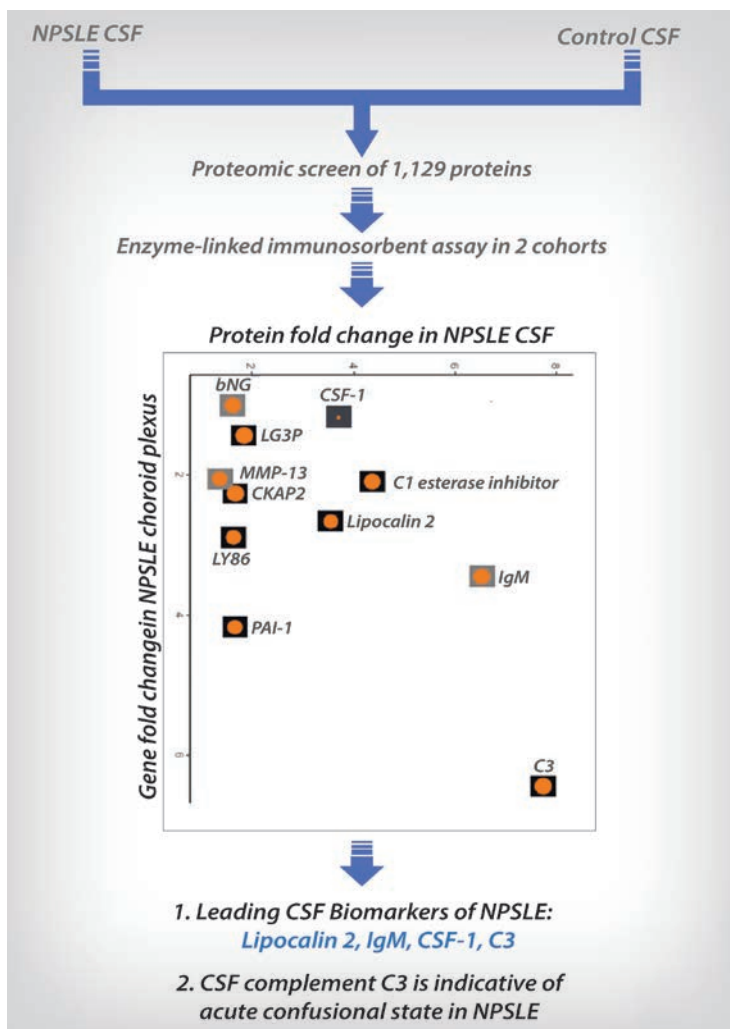
Shi et al found that serum from patients hospitalized with COVID-19 activated cultured endothelial cells to express surface adhesion molecules integral to inflammation and thrombosis, namely E-selectin, intercellular adhesion molecule 1 (ICAM-1), and vascular cell adhesion molecule 1 (VCAM-1). The presence of circulating aPLs was a strong marker of the ability of COVID-19 serum to activate endothelial cells, while depletion of total IgG from aPL-positive serum markedly reduced activation. Importantly, total IgG transferred the endothelial activation capacity of aPL-positive COVID serum to healthy control serum. It should be noted that all experiments were with total IgG fractions and not affinity-purified aPLs. Therefore, aPLs may mark antibody profiles in severe illness, quite possibly polyclonal, that activate the endothelium and steer the normally quiescent blood–vessel interface toward inflammation and coagulation.

Aptamer-Based Screen of Neuropsychiatric Lupus CSF Reveals Potential Biomarkers That Overlap With Choroid Plexus Transcriptome

Vanarsa et al, *Arthritis Rheumatol* 2022;74:1223–1234

CORRESPONDENCE

Chandra Mohan, MD, PhD: cmohan@central.uh.edu



SUMMARY

Forty to 91% of patients with lupus present with a wide variety of central or peripheral nervous system manifestations, collectively termed neuropsychiatric systemic lupus erythematosus (NPSLE). Currently, we do not have reliable biomarkers that can establish a definitive diagnosis of NPSLE. Vanarsa et al have carried out a broad proteomic screen of cerebrospinal fluid (CSF) from NPSLE patients using a library of aptamers.

Of the 1,129 CSF proteins interrogated, 23 proteins were significantly elevated in NPSLE CSF, compared to CSF from other neurologic disease controls and healthy controls. Interestingly, 11 proteins elevated in NPSLE CSF were also elevated in the choroid plexus in murine NPSLE, suggesting shared origins. Validation using an orthogonal platform confirmed the elevation of several of these proteins in NPSLE CSF drawn from 2 different cohorts (1 predominantly White cohort and 1 predominantly Chinese cohort), although ethnic differences were also noted. CSF α 2-macroglobulin, IgM, complement C3, macrophage CSF (M-CSF), and serine protease inhibitor G1 exhibited high specificity and positive predictive value for diagnosing NPSLE. Of these, M-CSF, IgM, and lipocalin 2 exhibited the highest diagnostic accuracy. Interestingly, 75% of the NPSLE patients with elevated CSF C3 had acute confusion.

Collectively, these studies highlight the diagnostic potential of M-CSF, IgM, and lipocalin 2 in NPSLE and warrant further validation. Based on previously reported mechanistic studies in murine models of NPSLE, M-CSF and lipocalin 2 are also likely to be pathogenic disease drivers and potential therapeutic targets.

KEY POINTS

- Comprehensive aptamer-based screens are powerful tools for identifying novel biomarkers for end-organ disease in lupus.
- M-CSF, IgM, and lipocalin 2 are potential diagnostic markers of NPSLE.
- Elevated CSF C3 may be a marker of pathogenic events leading to acute confusion in NPSLE.

EDITORIAL

Arthritis & Rheumatology: “Mid-Term” Report

Daniel H. Solomon,¹  Richard Bucala,²  Mariana J. Kaplan,³  and Peter A. Nigrovic⁴ 

As the current *Arthritis & Rheumatology* (A&R) editorial team approaches halfway into our 5-year term, we took stock of what is working and where we can make improvements. COVID-19 and COVID-19 manuscripts dominated the lives of our authors, reviewers, and editors for much of year 1 of the term. With many investigators out of the research setting, articles were finished and submitted, leading to a 50% increase in submissions for the first 6 months of our term. An amazing editorial team, staff, and academic editors handled the “surge” with characteristic grace. We balanced the need to publish COVID-19 work quickly with the requirement for scientific rigor, and only time will tell if A&R succeeded in achieving balance.

Initiatives in the first 2 years

After surviving the first wave of COVID-19, several initiatives were rolled out or strengthened during the first part of our term at A&R. First and foremost, A&R remains committed to publishing high-impact randomized controlled clinical trials (RCTs) in a timely manner. During 2021, A&R received 56 RCT submissions and published 20 of them (36%). These include a sham-controlled test of acupuncture for osteoarthritis (1), phase II testing of a new molecule for the treatment of systemic lupus erythematosus (2), a randomized withdrawal study in psoriatic arthritis (3), and multiple trials of urate-lowering agents for gout (4,5). We offer a fast-track review option with a time to first review of 10–14 days. Authors of RCTs (like all original articles) can submit a video summary of the accepted manuscript. A&R’s social media editor promotes all trials and their videos through the American College of Rheumatology (ACR) journal accounts on relevant social media platforms.

Commentaries published as “Notes From the Field” broadened the range of topics covered in A&R; this article type provides

authors a venue to comment on the policy, business, and ethics of rheumatology and rheumatic disease research. Recent papers comment on comparative safety studies of urate-lowering agents (6) and the treat-to-target paradigm from a patient perspective (7). We continue to encourage authors to reach out to editors with ideas for new commentaries. In response to the needs of clinicians, a new review type was initiated focusing on challenging clinical scenarios. This article type, “Expert Perspectives on Clinical Challenges,” has been well received by readers and helps balance our research content with pragmatic advice from world-leading clinicians. We welcome your ideas for future Expert Perspectives.

To render research findings easier to interpret, we have instituted new policies with respect to figures (8). The maximum figure size was increased from half a page to a page, enabling in-depth exploration of large data sets, and by editorial policy we require that individual data points be displayed wherever possible, largely prohibiting “dynamite plunger plots” that fail to clearly show subpopulations or outliers within a data set. We have begun routinely to request that authors revise figures to improve clarity, resolution, and aesthetic value.

Current directions

The editorial team strives to stay current with relevant societal trends in medicine, research, and publishing. We recognize the importance of promoting diversity and equity in the work published by A&R and have added an associate editor focused on these issues. We have developed a checklist for authors and updated the author instructions (<https://onlinelibrary.wiley.com/page/journal/23265205/homepage/forauthors.html>) to clarify how to describe sex, gender, race, and ethnicity in a study population. We recognize that this checklist will not apply to all studies and that

Dr. Kaplan contributed to this article in her personal capacity. The views expressed are her own and do not necessarily represent the views of the National Institutes of Health or the United States Government.

¹Daniel H. Solomon, MD, MPH: Brigham and Women’s Hospital, Boston, Massachusetts (Editor-in-Chief, *Arthritis & Rheumatology*); ²Richard Bucala, MD, PhD: Yale School of Medicine, New Haven, Connecticut (Deputy Editor, *Arthritis & Rheumatology*); ³Mariana J. Kaplan, MD: National Institute of Arthritis and Musculoskeletal and Skin Diseases, NIH, Bethesda, Maryland (Deputy Editor, *Arthritis & Rheumatology*); ⁴Peter A. Nigrovic, MD: Brigham and

Women’s Hospital and Boston Children’s Hospital, Boston, Massachusetts (Deputy Editor, *Arthritis & Rheumatology*).

Author disclosures are available at <https://onlinelibrary.wiley.com/action/downloadSupplement?doi=10.1002%2Fart.42131&file=art42131-sup-0001-Disclosureform.pdf>.

Address correspondence to Daniel H. Solomon, MD, MPH, Brigham and Women’s Hospital, 60 Fenwood Road, Boston, MA 02115. Email: dsolomon@bwh.harvard.edu.

Submitted for publication March 2, 2022; accepted in revised form March 25, 2022.

in some studies data were collected prior to the development of these new standards. However, over time, we expect that authors will collect data with the new standards in mind. *A&R* welcomes submissions that focus on diversity and equity issues in rheumatology.

We recognize the importance of succinct communication of research results in a format that is easy to transmit. Thus, *A&R* will promote the use of graphical or visual abstracts. These abstracts help promote research findings in a uniform visual manner to multiple audiences, including patients. To this end, we have collaborated with a graphics platform to create standardized templates, icons, and formats, simplifying the process for the authors of accepted manuscripts.

Finally, *A&R* has joined the modern era and will now allow publication of manuscripts that have appeared on preprint servers. While we were already receptive to basic/translational science manuscripts that were previously published on a preprint server, we have subsequently decided to allow all submissions that may have been published on a preprint server. The COVID-19 era has taught us all a lot about the importance of timely dissemination of research findings. While many manuscripts listed on preprint servers are not ultimately accepted after peer review, we do not want to limit authors' ability to disseminate their science, thereby soliciting input from the broader community before the final peer-reviewed version is published.

Journal performance

The Impact Factor of *A&R* has risen to 10.995 in 2021. We congratulate *Nature Reviews Rheumatology* and *Annals of the Rheumatic Diseases* on their astronomically high Impact Factors. Authors conducting research on rheumatic diseases have great options for target journals. *A&R* knows this and prides itself on promoting the research published in the journal: *A&R* articles were downloaded more than 4.3 million times in 2021; *A&R* articles were cited more than 16,730 times in 2020 (2021 statistics pending); and these articles received 7,120 mentions according to Altmetrics. The journal recently compiled an online issue containing the top 20 most mentioned articles, that we are providing as free access at [https://onlinelibrary.wiley.com/doi/toc/10.1002/\(ISSN\)2326-5205](https://onlinelibrary.wiley.com/doi/toc/10.1002/(ISSN)2326-5205). top-almetric.

While we recognize that the acceptance rate in *A&R* is low—13–14% for original articles—*A&R* endeavors to make the process as positive as possible by giving authors feedback quickly. Time until first decision averages 15 days, and time until first review for papers sent out for peer review averages 42 days. We have dedicated editors and peer reviewers who ensure high-quality feedback. *A&R* is always on the lookout for new expert reviewers. In fact, we are part of the ACR's Rheum With a (re)View initiative to train and recruit junior reviewers; feel free to send us your qualifications and we will consider you for future reviews.

Table 1. Unique topics of accepted manuscripts in *Arthritis & Rheumatology*, 2021

Topic	%
Rheumatoid arthritis	19.7
Systemic lupus erythematosus	11.3
Osteoarthritis	10.6
Vasculitis	7.9
Ankylosing spondylitis/psoriatic arthritis	6.9
COVID-19	5.2
Systemic sclerosis	5.1
Crystal arthritis	4.9
Autoinflammatory disease	3.7
Idiopathic inflammatory myopathies	3.7
Pain/fibromyalgia/spine	3.3
Pediatric rheumatic disease	2.8
Sjögren's syndrome	2.7
Bone/cartilage	1.7
Other*	10.5

* Includes rheumatology policy, Behçet's disease, relapsing poly-chondritis, IgG4-related disease, osteitis, sarcoidosis, and Lyme disease.

A&R strives to represent all types of rheumatic disease research, publishing on all rheumatic diseases (Table 1). Moreover, we include the full range of methods in our pages, with a near-even split between basic/translational and clinical research. *A&R* remains committed to publishing state-of-the-art basic and translational science that advances the field. Another important trend to note is the continued diversity of global regions represented in *A&R*. In 2021, 20% of accepted original articles were from Asia, 40% from Europe, 38% from North America, and 2% from the rest of the world.

A&R's authors benefit from expert professional manuscript editors who are well trained in rheumatic disease science publishing. As one of 3 official journals of the ACR, we collaborate closely with *Arthritis Care & Research* and *ACR Open Rheumatology*. Contents are complementary, editors share ideas, and authors benefit from the opportunity to transfer manuscripts seamlessly from one journal to another if appropriate.

We look forward to the next two and a half years of our tenure and hope you will continue to contribute and enjoy the contents of *A&R*. We exist to serve the rheumatology community; please let us know how we are doing!













REFERENCES

- Tu JF, Yang JW, Shi GX, Yu ZS, Li JL, Lin LL, et al. Efficacy of intensive acupuncture versus sham acupuncture in knee osteoarthritis: a randomized controlled trial. *Arthritis Rheumatol* 2021; 73:448–58.
- Isenberg D, Furie R, Jones NS, Guibord P, Galanter J, Lee C, et al. Efficacy, safety, and pharmacodynamic effects of the Bruton's tyrosine kinase inhibitor fenebrutinib (GDC-0853) in systemic lupus erythematosus: results of a phase II, randomized, double-blind, placebo-controlled trial. *Arthritis Rheumatol* 2021;73:1835–46.
- Coates LC, Pillai SG, Tahir H, Valter I, Chandran V, Kameda H, et al. Withdrawing ixekizumab in patients with psoriatic arthritis who

- achieved minimal disease activity: results from a randomized, double-blind withdrawal study. *Arthritis Rheumatol* 2021;73:1663–72.
4. Gaffo AL, Calhoun DA, Rahn EJ, Oparil S, Li P, Dudenbostel T, et al. Effect of serum urate lowering with allopurinol on blood pressure in young adults: a randomized, controlled, crossover trial. *Arthritis Rheumatol* 2021;73:1514–22.
 5. Khanna PP, Khanna D, Cutter G, Foster J, Melnick J, Jaafar S, et al. Reducing immunogenicity of pegloticase with concomitant use of mycophenolate mofetil in patients with refractory gout: a phase II, randomized, double-blind, placebo-controlled trial. *Arthritis Rheumatol* 2021;73:1523–32.
 6. Choi HK, Neogi T, Stamp LK, Terkeltaub R, Dalbeth N. Reassessing the cardiovascular safety of febuxostat: implications of the febuxostat versus allopurinol streamlined trial. *Arthritis Rheumatol* 2021;73:721–4.
 7. Schoemaker CG, de Wit MP. Treat-to-target from the patient perspective is bowling for a perfect strike. *Arthritis Rheumatol* 2021;73:9–11.
 8. Solomon DH, Binstadt BA, Felson DT, Nigrovic PA. A picture is worth a thousand words, but only if it is a good picture [editorial]. *Arthritis Rheumatol* 2021;73:912–3.

SPECIAL

The 2021 EULAR/American College of Rheumatology Points to Consider for Diagnosis, Management and Monitoring of the Interleukin-1 Mediated Autoinflammatory Diseases: Cryopyrin-Associated Periodic Syndromes, Tumour Necrosis Factor Receptor-Associated Periodic Syndrome, Mevalonate Kinase Deficiency, and Deficiency of the Interleukin-1 Receptor Antagonist

Micol Romano,¹ Z. Serap Arici,² David Piskin,¹ Sara Alehashemi,³  Daniel Aletaha,⁴  Karyl Barron,⁵ Susanne Bensele,⁶ Roberta A. Berard,¹  Lori Broderick,⁷ Fatma Dedeoglu,⁸  Michelle Diebold,¹ Karen Durrant,⁹ Polly Ferguson,¹⁰ Dirk Foell,¹¹  Jonathan S. Hausmann,¹²  Olcay Y. Jones,¹³ Daniel Kastner,¹⁴ Helen J. Lachmann,¹⁵ Ronald M. Laxer,¹⁶ Dorelia Rivera,¹⁷ Nicola Ruperto,¹⁸  Anna Simon,¹⁹ Marinka Twilt,⁶ Joost Frenkel,²⁰ Hal M. Hoffman,²¹ Adriana A. de Jesus,³ Jasmin B. Kuemmerle-Deschner,²²  Seza Ozen,²³  Marco Gattorno,¹⁸  Raphaela Goldbach-Mansky,³  and Erkan Demirkaya¹ 

Background. The interleukin-1 (IL-1) mediated systemic autoinflammatory diseases, including the cryopyrin-associated periodic syndromes (CAPS), tumour necrosis factor receptor-associated periodic syndrome (TRAPS), mevalonate kinase deficiency (MKD) and deficiency of the IL-1 receptor antagonist (DIRA), belong to a group of rare immunodysregulatory diseases that primarily present in early childhood with variable multiorgan involvement. When untreated, patients with severe clinical phenotypes have a poor prognosis, and diagnosis and management of these patients can be challenging. However, approved treatments targeting the proinflammatory cytokine IL-1 have been life changing and have significantly improved patient outcomes.

Objective. To establish evidence-based recommendations for diagnosis, treatment and monitoring of patients with IL-1 mediated autoinflammatory diseases to standardise their management.

Methods. A multinational, multidisciplinary task force consisting of physician experts, including rheumatologists, patients or caregivers and allied healthcare professionals, was established. Evidence synthesis, including systematic literature review and expert consensus (Delphi) via surveys, was conducted. Consensus methodology was used to formulate and vote on statements to guide optimal patient care.

Results. The task force devised five overarching principles, 14 statements related to diagnosis, 10 on therapy, and nine focused on long-term monitoring that were evidence and/or consensus-based for patients with IL-1 mediated diseases. An outline was developed for disease-specific monitoring of inflammation-induced organ damage progression and reported treatments of CAPS, TRAPS, MKD and DIRA.

Conclusion. The 2021 EULAR/American College of Rheumatology points to consider represent state-of-the-art knowledge based on published data and expert opinion to guide diagnostic evaluation, treatment and monitoring of patients with CAPS, TRAPS, MKD and DIRA, and to standardise and improve care, quality of life and disease outcomes.

This article is published simultaneously in *Annals of the Rheumatic Diseases* and was copyedited by *Annals of the Rheumatic Diseases*.

Supported by EULAR/American College of Rheumatology, and supported in part by the intramural research programme of the NIH institutes, NIAID, NHGRI and NIAMS.

Drs. Romano, Arici and Piskin contributed equally to this work.

Dr. Kuemmerle-Deschner's work was done in cooperation with ERN-RITA.*
*[Correction added after online publication 27 May 2022: a new paragraph was added to disclose Dr. Kuemmerle-Deschner's work as a member of ERN-RITA.]

¹Micol Romano, MD, David Piskin, MD, Roberta A. Berard, MD, Michelle Diebold, RN, Erkan Demirkaya, MD, MSc: University of Western

INTRODUCTION

Systemic autoinflammatory diseases (SAIDs) are a group of multisystem immunodysregulatory disorders caused primarily by the dysfunction of the innate immune system (1). Currently, SAIDs comprise a wide range of disorders with systemic and organ-specific inflammation in the absence of infections or autoimmunity (2–6). In a subset of genetically defined SAIDs, the pathogenesis is driven by increased release or signaling of the proinflammatory cytokine interleukin-1 (IL-1) (2,7,8).

The conditions addressed by this task force include the IL-1 mediated SAIDs (monogenic forms) that are most frequently evaluated by rheumatologists, and which have US Food and Drug Administration/European Medicines Agency (FDA/EMA) approval for IL-1 targeted therapies. Cryopyrin-associated periodic syndromes (CAPS) (9,10) or NLRP3-associated autoinflammatory diseases (NLRP3-AIDs) (11) are the spectrum of rare autosomal dominant autoinflammatory diseases caused by gain-of-function mutations in *NLRP3* (9,12–16), ranging from familial cold autoinflammatory syndrome (FCAS; mild NLRP3-AID phenotype), Muckle-Wells syndrome (MWS; moderate NLRP3-AID phenotype) to neonatal onset multisystem inflammatory disease/chronic infantile neurological cutaneous and articular (NOMID/CINCA; severe NLRP3-AID phenotype). The other IL-1 mediated SAIDs included are tumour necrosis factor receptor-associated periodic syndrome (TRAPS), an autosomal dominant disease caused by mutations in *TNFRSF1A* (17,18) encoding the tumour necrosis factor receptor type 1, and mevalonate kinase deficiency (MKD) caused by autosomal recessive loss-of-function mutations in the mevalonate kinase gene (*MVK*), resulting in a deficiency of mevalonate kinase enzyme (19–22). Lastly, deficiency of IL-1 receptor antagonist (DIRA) caused by biallelic deleterious loss-of-function mutations in the *IL1RN* gene encoding the IL-1 receptor antagonist was addressed by the task force (2). The most common IL-1 mediated autoinflammatory disease, familial Mediterranean fever, is not addressed, as EULAR-endorsed recommendations were published for this disease in 2016 (23).

IL-1 mediated SAIDs are caused by chronic systemic and organ-specific inflammation, leading to progressive organ

damage and dysfunction (24–27). Acute disease flares can be life-threatening and contribute to the high morbidity and mortality in untreated patients (17,28,29). In this rapidly evolving group of rare diseases, there is a need to harmonise care that reflects our current knowledge of genetics, diagnosis, treatment and monitoring for all patients globally.

The natural history of untreated patients with pathogenic mutations causing CAPS (10,30,31), TRAPS (18), MKD (32) and DIRA (2) has been characterised in the literature and forms the basis for the guidance on monitoring disease progression and organ damage. Disease severity is dependent on the level of systemic and organ-specific inflammation. Risk factors associated with adverse outcomes include specific mutations, clinically severe phenotypes, frequent and severe inflammatory episodes and organ damage at the time of initial presentation (17,33–36). The life-changing positive impact of treatments targeting IL-1 has been documented in patients with CAPS, TRAPS, MKD and DIRA. There is also mounting evidence for the benefits of maintenance treatment to prevent the progression of organ damage, thus pointing to the importance of early diagnosis and initiating treatment early in life (33,34,37,38).

An early and accurate genetic diagnosis allows for referral for genetic counselling, directs appropriate screening for potential complications, informs prognosis and improves our ability to define individual treatment goals and to tailor treatment decisions (33–37). Most patients with CAPS, TRAPS, MKD and DIRA are managed by paediatricians and paediatric specialists, and with effective treatments, adolescents and young adults are now reaching adulthood with expectations of a normal life span. They now face new challenges with transitioning care to adult rheumatologists comfortable with the management of these patients. Furthermore, pregnancy and other subspecialty needs (ie, surgery) are often not addressed adequately in the context of IL-1 mediated SAIDs. For some patients, the diagnosis may be delayed for decades, resulting in inadequate treatment and the development of permanent disabilities that may translate into special care needs.

The above considerations led to the convening of a task force that was charged with developing standardised guidance

Ontario, London, Ontario, Canada; ²Z. Serap Arici, MD: Sanliurfa Training and Research Hospital, Sanliurfa, Turkey; ³Sara Alehashemi, MD, MPH, Adriana A. de Jesus, MD, PhD: National Institute of Allergy and Infectious Diseases, NIH, Bethesda, Maryland; ⁴Daniel Aletaha, MD, MS, MBA: Medical University of Vienna, Vienna, Austria; ⁵Karyl Barron, MD: National Institute of Allergy and Immunology, NIH, Bethesda, Maryland; ⁶Susanne Benseler, MD, PhD, Marinka Twilt, MD, MSCE, PhD: University of Calgary, Calgary, Alberta, Canada; ⁷Lori Broderick, MD, PhD: University of California and Rady Children's Hospital, San Diego, California; ⁸Fatma Dedeoglu, MD: Harvard Medical School, Boston, Massachusetts; ⁹Karen Durrant, RN, BSN: Autoinflammatory Alliance and Kaiser Foundation Hospital, San Francisco, California; ¹⁰Polly Ferguson, MD: University of Iowa, Iowa City; ¹¹Dirk Foell, MD: University of Muenster, Muenster, Germany; ¹²Jonathan Hausmann, MD: Boston Children's Hospital and Beth Israel Deaconess Medical Center, Boston, Massachusetts; ¹³Olcay Y. Jones, MD: Walter Reed National Military Medical Center, Bethesda, Maryland; ¹⁴Daniel Kastner, MD: National Human Genome Research

Institute, NIH, Bethesda, Maryland; ¹⁵Helen J. Lachmann, MD: University College London, London, UK. ¹⁶Ronald M. Laxer, MD: The Hospital for Sick Children, University of Toronto, Toronto, Ontario, Canada; ¹⁷Dorelia Rivera: Autoinflammatory Alliance, San Francisco, California; ¹⁸Nicola Ruperto, MD, Marco Gattorno, MD: IRCCS Istituto Giannina Gaslini, Genoa, Italy; ¹⁹Anna Simon, MD: Radboud University Medical Centre, Nijmegen, The Netherlands; ²⁰Joost Frenkel, MD: Wilhelmina Kinderziekenhuis, Utrecht, The Netherlands; ²¹Hal M. Hoffman, MD: University of California and Rady Children's Hospital, San Diego, California; ²²Jasmin B. Kuemmerle-Deschner, MD: University Hospital Tubingen, Tubingen, Germany; ²³Seza Ozen, MD: Hacettepe University, Ankara, Turkey.

Address correspondence to Erkan Demirkaya, MD, MSc, FRCP, Division of Pediatric Rheumatology, University of Western Ontario, 800 Commissioners Road East B1-146, London, Ontario N6A 5W9, Canada. E-mail: Erkan.Demirkaya@lhsc.on.ca.

Submitted for publication November 5, 2021; accepted in revised form March 2, 2022.

for diagnosis, treatment and long-term monitoring of patients with CAPS, TRAPS, MKD and DIRA that target paediatricians, inter-nists and subspecialists (particularly rheumatologists). The statements were developed as a resource for physicians to facilitate management, for policy makers who have a role in authorising patients' access to diagnostic tools and treatment options, as well as for patients and caregivers to provide knowledge and allow for setting appropriate expectations. Finally, these guide-lines aim to standardise the level of care with a goal of improving quality of life and disease outcomes worldwide.

METHODS

With approval granted by the EULAR and the American College of Rheumatology (ACR) executive committees, the IL-1 mediated autoinflammatory diseases task force was convened to develop guidance on diagnosis, treatment and monitoring of four different IL-1 mediated SAIDs, including CAPS, TRAPS, MKD and DIRA. The task force was led by two conveners (ED and RG-M) and consisted of 19 paediatric and four adult rheumatologists, who were selected based on their expertise in the treatment and care of these patients. In addition, the task force included two healthcare professionals, three fellows and one patient representative from the Autoinflammatory Alliance and two methodologists. The 31 task force members were from 17 centres in seven different countries from across Europe, the United States and Canada. EULAR (39) and the ACR standardised operating procedures were followed during the project (see [online supplemental methods](#)). The first meeting was convened in August 2019 in Bethesda, Maryland, USA, to define the focus of the task force, which identified four IL-1 mediated SAIDs to be included in this points to consider project. In line with the EULAR standardised operating procedures, the target audience was defined as healthcare professionals, policy makers, health insurance companies, patients and their caregivers. The group worked to determine the PICO (Population, Intervention, Comparison, Outcome) questions related to diagnosis, monitoring and management of these diseases. Using the PICO questions defined during the first meeting, a systematic literature review was performed by three research fellows (MR, ZSA, DP) with support from a librarian (DH) and the senior methodologists (ED, DA) to identify relevant publications using PubMed, Embase and the Cochrane Library through August 2020.

Before the first consensus meeting, two surveys that included statements or items pertaining to diagnosis, treatment and long-term monitoring were distributed to all task force members via RedCap. The task force members were asked to indicate their agreement with each statement or item with yes or no. A free-text option was provided to capture every member's comments or suggestions for modification; and a request was made to add items to be addressed, edited or altered. Consensus was achieved using the Delphi technique. Draft statements with 80% or higher agreement were retained. Comments and suggestions

provided in the questionnaires were used to modify the draft statements and to add additional items. The revised and amended statements were then sent through a second round of questionnaires. After the two rounds, the draft statements were revised to incorporate all suggestions and reviewed by the steering committee members. These draft statements were then included for discussion at the consensus meetings.

Owing to the COVID-19 pandemic, three consensus meetings were held online between September and November 2020. At the consensus meetings, statements that did not reach a greater than 80% consensus were discussed in a round robin discussion, reworded, amended and refined and were then voted on again. If a statement did not achieve $\geq 80\%$ agreement after discussion, refinement and revoting, the statement was excluded. All statements that achieved $\geq 80\%$ agreement were considered a final statement for inclusion in the final version of the points to consider. For each statement, the Oxford levels of evidence (LoE) and the grade of the recommendation (GoR) were assigned based on the systematic literature review by the fellows under the supervision of the methodologist (40). The final statements annotated with the LoE and GoR were sent through an online survey to all task force members again; and each member was asked to provide their level of agreement (LoA) on a scale of 0 (absolutely disagree) to 10 (absolutely agree). The mean and SD of the LoA with each statement were calculated. The manuscript was reviewed and approved by all task force members and the EULAR/ACR executive committees before submission to the journal.

RESULTS

Systematic literature review

The details for the literature search strategy and summary of results are described in the online supplemental material at <https://onlinelibrary.wiley.com/doi/10.1002/art.42139>. Briefly, randomised controlled trials (RCTs), cohort studies, cross-sectional studies, case-control studies and case reports including more than three cases were included. Review articles, conference abstracts, book chapters, single case reports and articles written in a language other than English were excluded. For CAPS, of 2041 references identified, 72 studies were selected for inclusion. For TRAPS, of 1161 references identified, 47 studies were selected for inclusion. For MKD, of 1806 references identified, 51 studies were selected for inclusion. For DIRA, of 557 references identified, two studies were selected for inclusion. In total, from the 5565 references identified, 172 were included. After a group discussion that included the results of the systematic literature review, the consensus process was initiated.

Overarching principles

During the consensus meeting, seven overarching principles and 55 candidate statements were discussed and voted on.

The task force decided to merge two overarching principles. Owing to lack of agreement, the task force eliminated 26 statements (12 referring to CAPS, 6 to TRAPS, 2 to MKD and 6 to DIRA). The task force agreed on a final set of five overarching principles (Table 1) and 33 points to consider (Tables 2–4).

CAPS, TRAPS, MKD and DIRA typically present with complex clinical features and phenotypes in the neonatal or early childhood period; these include features of systemic and organ-specific inflammation (2,17,28,29,36) presenting with early onset of fever, abdominal pain, rash, musculoskeletal symptoms, neurologic manifestations and elevated biomarkers of systemic inflammation (17,35,41–45). The specific biomarkers of systemic inflammation included in this document are referred to as acute phase reactants and include: C-reactive protein (CRP), erythrocyte sedimentation rate (ESR), serum amyloid A protein (SAA) (46) and S100 proteins, which in most patients correlate with disease activity (41,47,48). The first goal (overarching principle A) is to recognise patients with potential monogenic IL-1 mediated SAIDs and to establish a multidisciplinary team for diagnosis, treatment and long-term management. Delay in treatment initiation can result in rapidly progressive

organ damage (24–27), morbidity and increased mortality (34,49,50). Overarching principle B outlines the need to initiate a clinical workup that assesses the extent of the inflammatory organ involvement and screens for treatment-related comorbidities, a process that often requires a multidisciplinary team of subspecialists (24,25,47). The third goal (overarching principle C) highlights the need for an accurate genetic diagnosis, which in many countries may be required to access the IL-1 blocking biological agents that prevent life-threatening complications (47,51,52), and facilitate access to supportive care.

The goals of treatment (overarching principle D) are to rapidly control disease activity by suppressing systemic and organ inflammation. IL-1 blockade has been FDA (53–55) and EMA (56,57) approved for CAPS, TRAPS, MKD and DIRA (49,58). Rapid disease control using these agents is critical in preventing the development of irreversible early inflammation-related organ damage, and minimising side effects from the use of other drugs that are ineffective and/or carry substantial toxicities.

There are currently no cures for these lifelong diseases. Overarching principle E outlines long-term monitoring goals

Table 1. Overarching principles for the diagnosis, treatment and monitoring of CAPS, TRAPS, MKD and DIRA*

Overarching principles		LoE	GoR	LoA (0–10), mean ± SD
A	Patients with the IL-1 mediated diseases CAPS, TRAPS, MKD and DIRA present with chronic or intermittent flares of systemic and organ inflammation that, if untreated, result in progressive organ damage, morbidity and increased mortality. A multidisciplinary team is required to diagnostically evaluate and manage patients with CAPS, TRAPS, MKD and DIRA, which includes evaluation of systemic inflammation, disease-associated complications and long-term treatment and management.	5	D	9.5 ± 0.7
B	Patients presenting with chronic or episodic flares of unexplained systemic inflammation (including elevations of CRP and ESR) and clinical features suggestive of CAPS, TRAPS, MKD and DIRA should receive a prompt diagnostic workup comprising: <ul style="list-style-type: none"> ▶ genetic testing ▶ clinical workup focusing on the extent of inflammatory organ involvement ▶ screening for disease and treatment-related comorbidities 	5	D	9.8 ± 0.6
C	A genetic diagnosis for CAPS, TRAPS, MKD and DIRA is required which facilitates initiation of targeted treatments, genetic counselling, and informs prognosis. Genetic testing using a next-generation sequencing (NGS) platform should be used to diagnose CAPS, TRAPS, MKD and DIRA.	4	C	8.9 ± 1.6
D	The goal of treatment is to control clinical signs and symptoms and normalise laboratory biomarkers of systemic inflammation using a treat-to-target approach.	5	D	9.6 ± 0.8
E	Long-term monitoring goals should focus on: <ul style="list-style-type: none"> ▶ adequate treatment adjusted to the needs of the growing child and prevention of systemic and organ-specific inflammatory manifestations ▶ fostering of self-management skills and medical decision-making ▶ initiating a transition programme to adult specialist care in adolescent patients 	5	D	9.6 ± 0.9

* Level of evidence (LoE): 1a: systematic review of randomised controlled trials (RCTs); 1b: individual RCT; 2a: systematic review of cohort studies; 2b: individual cohort study (including low-quality RCT); 3a: systematic review of case-control studies; 3b: individual case-control study; 4: case-series (and poor-quality cohort and case-control studies); 5: expert opinion without explicit critical appraisal, or based on physiology, bench research or “first principles”; grade of recommendation (GoR): A: based on consistent level 1 studies; B: based on consistent level 2 or 3 studies or extrapolations from level 1 studies; C: based on level 4 studies or extrapolations from level 2 or 3 studies; D: based on level 5 studies or on troublingly inconsistent or inconclusive studies of any level. CAPS = cryopyrin-associated periodic syndromes; CRP = C-reactive protein; DIRA = deficiency of the interleukin-1 receptor antagonist; ESR = erythrocyte sedimentation rate; LoA = level of agreement; MKD = mevalonate kinase deficiency; TRAPS = tumour necrosis factor receptor-associated periodic syndrome.

Table 2. Points to consider for the diagnosis of CAPS, TRAPS, MKD and DIRA*

	LoE	GoR	LoA (0–10), mean ± SD
1 Patients with clinical symptoms of CAPS, TRAPS, MKD and DIRA who do not carry any of the disease-causing mutations described here should be referred to specialty/research centres to guide further workup and treatment.	5	D	9.4 ± 1
Genetic workup			
2 Genetic testing using an NGS platform, if available, should be used to make a genetic diagnosis. ▶ Sanger sequencing of targeted genes known to cause CAPS (<i>NLRP3</i>), TRAPS (<i>TNFRSF1A</i>), MKD (<i>MVK</i>) and DIRA (<i>IL1RN</i>) can be used if the clinical suspicion is strong or to validate NGS.	4	D	9.4 ± 1.1
3 Deep sequencing in patients with CAPS and TRAPS may be needed to detect some somatic mutations that may not be identified by standard NGS or Sanger sequencing.	5	D	9.5 ± 1.1
CAPS specific			
4 Patients with low penetrance variants in <i>NLRP3</i> may present with clinical manifestations different from CAPS; their treatment response and prognosis may differ from “canonical” CAPS.	2	B	9.4 ± 1.2
TRAPS specific			
5 Patients with low penetrance variants in <i>TNFRSF1A</i> (ie, R121Q [previously referred to as: R92Q]) may present with clinical manifestations different from TRAPS and their treatment response and prognosis may differ from “canonical” TRAPS.	2	B	9.5 ± 1.2
DIRA specific			
6 In patients with DIRA, Sanger sequencing, WES or WGS may not detect large deletions in <i>IL1RN</i> , thus complicating a genetic diagnosis. ▶ In cases with a high clinical suspicion of DIRA and negative Sanger sequencing or WES/WGS, chromosomal microarray analysis (CMA) is recommended to detect large deletions. ▶ The use of deletion-specific primers, in countries with founder variants that include large deletions, is recommended.	3	B	9.3 ± 1.2
Clinical workup			
7 The clinical workup of systemic inflammation should include CRP, ESR and CBC with differential; if available SAA and S100 proteins may be assessed. ▶ Patients with longstanding untreated systemic inflammation need to be screened for the presence of amyloidosis.	5	D	9.7 ± 0.6
CAPS specific			
8 The following clinical features in the presence or absence of autosomal dominant inheritance should prompt consideration of a diagnostic workup of CAPS: ▶ urticaria-like rash ▶ cold/stress-triggered episodes ▶ sensorineural hearing loss ▶ chronic aseptic meningitis ▶ skeletal abnormalities	2	B	9.8 ± 0.5
9 The initial diagnostic workup should include an audiogram and an ophthalmologic examination. Lumbar puncture and a head MRI should be performed if clinically indicated.	5	D	9.8 ± 0.5
TRAPS specific			
10 The following clinical features should prompt consideration of a diagnostic workup of TRAPS: ▶ long-lasting fever episodes ▶ migratory rash ▶ periorbital oedema ▶ myalgia ▶ a positive family history	2	B	9.8 ± 0.5
MKD specific			
11 The following clinical features should prompt consideration of a diagnostic workup of MKD: ▶ age at onset <1 year ▶ gastrointestinal symptoms ▶ painful lymph nodes ▶ aphthous stomatitis ▶ a history of triggers of the periodic fever attack (ie, postvaccination) ▶ a maculopapular rash	2	B	9.8 ± 0.5
12 In patients with unexplained/undifferentiated inflammatory diseases, the presence of mevalonic acid in urine should prompt further diagnostic workup for MKD.	4	C	9.5 ± 0.7
DIRA specific			
13 The following clinical features particularly if occurring sporadically, should prompt consideration of a diagnostic workup of DIRA: ▶ pustular psoriasis-like rashes ▶ osteomyelitis (ie, CRMO-like disease, rib flaring and cloaking of the femoral head, odontoid lesions/osteomyelitis) ▶ absence of bacterial osteomyelitis ▶ nail changes (ie, onychomadesis)	5	D	9.6 ± 0.8

(Continued)

Table 2. (Cont'd)

	LoE	GoR	LoA (0–10), mean ± SD
14 For patients with suspected DIRA, X-ray examinations of the chest and upper and lower limbs and/or MRI/CT to assess the spine, including odontoid, should be included in the diagnostic workup to assess the extent of the inflammatory bone involvement. A dermatology consultation and skin biopsy should be considered as the presence of neutrophilic dermatosis with exocytosis of neutrophils and subcorneal pustules is highly suggestive of DIRA.	5	D	9.7 ± 0.8

* Level of evidence (LoE): 1a: systematic review of randomised controlled trials (RCTs); 1b: individual RCT; 2a: systematic review of cohort studies; 2b: individual cohort study (including low-quality RCT); 3a: systematic review of case-control studies; 3b: individual case-control study; 4: case-series (and poor-quality cohort and case-control studies); 5: expert opinion without explicit critical appraisal, or based on physiology, bench research or “first principles”; grade of recommendation (GoR): A: based on consistent level 1 studies; B: based on consistent level 2 or 3 studies or extrapolations from level 1 studies; C: based on level 4 studies or extrapolations from level 2 or 3 studies; D: based on level 5 studies or on troublingly inconsistent or inconclusive studies of any level. CAPS = cryopyrin-associated periodic syndromes; CBC = complete blood count; CRMO = chronic recurrent multifocal osteomyelitis; CRP = C-reactive protein; CT = computed tomography; DIRA = deficiency of the interleukin-1 receptor antagonist; ESR = erythrocyte sedimentation rate; LoA = level of agreement; MKD = mevalonate kinase deficiency; MRI = magnetic resonance imaging; NGS = next-generation sequencing; SAA = serum amyloid A; TRAPS = tumour necrosis factor receptor-associated periodic syndrome; WES = whole exome sequencing; WGS = whole genome sequencing.

that focus on evaluating disease activity, assessing and monitoring signs and symptoms of disease-specific organ inflammation, growth and development, and adjusting therapeutic doses according to growth, or control of symptoms and

inflammation. Monitoring should be developmentally appropriate, include adjustments for adolescence (59), be tailored to accommodate cognitive (ie, learning and behavioural disorders) and physical disabilities (ie, bone deformities, hearing

Table 3. Points to consider for the treatment of CAPS, TRAPS, MKD and DIRA*

	LoE	LoE	LoA (0–10), mean ± SD
15 IL-1 blocking therapy has become the preferred treatment and a therapeutic trial with IL-1 blocking treatment may be started when a strong clinical suspicion of a diagnosis of CAPS, TRAPS, MKD or DIRA is entertained.	4	C	9.5 ± 0.9
16 In the context of viral infections, including COVID-19, IL-1 blocking therapy should not be altered, as stopping treatment may lead to rebound inflammation.	4	C	9.5 ± 0.8
CAPS specific			
17 Treatment with IL-1 blockers is recommended standard of care and currently includes anakinra, ¹ canakinumab ² and rilonacept. ³	1 ² 2 ¹ 3 ¹	A B B	9.9 ± 0.3
18 Anakinra may be the most effective anti-IL-1 treatment for CNS disease.	2	B	9.6 ± 0.8
19 Higher and more frequent dosing with IL-1 blockers may be required to control disease activity in more severe cases and/or younger children to prevent complications. Less frequent dosing may be appropriate for patients with milder disease.	1	B	9.8 ± 0.5
TRAPS specific			
20 Anti-IL-1 drugs are more effective than traditional disease-modifying antirheumatic drugs (DMARDs) and other biologic DMARDs in achieving disease remission and preventing long-term complications.	4	C	9.6 ± 0.9
MKD specific			
21 In children with MKD, IL-1 blocking therapy is generally required. In patients without chronic systemic inflammation, on-demand IL-1 blockade should be attempted at the onset of flares.	4	C	9.4 ± 1.0
22 If anti-IL-1 is not effective or available, then anti-TNF agents should be considered.	3	B	9.3 ± 0.9
23 Glucocorticoids on demand may be effective in treating acute flares; however, frequent or long-term use is limited by side effects.	2	B	9.3 ± 1.0
DIRA specific			
24 In patients with DIRA, treatment with agents that block both IL-1α and IL-1β is recommended and includes anakinra and rilonacept. Both have shown benefit in controlling disease flares and in preventing long-term complications.	4	C	9.6 ± 0.8

* Level of evidence (LoE): 1a: systematic review of randomised controlled trials (RCTs); 1b: individual RCT; 2a: systematic review of cohort studies; 2b: individual cohort study (including low-quality RCT); 3a: systematic review of case-control studies; 3b: individual case-control study; 4: case-series (and poor-quality cohort and case-control studies); 5: expert opinion without explicit critical appraisal, or based on physiology, bench research or “first principles”; grade of recommendation (GoR): A: based on consistent level 1 studies; B: based on consistent level 2 or 3 studies or extrapolations from level 1 studies; C: based on level 4 studies or extrapolations from level 2 or 3 studies; D: based on level 5 studies or on troublingly inconsistent or inconclusive studies of any level. CAPS = cryopyrin-associated periodic syndromes; CNS = central nervous system; COVID-19 = coronavirus disease 2019; DIRA = deficiency of the interleukin-1 receptor antagonist; IL-1 = interleukin-1; LoA = level of agreement; MKD = mevalonate kinase deficiency; TNF = tumour necrosis factor; TRAPS = tumour necrosis factor receptor-associated periodic syndrome.

Table 4. Points to consider for the monitoring of CAPS, TRAPS, MKD and DIRA*

		LoE	GoR	LoA (0–10), mean ± SD
25	Disease activity and burden of disease should be monitored regularly depending on disease activity and severity, often requiring a multidisciplinary team. ▶ Symptom control can be monitored with validated tools that assess disease-specific symptoms, with patient-reported outcome and quality of life assessments and by recording missing school or work days. ▶ The frequency of the follow-up evaluations should be tailored to disease severity and clinical needs.	5	D	9.7 ± 0.6
26	Growth and development of children should be monitored at each visit.	5	D	9.9 ± 0.3
27	Systemic inflammation should be monitored by following up inflammatory markers, including peripheral neutrophilia, CRP and ESR. SAA and S100 protein may be used as inflammatory markers where available.	5	D	9.8 ± 0.5
28	Systemic inflammation may predispose to the development of amyloidosis, and patients should be monitored for the development of amyloidosis by monitoring proteinuria and microalbuminuria.	5	D	9.8 ± 0.5
29	Physicians should be aware of the increased risk of infections in patients with IL-1 targeted therapy, including respiratory tract infections with <i>Streptococcus pneumoniae</i> and skin infections due to <i>Staphylococci</i> .	1	B	9.8 ± 0.4
30	Patients should receive immunisations, in particular live-attenuated vaccines, in accordance with their regional policy, before beginning anti-IL-1 targeted therapy when possible.	5	D	9.2 ± 1.4
CAPS specific				
31	Monitoring of organ damage should be established based on disease manifestations and can include monitoring of hearing loss, eye disease, aseptic meningitis, CNS disease and bone disease.	5	D	9.7 ± 0.6
32	Patients with CNS and/or bone involvement should be assessed for developmental delay, the development of bone deformities and limb-length discrepancies.	5	D	9.7 ± 0.6
DIRA specific				
33	Normalisation of acute phase reactants and absence of inflammatory skin and bone findings is required to determine the adequate dose of IL-1 blocking treatment, and to monitor disease activity long term.	5	D	9.5 ± 0.8

* Level of evidence (LoE): 1a: systematic review of randomised controlled trials (RCTs); 1b: individual RCT; 2 a: systematic review of cohort studies; 2b: individual cohort study (including low-quality RCT); 3a: systematic review of case–control studies; 3b: individual case–control study; 4: case-series (and poor-quality cohort and case–control studies); 5: expert opinion without explicit critical appraisal, or based on physiology, bench research or “first principles”; grade of recommendation (GoR): A: based on consistent level 1 studies; B: based on consistent level 2 or 3 studies or extrapolations from level 1 studies; C: based on level 4 studies or extrapolations from level 2 or 3 studies; D: based on level 5 studies or on troublingly inconsistent or inconclusive studies of any level. CAPS = cryopyrin-associated periodic syndromes; CNS = central nervous system; CRP = C-reactive protein; DIRA = deficiency of the IL-1 receptor antagonist; ESR = erythrocyte sedimentation rate; IL-1 = interleukin-1; LoA = level of agreement; MKD = mevalonate kinase deficiency; SAA = serum amyloid A; TRAPS = tumour necrosis factor receptor-associated periodic syndrome.

and vision loss) (29,60) and prepare patients for transitioning to adult specialists. This transition can be challenging and lengthy and may put patients at risk of unfavourable outcomes. Therefore, the task force emphasised the need to include goals that foster self-management skills and medical decision-making (ie, including reproductive health) throughout the life of the patient (59,61).

Focus on the diagnosis of IL-1 mediated SAIDs, including recognising clinical diagnostic and damage-related features of the respective diseases, genetic testing, disease-specific clinical and laboratory workup and initiation of early treatment: points to consider 1–14.

Disease-specific clinical features of untreated CAPS, TRAPS, MKD and DIRA and the resulting organ damage have been characterised

in clinical descriptions of patient cohorts before anti-IL-1 treatment was used (2,17,36,62). These signs and symptoms form the basis of evidence-based classification criteria for CAPS (48), TRAPS and MKD (41) and are listed in Table 2—recommendations 8 (CAPS), 10 (TRAPS), 11 (MKD) and 13 (DIRA), respectively. In combination with the molecular analyses, these features help physicians to recognise disease-specific characteristics and differentiate these conditions from clinically complex diseases that can present with overlapping inflammatory manifestations, including systemic juvenile idiopathic arthritis, adult-onset Still’s disease, neoplasms, infections and autoimmune disorders (63,53).

Genetic workup: points to consider 2–6. Suggestive clinical features should trigger a genetic investigation, as genetic testing is a crucial component of an accurate diagnosis of CAPS,

TRAPS, MKD and DIRA (41,65). Next-generation sequencing (NGS) platforms are now widely used and are replacing the Sanger sequencing “gene by gene” approach (51,52,66–68). NGS is therefore generally recommended (52,63,66,69,70). In certain conditions, Sanger sequencing of a single gene may be cost-effective, such as in patients with a known familial disease or classic disease features. In some countries, Sanger sequencing may be the only modality of genetic testing available (52,71–73).

CAPS and TRAPS are autosomal dominant diseases caused by gain-of-function mutations in *NLRP3* and *TNFRSF1A* (18) genes, respectively, and can be familial (63,74) or caused by de novo mutations. In CAPS, de novo mutations are most frequently found in patients with severe phenotypes (7). Somatic mutations in these patients may be undetected by standard coverage of NGS and may require deep sequencing, though this analysis may not be available to all providers (51,74–77). In contrast, MKD and DIRA are caused by recessive loss-of-function mutations in *MVK* (78,79) and *IL1RN* (2) genes, respectively. In patients with clinical symptoms suggestive of MKD or DIRA, Sanger sequencing, whole exome sequencing and whole genome sequencing may not detect large deletions (2). If appropriate, chromosomal microarray analysis by comparative genomic hybridization array or by single nucleotide polymorphism array should be performed (2). For the genetic diagnosis of DIRA, PCR and sequencing using specific deletion breakpoint primers to screen reported *IL1RN* large deletions may aid the genetic evaluation in selected ethnic backgrounds (ie, Puerto Rico, Brazil, India) (2,80,81). If a genetic diagnosis cannot be made following routine genetic workup, patients should be referred to a research centre of excellence with expertise in the molecular diagnosis of SAIDs.

One significant challenge is the interpretation of genetic results that have not been classified or validated as pathogenic mutations, including variants of uncertain significance, that is, variants that have not been described previously or studied functionally, or likely benign variants that may be present in the general population at a relatively high frequency and could be low-penetrance mutations with inconsistent clinical significance. Patients with these genetic findings may display distinct clinical and biologic phenotypes, and can include IL-1 β and non-IL-1 β -mediated inflammatory pathway activation, which may have implications for their management, further emphasising the need for speciality care.

Clinical workup: points to consider 7–14. In IL-1-mediated SAIDs patients, systemic inflammation typically accompanies clinical signs and symptoms, which can be episodic/periodic or chronic/persisting (36,82). MKD, TRAPS and the mildest form of CAPS, known as FCAS, may in rare cases, present with intermittent episodes (flares of symptoms) separated by periods of perceived improvement (17,41,65,83–85). However, most patients except for patients with milder disease (ie,

some patients with FCAS and TRAPS) have evidence of chronic subclinical inflammation between episodes. Patients with more severe forms of CAPS such as MWS or NOMID/CINCA, or those with severe MKD with almost complete absence of the enzymatic activity of mevalonate kinase, or with DIRA, all present with chronic systemic inflammation that rarely spontaneously remits. In general, markers of systemic inflammation correlate with disease symptoms and risk of organ damage (75,86–88). Historically, CRP, ESR and, if available, SAA (46) have been used to assess systemic inflammation. Additionally, S100 proteins (89) have been used by some investigators as sensitive markers in research settings. How to best use S100 protein markers for patient care, given increased clinical availability, remains under investigation. The diagnostic workup across all four diseases is broadly similar and can be synchronised. Typical signs and symptoms of active disease (ie, hepatosplenomegaly), organ inflammation and damage should prompt a diagnostic workup (Tables 2 and 5).

The clinical presentation of the CAPS disease spectrum includes systemic inflammation and an urticaria-like rash with histologic features of a neutrophilic dermatosis involving eccrine glands, which is present in almost all patients (24,43,75,86,88,90–92). Cold-induced flares often last less than 24 hours and are most often observed in patients at the mild end of the disease spectrum (FCAS) (14,42). A negative localised cold challenge (ice cube test) differentiates FCAS from patients with cold urticaria (42). Progressive sensorineural hearing loss is often seen in moderately (MWS) and severely (NOMID/CINCA) affected patients (24,29,60,95) while neurologic findings (chronic aseptic meningitis, increased intracranial pressure, cognitive impairment) (87,93) and skeletal abnormalities (distal femur overgrowth, frontal bossing) are typically seen in NOMID/CINCA (75,86). Ophthalmologic involvement can vary and most typically includes conjunctivitis, but keratitis, episcleritis and anterior and/or posterior uveitis have also been described. Increased intracranial pressure may cause papilloedema and subsequent optic disc atrophy. Therefore, a slit lamp examination and retinal evaluation should be performed in all patients with CAPS at baseline (25,43,88). In patients with suspected neurologic involvement, brain imaging (28,94,95) and lumbar puncture may be needed to evaluate for elevated intracranial pressure or aseptic meningitis, while a specialised brain MRI scan can detect cochlear enhancement, cerebral atrophy and ventriculomegaly (87,96). Epiphysial bony overgrowth, commonly found around the knees, may be assessed by bone MRI or radiograph (25,26,92).

TRAPS is characterised by episodes of fever lasting more than 7 days, abdominal pain that can mimic an acute abdomen, variable chest pain and, rarely, testicular pain (17,41,70). Especially in adults, a subchronic disease course might be observed, with fatigue, diffuse limb pain and persistent elevation of acute phase reactants (17). Periorbital oedema and myalgias might herald the onset of an attack. Typical findings of a flare include painful, migratory skin plaques with hazy edges that are

Table 5. Disease specific monitoring of CAPS, TRAPS, MKD and DIRA*

For all diseases, systemic inflammation needs to be monitored		Frequency
A. Monitoring of systemic inflammation in all diseases		
	ESR, CRP, CBC+differential (granulocytosis), S100 proteins and SAA where available, hepatosplenomegaly, lymphadenopathy, fatigue	Each visit
	Urinalysis to monitor proteinuria (AA amyloidosis)	Every 6–12 months
	Monitor growth, BMD, sexual development	Each visit as indicated
B. Monitoring of disease-specific symptoms† and patient-related outcomes		
CAPS	Fever, rash (urticaria-like), progressive hearing loss, headaches, early morning nausea and vomiting, musculoskeletal symptoms, conjunctivitis, cognitive development (severe disease)	Each visit
TRAPS	Fever, rash (migratory), periorbital oedema, pain (abdomen, chest, testicular), myalgia	Each visit
MKD	Periodic fever attacks (including triggered sequencing), rash (urticarial or maculopapular), gastrointestinal symptoms (abdominal pain, diarrhoea, vomiting), cervical lymphadenopathy, aphthous stomatitis, cognitive impairment in severe cases	Each visit
DIRA	Pustular psoriasis-like rashes (pathergy), musculoskeletal (bone) pain (caused by osteomyelitis), nail changes	Each visit
Patient-related outcomes for all four diseases		QoL, PGA, PPGA, missing school/work days
C. Monitoring of organ manifestations/damage‡		
CAPS		
Amyloidosis	Urinalysis	Each visit
Hearing loss (S)	Audiogram	3–6 months until stable then every 6–12 months
Eye disease (S)	Ophthalmologic examination (vision, retina evaluation and slit lamp examination)	6–12 months
CNS disease (S)	Lumbar puncture, head MRI (with special examination of cochlea, cerebral atrophy and ventriculomegaly)	12–36 months depending on symptoms
Bone deformity (S)	Bone MRI, scanogram to monitor limb length, epiphysial overgrowth	12–36 months depending on symptoms
TRAPS		
Amyloidosis	Urinalysis	Each visit
Bone deformity (S)	Bone MRI, X-ray examination	12–36 months depending on symptoms
MKD		
Amyloidosis	Urinalysis	Each visit
Eye disease (S)	Ophthalmologic examination	As needed
Neurologic involvement (S)	Neuropsychological testing	As needed
DIRA		
Spinal and bone deformities (S)	Neck, spine MRI (vertebral osteomyelitis), bone X-ray/MRI, corrective surgery or spinal fusion	As needed
D. Monitoring of treatment-related complications (interleukin-1 blocking treatments)		
Infections	Clinical history, skin infections, other infections	Each visit
Laboratory work	CBC+differential, LFTs, urinalysis, renal function, lipid profile	Each visit

* BMD = bone mineral density; CAPS = cryopyrin-associated periodic syndromes; CBC = complete blood count; CNS = central nervous system; CRP = C-reactive protein; DIRA = deficiency of the interleukin-1 receptor antagonist; ESR = erythrocyte sedimentation rate; LFT = liver function test; MKD = mevalonate kinase deficiency; MRI = magnetic resonance imaging; SAA = serum amyloid A; TRAPS = tumour necrosis factor receptor-associated periodic syndrome.

† The following instruments can be used for symptom monitoring: autoinflammatory diseases activity index (AIDA), for damage assessment the Autoinflammatory Disease Damage Index (ADDI), for quality of life (QoL), physician global assessment (PGA), patient's/parent's global assessment (PPGA).

‡ (S) denotes may require subspecialty care.

erythematous, swollen and warm (3) and predominantly affect the limbs. Suspected fasciitis may be imaged by MRI (97). There is now consensus that population frequent variants of uncertain significance, such as R121Q (previously referred to as R92Q) should not be considered as pathogenic (17,45,98–103). Therefore, the interpretation of these variants should occur in the context of the inflammatory phenotype by an expert in the field if available.

Patients with MKD usually present in the first year of life (5,104) with recurrent episodes of fever lasting 4 to 6 days (104), gastrointestinal symptoms (severe abdominal pain with vomiting and diarrhoea), cervical lymphadenopathy, aphthous stomatitis and/or skin rash (urticarial or maculopapular) (32,64,84,105–110). The most severe form of MKD, namely mevalonic aciduria, presents with severe cognitive impairment, and patients can

present with hyperinflammation leading to macrophage activation syndrome (36) along with the clinical features described above (84,110,111). Febrile attacks triggered by vaccinations suggest a diagnosis of MKD (36,85,112–115).

High levels of circulating immunoglobulin D that were described formerly and led to the name hyper IgD syndrome have low diagnostic sensitivity and specificity (82,105,116,117). However, elevated urine mevalonate levels during disease flares, due to reduced MVK enzyme activity and accumulation of mevalonic acid, are more specific for MKD (118,119) and can be used to aid in diagnosis.

Patients with DIRA present with early-onset pustular rashes that can be triggered by mechanical stress (pathergy), with sterile osteomyelitis and nail changes (onychomadesis) (2,120). Although the inflammatory markers are typically highly elevated, fever may be absent. Vertebral involvement can include odontoid osteomyelitis, resulting in destruction and neck instability, vertebral block formation and gibbus-like spinal changes that need to be screened for by MRI or CT (2,120). In contrast to patients with CAPS, TRAPS and MKD, patients with DIRA rarely present with flare-associated fever. In patients with presumed DIRA, a diagnostic workup includes assessing peripheral neutrophilia and elevated inflammatory markers, determining bone involvement (ie, X-ray or bone MRI) and genetic testing (2,120). The differential diagnosis for DIRA includes chronic recurrent multifocal osteomyelitis (CRMO) (121,122), synovitis, acne, pustulosis, hyperostosis, osteitis (SAPHO) (123) syndrome and pustular psoriasis (124). Genetic testing for monogenic defects with overlapping clinical features should include *LPIN2*, *FGR*, *FBLIM1* for CRMO (125,126), *CARD14* for *CARD14*-mediated psoriasis (CAMPS) (127,128), *IL36RN* for deficiency of IL-36 receptor antagonist (127,128), *AP1S3* (128) for other pustular psoriasis and *MEFV* for pyrin-associated autoinflammation with neutrophilic dermatosis (129).

Focus on the treatment of IL-1 mediated diseases: points to consider 15–24. Disease management involves a shared decision-making approach and a combination of pharmacologic and non-pharmacologic interventions. The current standard of care for patients with CAPS, TRAPS, MKD and DIRA is subcutaneous IL-1 targeted biologic therapy when available (28,49,130–132). While the specific pharmacologic mechanisms, pharmacokinetics, disease indications and costs differ for each of the three available drugs, anakinra (Kineret), rilonacept (Arcalyst) and canakinumab (Ilaris), each blocks the effect of IL-1 β on the IL-1 receptor and downstream signaling, resulting in improved symptom control, as well as reduced systemic and tissue/organ inflammation. Anakinra is a recombinant IL-1 receptor antagonist with a short half-life that binds to the IL-1 receptor and blocks both IL-1 α and IL-1 β signaling (95,133–135). Rilonacept is a recombinant fusion protein with a relatively longer half-life that binds to both IL-1 α and IL-1 β (130,136,137). Canakinumab is a

human monoclonal antibody to IL-1 β with a long half-life (49,131,138,139). As expected for treatment of rare disorders, case reports and small patient series have demonstrated the success of IL-1 blockade across the spectrum of disease. The highest level of evidence, however, stems from pivotal studies including randomised studies in CAPS (137,140,141) (MWS and FCAS), in TRAPS and MKD (142), which have confirmed that rilonacept was effective in CAPS (137), and that canakinumab was efficacious in controlling and preventing flares in patients with CAPS (140) and with MKD and TRAPS (142), respectively (Table 3). The availability of these drugs varies significantly in different countries.

Aims of treatment are early control of disease activity, prevention of disease and treatment-related damage and optimal health-related quality of life (58,142). The ultimate goal of a treat-to-target approach is complete remission (37). In the absence of a consensus definition of remission or minimal disease activity for these diseases, remission has been defined for clinical studies and clinical monitoring as an absence of clinical symptoms and normal inflammatory markers. The instruments used to measure disease activity include daily symptom diary scores (28,95) or Auto-inflammatory Diseases Activity Index (AIDAI) (143), and a physician global assessment (PGA) and patient–parent global assessment (PPGA). The most commonly used inflammatory marker is CRP (also known as high sensitivity or cardio CRP in some countries), with levels of less than 5 mg/L or 10 mg/L indicating adequate control of inflammation (95,120,142). Minimal disease activity has been suggested as an alternative target if remission cannot be achieved. Definitions of remission and minimal disease activity and their validations are on the research agenda for autoinflammatory diseases (142,143).

Treat-to-target strategies aiming for low disease activity assessed by clinical symptoms and normalisation of serum markers of systemic inflammation are effective and used in the treatment of patients with IL-1 mediated SAIDs to find individualised and optimal dosing regimens for each patient and disease (37). IL-1 blocking therapies control inflammation in the absence of glucocorticoids (134,142,144). Treatment can delay or prevent development or progression of organ damage in patients with moderate or even severe disease activity (60,95,145). Management by a multidisciplinary team that includes subspecialists results in better disease control in patients with CAPS (37). To achieve and maintain optimal disease control, IL-1 targeted therapies need to be administered continuously in most patients, and the dose and/or frequency of administration should be adjusted for control of disease activity, normalisation of markers of systemic inflammation and for weight gain and appropriate development in the growing patient.

Medication dose adjustments for weight gain and growth and higher mg/kg doses to optimise treatment responses should be individualised for each patient (37,95). Some patients with CAPS may require more frequent or higher doses of these

Table 6. Treatments based on FDA, EMA* or expert panel consensus†

Disease	Treatment	Recommended dosing based on FDA, EMA or task force consensus	FDA	EMA	LoE
CAPS (NLRP3-AID) FCAS	Canakinumab	PD: 2–8 mg/kg/q8w AD: >40 kg, 150–600 mg/q8w	+	+	1B
	Rilonacept	PD: LD 4.4 mg/kg/q1w and MD 2.2 mg/kg/q1w AD: LD 320 mg/q1w and MD 160 mg/q1w	+	–	1B
MWS	Anakinra	1–2 mg/kg/day	–	+	4C
	Canakinumab‡	PD: 2–8 mg/kg/q8w‡ AD: >40 kg, 150–600 mg/q8w	+	+	1B
NOMID/CINCA	Rilonacept	PD: LD 4.4 mg/kg/q1w and MD 2.2 mg/kg/q1w AD: LD 320 mg/q1w and MD 160 mg/q1w	+	–	1B
	Anakinra	1–2 mg/kg/day	–	+	2B
	Anakinra Canakinumab§	1–8 mg/kg/day PD: 2–8 mg/kg/q4w§	+	+	2A 4C
TRAPS	Canakinumab	AD: >40 kg, 150–600 mg/q4w PD: 2–4 mg/kg/q4w	+	+	1B
MKD	Canakinumab	AD: >40 kg, 150–300 mg/q4w PD: 2–4 mg/kg/q4w	+	+	1B
DIRA	Anakinra	1–8 mg/kg/day	+	–	4C
	Rilonacept	PD: 4.4 mg/kg/q1w AD: LD 320 mg/q1w and MD 320 mg/q1w	+	–	4C

* Drug approvals, dosages may vary between different countries and local regulations should be followed in the respective countries (53–57).

† Level of evidence (LoE): 1a: systematic review of randomised controlled trials (RCTs); 1b: individual RCT; 2a: systematic review of cohort studies; 2b: individual cohort study (including low-quality RCT); 3a: systematic review of case-control studies; 3b: individual case-control study; 4: case-series (and poor-quality cohort and case-control studies); 5: expert opinion without explicit critical appraisal, or based on physiology, bench research or “first principles.” AD = adult dosage; CAPS = cryopyrin-associated periodic syndromes; CINCA = chronic infantile neurologic cutaneous articular syndrome; DIRA = deficiency of the interleukin-1 receptor antagonist; EMA = European Medicines Agency; FCAS = familial cold autoinflammatory syndrome; FDA = US Food and Drug Administration; LD = loading dose; MD = maintenance dose; MKD = mevalonate kinase deficiency; MWS = Muckle-Wells syndrome; NOMID = neonatal onset multisystem inflammatory disease; PD = paediatric dosage; TRAPS = tumour necrosis factor receptor-associated periodic syndrome.

‡ Canakinumab is approved by the FDA and EMA for the treatment of CAPS at the same dosing regimens for FCAS and MWS; however, some patients with MWS may require more frequent dosing according to the expert panel.

§ Although canakinumab was approved by the EMA for the treatment of CAPS at the same dosing regimens for all three disease severity phenotypes (which also includes patients with NOMID/CINCA), the study submitted for approval only included five patients with NOMID/CINCA and a subanalysis in patients with NOMID/CINCA was not performed. The dosing frequency required for patients with NOMID is typically every 4 weeks. We therefore added the panel’s recommendation as 4C in the dosing table (149,153,174).

medicines than that approved by FDA or EMA (Table 6), such as dosing of canakinumab more often than the approved frequency of every 8 weeks, if patients have not achieved remission (34,37,141). On-demand regimens may be used in selected patients with MKD, TRAPS and FCAS who have very mild disease and/or episodic disease manifestations and who maintain normal inflammatory markers in between episodes (146,147). Patients with severe disease manifestations, such as those with NOMID/CINCA, may require frequent adjustments and higher doses than patients with less severe diseases (Table 6) (37,95,141). There is a potential clinical advantage of using anakinra for patients with severe CAPS, especially for those with neurologic disease (148,149). Patients with *NLRP3* variants that have not been validated as pathogenic (ie, V198M, R488K, Q703K) may respond to IL-1 blockade, and specific recommendations have previously been published (150,151). To improve symptom control, non-steroidal anti-inflammatory drugs may be efficacious when used

together with IL-1 targeted therapy. Ongoing efficacy and a beneficial long-term safety profile have been demonstrated for the long-term use of all three IL-1 blockers (anakinra, rilonacept and canakinumab) in CAPS, although direct comparative studies are lacking (44,49,130,134,136–139,152–157).

A large body of evidence suggests that IL-1 inhibitors should be considered as the preferred treatment for TRAPS (100). Although anakinra was the first IL-1 blocker successfully used in patients with TRAPS in small series and observational registries (100,131,145,158), the long-acting anti-IL-1 β monoclonal antibody, canakinumab is currently the only IL-1 blocker that the FDA and EMA have approved for the treatment of patients with TRAPS (54,57) (Table 6). Individual patients with TRAPS may respond to treatment with short-term glucocorticoids or etanercept; however, responses often wane and patients should be monitored for increased disease activity (45,100,159). Patients with *TNFRSF1A* variants that are not classified as pathogenic (ie,

D41E, I57S, P75L, R121Q, N145S [previously referred to as: D12E, I28E, P46L, R92Q, N116S, respectively]) do not have TRAPS; however, they may still have signs of clinical autoinflammation requiring treatment with colchicine or biologic therapies (100).

Anakinra and canakinumab have been used in children with MKD with success, but only canakinumab has been evaluated in a randomised study and approved by the FDA and EMA (54,57,142,146). Some patients with MKD with milder disease phenotypes, characterised by occasional attacks separated by symptom-free periods, can be managed with on-demand treatment (146). Glucocorticoids may also be beneficial during flares, but their extended use is limited by adverse effects (146). The panel suggested the use of IL-1 blockade, but noted that treatment could be switched to anti-tumour necrosis factor (anti-TNF) agents, if IL-1 blockade is not available or is ineffective (146).

Anakinra and rilonacept both block IL-1 α and IL-1 β and should be used for patients with DIRA (2,80,81,120). The FDA recently approved both anakinra and rilonacept for treatment of DIRA (53,55). Blocking IL-1 α may be necessary to completely block bone inflammation, as observed in a patient who developed osteitis during treatment with canakinumab, which only blocks IL-1 β . While anakinra has been used initially in all patients with DIRA to achieve disease control, rilonacept can be used to maintain remission (120). Doses of IL-1 blocking therapies required for disease control in patients with DIRA have typically been lower than those required in patients with severe CAPS-NOMID/CINCA. Long-term sustained and complete remission is an achievable goal of treatment for patients with DIRA.

For all IL-1 mediated SAIDs, individualised dose adjustments of IL-1 blocking agents may be necessary in young patients or in those with severe disease. In infants and preschool-aged children, twice daily dosing of anakinra may be required for control of disease activity. This is probably due to the higher liver blood flow, which increases the hepatic clearance of drugs owing to the larger ratio of liver to total body mass in children than in adults (160). Some older patients with severe and difficult to control disease, including central nervous system disease, may also achieve improved disease control with twice daily dosing. While canakinumab is approved by the EMA for CAPS-NOMID/CINCA at a frequency of every 8 weeks, supporting evidence suggests that this may be inadequate, so the consensus of experts recommends more frequent dosing up to every 4 weeks for these severely affected patients based on clinical experience and numerous reports (34,37,141). This is consistent with dose frequency for other SAIDs, and with EMA-provided consumer medical information for patients with inadequate responses (57).

Focus on monitoring of IL-1 mediated SAIDs: CAPS, TRAPS, MKD and DIRA: points to consider 25–33. Ongoing management includes adjustment of pharmacologic

therapy, monitoring of disease activity, development of disease-related complications and recognition of drug toxicity. Additionally, individual focus on the needs of the growing child, adolescent, adult or even elderly should include age-appropriate and developmentally appropriate measures that foster self-management skills, encourage shared medical decision-making, address reproductive health issues and facilitate timely and effective transition to adult medical care (47,161,162) (Table 4).

Appropriate management of patients with IL-1 mediated SAIDs necessitates a multidisciplinary team of local primary care givers working together with experienced physicians, rheumatologists and other specialists on a case-by-case basis that can include, but is not limited to, immunologists, ophthalmologists, otolaryngologists, nephrologists, neurologists and genetic counsellors, as well as physiotherapists, occupational therapists and psychosocial specialists (47,161,163). The management of patients, particularly those with cognitive (ie, learning and behavioural disorders) and those with physical disabilities (ie, bone deformities, hearing and vision loss) (29,60), is complex. The physical, mental, psychosocial health and social functioning of entire families should be considered. Individualised support services, including, but not limited to, psychosocial support, genetic counselling, cognitive and learning support, school accommodations and occupational therapy and physiotherapy, may be needed to manage these challenges (110,161,163,164). Some adult patients may have increased difficulties due to their disease and chronic organ involvement that may require accommodations for work, or other aspects of their daily life.

Long-term monitoring requires age-appropriate dose adjustment of IL-1 blocking treatment to maintain control of systemic and organ-specific inflammatory manifestations, and of laboratory markers (49,130,134,135,139,157). Systemic inflammation should be monitored by following up inflammatory markers, which include peripheral neutrophilia (165), CRP and ESR. SAA and S100 protein may be used as inflammatory markers where available (45,131).

Chronic systemic inflammation can have significant effects on growth and development, and ongoing inflammation may predispose to AA amyloidosis (27). Patients with IL-1 mediated SAIDs need continuous and developmentally appropriate care during and beyond adolescence. However, up to half of adolescent patients are not appropriately transferred to adult specialist care owing to general lack of transition readiness, inadequately robust quality indicators and insufficient understanding of the needs of adolescents. This population is therefore at particular risk of unfavourable outcomes (59,61). Relevant for this group are complications related to amyloidosis, hearing loss and vision loss. Although AA amyloidosis has become less common with the early initiation of anti-IL-1 targeted treatment, adults who have had longstanding uncontrolled disease should be closely

monitored (49,100,140). The task force recommended that proteinuria should be evaluated every 6 months in all patients with IL-1 mediated SAIDs, particularly in patients with a positive family history of amyloidosis as they may have other factors, including genetic variants contributing to the development of amyloidosis (ie, SAA1 variants).

Disease-specific monitoring plans that take into account the different disease manifestations in CAPS, TRAPS, MKD and DIRA are outlined in Table 4. Hearing loss, central nervous system disease, bone deformities, renal failure due to amyloidosis and visual loss are the most severe organ manifestations in patients with CAPS (62). In patients with TRAPS the disease may progress from longer-lasting episodes of fever, migratory and painful rash, to a more chronic disease course with persistent inflammation in the absence of the typical fever episodes, which may still represent an important risk factor for the development of AA amyloidosis (27), and are an indication for long-term treatment with biological disease-modifying antirheumatic drugs (131,145). Rare MKD-associated manifestations include retinitis pigmentosa and hearing loss. Therefore, ophthalmologic evaluations and audiograms should be included as clinically indicated (32,35,36,118). Secondary hemophagocytosis in the context of infections has been reported and should be considered in the situation of severe disease flares in MKD (35,36,82). For all IL-1-mediated SAIDs, appropriate monitoring aims to limit or prevent complications of inflammation and disease-associated damage through ongoing individualised treatment, while encouraging the best possible quality of life for patients and families (161).

Beyond objective laboratory measurements, patient-reported outcomes and disease assessment tools can be helpful in the monitoring of disease symptoms. Patient- or physician-reported outcomes (110,166,167) can include measures of health-related quality of life (47,168,169), disease activity (143) (ie, Auto-inflammatory Diseases Activity Index [AIDAI] for CAPS, TRAPS and MKD) (100,143,154,166,169,170), global assessment scales for physicians and patients/parents (142) (PGA, PPGA) and assessment of disease-related organ damage (167) (ie, Auto-inflammatory Diseases Damage Index [ADDI]) that are listed in Table 5. Questions about performance at school and work place and recording missing school/work days help assess the burden of disease and guide revisions to the treatment plan (163). The safety profile for IL-1 blocking treatment has generally been favourable. However, monitoring for infection, particularly respiratory tract infections with *Streptococcus pneumoniae* and skin infections due to *Staphylococcus*, is recommended (142). Even though in some conditions, such as MKD, vaccination may lead to a disease flare, patients should be vaccinated in accordance with regional recommendations (171). This includes pneumococcal vaccines, including the polysaccharide vaccine (Pneumovax) in patients with CAPS, as benefits generally outweigh the potential risks of local and systemic reactions

(49,172). Patients who are receiving, or planning to initiate, anti-IL-1 targeted therapy should receive pneumococcal vaccinations. While it is preferable to administer vaccines before starting treatment, it is also acceptable to do so during treatment (49). Preliminary data suggest that an adequate antibody response to vaccines occurs in patients receiving canakinumab (49). Whether vaccines against COVID-19 have the potential to provoke disease flares is unknown; theoretical concerns about disease flare in IL-1 mediated SAIDs caused by RNA vaccines exist. However, there are currently insufficient data to make recommendations regarding COVID-19 vaccines.

Data on IL-1 treatment in pregnancy is limited (100,162,173). In women with IL-1 mediated SAIDs who require biological treatment and are considering pregnancy, a benefit-risk discussion should be held before conception, including the risk of untreated disease to mother and fetus compared with the risk of continuing biologic agents. At present, regulatory advice and clinical case series reports support the use of anakinra rather than any other anti-IL-1 agent in pregnancy (100).

CONCLUSION

In recent years, we have learnt more about the phenotypic breadth and pathogenesis of IL-1 mediated SAIDs, which has led to a more efficient diagnosis and better treatment and monitoring of these diseases. An improved understanding of the pathogenesis and presentation of patients with IL-1 mediated SAIDs, along with the development of effective treatments, has dramatically improved our ability to diagnose and treat patients. As formalised training in the diagnosis and management of IL-1 mediated SAIDs is variable, many physicians, including rheumatologists, lack the knowledge to optimally manage these patients. The task force aims to raise awareness and assist both specialists and primary healthcare providers in managing patients with IL-1 mediated SAIDs. The panel has also highlighted the distinguishing clinical features of CAPS, TRAPS, MKD and DIRA in the suggested recommendations. These points for consideration attempt to address the unmet needs for guidance based on a EULAR and ACR consensus process for diagnosing, managing and treating CAPS, TRAPS, MKD and DIRA.

The task force included specialists with broad expertise in managing patients with IL-1 mediated autoinflammatory diseases, representing different countries, disease interests and practice environments. Owing to the rarity of these disorders, statements have been developed based on low level of evidence and on expert opinion, which will probably require revisions as new knowledge is generated. Multicentre collaborative efforts, prospective registries and randomised trials will help to define optimal treatment strategies to relieve patient symptoms and to further improve long-term clinical outcomes. The panel also suggests areas for future research (Box 1).

Box 1: Research agenda

- ▶ To create transition clinics for patients with these rare disorders and optimise treatment during this vulnerable period
- ▶ To evaluate best treatment options during pregnancy and their effect on the fetus and newborn
- ▶ To establish biobanks for biomarker studies to validate the markers that best correlate with disease activity and severity
- ▶ To evaluate the effect of vaccination in triggering or exacerbating disease activity in patients with interleukin 1(IL-1) mediated systemic autoinflammatory diseases while receiving or not receiving treatment with biologic disease-modifying antirheumatic drugs and/or glucocorticoids
- ▶ To identify novel therapeutic targets and treatments
- ▶ To establish multicentre collaborative efforts to address:
 - Development of prospectively enrolling registries
 - Better characterisation of phenotype-genotype correlations
 - Pathophysiology of organ damage in IL-1 mediated disorders
 - Validation of remission criteria for each disease, including patient-reported outcome measures
 - Development of minimal disease activity criteria, response criteria
 - Understanding of additional factors (epigenetics, environment) defining the disease course
- ▶ Continuation of defining long-term outcomes, assessing long-term safety of biological agents in IL-1 mediated disorders, updating and refining disease-specific outcome measurements for measuring disease activity and severity

ACKNOWLEDGMENTS

The task force gratefully thanks the librarian Darren Hamilton (London Health Sciences Centre, London, Ontario, Canada) for his contribution to the systematic literature search, Brian Feldman, Hayyah Clairman and Natasha Naraidoo for their support in conducting the Delphi process using questionnaires on the RedCap platform and EULAR, and EULAR and the ACR for financial and logistical support. This project is part of a series of "points to consider" consensus efforts to standardise the diagnosis and care of patients with the three major groups of known autoinflammatory diseases including 1. The IL-1 mediated diseases CAPS, TRAPS, MKD and DIRA; 2. The autoinflammatory interferonopathies chronic atypical neutrophilic dermatosis with lipodystrophy and elevated temperature (CANDLE), STING-associated vasculopathy with onset in infancy (SAVI) and Aicardi-Goutieres syndrome (AGS) and 3. The early diagnosis and management of inflammatory conditions with the potential progression to hemophagocytic lymphohistiocytosis/macrophage activation syndrome (HLH/MAS). We would like to acknowledge, and are grateful for, the generous and invaluable financial and organisational support from the Autoinflammatory Alliance and the Systemic JIA Foundation. The Autoinflammatory Alliance substantially contributed to an international meeting and workgroup organisation in August 2019 that developed the outline of the points to consider project. The funds for this project came largely from patient fundraisers, online fundraising and the work of countless volunteers who made this project possible.

AUTHOR CONTRIBUTIONS

All authors contributed to the formulation of the points to consider. In detail: the steering committee of the task force (ED, RG-M, MG, JBK-D, HH, SO, JF, AAd-J) defined the research questions for the

systematic literature review (SLR). The SLR was conducted by MR, ZSA, DP with support from a librarian (DH) under supervision of a senior methodologist (ED). MR, ZSA, DP extracted the data. ED, RG-M, MG, JBK-D, HH, SO, JF and AAd-J synthesised the results from SLR and the Delphi questionnaires and generated draft statements. The manuscript was drafted by MR, ZSA and DP and revised in detail by the steering group members and received a final review by the convenors. DA oversaw the proceedings and provided advice of this points to consider project as EULAR methodologist. All other authors participated in the task force meetings, in two pre-meeting Delphi questionnaires, and suggested and agreed upon the research questions. All members read the final statements prior to the drafting of the manuscript, discussed results and made contributions to the text. All authors approved the final version of the manuscript.

COMPETING INTERESTS

DA: received grants from AbbVie, Amgen, Lilly, Novartis, Roche, Sobi and Sanofi; received consulting fees from AbbVie, Amgen, Lilly, Merck, Novartis, Pfizer, Roche and Sandoz; received lecture fees from Lilly, Merck, Pfizer, Roche and Sandoz. RB: received consultation fees from Sandoz and Roche. LB: received grants from Novartis and Regeneron. FD: received consulting fees from Novartis. KLD: is the president of the Autoinflammatory Alliance. PF: received grants from NIH and CARRA; consulting fees from Novartis. DF: received grants from Novartis and Sobi; received consultation fees from Boehringer Ingelheim, Chugai-Roche, Merck, Novartis and Sobi; received lecture fees from Novartis, Peer Voice and Sobi. JH: received grants from CARRA and Sobi; consultation fees from Novartis, Biogen and Pfizer. RML: received consultation fees from Novartis and he is participating on a Data Safety Monitoring/Advisory Board of Sobi, Novartis and Sanofi. NR: received consulting fees from Ablynx, Amgen, AstraZeneca-Medimmune, Aurinia, Bayer, Bristol Myers Squibb, Cambridge Healthcare Research, Celgene, Domain Therapeutic, Eli Lilly, EMD Serono, GSK, Idorsia, Janssen, Novartis, Sobi, Pfizer and UCB; received lecture fees from Eli Lilly, GSK, Pfizer, Sobi and UCB; he is member of advisory boards of Pfizer and Eli Lilly. HH: received grants from Bristol Myers Squibb, Jecure, Takeda and Zomagen; received consulting fees from Novartis, Regeneron, Sobi and Aclaris, received advisory board fees from Novartis and IFM. JBK-D: received grants from Novartis and Sobi; received consulting fees from Novartis; received payment for lectures from Novartis and Sobi; received advisory board fees from Novartis. SO: lectures fees from Novartis and Sobi; meeting support from Sobi, AbbVie and Pfizer; advisory board payment from Novartis. MG: received grants from Novartis; received consultation and lecture fees from Novartis and Sobi. RG-M: received study support under government CRADAs from Eli Lilly, IFM and Sobi. ED: received grants from Sobi.

REFERENCES

1. Masters SL, Simon A, Aksentijevich I, Kastner DL. Horror autoinflammatory: the molecular pathophysiology of autoinflammatory disease (*). *Annu Rev Immunol* 2009;27:621–68.
2. Aksentijevich I, Masters SL, Ferguson PJ, Dancy P, Frenkel J, van Royen-Kerkhoff A, et al. An autoinflammatory disease with deficiency of the interleukin-1-receptor antagonist. *N Engl J Med* 2009;360:2426–37.
3. Toro JR, Aksentijevich I, Hull K, Dean J, Kastner DL. Tumor necrosis factor receptor-associated periodic syndrome: a novel syndrome with cutaneous manifestations. *Arch Dermatol* 2000;136:1487–94.
4. Van Der Meer JW, Radl J, Meyer CL, Vossen J, Van Nieuwkoop J, Lobatto S, et al. Hyperimmunoglobulinaemia D and periodic fever: a new syndrome. *Lancet* 1984;323:1087–90.
5. Drenth JP, Haagsma CJ, van der Meer JW. Hyperimmunoglobulinemia D and periodic fever syndrome: the clinical spectrum in a series

- of 50 patients. International Hyper-IgD Study Group. *Medicine* (Baltimore) 1994;73:133–44.
6. Aksentijevich I, Putnam CD, Remmers EF, Mueller JL, Le J, Kolodner RD, et al. The clinical continuum of cryopyrinopathies: novel CIAS1 mutations in North American patients and a new cryopyrin model. *Arthritis Rheum* 2007;56:1273–85.
 7. Aksentijevich I, Nowak M, Mallah M, Chae JJ, Watford WT, Hofmann SR, et al. De novo CIAS1 mutations, cytokine activation, and evidence for genetic heterogeneity in patients with neonatal-onset multisystem inflammatory disease (NOMID): a new member of the expanding family of pyrin-associated autoinflammatory diseases. *Arthritis Rheum* 2002;46:3340–8.
 8. Drenth JP, Göertz J, Daha MR, van der Meer JW. Immunoglobulin D enhances the release of tumor necrosis factor- α , and interleukin-1 β as well as interleukin-1 receptor antagonist from human mononuclear cells. *Immunology* 1996;88:355–62.
 9. Feldmann J, Prieur AM, Quartier P, Berquin P, Certain S, Cortis E, et al. Chronic infantile neurological cutaneous and articular syndrome is caused by mutations in CIAS1, a gene highly expressed in polymorphonuclear cells and chondrocytes. *Am J Hum Genet* 2002;71:198–203.
 10. Kile RL, Rusk HA. A case of cold urticaria with an unusual family history. *JAMA* 1940;114:1067–8.
 11. Ben-Chetrit E, Gattorno M, Gul A, Kastner DL, Lachmann HJ, Touitou I, et al. Consensus proposal for taxonomy and definition of the autoinflammatory diseases (AIDs): a Delphi study. *Ann Rheum Dis* 2018;77:1558–65.
 12. Agostini L, Martinon F, Burns K, McDermott MF, Hawkins PN, Tschopp J. NALP3 forms an IL-1 β -processing inflammasome with increased activity in Muckle-Wells autoinflammatory disorder. *Immunity* 2004;20:319–25.
 13. Awad F, Assrawi E, Jumeau C, Odent S, Despert V, Cam G, et al. The NLRP3 p.A441V mutation in NLRP3-AID pathogenesis: functional consequences, phenotype-genotype correlations and evidence for a recurrent mutational event. *ACR Open Rheumatol* 2019;1:267–76.
 14. Johnstone RF, Dolen WK, Hoffman HM. A large kindred with familial cold autoinflammatory syndrome. *Ann Allergy Asthma Immunol* 2003;90:233–7.
 15. Wang L, Manji GA, Grenier JM, Al-Garawi A, Merriam S, Lora JM, et al. PYPAF7, a novel PYRIN-containing Apaf1-like protein that regulates activation of NF- κ B and caspase-1-dependent cytokine processing. *J Biol Chem* 2002;277:29874–80.
 16. Neven B, Callebaut I, Prieur AM, Feldmann J, Bodemer C, Lepore L, et al. Molecular basis of the spectral expression of CIAS1 mutations associated with phagocytic cell-mediated autoinflammatory disorders CINCA/NOMID, MWS, and FCU. *Blood* 2004;103:2809–15.
 17. Lachmann HJ, Papa R, Gerhold K, Obici L, Touitou I, Cantarini L, et al. The phenotype of TNF receptor-associated autoinflammatory syndrome (TRAPS) at presentation: a series of 158 cases from the Eurofever/EUROTRAPS international registry. *Ann Rheum Dis* 2014;73:2160–7.
 18. McDermott MF, Aksentijevich I, Galon J, McDermott EM, Ogunkolade BW, Centola M, et al. Germline mutations in the extracellular domains of the 55 kDa TNF receptor, TNFR1, define a family of dominantly inherited autoinflammatory syndromes. *Cell* 1999;97:133–44.
 19. D’Osualdo A, Picco P, Caroli F, Gattorno M, Giacchino R, Fortini P, et al. MVK mutations and associated clinical features in Italian patients affected with autoinflammatory disorders and recurrent fever. *Eur J Hum Genet* 2005;13:314–20.
 20. Drenth JP, Mariman EC, Van der Velde-Visser SD, Ropers HH, Van der Meer JW. Location of the gene causing hyperimmunoglobulinemia D and periodic fever syndrome differs from that for familial Mediterranean fever. International Hyper-IgD Study Group. *Hum Genet* 1994;94:616–20.
 21. Lainka E, Neudorf U, Lohse P, Timmann C, Bielak M, Stojanov S, et al. Incidence and clinical features of hyperimmunoglobulinemia D and periodic fever syndrome (HIDS) and spectrum of mevalonate kinase (MVK) mutations in German children. *Rheumatol Int* 2012;32:3253–60.
 22. Simon A, Cuisset L, Vincent MF, Van der Velde-Visser SD, Delpach M, Van der Meer JW, et al. Molecular analysis of the mevalonate kinase gene in a cohort of patients with the hyper-IgD and periodic fever syndrome: its application as a diagnostic tool. *Ann Intern Med* 2001;135:338–43.
 23. Ozen S, Demirkaya E, Erer B, Livneh A, Ben-Chetrit E, Giancane G, et al. EULAR recommendations for the management of familial Mediterranean fever. *Ann Rheum Dis* 2016;75:644–51.
 24. Ahmadi N, Brewer CC, Zalewski C, King KA, Butman JA, Plass N, et al. Cryopyrin-associated periodic syndromes: otolaryngologic and audiologic manifestations. *Otolaryngol Head Neck Surg* 2011;145:295–302.
 25. Dollfus H, Hafner R, Hofmann HM, Russo RA, Denda L, Gonzales LD, et al. Chronic infantile neurological cutaneous and articular/neonatal onset multisystem inflammatory disease syndrome: ocular manifestations in a recently recognized chronic inflammatory disease of childhood. *Arch Ophthalmol* 2000;118:1386–92.
 26. Hill SC, Namde M, Dwyer A, Poznanski A, Canna S, Goldbach-Mansky R. Arthropathy of neonatal onset multisystem inflammatory disease (NOMID/CINCA). *Pediatr Radiol* 2007;37:145–52.
 27. Lane T, Loeffler JM, Rowczenio DM, Gilbertson JA, Bybee A, Russell TL, et al. AA amyloidosis complicating the hereditary periodic fever syndromes. *Arthritis Rheum* 2013;65:1116–21.
 28. Goldbach-Mansky R, Dailey NJ, Canna SW, Gelabert A, Jones J, Rubin BI, et al. Neonatal-onset multisystem inflammatory disease responsive to interleukin-1 β inhibition. *N Engl J Med* 2006;355:581–92.
 29. Koitschev A, Gramlich K, Hansmann S, Benseler S, Plontke SK, Koitschev C, et al. Progressive familial hearing loss in Muckle-Wells syndrome. *Acta Oto-Laryngologica* 2012;132:756–62.
 30. Prieur AM, Griscelli C, Lampert F, Truckenbrodt H, Guggenheim MA, Lovell DJ, et al. A chronic, infantile, neurological, cutaneous and articular (CINCA) syndrome: a specific entity analysed in 30 patients. *Scand J Rheumatol Suppl* 1987;66:57–68.
 31. Muckle TJ, Wells M. Urticaria, deafness, and amyloidosis: a new heredo-familial syndrome. *Q J Med* 1962;31:235–48.
 32. Simon A, Kremer HP, Wevers RA, Scheffer H, De Jong JG, Van Der Meer JW, et al. Mevalonate kinase deficiency: evidence for a phenotypic continuum. *Neurology* 2004;62:994–7.
 33. Kümmerle-Deschner JB, Tyrrell PN, Reess F, Kötter I, Lohse P, Girschick H, et al. Risk factors for severe Muckle-Wells syndrome. *Arthritis Rheum* 2010;62:3783–91.
 34. Caorsi R, Lepore L, Zulian F, Alessio M, Stabile A, Insalaco A, et al. The schedule of administration of canakinumab in cryopyrin associated periodic syndrome is driven by the phenotype severity rather than the age. *Arthritis Res Ther* 2013;15:R33.
 35. Papa R, Doglio M, Lachmann HJ, Ozen S, Frenkel J, Simon A, et al. A web-based collection of genotype-phenotype associations in hereditary recurrent fevers from the Eurofever registry. *Orphanet J Rare Dis* 2017;12:167.
 36. Ter Haar NM, Jeyaratnam J, Lachmann HJ, Simon A, Brogan PA, Doglio M, et al. The phenotype and genotype of mevalonate kinase deficiency: a series of 114 cases from the Eurofever registry. *Arthritis Rheumatol* 2016;68:2795–805.
 37. Kümmerle-Deschner JB, Hofer F, Endres T, Kortus-Goetze B, Blank N, Weissbarth-Riedel E, et al. Real-life effectiveness of

- canakinumab in cryopyrin-associated periodic syndrome. *Rheumatology (Oxford)* 2016;55:689–96.
38. Kuemmerle-Deschner JB, Koitschev A, Tyrrell PN, Plontke SK, Deschner N, Hansmann S, et al. Early detection of sensorineural hearing loss in Muckle-Wells-syndrome. *Pediatr Rheumatol Online J* 2015;13:43.
 39. Van der Heijde D, Aletaha D, Carmona L, Edwards CJ, Kvien TK, Kouloumas M, et al. 2014 update of the EULAR standardised operating procedures for EULAR-endorsed recommendations. *Ann Rheum Dis* 2015;74:8–13.
 40. OCEBM Levels of Evidence Working Group. Oxford Centre for Evidence-Based Medicine: levels of evidence (March 2009). 2009. URL: <https://www.cebm.net/2009/06/oxford-centre-evidence-based-medicine-levels-evidence-march-2009/>.
 41. Gattorno M, Hofer M, Federici S, Vanoni F, Bovis F, Aksentijevich I, et al. Classification criteria for autoinflammatory recurrent fevers [review]. *Ann Rheum Dis* 2019;78:1025–32.
 42. Haas N, Küster W, Zuberbier T, Henz BM. Muckle-Wells syndrome: clinical and histological skin findings compatible with cold air urticaria in a large kindred. *Br J Dermatol* 2004;151:99–104.
 43. Kuemmerle-Deschner JB, Lohse P, Koetter I, Dannecker GE, Reess F, Ummerhofer K, et al. NLRP3 E311K mutation in a large family with Muckle-Wells syndrome: description of a heterogeneous phenotype and response to treatment. *Arthritis Res Ther* 2011; R196.
 44. Kuemmerle-Deschner JB, Wittkowski H, Tyrrell PN, Koetter I, Lohse P, Ummerhofer K, et al. Treatment of Muckle-Wells syndrome: analysis of two IL-1-blocking regimens. *Arthritis Res Ther* 2013;15:R64.
 45. Ozen S, Kuemmerle-Deschner JB, Cimaz R, Livneh A, Quartier P, Kone-Paut I, et al. International retrospective chart review of treatment patterns in severe familial Mediterranean fever, tumor necrosis factor receptor-associated periodic syndrome, and mevalonate kinase deficiency/hyperimmunoglobulinemia D syndrome. *Arthritis Care Res (Hoboken)* 2017;69:578–86.
 46. Pastore S, Paloni G, Caorsi R, Ronfani L, Taddio A, Lepore L, et al. Serum amyloid protein A concentration in cryopyrin-associated periodic syndrome patients treated with interleukin-1 β antagonist. *Clin Exp Rheumatol* 2014;32 Suppl:S63–S6.
 47. Chuamanochan M, Weller K, Feist E, Kallinich T, Maurer M, Kummerle-Deschner J, et al. State of care for patients with systemic autoinflammatory diseases – results of a tertiary care survey. *World Allergy Organ J* 2019;12.
 48. Kuemmerle-Deschner JB, Ozen S, Tyrrell PN, Kone-Paut I, Goldbach-Mansky R, Lachmann H, et al. Diagnostic criteria for cryopyrin-associated periodic syndrome (CAPS). *Ann Rheum Dis* 2017;76:942–7.
 49. Brogan PA, Hofer M, Kuemmerle-Deschner JB, Kone-Paut I, Roesler J, Kallinich T, et al. Rapid and sustained long-term efficacy and safety of canakinumab in patients with cryopyrin-associated periodic syndrome ages five years and younger. *Arthritis Rheumatol* 2019;71:1955–63.
 50. Rodrigues F, Philit JB, Giurgea I, Anglicheau D, Roux JJ, Hoyeau N, et al. AA amyloidosis revealing mevalonate kinase deficiency: a report of 20 cases including two new French cases and a comprehensive review of literature [review]. *Semin Arthritis Rheum* 2020; 50:1370–3.
 51. Dingulu G, Georjin-Lavialle S, Koné-Paut I, Pillet P, Pagnier A, Merlin E, et al. Validation of the new classification criteria for hereditary recurrent fever in an independent cohort: experience from the JIR Cohort Database. *Rheumatology (Oxford)*. 2020;59: 2947–52.
 52. Shinar Y, Ceccherini I, Rowczenio D, Aksentijevich I, Arostegui J, Ben-Chétrit E, et al. ISSAID/EMQN Best Practice Guidelines for the Genetic Diagnosis of Monogenic Autoinflammatory Diseases in the Next-Generation Sequencing Era. *Clin Chem*. 2020;66:525–36.
 53. Highlights of Prescribing Information: Kineret. US Food and Drug Administration, 2020. URL: https://www.accessdata.fda.gov/drugsatfda_docs/label/2020/103950s5189lbl.pdf.
 54. Highlights of Prescribing Information: Ilaris. US Food and Drug Administration, 2020. URL: https://www.accessdata.fda.gov/drugsatfda_docs/label/2020/125319s097lbl.pdf.
 55. Highlights of Prescribing Information: Arcalyst. US Food and Drug Administration, 2021. URL: https://www.accessdata.fda.gov/drugsatfda_docs/label/2021/125249s049lbl.pdf.
 56. Kineret. European Medicines Agency, 2020 URL: <https://www.ema.europa.eu/en/medicines/human/EPAR/kineret>.
 57. Ilaris. European Medicines Agency, 2021 URL: <https://www.ema.europa.eu/en/medicines/human/EPAR/ilaris>.
 58. Gattorno M, Obici L, Cattalini M, Tormey V, Abrams K, Davis N, et al. Canakinumab treatment for patients with active recurrent or chronic TNF receptor-associated periodic syndrome (TRAPS): an open-label, phase II study. *Ann Rheum Dis* 2017;76:173–8.
 59. Hausmann JS, O'Hare K. Improving the transition from pediatric to adult care for adolescents and young adults with autoinflammatory diseases. In: *Auto-inflammatory syndromes*. Heidelberg: Springer; 2019. p. 249–59.
 60. Kuemmerle-Deschner JB, Koitschev A, Ummerhofer K, Hansmann S, Plontke SK, Koitschev C, et al. Hearing loss in Muckle-Wells syndrome. *Arthritis Rheum* 2013;65:824–31.
 61. Foster HE, Minden K, Clemente D, Leon L, McDonagh JE, Kamphuis S, et al. EULAR/PReS standards and recommendations for the transitional care of young people with juvenile-onset rheumatic diseases. *Ann Rheum Dis* 2017;76:639–46.
 62. Levy R, Gérard L, Kuemmerle-Deschner J, Lachmann HJ, Koné-Paut I, Cantarini L, et al. Phenotypic and genotypic characteristics of cryopyrin-associated periodic syndrome: a series of 136 patients from the Eurofever Registry. *Ann Rheum Dis* 2015;74: 2043–9.
 63. Fingerhutova S, Franova J, Hlavackova E, Jancova E, Prochazkova L, Berankova K, et al. Muckle-Wells syndrome across four generations in one Czech family: natural course of the disease. *Front Immunol* 2019;10:802.
 64. Gattorno M, Caorsi R, Meini A, Cattalini M, Federici S, Zulian F, et al. Differentiating PFAPA syndrome from monogenic periodic fevers. *Pediatrics* 2009;124:e721–8.
 65. Federici S, Sormani MP, Ozen S, Lachmann HJ, Amaryan G, Woo P, et al. Evidence-based provisional clinical classification criteria for autoinflammatory periodic fevers. *Ann Rheum Dis* 2015;74: 799–805.
 66. Hua Y, Wu D, Shen M, Yu K, Zhang W, Zeng X. Phenotypes and genotypes of Chinese adult patients with systemic autoinflammatory diseases. *Semin Arthritis Rheum* 2019;49:446–52.
 67. Lasiglie D, Mensa-Vilaro A, Ferrera D, Caorsi R, Penco F, Santamaria G, et al. Cryopyrin-associated periodic syndromes in Italian patients: evaluation of the rate of somatic NLRP3 mosaicism and phenotypic characterization. *J Rheumatol* 2017;44:1667–73.
 68. Nakagawa K, Gonzalez-Roca E, Souto A, Umabayashi H, Campistol JM, Canellas J, et al. Somatic NLRP3 mosaicism in Muckle-Wells syndrome. a genetic mechanism shared by different phenotypes of cryopyrin-associated periodic syndromes. *Ann Rheum Dis* 2015;74:603–10.
 69. Tanaka N, Izawa K, Saito MK, Sakuma M, Oshima K, Ohara O, et al. High incidence of NLRP3 somatic mosaicism in patients with chronic infantile neurologic, cutaneous, articular syndrome: results of an international multicenter collaborative study. *Arthritis Rheum* 2011; 63:3625–32.

70. Ueda N, Ida H, Washio M, Miyahara H, Tokunaga S, Tanaka F, et al. Clinical and genetic features of patients with TNFRSF1A variants in Japan: findings of a nationwide survey. *Arthritis Rheumatol* 2016; 68:2760–71.
71. Jesus AA, Fujihira E, Watase M, Terreri MT, Hilario MO, Carneiro-Sampaio M, et al. Hereditary autoinflammatory syndromes: a Brazilian multicenter study. *J Clin Immunol* 2012;32:922–32.
72. Karagianni P, Nezos A, Ioakeim F, Tzioufas AG, Moutsopoulos HM. Analysis of NLRP3, MVK and TNFRSF1A variants in adult Greek patients with autoinflammatory symptoms. *Clin Exp Rheumatol* 2018;36 Suppl:86–9.
73. Vergara C, Borzutzky A, Gutierrez MA, Iacobelli S, Talesnik E, Martinez ME, et al. Clinical and genetic features of hereditary periodic fever syndromes in Hispanic patients: the Chilean experience. *Clin Rheumatol* 2012;31:829–34.
74. Dode C, Le Du N, Cuisset L, Letourneur F, Berthelot JM, Vaudour G, et al. New mutations of CIAS1 that are responsible for Muckle-Wells syndrome and familial cold urticaria: a novel mutation underlies both syndromes. *Am J Hum Genet* 2002;70:1498–506.
75. Caroli F, Pontillo A, D'Ossualdo A, Travan L, Ceccherini I, Crovella S, et al. Clinical and genetic characterization of Italian patients affected by CINCA syndrome. *Rheumatology (Oxford)* 2007;46:473–8.
76. Mehr S, Allen R, Boros C, Adib N, Kakakios A, Turner PJ, et al. Cryopyrin-associated periodic syndrome in Australian children and adults: epidemiological, clinical and treatment characteristics. *J Paediatr Child Health* 2016;52:889–95.
77. Rowczenio DM, Gomes SM, Arostegui JI, Mensa-Vilaro A, Omoyinmi E, Trojer H, et al. Late-onset cryopyrin-associated periodic syndromes caused by somatic NLRP3 mosaicism: UK single center experience. *Front Immunol* 2017;8:1410.
78. Federici L, Rittore-Domingo C, Koné-Paut I, Jorgensen C, Rodière M, Le Quellec A, et al. A decision tree for genetic diagnosis of hereditary periodic fever in unselected patients. *Ann Rheum Dis* 2006;65:1427–32.
79. Munoz MA, Jurczyk J, Simon A, Hissaria P, Arts RJ, Coman D, et al. Defective protein prenylation in a spectrum of patients with mevalonate kinase deficiency. *Front Immunol* 2019;10:1900.
80. Jesus AA, Osman M, Silva CA, Kim PW, Pham TH, Gadina M, et al. A novel mutation of IL1RN in the deficiency of interleukin-1 receptor antagonist syndrome: description of two unrelated cases from Brazil. *Arthritis Rheum* 2011;63:4007–17.
81. Mendonca LO, Malle L, Donovan FX, Chandrasekharappa SC, Montealegre Sanchez GA, Garg M, et al. Deficiency of interleukin-1 receptor antagonist (DIRA): report of the first Indian patient and a novel deletion affecting IL1RN. *J Clin Immunol* 2017;37:445–51.
82. Tanaka T, Yoshioka K, Nishikomori R, Sakai H, Abe J, Yamashita Y, et al. National survey of Japanese patients with mevalonate kinase deficiency reveals distinctive genetic and clinical characteristics. *Mod Rheumatol* 2019;29:181–7.
83. Al-Mayouf SM, Almutairi A, Albrawi S, Fathalla BM, Alzyoud R, AlEnazi A, et al. Pattern and diagnostic evaluation of systemic autoinflammatory diseases other than familial Mediterranean fever among Arab children: a multicenter study from the Pediatric Rheumatology Arab Group (PRAG). *Rheumatol Int* 2020;40:49–56.
84. Bader-Meunier B, Florkin B, Sibilia J, Acquaviva C, Hachulla E, Grateau G, et al. Mevalonate kinase deficiency: a survey of 50 patients. *Pediatrics* 2011;128:e152–9.
85. Berody S, Galeotti C, Kone-Paut I, Piram M. A retrospective survey of patients's journey before the diagnosis of mevalonate kinase deficiency. *Joint Bone Spine* 2015;82:240–4.
86. Houx L, Hachulla E, Kone-Paut I, Quartier P, Touitou I, Guennoc X, et al. Musculoskeletal symptoms in patients with cryopyrin-associated periodic syndromes: a large database study. *Arthritis Rheumatol* 2015;67:3027–36.
87. Kilic H, Sahin S, Duman C, Adrovic A, Barut K, Turanli ET, et al. Spectrum of the neurologic manifestations in childhood-onset cryopyrin-associated periodic syndrome. *Eur J Paediatr Neurol* 2019;23:466–72.
88. Sobolewska B, Angermair E, Deuter C, Doycheva D, Kuemmerle-Deschner J, Zierhut M. NLRP3 A439V mutation in a large family with cryopyrin-associated periodic syndrome: description of ophthalmologic symptoms in correlation with other organ symptoms. *J Rheumatol* 2016;43:1101–6.
89. Wittkowski H, Kuemmerle-Deschner JB, Austermann J, Holzinger D, Goldbach-Mansky R, Gramlich K, et al. MRP8 and MRP14, phagocyte-specific danger signals, are sensitive biomarkers of disease activity in cryopyrin-associated periodic syndromes. *Ann Rheum Dis* 2011;70:2075–81.
90. Cuisset L, Jeru I, Dumont B, Fabre A, Cochet E, Le Bozec J, et al. Mutations in the autoinflammatory cryopyrin-associated periodic syndrome gene: epidemiological study and lessons from eight years of genetic analysis in France. *Ann Rheum Dis* 2011;70:495–9.
91. Kuemmerle-Deschner JB, Samba SD, Tyrrell PN, Koné-Paut I, Marie I, Deschner N, et al. Challenges in diagnosing Muckle-Wells syndrome: identifying two distinct phenotypes. *Arthritis Care Res (Hoboken)* 2014;66:765–72.
92. Li C, Tan X, Zhang J, Li S, Mo W, Han T, et al. Gene mutations and clinical phenotypes in 15 Chinese children with cryopyrin-associated periodic syndrome (CAPS). *Sci China Life Sci* 2017;60:1436–44.
93. Kitley JL, Lachmann HJ, Pinto A, Ginsberg L. Neurologic manifestations of the cryopyrin-associated periodic syndrome. *Neurology* 2010;74:1267–70.
94. Eroglu FK, Kasapcopur O, Besbas N, Ozaltin F, Bilginer Y, Barut K, et al. Genetic and clinical features of cryopyrin-associated periodic syndromes in Turkish children. *Clin Exp Rheumatol* 2016;34 Suppl: S115–20.
95. Sibley CH, Plass N, Snow J, Wiggs EA, Brewer CC, King KA, et al. Sustained response and prevention of damage progression in patients with neonatal-onset multisystem inflammatory disease treated with anakinra: a cohort study to determine three- and five-year outcomes. *Arthritis Rheum* 2012;64:2375–86.
96. Lauro CF, Goldbach-Mansky R, Schmidt M, Quezado ZM. The anesthetic management of children with neonatal-onset multisystem inflammatory disease. *Anesth Analg* 2007;105:351–7.
97. Quillinan N, Mohammad A, Mannion G, O'Keeffe D, Bergin D, Coughlan R, et al. Imaging evidence for persistent subclinical fasciitis and arthritis in tumour necrosis factor receptor-associated periodic syndrome (TRAPS) between febrile attacks. *Ann Rheum Dis* 2010; 69:1408–9.
98. Lainka E, Neudorf U, Lohse P, Timmann C, Stojanov S, Huss K, et al. Incidence of TNFRSF1A mutations in German children: epidemiological, clinical and genetic characteristics. *Rheumatology (Oxford)* 2009;48:987–91.
99. D'Ossualdo A, Ferlito F, Prigione I, Obici L, Meini A, Zulian F, et al. Neutrophils from patients with TNFRSF1A mutations display resistance to tumor necrosis factor-induced apoptosis: pathogenetic and clinical implications. *Arthritis Rheum* 2006;54:998–1008.
100. Papa R, Lane T, Minden K, Touitou I, Cantarini L, Cattalini M, et al. INSAID variant classification and Eurofever Criteria Guide optimal treatment strategy in patients with TRAPS: data from the Eurofever registry. *J Allergy Clin Immunol Pract* 2021;9:783–91.
101. Pelagatti MA, Meini A, Caorsi R, Cattalini M, Federici S, Zulian F, et al. Long-term clinical profile of children with the low-penetrance R92Q mutation of the TNFRSF1A gene. *Arthritis Rheum* 2011;63:1141–50.
102. Ravet N, Rouaghe S, Dodé C, Bienvenu J, Stirnemann J, Lévy P, et al. Clinical significance of P46L and R92Q substitutions in the



- tumour necrosis factor superfamily 1A gene. *Ann Rheum Dis* 2006; 65:1158–62.
103. Ruiz-Ortiz E, Iglesias E, Soriano A, Buján-Rivas S, Español-Rego M, Castellanos-Moreira R, et al. Disease phenotype and outcome depending on the age at disease onset in patients carrying the R92Q low-penetrance variant in TNFRSF1A gene. *Front Immunol* 2017;8:299.
 104. Livneh A, Drenth JP, Klasen IS, Langevitz P, George J, Shelton DA, et al. Familial Mediterranean fever and hyperimmunoglobulinemia D syndrome: two diseases with distinct clinical, serologic, and genetic features. *J Rheumatol* 1997;24:1558–63.
 105. Ammouri W, Cuisset L, Rouaghe S, Rolland MO, Delpech M, Grateau G, et al. Diagnostic value of serum immunoglobulinaemia D level in patients with a clinical suspicion of hyper IgD syndrome. *Rheumatology (Oxford)* 2007;46:1597–600.
 106. Drenth JP, Boom BW, Toonstra J, Van der Meer JW. Cutaneous manifestations and histologic findings in the hyperimmunoglobulinemia D syndrome. International Hyper IgD Study Group. *Arch Dermatol* 1994;130:59–65.
 107. Loeliger AE, Kruize AA, Bijlsma JW, Loeliger AE, Derksen RH. Arthritis in hyperimmunoglobulinaemia D. *Ann Rheum Dis* 1993; 52:81.
 108. Oretti C, Barbi E, Marchetti F, Lepore L, Ventura A, D’Ossualdo A, et al. Diagnostic challenge of hyper-IgD syndrome in four children with inflammatory gastrointestinal complaints. *Scand J Gastroenterol* 2006;41:430–6.
 109. Stojanov S, Lohse P, Lohse P, Hoffmann F, Renner ED, Zellerer S, et al. Molecular analysis of the MVK and TNFRSF1A genes in patients with a clinical presentation typical of the hyperimmunoglobulinemia D with periodic fever syndrome: a low-penetrance TNFRSF1A variant in a heterozygous MVK carrier possibly influences the phenotype of hyperimmunoglobulinemia D with periodic fever syndrome or vice versa. *Arthritis Rheum* 2004;50:1951–8.
 110. Van Der Hilst JC, Bodar EJ, Barron KS, Frenkel J, Drenth JP, Van Der Meer JW, et al. Long-term follow-up, clinical features, and quality of life in a series of 103 patients with hyperimmunoglobulinemia D syndrome. *Medicine* 2008;87:301–10.
 111. De Pieri C, Taddio A, Insalaco A, Barbi E, Lepore L, Ventura A, et al. Different presentations of mevalonate kinase deficiency: a case series. *Clin Exp Rheumatol* 2015;33:437–42.
 112. Durel CA, Aouba A, Bienvenu B, Deshayes S, Coppere B, Gombert B, et al. Observational study of a French and Belgian multicenter cohort of 23 patients diagnosed in adulthood with mevalonate kinase deficiency. *Medicine (Baltimore)* 2016;95:e3027.
 113. Frenkel J, Houten SM, Waterham HR, Wanders RJ, Rijkers GT, Duran M, et al. Clinical and molecular variability in childhood periodic fever with hyperimmunoglobulinemia D. *Rheumatology* 2001;40: 579–84.
 114. Haraldsson A, Weemaes CM, De Boer AW, Bakkeren JA, Stoelinga GB. Immunological studies in the hyper-immunoglobulin D syndrome. *J Clin Immunol* 1992;12:424–8.
 115. Tas DA, Dinkci S, Erken E. Different clinical presentation of the hyper-immunoglobulin D syndrome (HIDS) (four cases from Turkey). *Clin Rheumatol* 2012;31:889–93.
 116. De Dios Garcia-Diaz J, Alvarez-Blanco MJ. High IgD could be a non-pathogenetic diagnostic marker of the hyper-IgD and periodic fever syndrome. *Ann Allergy Asthma Immunol* 2001;86:587.
 117. Stabile A, Compagnone A, Napodano S, Raffaele CG, Patti M, Rigante D. Mevalonate kinase genotype in children with recurrent fevers and high serum IgD level. *Rheumatol Int* 2013;33:3039–42.
 118. Jeyaratnam J, Ter Haar NM, de Sain-van der Velden MG, Waterham HR, van Gijn ME, Frenkel J. Diagnostic value of urinary mevalonic acid excretion in patients with a clinical suspicion of mevalonate kinase deficiency (MKD). *JIMD Rep* 2016;27:33–8.
 119. Poll-The BT, Frenkel J, Houten SM, Kuis W, Duran M, De Koning TJ, et al. Mevalonic aciduria in 12 unrelated patients with hyperimmunoglobulinemia D and periodic fever syndrome. *J Inher Metab Dis* 2000;23:363–6.
 120. Garg M, de Jesus AA, Chapelle D, Dancey P, Herzog R, Rivas-Chacon R, et al. Riloncept maintains long-term inflammatory remission in patients with deficiency of the IL-1 receptor antagonist. *JCI Insight* 2017;2:e94838.
 121. Kuemmerle-Deschner JB, Welzel T, Hoertnagel K, Tsiflikas I, Hospach A, Liu X, et al. New variant in the IL1RN-gene (DIRA) associated with late-onset, CRMO-like presentation. *Rheumatology (Oxford)* 2020;59:3259–63.
 122. Beck C, Girschick HJ, Morbach H, Schwarz T, Yimam T, Frenkel J, et al. Mutation screening of the IL-1 receptor antagonist gene in chronic non-bacterial osteomyelitis of childhood and adolescence. *Clin Exp Rheumatol* 2011;29:1040–3.
 123. Thacker PG, Binkovitz LA, Thomas KB. Deficiency of interleukin-1-receptor antagonist syndrome: a rare auto-inflammatory condition that mimics multiple classic radiographic findings. *Pediatr Radiol* 2012;42:495–8.
 124. Minkis K, Aksentijevich I, Goldbach-Mansky R, Magro C, Scott R, Davis JG, et al. Interleukin 1 receptor antagonist deficiency presenting as infantile pustulosis mimicking infantile pustular psoriasis. *Arch Dermatol* 2012;148:747–52.
 125. Cox AJ, Zhao Y, Ferguson PJ. Chronic recurrent multifocal osteomyelitis and related diseases: update on pathogenesis. *Curr Rheumatol Rep* 2017;19:18.
 126. Abe K, Cox A, Takamatsu N, Velez G, Laxer RM, Tse SM, et al. Gain-of-function mutations in a member of the Src family kinases cause autoinflammatory bone disease in mice and humans. *Proc Natl Acad Sci U S A* 2019;116:11872–7.
 127. De Jesus AA, Goldbach-Mansky R. Monogenic autoinflammatory diseases: concept and clinical manifestations. *Clin Immunol* 2013; 147:155–74.
 128. Takeichi T, Akiyama M. Generalized pustular psoriasis: clinical management and update on autoinflammatory aspects. *Am J Clin Dermatol* 2020;21:227–36.
 129. Van Nieuwenhove E, De Langhe E, Dooley J, Van Den Oord J, Shahrooei M, Parvaneh N, et al. Phenotypic analysis of pyrin-associated autoinflammation with neutrophilic dermatosis patients during treatment. *Rheumatology (Oxford)* 2021;60:5436–46.
 130. Hoffman HM, Throne ML, Amar NJ, Cartwright RC, Kivitz AJ, Soo Y, et al. Long-term efficacy and safety profile of riloncept in the treatment of cryopyrin-associated periodic syndromes: results of a 72-week open-label extension study. *Clin Ther* 2012;34:2091–103.
 131. Obici L, Meini A, Cattalini M, Chicca S, Galliani M, Donadei S, et al. Favourable and sustained response to anakinra in tumour necrosis factor receptor-associated periodic syndrome (TRAPS) with or without AA amyloidosis. *Ann Rheum Dis* 2011;70:1511–2.
 132. Rossi-Semerano L, Fautrel B, Wendling D, Hachulla E, Galeotti C, Semerano L, et al. Tolerance and efficacy of off-label anti-interleukin-1 treatments in France: a nationwide survey. *Orphanet J Rare Dis* 2015;10:19.
 133. Kuemmerle-Deschner JB, Tyrrell PN, Koetter I, Wittkowski H, Bialkowski A, Tzaribachev N, et al. Efficacy and safety of anakinra therapy in pediatric and adult patients with the autoinflammatory Muckle-Wells syndrome. *Arthritis Rheum* 2011;63:840–9.
 134. Kullenberg T, Lofqvist M, Leinonen M, Goldbach-Mansky R, Olivecrona H. Long-term safety profile of anakinra in patients with severe cryopyrin-associated periodic syndromes. *Rheumatology (Oxford)* 2016;55:1499–506.
 135. Neven B, Marvillet I, Terrada C, Ferster A, Boddaert N, Couloignier V, et al. Long-term efficacy of the interleukin-1 receptor antagonist anakinra in ten patients with neonatal-onset multisystem inflammatory

- disease/chronic infantile neurologic, cutaneous, articular syndrome. *Arthritis Rheum* 2010;62:258–67.
136. Goldbach-Mansky R, Shroff SD, Wilson M, Snyder C, Plehn S, Barham B, et al. A pilot study to evaluate the safety and efficacy of the long-acting interleukin-1 inhibitor rilonacept (interleukin-1 Trap) in patients with familial cold autoinflammatory syndrome. *Arthritis Rheum* 2008;58:2432–42.
 137. Hoffman HM, Throne ML, Amar NJ, Sebai M, Kivitz AJ, Kavanaugh A, et al. Efficacy and safety of rilonacept (interleukin-1 Trap) in patients with cryopyrin-associated periodic syndromes: results from two sequential placebo-controlled studies. *Arthritis Rheum* 2008;58:2443–52.
 138. Kuemmerle-Deschner JB, Ramos E, Blank N, Roesler J, Felix SD, Jung T, et al. Canakinumab (ACZ885, a fully human IgG1 anti-IL-1 β mAb) induces sustained remission in pediatric patients with cryopyrin-associated periodic syndrome (CAPS). *Arthritis Res Ther* 2011;13:R34.
 139. Yokota S, Imagawa T, Nishikomori R, Takada H, Abrams K, Lheritier K, et al. Long-term safety and efficacy of canakinumab in cryopyrin-associated periodic syndrome: results from an open-label, phase III pivotal study in Japanese patients. *Clinical Exp Rheumatol* 2017;35 Suppl:S19–26.
 140. Lachmann HJ, Kone-Paut I, Kuemmerle-Deschner JB, Leslie KS, Hachulla E, Quartier P, et al. Use of canakinumab in the cryopyrin-associated periodic syndrome. *N Engl J Med* 2009;360:2416–25.
 141. Kuemmerle-Deschner JB, Hachulla E, Cartwright R, Hawkins PN, Tran TA, Bader-Meunier B, et al. Two-year results from an open-label, multicentre, phase III study evaluating the safety and efficacy of canakinumab in patients with cryopyrin-associated periodic syndrome across different severity phenotypes. *Ann Rheum Dis* 2011;70:2095–102.
 142. De Benedetti F, Gattorno M, Anton J, Ben-Chetrit E, Frenkel J, Hoffman HM, et al. Canakinumab for the treatment of auto-inflammatory recurrent fever syndromes. *N Engl J Med* 2018;378:1908–19.
 143. Piram M, Koné-Paut I, Lachmann HJ, Frenkel J, Ozen S, Kuemmerle-Deschner J, et al. Validation of the auto-inflammatory diseases activity index (AIDAI) for hereditary recurrent fever syndromes. *Ann Rheum Dis* 2014;73:2168–73.
 144. Koné-Paut I, Galeotti C. Current treatment recommendations and considerations for cryopyrin-associated periodic syndrome. *Expert Rev Clin Immunol* 2015;11:1083–92.
 145. Ter Haar N, Lachmann H, Özen S, Woo P, Uziel Y, Modesto C, et al. Treatment of autoinflammatory diseases: results from the Eurofever Registry and a literature review. *Ann Rheum Dis* 2013;72:678–85.
 146. Bodar EJ, Kuijk LM, Drenth JP, van der Meer JW, Simon A, Frenkel J. On-demand anakinra treatment is effective in mevalonate kinase deficiency. *Ann Rheum Dis* 2011;70:2155–8.
 147. Grimwood C, Despert V, Jeru I, Hentgen V. On-demand treatment with anakinra: a treatment option for selected TRAPS patients. *Rheumatology (Oxford)* 2015;54:1749–51.
 148. Fox E, Jayaprakash N, Pham TH, Rowley A, McCully CL, Pucino F, et al. The serum and cerebrospinal fluid pharmacokinetics of anakinra after intravenous administration to non-human primates. *J Neuroimmunol* 2010;223:138–40.
 149. Rodriguez-Smith J, Lin YC, Tsai WL, Kim H, Montealegre-Sanchez G, Chapelle D, et al. Cerebrospinal fluid cytokines correlate with aseptic meningitis and blood–brain barrier function in neonatal-onset multisystem inflammatory disease: central nervous system biomarkers in neonatal-onset multisystem inflammatory disease correlate with central nervous system inflammation. *Arthritis Rheumatol* 2017;69:1325–36.
 150. Kuemmerle-Deschner JB, Verma D, Endres T, Broderick L, de Jesus AA, Hofer F, et al. Clinical and molecular phenotypes of low-penetrance variants of NLRP3: diagnostic and therapeutic challenges. *Arthritis Rheumatol* 2017;69:2233–40.
 151. Schuh E, Lohse P, Ertl-Wagner B, Witt M, Krumbholz M, Frankenberger M, et al. Expanding spectrum of neurologic manifestations in patients with NLRP3 low-penetrance mutations. *Neurol Neuroimmunol Neuroinflamm* 2015;2:e109.
 152. Elmi AA, Wynne K, Cheng IL, Eleftheriou D, Lachmann HJ, Hawkins PN, et al. Retrospective case series describing the efficacy, safety and cost-effectiveness of a vial-sharing programme for canakinumab treatment for paediatric patients with cryopyrin-associated periodic syndrome. *Pediatr Rheumatol Online J* 2019;17:36.
 153. Imagawa T, Nishikomori R, Takada H, Takeshita S, Patel N, Kim D, et al. Safety and efficacy of canakinumab in Japanese patients with phenotypes of cryopyrin-associated periodic syndrome as established in the first open-label, phase-3 pivotal study (24-week results). *Clin Exp Rheumatol* 2013;31:302–9.
 154. Kone-Paut I, Quartier P, Fain O, Grateau G, Pillet P, Le Blay P, et al. Real-world experience and impact of canakinumab in cryopyrin-associated periodic syndrome: results from a French observational study. *Arthritis Care Res* 2017;69:903–11.
 155. Lepore L, Paloni G, Caorsi R, Alessio M, Rigante D, Ruperto N, et al. Follow-up and quality of life of patients with cryopyrin-associated periodic syndromes treated with Anakinra. *J Pediatr* 2010;157:310–5.
 156. Russo RA, Melo-Gomes S, Lachmann HJ, Wynne K, Rajput K, Eleftheriou D, et al. Efficacy and safety of canakinumab therapy in paediatric patients with cryopyrin-associated periodic syndrome: a single-centre, real-world experience. *Rheumatology (Oxford)* 2014;53:665–70.
 157. Wiken M, Hallen B, Kullenberg T, Koskinen LO. Development and effect of antibodies to anakinra during treatment of severe CAPS: sub-analysis of a long-term safety and efficacy study. *Clin Rheumatol* 2018;37:3381–6.
 158. Gattorno M, Pelagatti MA, Meini A, Obici L, Barcellona R, Federici S, et al. Persistent efficacy of anakinra in patients with tumor necrosis factor receptor-associated periodic syndrome. *Arthritis Rheum* 2008;58:1516–20.
 159. Bulua AC, Mogul DB, Aksentijevich I, Singh H, He DY, Muenz LR, et al. Efficacy of etanercept in the tumor necrosis factor receptor-associated periodic syndrome: a prospective, open-label, dose-escalation study. *Arthritis Rheum* 2012;64:908–13.
 160. Batchelor HK, Marriott JF. Paediatric pharmacokinetics: key considerations. *Br J Clin Pharmacol* 2015;79:395–404.
 161. Erbis G, Schmidt K, Hansmann S, Sergiichuk T, Michler C, Kuemmerle-Deschner JB, et al. Living with autoinflammatory diseases: identifying unmet needs of children, adolescents and adults. *Pediatr Rheumatol Online J* 2018;16:81.
 162. Youngstein T, Hoffmann P, Gul A, Lane T, Williams R, Rowczenio DM, et al. International multi-centre study of pregnancy outcomes with interleukin-1 inhibitors. *Rheumatology (Oxford)* 2017;56:2102–8.
 163. Mamoudiy N, Maurey H, Marie I, Kone-Paut I, Deiva K. Neurological outcome of patients with cryopyrin-associated periodic syndrome (CAPS). *Orphanet J Rare Dis* 2017;12:33.
 164. Kuemmerle-Deschner JB, Quartier P, Kone-Paut I, Hentgen V, Marzan KA, Dedeoglu F, et al. Burden of illness in hereditary periodic fevers: a multinational observational patient diary study. *Clin Exp Rheumatol* 2020;38 Suppl:26–34.
 165. Torene R, Nirmala N, Obici L, Cattalini M, Tormey V, Caorsi R, et al. Canakinumab reverses overexpression of inflammatory response genes in tumour necrosis factor receptor-associated periodic syndrome. *Ann Rheum Dis* 2017;76:303–9.
 166. Kone-Paut I, Lachmann HJ, Kuemmerle-Deschner JB, Hachulla E, Leslie KS, Mouy R, et al. Sustained remission of symptoms and

- improved health-related quality of life in patients with cryopyrin-associated periodic syndrome treated with canakinumab: results of a double-blind placebo-controlled randomized withdrawal study. *Arthritis Res Ther* 2011;13:R202.
167. Ter Haar NM, Annink KV, Al-Mayouf SM, Amaryan G, Anton J, Barron KS, et al. Development of the autoinflammatory disease damage index (ADDI). *Ann Rheum Dis* 2017;76:821–30.
168. Hoffman HM, Wolfe F, Belomestnov P, Mellis SJ. Cryopyrin-associated periodic syndromes: development of a patient-reported outcomes instrument to assess the pattern and severity of clinical disease activity. *Curr Med Res Opin* 2008;24:2531–43.
169. Mulders-Manders CM, Kanters TA, Van Daele PL, Hoppenreijns E, Legger GE, Van Laar JA, et al. Decreased quality of life and societal impact of cryopyrin-associated periodic syndrome treated with canakinumab: a questionnaire based cohort study. *Orphanet J Rare Dis* 2018;13.
170. Piram M, Frenkel J, Gattorno M, Ozen S, Lachmann HJ, Goldbach-Mansky R, et al. A preliminary score for the assessment of disease activity in hereditary recurrent fevers: results from the AIDAI (Auto-Inflammatory Diseases Activity Index) consensus conference. *Ann Rheum Dis* 2011;70:309–14.
171. Jeyaratnam J, ter Haar NM, Lachmann HJ, Kasapcopur O, Ombrello AK, Rigante D, et al. The safety of live-attenuated vaccines in patients using IL-1 or IL-6 blockade: an international survey. *Pediatr Rheumatol* 2018;16.
172. Jaeger VK, Hoffman HM, van der Poll T, Tilson H, Seibert J, Speziale A, et al. Safety of vaccinations in patients with cryopyrin-associated periodic syndromes: a prospective registry based study. *Rheumatology (Oxford)* 2017;56:1484–91.
173. Chang Z, Spong CY, Jesus AA, Davis MA, Plass N, Stone DL, et al. Anakinra use during pregnancy in patients with cryopyrin-associated periodic syndromes (CAPS). *Arthritis Rheumatol* 2014;66:3227–32.
174. Sibley CH, Chioato A, Felix S, Colin L, Chakraborty A, Plass N, et al. A 24-month open-label study of canakinumab in neonatal-onset multisystem inflammatory disease. *Ann Rheum Dis* 2015;74:1714–9.

REVIEW

The Conundrum of Lung Disease and Drug Hypersensitivity-like Reactions in Systemic Juvenile Idiopathic Arthritis

Bryce A. Binstadt¹  and Peter A. Nigrovic² 

An unusual form of lung disease has begun to affect some children with systemic juvenile idiopathic arthritis (JIA), coincident with increasing utilization of interleukin-1 (IL-1) and IL-6 antagonists. Many children with systemic JIA-associated lung disease (SJIA-LD) have a history of clinical and laboratory features resembling drug reaction with eosinophilia and systemic symptoms (DRESS), a presentation now convincingly associated with HLA-DRB1*15. Treatment of DRESS typically requires drug discontinuation, a daunting prospect for clinicians and families who rely upon these agents. Here we review SJIA-LD and its associated DRESS-like phenotype. We suggest an alternative explanation, the cytokine plasticity hypothesis, proposing that IL-1 and IL-6 blockers modulate the milieu in which T cells develop, leading to a pathologic immune response triggered through exposure to common microbes, or to other exogenous or endogenous antigens, rather than to the drugs themselves. This hypothesis differs from DRESS in mechanism but also in clinical implications, predicting that control of pathogenic T cells could permit continued use of IL-1 and IL-6 antagonists in some individuals. The spectrum posed by these two hypotheses provides a conceptual framework that will guide investigation into the pathogenesis of SJIA-LD and may open up new therapeutic avenues for patients with systemic JIA.

INTRODUCTION

The pediatric rheumatology community is worried. Some children with systemic juvenile idiopathic arthritis (JIA) are developing an unusual, sometimes life-threatening, condition termed systemic JIA-associated lung disease (SJIA-LD) (1–4). The emergence of SJIA-LD has coincided with increasing use of blockers of interleukin-1 (IL-1; anakinra, canakinumab, and rarely rilonacept) or IL-6 (tocilizumab), and most children with SJIA-LD have a history of exposure to one or more of these agents (2,3). Recent work by Saper et al linked these reactions to the HLA class II allele DRB1*15, prompting the suggestion that SJIA-LD arises through an IL-1/IL-6 blocker-induced drug-induced hypersensitivity syndrome (DIHS) or even drug reaction with eosinophilia and systemic symptoms (DRESS) (5). These observations place clinicians, patients, and families in an extremely difficult

conundrum. IL-1 and IL-6 antagonists have transformed systemic JIA from the most destructive arthritis of childhood into a disease with an excellent prognosis for most patients (6–11). But if these biologics are potentially harmful, even life-threatening, what are we to do?

Here we review the available data supporting the suggestion that allergic-type responses and SJIA-LD reflect hypersensitivity to IL-1 and IL-6 antagonists—a proposal we term the “DRESS hypothesis”—and present an alternative, the “cytokine plasticity hypothesis,” that differs in mechanism and in clinical implications. We present this alternative not because we believe that the DRESS hypothesis is necessarily incorrect but because articulating alternate explanations is sound scientific practice. Considering these hypotheses, potentially together with others, will shape the scientific agenda and thereby help us to understand the relationship between IL-1 and IL-6 blockade, DIHS-type reactions, and

Dr. Binstadt's work was supported by the National Heart, Lung, and Blood Institute, NIH (award R01-HL-121093), the National Institute of Allergy and Infectious Diseases, NIH (award R21-AI-149334), and an Innovative Research Award from the Rheumatology Research Foundation. Dr. Nigrovic's work was supported by the National Institute of Arthritis and Musculoskeletal and Skin Diseases, NIH (awards 2R01-AR-065538, R01-AR-075906, R01-AR-073201, and 2P30-AR-070253), the Fundación Bechara, and the Arbuckle Family Fund for Arthritis Research.

¹Bryce A. Binstadt, MD, PhD: University of Minnesota, Minneapolis; ²Peter A. Nigrovic, MD: Boston Children's Hospital and Brigham and Women's Hospital, Boston, Massachusetts.

Author disclosures are available at <https://onlinelibrary.wiley.com/action/downloadSupplement?doi=10.1002%2Fart.42137&file=art42137-sup-0001-Disclosureform.pdf>.

Address correspondence to Bryce A. Binstadt, MD, PhD, Division of Rheumatology, Allergy & Immunology, Academic Office Building, AO-10, 2450 Riverside Avenue S., Minneapolis, MN 55454 (email: binstadt@umn.edu); or to Peter A. Nigrovic, MD, Division of Immunology, Boston Children's Hospital, Karp 10211, One Blackfan Circle, Boston, MA 02115 (email: peter.nigrovic@childrens.harvard.edu).

Submitted for publication January 24, 2022; accepted in revised form April 6, 2022.

SJIA-LD, while guiding clinical decision-making for patients with systemic JIA and its adult counterpart, adult-onset Still's disease.

Systemic JIA-associated lung disease

Following isolated case reports of pulmonary involvement in systemic JIA in the pre-biologic era (12,13), Kimura and colleagues reported in 2013 a series of 25 patients with systemic JIA and lung disease, including pulmonary arterial hypertension, interstitial lung disease, and alveolar proteinosis. Mortality was high (68%). Most patients had been treated with IL-1 and/or IL-6 antagonists, raising the concern that these agents might have contributed to lung complications (1). In 2019, two groups reported an additional 70 patients with SJIA-LD (2,3). Where lung histology was available, in many cases it resembled pulmonary alveolar proteinosis (PAP), a condition in which alveolar macrophages fail to clear surfactant and other material from the air-space. Risk factors for SJIA-LD included onset of systemic JIA before age 2 years, a history of macrophage activation syndrome (MAS), trisomy 21, and use of IL-1 and/or IL-6 blockers. Intriguingly, almost 40% of children had experienced anaphylactic reactions to tocilizumab, which is very unusual in other contexts. These studies noted increasing incidence of SJIA-LD over the past two decades, roughly paralleling the increased use of IL-1 and IL-6 blockers (2,3). In one center in the US, SJIA-LD affected 5 of 74 new patients with systemic JIA (7%), though the European Pharmachild Registry of 306 systemic JIA patients treated with anakinra identified only one with SJIA-LD (0.3%) (3,14).

These reports raised several questions: Does exposure to IL-1 or IL-6 blockade cause SJIA-LD? What underlies the apparent geographic variability in SJIA-LD incidence? Might IL-1 or IL-6 blockade permit an as-yet undefined pathogen to drive SJIA-LD? Could there be confounding by indication—in other words, if IL-1 and IL-6 blockade are used preferentially in the patients who are also the most likely to develop SJIA-LD, could the association be true but not causal? Could reduced reliance on corticosteroids, methotrexate, and other agents play a role? One of us entertained these possibilities two years ago (4). Do we have better insight now?

Importantly, one of the 18 patients (6%) with SJIA-LD reported by Schulert and colleagues had not received IL-1 or IL-6 antagonists (3). Among the 61 patients reported by Saper and colleagues, 15 (25%) had no exposure before disease onset (2), a result echoed in a European cohort in which 7 of 26 subjects with SJIA-LD (27%) had never received IL-1 or IL-6 blockade (ref. 15 and Bracaglia C: personal communication).

What do we know about the pathogenesis of SJIA-LD? In all series, patients with a history of MAS are at greater risk for SJIA-LD (1–3). Schulert and colleagues reported that patients with SJIA-LD exhibit higher levels of serum IL-18; increased levels of interferon- γ (IFN γ), IL-18, CXCL9, and CXCL10 in bronchoalveolar lavage fluid; and lung transcriptional profiles demonstrating

up-regulation of IFN γ and T cell activation networks, features that echo aspects of the pathogenesis of MAS (3). Using a mouse model of MAS induced by repeated administration of the Toll-like receptor 9 agonist CpG, Schulert's group identified CD4+ T cell-predominant IFN γ -dependent pulmonary inflammation, although not PAP (16). By contrast, T cell overexpression of T-bet, the Th1 master transcription factor, impairs macrophage development and results in PAP-like lung disease in mice (17). Clinical experience indicating that SJIA-LD and MAS may respond favorably to blocking IFN γ with emapalumab supports the notion of a pathogenic role of Th1-type inflammation in both conditions (18,19).

Chen and colleagues recently reported the results of serum proteomic analysis of patients with SJIA-LD and related conditions, identifying 20 proteins with elevated levels and 6 with decreased levels in SJIA-LD independent of MAS (20). Unexpectedly, up-regulated proteins included chemokines associated with Th2 responses: CCL11/eotaxin 1 and CCL17/thymus activation-related chemokine, the latter sometimes elevated in DRESS (21–25). Also up-regulated were the lung adhesion molecule intercellular adhesion molecule 5 (ICAM-5) and the ICAM-5–cleaving matrix metalloproteinase 7. ICAM-5 was elevated in other forms of interstitial lung disease, but since it is not otherwise increased in systemic JIA the authors propose ICAM-5 as a valuable biomarker of SJIA-LD. Intriguingly, in some subjects the SJIA-LD proteome profile occurred in the absence of high MAS activity, suggesting the possibility of an “independent origin” of MAS and SJIA-LD, meaning that MAS and SJIA-LD are driven by distinct pathogenic mechanisms, rather than a “sequential” model in which MAS directly predisposes to SJIA-LD (20).

DRB1*15:XX and DIHS/DRESS-like reactions

A recent report by Saper and colleagues sought to better understand adverse outcomes in children receiving IL-1/IL-6 antagonists by comparing 66 subjects with systemic JIA and apparent drug reactions to 65 “drug-tolerant” systemic JIA controls (5). Features of DRESS among the first group included eosinophilia, elevation of hepatic transaminases, and non-evanescent rash, including facial edema characteristic of DRESS but unusual in systemic JIA. Critically, DRB1*15 was vastly overrepresented among patients with systemic JIA and DIHS-like reactions (75–93%) compared to drug-tolerant patients, of whom 0% carried DRB1*15:01 and 18% carried any allele of DRB1*15. (DRB1*15:01 predominates in White subjects whereas 15:03 and 15:06 are more common in non-White subjects [26]; we follow the convention of Saper and colleagues and use the term DRB1*15:XX to encompass all of these [5].) The fact that none of the 65 “drug-tolerant” patients carried DRB1*15:01, an allele carried by 6–28% of individuals in the US (26), suggests that the large majority of systemic JIA patients with this risk allele react adversely to the introduction of drug. Among patients with

DIHS-like reactions, 82% with SJIA-LD and 72% without SJIA-LD expressed DRB1*15:XX; this allele is therefore a risk factor for DIHS-like reactions, not for SJIA-LD independent of such reactions. However, because SJIA-LD occurred predominantly among patients with DIHS-like reactions, these phenotypes are closely linked. MAS was also far more common in patients with DIHS-like reactions (64% versus 3% in drug-tolerant controls), prompting the authors to speculate that DRESS might directly provoke MAS, although potential mechanisms were not explored (5). Echoing these findings, in the recent study by Chen and colleagues, DRB1*15:XX was present in 87% of the subjects with SJIA-LD in whom HLA typing was available, and all had prior exposure to IL-1 or IL-6 blockade (20).

To classify patients as having DRESS, Saper and colleagues (5) used the well-accepted Registry of severe cutaneous adverse reactions (RegiSCAR) criteria incorporating 8 clinical features: fever, lymphadenopathy, eosinophilia, atypical lymphocytosis, rash, skin histology, organ involvement (including hepatic transaminase elevation), and persistence of symptoms for 15 days or more after drug withdrawal (27,28). Since many of these features overlap with those of active systemic JIA, a typical systemic JIA patient could score in the range of “possible/probable” DRESS, potentially complicating the use of the RegiSCAR criteria in this context. The authors were careful to point out, however, that most patients met RegiSCAR criteria floridly and many exhibited facial edema and eosinophilia not typical of systemic JIA (29). Saper et al (5) observed that patients who discontinued biologics did better than those in whom treatment continued or was reintroduced, although many SJIA-LD patients remain stable or even improve despite ongoing exposure to IL-1/IL-6 blockade (ref. 3 and personal experience of the authors), unusual for DRESS, which typically progresses until the offending agent is discontinued. How can we understand what is going on in these patients, using the critical insight provided by the newly-recognized DRB1*15:XX association as the stepping-off point?

HLA class II and CD4+ T cells in systemic JIA

DRB1*15:XX is part of the class II major histocompatibility complex (MHC) system. MHC II presents peptide antigens to CD4+ T cells, allowing them to recognize antigen, become activated, and undergo clonal expansion. As they do so, they differentiate from naïve (Th0) cells into more specialized cell subsets, including Th1 (making cytokines such as IFN γ), Th2 (making cytokines such as IL-4), Th17 (making cytokines such as IL-17), and Treg cells, depending on the milieu in which the T cell develops.

DRB1*15:XX is not the first MHC II allele linked to systemic JIA or its complications. In 2015, Ombrello and colleagues observed that DRB1*11 and its associated haplotype (DRB1*11; DQA1*05-DQB1*03) predisposes to development of systemic JIA, drawing renewed attention to the potential involvement of CD4+ T cells in this disorder, despite its autoinflammatory-like

phenotype (30,31). However, DRB1*11 was not associated with development of DIHS-like responses, and its odds ratio for incident systemic JIA (~2.3) was much lower than that of DRB1*15:XX with apparent DIHS (~40.8) (5,30). Thus, these two MHC II alleles play very different roles: DRB1*11 predisposes to systemic JIA but not otherwise to SJA-LD, whereas DRB1*15:XX predisposes for DIHS-type responses in patients who already have systemic JIA.

A key concept in T cell biology is phenotypic plasticity (for review, see refs. 32–36). CD4+ T cells exposed to cytokines and other cues can convert from Treg cells to Th17 cells and vice versa (37–39), from Th17 cells to Th1 cells (40–42), and from Th1 and Th17 cells to Th2 cells (43,44). This propensity grounds the so-called “biphasic hypothesis” of systemic JIA, which proposes that the IL-1/IL-6-rich environment of early systemic JIA skews T cells away from beneficial Treg cells and toward pathogenic Th17 cells, thereby mediating chronic arthritis (31,45). While the biphasic hypothesis remains unconfirmed, some supportive evidence has emerged. Omoyinmi and colleagues observed enrichment of circulating Th1 and Th17 cells in patients with systemic JIA (46). Henderson and colleagues found a Th17 gene expression signature among T cells in systemic JIA synovial fluid and blood, predominantly among unusual IL-17–producing Treg cells in acute disease and among effector Th17 cells in chronic disease, although the latter expressed little IL-17 protein (47). These findings plausibly reflect the known role of IL-1 and IL-6 in Th17 polarization and maintenance, since early IL-1 blockade largely abrogated Treg cell IL-17 expression (38,47–49). In chronic systemic JIA, effector Th cells also up-regulated TNF, IFN α , and IFN γ pathways, underscoring the complexity of the adaptive immune response (47). Not explored in that study was whether IL-1 blockade led to an alternative cytokine polarization pattern, in either the Treg or Th cells, except that the Treg cells appeared not to express IFN γ protein. Analogously, Kessel and colleagues found IL-17–expressing $\gamma\delta$ T cells in systemic JIA, potentially reflecting cytokine-driven lymphocyte polarization beyond conventional CD4+ T cells (50). To date, no study has provided comparable analysis of T cell cytokine/gene expression in systemic JIA with DIHS-like features.

The DRESS hypothesis revisited

With this background, we can better consider how DRB1*15:01 might lead to DIHS-like reactions to IL-1 and IL-6 blockers. Saper and colleagues propose that anakinra, canakinumab, and tocilizumab, or their excipients (the vehicle and its associated components) drive pathogenic T cell responses as antigens or by otherwise changing antigen presentation (5). Strengths of this hypothesis are the DRESS-like phenotype of many drug-exposed patients with systemic JIA; the improvement reported in some patients after drug discontinuation; the clinical deterioration observed in some patients who continue to receive

the drug; and the extremely striking MHC II association, strongly implicating an antigen-directed response.

The DRESS hypothesis also faces some conceptual hurdles. Anakinra (IL-1 receptor antagonist [IL-1Ra]) shares no antigen-length peptides with canakinumab or tocilizumab. Indeed, aside from an N-terminal methionine, anakinra is identical to endogenous IL-1Ra and should therefore have limited antigenic potential. The only excipient shared by these agents is polysorbate-80, an emulsifier that prevents protein aggregation. Polysorbate-80 is found in most monoclonal antibodies and in many vaccines. Since polysorbate-80 is a heterogeneous chemical product, it is conceivable that something might be different about the preparation employed in IL-1/IL-6 antagonists; however, its ubiquity renders this excipient a poor candidate trigger for DRESS.

Importantly, drugs can cause DRESS even if they are not themselves the antigen (51). First, they can bind covalently to endogenous proteins; these haptenated antigens are then recognized by T cells as foreign. Second, drugs can bind non-covalently to the MHC and/or the T cell receptor (TCR) outside of the antigen binding pocket, leading to T cell activation in a manner reminiscent of bacterial superantigens, agents that can even display HLA class II allele specificity (52). Third, drugs can bind within or otherwise modify the MHC groove, altering peptide specificity such that certain self-peptides now appear foreign. IL-1 and IL-6 blockers could each be capable of one of these interactions with DRB1*15:XX, despite their structural differences, or they could induce DIHS via a new type of interaction yet to be described. The possibility that any—actually, all—of these drugs interact with DRB1*15:XX to stimulate CD4+ T cells can (and should!) be tested directly in vitro, for example by using activation-induced marker or similar sensitive assays to identify antigen-specific CD4+ T cells in patients (53).

Anakinra, canakinumab, and tocilizumab are used in diseases other than systemic JIA, such as rheumatoid arthritis, polyarticular JIA, giant cell arteritis, and autoinflammatory diseases. In the Canakinumab Antiinflammatory Thrombosis Outcome Study (CANTOS) trial, almost 7,000 individuals with atherosclerotic cardiovascular disease and persistent C-reactive protein elevation were treated with canakinumab for 48 months (54). Given a carrier frequency of DRB1*15:XX of 15–29% in the US (26), one might have predicted DIHS/DRESS to develop regularly in these patient groups—something that simply hasn't happened, apart from isolated case reports cited by Saper and colleagues (5). They did observe 4 patients with Kawasaki disease (KD) with suspected anakinra reactions (defined as an increase in eosinophil count of >50% compared to baseline), of whom 3 of 4 carried DRB1*15:XX, in contrast to 2 of 15 “drug-tolerant” patients with KD (5). This small series is intriguing but might well reflect something shared in the hyperinflammatory milieu of systemic JIA and KD—that is, a “drug–disease” interaction. We present below one proposal for such an interaction.

An additional concern is that most HLA associations with DIHS/DRESS are with MHC class I alleles, although well-described exceptions exist, including the association of DRB1*15:01 with Stevens-Johnson syndrome/toxic epidermal necrolysis in Han Chinese subjects (55,56). Why MHC I predominates over MHC II is not entirely clear but may have to do with another interesting observation: DRESS is often accompanied by reactivation of human herpesvirus 6 (HHV-6) and other herpesviruses such as Epstein-Barr virus (EBV). One theory is that the expanded MHC I-restricted CD8+ T cell clones that recognize reactivating herpesviruses coincidentally cross-recognize drug, inducing DRESS via molecular mimicry (57). Whether reactivation or de novo infection with HHV-6, EBV, or other herpesviruses occurs in patients with systemic JIA and DIHS needs to be explored, particularly since CD8+ T cell responses could underlie the increase in IFN γ production and T cell activation profile observed in SJIA-LD (3). It is worth noting that the DRESS hypothesis requires that 3 structurally distinct biologics each represent an outlier among known drug–MHC–DRESS associations, and then each (coincidentally) with the same MHC II allele.

A final issue, noted above, is that ~25% of patients with SJIA-LD have never been exposed to IL-1 or IL-6 blockers, seemingly excluding any pathogenic role for biologic therapy in this subset of patients. It will be interesting to investigate whether eosinophilia or other DRESS-like manifestations occur in patients with systemic JIA not exposed to biologics, and if so whether such patients express DRB1*15:XX. Such patients would not have been detected by the recent study by Saper et al (5) since its case–control design required all patients to be drug-exposed.

The cytokine plasticity hypothesis

Boiled down, the key feature of the DRESS hypothesis is that IL-1 and IL-6 blockers drive DIHS via *antigen presentation*—either as the source of peptide or by altering the peptide–MHC II–TCR complex. We propose instead an alternative we term the cytokine plasticity hypothesis, that it is the *biologic activity* of IL-1 and IL-6 blockers that sets the stage for DIHS-like reactions and even SJIA-LD in predisposed patients.

The association of DRB1*15:XX implies a pathogenic role for CD4+ T cells. The antigens recognized by these T cells could originate from self-proteins, commensal organisms, pathogens, or other exposures. For the sake of the cytokine plasticity hypothesis, the identity of the antigen is not crucial. Rather, as with the biphasic hypothesis, the key is the inherent susceptibility of CD4+ T cells to change phenotype in response to environmental cues.

Prior to treatment, patients with systemic JIA will have a diverse population of CD4+ T cells, potentially including expanded Th and Treg cell clones. Through genetic, environmental, age-dependent, and stochastic factors, patients will differ from one another in the balance of Th effector profiles among

these clones. Some clones exhibit Th17 features, as identified by Henderson and colleagues (47), whereas others exhibit Th1 or Th2 differentiation. The cytokine plasticity hypothesis proposes that biologics shift the balance of some of these T cells away from the IL-1/IL-6-driven Th17 phenotype. In patients predisposed to develop SJIA-LD, we speculate that the phenotypic switch is predominantly from Th17 to Th1, with associated production of IFN γ . Such a Th switch could be facilitated by other risk factors epidemiologically associated with SJIA-LD, including (again speculatively) young age, high levels of circulating IL-18 and other mediators (58–60), and trisomy 21. For example, trisomy 21 is associated with up-regulation of IFN γ and its receptor (61), expansion of Th1 and Th1/Th17 T cells (62), and higher levels of other proinflammatory cytokines including TNF and IL-6 (63). By contrast, for clones exhibiting a Th2 bias, blocking IL-1 or IL-6 might promote Th17-to-Th2 conversion leading to a DIHS-type response. Under the right conditions, such clonal skew could happen even in the absence of exogenous manipulation, enabling the cytokine plasticity hypothesis to account for patients who develop SJIA-LD *without* exposure to IL-1 or IL-6 antagonists.

How might DRB1*15:XX predispose to DIHS/DRESS-like reactions and/or SJIA-LD under the cytokine plasticity hypothesis? One pathway is suggested by the association of HLA–DRB1*15:01 with allergic bronchopulmonary aspergillosis (ABPA) (64,65). Experimental data show that this risk allele skews T cells to differentiate toward Th2 rather than Th1 cells when encountering *Aspergillus fumigatus*, resulting in allergy-like hypersensitivity instead of pathogen clearance (66). In patients with systemic JIA carrying DRB1*15:XX, IL-1 or IL-6 blockade might favor expansion of related Th2 clones in response to *Aspergillus*, leading to a DIHS-type response. Importantly, this possibility generates testable predictions: these systemic JIA patients might have elevated *Aspergillus*-specific IgE titers, CD4+ T cells activatable *in vitro* in response to *Aspergillus*-derived peptides, or tetramer-binding

CD4+ T cells specific for *Aspergillus*-derived peptides presented by DRB1*15:XX. Of course, the universe of allergens/antigens is vast. Cross-reactivity to foreign antigens has been proposed to drive the risk of multiple sclerosis associated with DRB1*15:XX, implicating peptides from EBV and from the abundant gut gram negative anaerobe *Akkermansia muciniphila*, including some peptides that (as with ABPA) favor Th2-predominant responses, although the mechanisms underlying this MHC class II-influenced Th2 skewing remain unknown (66,67). Endogenous antigens, potentially modulated with the inflammatory milieu of systemic JIA, might also be presented. The central point is that a wide range of DRB1*15:XX-presented antigens are plausible drivers of SJIA-LD under the cytokine plasticity hypothesis.

Like the DRESS hypothesis, the cytokine plasticity hypothesis confronts certain challenges. The clonal shifts proposed remain to be confirmed experimentally. Acute anaphylactic reactions to tocilizumab are difficult to explain under the cytokine plasticity hypothesis, although IgE-mediated reactions are also uncharacteristic of DRESS (68). Why are patients with systemic JIA (and possibly KD) susceptible to this complication while those with other inflammatory diseases remain protected? How does the Th1 and/or Th2 shift cause alveolar macrophage dysfunction manifesting as PAP—also an unusual pulmonary manifestation of DRESS (69)? Most of these mechanistic unknowns are shared with the DRESS hypothesis.

The cytokine plasticity hypothesis also has strengths (Table 1). Most importantly, it explains how biologic-naïve patients might develop the same phenotype as biologic-exposed children. By invoking non-drug antigens as the disease trigger, it explains how reactions to 3 structurally unrelated biologics could share the same HLA association, and potentially why the incidence of DRESS-like reactions and of SJIA-LD varies across regions of the world, with age, and with duration from first exposure to drug

Table 1. Comparison of two hypotheses to explain how IL-1 or IL-6 blocking agents might contribute to systemic JIA-associated DIHS and/or systemic JIA-associated lung disease*

	Explained by DRESS hypothesis	Explained by cytokine plasticity hypothesis
Eosinophilia	Yes	Yes
Rash	Yes	Yes
HLA class II association	Usually class I	Yes
Drug exposure in many	Yes	Yes
No drug exposure in some	No	Yes
Structurally unrelated but biologically similar drugs	No	Yes
Low frequency of DIHS in other diseases treated with these drugs	No	Yes
Anakinra is a self protein	No	Yes
Many patients can continue drug	No	Yes
Possibility of foreign antigen	No	Yes
Pulmonary alveolar proteinosis	Unclear	Unclear

* IL-1 = interleukin-1; JIA = juvenile idiopathic arthritis; DIHS = drug-induced hypersensitivity syndrome; DRESS = drug reaction with eosinophilia and systemic symptoms.

(7,14,70,71). To the extent that corticosteroids and other nonbiologic immunomodulators keep pathogenic T cells in check, the cytokine plasticity hypothesis offers a plausible mechanism by which reduced reliance on these agents might contribute to the increasing incidence of SJIA-LD. Finally, whereas DRESS progresses with continued drug exposure, the cytokine plasticity hypothesis implies that some patients could remain stable or even improve despite ongoing IL-1/IL-6 blockade if the pathogenic cytokine/cellular milieu is otherwise remediated—a difference of major clinical importance.

Two hypotheses and next steps

We present two hypotheses to explain the association of adverse reactions to IL-1 or IL-6 blockade with DRB1*15:XX (Figure 1). Other hypotheses could also be entertained. For example, the HLA association might reflect not DRB1*15 itself but instead another linked gene (*C2*, *C4*, *HSP*, and *TNF* are encoded nearby). SJIA-LD might arise through an

infection yet to be identified, potentially one to which systemic JIA patients with particular HLA alleles and receiving cytokine antagonists are especially susceptible. Even if not exhaustive of all possible explanations, the contrast between the DRESS hypothesis and the cytokine plasticity hypothesis provides a useful foundation to develop a scientific agenda for future research (Table 2).

The main differences between these ideas are the roles of the IL-1 and IL-6 blocking drugs and the identities of the DRB1*15:XX-presented antigens. Under the first hypothesis, the drugs cause disease via antigen presentation. Under the second, the drugs alter the cytokine milieu in which Th and other cells develop and differentiate. A key experimental question is whether patients with systemic JIA and DIHS/DRESS-like syndromes and/or SJIA-LD have T cells that react to these drugs, or not. If the second hypothesis is correct, defining the critical antigens could begin with investigation of DRB1*15-presented pathogens, including *Aspergillus*, EBV, and *Akkermansia muciniphila*, and by testing whether onset of DIHS-like responses and/or SJIA-LD coincides

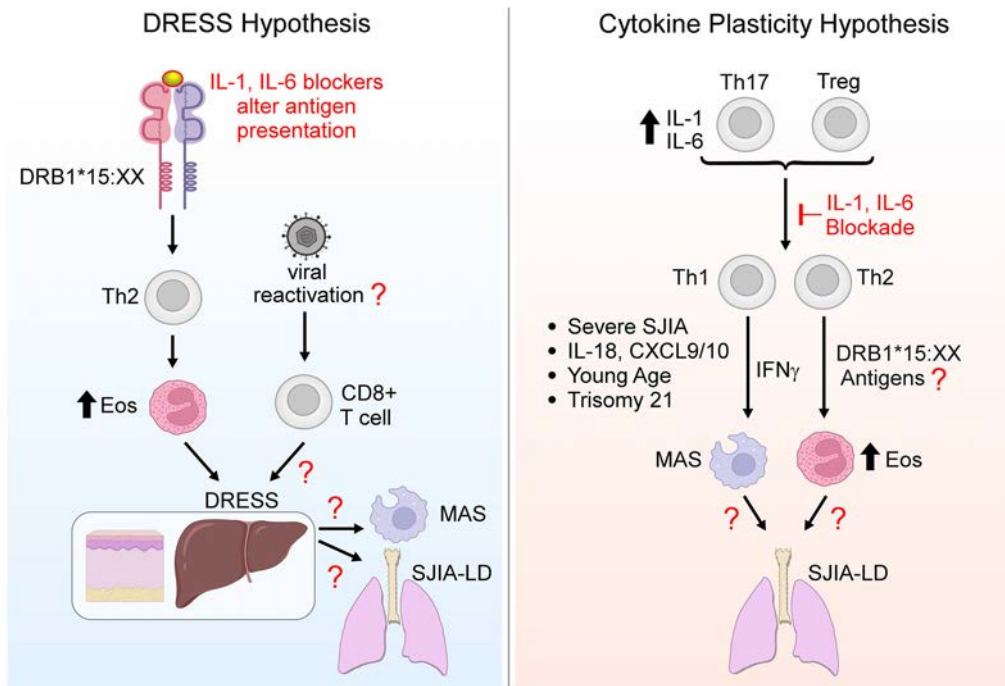


Figure 1. Two hypotheses regarding the relationship between systemic juvenile idiopathic arthritis (SJIA), major histocompatibility complex (MHC) class II, and adverse outcomes after interleukin-1 (IL-1) and IL-6 blockade. In the drug reaction with eosinophilia and systemic symptoms (DRESS) hypothesis, IL-1 and IL-6 antagonists alter antigen presentation by MHC class II to CD4+ T cells, leading to Th2-dominated DRESS. Many DRESS reactions involve herpesvirus reactivation and thus CD8+ T cell activation, factors yet to be studied in systemic JIA. DRESS may then predispose to macrophage activation syndrome (MAS) and/or systemic JIA-associated lung disease (SJIA-LD) through pathways still to be defined. Under the cytokine plasticity hypothesis, elevated IL-1 and IL-6 levels in systemic JIA lead to Th17 skewing in CD4+ Th and Treg cells. Blocking IL-1 or IL-6 converts these cells to interferon- γ (IFN γ)-producing Th1 cells and/or IL-4-producing Th2 cells, in particular CD4+ T cells recognizing HLA-DRB1*15:XX-presented antigens (exogenous or endogenous). Some patients may undergo analogous transitions without exposure to therapeutics. The resulting clones lead to DRESS-like reactions and/or SJIA-LD through pathways still to be defined. Risk factors include severe systemic JIA; increased levels of IL-18, CXCL9, and CXCL10; young age; and trisomy 21. The critical difference between these hypotheses is the contribution of the IL-1 and IL-6 blocking agents. Eos = eosinophils. Created in part using BioRender.

Table 2. Key research foci and questions for systemic JIA investigators*

Clinical research
Develop classification criteria for DIHS/DRESS-like reactions in systemic JIA and for SJIA-LD
Collect HLA class II typing on large, diverse, well-characterized populations of systemic JIA patients
Translational research
Determine if HHV-6 (or other viral reactivation) occurs in DIHS/DRESS-like reactions in systemic JIA
Determine if DIHS/DRESS-like reactions or SJIA-LD are associated with prior <i>Aspergillus</i> or EBV exposure or the presence of <i>Akkermansia muciniphila</i> in gut microbiome
Basic research
Determine if IL-1/IL-6 blockers activate CD4 T cells in a DRB1*15:XX-dependent manner
Characterize the Th cell gene/cytokine expression profile of “high-risk” systemic JIA versus typical systemic JIA
Understand mechanisms driving pulmonary alveolar proteinosis in systemic JIA

* JIA = juvenile idiopathic arthritis; DIHS = drug-induced hypersensitivity syndrome; DRESS = drug reaction with eosinophilia and systemic symptoms; SJIA-LD = systemic JIA-associated lung disease; HHV-6 = human herpesvirus 6; EBV = Epstein-Barr virus; IL-1 = interleukin-1.

with EBV seroconversion, as observed recently for multiple sclerosis (72).

Notably, the cytokine and chemokine milieu of systemic JIA, MAS, DIHS/DRESS-like syndromes, and SJIA-LD may not differentiate the two hypotheses. Under either, patients with DIHS-like reactions will likely exhibit a Th2 profile, patients with MAS/SJIA-LD will exhibit a Th1 profile, and some patients may have both. It will be essential to evaluate patients who have not been previously exposed to IL-1 or IL-6 blockers and yet go on to develop DIHS-like reactions and/or SJIA-LD, as well as to study patients with SJIA-LD risk factors, such as young age, a history of MAS, and trisomy 21. Such patients might for example exhibit a Th1-predominant profile even before development of SJIA-LD, in contrast to the Th17 profile described in other patients with systemic JIA (46,47). Importantly, basic investigations of the mechanisms of PAP in systemic JIA are needed, as neither hypothesis clearly delineates how this pathology arises, although the observation that PAP arises in mice whose T cells overexpress the Th1 transcription factor T-bet represents an enticing clue (17).

Fundamentally, what the field needs most is detailed information about more patients. This will require coordinated efforts of clinicians and basic and translational investigators. Thankfully, the Childhood Arthritis and Rheumatology Research Alliance, the Paediatric Rheumatology International Trials Organisation, the Paediatric Rheumatology European Society, and other collaborative networks are well-positioned to collect clinical data on a broad range of patients with systemic JIA. For investigative discovery, it will be informative to collect HLA typing on all subjects with systemic JIA. Organized efforts to harvest T cells from both DRB1*15:XX-positive and -negative subjects will be critical to determine if subjects with DIHS-like reactions have drug-reactive

T cells and to explore other candidate antigens. Analyzing the apparently rare patients with systemic JIA who express DRB1*15:XX but do *not* develop DIHS-like reactions in response to IL-1 or IL-6 blockade could reveal protective factors, for instance more liberal use of corticosteroids and other immunomodulators. Basic investigations in DRB1*15:01 (DR2)-transgenic mice in conjunction with existing models of systemic JIA might also be informative, as it has been in ABPA (66).

While the field works to understand disease pathogenesis in greater depth, the immediate challenge is how to care for our patients. Should clinical HLA typing be performed on all patients with systemic JIA, and should detection of DRB1*15:XX be considered a contraindication to IL-1 and IL-6 blockade? Should patients who develop eosinophilia, transaminase elevation, or rash while receiving IL-1 or IL-6 blockade stop the drug immediately and thereafter avoid these biologics altogether? If so, what other therapies could be substituted? Avoiding the offending agents makes sense under the DRESS hypothesis, based on the observation from Saper and colleagues that the 26% of their patients with DRESS-like reactions who stopped IL-1 or IL-6 blockade demonstrated resolution of eosinophilia, rash, and transaminase elevation, whereas some of those who continued treatment had worse outcomes, including death (5). The difficulty is that IL-1 and IL-6 blocking agents are exquisitely effective for systemic JIA, with few available alternatives. Many rheumatologists (and families) are therefore understandably hesitant to discontinue them, particularly in the sickest children—a key confounder in the comparison between patients who tolerated stopping biologics and patients who had to continue or even restart these agents. Saper and colleagues reported resolution of SJIA-LD in 3 patients in whom IL-1 or IL-6 blockade was stopped within 6 weeks of detection of SJIA-LD; they further suggested that longer duration of biologic exposure might increase the risk of SJIA-LD, although this is again confounded by indication, as patients with more severe systemic JIA are more likely to be receiving biologics longer (73). In contrast, Schulert et al elected to maintain IL-1 or IL-6 blockade in all 18 patients in their SJIA-LD series, with clinical stability in 14 patients and even improved lung disease in 3 (3). The cytokine plasticity hypothesis suggests that it is premature to assume that drug discontinuation is the only correct answer to DIHS-like reactions and/or SJIA-LD, although in some patients it may be useful to interrupt therapy.

The framework of the cytokine plasticity hypothesis provides a new way to approach clinical questions. Highly targeted biologics could be *too* specific for some patients with systemic JIA, shifting the cytokine milieu without providing sufficient global immune suppression. Perhaps patients at particular risk of DIHS-like reactions and SJIA-LD (those with DRB1*15:XX, young age, severe disease with MAS, or trisomy 21) are not good candidates for monotherapy with IL-1 or IL-6 antagonists. Instead, these patients might benefit from therapeutic strategies that combine these biologics with corticosteroids and/or agents that target T

cells (e.g., methotrexate, mycophenolate mofetil, tacrolimus, abatacept) to address both innate and adaptive immune contributors. Where possible, we think it is reasonable to perform HLA typing on all patients with systemic JIA at disease onset and to monitor all patients with care when using IL-1 or IL-6 blockers since adverse reactions can occur even in patients lacking the risk alleles. However, we would not avoid starting IL-1 and IL-6 antagonists while awaiting these results and believe that IL-1 or IL-6 blockade should remain an important component of initial therapy for most patients with new-onset systemic JIA, even if risk alleles are present.

How best to treat patients who do progress to SJIA-LD remains an enormous and important challenge for the field. In addition to the T cell targeting agents mentioned above, clinicians are currently using JAK inhibitors, the anti-IFN γ monoclonal antibody emapalumab, and other approaches. Prospective studies to evaluate these therapeutic approaches are necessary and should be supported by our field's collaborative research groups. Most importantly, patients and families need reassurance that their care team is fully informed about these emerging concerns, paying close attention to the known risk factors, and working alongside them to develop thoughtful, tailored treatment plans.

Conclusions

Pediatric rheumatology faces a conundrum posed by the twin complications of DIHS-like reactions and SJIA-LD. We present two reasonable explanations for these phenomena—the DRESS hypothesis and the cytokine plasticity hypothesis. Our hope is that consideration of these alternatives, potentially together with others, will stimulate targeted studies across clinical, translational, and basic domains. Our patients are counting on us.

ACKNOWLEDGMENTS

The authors thank Lauren Henderson, David Hoytema van Konijnenburg, Marc Jenkins, Ronald Laxer, Pui Lee, Shawn Mahmud, Elizabeth Mellins, Michael Ombrello, Elizabeth Phillips, Vivian Saper, and the reviewers for their insightful ideas and constructive comments.

AUTHOR CONTRIBUTIONS

Drs. Binstadt and Nigrovic drafted the article, revised it critically for important intellectual content, and approved the final version to be published.

REFERENCES


- Kimura Y, Weiss JE, Haroldson KL, Lee T, Punaro M, Oliveira S, et al. Pulmonary hypertension and other potentially fatal pulmonary complications in systemic juvenile idiopathic arthritis. *Arthritis Care Res (Hoboken)* 2013;65:745–52.
- Saper VE, Chen G, Deutsch GH, Guillerman RP, Birgmeier J, Jagadeesh K, et al. Emergent high fatality lung disease in systemic juvenile arthritis. *Ann Rheum Dis* 2019;78:1722–31.
- Schulert GS, Yasin S, Carey B, Chalk C, Do T, Schapiro AH, et al. Systemic juvenile idiopathic arthritis-associated lung disease: characterization and risk factors. *Arthritis Rheumatol* 2019;71:1943–54.
- Nigrovic PA. Storm warning: lung disease in systemic juvenile idiopathic arthritis [editorial]. *Arthritis Rheumatol* 2019;71:1773–75.
- Saper VE, Ombrello MJ, Tremoulet AH, Montero-Martin G, Prahalad S, Canna S, et al. Severe delayed hypersensitivity reactions to IL-1 and IL-6 inhibitors link to common HLA-DRB1*15 alleles. *Ann Rheum Dis* 2022;81:406–15.
- Nigrovic PA, Mannion M, Prince FH, Zeff A, Rabinovich CE, van Rossum MA, et al. Anakinra as first-line disease-modifying therapy in systemic juvenile idiopathic arthritis: report of forty-six patients from an international multicenter series. *Arthritis Rheum* 2011;63:545–55.
- Ter Haar NM, van Dijkhuizen EH, Swart JF, van Royen-Kerkhof A, El Idriiss A, Leek AP, et al. Treatment to target using recombinant interleukin-1 receptor antagonist as first-line monotherapy in new-onset systemic juvenile idiopathic arthritis: results from a five-year follow-up study. *Arthritis Rheumatol* 2019;71:1163–73.
- Quartier P, Allantaz F, Cimaz R, Pillet P, Messiaen C, Bardin C, et al. A multicentre, randomised, double-blind, placebo-controlled trial with the interleukin-1 receptor antagonist anakinra in patients with systemic-onset juvenile idiopathic arthritis (ANAJIS trial). *Ann Rheum Dis* 2011;70:747–54.
- De Benedetti F, Brunner HI, Ruperto N, Kenwright A, Wright S, Calvo I, et al. Randomized trial of tocilizumab in systemic juvenile idiopathic arthritis. *N Engl J Med* 2012;367:2385–95.
- Yokota S, Imagawa T, Mori M, Miyamae T, Aihara Y, Takei S, et al. Efficacy and safety of tocilizumab in patients with systemic-onset juvenile idiopathic arthritis: a randomised, double-blind, placebo-controlled, withdrawal phase III trial. *Lancet* 2008;371:998–1006.
- Ruperto N, Brunner HI, Quartier P, Constantin T, Wulffraat N, Horneff G, et al. Two randomized trials of canakinumab in systemic juvenile idiopathic arthritis. *N Engl J Med* 2012;367:2396–406.
- Padeh S, Laxer RM, Silver MM, Silverman ED. Primary pulmonary hypertension in a patient with systemic-onset juvenile arthritis. *Arthritis Rheum* 1991;34:1575–9.
- Schultz R, Mattila J, Gappa M, Verronen P. Development of progressive pulmonary interstitial and intra-alveolar cholesterol granulomas (PICG) associated with therapy-resistant chronic systemic juvenile arthritis (CJA). *Pediatr Pulmonol* 2001;32:397–402.
- Giancane G, Papa R, Vastert S, Bagnasco F, Swart JF, Quartier P, et al. Anakinra in patients with systemic juvenile idiopathic arthritis: long-term safety from the Pharmachild registry. *J Rheumatol* 2022; 49:398–407.
- Bracaglia C, Minoia F, Kessel C, Vastert S, Pardeo M, Arduini A, et al. Systemic juvenile idiopathic arthritis associated lung disease in Europe [abstract]. *Pediatr Rheumatol Online J* 2021;19 Suppl:P53.
- Gao DK, Salomonis N, Henderlight M, Woods C, Thakkar K, Grom AA, et al. IFN- γ is essential for alveolar macrophage-driven pulmonary inflammation in macrophage activation syndrome. *JCI Insight* 2021;6.
- Iriguchi S, Kikuchi N, Kaneko S, Noguchi E, Morishima Y, Matsuyama M, et al. T-cell-restricted T-bet overexpression induces aberrant hematopoiesis of myeloid cells and impairs function of macrophages in the lung. *Blood* 2015;125:370–82.
- De Benedetti F, Brogan P, Bracaglia C, Pardeo M, Marucci G, Sacco E, et al. Emapalumab (anti-interferon- γ monoclonal antibody) in patients with macrophage activation syndrome (MAS) complicating systemic juvenile idiopathic arthritis (sJIA) [abstract]. *Arthritis Rheumatol* 2020;72 Suppl 4. URL: <https://acrabstracts.org/abstract/emapalumab-anti-interferon-gamma-monoclonal-antibody-in-patients-with-macrophage-activation-syndrome-mas-complicating-systemic-jvenile-idiopathic-arthritis-sjia/>.

19. Arduini A, Pardeo M, De Matteis A, Marucci G, Caiello I, Prencipe G, et al. Efficacy of emapalumab in chronic/relapsing macrophage activation syndrome in systemic juvenile idiopathic arthritis with lung and liver involvement [abstract]. *Pediatr Rheumatol Online J* 2021;19 Suppl:P146.
20. Chen G, Deutsch GH, Schulert G, Zheng H, Jang S, Trapnell B, et al. Identification of distinct inflammatory programs and biomarkers in systemic juvenile idiopathic arthritis and related lung disease by serum proteome analysis. *Arthritis Rheumatol* 2022;74:1273–1285.
21. Ogawa K, Morito H, Hasegawa A, Daikoku N, Miyagawa F, Okazaki A, et al. Identification of thymus and activation-regulated chemokine (TARC/CCL17) as a potential marker for early indication of disease and prediction of disease activity in drug-induced hypersensitivity syndrome (DIHS)/drug rash with eosinophilia and systemic symptoms (DRESS). *J Dermatol Sci* 2013;69:38–43.
22. Ogawa K, Morito H, Hasegawa A, Miyagawa F, Kobayashi N, Watanabe H, et al. Elevated serum thymus and activation-regulated chemokine (TARC/CCL17) relates to reactivation of human herpesvirus 6 in drug reaction with eosinophilia and systemic symptoms (DRESS)/drug-induced hypersensitivity syndrome (DIHS). *Br J Dermatol* 2014;171:425–7.
23. Komatsu-Fujii T, Chinuki Y, Niihara H, Hayashida K, Ohta M, Okazaki R, et al. The thymus and activation-regulated chemokine (TARC) level in serum at an early stage of a drug eruption is a prognostic biomarker of severity of systemic inflammation. *Allergol Int* 2018; 67:90–95.
24. Choudhary R, Vinay K, Srivastava N, Bishnoi A, Kamat D, Parsad D, et al. Clinical, biochemical, and serologic predictors of drug reaction with eosinophilia and systemic symptoms syndrome: a prospective case-control study. *J Am Acad Dermatol* 2021;85:901–09.
25. Wang F, He D, Tang X, Zhang X. Chemokine expression in diverse nonimmediate drug hypersensitivity reactions: focus on thymus activation-regulated chemokine, cutaneous T-cell-attracting chemokine, and interleukin-10. *Ann Allergy Asthma Immunol* 2014;113: 204–8.
26. Maiers M, Gragert L, Klitz W. High-resolution HLA alleles and haplotypes in the United States population. *Hum Immunol* 2007;68: 779–88.
27. Kardaun SH, Sidoroff A, Valeyrie-Allanore L, Halevy S, Davidovici BB, Mockenhaupt M, et al. Variability in the clinical pattern of cutaneous side-effects of drugs with systemic symptoms: does a DRESS syndrome really exist? *Br J Dermatol* 2007;156:609–11.
28. Kardaun SH, Sekula P, Valeyrie-Allanore L, Liss Y, Chu CY, Creamer D, et al. Drug reaction with eosinophilia and systemic symptoms (DRESS): an original multisystem adverse drug reaction. Results from the prospective RegiSCAR study. *Br J Dermatol* 2013;169: 1071–80.
29. Musette P, Janela B. New insights into drug reaction with eosinophilia and systemic symptoms pathophysiology. *Front Med (Lausanne)* 2017;4:179.
30. Ombrello MJ, Remmers EF, Tachmazidou I, Grom A, Foell D, Haas JP, et al. HLA-DRB1*11 and variants of the MHC class II locus are strong risk factors for systemic juvenile idiopathic arthritis. *Proc Natl Acad Sci U S A* 2015;112:15970–5.
31. Nigrovic PA. Autoinflammation and autoimmunity in systemic juvenile idiopathic arthritis. *Proc Natl Acad Sci U S A* 2015;112:15785–6.
32. Stadhouders R, Lubberts E, Hendriks RW. A cellular and molecular view of T helper 17 cell plasticity in autoimmunity. *J Autoimmun* 2018;87:1–15.
33. Mazzoni A, Maggi L, Liotta F, Cosmi L, Annunziato F. Biological and clinical significance of T helper 17 cell plasticity. *Immunology* 2019; 158:287–95.
34. Bluestone JA, Mackay CR, O’Shea JJ, Stockinger B. The functional plasticity of T cell subsets. *Nat Rev Immunol* 2009;9:811–6.
35. DuPage M, Bluestone JA. Harnessing the plasticity of CD4(+) T cells to treat immune-mediated disease. *Nat Rev Immunol* 2016;16: 149–63.
36. Cerboni S, Gehrman U, Preite S, Mitra S. Cytokine-regulated Th17 plasticity in human health and diseases. *Immunology* 2021;163:3–18.
37. Koenen HJ, Smeets RL, Vink PM, van Rijssen E, Boots AM, Joosten I. Human CD25highFoxp3pos regulatory T cells differentiate into IL-17-producing cells. *Blood* 2008;112:2340–52.
38. Deknuydt F, Bioley G, Valmori D, Ayyoub M. IL-1 β and IL-2 convert human Treg into T(H)17 cells. *Clin Immunol* 2009;131:298–307.
39. Gagliani N, Vesely MC, Iseppon A, Brockmann L, Xu H, Palm NW, et al. Th17 cells transdifferentiate into regulatory T cells during resolution of inflammation. *Nature* 2015;523:221–5.
40. Hirota K, Duarte JH, Veldhoen M, Hornsby E, Li Y, Cua DJ, et al. Fate mapping of IL-17-producing T cells in inflammatory responses. *Nat Immunol* 2011;12:255–63.
41. Gaublotte JT, Yosef N, Lee Y, Gertner RS, Yang LV, Wu C, et al. Single-cell genomics unveils critical regulators of Th17 cell pathogenicity. *Cell* 2015;163:1400–12.
42. Schnell A, Huang L, Singer M, Singaraju A, Barilla RM, Regan BM, et al. Stem-like intestinal Th17 cells give rise to pathogenic effector T cells during autoimmunity. *Cell* 2021;184:6281–98.
43. Moon HG, Tae YM, Kim YS, Jeon SG, Oh SY, Gho YS, et al. Conversion of Th17-type into Th2-type inflammation by acetyl salicylic acid via the adenosine and uric acid pathway in the lung. *Allergy* 2010;65: 1093–103.
44. Panzer M, Sitte S, Wirth S, Drexler I, Sparwasser T, Voehringer D. Rapid in vivo conversion of effector T cells into Th2 cells during helminth infection. *J Immunol* 2012;188:615–23.
45. Nigrovic PA. Is there a window of opportunity for treatment of systemic juvenile idiopathic arthritis? [review]. *Arthritis Rheumatol* 2014; 66:1405–13.
46. Omoyinmi E, Hamaoui R, Pesenacker A, Nistala K, Moncrieffe H, Ursu S, et al. Th1 and Th17 cell subpopulations are enriched in the peripheral blood of patients with systemic juvenile idiopathic arthritis. *Rheumatology (Oxford)* 2012;51:1881–6.
47. Henderson LA, Hoyt KJ, Lee PY, Rao DA, Jonsson AH, Nguyen JP, et al. Th17 reprogramming of T cells in systemic juvenile idiopathic arthritis. *JCI Insight* 2020;5.
48. Zhou L, Ivanov II, Spolski R, Min R, Shenderov K, Egawa T, et al. IL-6 programs T(H)-17 cell differentiation by promoting sequential engagement of the IL-21 and IL-23 pathways. *Nat Immunol* 2007;8:967–74.
49. Harbour SN, DiToro DF, Witte SJ, Zindl CL, Gao M, Schoeb TR, et al. TH17 cells require ongoing classic IL-6 receptor signaling to retain transcriptional and functional identity. *Sci Immunol* 2020;5.
50. Kessel C, Lippitz K, Weinhage T, Hinze C, Wittkowski H, Holzinger D, et al. Proinflammatory cytokine environments can drive interleukin-17 overexpression by $\gamma\delta$ T cells in systemic juvenile idiopathic arthritis. *Arthritis Rheumatol* 2017;69:1480–94.
51. White KD, Chung WH, Hung SI, Mallal S, Phillips EJ. Evolving models of the immunopathogenesis of T cell-mediated drug allergy: the role of host, pathogens, and drug response. *J Allergy Clin Immunol* 2015; 136:219–34.
52. Scholl PR, Diez A, Karr R, Sekaly RP, Trowsdale J, Geha RS. Effect of isotypes and allelic polymorphism on the binding of staphylococcal exotoxins to MHC class II molecules. *J Immunol* 1990;144:226–30.
53. Reiss S, Baxter AE, Cirelli KM, Dan JM, Morou A, Daigneault A, et al. Comparative analysis of activation induced marker (AIM) assays for sensitive identification of antigen-specific CD4 T cells. *PLoS One* 2017;12:e0186998.
54. Ridker PM, Everett BM, Thuren T, MacFadyen JG, Chang WH, Ballantyne C, et al. Antiinflammatory therapy with canakinumab for atherosclerotic disease. *N Engl J Med* 2017;377:1119–31.

55. Yang SC, Chen CB, Lin MY, Zhang ZY, Jia XY, Huang M, et al. Genetics of severe cutaneous adverse reactions. *Front Med (Lausanne)* 2021;8:652091.
56. Wang W, Hu FY, Wu XT, An DM, Yan B, Zhou D. Genetic predictors of Stevens-Johnson syndrome and toxic epidermal necrolysis induced by aromatic antiepileptic drugs among the Chinese Han population. *Epilepsy Behav* 2014;37:16–9.
57. Niu J, Jia Q, Ni Q, Yang Y, Chen G, Yang X, et al. Association of CD8(+) T lymphocyte repertoire spreading with the severity of DRESS syndrome. *Sci Rep* 2015;5:9913.
58. Schulert GS. The IL-18/IFN γ axis in systemic JIA and MAS—new answers, more questions. *Rheumatology (Oxford)* 2021;60:3045–47.
59. Hinze T, Kessel C, Hinze CH, Seibert J, Gram H, Foell D. A dysregulated interleukin-18-interferon- γ -CXCL9 axis impacts treatment response to canakinumab in systemic juvenile idiopathic arthritis. *Rheumatology (Oxford)* 2021;60:5165–74.
60. Bracaglia C, de Graaf K, Marafon DP, Guilhot F, Ferlin W, Prencipe G, et al. Elevated circulating levels of interferon- γ and interferon- γ -induced chemokines characterise patients with macrophage activation syndrome complicating systemic juvenile idiopathic arthritis. *Ann Rheum Dis* 2017;76:166–72.
61. Sullivan KD, Lewis HC, Hill AA, Pandey A, Jackson LP, Cabral JM, et al. Trisomy 21 consistently activates the interferon response. *Elife* 2016;5.
62. Araya P, Waugh KA, Sullivan KD, Nunez NG, Roselli E, Smith KP, et al. Trisomy 21 dysregulates T cell lineages toward an autoimmunity-prone state associated with interferon hyperactivity. *Proc Natl Acad Sci U S A* 2019;116:24231–41.
63. Sullivan KD, Evans D, Pandey A, Hraha TH, Smith KP, Markham N, et al. Trisomy 21 causes changes in the circulating proteome indicative of chronic autoinflammation. *Sci Rep* 2017;7:14818.
64. Patel G, Greenberger PA. Allergic bronchopulmonary aspergillosis. *Allergy Asthma Proc* 2019;40:421–24.
65. Chauhan B, Santiago L, Hutcheson PS, Schwartz HJ, Spitznagel E, Castro M, et al. Evidence for the involvement of two different MHC class II regions in susceptibility or protection in allergic bronchopulmonary aspergillosis. *J Allergy Clin Immunol* 2000;106:723–9.
66. Koehm S, Slavin RG, Hutcheson PS, Trejo T, David CS, Bellone CJ. HLA-DRB1 alleles control allergic bronchopulmonary aspergillosis-like pulmonary responses in humanized transgenic mice. *J Allergy Clin Immunol* 2007;120:570–7.
67. Wang J, Jelcic I, Muhlenbruch L, Haunerding V, Toussaint NC, Zhao Y, et al. HLA-DR15 molecules jointly shape an autoreactive T cell repertoire in multiple sclerosis. *Cell* 2020;183:1264–81.
68. Park EH, Lee EY, Shin K, Kim HA. Tocilizumab-induced anaphylaxis in patients with adult-onset Still's disease and systemic juvenile idiopathic arthritis: a case-based review. *Rheumatol Int* 2020;40:791–98.
69. Taweeseedt PT, Nordstrom CW, Stoeckel J, Dumic I. Pulmonary manifestations of drug reaction with eosinophilia and systemic symptoms (DRESS) syndrome: a systematic review. *Biomed Res Int* 2019;2019:7863815.
70. Brunner HI, Quartier P, Alexeeva E, Constantin T, Kone-Paut I, Marzan K, et al. Efficacy and safety of canakinumab in patients with systemic juvenile idiopathic arthritis with and without fever at baseline: results from an open-label, active-treatment extension study. *Arthritis Rheumatol* 2020;72:2147–58.
71. Pardeo M, Rossi MN, Marafon DP, Sacco E, Bracaglia C, Passarelli C, et al. Early treatment and IL1RN single-nucleotide polymorphisms affect response to anakinra in systemic juvenile idiopathic arthritis. *Arthritis Rheumatol* 2021;73:1053–61.
72. Bjornevik K, Cortese M, Healy BC, Kuhle J, Mina MJ, Leng Y, et al. Longitudinal analysis reveals high prevalence of Epstein-Barr virus associated with multiple sclerosis. *Science* 2022;375:296–301.
73. Saper V, Prahalad S, Canna S, Abul-Aziz R, Alvarez M, Bingham C, et al. Effect of drug withdrawal on interleukin-1 or interleukin-6 inhibitor associated diffuse lung disease [abstract]. *Arthritis Rheumatol* 2021; 73 Suppl 10. URL: <https://acrabstracts.org/abstract/effect-of-drug-withdrawal-on-interleukin-1-or-interleukin-6-inhibitor-associated-diffuse-lung-disease/>.

COVID-19

Endothelial Cell-Activating Antibodies in COVID-19

Hui Shi,¹ Yu Zuo,² Sherwin Navaz,² Alyssa Harbaugh,² Claire K. Hoy,² Alex A. Gandhi,² Gautam Sule,² Srilakshmi Yalavarthi,² Kelsey Gockman,² Jacqueline A. Madison,² Jintao Wang,³ Melanie Zuo,² Yue Shi,⁴ Michael D. Maile,² Jason S. Knight,²  and Yogendra Kanthi⁵

Objective. While endothelial dysfunction has been implicated in the widespread thromboinflammatory complications of COVID-19, the upstream mediators of endotheliopathy remain, for the most part, unknown. This study was undertaken to identify circulating factors contributing to endothelial cell activation and dysfunction in COVID-19.

Methods. Human endothelial cells were cultured in the presence of serum or plasma from 244 patients hospitalized with COVID-19 and plasma from 100 patients with non-COVID-19-related sepsis. Cell adhesion molecules (E-selectin, vascular cell adhesion molecule 1, and intercellular adhesion molecule 1 [ICAM-1]) were quantified using in-cell enzyme-linked immunosorbent assay.

Results. Serum and plasma from COVID-19 patients increased surface expression of cell adhesion molecules. Furthermore, levels of soluble ICAM-1 and E-selectin were elevated in patient serum and correlated with disease severity. The presence of circulating antiphospholipid antibodies was a strong marker of the ability of COVID-19 serum to activate endothelium. Depletion of total IgG from antiphospholipid antibody-positive serum markedly reduced the upregulation of cell adhesion molecules. Conversely, supplementation of control serum with patient IgG was sufficient to trigger endothelial activation.

Conclusion. These data are the first to indicate that some COVID-19 patients have potentially diverse antibodies that drive endotheliopathy, providing important context regarding thromboinflammatory effects of autoantibodies in severe COVID-19.

INTRODUCTION

There are several likely synergistic mechanisms by which SARS-CoV-2 infection may result in COVID-19-associated coagulopathy, including cytokine release that activates leukocytes, endothelium, and platelets; the direct activation of various cells by viral infection; and high levels of intravascular neutrophil extracellular traps (NETs) (1). The latter are inflammatory cell remnants that contribute to thrombosis (2). COVID-19-associated coagulopathy may

manifest with thrombosis in venous, arterial, and microvascular circuits. The incidence of venous thromboembolism is particularly notable in severe COVID-19 (10–35%), with autopsy specimen findings suggesting that it affects as many as 60% of patients in association with COVID-19-related mortality (3).

Recently, there have been several descriptions of what appears to be de novo autoantibody formation in individuals with severe COVID-19. One example replicated in multiple studies is the detection of antibodies similar to the antiphospholipid

Dr. Y. Zuo's work was supported by the Rheumatology Research Foundation and the Arthritis National Research Foundation. Dr. Madison's work was supported by the VA Healthcare System. Dr. Knight's work was supported by the Rheumatology Research Foundation, the Michigan Medicine Frankel Cardiovascular Center, the A. Alfred Taubman Medical Research Institute, the NIH (grant R01-HL-115138), Burroughs Wellcome Fund, and the Lupus Research Alliance. Dr. Kanthi's work was supported by the Intramural Research Program of the National Heart, Lung, and Blood Institute, NIH, the Lasker Foundation, the University of Michigan Frankel Cardiovascular Center, the A. Alfred Taubman Medical Research Institute, and the Falk Medical Research Trust Catalyst Award.

¹Hui Shi, MD, PhD: University of Michigan, Ann Arbor, and Shanghai Jiao Tong University School of Medicine, Shanghai, China; ²Yu Zuo, MD, Sherwin Navaz, BS, Alyssa Harbaugh, BS, Claire K. Hoy, BS, Alex A. Gandhi, BS, Gautam Sule, PhD, Srilakshmi Yalavarthi, MS, Kelsey Gockman, BS, Jacqueline

A. Madison, MD, Melanie Zuo, MD, Michael D. Maile, MD, Jason S. Knight, MD, PhD: University of Michigan, Ann Arbor; ³Jintao Wang, PhD: National Heart, Lung and Blood Institute, Bethesda, Maryland; ⁴Yue Shi, PhD: Shanghai University of Sport, Shanghai, China; ⁵Yogendra Kanthi, MD: National Heart, Lung and Blood Institute, Bethesda, Maryland, and University of Michigan, Ann Arbor.

Author disclosures are available at <https://onlinelibrary.wiley.com/action/downloadSupplement?doi=10.1002%2Fart.42094&file=art42094-sup-0001-Disclosureform.pdf>.

Address correspondence to Jason S. Knight, MD, PhD, 1150 West Medical Center Drive, Ann Arbor, Michigan (email: jsknight@umich.edu); or to Yogendra Kanthi, MD, Clinical Center, 10 Center Drive, Bethesda, Maryland (yogen.kanthi@nih.gov).

Submitted for publication August 24, 2021; accepted in revised form February 13, 2022.

antibodies (aPLs) that mediate antiphospholipid syndrome (APS) in the general population. In APS, persistent autoantibodies are formed to phospholipids and phospholipid-binding proteins, such as prothrombin and β_2 -glycoprotein I (β_2 GPI). These autoantibodies then engage cell surfaces, where they activate endothelial cells, platelets, and neutrophils and thereby trigger thrombosis in the blood vessel wall interface. While viral infections have long been known to trigger transient aPLs (4), the mechanisms by which these potentially short-lived antibodies may be pathogenic have not been thoroughly characterized. To this end, our group recently found that IgG fractions from COVID-19 patients were enriched for aPLs and amplified thrombosis when injected into mice (5). Intriguingly, the circulating B cell compartment in COVID-19 appears similar to lupus, an autoimmune disease whereby naive B cells rapidly become antibody-producing cells using an extrafollicular pathway (6), and, in doing so, bypass the normal germinal center tolerance checkpoints against autoimmunity.

Here, we were initially interested in the extent to which circulating NET remnants might be an important activator of endothelial cells. We then also turned our attention to aPLs as potential markers of COVID-19 serum and polyclonal IgG fractions with strong endothelial cell-activating potential.

MATERIALS AND METHODS

For detailed methods see Supplementary Materials and Methods (available on the *Arthritis & Rheumatology* website at <http://onlinelibrary.wiley.com/doi/10.1002/art.42094>). This study complied with all relevant ethics regulations and was approved by the Institutional Review Board of the University of Michigan (approval nos. HUM00179409 and HUM00131596).

Serum and plasma samples from COVID-19 patients and cell culture conditions. All 118 patients in the primary cohort and 126 patients in the second cohort had a confirmed COVID-19 diagnosis based on US Food and Drug Administration-approved RNA testing. Human umbilical vein endothelial cells (HUVECs) were cultured in endothelial cell growth basal medium 2 (CC-3156; Lonza) supplemented with EGM-2 MV SingleQuot kit (CC-4147; Lonza).

Protocols for purification of human IgG, in-cell enzyme-linked immunosorbent assay (ELISA), and characterization of neutrophil adhesion. IgG was purified as described previously (5). In-cell ELISA and neutrophil adhesion were also conducted according to protocols described previously (7).

Quantification of antibodies and biomarkers. We quantified aPLs using Quanta Lite kits (Inova Diagnostics). Soluble E-selectin and intercellular adhesion molecule 1 (ICAM-1) levels were quantified by ELISA (DY724 and DY720; R&D Systems).

Myeloperoxidase (MPO)-DNA complexes were quantified as previously described (8). Cell-free DNA was quantified using a Quant-iT PicoGreen double-stranded DNA Assay kit (P11496; Invitrogen). Citrullinated histone H3 was quantified by ELISA (501620; Cayman Chemical), and calprotectin was quantified by ELISA (DY8226; R&D Systems).

RESULTS

Activation of HUVECs by COVID-19 serum. Serum samples were collected from 118 patients hospitalized with COVID-19 at an academic hospital. The mean age of patients in this cohort was 62 years, 47% of patients were women, and 42% were Black African Americans (Supplementary Table 1, <http://onlinelibrary.wiley.com/doi/10.1002/art.42094>); 35% were receiving mechanical ventilation. Serum from COVID-19 patients was added to early-passage HUVECs, and the expression of cell adhesion molecules was determined after 6 hours using a custom in-cell ELISA compatible with a biosafety level 3 facility per institutional guidelines (Figure 1A). As compared to serum samples from 38 healthy controls, the samples from COVID-19 patients triggered an activated endothelial cell phenotype, as evidenced by increased surface expression of the cell adhesion molecules E-selectin (Figure 1B and Supplementary Figure 1A, <http://onlinelibrary.wiley.com/doi/10.1002/art.42094>), vascular cell adhesion molecule 1 (VCAM-1) (Figure 1C and Supplementary Figure 1B), and ICAM-1 (Figure 1D and Supplementary Figure 1C). Relative activation (as compared to unstimulated cells) was similar to activation observed with 20 ng/ml tumor necrosis factor stimulation, which was included in all experiments as a positive control (Supplementary Figure 2, <http://onlinelibrary.wiley.com/doi/10.1002/art.42094>).

We obtained sufficient serum from an additional 126 hospitalized patients with COVID-19 to expand ICAM-1 testing. These patients had similar clinical severity profiles compared to the original 118 patients (see Supplementary Table 1 <http://onlinelibrary.wiley.com/doi/10.1002/art.42094>) and had similarly up-regulated expression of surface ICAM-1 (Supplementary Figure 3). Considering all 244 patients together, serum from patients requiring mechanical ventilation up-regulated ICAM-1 more strongly than serum from patients who were hospitalized but did not require mechanical ventilation ($P < 0.01$) (Figure 1E). We also measured levels of soluble ICAM-1 and E-selectin in patient serum. We found significantly higher levels of both soluble ICAM-1 and E-selectin in COVID-19 serum as compared to healthy control serum (Figure 1F and Supplementary Figure 4, <http://onlinelibrary.wiley.com/doi/10.1002/art.42094>). Soluble ICAM-1 levels positively correlated with HUVEC ICAM-1 expression (Figure 1G), as well as with clinical parameters that correlated with severity, including C-reactive protein level ($r = 0.27$, $P = 0.0002$), D-dimer ($r = 0.29$, $P = 0.0001$), and oxygenation efficiency ($r = -0.37$, $P < 0.0001$) (Supplementary Figure 5, <http://onlinelibrary.wiley.com/doi/10.1002/art.42094>). Soluble

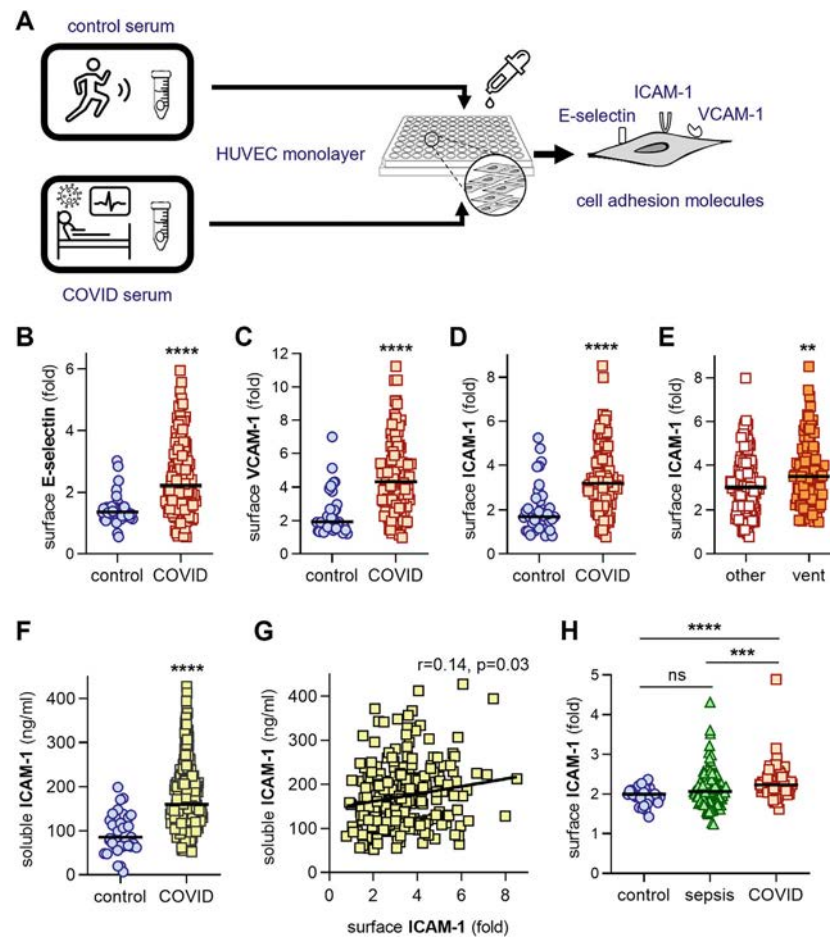


Figure 1. Activation of human umbilical vein endothelial cells (HUVECs) by control or COVID-19 serum. **A**, Schematic workflow of in-cell enzyme-linked immunosorbent assay is shown. HUVECs were cultured for 6 hours with serum from either healthy controls (collected prepandemic) ($n = 38$) or patients hospitalized with COVID-19 ($n = 118$). **B–D**, Cells were fixed, and surface expression of E-selectin (**B**), vascular cell adhesion molecule 1 (VCAM-1) (**C**), or intercellular adhesion molecule 1 (ICAM-1) (**D**) was quantified. **E**, Beyond the 118 COVID-19 patients tested in **D**, surface expression of ICAM-1 was tested in an additional 126 unique patient samples. Patients requiring mechanical ventilation (vent) ($n = 101$) were compared to hospitalized patients who did not receive mechanical ventilation ($n = 143$). **F**, Serum from healthy controls ($n = 37$) and from COVID-19 patients ($n = 232$) was assessed for soluble ICAM-1. **G**, In samples from COVID-19 patients, the correlation between expression levels of soluble ICAM-1 and HUVEC expression of surface ICAM-1 was assessed by Spearman's test. **H**, HUVECs were cultured for 6 hours with plasma from healthy controls ($n = 36$), patients with non-COVID-19-related sepsis admitted to the intensive care unit ($n = 100$), or patients hospitalized with COVID-19 ($n = 72$). Cells were then fixed, and surface expression of ICAM-1 was quantified. In **B–F** and **H**, symbols represent individual subjects; bars show the median. In **B–F**, ** = $P < 0.01$; *** = $P < 0.001$; **** = $P < 0.0001$, by Mann-Whitney test in **B–F** and by Kruskal-Wallis test with Dunn's correction for multiple comparisons in **H**. NS = not significant.

E-selectin had similar correlations to all of the above (Supplementary Figure 4).

To determine the extent to which this phenomenon might extend to critically ill patients without COVID-19, 100 age- and comorbidity-matched patients with non-COVID-19-related sepsis (Supplementary Table 2, <http://onlinelibrary.wiley.com/doi/10.1002/art.42094>) admitted to the intensive care unit (plasma obtained in the pre-COVID-19 era) were matched with patients in our COVID-19 cohort ($n = 72$ available plasma samples). More patients in the non-COVID-19-related sepsis cohort required mechanical ventilation (65% versus 46%). We then stimulated HUVECs with plasma and determined levels of surface

expression of ICAM-1. While a subset of the non-COVID-19-related sepsis plasma elicited high levels of expression of surface ICAM-1, that group as a whole was not significantly different from the control group (Figure 1H). Additionally, COVID-19 plasma demonstrated greater activation than either control or non-COVID-19-related sepsis plasma (Figure 1H). Taken together, these data indicate that COVID-19 serum and plasma contain factors capable of activating endothelial cells.

Association of NET remnants and other biomarkers with the endothelial cell-activating potential of COVID-19 serum. Given that NETs are known activators of endothelial cells,

Table 1. Correlation of HUVEC cell adhesion molecule expression with aPL expression in COVID-19 patients*

	E-selectin		VCAM-1		ICAM-1	
	r	P	r	P	r	P
aPLs						
IgG aCL	0.446	<0.0001	0.421	<0.0001	0.346	<0.001
IgM aCL	0.369	<0.0001	0.252	<0.01	0.357	<0.0001
IgG anti- β_2 GPI	0.156	NS	0.213	<0.05	0.076	NS
IgM anti- β_2 GPI	0.009	NS	0.047	NS	0.150	NS
IgG aPS/PT	0.432	<0.0001	0.252	<0.01	0.299	<0.001
IgM aPS/PT	0.254	<0.01	0.115	NS	0.276	<0.01
NET remnants						
Cell-free DNA	0.073	NS	0.237	<0.05	0.135	NS
MPO-DNA complexes	0.156	NS	0.256	<0.01	0.277	<0.01
Cit-H3	0.079	NS	0.224	<0.05	0.076	NS
Other biomarkers						
C-reactive protein	-0.008	NS	0.173	NS	0.003	NS
D-dimer	0.175	NS	0.133	NS	0.258	<0.05
Calprotectin	0.206	<0.05	0.203	<0.05	0.197	<0.05

* Correlations were determined by Spearman's test. HUVEC = human umbilical vein endothelial cell; aPL = anti-phospholipid antibody; VCAM-1 = vascular cell adhesion molecule 1; ICAM-1 = intercellular adhesion molecule 1; aCL = anticardiolipin; NS = not significant; β_2 GPI = β_2 -glycoprotein I; aPS/PT = antiphosphatidylserine/prothrombin; NET = neutrophil extracellular trap; MPO-DNA = myeloperoxidase-DNA; Cit-H3 = citrullinated histone H3.

we investigated whether NET remnants might predict the ability of a particular COVID-19 serum sample to up-regulate levels of surface E-selectin, VCAM-1, and ICAM-1. Specifically, we measured NETs in COVID-19 serum ($n = 118$) via quantification of cell-free DNA, myeloperoxidase (MPO)-DNA complexes, and citrullinated histone H3 (Cit-H3) (Table 1). Serum MPO-DNA complexes moderately correlated with surface expression of both VCAM-1 ($r = 0.26$, $P < 0.01$) and ICAM-1 ($r = 0.28$, $P < 0.01$). Cell-free DNA and Cit-H3 both correlated only with VCAM-1 ($r = 0.24$, $P < 0.05$ and $r = 0.22$, $P < 0.05$, respectively) (Table 1). Beyond these relatively specific markers of NETs, we also investigated correlations with more general markers of thromboinflammation, including C-reactive protein, D-dimer, and calprotectin (the latter previously shown to be an early predictor of respiratory failure in COVID-19). Of the 3, only calprotectin positively correlated with expression of all 3 endothelial cell surface markers ($r = 0.19$ - 0.20 , $P < 0.05$), while D-dimer correlated with ICAM-1 only ($r = 0.26$, $P < 0.05$) (Table 1). Taken together, these data demonstrate modest correlations between NETs/thromboinflammation and the ability of COVID-19 serum to activate endothelial cells.

Association of aPLs with the endothelial cell-activating potential of COVID-19 serum. We reasoned that COVID-19-associated autoreactive antibodies might activate endothelial cells. In pursuit of such antibody fractions, we focused on the IgG and IgM isotypes of 3 types of aPLs: anticardiolipin antibodies (aCLs), anti- β_2 GPI, and antiphosphatidylserine/prothrombin (aPS/PT). As shown in Supplementary Table 3 (<http://onlinelibrary.wiley.com/doi/10.1002/art.42094>), 45% of subjects were positive for at least 1 antibody based on the manufacturer's cutoff, and 25% were positive using a more stringent

cutoff of ≥ 40 . The vast majority of positive findings were either aCL positivity (for IgG and IgM, values were 3% and 25% of the cohort, respectively) or aPS/PT positivity (for IgG and IgM, values were 24% and 15% of the cohort, respectively). It should also be noted that there were strong correlations among many of the antibodies, for example IgG aCL and IgG aPS/PT ($r = 0.51$, $P < 0.0001$) and IgM aCL and IgM aPS/PT ($r = 0.53$, $P < 0.0001$) (all correlations are shown in Supplementary Table 4, <http://onlinelibrary.wiley.com/doi/10.1002/art.42094>). Furthermore, aPL levels correlated, to some extent, with clinical biomarkers, especially levels of circulating NETs (Supplementary Table 5, <http://onlinelibrary.wiley.com/doi/10.1002/art.42094>). None of the aPLs were detected at significant levels in the healthy control serum (2 positive test results) and plasma (1 positive test result) in this study (Supplementary Tables 6 and 7, <http://onlinelibrary.wiley.com/doi/10.1002/art.42094>).

Interestingly, we detected strong correlations between aCL and aPS/PT antibodies and the 3 markers of endothelial cell activation (E-selectin, VCAM-1, and ICAM-1) (Table 1). The only correlation that was not significant was between IgM aPS/PT and VCAM-1 (Table 1). We additionally performed a logistic regression analysis after setting a positive/negative threshold for cell adhesion molecule up-regulation that was 2 standard deviations greater than the control mean (Supplementary Table 8, <http://onlinelibrary.wiley.com/doi/10.1002/art.42094>). IgG aCL levels were significantly higher in E-selectin- and VCAM-1-positive patients ($P = 0.001$ and $P = 0.003$, respectively), while IgG aPS/PT levels were significantly higher in ICAM-1-positive patients ($P = 0.018$). We also measured the same aPL levels in the aforementioned non-COVID-19-related sepsis cohort (Supplementary Table 9, <http://onlinelibrary.wiley.com/doi/10.1002/art.42094>). Of 100 patients, 29 were positive for any aPL, with 23 patients positive at the more

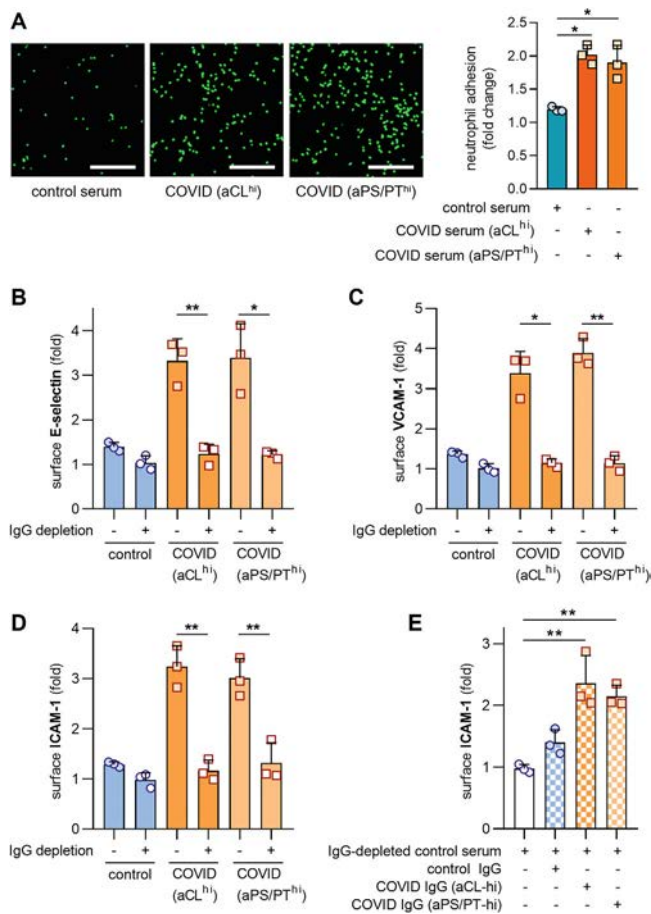


Figure 2. Depletion of IgG from sera with high levels of anticardiolipin (aCL) and antiphosphatidylserine/prothrombin (aPS/PT) antibodies alleviates HUVEC activation. **A**, Serum was pooled from 3 IgG aCL-positive patients, 5 IgG aPS/PT-positive patients, or 3 healthy donors. HUVEC monolayers were treated with 2.5% COVID-19 serum or control serum for 4 hours, and calcein AM-labeled neutrophils were added as described in Materials and Methods. Representative photomicrographs are shown (left) (bars = 200 μ m) and results were quantified (right). **B–D**, IgG was depleted from each of the aforementioned pools. Activation of HUVECs, defined by surface expression of E-selectin (**B**), VCAM-1 (**C**), or ICAM-1 (**D**), was determined after culture for 6 hours. The experiment was repeated on 3 different days. **E**, IgG (100 μ g/ml) was purified from the pooled samples in **A–C**, and then spiked into IgG-depleted control serum. HUVEC activation, defined by surface expression of ICAM-1, was determined after culture for 6 hours. Symbols represent individual samples; bars show the mean \pm SD from 3 independent experiments. * = $P < 0.05$; ** = $P < 0.01$, by one-way analysis of variance with Dunn's correction, or Tukey's correction or by 2-sided paired t -test. See Figure 1 for other definitions.

stringent cutoff of ≥ 40 . In contrast to the COVID-19 cohort, the vast majority of tests showed positivity for IgM aPS/PT, the levels of which correlated with the ability of plasma to up-regulate ICAM-1 ($r = 0.29$, $P < 0.01$) (Supplementary Table 10, <http://onlinelibrary.wiley.com/doi/10.1002/art.42094>). To summarize, we detected correlations between various aPLs and endothelial

cell activation in COVID-19, and to some extent in non-COVID-19-related sepsis.

Increased neutrophil adhesion upon serum-mediated HUVEC activation. To determine whether up-regulation of E-selectin, VCAM-1, and ICAM-1 is associated with increased adhesive functions of HUVECs, we performed a neutrophil adhesion assay. We pooled serum from 3 COVID-19 patients with positive IgG aCL activity (mean 29 IgG phospholipid units/ml) and from a separate 5 COVID-19 patients with positive IgG aPS/PT activity (mean 54). We then stimulated HUVECs with the pooled serum. Compared to control serum, both COVID-19 samples demonstrated significantly increased adhesion of neutrophils to endothelial cells (Figure 2A).

Depletion of IgG alleviates HUVEC activation. We next sought to determine the extent to which total IgG fractions from COVID-19 patients could directly activate HUVECs. To this end, we subjected the aforementioned pooled serum (IgG aCL- and IgG aPS/PT-positive) to either mock depletion or IgG depletion. IgG depletion did not result in a significant reduction of other serum proteins of note, such as calprotectin (Supplementary Figure 6, <http://onlinelibrary.wiley.com/doi/10.1002/art.42094>). As compared to mock depletion, total IgG depletion completely abrogated the ability of both pooled sample groups to up-regulate E-selectin (Figure 2B), VCAM-1 (Figure 2C), and ICAM-1 in endothelial cells (Figure 2D). We next purified a small quantity of total IgG from each group of pooled serum and added it to control serum that had been depleted of its own IgG. The COVID-19 IgG-supplemented control serum demonstrated an ability to increase expression of surface levels of ICAM-1 (Figure 2E). In contrast, IgG purified from COVID-19 serum that tested negative for both IgG aCL and IgG aPS/PT did not have increased expression of ICAM-1 (Supplementary Figure 7, <http://onlinelibrary.wiley.com/doi/10.1002/art.42094>). Taken together, these data indicate that the presence of aPLs correlates with activation of endothelial cells in the presence of IgG in the serum of patients with COVID-19.

DISCUSSION

In the current study, we show that serum from COVID-19 patients activated cultured endothelial cells that express surface adhesion molecules integral to inflammation and thrombosis, namely ICAM-1, E-selectin, and VCAM-1. Furthermore, we found that, for at least a subset of serum samples from COVID-19 patients, activation could be mitigated by depleting total IgG. The role of aPLs in activating endothelial cells has been demonstrated both in vitro and in vivo (9). For example, IgG fractions from APS patients have long been known to activate HUVECs, as indicated by increased monocyte adherence and increased expression of adhesion molecules. It is intriguing that while most characterization of endothelium in APS has focused on activation

of the endothelium by anti- β_2 GPI antibodies (10), these were only rarely detected in our cohort. An interesting recent study demonstrated activation of endothelium in APS by phospholipid-binding, cofactor-independent antibodies (11). Of course, it should be noted that all experiments performed in our study were with total IgG fractions and not affinity-purified aPLs. Therefore, aPLs may mark antibody profiles in severe illness (possibly polyclonal) that activate endothelium and influence inflammation and coagulation at the normally quiescent blood–vessel wall interface.

In addition to our findings (5), several other studies (12) have also provided evidence of the *de novo* formation of pathogenic autoantibodies in COVID-19. For example, in an interesting study, a high-throughput autoantibody discovery technique was used to screen a cohort of COVID-19 patients for autoantibodies against 2,770 extracellular and secreted proteins (13). That study found that there is a tendency for autoantibodies to be directed against immunomodulatory proteins, including cytokines, chemokines, complement components, and cell surface proteins. This is further supported by our data suggesting correlations among aPL species in serum from COVID-19 patients.

Beyond COVID-19, we were intrigued to find that ~25% of patients with non-COVID-19-related sepsis had at least 1 positive aPL test, mostly IgM aPS/PT. Given that IgM aPS/PT levels correlated with plasma activation of endothelial cells, we hypothesize a similar autoreactive antibody-mediated, endothelial cell-activating mechanism may occur in some patients with sepsis, a state in which interaction between the infection and the host immune response disrupts the vasculature (14). Of particular note, infections causing critical illness have long been known to be potential triggers of autoantibodies, and in particular aPLs (4,15). Although infection-associated aPLs have typically been described as transient (16), a recent systematic review showed that ~33% of individuals positive for aPLs in the setting of a virus-associated thrombotic event continue to have persistent aPL positivity for at least several months (15). Based on our data, studies with long-term clinical and serologic follow-up may be necessary to better define the natural history of COVID-19 and non-COVID-19-related sepsis.

There are several potential clinical implications of our findings. One consideration that warrants further investigation is whether patients with severe COVID-19 should be screened for aPLs to evaluate their risk of thrombosis and progression to respiratory failure, and whether patients with high aPL titers might benefit from treatments used in traditional cases of severe APS such as therapeutic anticoagulation, complement inhibition, and plasmapheresis. At the same time, determining the extent to which aPLs are direct mediators of the endothelial cell phenotypes observed here, and better understanding of which polyclonal antibody fractions are most likely to activate endothelial cells are important questions warranting future research. Our study has additional limitations, including lacking a direct readout of macrovascular thrombosis (available in other well-conducted studies [17]) given aggressive anticoagulation used at our center early in

the pandemic and a currently incomplete understanding of the mechanisms by which aPL-associated IgG fractions activate endothelial cells. However, given the urgency of COVID-19 research, we believe these issues are counterbalanced by our relatively large sample size and the previously unknown discovery of endothelial cell-activating antibody profiles in some COVID-19 serum. Indeed, these data also provide context for diffuse organ involvement of COVID-19, where a nonspecific humoral immune response to illness may disrupt the normally quiescent endothelium and increase vascular inflammation. As we await definitive solutions to the pandemic, these findings provide important context to the complex interplay between SARS-CoV-2 infection, the human immune system, and vascular immunobiology.

ACKNOWLEDGMENTS

We would like to thank all the individuals with COVID-19 and those with non-COVID-19-related sepsis who participated in this study, as well as the frontline workers during the pandemic.

AUTHOR CONTRIBUTIONS

All authors were involved in drafting the article or revising it critically for important intellectual content, and all authors approved the final version to be published. Drs. Knight and Kanthi had full access to all of the data in the study and take responsibility for the integrity of the data and the accuracy of the data analysis.

Study conception and design. Shi, Zuo, Maile, Knight, Kanthi.

Acquisition of data. Shi, Zuo, Navaz, Harbaugh, Hoy, Gandhi, Sule, Yalavarthi, Gockman, Madison, Wang, Zuo, Shi.

Analysis and interpretation of data. Shi, Zuo, Maile, Knight, Kanthi.

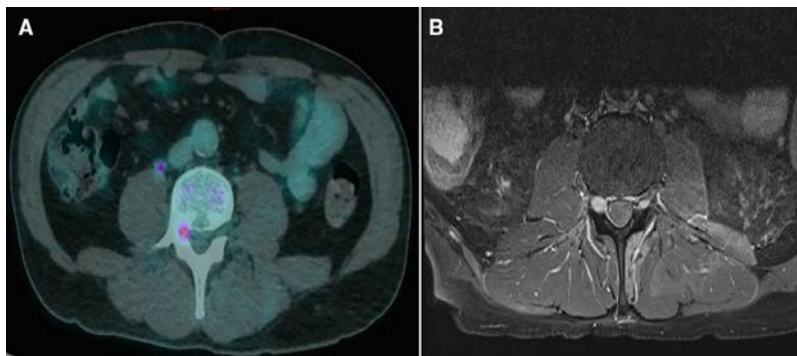
REFERENCES

1. Zuo Y, Yalavarthi S, Shi H, Gockman K, Zuo M, Madison JA, et al. Neutrophil extracellular traps in COVID-19. *JCI Insight* 2020;5: e138999.
2. Middleton EA, He XY, Denorme F, Campbell RA, Ng D, Salvatore SP, et al. Neutrophil extracellular traps contribute to immunothrombosis in COVID-19 acute respiratory distress syndrome. *Blood* 2020;136:1169–79.
3. Wichmann D, Sperhake JP, Lütgehetmann M, Steurer S, Edler C, Heinemann A, et al. Autopsy findings and venous thromboembolism in patients with COVID-19: a prospective cohort study. *Ann Intern Medicine* 2020;173:268–77.
4. Abdel-Wahab N, Talathi S, Lopez-Olivo MA, Suarez-Almazor ME. Risk of developing antiphospholipid antibodies following viral infection: a systematic review and meta-analysis. *Lupus* 2018;27:572–83.
5. Zuo Y, Estes SK, Ali RA, Gandhi AA, Yalavarthi S, Shi H, et al. Prothrombotic autoantibodies in serum from patients hospitalized with COVID-19. *Sci Transl Med* 2020;12:eabd3876.
6. Woodruff MC, Ramonell RP, Nguyen DC, Cashman KS, Saini AS, Haddad NS, et al. Extrafollicular B cell responses correlate with neutralizing antibodies and morbidity in COVID-19. *Nat Immunol* 2020; 21:1506–16.
7. Shi H, Gandhi AA, Smith SA, Wang Q, Chiang D, Yalavarthi S, et al. Endothelium-protective, histone-neutralizing properties of the polyanionic agent defibrotide. *JCI Insight* 2021;6: e149149.
8. Kessenbrock K, Krumbholz M, Schonermarck U, Back W, Gross WL, Werb Z, et al. Netting neutrophils in autoimmune small-vessel vasculitis. *Nat Med* 2009;15:623–5.

9. Pierangeli SS, Colden-Stanfield M, Liu X, Barker JH, Anderson GL, Harris EN. Antiphospholipid antibodies from antiphospholipid syndrome patients activate endothelial cells in vitro and in vivo. *Circulation* 1999;99:1997–2002.
10. Allen KL, Fonseca FV, Betapudi V, Willard B, Zhang J, McCrae KR. A novel pathway for human endothelial cell activation by antiphospholipid/anti- β 2 glycoprotein I antibodies. *Blood* 2012;119:884–93.
11. Muller-Calleja N, Hollerbach A, Royce J, Ritter S, Pedrosa D, Madhusudhan T, et al. Lipid presentation by the protein C receptor links coagulation with autoimmunity. *Science* 2021;371:eabc0956.
12. Chang SE, Feng A, Meng W, Apostolidis SA, Mack E, Artandi M, et al. New-Onset IgG autoantibodies in hospitalized patients with COVID-19. *Nat Commun* 2021;12:5417.
13. Wang EY, Mao T, Klein J, Dai Y, Huck JD, Jaycox JR, et al. Diverse functional autoantibodies in patients with COVID-19. *Nature* 2021;595:283–8.
14. Colling ME, Tourdot BE, Kanthi Y. Inflammation, infection and venous thromboembolism [review]. *Circ Res* 2021;128:2017–36.
15. Abdel-Wahab N, Lopez-Olivo MA, Pinto-Patarroyo GP, Suarez-Almazor ME. Systematic review of case reports of antiphospholipid syndrome following infection. *Lupus* 2016;25:1520–31.
16. Blank M, Asherson RA, Cervera R, Shoenfeld Y. Antiphospholipid syndrome infectious origin. *J Clin Immunol* 2004;24:12–23.
17. Borghi MO, Beltagy A, Garrafa E, Curreli D, Cecchini G, Bodio C, et al. Anti-phospholipid antibodies in COVID-19 are different from those detectable in the anti-phospholipid syndrome. *Front Immunol* 2020;11:584241.

DOI 10.1002/art.42108

Clinical Images: Motor deficiency and radicular pain secondary to sarcoidosis



The patient, a previously healthy 65-year-old man, presented with right L4 radiculopathy and motor deficit. Before presentation, he had asthenia for 1 month, which was associated with a weight loss of 5 kg. Physical examination revealed a complete leg extension deficit, absence of patellar reflex, and paresthesias of the anterolateral side of the right thigh. Spinal magnetic resonance imaging (MRI) showed no disc herniation. Laboratory investigations revealed a slightly elevated C-reactive protein level of 8.6 mg/liter and normal calcium and phosphate levels. His cerebrospinal fluid contained 1 white blood cell/mm³ and showed a total protein level of 0.42 gm/liter. Further analyses of the cerebrospinal fluid included testing for viruses, bacteria, and other immunologic factors, all of which yielded negative results. The angiotensin-converting enzyme level was normal. An electromyogram showed signs of denervation in the right L3 and L4 regions. Positron emission tomography showed an intense focal hypermetabolism in the right L4 root (A) and multiple hypermetabolic mediastinal lymphadenopathies. Lymphoma was the suspected diagnosis. The patient underwent intravenous administration of gadolinium-based contrast agent followed by fat-suppressed T1-weighted MRI, which showed an enlargement of the right L4 dorsal root ganglion (B). Biopsy findings of mediastinal lymphadenopathy confirmed a diagnosis of sarcoidosis. The patient's symptoms quickly disappeared after initiation of glucocorticoid treatment. Sarcoidosis is an inflammatory disease that, like some lymphomas, can present as radicular pain and deficiency (1,2). The clinician should be alert to this possibility.

Author disclosures are available at <https://onlinelibrary.wiley.com/action/downloadSupplement?doi=10.1002%2Fart.42108&file=art42108-sup-0001-Disclosureform.pdf>.

1. Shono T, Tamai M, Kobayashi M, Wakasaki H, Furuta H, Nakao T, et al. Neurosarcoidosis with spinal root pain as the first symptom. *Intern Med* 2004;43:873–7.
2. Santos E, Scolding NJ. Neurolymphomatosis mimicking neurosarcoidosis: a case report. *J Med Case Rep* 2010;4:5.

Coralie Humann
 Caroline Raymond, MD
 CHRU de Besançon
 Besançon, France
 Daniel Wendling, MD, PhD 
 Frank Verhoeven, MD, PhD 
 CHRU de Besançon
 and Franche-Comté University
 Besançon, France

BRIEF REPORT

The Prominent Role of Hematopoietic Peptidyl Arginine Deiminase 4 in Arthritis: Collagen- and Granulocyte Colony-Stimulating Factor–Induced Arthritis Model in C57BL/6 Mice

Shoichi Fukui,¹  Sarah Gutch,² Saeko Fukui,² Deya Cherpokova,¹ Karen Aymonnier,¹ Casey E. Sheehy,² Long Chu,² and Denisa D. Wagner¹

Objective. Genome-wide association studies have connected *PADI4*, encoding peptidylarginine deiminase 4 (PAD4), with rheumatoid arthritis (RA). PAD4 promotes neutrophil extracellular trap (NET) formation. This study was undertaken to investigate the origin of PAD4 and the importance of NET formation in a C57BL/6 mouse model of arthritis.

Methods. To permit the effective use of C57BL/6 mice in the collagen-induced arthritis (CIA) model, we introduced the administration of granulocyte colony-stimulating factor (G-CSF) for 4 consecutive days in conjunction with the booster immunization on day 21. Mice with global *Padi4* deficiency (*Padi4*^{−/−}) and mice with hematopoietic lineage-specific *Padi4* deficiency (*Padi4*^{Vav1Cre/+}) were evaluated in the model.

Results. G-CSF significantly increased the incidence and severity of CIA. G-CSF–treated mice showed elevated citrullinated histone H3 (Cit-H3) levels in plasma, while vehicle-treated mice did not. Immunofluorescence microscopy revealed deposition of Cit-H3 in synovial tissue in G-CSF–treated mice. *Padi4*^{−/−} mice developed less severe arthritis and had lower levels of serum interleukin-6 and plasma Cit-H3, lower levels of Cit-H4 in synovial tissue, and less bone erosion on micro-computed tomography than *Padi4*^{+/+} mice in the G-CSF–modified CIA model. Similarly, *Padi4*^{Vav1Cre/+} mice developed less severe arthritis, compared with *Padi4*^{fl/fl} mice, and presented the same phenotype as *Padi4*^{−/−} mice.

Conclusion. We succeeded in developing an arthritis model suitable for use in C57BL/6 mice that is fully compliant with high animal welfare standards. We observed a >90% incidence of arthritis in male mice and detectable NET markers. This model, with some features consistent with human RA, demonstrates that hematopoietic PAD4 is an important contributor to arthritis development and may prove useful in future RA research.

INTRODUCTION

Rheumatoid arthritis (RA) is a chronic systemic inflammatory autoimmune disorder characterized by persistent joint inflammation resulting in cartilage and bone damage, disability, and systemic complications. One hallmark of RA is the presence of autoantibodies to citrullinated proteins. A genome-wide association study (GWAS) of RA patients demonstrated an association with *PADI4*, which encodes peptidylarginine deiminase 4 (PAD4) (1).

PAD4 is an enzyme that converts positively charged arginine to neutral citrulline and thus modifies immunologic epitopes and protein function. PAD4 plays a role in releasing neutrophil extracellular traps (NETs) by citrullinating histones, which leads to the decondensation of chromatin (2).

Padi4 deficiency alleviates arthritis and autoantibody production in inflammatory arthritis induced in mice overexpressing tumor necrosis factor (3), collagen-induced arthritis (CIA) in DBA/1 mice (4) and glucose-6-phosphate isomerase–induced arthritis in DBA/1 mice (5). However, *Padi4*-deficient mice in the

Dr. Shoichi Fukui's work was supported by a Grant-in-Aid for Japan Society for the Promotion of Science Fellows and by the Uehara Memorial Foundation. Dr. Wagner's work was supported by a grant from the NIH (National Heart, Lung, and Blood Institute grant R35-HL-135765).

¹Shoichi Fukui, MD, PhD, Deya Cherpokova, PhD, Karen Aymonnier, PhD, Denisa D. Wagner, PhD: Boston Children's Hospital and Harvard Medical School, Boston, Massachusetts; ²Sarah Gutch, BS, Saeko Fukui, MD, Casey E. Sheehy, BS, Long Chu, BS: Boston Children's Hospital, Boston, Massachusetts.

Author disclosures are available at <https://onlinelibrary.wiley.com/action/downloadSupplement?doi=10.1002%2Fart.42093&file=art42093-sup-0001-Disclosureform.pdf>.

Address correspondence to Denisa D. Wagner, PhD, 1 Blackfan Circle, 9th Floor, Boston, MA 02115. Email: denisa.wagner@childrens.harvard.edu.

Submitted for publication August 26, 2021; accepted in revised form February 9, 2022.

K/BxN serum-transfer model of arthritis showed an absence of NETs, but did not demonstrate an amelioration of arthritis *in vivo* (6). These inconsistent results suggest that the effect of *Padi4* may depend on the particular murine model, more specifically whether NET-dependent or NET-independent pathways are essential. Thus, further evaluation of the contribution of *Padi4* to murine arthritis is needed in a manner that meets current animal welfare criteria.

We hypothesized that the effects of *Padi4* observed in the mouse model of CIA are dependent on NETs, and more specifically hematopoietic cell-associated *Padi4*. Because we had *Padi4*-deficient mice on a C57BL/6 background, we aimed to induce CIA in that strain. However, susceptibility to CIA is linked to specific major histocompatibility complex class II genes (7), and the C57BL/6 mouse strain is not highly susceptible to CIA. Despite attempts to improve the protocol, CIA in C57BL/6 mice is associated with a lower disease incidence and severity and more variability than seen in more susceptible mouse strains such as DBA/1 (8). Additionally, concerns regarding animal welfare, including pain and distress in mice, made it impossible for us to use the original CIA protocol (9). Specifically, the use of Freund's complete adjuvant (CFA) including heat-killed *Mycobacterium tuberculosis* in the booster immunization is not allowed in most institutions (7). Therefore, we sought to develop a novel murine arthritis model on the C57BL/6 background to address our hypothesis using 2 strains of genetically engineered mice.

MATERIALS AND METHODS

Animals. Wild-type C57BL/6 mice were bred in house. *Padi4*^{-/-} mice were originally generated by Y. Wang (10) and backcrossed with C57BL/6J mice. They were bred in house, and littermates were derived from heterozygous-by-heterozygous crosses. *Padi4*^{fl/fl} mice (stock no. 026708), previously described by Hemmers et al (11), and *Vav1-iCre* mice (stock no. 008610) were purchased from The Jackson Laboratory and intercrossed to generate mice lacking *Padi4* in the hematopoietic lineage (*Padi4*^{Vav1Cre/+}) following a female Cre+ (carrier) and male Cre- (noncarrier) breeding strategy recommended by Joseph et al (12). The abrogated *Padi4* expression in *Padi4*^{Vav1Cre/+} mouse neutrophils was confirmed in our previous study (13). All mice were housed in the animal facility of Boston Children's Hospital and were kept free from specific pathogens. Experimental protocols were approved by the Institutional Animal Care and Use Committee of Boston Children's Hospital (protocol number 20-01-4096R).

Induction and evaluation of CIA. Male mice ages 8–12 weeks were immunized with an emulsion of CFA (catalog no. 7023; Chondrex) and 100 µg of chicken type II collagen (catalog no. 20012; Chondrex) in a 1:1 mixture (total 100 µl) injected

intradermally into the base of the tail on day 0. On day 21, a booster immunization of type II collagen with Freund's incomplete adjuvant (IFA) (catalog no. 7002; Chondrex) was administered intradermally at a site proximal to the first injection site. The severity of arthritis was evaluated using the following clinical scoring system for each limb: 0 = normal; 1 = swelling in 1 digit; 2 = swelling in >1 digit or wrist or ankle joint; 3 = swelling in the entire paw; and 4 = deformity and/or ankylosis. The maximum score was 16 per mouse. Two evaluators (one who knew the group allocation and one who did not) independently scored arthritis severity and arrived at an agreement on final scores.

Administration of granulocyte colony-stimulating factor (G-CSF). Recombinant human G-CSF (filgrastim [Neupogen]; Amgen) was injected at 10 µg peritoneally once daily from day 20 to day 23. Sterile saline was used as the vehicle control.

Immunofluorescence microscopy. Sections were fixed in zinc fixative (100 mmoles/liter Tris HCl, 37 mmoles/liter zinc chloride, 23 mmoles/liter zinc acetate, and 3.2 mmoles/liter calcium acetate), permeabilized with 0.1% Triton X and 0.1% sodium citrate for 10 minutes at 4°C, blocked with 3% bovine serum albumin in phosphate buffered saline with 0.05% Tween 20 for 1 hour at room temperature, and incubated with primary antibodies against Cit-H3 (1:1,000) (catalog no. ab5103; Abcam) and Ly6G (1:500) (catalog no. 551459; BD PharMingen) overnight at 4°C. After washes, the sections were incubated with appropriate Alexa Fluor-conjugated secondary antibodies (1:1,500) (catalog no. A-21206 [Alexa Fluor 488-conjugated anti-rabbit] and catalog no. A-21434 [Alexa Fluor 555-conjugated anti-rat]; Life Technologies) for 2 hours at room temperature. Hoechst 33342 (1:10,000) (catalog no. H3570; Invitrogen) was used to counterstain DNA. Images were obtained with a Zeiss Axiovert 200M wide-field fluorescence microscope with Zeiss AxioVision software.

Statistical analysis. Data are presented as the median and interquartile range for quantitative variables. We assessed the association between quantitative variables using Wilcoxon's rank sum test. For evaluation of the changes in plasma double-stranded DNA (dsDNA) and Cit-H3 levels, we used Wilcoxon's signed rank test. The cumulative incidence of arthritis was estimated using the Kaplan-Meier method and log rank test. Bonferroni correction was used for multiple comparisons. All tests were 2-sided, and *P* values less than 0.05 were considered significant. All statistical analyses were performed using GraphPad Prism software, version 7.0.

See the Supplementary Methods, available on the *Arthritis & Rheumatology* website at <http://onlinelibrary.wiley.com/doi/10.1002/art.42093>, for details on enzyme-linked immunosorbent assay (ELISA), dsDNA measurement, micro-computed tomography (micro-CT), histologic evaluation, and immunoblotting.

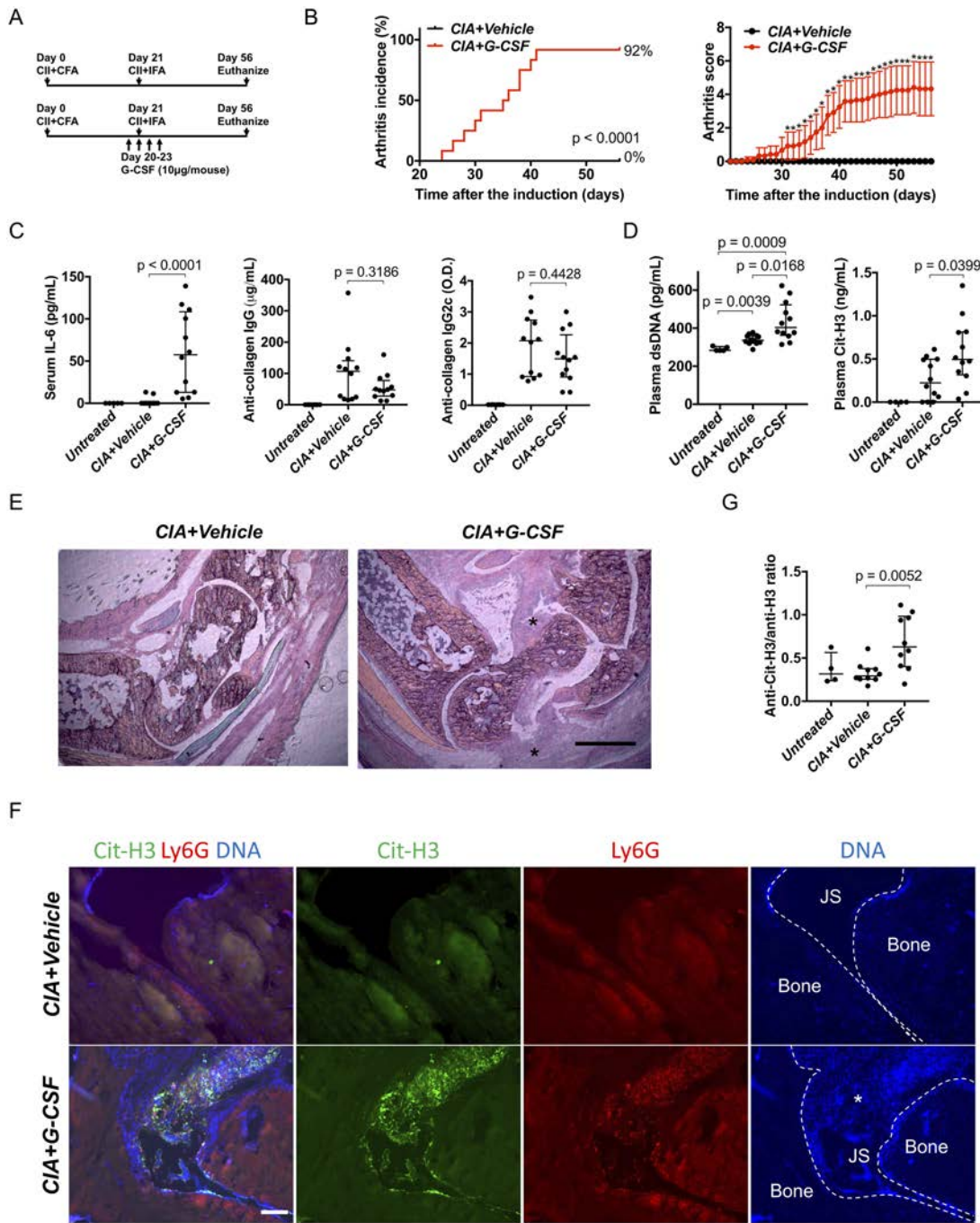


Figure 1. Exacerbation of collagen-induced arthritis (CIA) in C57BL/6 mice after addition of an injection of granulocyte colony-stimulating factor (G-CSF). **A**, Schedule of injection with type II collagen (CII) and Freund’s complete adjuvant (CFA) and type II collagen and Freund’s incomplete adjuvant (IFA). **B**, Arthritis incidence and severity in mice with CIA treated with vehicle and mice with CIA treated with G-CSF (n = 12 per group). For arthritis severity, values are the mean and 95% confidence interval. * = P < 0.05 by Wilcoxon’s rank sum test. **C** and **D**, Serum levels of interleukin-6 (IL-6), anti-collagen IgG antibody, and anti-collagen IgG2c antibody on day 56 (**C**) and plasma levels of double-stranded DNA (dsDNA) and citrullinated histone H3 (Cit-H3) on day 22 (**D**). Circles represent individual mice (n = 12 per group); horizontal lines and error bars show the median and interquartile range (IQR). **E**, Representative images of hematoxylin and eosin staining of mouse ankle joints. **Asterisks** indicate expansion of synovial tissue. Bar = 500 µm. **F**, Representative images of immunostaining for Cit-H3 and Ly6G in mouse ankle joints. **Asterisk** indicates synovial tissue. **JS** = joint space. Bar = 100 µm. **G**, Ratio of anti-Cit-H3 antibody to anti-native H3 antibody, calculated from enzyme-linked immunosorbent assay optical density values. Circles represent individual mice (n = 4 untreated mice; n = 10 mice with CIA treated with vehicle, and n = 10 mice with CIA treated with G-CSF); horizontal lines and error bars show the median and IQR.

RESULTS

We tested the CIA model in C57BL/6 mice. In the original protocol, induction of CIA in C57BL/6 mice required 2 injections of an emulsion of type II collagen and CFA (9). However, the use of the second injection of CFA is not allowed in most institutions (7), including Boston Children's Hospital, because of the pain and distress caused to mice. Therefore, we used 1 injection of type II collagen with CFA on day 0 and 1 injection of type II collagen with IFA on day 21 (Figure 1A). Previous studies using this protocol demonstrated an arthritis incidence of 0% (14) to 50–80% (15). In our study, no wild-type mice subjected to this protocol developed arthritis (data not shown). We hypothesized that priming neutrophils with G-CSF would induce arthritis because G-CSF primes neutrophils to induce NETs (16) and exacerbates CIA in DBA/1 mice (17). We administered G-CSF daily for 4 consecutive days beginning 1 day before the second type II collagen injection (Figure 1A). Eleven of 12 G-CSF-treated mice developed arthritis, while none of the vehicle-treated mice developed arthritis (Figure 1B). Mice treated with G-CSF only did not develop arthritis (data not shown).

G-CSF increased the neutrophil count in peripheral blood ~2-fold (Supplementary Figure 1A, available on the *Arthritis & Rheumatology* website at <http://onlinelibrary.wiley.com/doi/10.1002/art.42093>). G-CSF-treated mice showed higher serum levels of interleukin-6 (IL-6) on day 56 compared with vehicle-treated mice (Figure 1C). Because C57BL/6 mice produce IgG2c antibodies instead of IgG2a antibodies (9), we measured serum anti-type II collagen IgG2c antibodies along with anti-type II collagen IgG antibodies; there were no differences between vehicle-treated and G-CSF-treated mice (Figure 1C). We measured plasma levels of dsDNA and citrullinated histone H3 (Cit-H3) as NET biomarkers on day 22. G-CSF-treated mice showed higher plasma levels of NET markers than vehicle-treated mice (Figure 1D).

When evaluated histopathologically (by hematoxylin and eosin [H&E] staining), G-CSF-treated mice showed expansion of synovial tissue in the joint space, while vehicle-treated mice exhibited no such expansion (Figure 1E). Immunofluorescence microscopy revealed lesions positive for Cit-H3 and Ly6G (a mouse neutrophil marker) with DNA within the joint space and on the joint surface in G-CSF-treated mice (Figure 1F). In contrast, vehicle-treated mice showed no lesion with Cit-H3, Ly6G, and DNA. Finally, we sought to detect serum anti-Cit-H3 antibodies, which are one type of anti-citrullinated protein antibody (ACPA) present in the sera of RA patients (18). ELISA detected anti-native H3 antibodies and anti-Cit-H3 antibodies in serum in both G-CSF-treated and vehicle-treated mice (Supplementary Figure 1B). When the relative value of anti-Cit-H3 antibody to anti-native H3 antibody was calculated, G-CSF-treated mice showed a significantly higher ratio of anti-Cit-H3 antibody to anti-native H3 antibody than vehicle-treated mice (Figure 1G).

Based on data showing the enrichment of citrullinated histones, we sought to investigate the contribution of PAD4 in the process. We induced arthritis in littermate *Padi4*^{+/+} and *Padi4*^{-/-} mice using the G-CSF-modified CIA model (Figure 2A). *Padi4* deficiency reduced arthritis incidence and severity (Figure 2B). *Padi4*^{-/-} mice had reduced serum IL-6 and anti-type II collagen IgG antibody levels on day 56, but similar anti-type II collagen IgG2c antibody levels, compared with *Padi4*^{+/+} mice (Figure 2C). *Padi4*^{-/-} mice showed less of an increase in plasma dsDNA and Cit-H3 levels from day 20 to day 22 than *Padi4*^{+/+} mice (Figure 2D). When evaluated by micro-CT, fewer areas of eroded bone surface were observed in *Padi4*^{-/-} mice (Figure 2E). H&E staining of mouse ankle joints (exudate and infiltrate) revealed that *Padi4*^{-/-} mice had a less severe arthritis phenotype than *Padi4*^{+/+} mice (Figure 2F). Immunofluorescence microscopy revealed lesions positive for Cit-H3 and Ly6G, and DNA within the joint space and on the bone surface, in *Padi4*^{+/+} mice but not in *Padi4*^{-/-} mice (Figure 2G). Synovial tissue from *Padi4*^{-/-} mice contained lower levels of myeloperoxidase (MPO) and Cit-H4 compared with that from *Padi4*^{+/+} mice (Figure 2H). *Padi4*^{-/-} mice also demonstrated a significantly lower ratio of anti-Cit-H3 antibody to anti-native H3 antibody compared with *Padi4*^{+/+} mice (Figure 2I and Supplementary Figure 1C).

Fibroblasts are the main constituents of RA synovial tissue, and their origins possibly consist of resident fibroblasts, pericytes, and mesenchymal stem cells (19). Because fibroblast-like synoviocytes from RA patients express PAD4 (20), the origin of PAD4 is of interest. To address this issue, we used hematopoietic lineage-specific *Padi4*-knockout mice (*Padi4*^{Vav1Cre/+}) in the G-CSF-modified CIA model. We confirmed that organ expression of *Padi4* RNA was comparable in *Padi4*^{Vav1Cre/+} mice and *Padi4*^{fl/fl} mice (Supplementary Figure 2A, available on the *Arthritis & Rheumatology* website at <http://onlinelibrary.wiley.com/doi/10.1002/art.42093>). Additionally, we confirmed *Padi4* protein expression in peripheral blood and the absence of *Padi4* protein expression in endothelial cells of the aorta (Supplementary Figure 2B) because *Vav1-iCre* is expressed in endothelial cells (12).

Padi4^{Vav1Cre/+} mice had reduced arthritis incidence and severity compared with littermate *Padi4*^{fl/fl} mice (Figure 3A). *Padi4*^{Vav1Cre/+} mice had reduced serum levels of IL-6; however, they had serum levels of anti-type II collagen IgG antibody and anti-type II collagen IgG2c antibody comparable to those in *Padi4*^{fl/fl} mice on day 56 (Figure 3B). An increase in plasma dsDNA and Cit-H3 from day 20 to day 22 was detected in *Padi4*^{fl/fl} mice but not in *Padi4*^{Vav1Cre/+} mice (Figure 3C). *Padi4*^{Vav1Cre/+} mice showed fewer areas of eroded bone surface on micro-CT compared with *Padi4*^{fl/fl} mice (Figure 3D). Immunofluorescence microscopy revealed lesions positive for Cit-H3 and Ly6G, and DNA within the joint space and on the bone surface, in *Padi4*^{fl/fl} mice but not in *Padi4*^{Vav1Cre/+} mice (Figure 3E).

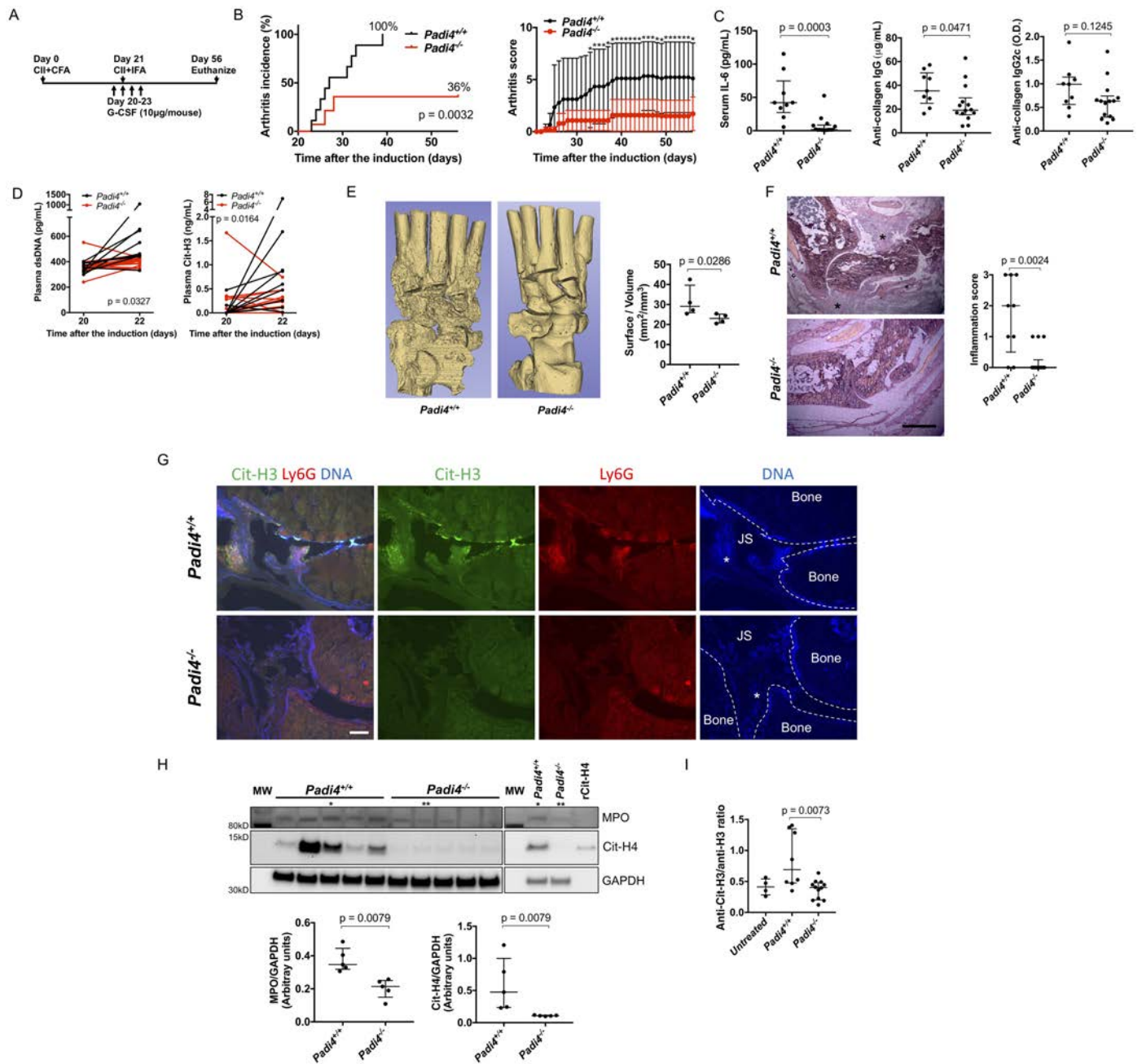


Figure 2. Comparison of the effects of the G-CSF-modified CIA model on *Padi4*^{+/+} mice and littermate *Padi4*^{-/-} mice. **A**, Injection schedule. **B**, Arthritis incidence and severity in *Padi4*^{+/+} mice (n = 9) and *Padi4*^{-/-} mice (n = 14). For arthritis severity, values are the mean and 95% confidence interval. * = *P* < 0.05 by Wilcoxon’s rank sum test. **C**, Serum levels of IL-6, anti-collagen IgG antibody, and anti-collagen IgG2c antibody on day 56. **D**, Change in plasma levels of dsDNA and Cit-H3 from day 20 to day 22 in *Padi4*^{+/+} mice (n = 9) and *Padi4*^{-/-} mice (n = 14). *P* values were determined by Wilcoxon’s signed rank test. **E**, Representative micro-computed tomography images of the mouse ankle joints (left) and quantification of eroded joint surface (right). **F**, Representative images of hematoxylin and eosin staining of mouse ankle joints (left) and inflammation score on a scale of 0 (no inflammation) to 3 (severely inflamed joint), determined by the number of inflammatory cells in the synovial cavity (exudate) and synovial tissue (infiltrate). **Asterisks** indicate proliferated synovial tissue. Bar = 500 µm. **G**, Representative images of immunostaining for Cit-H3 and Ly6G in mouse ankle joints. **Asterisks** indicate synovial tissue. Bar = 100 µm. **H**, Blot (top) and quantification by densitometry (bottom) of myeloperoxidase (MPO), Cit-H4, and GAPDH levels in synovial tissue from *Padi4*^{+/+} mice and *Padi4*^{-/-} mice. Recombinant Cit-H4 (rCit-H4) was used as a positive control. Values are the expression relative to GAPDH. Single and double asterisks indicate the same samples, respectively. **I**, Ratio of anti-Cit-H3 antibody to anti-native H3 antibody, calculated from enzyme-linked immunosorbent assay optical density values, in *Padi4*^{+/+} mice and *Padi4*^{-/-} mice. In **C**, **E**, **F**, **H**, and **I**, circles represent individual mice (n = 9 *Padi4*^{+/+} mice and n = 14 *Padi4*^{-/-} mice in **C** and **F**; n = 4 per group in **E**; n = 5 per group in **H**; and n = 4 untreated mice, 8 *Padi4*^{+/+} mice, and 12 *Padi4*^{-/-} mice in **I**); horizontal lines and error bars show the median and IQR. See Figure 1 for other definitions.

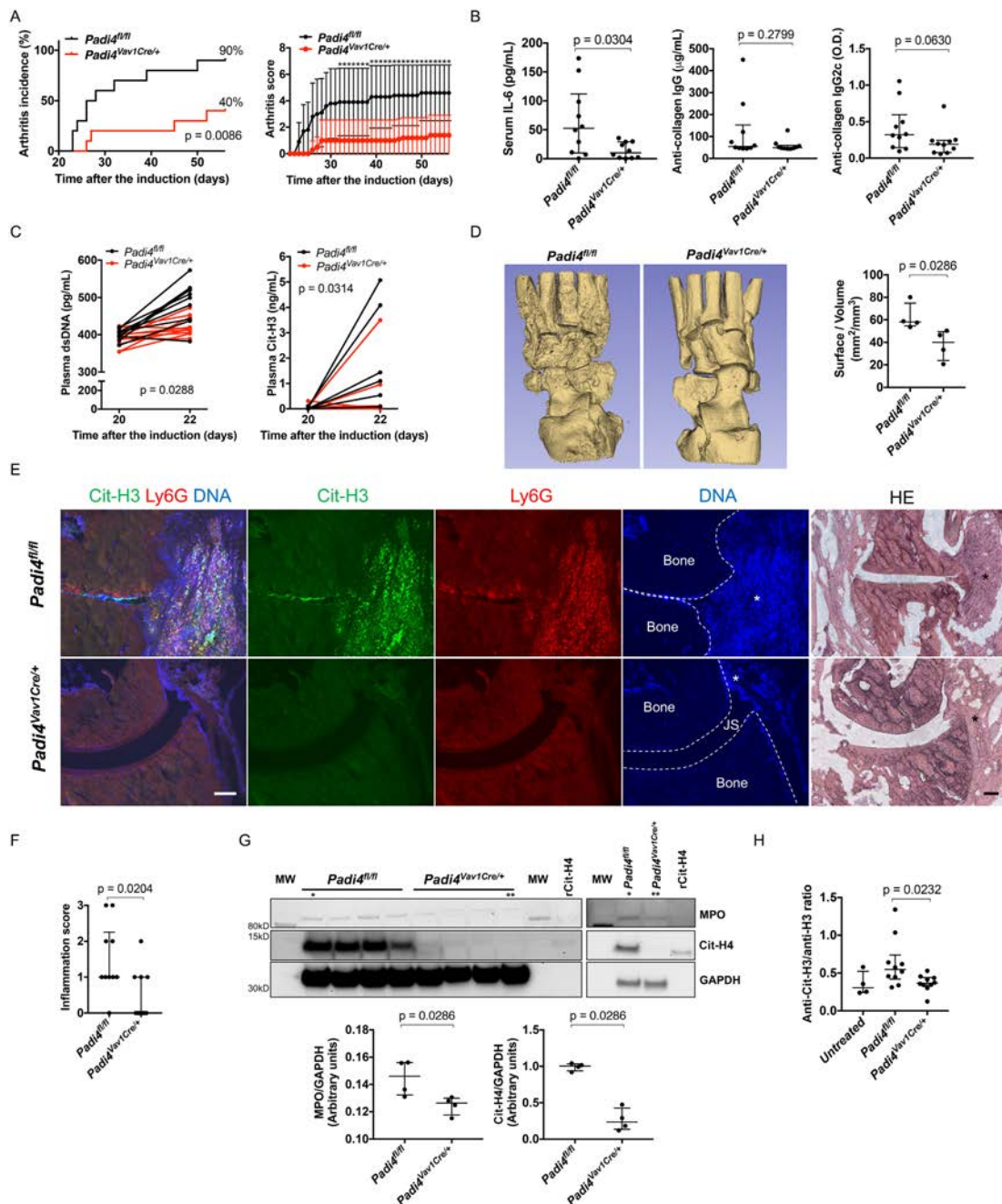


Figure 3. Comparison of the effects of the G-CSF-modified CIA model on *Padi4^{fl/fl}* mice and littermate *Padi4^{Vav1Cre/+}* mice. **A**, Arthritis incidence and severity in *Padi4^{fl/fl}* mice ($n = 10$) and *Padi4^{Vav1Cre/+}* mice ($n = 10$) treated according to the schedule shown in Figure 2A. For arthritis severity, values are the mean and 95% confidence interval. * = $P < 0.05$ by Wilcoxon's rank sum test. **B**, Serum levels of IL-6, anti-collagen IgG antibody, and anti-collagen IgG2c antibody on day 56. **C**, Change in plasma levels of dsDNA and Cit-H3 from day 20 to day 22 in *Padi4^{fl/fl}* mice ($n = 10$) and *Padi4^{Vav1Cre/+}* mice ($n = 10$). P values were determined by Wilcoxon's signed rank test. **D**, Representative micro-computed tomography images of the mouse ankle joints (left) and quantification of eroded joint surface (right). **E**, Representative images of immunostaining for Cit-H3 and Ly6G, and hematoxylin and eosin (H&E) staining, in mouse ankle joints. Asterisks indicate proliferated synovial tissue. Bars = 100 μ m. **F**, Inflammation score on a scale of 0 (no inflammation) to 3 (severely inflamed joint), determined by the number of inflammatory cells in the synovial cavity (exudate) and synovial tissue (infiltrate). **G**, Blot (top) and quantification by densitometry (bottom) of myeloperoxidase (MPO), Cit-H4, and GAPDH levels in synovial tissue from *Padi4^{fl/fl}* and *Padi4^{Vav1Cre/+}* mice. Recombinant Cit-H4 (rCit-H4) was used as a positive control. Values are the expression relative to GAPDH. Single and double asterisks indicate the same samples, respectively. **H**, Ratio of anti-Cit-H3 antibody to anti-native H3 antibody, calculated from enzyme-linked immunosorbent assay optical density values, in *Padi4^{fl/fl}* mice and *Padi4^{Vav1Cre/+}* mice. In **B**, **D**, and **F–H**, circles represent individual mice ($n = 10$ per group in **B** and **F**; $n = 4$ per group in **D** and **G**; and $n = 4$ untreated mice, 10 *Padi4^{fl/fl}* mice, and 10 *Padi4^{Vav1Cre/+}* mice in **H**); bars show the median and IQR. See Figure 1 for other definitions.

Padi4^{Vav1Cre/+} mice showed reduced inflammation of joint tissue, which was significant when semiquantified (Figure 3F). Synovial tissue from *Padi4*^{Vav1Cre/+} mice contained lower levels of MPO and Cit-H4 compared with that from *Padi4*^{fl/fl} mice (Figure 3G). *Padi4*^{Vav1Cre/+} mice also displayed a lower ratio of anti-Cit-H3 antibody to anti-native H3 antibody compared with *Padi4*^{fl/fl} mice (Figure 3H and Supplementary Figure 1D).

DISCUSSION

There are conflicting data on the susceptibility of C57BL/6 mice to CIA, ranging from no incidence (14) and less severity (21) to 50–80% incidence with mild severity (15). Even with the use of the well-known protocol, authors have described variability in results (15). Pepsin used to prepare homemade collagen has been reported to be strongly immunogenic and essential for arthritis development (8). This finding may be one of the reasons for the variability in incidence and severity observed in the model.

The G-CSF-modified CIA model demonstrated reliably high arthritis incidence (90–100%) and severity suitable to compare different treatment groups. This model is considerate of animal welfare and acceptable to Institutional Animal Care and Use Committees. Additionally, in contrast to the previously described protocol for inducing CIA in C57BL/6 mice using homemade collagen (15), our protocol uses commercially available collagen.

The presence of anti-type II collagen antibody is thought to correlate with the development of arthritis (7). However, G-CSF-treated mice presented levels of anti-type II collagen IgG and IgG2c comparable with those in vehicle-treated mice. This finding suggests that the production of anti-type II collagen IgG is not sufficient for the development of arthritis in G-CSF-modified CIA, and other factors induced by G-CSF must be important.

Our G-CSF-modified CIA model has interesting features. The detection of Cit-H4 in synovial tissue is consistent with the detection of Cit-H4 bound to ACPAs in RA synovial fluid (22). Additionally, serum anti-Cit-H3 antibody mimics RA, as it is detected in RA patients (18). NETs are the likely origin of the citrullinated proteins in RA (23). These features are helpful for studying the relationship between citrullinated antigens and autoantibodies in RA.

The importance of G-CSF in arthritis has been shown in both clinical and basic studies. There are several case reports of G-CSF exacerbating RA (24), and a clinical study has demonstrated RA flares after filgrastim (G-CSF) administration (25). In a mouse study, injection of G-CSF exacerbated the severity of CIA in DBA/1 mice (17). Our results indicating that G-CSF-modified CIA causes arthritis accompanied with NET biomarkers in plasma and synovial tissue represent a novel insight into the possible mechanism of the effects of G-CSF on arthritis, as well as the effects of G-CSF on neutrophil elevation. We showed that G-CSF exerts its effects primarily through PAD4, as evidenced

by the fact that *Padi4*^{-/-} mice and *Padi4*^{Vav1Cre/+} mice were significantly protected against G-CSF-modified CIA. G-CSF might promote neutrophil priming for NET formation, and PAD4-dependent NETs could act as an adjuvant in arthritis. The remaining arthritis-enhancing effect of G-CSF may be on blood cells other than neutrophils, other citrullinating enzymes, or noncitrullination processes.

This study has some limitations. We need to consider the influence of *Padi4* expressed not only in neutrophils, but also in monocytes and macrophages in the pathogenesis of this model. Additionally, in our study, most sera from mice reacted more strongly with native H3 peptides than with Cit-H3 peptides, although ACPAs bind the citrullinated peptides much more strongly than the native peptides in RA patients. Therefore, the anti-Cit-H3 antibody played only a limited pathologic role in this study, and controversies regarding the detection of ACPAs in mouse models of arthritis (26) should be considered. Although our G-CSF-modified CIA model has some features seen in human RA, we need to be aware of the differences between human RA and this model. Another limitation is that we used only male mice in this study, whereas RA is seen predominantly in females. In a preliminary study, we found an arthritis incidence of 60% in female mice in this model (Supplementary Figure 3, available on the *Arthritis & Rheumatology* website at <http://onlinelibrary.wiley.com/doi/10.1002/art.42093>); thus, it is likely the model could be adapted for use in female mice in the future.

In conclusion, we have demonstrated that G-CSF administration around the time of the booster collagen immunization significantly improves the CIA model in C57BL/6 mice, resulting in a ≥90% incidence of arthritis, accompanied by markers of NET formation in plasma and synovial tissue. Importantly, this model addresses previous concerns regarding animal welfare. Finally, we determined that hematopoietic cell-associated PAD4 promotes arthritis development in the G-CSF-modified CIA model. This model may prove to be of value in future RA research and the development of drugs targeting this disease.

ACKNOWLEDGMENTS

We thank Dr. Bruce Ewenstein for critical reading of the manuscript and Ms. Kristen Douthit for language editing and proofreading.

AUTHOR CONTRIBUTIONS

All authors were involved in drafting the article or revising it critically for important intellectual content, and all authors approved the final version to be published. Dr. Shoichi Fukui had full access to all of the data in the study and takes responsibility for the integrity of the data and the accuracy of the data analysis.

Study conception and design. Shoichi Fukui, Wagner.





Acquisition of data. Shoichi Fukui, Gutch, Saeko Fukui, Cherpokova, Aymonnier, Sheehy, Chu.

Analysis and interpretation of data. Shoichi Fukui, Gutch, Saeko Fukui, Cherpokova, Aymonnier, Sheehy, Chu, Wagner.

REFERENCES

1. Suzuki A, Yamada R, Chang X, Tokuhiro S, Sawada T, Suzuki M, et al. Functional haplotypes of PAD4, encoding citrullinating enzyme peptidylarginine deiminase 4, are associated with rheumatoid arthritis. *Nat Genet* 2003;34:395–402.
2. Wang Y, Li M, Stadler S, Correll S, Li P, Wang D, et al. Histone hypercitrullination mediates chromatin decondensation and neutrophil extracellular trap formation. *J Cell Biol* 2009;184:205–13.
3. Shelef MA, Sokolove J, Lahey LJ, Wagner CA, Sackmann EK, Warner TF, et al. Peptidylarginine deiminase 4 contributes to tumor necrosis factor α -induced inflammatory arthritis. *Arthritis Rheumatol* 2014;66:1482–91.
4. Suzuki A, Kochi Y, Shoda H, Seri Y, Fujio K, Sawada T, et al. Decreased severity of experimental autoimmune arthritis in peptidylarginine deiminase type 4 knockout mice. *BMC Musculoskelet Disord* 2016;17:205.
5. Seri Y, Shoda H, Suzuki A, Matsumoto I, Sumida T, Fujio K, et al. Peptidylarginine deiminase type 4 deficiency reduced arthritis severity in a glucose-6-phosphate isomerase-induced arthritis model. *Sci Rep* 2015;5:13041.
6. Rohrbach AS, Hemmers S, Arandjelovic S, Corr M, Mowen KA. PAD4 is not essential for disease in the K/BxN murine autoantibody-mediated model of arthritis. *Arthritis Res Ther* 2012;14:R104.
7. Brand DD, Latham KA, Rosloniec EF. Collagen-induced arthritis. *Nat Protoc* 2007;2:1269–75.
8. Bäcklund J, Li C, Jansson E, Carlsen S, Merky P, Nandakumar KS, et al. C57BL/6 mice need MHC class II Aq to develop collagen-induced arthritis dependent on autoreactive T cells. *Ann Rheum Dis* 2013;72:1225–32.
9. Campbell IK, Hamilton JA, Wicks IP. Collagen-induced arthritis in C57BL/6 (H-2b) mice: new insights into an important disease model of rheumatoid arthritis. *Eur J Immunol* 2000;30:1568–75.
10. Li P, Li M, Lindberg MR, Kennett MJ, Xiong N, Wang Y. PAD4 is essential for antibacterial innate immunity mediated by neutrophil extracellular traps. *J Exp Med* 2010;207:1853–62.
11. Hemmers S, Tejaro JR, Arandjelovic S, Mowen KA. PAD4-mediated neutrophil extracellular trap formation is not required for immunity against influenza infection. *PLoS One* 2011;6:e22043.
12. Joseph C, Quach JM, Walkley CR, Lane SW, Lo Celso C, Purton LE. Deciphering hematopoietic stem cells in their niches: a critical appraisal of genetic models, lineage tracing, and imaging strategies [review]. *Cell Stem Cell* 2013;13:520–33.
13. Münzer P, Negro R, Fukui S, di Meglio L, Aymonnier K, Chu L, et al. NLRP3 inflammasome assembly in neutrophils is supported by PAD4 and promotes NETosis under sterile conditions. *Front Immunol* 2021;12:1–16.
14. Stevanin M, Busso N, Chobaz V, Pigni M, Ghassem-Zadeh S, Zhang L, et al. CD11b regulates the Treg/Th17 balance in murine arthritis via IL-6. *Eur J Immunol* 2017;47:637–45.
15. Inglis JJ, Simelyte E, McCann FE, Criado G, Williams RO. Protocol for the induction of arthritis in C57BL/6 mice. *Nat Protoc* 2008;3:612–8.
16. Demers M, Wong SL, Martinod K, Gallant M, Cabral JE, Wang Y, et al. Priming of neutrophils toward NETosis promotes tumor growth. *Oncoimmunology* 2016;5:1–9.
17. Campbell IK, Rich MJ, Bischof RJ, Hamilton JA. The colony-stimulating factors and collagen-induced arthritis: exacerbation of disease by M-CSF and G-CSF and requirement for endogenous M-CSF. *J Leukoc Biol* 2000;68:144–50.
18. Janssen KM, de Smit MJ, Withaar C, Brouwer E, van Winkelhoff AJ, Vissink A, et al. Autoantibodies against citrullinated histone H3 in rheumatoid arthritis and periodontitis patients. *J Clin Periodontol* 2017;44:577–84.
19. Matsuo Y, Saito T, Yamamoto A, Kohsaka H. Origins of fibroblasts in rheumatoid synovial tissues: implications from organ fibrotic models. *Mod Rheumatol* 2018;28:579–82.
20. Sorice M, Iannuccelli C, Manganelli V, Capozzi A, Alessandri C, Lococo E, et al. Autophagy generates citrullinated peptides in human synoviocytes: a possible trigger for anti-citrullinated peptide antibodies. *Rheumatology (Oxford)* 2016;55:1374–85.
21. Svendsen P, Etzerodt A, Deleuran BW, Moestrup SK. Mouse CD163 deficiency strongly enhances experimental collagen-induced arthritis. *Sci Rep* 2020;10:1–12.
22. Meng X, Ezzati P, Smolik I, Bernstein CN, Hitchon CA, El-Gabalawy HS. Characterization of autoantigens targeted by anti-citrullinated protein antibodies in vivo: prominent role for epitopes derived from histone 4 proteins. *PLoS One* 2016;11:1–14.
23. Khandpur R, Carmona-Rivera C, Vivekanandan-Giri A, Gizinski A, Yalavarthi S, Knight JS, et al. NETs are a source of citrullinated autoantigens and stimulate inflammatory responses in rheumatoid arthritis. *Sci Transl Med* 2013;5:178ra40.
24. Cornish AL, Campbell IK, McKenzie BS, Chatfield S, Wicks IP. G-CSF and GM-CSF as therapeutic targets in rheumatoid arthritis [review]. *Nat Rev Rheumatol* 2009;5:554–9.
25. Snowden JA, Biggs JC, Milliken ST, Fuller A, Staniforth D, Passuello F, et al. A randomised, blinded, placebo-controlled, dose escalation study of the tolerability and efficacy of filgrastim for haemopoietic stem cell mobilisation in patients with severe active rheumatoid arthritis. *Bone Marrow Transplant* 1998;22:1035–41.
26. Willis VC, Gizinski AM, Banda NK, Causey CP, Knuckley B, Cordova KN, et al. N- α -benzoyl-N5-(2-chloro-1-iminoethyl)-L-ornithine amide, a protein arginine deiminase inhibitor, reduces the severity of murine collagen-induced arthritis. *J Immunol* 2011;100:1620.

IgG Anti-Citrullinated Protein Antibody Variable Domain Glycosylation Increases Before the Onset of Rheumatoid Arthritis and Stabilizes Thereafter: A Cross-Sectional Study Encompassing ~1,500 Samples

Theresa Kissel,¹  Lise Hafkenscheid,² Tineke J. Wesemael,¹ Mami Tamai,³ Shin-ya Kawashiri,³ 
Atsushi Kawakami,³ Hani S. El-Gabalawy,⁴ Dirkjan van Schaardenburg,⁵ Solbritt Rantapää-Dahlqvist,⁶ 
Manfred Wuhler,¹ Annette H. M. van der Helm-van Mil,¹ Cornelia F. Allaart,¹ Diane van der Woude,¹
Hans U. Scherer,¹  Rene E. M. Toes,¹ and Tom W. J. Huizinga¹

Objective. The autoimmune response in rheumatoid arthritis (RA) is marked by the presence of anti-citrullinated protein antibodies (ACPAs). A notable feature of IgG ACPA is the abundant expression of *N*-linked glycans in the variable domain. However, the presence of ACPA variable domain glycosylation (VDG) across disease stages, and its response to therapy, are poorly described. To understand its dynamics, we investigated the abundance of IgG ACPA VDG in 1,498 samples from individuals in different clinical stages.

Methods. Using liquid chromatography, we analyzed IgG ACPA VDG profiles in 7 different cohorts from Japan, Canada, The Netherlands, and Sweden. We assessed 106 healthy individuals, 228 individuals with presymptomatic RA, 277 individuals with arthralgia, 307 patients with new-onset/early RA, and 117 RA patients after prespecified treatment regimens. Additionally, we measured VDG in 234 samples from patients with RA who did or did not achieve long-term drug-free remission (DFR) during up to 16 years follow-up.

Results. IgG ACPA VDG significantly increased ($P < 0.0001$) toward disease onset and was associated with ACPA levels and epitope spreading prior to diagnosis. A slight increase in VDG was observed in patients with established RA, with a moderate influence of treatment ($P = 0.007$). In patients in whom DFR was later achieved, IgG ACPA VDG was already reduced at the time of RA onset.

Conclusion. The abundance of IgG ACPA VDG increases toward RA onset and correlates with maturation of the ACPA response. While IgG ACPA VDG levels are fairly stable in established disease, a lower degree of VDG at RA onset correlates with DFR. Although the underlying biologic mechanisms remain elusive, our data support the concept that VDG relates to an expansion of the ACPA response in the pre-disease phase and contributes to disease development.

Supported by ReumaNederland (grants 17-1-402 and 08-1-34), the IMI funded project RTCure (777357), ZonMw TOP (grant 91214031), Target to BI (LSHM18055-5GF), the Swedish Research Council (VR 2017-00650), King Gustaf V's 80-Year Fund, King Gustaf V's and Queen Victoria's Fund, the Swedish Rheumatism Association, and the Canadian Institutes of Health Research MOP grant (77700). Dr. Scherer is recipient of an NWO-ZonMw clinical fellowship (90714509), an NWO-ZonMw VENI grant (91617107), an NWO-ZonMw VIDI grant (09150172010067), and a ZonMw Enabling Technology Hotels grant (435002030) and has received support from the Dutch Arthritis Foundation (15-2-402 and 18-1-205). Dr. Toes is recipient of a European Research Council (ERC) advanced grant (AdG2019-884796).

¹Theresa Kissel, MSc, Tineke J. Wesemael, MSc, Manfred Wuhler, PhD, Annette H. M. van der Helm-van Mil, MD, PhD, Cornelia F. Allaart, MD, PhD, Diane van der Woude, MD, PhD, Hans U. Scherer, MD, PhD, Rene E. M. Toes, PhD, Tom W. J. Huizinga, MD, PhD: Leiden University Medical Center, Leiden, The Netherlands; ²Lise Hafkenscheid, PhD: Leiden University Medical Center,

Leiden, The Netherlands, and Technical University of Denmark, Lyngby, Denmark; ³Mami Tamai, MD, PhD, Shin-ya Kawashiri, MD, PhD, Atsushi Kawakami, MD, PhD: Nagasaki University Graduate School of Biomedical Sciences, Nagasaki, Japan; ⁴Hani S. El-Gabalawy, MD: University of Manitoba, Winnipeg, Manitoba, Canada; ⁵Dirkjan van Schaardenburg, MD, PhD: Amsterdam Rheumatology and Immunology Center and Amsterdam Academic Medical Center, Amsterdam, The Netherlands; ⁶Solbritt Rantapää-Dahlqvist, MD, PhD: Umeå University, Umeå, Sweden.

Author disclosures are available at <https://onlinelibrary.wiley.com/action/downloadSupplement?doi=10.1002%2Fart.42098&file=art42098-sup-0001-Disclosureform.pdf>.

Address correspondence to Rene E. M. Toes, PhD, Leiden University Medical Center, Department of Rheumatology, Albansudreef 2, PO Box 9600, 2300 RC Leiden, The Netherlands. Email: R.E.M.Toes@lumc.nl.

Submitted for publication August 26, 2021; accepted in revised form February 15, 2022.

INTRODUCTION

Rheumatoid arthritis (RA) is a prevalent, slowly evolving autoimmune disease in which arthralgia is an important pre-disease manifestation. The autoimmune response that is the most specific for RA is characterized by the presence of anti-citrullinated protein antibodies (ACPAs), which can be present several years before the onset of clinical symptoms. ACPA-positive patients have a more severe disease course and are less likely to achieve drug-free remission (DFR) as compared to seronegative patients (1). ACPA responses are known to be dynamic during the transition toward RA, as an increase in ACPA levels combined with a broader epitope recognition profile is associated with the development of clinical symptoms (2). Autoantibody levels are, however, not associated with long-term treatment response and do not predict DFR (3).

Glycomic analysis has revealed that IgG ACPAs are abundantly glycosylated in their antigen-binding fragments, expressing complex-type variable domain glycans that are mainly disialylated and bisected (4). Variable domain glycosylation (VDG) on >90% of the autoantibodies is a notable characteristic of IgG ACPA and distinguishes the molecules from conventional IgG antibodies, which display, next to the conserved presence of glycans in the Fc region, a considerably lower VDG of ~12–14% (4,5). Glycosylation sites required for the attachment of variable domain glycans are introduced by somatic hypermutation (6).

Although the role and dynamics of IgG ACPA Fc glycans have been studied extensively (7–10), little is known about the expression levels or potential biologic implications of variable domain glycans on ACPA. As carbohydrates might encode important biologic information and possibly affect cellular functions, it is important to understand VDG dynamics over time in relation to the disease course of RA. Previously, we showed that IgG ACPA VDG can occur several years before RA onset. In a Canadian population, IgG ACPA VDG was predictive of disease development (11,12). However, how IgG ACPA VDG changes between clinical disease states from healthy, symptom-free individuals to individuals with arthralgia to patients at RA onset and with established RA has not been elucidated. Additionally, it is unclear whether VDG levels are associated with treatment outcomes, predict DFR and disease flares, or can be modified by treatment.

To understand the characteristics and action of variable domain glycans and thereby their possible contribution to autoreactive B cell responses in RA, we cross-sectionally investigated the presence and abundance of IgG ACPA VDG in 1,498 samples from an ethnically diverse group of individuals in various stages of disease (Table 1). By analyzing samples from a well-controlled treatment strategy trial (the Improved [Induction Therapy with Methotrexate and Prednisone in Rheumatoid or Very Early Arthritic Disease] study) that aimed to assess the most effective strategy for inducing remission in early RA (13), we investigated longitudinal changes in VDG in established RA after treatment

escalation or treatment tapering. Finally, we longitudinally analyzed IgG ACPA VDG changes in patients from the Leiden Early Arthritis Clinic (EAC) in whom sustained (>1 year) DFR (SDFR) was achieved and those who experienced late disease flares, with an extensive follow-up of up to 16 years (14).

PATIENTS AND METHODS

Study cohorts. IgG ACPA VDG was analyzed in 1,498 serum samples from individuals in different clinical disease stages including 121 ACPA-negative RA control samples. Descriptive data on the cohorts are presented in Table 1. Additionally, 247 healthy donor and 150 ACPA-positive RA control samples, obtained at the Leiden University Medical Center outpatient rheumatology clinic, were assessed to verify the methodology used. Details on patient and public involvement and ethical considerations in the recruitment of individuals and of the study cohorts are available in Supplementary Methods, on the *Arthritis & Rheumatology* website at <https://onlinelibrary.wiley.com/doi/10.1002/art.42098>.

Cohort 1, healthy, symptom free (Nagasaki, Japan). Cohort 1 consisted of healthy symptom-free individuals (n = 58) enrolled in the Nagasaki Island Study (a community-based prospective cohort study based on resident health examinations) (15) who tested positive for ACPA. The individuals included in the study cohort had no joint symptoms at the time of the most recent resident health examination. These individuals were followed up for a period of up to 3 years. Nine of them (15.5%) developed RA during follow-up.

Cohort 2, healthy and RA onset (Manitoba, Canada). Members of cohort 2 were part of the longitudinal research project Early Identification of Rheumatoid Arthritis in First Nations, based at the Arthritis Centre, the University of Manitoba (16). Forty-eight samples from healthy individuals (first-degree relatives of patients with RA) were included, as were paired samples obtained from 25 individuals prior to RA onset and in the absence of joint-symptoms, and at the time of diagnosis of clinically apparent RA.

Cohort 3, presymptomatic and after RA onset/early RA (Umeå, Sweden). Cohort 3 comprised 354 samples from the Northern Sweden Health and Disease Study or the Västerbotten Intervention Project. Blood samples were collected and stored in a biorepository (the Northern Sweden Medical Research Biobank). Individuals were considered to have RA if they fulfilled the 1987 American College of Rheumatology classification criteria (17). Two hundred twenty-eight individuals from the cohort were retrospectively identified as having donated blood before the onset of signs or symptoms of joint disease (defined as presymptomatic), with a median time from blood sampling to onset of signs/symptoms of 4.7 years (interquartile range [IQR] 5.9 years). For 126 individuals (defined as having early RA), blood was obtained 0.5–1.5 years after RA diagnosis (18).

Table 1. Characteristics of the study cohorts*

Cohort (location), diagnosis	Female	Age, mean \pm SD years	Arthritis/RA at follow-up	VDG positive	VDG, median (IQR) %	ACPA positive	ACPA level, median (IQR) AU/ml†	ACPA assay
Cohort 1 (Nagasaki, Japan), healthy, symptom free (n = 58)	38 (66)	67 \pm 9.9	9 (15.5)	48 (83.8)	58.1 (35.6)	58 (100)	35.8	CLEIA (STACIA MEBLUX CCP test; MBL) (15)
Cohort 2 (Manitoba, Canada) Healthy (n = 48) RA onset (n = 25)	32 (66.7) 19 (76)	37.6 \pm 13.5 42 \pm 14.7	31 (64.6) –	42 (33.3) 21	44.9 (69.3) 99.9 (46.1)	37 (77.1) 22	54 (135.5) 200 (103.3)	CCP-2 kit (Inova Diagnostics) (16) CCP-2 kit (Inova Diagnostics) (16)
Cohort 3 (Umeå, Sweden) Presymptomatic (n = 228) 0.5–1.5 years after RA onset (n = 126)	145 (64) 78 (61)	52.2 \pm 9.4 59.7 \pm 9.3	228 (100) –	105 (46.1) 116 (92.1)	97.4 (53.5) 94.2 (50.8)	168 (73.7) 125 (98.4)	126.7 (455.5) 592.9 (725.3)	Immunoscan RA anti-CCP-2 EIA (Euro Diagnostica) (18) Immunoscan RA anti-CCP-2 EIA (Euro Diagnostica) (18)
Cohort 4 (Amsterdam, Reade, The Netherlands), arthralgia (n = 239)	185 (77)	48.3 \pm 11.6	137 (57.3)	211 (87.9)	75.3 (49)	239 (100)	358 (1,351)	Anti-CCP ELISA (Axis-Shield) (19)
Cohort 5 (Leiden, The Netherlands; CSA Study) Arthralgia (n = 38) RA onset (n = 26)	29 (76.3) 22 (84.6)	48.3 \pm 12.5 48.1 \pm 12.5	26 (68.4) –	27 (71.1) 18 (69.2)	70.4 (28.8) 59.1 (49.1)	33 (86.8) 21 (80.8)	123 (324) 25.5 (266.8)	Anti-CCP-2 ELISA (Euro Diagnostica) (23) Anti-CCP-2 ELISA (Euro Diagnostica) (23)
Cohort 6 (Leiden, The Netherlands; Improved study) RA onset (n = 130) 4 months after RA onset (n = 117) 8 months after RA onset (n = 112) 12 months after RA onset (n = 117)	88 (67.7) 79 (67.5) 78 (69.6) 78 (66.7)	51.1 \pm 12.5 50.6 \pm 12.8 50.7 \pm 12.4 51.0 \pm 12.4	– – – –	117 (90) 78 (66.7) 86 (76.8) 98 (83.8)	96 (48.2) 95.9 (45.1) 101.7 (50.3) 105.2 (48.1)	130 (100) 117 (100) 112 (100) 117 (100)	903.3 (1,101.2) 449.9 (806.9) 602 (1,061.8) 651.7 (962.5)	In-house anti-CCP-2 ELISA (3,22) In-house anti-CCP-2 ELISA (3,22) In-house anti-CCP-2 ELISA (3,22) In-house anti-CCP-2 ELISA (3,22)
Cohort 7 (Leiden, The Netherlands; EAC) RA onset, DFR not achieved (n = 59) RA onset, DFR achieved (n = 36) Pre-remission (n = 52) DFR (n = 41) SDFR (n = 35) DFR with late flares (n = 11)	42 (71.2) 24 (66.7) 37 (71.2) 27 (65.9) 27 (77.1) 7 (63.6)	49.7 \pm 14.5 50.8 \pm 13.1 54.2 \pm 14.8 58.5 \pm 13.6 54.6 \pm 15.1 69.4 \pm 14.8	– – – – – –	59 (100) 32 (89) 37 (71) 30 (73.2) 22 (62.9) 9 (81.8)	83.8 (46) 61.4 (35) 74.05 (30) 67.7 (41.5) 73.5 (42) 78.3 (26.9)	59 (100) 29 (80.6) 38 (73) 33 (80) 29 (82.9) 10 (91)	7,340 (5,984) 1,933 (7,296) 3,583 (5,302) 3,010 (8,975) 2,626 (6,765) 4,210 (10,709)	In-house anti-CCP-2 ELISA (3,22) In-house anti-CCP-2 ELISA (3,22) In-house anti-CCP-2 ELISA (3,22) In-house anti-CCP-2 ELISA (3,22) In-house anti-CCP-2 ELISA (3,22) In-house anti-CCP-2 ELISA (3,22)

* Except where indicated otherwise, values are the number (%). RA = rheumatoid arthritis; VDG = variable domain glycosylation; IQR = interquartile range; CCP = cyclic citrullinated peptide; EIA = enzyme immunoassay; ELISA = enzyme-linked immunosorbent assay; CSA = Clinically Suspect Arthralgia; EAC = Early Arthritis Cohort; DFR = drug-free remission; SDFR = sustained DFR.

† Anti-citrullinated protein antibody (ACPA) levels were determined with various assays/standards and thus are not directly comparable with one another.

Cohort 4, arthralgia (Amsterdam, Reade, The Netherlands). Patients in cohort 4 were ACPA-positive individuals with arthralgia ($n = 239$) who were seen at rheumatology outpatient clinics in the Amsterdam area (19). These individuals were followed up for a period of up to 10 years, during which 137 (57.3%) developed arthritis.

Cohort 5, arthralgia and RA onset (Leiden, The Netherlands). Individuals at risk of RA development were recruited for the prospective Clinically Suspect Arthralgia (CSA) cohort at the Leiden University Medical Center outpatient rheumatology clinic and followed up longitudinally (20). Thirty-eight patients with arthralgia from the CSA were included as cohort 5 in the present study. Paired samples from 26 of these patients were studied, i.e., a sample obtained at the time of arthralgia pre-RA diagnosis and a sample obtained at the time of diagnosis of clinically apparent RA.

Cohort 6, RA onset and established RA after treatment (Leiden, The Netherlands). Cohort 6 consisted of patients with RA who were recruited at 12 hospitals in the western area of The Netherlands and were included in the Improved study. The aim of this multicenter randomized controlled trial was to assess the achievement of DFR with treatment alteration every 4 months. Initial treatment was methotrexate (MTX) and prednisone. Prednisone was tapered in patients whose RA was in early remission (defined as a Disease Activity Score [DAS] of <1.6) (21) at 4 months. If disease was still in remission at 8 months, MTX was also tapered. If the DAS was ≥ 1.6 after prednisone was stopped, it was restarted. Patients in whom early remission was not achieved were randomized to 1 of 2 treatment arms: MTX, prednisone, hydroxychloroquine, and sulfasalazine combination (arm 1) or MTX and adalimumab combination (arm 2) (13). Serum samples obtained at the time of RA onset ($n = 130$) and at 4 months ($n = 117$), 8 months ($n = 112$), and 12 months ($n = 117$) after diagnosis and prespecified treatment were assessed in the present study.

Cohort 7, RA onset, DFR, SDFR, and late disease flares (Leiden, The Netherlands). Members of cohort 7 were patients from the Leiden EAC (14). Samples obtained at the time of RA onset from individuals in whom DFR was not later achieved ($n = 59$) and individuals in whom DFR was later achieved ($n = 36$) were assessed. Patients in whom DFR was later achieved were followed up longitudinally for up to 16 years; samples obtained at RA onset ($n = 36$), during the pre-remission phase ($n = 52$), DFR ($n = 41$), SDFR ($n = 35$), and at the time of late disease flares ($n = 11$) were included. DFR was defined as the absence of clinical synovitis (swollen joints at physical examination) after discontinuation of disease-modifying antirheumatic drug (DMARD) treatment (including systemic/intraarticular glucocorticoids). In the 41 patients in whom DFR was achieved, DMARD treatment was stopped after a median of 2.9 years (IQR 1.0–4.9 years). SDFR was defined as the absence of clinical synovitis after cessation of DMARD treatment, that persisted for ≥ 1 year. SDFR was achieved in the 35 patients after a median of 2.8 years of DMARD treatment (IQR 2.0–5.2 years) and was maintained for a median of

7.1 years (IQR 4.5–11.2 years) after DMARD cessation, demonstrating the sustainability of DMARD-free remission. Flare was defined as the recurrence of clinical synovitis on joint examination. Among patients in whom SDFR was achieved, data in the medical records were reviewed through September 2021.

Laboratory analyses. IgG ACPA levels in serum samples were analyzed using standard and commercially available anti-cyclic citrullinated peptide (anti-CCP) assays or in-house anti-CCP2 enzyme-linked immunosorbent assays (ELISAs) as previously described (3,15–17,19,22,23). ACPA fine specificity of samples from cohort 6 was determined using in-house anti-citrullinated vimentin 59–74, anti-citrullinated fibrinogen $\beta 36$ –52 and $\alpha 27$ –43, and anti-citrullinated enolase 5–20 ELISAs as previously described (3). ACPA fine specificity of samples from cohort 4 was determined using in-house IgG anti-citrullinated vimentin 60–75, anti-citrullinated fibrinogen $\beta 36$ –52, $\alpha 60$ –74, and $\alpha 36$ –50, and anti-citrullinated enolase 5–21 ELISAs.

IgG ACPA capture and VDG analysis using liquid chromatography. Capture of IgG ACPA, total glycan release, and glycan labeling and purification were performed as previously described (11). Briefly, ACPAs were affinity isolated from 25- μ l serum samples using NeutrAvidin Plus resin (Thermo Scientific) coupled with 0.1 μ g/ μ l CCP-2-biotin followed by IgG capture using FcXL affinity beads (Thermo Scientific). *N*-linked glycans were released using 0.5 units of PNGaseF (Roche), subsequently labeled with 2-anthranilic acid and 2-picoline borane, and hydrophobic interaction liquid chromatography–solid-phase extraction purified using GHP membrane filter plates (Pall Life Sciences). Ultra high-performance liquid chromatography was performed on a Dionex Ultimate 3000 instrument (ThermoFisher Scientific), an FLR fluorescence detector set, and an Acquity BEH Glycan column (Waters). Separation and glycan peak alignment were performed as previously described (11). HappyTools, version 0.0.2, was used for calibration and peak integration (24). The *N*-linked glycan abundance in each peak was expressed as the total integrated area under the curve. The cutoff was defined based on phosphate buffered saline control (blank) and blood samples from ACPA-negative healthy control subjects in the Leiden area, excluding outliers (below 1.5 \times the 25th percentile or above 1.5 \times the 75th percentile). The percentage IgG ACPA VDG was calculated based on the formula (sum of the most abundant variable domain glycans/sum of the most abundant Fc glycans) \times 100, or $([G2FBS1 + G2FS2 + G2FBS2]/[G0F + G1F + G2F]) \times 100$, where G0/G1/G2 represents A-/mono-/di-galactosylated, F represents core fucosylated, B represents bisecting *N*-acetylglucosamine (GlcNAc), and S1/S2 represents mono-/disialylated (12). The glycan traits were selected based on previous observations showing their exclusive presence on either the variable domain or the Fc domain of IgG ACPA molecules (12,25). The sum of the Fc glycans (the amount of *N*-linked

glycans attached to the conserved Asn297 in the Fc domain of IgG antibodies) remains constant.

Statistical analysis. Continuous data were analyzed using nonparametric methods (Kruskal-Wallis test for unpaired groups and Mann-Whitney U test for 2 unpaired groups) and parametric tests (mixed-effects analysis for matched paired samples accounting for missing values) when appropriate. The mixed-effects analysis model using restricted maximum likelihood is comparable to repeated-measures analysis of variance with regard to *P* values and multiple comparisons tests, but can accommodate missing values. Correlations between IgG ACPA levels (log transformed) and percentages of VDG were assessed with Pearson's correlation

coefficient. *P* values (all 2-sided) less than 0.05 were considered significant. Logistic and ordinal regression analyses were performed in cohort 4 and cohort 6 to investigate the association of IgG ACPA VDG/IgG ACPA levels with epitope spreading, remission, and early DFR. The unstandardized coefficient (B) represents the mean change in the response given a 1-unit change in the predictor. The longitudinal and repeated-measures data from cohort 6 were analyzed by generalized estimating equation (GEE) analysis, as previously described (3). GEE analysis was used to assess VDG changes over time and associations with treatment. The specific covariates and dependent variables are listed in the supplementary tables (<https://onlinelibrary.wiley.com/doi/10.1002/art.42098>). Statistical calculations were performed using Stata, version 16.1.

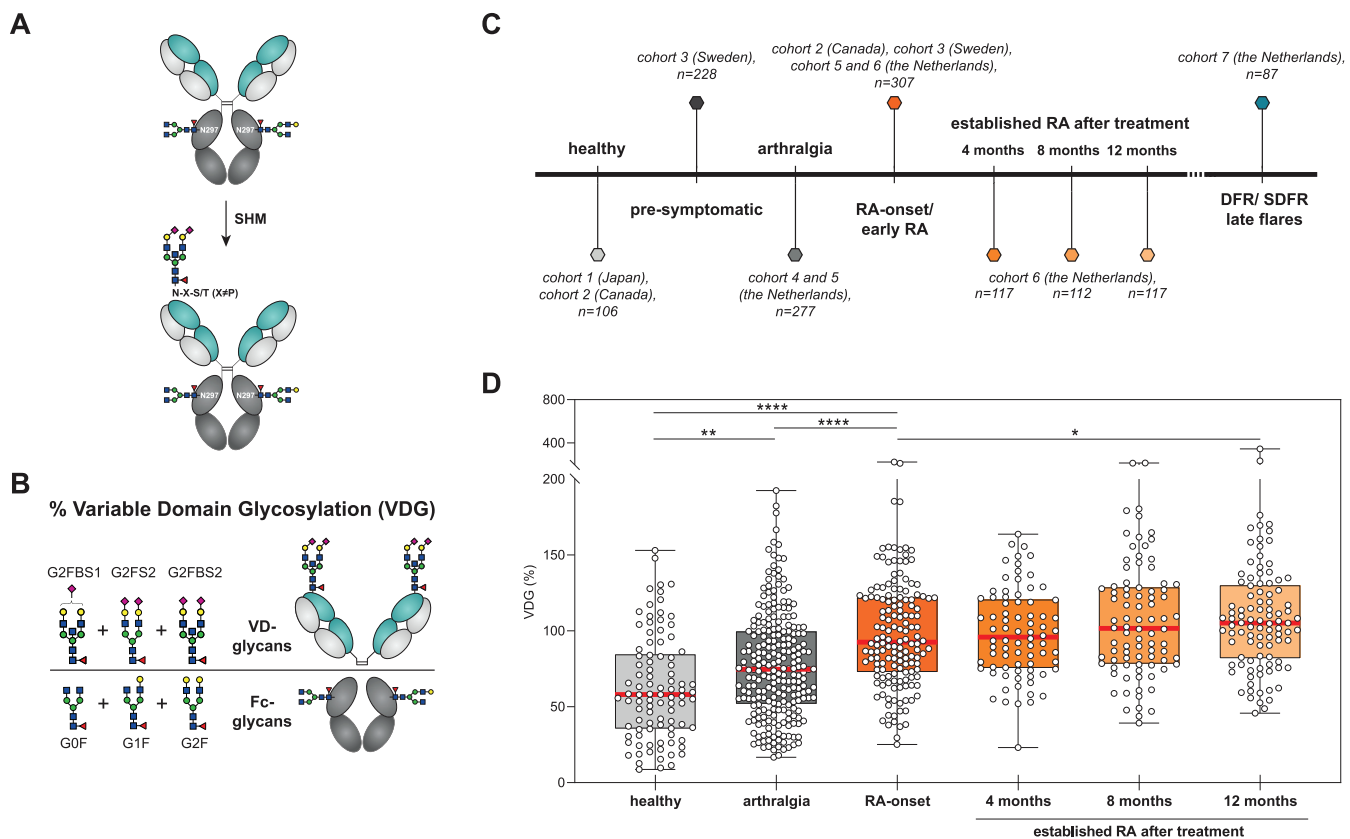


Figure 1. Percentage variable domain glycosylation in IgG anti-citrullinated protein antibodies (ACPAs) from healthy individuals, patients with arthralgia, and patients with rheumatoid arthritis (RA) in different disease stages. **A**, Depiction of the process by which IgG carries *N*-glycans at each N297 residue in the Fc domain and can acquire additional *N*-linked glycosylation sites (N-X-S/T, X ≠ P) in the variable domain by somatic hypermutation (SHM) (6). **B**, Depiction of the calculation of IgG ACPA VDG, i.e., (sum of the most abundant variable domain glycoforms/sum of the most abundant Fc glycoforms) × 100, or [(G2FBS1 + G2FS2 + G2FBS2)/(G0F + G1F + G2F)] × 100, where G0/G1/G2 represents A-/mono-/di-galactosylated, F represents core fucosylated, B represents bisecting *N*-acetylglucosamine (GlcNAc), and S1/S2 represents mono-/di-sialylated. The selected glycan traits are exclusively present on either the variable domain or the Fc domain of IgG ACPA. GlcNAc is shown as blue squares, mannose as green circles, galactose as yellow circles, fucose as red triangles, and *N*-acetylneuraminic acid as pink diamonds. **C**, “Timeline” of clinical disease stages, the corresponding analyzed cohorts, and numbers of samples analyzed. **D**, Percentage IgG ACPA VDG, measured by liquid chromatography, in healthy individuals, patients with arthralgia, patients at the time of RA onset, and patients with established RA 4 months, 8 months, and 12 months after institution of prespecified treatment. Data are presented as box and whisker plots, where the boxes represent the 25th to 75th percentiles, the lines within the boxes represent the median, and the whiskers represent the minimum to maximum values. Circles represent individual samples. The cross-sectional data sets from cohorts 1, 2, 4, and 5 were analyzed by Kruskal-Wallis test with Dunn's post hoc test. The longitudinally obtained data from cohort 6 were analyzed by generalized estimating equation. * = *P* = 0.037; ** = *P* = 0.0032; **** = *P* < 0.0001. DFR = drug-free remission; SDRF = sustained drug-free remission.

RESULTS

IgG ACPA variable domain glycosylation increases toward disease onset and remains stable in established RA.

To provide a comprehensive overview of the presence and abundance of IgG ACPA VDG (Figures 1A and B), we analyzed 1,377 ACPA-positive and 121 ACPA-negative samples from individuals in different clinical disease stages (Figure 1C and Table 1). Comparable to the results of previous studies (11,12), we found that variable domain glycans were already present in high percentages (median 56.2%) on IgG ACPA from healthy individuals without symptoms ($n = 106$) (Figure 1D). Cross-sectional analysis revealed a significant increase in VDG (median 74.7%) in

individuals with clinically identified arthralgia ($n = 277$) compared to healthy individuals (Figure 1D).

A further significant increase in VDG of 18% was observed in samples obtained at the time of RA onset ($n = 181$) (median VDG 92.6% in the combined data sets) (Figure 1D and Table 1). This was, however, not apparent in all individual sample sets, as changes in VDG between the arthralgia phase and RA onset could not be observed in the statistically underpowered longitudinal data set from cohort 5, presumably because the individuals with clinically suspected arthralgia were tested only shortly before the onset of arthralgia (Supplementary Figure 1, on the *Arthritis & Rheumatology* website at <https://onlinelibrary.wiley.com/doi/10.1002/art.42098>), and an increase in VDG could have occurred

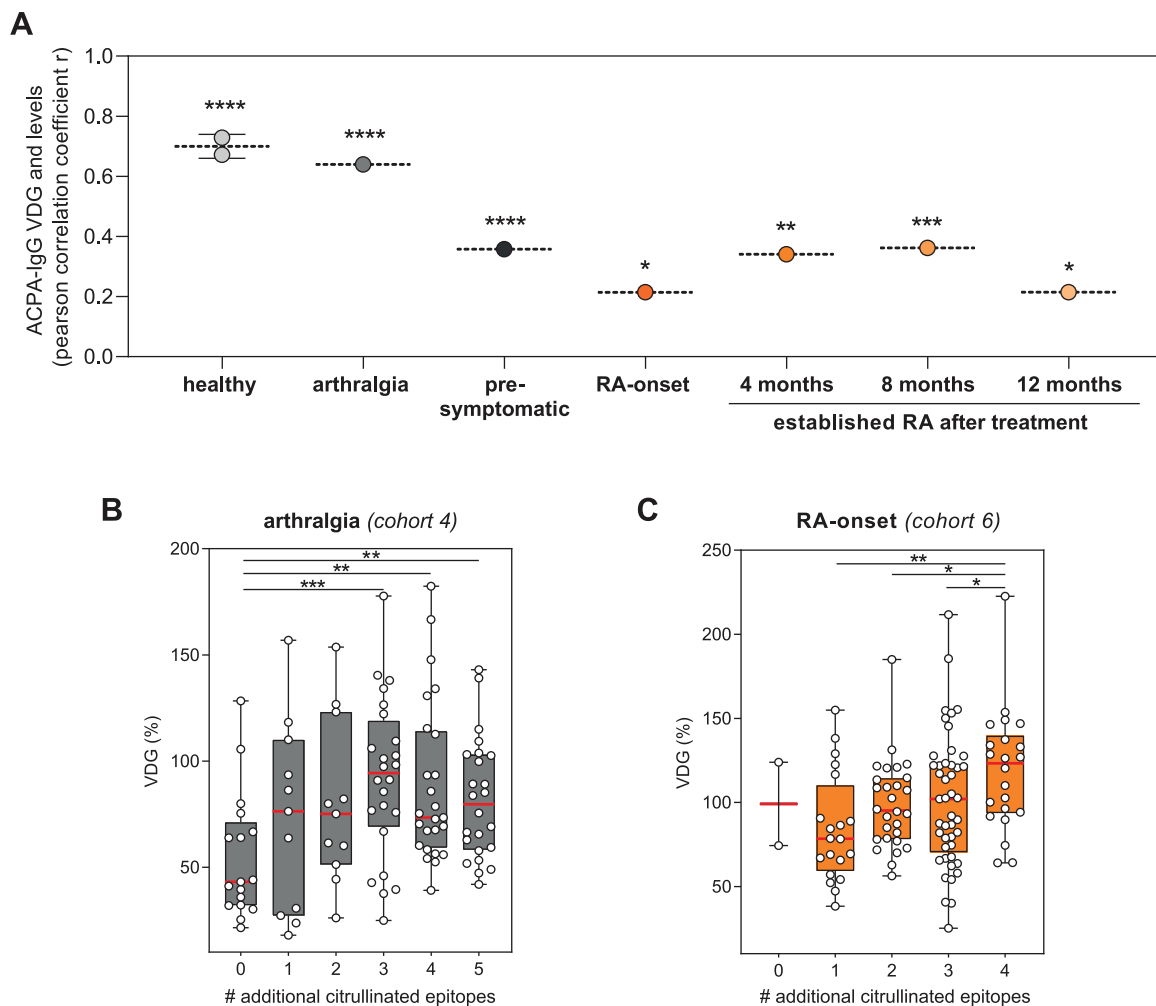


Figure 2. Correlation of IgG ACPA VDG with IgG ACPA levels and epitope spreading (maturation of the ACPA response). **A**, Pearson's correlation coefficients for the correlation between IgG ACPA VDG and IgG ACPA levels across different disease stages. * = $P < 0.05$; ** = $P < 0.005$; *** = $P < 0.001$; **** = $P < 0.0001$. For healthy individuals, values from 2 different cohorts are shown. **B**, VDG percentage on IgG ACPA from individuals with arthralgia, isolated using cyclic citrullinated peptide 2 and tested for binding to 5 additional citrullinated antigens (citrullinated vimentin 60–75, citrullinated fibrinogen β 36–52, α 60–74, and α 36–50, and citrullinated enolase 5–21). ** = $P < 0.01$; *** = $P = 0.0006$. **C**, VDG percentage in IgG ACPA from patients at the time of RA onset, isolated using cyclic citrullinated peptide 2 and tested for recognition of 4 additional citrullinated antigens (citrullinated vimentin 59–74, citrullinated fibrinogen β 36–52 and α 27–43, and citrullinated enolase 5–20). * = $P < 0.05$; ** = $P = 0.001$. In **B** and **C**, data are presented as box and whisker plots, where the boxes represent the 25th to 75th percentiles, the lines within the boxes represent the median, and the whiskers represent the minimum to maximum values. Circles represent individual samples. See Figure 1 for definitions.

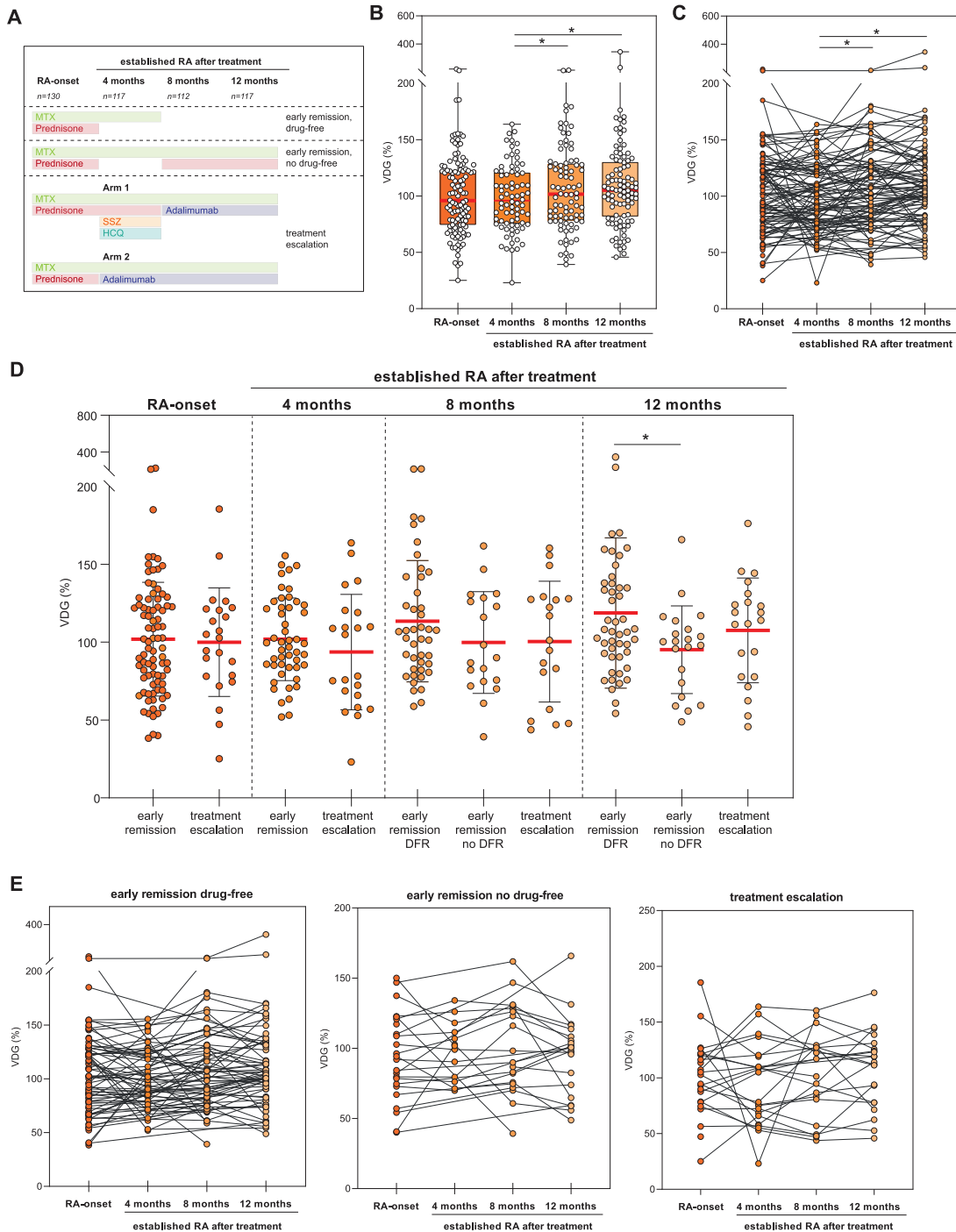


Figure 3. Longitudinal analysis of IgG ACPA VDG at the time of RA onset and in established RA after treatment (cohort 6). **A**, Treatment protocol. **B**, Longitudinal data on VDG percentage on IgG ACPA by time since RA onset. Data are presented as box and whisker plots, where the boxes represent the 25th to 75th percentiles, the lines within the boxes represent the median, and the whiskers represent the minimum to maximum values. Circles represent individual samples. Data were analyzed by mixed-effects analysis using restricted maximum likelihood and Tukey's test. **C**, Longitudinal data by time since RA onset, represented as matched pairs. **D**, VDG percentage in IgG ACPA by treatment group (early remission [drug-free], early remission [no drug-free], and treatment escalation) at each assessed time point since RA onset. Data were analyzed by one-way analysis of variance with Fisher's least significant difference test. Horizontal and vertical bars show the mean \pm SD. Circles represent individual samples. **E**, Longitudinal data by time since RA onset within each treatment group, represented as matched pairs. * = $P < 0.05$. MTX = methotrexate; SSZ = sulfasalazine; HCQ = hydroxychloroquine (see Figure 1 for other definitions).

earlier. Patients presenting with arthralgia, regardless of whether they did or did not subsequently develop RA, displayed lower VDG than patients tested at the time of RA onset (Supplementary Figure 2E, <https://onlinelibrary.wiley.com/doi/10.1002/art.42098>). In samples from patients with established RA after prespecified treatment ($n = 346$), IgG ACPA VDG remained stable, with only a moderate increase after 12 months, to a median of 105.2% (Figure 1D). As previously shown (11), an increase in IgG ACPA VDG toward the time of RA onset was also observed in a Swedish population of ACPA-positive individuals

who later developed RA. The extended data set used here also exhibited a rise in VDG when analyzed per individual in a longitudinal manner (26) (Supplementary Figure 2D); however, there was no significant difference on cross-sectional analysis (Supplementary Figure 2C).

Overall, the results showed that the presence of variable domain glycans on IgG ACPA was lower in healthy individuals and increased toward RA development. However, in established disease, no further progression of IgG ACPA VDG was observed in this cross-sectional analysis.

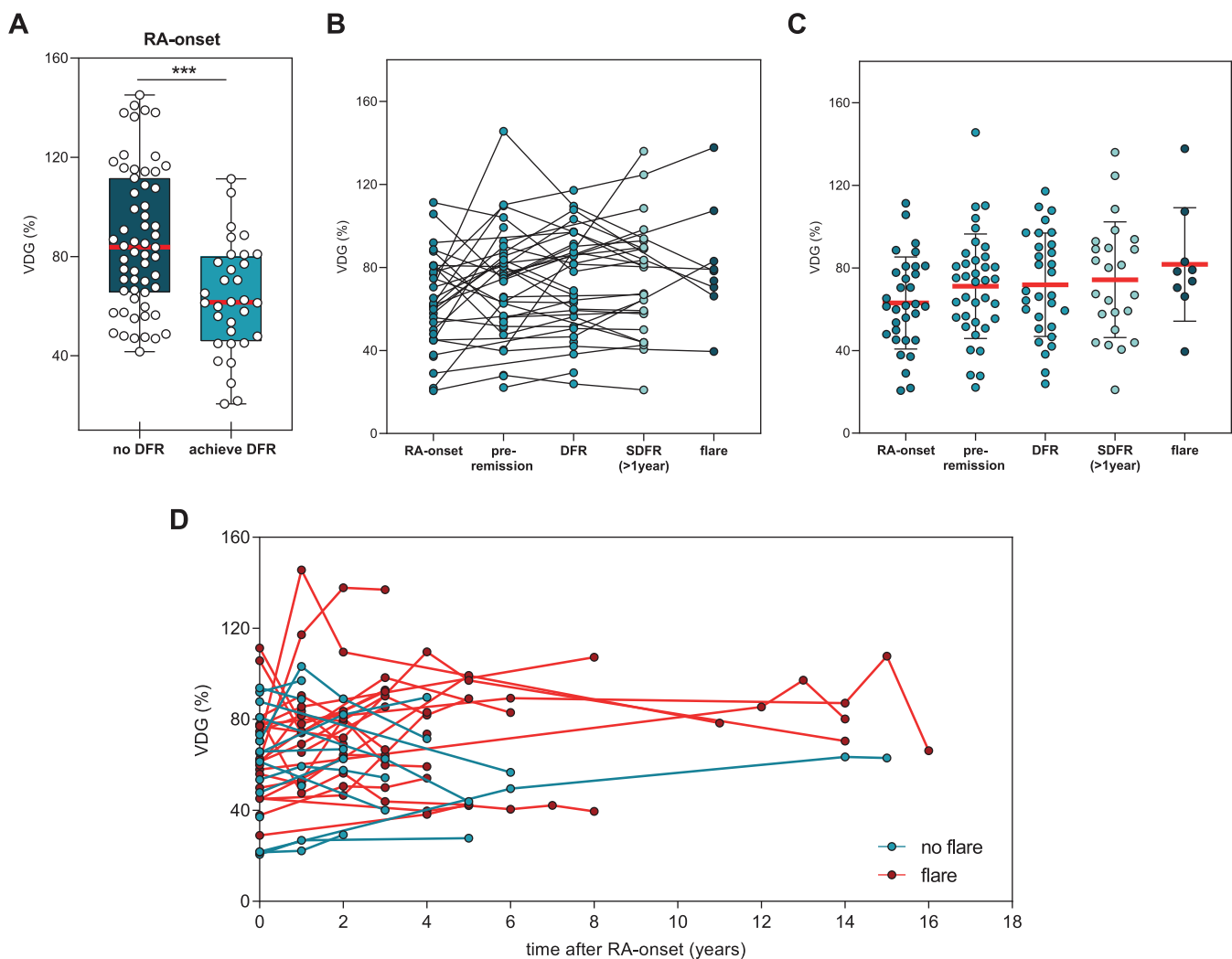


Figure 4. Cross-sectional and longitudinal analysis of IgG ACPA VDG at the time of RA onset and during DFR (cohort 7). **A**, VDG percentage on IgG ACPA at the time of RA onset in individuals in whom DFR was not achieved and those in whom DFR was achieved. DFR was defined as the absence of clinical synovitis after discontinuation of disease-modifying antirheumatic drug treatment. Data are presented as box and whisker plots, where the boxes represent the 25th to 75th percentiles, the lines within the boxes represent the median, and the whiskers represent the minimum to maximum values. *** = $P < 0.0001$ by Mann-Whitney U test. **B**, Data on VDG percentage on IgG ACPA in matched paired samples from patients at the time of RA onset, pre-remission, during DFR, during SDFR, and during late disease flares. Flare was defined as the recurrence of clinical synovitis on joint examination. **C**, IgG ACPA VDG data by group (RA onset, pre-remission, DFR, SDFR, flare). Horizontal and vertical bars show the mean \pm SD. Circles represent individual samples. **D**, IgG ACPA VDG data by assessment time point in longitudinally assessed samples from patients who did and those who did not experience late flares. Circles represent individual samples. See Figure 1 for definitions.

Interconnection between the increase in variable domain glycosylation and maturation of the ACPA immune response. To obtain further insights into IgG ACPA VDG, we investigated the possible association between VDG percentages and the “maturation” of the ACPA response by analyzing IgG ACPA levels and the broadness of the citrullinated epitope recognition profile. Pearson’s correlation analysis revealed a strong, highly significant correlation between VDG percentages and IgG ACPA levels among healthy individuals ($r = 0.672$ and $r = 0.728$ in cohorts 1 and 2, respectively) and among individuals with arthralgia ($r = 0.640$) (Figure 2A and Supplementary Figure 3, <https://onlinelibrary.wiley.com/doi/10.1002/art.42098>). At RA onset and in established RA after prespecified treatment, however, we observed only moderate correlations ($r = 0.214, 0.341, 0.362,$ and 0.215 at RA onset and after 4, 8, and 12 months of treatment, respectively) (Figure 2A and Supplementary Figure 2E, <https://onlinelibrary.wiley.com/doi/10.1002/art.42098>). Likewise, our data revealed that IgG ACPA with increased VDG showed a significantly broader recognition profile toward multiple citrullinated epitopes (Figures 2B and C). Ordinal regression analyses confirmed these findings in individuals with arthralgia ($P < 0.001$) (Supplementary Table 1, <https://onlinelibrary.wiley.com/doi/10.1002/art.42098>) as well as in patients at the time of RA onset ($P = 0.004$) and over time after treatment ($P < 0.001$) (Supplementary Table 2, <https://onlinelibrary.wiley.com/doi/10.1002/art.42098>). Thus, IgG ACPA VDG is associated with IgG ACPA levels and the breadth of the epitope recognition profile, suggesting that these two features of the ACPA response are interconnected.

Impact of immunosuppression on IgG ACPA variable domain glycosylation. We took advantage of the design of the Improved study (Figure 3A) to investigate whether IgG ACPA VDG predicts early remission in RA or is associated with the intensity of immunosuppression. First, we used the longitudinal data set to identify changes in IgG ACPA VDG over time by analyzing paired samples from patients at RA onset ($n = 130$) versus at 4 months ($n = 117$), 8 months ($n = 112$), and 12 months ($n = 117$) after disease development. Variable domain glycans appeared to be steadily and abundantly expressed on IgG ACPA after the onset of RA, although minor changes in expression levels were observed over time.

A slight but nonsignificant decrease was observed 4 months after disease onset and initiation of treatment with MTX and prednisone (Figures 3B and C and Supplementary Table 3, <https://onlinelibrary.wiley.com/doi/10.1002/art.42098>). Previous studies have shown a similar decline of IgG ACPA levels after initiation of treatment (3), providing further evidence of a correlation between VDG and IgG ACPA levels. After 4 months, prednisone was tapered such that patients were then treated with MTX only, if early remission (DAS < 1.6) had been achieved. If early remission was not achieved, patients were randomized to 1 of 2 treatment escalation arms, i.e., combination treatment with MTX,

prednisone, hydroxychloroquine, and sulfasalazine or combination treatment with MTX and adalimumab (13) (Figure 3A). At 8 months, individuals in the early remission group either continued MTX treatment combined with prednisone (no drug-free group) or, if disease remission persisted, their medication was tapered (drug-free group). Individuals in the treatment escalation group (arms 1 and 2) continued MTX treatment, in combination with adalimumab. Overall, irrespective of the treatment arm, VDG had increased moderately but significantly at 12 months after RA onset ($P = 0.037$) (Supplementary Table 3).

When the different treatment groups were compared, marginal but statistically significant effects of immunosuppression on IgG ACPA VDG were observed, with a reduction in VDG 12 months after RA onset (Figures 3D and E and Supplementary Figure 4A, <https://onlinelibrary.wiley.com/doi/10.1002/art.42098>), though not at 4 months or 8 months. This moderate but significant negative effect of immunosuppression on VDG was confirmed by GEE analysis of changes over time (8 months versus 12 months) (regression coefficient [B] 12.27 [95% confidence interval $-7.32, 31.87$] in the early remission, drug-free group versus 6.42 [95% confidence interval $-0.35, 13.10$] in the early remission, no drug-free and treatment escalation group; $P = 0.007$) (Supplementary Table 4, <https://onlinelibrary.wiley.com/doi/10.1002/art.42098>) and was similar to previously reported findings with regard to IgG ACPA levels (3). Last, we investigated whether VDG percentage at RA onset predicts remission after 4 months and drug-free remission within the first year. Similar to IgG ACPA levels (3), VDG percentages did not predict early drug-free remission (Supplementary Table 5, <https://onlinelibrary.wiley.com/doi/10.1002/art.42098>). Collectively, these results show that IgG ACPA variable domain glycans are expressed at a persistently high level in established RA and show a slight but statistically significant decrease upon immunosuppression.

Decreased VDG during active disease in patients in whom sustained DFR is later achieved. As a next step, we performed cross-sectional and longitudinal analyses of IgG ACPA VDG in individuals in whom long-term DFR was achieved or who experienced DFR with late flares. We made use of the unique EAC database including patients who were followed up for a period of up to 16 years after disease onset. Using this database, we were able to identify 41 individuals in whom DFR had been achieved and 35 patients in whom SDFR (> 1 year) had been achieved. Longitudinal samples obtained from the same patient at RA onset ($n = 36$), during active disease (pre-remission) ($n = 52$), during DFR ($n = 41$), during SDFR ($n = 35$), and when experiencing late disease flares ($n = 11$) were assessed. Again, the data showed that variable domain glycans are stably expressed in established RA. Intriguingly, however, patients in whom DFR was achieved during follow-up ($n = 36$) showed significantly reduced IgG ACPA VDG at the onset of disease compared to age- and sex-matched patients with persistently high disease activity (DAS > 3) ($n = 59$) (median VDG at disease onset 61.4%

versus 83.8%) (Figure 4A and Table 1). In contrast, no statistically significant changes were observed when the IgG ACPA VDG percentages were determined over time in the DFR group or any of the other groups analyzed (Figures 4B–D). Thus, these longitudinal data confirm that IgG ACPAs express a constant amount of variable domain glycans after RA onset. The cross-sectional data also indicate that among individuals in whom long-term DFR is achieved, fewer glycans are present on IgG ACPA variable domains at the time of RA onset.

DISCUSSION

A key important characteristic of IgG autoantibodies from patients with RA is the abundant presence of bisected and disialylated glycans in the variable domain. To gain insight into the introduction and occurrence of this unusual antibody feature across different disease stages, we assessed IgG ACPAs in ~1,500 samples from 852 individuals in different clinical disease stages. Moreover, we analyzed the effect of therapy on the degree of VDG on ACPAs. The large sample size increased the power of our study, and we demonstrated that IgG ACPA VDG correlates strongly with the maturation of the ACPA immune response prior to disease onset, while no correlation with age was observed. We found that the abundance of IgG ACPA VDG increased significantly from the time these ACPA-positive individuals were healthy and symptom-free (58.1%) toward the pre-RA phase (arthralgia) (74.7%), with a further increase around the time of disease onset (92.6%). Thus, our data strongly indicate that an increase in IgG ACPA VDG occurs in the asymptomatic phase, with a further increase during progression to arthralgia and ultimately RA diagnosis, although the latter notion requires further detailed research with longitudinal sampling.

In established RA, we noted constant high expression of glycans on the variable domain of IgG ACPA, with a slight, but significant, increase after 12 months (105.2%). This is consistent with our previous observations, estimating >90% VDG on IgG ACPA in RA (4), as well as the finding that >80% of ACPA B cell receptors in RA express *N*-linked glycosylation sites in the variable region (27). Our longitudinal data from cohort 6 depict increased VDG levels in individuals in whom treatment was tapered, while patients who received more intensive treatment showed reduced IgG ACPA VDG profiles over time ($P = 0.007$). This significant impact of immunosuppression was also observed for IgG ACPA levels (22), confirming the correlation between IgG ACPA levels and VDG, which was strongest in the pre-disease phase. These findings are also in accordance with the notion that variable domain glycans could have a regulatory impact on the ACPA immune response. In this respect, it is intriguing to note that the HLA shared epitope alleles predispose to ACPA harboring VDG rather than to ACPA in general (11), thus linking ACPA VDG with the major genetic risk factor for RA. Indeed, a more in-depth longitudinal analysis of the correlation between the presence of

predisposing HLA–DR4 genes and the presence of VDG revealed a shorter “transit time” to RA in HLA–DR4–positive pre-disease individuals who still displayed relatively low levels of ACPA variable domain glycans, as compared to HLA–DR4–negative individuals with similar ACPA variable domain glycan levels (26).

Of note, in the longitudinal analysis we observed that individuals in whom long-term DFR is achieved exhibit lower VDG profiles at disease onset (61.4%) compared to patients in whom long-term DFR is not achieved (83.8%). The relevance of these findings is unknown, although it is remarkable that long-term DFR, a relatively rare event in ACPA-positive RA, was associated with lower VDG on ACPAs.

Importantly, reduced IgG ACPA levels are not the cause of lower VDG, which was controlled by titrating IgG ACPA into healthy serum samples to enable maintenance of a high degree of VDG (Supplementary Figure 5B, on the *Arthritis & Rheumatology* website at <https://onlinelibrary.wiley.com/doi/10.1002/art.42098>). Thus it is tempting to speculate that variable domain glycans serve as an additional “hit” determining the fate of the autoreactive B cell response and thereby exert an impact on ACPA levels.

Together with previous data showing that *N*-linked glycan sites are selectively introduced into ACPA B cell receptor sequences upon somatic hypermutation (27) and that variable domain glycan levels are significantly elevated in ACPA-positive individuals who subsequently develop RA (12), our results provide evidence that a glycan attached to the variable domain fosters a breach of tolerance of autoreactive B cells. As carbohydrates are known to affect cellular functions, ACPA-expressing B cells may gain a selection advantage when abundantly expressing glycans in their variable domains. The disialylated, and thus negatively charged, glycans attached to the variable domain, which also have a large steric requirement, might modulate binding to autoantigens or affect B cell receptor signaling of citrullinated antigen-directed B cells. Further, we cannot rule out a possible role of variable domain glycans in effector mechanism, and thereby, autoantibody-mediated inflammation, similar to findings for Fc glycans. In addition to these areas for further research, it would be interesting to investigate changes in specific variable domain glycan traits in more depth, as altered glycan composition could be associated with defined biologic implications, as also observed for Fc glycans. Recent studies have shown, for example, that not only Fc glycans on total IgG, but also variable domain glycans on IgG ACPA, show a decrease in the bisecting GlcNAc after COVID-19 (28,29). Interestingly, variable domain glycans are not only a feature of IgG ACPA in RA, but have also been described in other human autoimmune responses, such as in antineutrophil cytoplasmic antibody-associated vasculitis and Sjögren's syndrome, and have been observed on anti-hinge and antidrug antibodies (30–32).

A limitation of our study is that VDG profiles could be detected in only 70% of the samples analyzed, mainly due to a limited amount of serum available for the IgG ACPA capturing

and subsequent glycan analysis or to low IgG ACPA levels, as observed in the group of healthy individuals. Especially for rare disease stages, such as for the “DFR with late flares” group, only a limited number of samples were available to us. In addition, ACPAs were captured using the highly sensitive and specific antigen CCP-2. However, it cannot be excluded that certain ACPA molecules that recognize different citrullinated epitopes and do not interact with CCP-2 were omitted from the analysis. Importantly though, we did not observe an effect of VDGs on binding affinity to CCP-2 (data not shown), making selection bias toward higher or lower glycosylated ACPAs unlikely. Another limitation of the study is that conclusions are mainly based on cross-sectional data derived from samples collected at different sites. Although collection of such data from one site would be highly challenging, the analyses of samples from different sites could be hampered by site-specific effects. Importantly, however, we also observed an increase in IgG ACPA VDG toward the time of RA onset in the longitudinal data set from cohort 3, including paired samples obtained from individuals when they were presymptomatic and after RA onset, over a period of 15 years, as also previously described (26). Furthermore, our findings of IgG ACPA variable domain glycan levels were concordant across different cross-sectional cohorts of healthy individuals (58.1% and 44.9%) or individuals with arthralgia (75.3% and 70.4%).

In summary, we have provided a comprehensive overview of the expression of variable domain glycans on IgG ACPA over various clinical disease stages in RA. Although the biologic implications of variable domain glycans attached to antibodies in general and to ACPAs specifically are still largely unexplored, our data show that they are a key characteristic of ACPAs across disease stages in individuals of different ethnicities who develop RA. Our results demonstrate an increase in VDG toward the time of disease onset and, taken together with previous data indicating a selective introduction of these *N*-linked glycan sites, suggest that variable domain glycans may serve as a trigger for the maturation of the ACPA immune response. It will therefore be useful to understand the biologic impact of variable domain glycans on the ACPA immune response and its detailed clinical implications.

ACKNOWLEDGMENTS

The authors would like to thank personnel of the Department of Biobank Research (Umeå University), the Västerbotten Intervention Programme (Västerbotten, Sweden), the Northern Sweden MONICA study, and the County Council of Västerbotten for providing data and samples. We are grateful to Dr. Jan Wouter Drijfhout (Leiden University Medical Center) for providing the CCP-2 peptide, Carolien Koeleman (Leiden University Medical Center) for expert assistance with liquid chromatography, and Ellis Niemantsverdriet and Marloes Verstappen (Leiden University Medical Center) for assistance with sample and data collection.

AUTHOR CONTRIBUTIONS

All authors were involved in drafting the article or revising it critically for important intellectual content, and all authors approved the final

version to be published. Ms. Kissel had full access to all of the data in the study and takes responsibility for the integrity of the data and the accuracy of the data analysis.

Study conception and design. Kissel, Hafkenscheid, Tamai, Kawashiri, Kawakami, El-Gabalawy, van Schaardenburg, Rantapää-Dahlqvist, Wuhler, van der Helm-van Mil, Allaart, van der Woude, Scherer, Toes, Huizinga.

Acquisition of data. Kissel, Hafkenscheid.


Analysis and interpretation of data. Kissel, Wesemael, Wuhler, van der Helm-van Mil, van der Woude, Scherer, Toes, Huizinga.

REFERENCES

1. Van der Kooij SM, Goekoop-Ruiterman YP, de Vries-Bouwstra JK, Guler-Yuksel M, Zwinderman AH, Kerstens PJ, et al. Drug-free remission, functioning and radiographic damage after 4 years of response-driven treatment in patients with recent-onset rheumatoid arthritis. *Ann Rheum Dis* 2009;68:914–21.
2. Willemze A, Trouw LA, Toes RE, Huizinga TW. The influence of ACPA status and characteristics on the course of RA [review]. *Nat Rev Rheumatol* 2012;8:144–52.
3. de Moel EC, Derksen V, Trouw LA, Bang H, Collee G, Lard LR, et al. In rheumatoid arthritis, changes in autoantibody levels reflect intensity of immunosuppression, not subsequent treatment response. *Arthritis Res Ther* 2019;21:28.
4. Hafkenscheid L, Bondt A, Scherer HU, Huizinga TW, Wuhler M, Toes RE, et al. Structural analysis of variable domain glycosylation of anti-citrullinated protein antibodies in rheumatoid arthritis reveals the presence of highly sialylated glycans. *Mol Cell Proteomics* 2017;16:278–87.
5. Kasermann F, Boerema DJ, Rueggsegger M, Hofmann A, Wymann S, Zuercher AW, et al. Analysis and functional consequences of increased Fab-sialylation of intravenous immunoglobulin (IVIg) after lectin fractionation. *PLoS One* 2012;7:e37243.
6. Vergoesen RD, Slot LM, Hafkenscheid L, Koning MT, van der Voort EI, Grooff CA, et al. B-cell receptor sequencing of anti-citrullinated protein antibody (ACPA) IgG-expressing B cells indicates a selective advantage for the introduction of *N*-glycosylation sites during somatic hypermutation. *Ann Rheum Dis* 2018;77:956–8.
7. Rombouts Y, Ewing E, van de Stadt LA, Selman MH, Trouw LA, Deelder AM, et al. Anti-citrullinated protein antibodies acquire a pro-inflammatory Fc glycosylation phenotype prior to the onset of rheumatoid arthritis. *Ann Rheum Dis* 2015;74:234–41.
8. Scherer HU, van der Woude D, Ioan-Facsinay A, el Bannoudi H, Trouw LA, Wang J, et al. Glycan profiling of anti-citrullinated protein antibodies isolated from human serum and synovial fluid. *Arthritis Rheum* 2010; 62:1620–9.
9. Bondt A, Hafkenscheid L, Falck D, Kuijper TM, Rombouts Y, Hazes JM, et al. ACPA IgG galactosylation associates with disease activity in pregnant patients with rheumatoid arthritis. *Ann Rheum Dis* 2018;77:1130–6.
10. Ercan A, Cui J, Chatterton DE, Deane KD, Hazen MM, Brintnell W, et al. Aberrant IgG galactosylation precedes disease onset, correlates with disease activity, and is prevalent in autoantibodies in rheumatoid arthritis. *Arthritis Rheum* 2010;62:2239–48.
11. Kissel T, van Schie KA, Hafkenscheid L, Lundquist A, Kokkonen H, Wuhler M, et al. On the presence of HLA-SE alleles and IgG ACPA variable domain glycosylation in the phase preceding the development of rheumatoid arthritis. *Ann Rheum Dis* 2019;78:1616–20.
12. Hafkenscheid L, de Moel E, Smolik I, Tanner S, Meng X, Jansen BC, et al. *N*-linked glycans in the variable domain of IgG anti-citrullinated protein antibodies predict the development of rheumatoid arthritis. *Arthritis Rheumatol* 2019;71:1626–33.

13. Heimans L, Wevers-de Boer KV, Visser K, Goekoop RJ, van Oosterhout M, Harbers JB, et al. A two-step treatment strategy trial in patients with early arthritis aimed at achieving remission: the IMPROVED study. *Ann Rheum Dis* 2014;73:1356–61.
14. Van Aken J, van Bilsen JH, Allaart CF, Huizinga TW, Breedveld FC. The Leiden Early Arthritis Clinic. *Clin Exp Rheumatol* 2003;21 Suppl: S100–5.
15. Kawashiri SY, Tsuji Y, Tamai M, Nonaka F, Nobusue K, Yamanashi H, et al. Effects of cigarette smoking and human T-cell leukaemia virus type 1 infection on anti-citrullinated peptide antibody production in Japanese community-dwelling adults: the Nagasaki Islands Study. *Scand J Rheumatol* 2020;22:1–4.
16. Smolik I, Robinson DB, Bernstein CN, El-Gabalawy HS. First-degree relatives of patients with rheumatoid arthritis exhibit high prevalence of joint symptoms. *J Rheumatol* 2013;40:818–24.
17. Arnett FC, Edworthy SM, Bloch DA, McShane DJ, Fries JF, Cooper NS, et al. The American Rheumatism Association 1987 revised criteria for the classification of rheumatoid arthritis. *Arthritis Rheum* 1988;31:315–24.
18. Rantapää-Dahlqvist S, de Jong BA, Berglin E, Hallmans G, Wadell G, Stenlund H, et al. Antibodies against cyclic citrullinated peptide and IgA rheumatoid factor predict the development of rheumatoid arthritis. *Arthritis Rheum* 2003;48:2741–9.
19. Bos WH, Wolbink GJ, Boers M, Tjhuis GJ, de Vries N, van der Horst-Bruinsma IE, et al. Arthritis development in patients with arthralgia is strongly associated with anti-citrullinated protein antibody status: a prospective cohort study. *Ann Rheum Dis* 2010;69:490–4.
20. Newsum EC, van der Helm-van Mil AH, Kaptein AA. Views on clinically suspect arthralgia: a focus group study. *Clin Rheumatol* 2016;35: 1347–52.
21. Van der Heijde DM, van 't Hof MA, van Riel PL, Theunisse LM, Lubberts EW, van Leeuwen MA, et al. Judging disease activity in clinical practice in rheumatoid arthritis: first step in the development of a disease activity score. *Ann Rheum Dis* 1990;49:916–20.
22. De Moel EC, Derksen V, Stoeken G, Trouw LA, Bang H, Goekoop RJ, et al. Baseline autoantibody profile in rheumatoid arthritis is associated with early treatment response but not long-term outcomes. *Arthritis Res Ther* 2018;20:33.
23. Van Steenberg HW, Mangnus L, Reijniere M, Huizinga TW, van der Helm-van Mil AH. Clinical factors, anticitrullinated peptide antibodies and MRI-detected subclinical inflammation in relation to progression from clinically suspect arthralgia to arthritis. *Ann Rheum Dis* 2016;75:1824–30.
24. Jansen BC, Hafkenscheid L, Bondt A, Gardner RA, Hendel JL, Wuhler M, et al. HappyTools: a software for high-throughput HPLC data processing and quantitation. *PLoS One* 2018;13:e0200280.
25. Rombouts Y, Willemze A, van Beers JJ, Shi J, Kerkman PF, van Toorn L, et al. Extensive glycosylation of IgG ACPA variable domains modulates binding to citrullinated antigens in rheumatoid arthritis. *Ann Rheum Dis* 2016;75:578–85.
26. Kissel T, van Wesemael TJ, Lundquist A, Kokkonen H, Kawakami A, Tamai M, et al. Genetic predisposition (HLA-SE) is associated with IgG ACPA variable domain glycosylation in the predisease phase of RA [letter]. *Ann Rheum Dis* 2021;81:141–3.
27. Vergoesen RD, Slot LM, van Schaik BD, Koning MT, Rispens T, van Kampen AH, et al. N-glycosylation site analysis of citrullinated antigen-specific B-cell receptors indicates alternative selection pathways during autoreactive B-cell development. *Front Immunol* 2019; 10:2092.
28. Derksen V, Kissel T, Lamers-Karnebeek FB, van der Bijl AE, Venhuizen AC, Huizinga TW, et al. Onset of rheumatoid arthritis after COVID-19: coincidence or connected? *Ann Rheum Dis* 2021. DOI: [10.1136/annrheumdis-2021-219859](https://doi.org/10.1136/annrheumdis-2021-219859). E-pub ahead of print.
29. Chakraborty S, Gonzalez J, Edwards K, Mallajosyula V, Buzzanco AS, Sherwood R, et al. Proinflammatory IgG Fc structures in patients with severe COVID-19. *Nat Immunol* 2021;22:67–73.
30. Vletter EM, Koning MT, Scherer HU, Veelken H, Toes RE. A comparison of immunoglobulin variable region N-linked glycosylation in healthy donors, autoimmune disease and lymphoma. *Front Immunol* 2020;11:241.
31. Biermann MH, Griffante G, Podolska MJ, Boeltz S, Sturmer J, Munoz LE, et al. Sweet but dangerous: the role of immunoglobulin G glycosylation in autoimmunity and inflammation. *Lupus* 2016;25: 934–42.
32. Van de Bovenkamp FS, Derksen NI, Ooijevaar-de Heer P, van Schie KA, Kruihof S, Berkowska MA, et al. Adaptive antibody diversification through N-linked glycosylation of the immunoglobulin variable region. *Proc Natl Acad Sci U S A* 2018;115:1901–6.

Epigenetic Regulation of Nutrient Transporters in Rheumatoid Arthritis Fibroblast-like Synoviocytes

Alyssa Torres,¹  Brian Pedersen,¹ Isidoro Cobo,¹ Rizi Ai,¹ Roxana Coras,² Jessica Murillo-Saich,¹ Gyrid Nygaard,¹ Elsa Sanchez-Lopez,³ Anne Murphy,³ Wei Wang,¹ Gary S. Firestein,¹ and Monica Guma⁴

Objective. Since previous studies indicate that metabolism is altered in rheumatoid arthritis (RA) fibroblast-like synoviocytes (FLS), we undertook this study to determine if changes in the genome-wide chromatin and DNA states in genes associated with nutrient transporters could help to identify activated metabolic pathways in RA FLS.

Methods. Data from a previous comprehensive epigenomic study in FLS were analyzed to identify differences in genome-wide states and gene transcription between RA and osteoarthritis. We utilized the single nearest genes to regions of interest for pathway analyses. Homer promoter analysis was used to identify enriched motifs for transcription factors. The role of solute carrier transporters and glutamine metabolism dependence in RA FLS was determined by small interfering RNA knockdown, functional assays, and incubation with CB-839, a glutaminase inhibitor. We performed ¹H nuclear magnetic resonance to quantify metabolites.

Results. The unbiased pathway analysis demonstrated that solute carrier-mediated transmembrane transport was one pathway associated with differences in at least 4 genome-wide states or gene transcription. Thirty-four transporters of amino acids and other nutrients were associated with a change in at least 4 epigenetic marks. Functional assays revealed that solute carrier family 4 member 4 (SLC4A4) was critical for invasion, and glutamine was sufficient as an alternate source of energy to glucose. Experiments with CB-839 demonstrated decreased RA FLS invasion and proliferation. Finally, we found enrichment of motifs for c-Myc in several nutrient transporters.

Conclusion. Our findings demonstrate that changes in the epigenetic landscape of genes are related to nutrient transporters, and metabolic pathways can be used to identify RA-specific targets, including critical solute carrier transporters, enzymes, and transcription factors, to develop novel therapeutic agents.

INTRODUCTION

Metabolomic studies have shown that rheumatoid arthritis (RA) is associated with metabolic disruption (1,2). This is likely a reflection of the increased bioenergetic and biosynthetic demands of chronic inflammation and changes in nutrient and oxygen availability in tissue during inflammation. The synovial membrane lining layer is the principal site of inflammation in RA (3). Fibroblast-like synoviocytes (FLS) transform in RA to overproduce enzymes, which degrade cartilage and bone, and

overproduce cytokines, which promote immune cell infiltration (4,5). Prior studies from our group and others have shown that several metabolic changes in FLS from RA patients may be therapeutically targetable (6–9). These metabolic changes could be targeted without compromising systemic homeostasis as a novel combination therapy independent of systemic immunosuppression.

Recent studies in cancer and other activated cells revealed similar metabolic changes (10). These changes often involve increased expression of nutrient transporters to supplement the

The content is solely the responsibility of the authors and does not necessarily represent the official views of the National Institutes of Health.

Supported by the NIH (diversity supplement to Ms. Torres, and grants T32-AR-064194 to Drs. Coras and Murillo-Saich, K01-AR-077111 to Dr. Sanchez-Lopez, NS-087611 to Dr. Murphy, P30-AR-073761 to Drs. Wang and Firestein, R01-AR-073324 to Dr. Guma, and NS-047101 to the University of California San Diego Microscopy Core), and by a European Molecular Biology Organization long-term fellowship (ALTF-960-2018) to Dr. Cobo.

¹Alyssa Torres, BS, Brian Pedersen, MD, Isidoro Cobo, PhD, Rizi Ai, PhD, Jessica Murillo-Saich, PhD, Gyrid Nygaard, PhD, Wei Wang, PhD, Gary S. Firestein, MD: University of California, San Diego; ²Roxana Coras, MD: University of California, San Diego, and Autonomous University of Barcelona,

Spain; ³Elsa Sanchez-Lopez, PhD, Anne Murphy, PhD: VA Medical Center, San Diego, California; ⁴Monica Guma, MD, PhD: University of California, San Diego, Autonomous University of Barcelona, Spain, and VA Medical Center, San Diego, California.

Ms. Torres and Dr. Pedersen contributed equally to this work.

Author disclosures are available at <https://onlinelibrary.wiley.com/action/downloadSupplement?doi=10.1002%2Fart.42077&file=art42077-sup-0001-Disclosureform.pdf>.

Address correspondence to Monica Guma, MD, PhD, University of California, San Diego, 9500 Gilman Drive MC 0663, La Jolla, CA 92093-0663. Email: mguma@health.ucsd.edu.

Submitted for publication January 25, 2021; accepted in revised form January 25, 2022.

elevated needs of the activated cell (11). Nutrient transporters, with the solute carrier transporter families that contain ~400 genes and 52 subfamilies, among others, serve as metabolic gates for cells by mediating transport of several different nutrients and metabolites such as glucose, amino acids, vitamins, neurotransmitters, and inorganic/metal ions (12). For instance, an elevated level of glutamine transporters that correlates with increased glutamine metabolism has been observed in activated cells in cancer (13) and other diseases including neurodegenerative diseases (14) and arthritis (15). In response to these metabolic changes, glutamine can ultimately assist in the tricarboxylic acid cycle as an alternative carbon source to glucose. Other recent studies have shown the effects of solute carrier transporters in nutrients other than glutamine in both FLS and lymphocytes in arthritis (16,17). Other studies of non-amino acid transporter roles in cancer explored the roles of mitochondrial carriers (18), zinc transporters (19), and bicarbonate transporters (20), to name a few.

Epigenetic alterations, such as DNA methylation and histone modification, might contribute to disease pathogenesis by enhancing chromatin accessibility to activate gene coding for these nutrient transporters (21,22). Of interest, several studies have demonstrated epigenetic changes in FLS (DNA methylation, histone modification, and microRNA expression) (23,24). Comprehensive epigenomic characterization of RA FLS was recently described (25). Since previous studies indicate that metabolism is altered in RA FLS, we hypothesized that changes in the histone landscape of genes associated with nutrient transporters correlate with differences in expression and would help identify activated metabolic pathways and thus targets for RA pathogenesis. Therefore, studying epigenetic changes in nutrient transporters not only may help us identify important metabolic pathways, but also could lead to the identification of specific nutrients and transporters essential to creating a metabolic shift in inflamed tissue. Targeting these specific nutrients and pathways could result in an insufficient energy supply and thus reduce the aggressive phenotype of FLS involved in the pathogenesis of RA.

MATERIALS AND METHODS

More detailed methods are provided in Supplementary Methods (available on the *Arthritis & Rheumatology* website at <http://onlinelibrary.wiley.com/doi/10.1002/art.42077/abstract>).

Genome-wide data sets. A total of 191 genome-wide data sets were generated from 11 RA FLS samples and 11 osteoarthritis (OA) FLS samples, which we characterized in our previous study (25) and deposited in the GEO (GEO accession no. GSE112658). Briefly, our data sets include 130 histone modification data sets, 22 open chromatin data sets, 20 RNA-Seq data sets, and 19 DNA methylation data sets. Six histone modification marks were analyzed, including histone H3 lysine 4 trimethylation

(H3K4me3) (associated with promoter regions), H3K4me1 (associated with enhancer regions), H3K27ac (associated with increased activation of promoter and enhancer regions), H3K36me3 (associated with transcribed regions), H3K27me3 (associated with polycomb repression), and H3K9me3 (associated with heterochromatin regions). Additional epigenomic marks include open chromatin regions, profiled with assay for transposase-accessible chromatin with sequencing (ATAC-seq), denoting regions of accessible chromatin, and are typically associated with regulator binding. DNA methylation, commonly associated with repressed regulatory regions, was profiled with whole-genome bisulfite sequencing (WGBS), and RNA-Seq was used to measure gene expression levels. Images were generated using Integrative Genomics Viewer version 2.3.98. Epigenetic analysis of the nutrient transporters was conducted as previously described (25).

Human FLS. FLS were extracted from the joints of RA patients or OA patients undergoing total joint replacement as previously described (26). RA FLS and OA FLS were grown in Dulbecco's modified Eagle's medium (DMEM) without sodium pyruvate, supplemented with 10% fetal bovine serum (FBS), 2 mM L-glutamine, 100 units/ml penicillin, and 100 µg/ml streptomycin. Experiments testing glucose and glutamine concentrations were conducted with dialyzed FBS (no. A3382001; Gibco) in DMEM without glucose, glutamine, phenol red, and sodium pyruvate (no. A1443001; Gibco). In experiments testing the lack of various amino acids without glucose, we used dialyzed FBS (no. A24939-01; Gibco) in DMEM without glucose, sodium pyruvate, phenol red, lysine, and arginine.

RNA-Seq. In total, 4 RA FLS cell lines and 3 OA FLS cell lines were plated 100,000 cells per well on a 6-well plate, starved overnight in 1% dialyzed serum, and stimulated with either 2 mM or 25 mM of glucose in 6 mM of glutamine for 5 hours. RNA-Seq was performed and analyzed as described elsewhere (27–29) and in Supplementary Methods (<http://onlinelibrary.wiley.com/doi/10.1002/art.42077/abstract>).

Gene set enrichment analysis (GSEA). To analyze signaling pathways regulated by differentially expressed genes, we used the Molecular Signature Database of GSEA (30–32) and computed the overlaps with data sets from Pathway Interaction Database, Reactome, WikiPathways, Hallmark, or KEGG as indicated in the figures and Supplementary Methods (<http://onlinelibrary.wiley.com/doi/10.1002/art.42077/abstract>).

Experiments with ¹H nuclear magnetic resonance (NMR) imaging. A total of ~600,000 RA FLS were starved of glutamine and glucose for 4 hours and then incubated in either DMSO or the glutaminase inhibitor CB-839 (300 nM) along with 10 ng/ml of platelet-derived growth factor (PDGF) for 4 hours in



Figure 1. Unsupervised analysis of metabolic pathways associated with differentially modified genome-wide chromatin and DNA states and gene expression in rheumatoid arthritis (RA) fibroblast-like synoviocytes (FLS) compared to osteoarthritis FLS. **A**, Metabolic-related pathways and their occurrences in RA FLS. **B**, Metabolic pathways according to histone modification, whole-genome bisulfite sequencing, assay for transposase-accessible chromatin with sequencing (ATAC-seq), and RNA sequencing. PI3K = phosphatidylinositol 3-kinase; SLC = solute carrier; LPA = lysophosphatidic acid receptor; HIF-1 α = hypoxia-inducible factor 1 α ; PIP3 = phosphatidylinositol 3-trisphosphate; H3K4me3 = histone H3 lysine 4 trimethylation; SREBF = sterol regulatory element binding transcription factor 1; mTOR = mechanistic target of rapamycin.

medium with 6 mM glutamine without glucose for metabolite extraction, as described elsewhere (33–35) and in Supplementary Methods (<http://onlinelibrary.wiley.com/doi/10.1002/art.42077/abstract>).

Acquisition and processing of NMR. NMR spectra were recorded using a 600 MHz Bruker Avance III NMR spectrometer fitted with a 1.7-mm triple resonance cryoprobe. We used the standard Bruker pulse sequence "noesygppr1d" with a mixing

time of 500 msec. A daily quality assurance procedure was performed before sample data acquisition, involving temperature checks and calibration, including shim calibration and water suppression quality. The data were collected at the NMR facility at the University of California San Diego Skaggs School of Pharmacy and Pharmaceutical Sciences.

Identification and quantification of metabolites.

Metabolites were identified using Chenomx NMR suite 8.5 professional 600 MHz version 11 software, which contains a library of compounds to match peaks of metabolites according to chemical shifts. Metabolite concentrations were normalized according to TSP-d4 (no. 269913; MilliporeSigma). Cell pellets were normalized according to protein quantification using Bradford. Supernatant concentrations were determined after subtraction from control values in complete DMEM; negative values suggest that the metabolite has been consumed by cells in culture (metabolite concentrations are in μM).

Statistical analysis. Statistical analysis was performed using GraphPad Prism software version 8. Results are the mean \pm SD. Normality of variables was assessed using a Kolmogorov-Smirnov normality test or Shapiro-Wilk normality test. For comparison between >2 conditions, ordinary one-way analysis of variance (ANOVA) or Kruskal-Wallis tests were used depending on normality of the distribution of the variables, followed by Tukey's multiple comparisons test or Dunn's multiple comparisons test, respectively. *P* values less than 0.05 by 2-sided test were considered significant. Heatmaps generated with R software show Pearson's correlation coefficients for gene expression. Correlation ranges were from -1 to 1 . The greater the R^2 value, the better the model. Pearson's correlation coefficients between -0.3 and -0.5 or 0.3 and 0.5 were considered weak, correlations between -0.5 and -0.7 or 0.5 and 0.7 were considered moderate, and correlations from <-0.7 to >0.7 were considered strong. Our sample size of 10 RA FLS and 10 OA FLS was used to detect a Pearson's correlation coefficient of 0.7 with 80% power ($\alpha = 0.05$, by 2-tailed test).

RESULTS

Unsupervised analysis of metabolic pathways associated with differential marks between OA FLS and RA FLS. Histone modification, WGBS, ATAC-seq, and RNA-Seq data were individually analyzed to identify metabolic pathways associated with differential genome-wide chromatin and DNA states and gene expression between OA FLS and RA FLS. Interestingly, in addition to the significant enrichment of pathways involved in inflammation, immune response, matrix regulation, and cell migration (see Supplementary File 1, <http://onlinelibrary.wiley.com/doi/10.1002/art.42077/abstract>), we identified several enriched metabolic-related pathways in RA

FLS. The metabolic-related pathways and number of occurrences of pathways are shown in Figure 1A, and Figure 1B shows the pathways according to histone modification, WGBS, ATAC-seq, and RNA-Seq.

Interestingly, enriched metabolic pathways were only associated with changes in activating histone marks linked to increased expression of downstream genes, such as H3K4me1, H3K4me3, and H3K27ac, but not repressive histone marks, such as H3K9me3, H3K27me3, or H3K36me3. Pathways associated with >5 differentially modified genome-wide chromatin and DNA states between OA FLS and RA FLS included phosphatidylinositol 3-kinase (PI3K)/Akt signaling and metabolism of carbohydrates. PI3K/Akt signaling is a well-known pathway involved in metabolic reprogramming and metabolism of carbohydrates, and our group and others previously described that PI3K-Akt plays an important role in the aggressive phenotype of FLS (36–40). The solute carrier-mediated transmembrane transport pathway is another pathway that stood out as significant. These data indicate that changes in chromatin accessibility and activation of regulatory regions associated with metabolic genes is a feature of FLS in RA.

Solute carrier-mediated transmembrane transporters with differential marks between OA FLS and RA FLS.

Findings from our epigenetic analyses suggest a role for solute carrier transporters in RA FLS. We conducted a supervised analysis of the epigenetic changes in genes from the solute carrier transporter families. Data regarding histone modification, WGBS, ATAC-seq, and RNA-Seq corresponding to ~ 350 genomically encoded genes of the solute carrier transporter family were probed to determine differences between RA and OA (Supplementary File 2, <http://onlinelibrary.wiley.com/doi/10.1002/art.42077/abstract>). Of these solute carrier genes, 78 were associated with at least 3 differentially modified genome-wide chromatin and DNA states between OA FLS and RA FLS, and 32 genes were associated with at least 4 differentially modified states (Supplementary File 2). We performed a pathway analysis of these 78 genes to identify predominant nutrient transporters (Figure 2A). Other than hexose transporters (which include glucose and fructose), more significant transporters were classified as amino acid transporters.

Figure 2B details the genes with >4 differentially modified marks comparing RA FLS and OA FLS. H3K27ac and H3K4me1 were the most commonly differentially changed histone modifications and correlated with significant changes in ATAC-seq. These transporters were mostly related to amino acid transporters, including glutamine transporters (solute carrier family 38 member 1 [SLC38A1], SLC38A4, SLC7A11, SLC7A5, SLC7A8, SLC1A4) (Figure 2B). Other transporters that were differentially regulated between OA and RA were ion transporters including zinc and bicarbonate transporters, such as SLC4A4, a

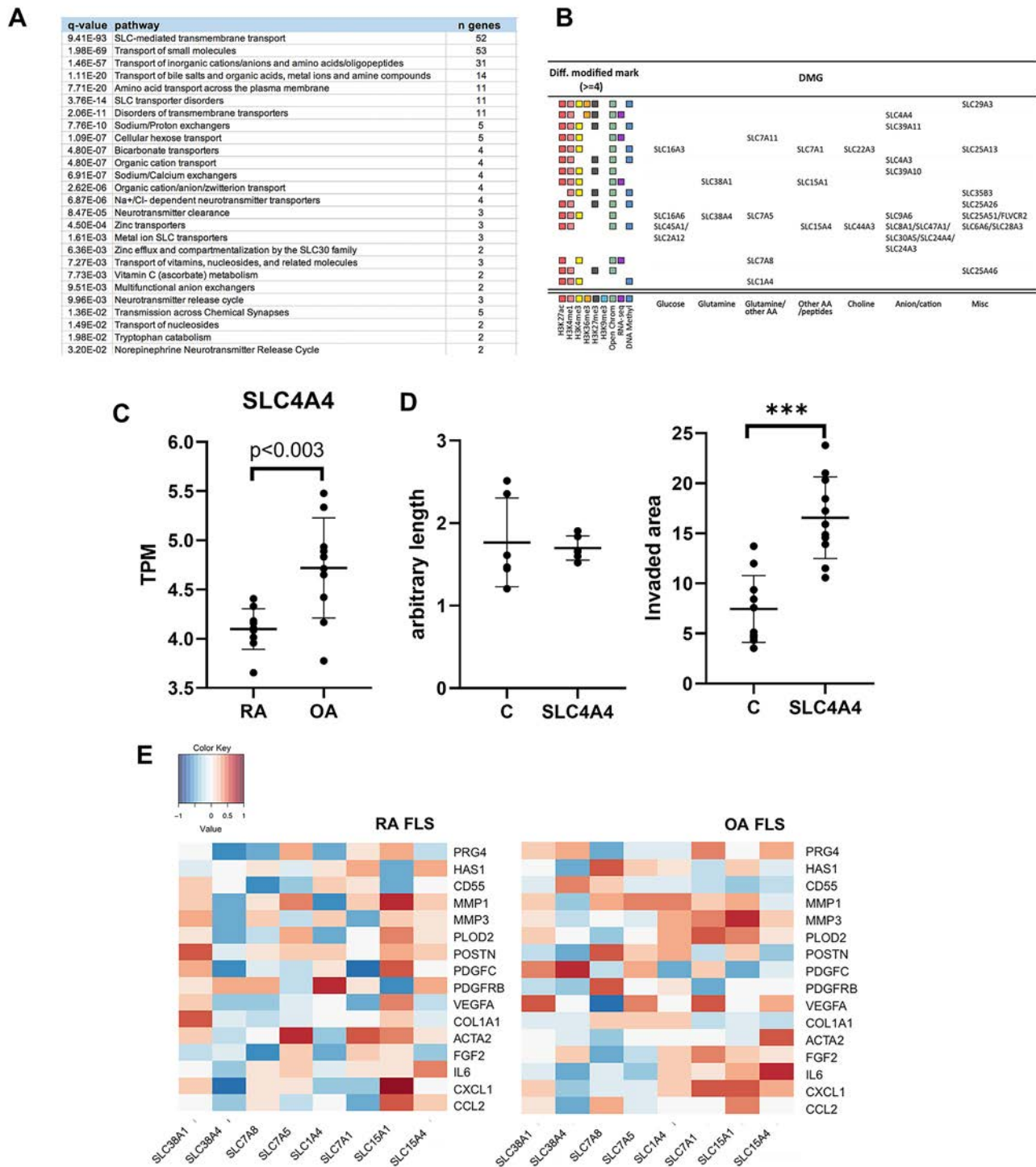


Figure 2. Supervised analysis of solute carrier-mediated transmembrane transporters showing differential marks between osteoarthritis (OA) FLS and RA FLS. **A**, Reactome pathway analysis of the 78 genes associated with differential modifications in at least 3 genome-wide chromatin and DNA states between OA FLS and RA FLS to identify predominant nutrient transporters. **B**, Number and type of dynamic chromatin changes for each of the listed posttranslational histone modifications, ATAC-seq, RNA sequencing, and whole-genome bisulfite sequencing signaling between OA FLS and RA FLS in the 32 genes associated with differential (Diff.) modifications in at least 4 genome-wide chromatin and DNA states. **C**, Expression of *SLC4A4* as assessed by RNA-Seq (transcripts per million [TPM]). Each symbol represents one RA cell line or one OA cell line. **D**, Results of transfection of RA cells (in medium with glucose and glutamine) with solute carrier family 4 member 4 (*SLC4A4*) small interfering RNA to assess cell migration with a scratch assay (left) and to assess cell invasion after plating the cells in Matrigel (right). Each symbol represents each replicate between 3 cell lines. *** = $P < 0.001$ by 2-tailed t test. In **C** and **D**, horizontal lines and error bars show the mean \pm SD. **E**, Heatmap showing gene expression associations between amino acid (AA)-related solute carrier transporters and genes related to aggressive FLS behavior in 10 RA FLS and 10 OA FLS cell lines. Color key shows the strength and direction of the correlation as determined by Pearson's correlation coefficient. DMG = differentially modified gene (see Figure 1 for other definitions). Color figure can be viewed in the online issue, which is available at <http://onlinelibrary.wiley.com/doi/10.1002/art.42077/abstract>.

bicarbonate transporter that is heavily differentially regulated between OA FLS and RA FLS (Figure 2B) with comparatively higher expression in OA FLS (Figure 2C). Of note, small interfering RNA (siRNA) knockdown of *SLC4A4* resulted in increased invasion, but not migration, compared to the control siRNA, suggesting that this transporter is repressed in RA FLS to increase its aggressive phenotype (Figure 2D and Supplementary Figure 1A, <http://onlinelibrary.wiley.com/doi/10.1002/art.42077/abstract>). Supplementary Figure 1B depicts significant solute carrier transporter genes that have >4 differentially modified marks comparing RA FLS and OA FLS and their location in the cell (<http://onlinelibrary.wiley.com/doi/10.1002/art.42077/abstract>).

We also performed analyses and found correlations between the expression of nutrient transporters that were more differentially marked between 10 RA FLS and 10 OA FLS cell lines and the expression of various genes related to FLS-relevant functions including synovial fluid molecules (*PRG4* and *HAS1*), matrix metalloproteinases (*MMP1*, *MMP3*), *IL6*, chemokines (*CXCL1*, *CCL2*), genes involved in cell invasion and migration (*POSTN*, *PLOD2*, *ACTA2*, *PDGFC*) and angiogenesis (*VEGF*, *FGF2*), and genes involved in fibrosis (*PLOD2*, *COL1A1*) (4–6,36,41–44).

Our findings demonstrated an association between amino acid-related solute carrier transporters (Figure 2E) and other nutrient-related solute carrier transporters (Supplementary Figure 1C, <http://onlinelibrary.wiley.com/doi/10.1002/art.42077/abstract>). Several solute carrier transporters moderately or strongly correlated with these genes in both OA FLS and RA FLS, for instance between *SLC15A4* and *IL6*, suggesting a critical role of this transporter in interleukin-6 (IL-6) expression in all synovial fibroblasts. Of interest, 2 transporters, *SLC38A1* (a glutamine transporter) and *SLC15A1* (a dipeptide L-alanyl-L-glutamine transporter) moderately or strongly correlated ($r > 0.5$) with >1 of these genes, including genes for chemokines (*CXCL1*, *CCL2*), genes for matrix metalloproteinases (*MMP1*), and genes involved in cell invasion in RA FLS (*POSTN*, *PLOD2*, and *PDGFC*).

The expression of solute carrier 39 transporters, which controls the influx of zinc into the cytoplasm, but not expression of solute carrier 30 transporters, which controls the efflux of zinc, moderately-to-strongly correlated with these genes in RA FLS but not in OA FLS (Supplementary Figure 1C, <http://onlinelibrary.wiley.com/doi/10.1002/art.42077/abstract>). In OA FLS, other solute carrier transporters moderately or strongly correlated with

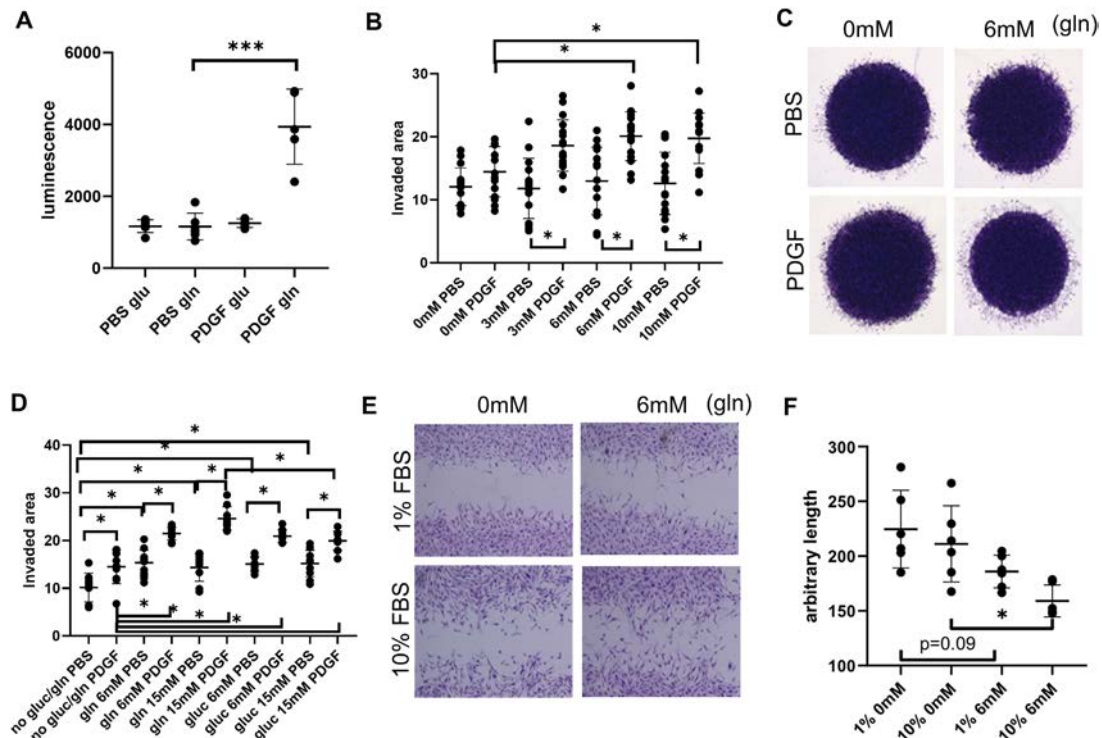


Figure 3. Glutamine availability enhances invasion and migration of RA FLS. **A**, Quantification of luminescence of RA FLS was used to measure intracellular glutamine (gln) and glutamate (glu) levels in cell cultures after removal of glucose and 2-hour stimulation with platelet-derived growth factor (PDGF). **B–D**, RA FLS were starved overnight without glucose (gluc) and then starved of glutamine for 4 hours, plated for invasion, and stimulated with various amounts of glutamine with or without PDGF. Quantification of the results (**B** and **D**) and images of RA FLS invasion in representative samples (**C**) are shown. **E** and **F**, RA FLS were plated and starved overnight in medium with 0.1% fetal bovine serum (FBS). Medium without glucose was added along with various concentrations of glutamine, and scratch assays were used to assess cell migration in cultures with 1% or 10% dialyzed FBS. Representative images of RA FLS migration (**E**) and quantification of results (**F**) are shown. Each symbol represents the mean of 3–4 FLS cell lines. Horizontal lines and error bars show the mean \pm SD. * = $P < 0.05$; *** = $P < 0.001$, by one-way analysis of variance followed by Tukey's multiple comparisons test. PBS = phosphate buffered saline (see Figure 1 for other definitions). Color figure can be viewed in the online issue, which is available at <http://onlinelibrary.wiley.com/doi/10.1002/art.42077/abstract>.

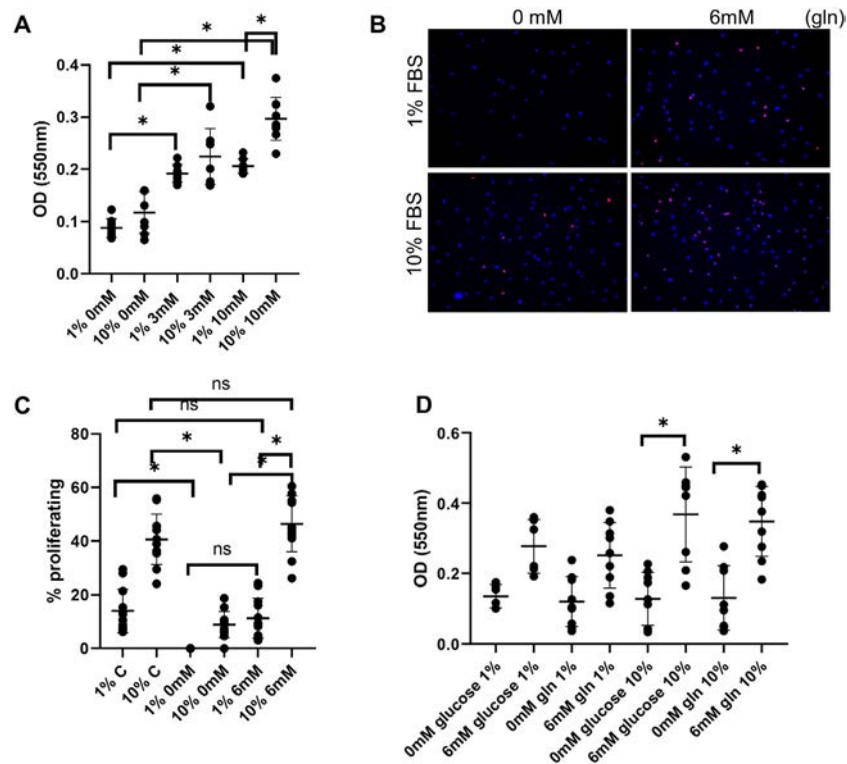


Figure 4. Glutamine (gln) availability enhances proliferation of RA FLS. **A**, RA FLS were plated, starved overnight with 0.1% fetal bovine serum (FBS), and stimulated with various amounts of glutamine without glucose. MTT was added after 4 days of stimulation. **B** and **C**, FLS were starved overnight with medium containing 0.1% FBS without glucose and with different concentrations of glutamine and were left to proliferate for 4 days. Representative images are shown for cells cultured either without glutamine (0 mM) or with 6 mM glutamine in 1% or 10% dialyzed FBS, and stained with Hoechst 33342 (blue) dye to assess proportions of positive cells and EdU to assess cell proliferation (**B**). Results were quantified as the percentage of EdU-positive cells among the total number of Hoechst 33342-positive cells (**C**), and as the optical density of staining intensity after 7-day MTT assay of FLS stimulated with either glucose or glutamine in 1% or 10% FBS (**D**). Each symbol represents the mean of 3 FLS cell lines. Horizontal lines and error bars show the mean \pm SD. * = $P < 0.05$ by one-way analysis of variance followed by Tukey's multiple comparisons test. C = control treatment with Dulbecco's modified Eagle's medium with 25 mM glucose and 6 mM glutamine; NS = not significant (see Figure 1 for other definitions). Color figure can be viewed in the online issue, which is available at <http://onlinelibrary.wiley.com/doi/10.1002/art.42077/abstract>.

>1 of these genes, including *SLC15A4* (histidine carrier) and *SLC7A1* (alanine, serine, cysteine, and threonine transporter). As recent evidence emphasizes the emergent role of FLS-mediated synovitis in OA (45), these differential correlations in RA FLS and OA FLS suggest different key FLS transporters in both diseases.

Effect of glutamine availability on invasion, migration, and proliferation, but not on cytokine secretion, in RA FLS.

Between OA FLS and RA FLS, among other nutrients, some of the most significantly heavily differentially regulated solute carrier transporters were related to amino acid transporters (Figure 2B), specifically glutamine transporters (*SLC38A1*, *SLC38A4*, *SLC7A11*, *SLC7A5*, *SLC7A8*, *SLC1A4*). We tested whether glutamine metabolism was important for the aggressive FLS phenotype. We first determined glutamine uptake by measuring intracellular levels after glucose starvation with or without additional PDGF stimulation. As shown in Figure 3A, intracellular glutamine levels increased after PDGF stimulation of RA FLS.

We then tested whether an increase in glutamine availability would enhance the invasive phenotype of RA FLS. As shown in Figures 3B and C, an increase in the amount of glutamine in the medium increased RA FLS invasiveness under a state of glucose deprivation. These results were not observed when RA FLS were treated with different concentrations of arginine or lysine (Supplementary Figure 2A, <http://onlinelibrary.wiley.com/doi/10.1002/art.42077/abstract>). Of interest, when comparing the effects of either glucose or glutamine in the medium, RA FLS efficiently used either carbon source during invasion (Figure 3D). In addition, migration was also dependent on glutamine in RA FLS (Figure 3E). Of note, OA FLS had more heterogeneous glutamine dependence during migration (Supplementary Figure 2B).

In Figures 4A–C, viability measured by an MTT assay and proliferation measured by an EdU assay showed glutamine dependence in the absence of glucose in RA FLS. As with migration, RA FLS were found to also use glutamine in the absence of glucose for proliferation (Figure 4D). OA FLS showed a pattern of proliferation similar to that of RA FLS (Supplementary Figure 2C). Of note, MMP-3, IL-6, and C-C motif chemokine ligand 2 secretion after

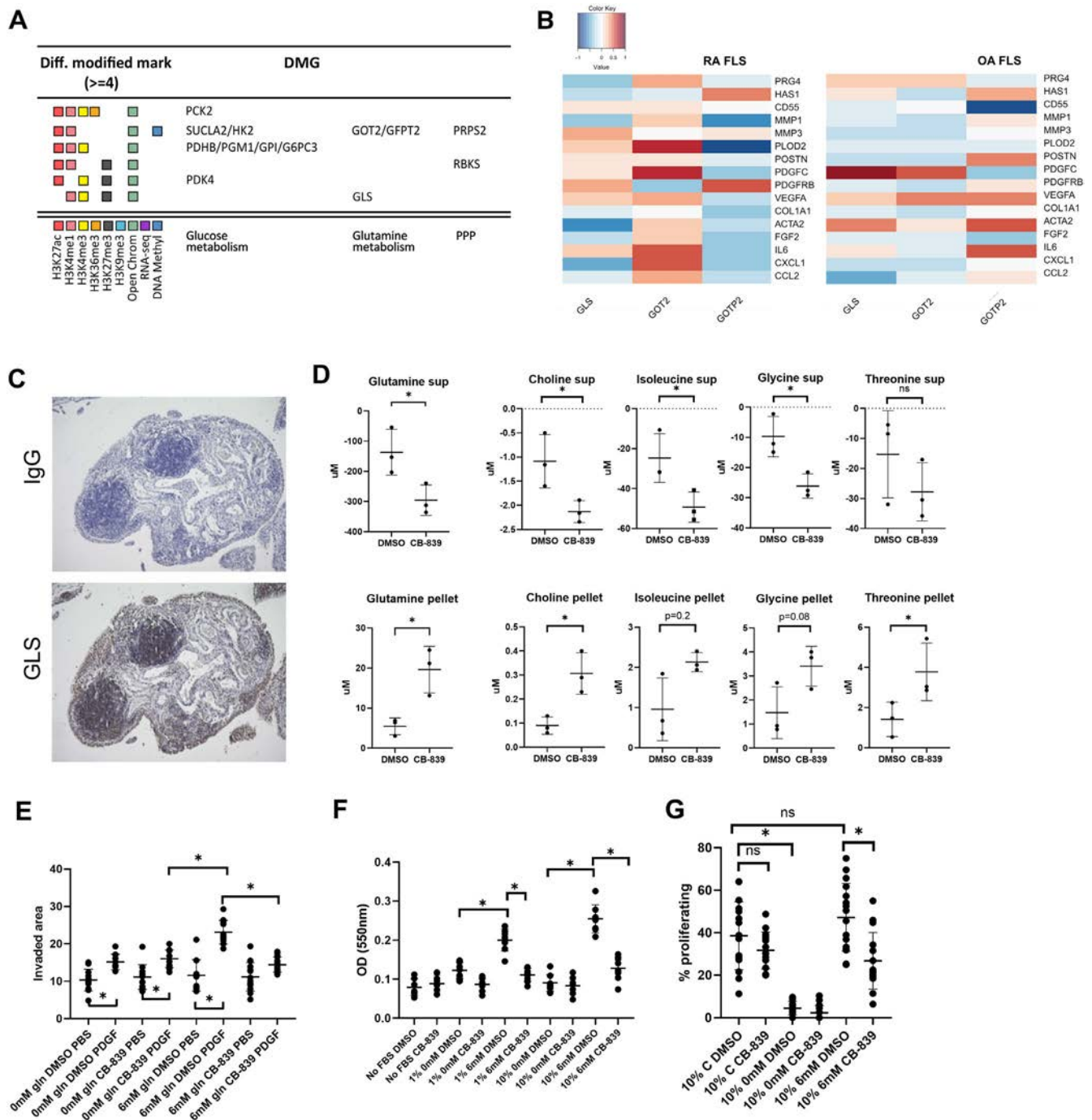


Figure 5. Effect of glutaminase inhibition on FLS invasion and proliferation. **A**, Number and type of dynamic chromatin changes of genes with at least 4 differential (Diff.) marks between osteoarthritis (OA) FLS and RA FLS. **B**, Heatmaps showing the association between glutamine-related genes and genes related to aggressive FLS behavior in 10 RA FLS and 10 OA FLS cell lines. Color key shows the strength and direction of the correlation as determined by Pearson's correlation coefficient. **C**, Representative images showing the distribution of glutaminase (GLS) expression in RA synovial tissue. **D**, One-dimensional ^1H nuclear magnetic resonance spectrum and concentration of glutamine in pellet and supernatant (sup) in cultures containing 3 RA FLS cell lines after 4 hours of platelet-derived growth factor (PDGF) stimulation with or without CB-839 ($10\ \mu\text{M}$). **E**, Quantification of invasion of RA FLS. Cells were plated on Matrigel, deprived of glucose, and treated with glutamine with or without CB-839. **F**, Results of 4-day MTT assay of RA FLS deprived of glucose under the indicated conditions. **G**, EdU assay assessing proliferation of RA FLS with or without CB-839. Results are expressed as a percentage of EdU-expressing cells among the total number of cells. In **D–G**, each symbol represents the mean of 4 RA cell lines. Horizontal lines and error bars show the mean \pm SD. * = $P < 0.05$ by 2-tailed t -test in **D** and by one-way analysis of variance in **E–G**. DMG = differentially modified gene; PPP = pentose phosphate pathway; GOT2 = glutamic-oxaloacetic transaminase 2; C = control treatment with Dulbecco's modified Eagle's medium with 25 mM glucose and 6 mM glutamine; PBS = phosphate buffered saline; NS = not significant (see Figure 1 for other definitions). Color figure can be viewed in the online issue, which is available at <http://onlinelibrary.wiley.com/doi/10.1002/art.42077/abstract>.

PDGF and tumor necrosis factor stimulation were not glutamine dependent (Supplementary Figures 3A and B). However siRNA knockdown of *SLC38A1*, one of the glutamine transporters that was heavily differentially marked between OA and RA (for which expression was significantly up-regulated in RA FLS compared to OA FLS) did not decrease invasion or migration. This suggests some redundancy in roles of the glutamine transporters (Supplementary Figures 3C–E).

Glutamine pathway-related enzymes and the differential marking between OA FLS and RA FLS. Since targeting an enzyme appeared to be a more feasible approach to inhibit the glutamine metabolic pathway than targeting several transporters involved in glutamine transport, we analyzed the enzymes related to the glutamine pathway. We analyzed 19 genomically encoded genes of glutamine-related enzymes in the different data sets of histone marks, RNA-Seq, ATAC-seq, and WGBS to find differences between RA and OA samples (Supplementary File 3, <http://onlinelibrary.wiley.com/doi/10.1002/art.42077/abstract>). Given that glucose metabolism is associated with the aggressive phenotype of FLS (38–40) and that glucose transporters were also differentially marked between RA FLS and OA FLS, we also analyzed 83 generically encoded genes related to glucose metabolism (Supplementary File 3, <http://onlinelibrary.wiley.com/doi/10.1002/art.42077/abstract>).

The type of dynamic chromatin changes for each of the listed posttranslational histone modifications, ATAC-seq, RNA-Seq, and WGBS signaling of genes associated with at least 4 differentially modified genome-wide chromatin and DNA states in RA FLS compared to OA FLS are shown in Figure 5A and Supplementary Figure 4A (<http://onlinelibrary.wiley.com/doi/10.1002/art.42077/abstract>). Several glucose metabolism-related genes were heavily differentially marked and correlated with significant changes in ATAC-seq, including *PCK2*, *PDHB*, and *PGM1*. Of interest the gene for hexokinase 2 (HK-2), a glycolytic enzyme recently described as a key gene in regulating the aggressive phenotype in RA FLS (26,46), was also heavily differentially marked. HK-2 was also the gene that moderately-to-strongly correlated with genes related to the aggressive phenotype of RA FLS (Supplementary Figure 4B, <http://onlinelibrary.wiley.com/doi/10.1002/art.42077/abstract>). Our epigenetic analysis also revealed that glutaminase, glutamic-oxaloacetic transaminase 2 (GOT-2), and glutamine-fructose-6-phosphate transaminase 2 (GFPT-2) were the glutamine metabolism-related enzymes that were more differentially marked between RA FLS and OA FLS. Glutaminase and GOT-2 appeared to be more critical in RA FLS, and GFPT-2 was more critical in OA FLS (Figure 5B).

Glutaminase, a key target for the aggressive phenotype of FLS. Glutaminase, which is responsible for the conversion of glutamine to glutamate, plays a vital role in up-regulating cell metabolism for tumor cell growth and is considered a valuable

therapeutic target for cancer treatment. Several glutaminase inhibitors have been developed and are currently being evaluated in phase I and phase II clinical trials. Thus, we focused on glutaminase to determine whether glutaminase could be a feasible target for the aggressive phenotype of FLS. Our findings showed that glutaminase was expressed in both the lining and sublining layer of RA synovial tissue (Figure 5C).

We then investigated the effect of CB-839 compound, an inhibitor of glutaminase, on FLS metabolism, proliferation, and invasion. We first analyzed the metabolic effect of CB-839 after PDGF stimulation. The effect of the inhibitor on glutamine levels is shown in Supplementary Figure 5A (<http://onlinelibrary.wiley.com/doi/10.1002/art.42077/abstract>). As expected, there was a significant increase in intracellular glutamine in the presence of the inhibitor. Interestingly, levels of other intracellular nutrients, including choline, isoleucine, glycine, and threonine, also increased with CB-839 (Figure 5D and Supplementary Figures 5B and C, <http://onlinelibrary.wiley.com/doi/10.1002/art.42077/abstract>). Results from MTT viability assays revealed that CB-839 was nontoxic at a wide range of concentrations (Supplementary Figure 5D) and CB-839 (300 nM) significantly reduced RA FLS invasion (Figure 5E) and proliferation (Figures 5F and G) but only under glucose-free conditions (Figure 5E and Supplementary Figure 5E).

Effect of c-Myc, a key transcription factor for the aggressive phenotype of FLS. To determine the regulation of nutrient transporters in RA FLS, we performed a motif enrichment analysis of the promoters of the solute carrier genes exhibiting differential ATAC-seq signaling between RA FLS and OA FLS (Supplementary Figure 6A, <http://onlinelibrary.wiley.com/doi/10.1002/art.42077/abstract>). In addition, we performed an analysis of the motifs of the promoter regions of genes with differential modifications in at least 4 genome-wide chromatin and DNA states and found enrichment of motifs for c-Myc and the nuclear receptors TLX, retinoic acid receptor-related orphan nuclear receptor α (ROR α), and ROR γ (Figure 6A). The number of putative c-Myc binding sites in the analyzed solute carrier transporters are shown in Supplementary Figure 6B (<http://onlinelibrary.wiley.com/doi/10.1002/art.42077/abstract>). Some solute carriers, including transporters involved in lactate/pyruvate (SLC16A3 and SLC16A6), zinc (SLC39A10), and amino acids (SLC38A1 and SLC7A8) had a high number of putative binding sites. Importantly, c-Myc was expressed in the lining of RA tissue (Figure 6B), and c-Myc inhibition in FLS altered the intracellular levels of pyruvate and several amino acids, including glutamine, pyruvate, succinate, alanine, and valine, suggesting changes in their transport and/or FLS metabolic pathways (Figure 6C and Supplementary Figure 6C, <http://onlinelibrary.wiley.com/doi/10.1002/art.42077/abstract>).

Since c-Myc is known to regulate the expression of genes, especially in conditions with glucose starvation (47), and RA FLS

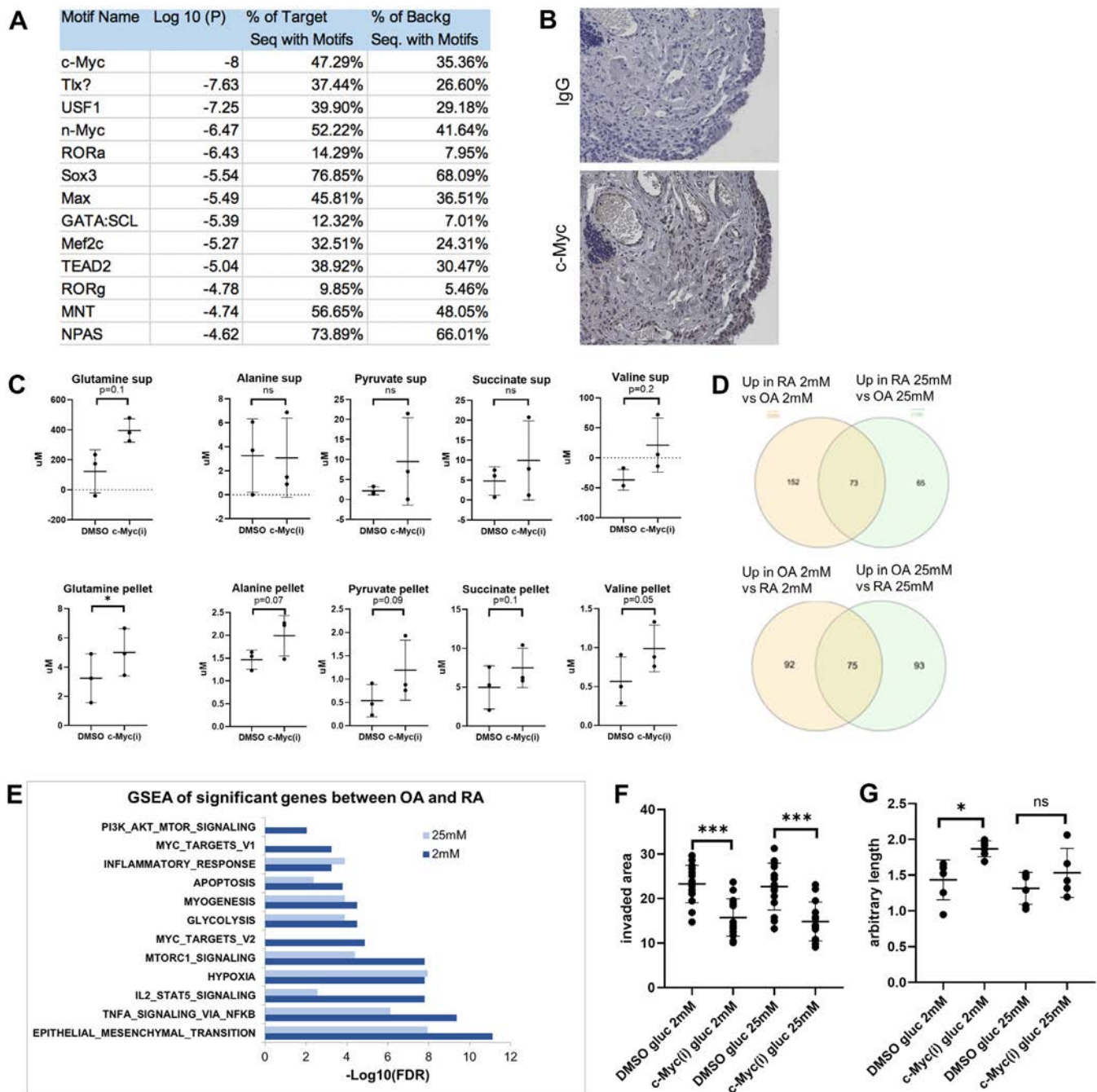


Figure 6. Effect of c-Myc inhibition on FLS invasion and proliferation. **A**, Motif analysis of promoters of genes associated with alterations in at least 4 genome-wide states. **B**, Representative images showing the distribution of c-Myc expression in RA synovial tissue. **C**, Concentration of metabolites in pellet and supernatant (sup) obtained from 1-dimensional ^1H nuclear magnetic resonance spectrum analysis using 3 RA cell lines in 1% dialyzed medium with 6 mM glutamine with or without c-Myc inhibitor ($10\ \mu\text{M}$) for 24 hours. **D**, Venn diagram showing significantly up-regulated genes in 4 RA FLS cell lines compared to 3 osteoarthritis (OA) FLS cell lines in 25 mM and 2 mM of medium (top) and significantly up-regulated genes in OA compared to RA FLS in 25 mM or 2 mM of medium (bottom). **E**, Gene set enrichment analysis (GSEA) using hallmark data sets differentially expressed between RA FLS and OA FLS in 25 mM or 2 mM glucose (gluc). **F** and **G**, Results of invasion (**F**) and migration (**G**) experiments, in which RA FLS were plated in 1% dialyzed medium with 6 mM glutamine and either 2 mM or 25 mM glucose, with or without c-Myc inhibitor (c-Myc[i]) ($10\ \mu\text{M}$). In **C**, **F**, and **G**, each symbol represents the mean of 3 cell lines. Horizontal lines and error bars show the mean \pm SD. * = $P < 0.05$; *** = $P < 0.001$, by one-way analysis of variance followed by Tukey's multiple comparisons test. Tlx = tailless homolog; USF = upstream stimulatory factor; RORa = retinoic acid receptor-related orphan nuclear receptor; TEAD2 = transcription-enhancer factor domain 2; MNT = MAX network transcriptional repressor; NPAS = neuronal PAS; FDR = false discovery rate; NS = not significant (see Figure 1 for other definitions). Color figure can be viewed in the online issue, which is available at <http://onlinelibrary.wiley.com/doi/10.1002/art.42077/abstract>.

kept its aggressive phenotype even with glucose deprivation, we investigated whether c-Myc was also involved in the regulation of RA FLS phenotypes under deprivation. We performed RNA sequencing for 4 RA FLS and 3 OA FLS cell lines incubated with 25 mM or 2 mM of glucose for 5 hours to determine which signaling pathways are deregulated upon glucose deprivation. The differential expression analysis showed 225 up-regulated genes in RA cells versus OA cells with 2 mM glucose, 138 unregulated genes in RA cells versus OA cells each with 25 mM glucose, 167 down-regulated genes in RA cells versus OA cells each with 2 mM glucose, and 168 down-regulated genes in RA cells versus OA cells each with 25 mM glucose (Figure 6D). GSEA of differentially expressed genes between RA cells and OA cells with either 2 mM or 25 mM of glucose showed activation of Myc targets and PI3K/Akt signaling that were only differently activated in the cultures with 2 mM glucose and RA FLS versus 2 mM glucose and OA FLS (Figure 6E). These results suggest that Myc and PI3K/Akt pathways are involved in the distinct response of RA FLS under glucose starvation. Upon investigation of the effect of a c-Myc inhibitor on RA FLS at a viable dosage (Supplementary Figure 6D), c-Myc inhibition attenuated RA FLS migration and invasion (Figures 6F and G). Of note, the c-Myc inhibitor significantly attenuated RA FLS migration only when the cells were cultured in 2 mM of glucose and not in 25 mM of glucose, but interestingly RA FLS invasion was equally attenuated with either dose of glucose.

DISCUSSION

The differences in epigenetic changes of metabolic genes in OA FLS versus RA FLS are largely unknown. Here, we described epigenetic changes in metabolic genes related to solute carrier transporters that differed between RA FLS and OA FLS. Our current findings might help to better understand the increased demand for nutrients in RA synovial cells (1). For instance, when glucose demand is high in RA synovium, the up-regulation of glutamine transporters may allow FLS to utilize other sources of energy. Our results showed that glutamine served as an alternate carbon source in the absence of glucose. In addition, RA FLS did not utilize other amino acids such as lysine and arginine. Even though FLS appeared to facilitate uptake of other amino acids and nutrients during glutaminase inhibition, they did not have a role in invasion or proliferation. Of interest, OA FLS also utilized glutamine, although we were unable to detect large differences in *in vitro* glutamine metabolism between OA FLS and RA FLS in these conditions. This could indicate that either the overall differences in glutamine metabolism between OA FLS and RA FLS were subtle in cell culture or that we could not mimic *in vivo* inflamed synovial conditions in which RA FLS would have greater glutamine metabolic changes than OA FLS.

Our results also suggest that inhibiting glutamine metabolism with a glutaminase inhibitor (CB-839) could potentially suppress

aggressive features of RA FLS, such as invasion, migration, and proliferation (48). Even though the differences in OA FLS are small, the important role of glutamine in these functions suggests that they could be important in the context of rheumatoid synovitis. Glutamine metabolism has also been a focus in recent years for other diseases such as cancer (49,50), and clinical trials using glutaminase inhibitors are under way in cancer research (50). Since glutamine metabolism does not seem to play a role in cytokine secretion, inhibition of glutamine metabolism would mostly target the aggressive phenotype of FLS and could complement current immunotherapies. In addition, inhibiting the glutaminase enzyme could prove to be more effective than knockdown of certain solute carrier glutamine transporters, since they may have a redundant function.

Future studies are needed to investigate the roles of glutamine and other amino acid transporters (such as SLC7A11) in more depth in order to inhibit their aggressive phenotype and promote only essential homeostatic FLS functions. Tracing experiments, and not just paired supernatant–pellet concentrations, are needed to better determine changes in amino acid levels and the role of these amino acid transporters. Of note, solute carrier transporters have long been used as a drug target in RA, since sulfasalazine is a nonspecific inhibitor of SLC7A11, which facilitates the import and export of the amino acids glutamate and cystine.

Other nutrient transporters are potential therapeutic targets. Findings from our epigenetic analysis could help prioritize the transporters and target specific activated metabolic pathways in synovial RA. For example, many other transporters specific to choline, ions like zinc, sodium, and calcium, as well as bicarbonate, nucleosides, lactate, and mitochondrial carriers are differentially regulated between RA and OA. A prior study from our group described a role of choline in RA FLS phenotypes (51). Our analysis indicated that SLC22A3 and SLC44A3 are potential key choline transporters in FLS. The role of zinc in RA FLS was also recently described (52). SLC39A10 and SLC39A11 may be promising candidates for targeted inhibition of zinc transport. Although our correlation analysis highlighted specific FLS transporters in both OA cell lines and RA cell lines, the results need to be interpreted with caution given the limited power of the analysis and the need for additional biologic validation.

Our findings also suggest a possible role for bicarbonate transporters, mitochondrial carriers, and nucleosides in RA pathogenesis and indicate that they might also be attractive transporter targets in RA. Bicarbonate transporters have large roles in regulating pH in cancer through the SLC4 family of transporters (20). These transporters seem to have different roles that serve different purposes, which need further exploration. For example, SLC4A4 is up-regulated in breast cancer cells and its knockdown reduces migration (20). However, in FLS, the expression of SLC4A4 transporter is higher in OA than in RA, and down-

regulation further increases expression of the invasive phenotype of RA FLS but does not increase migration. Of note, migration across a surface and invasion into the extracellular matrix are distinct biologic functions and involve distinct patterns of gene expression, such as proteases, to degrade the matrix at the leading edge. The SLC25 family is composed of mitochondrial carriers which have been identified as biomarkers in cancers and regulate several different types of substrates, such as amino acids, nucleotides, carboxylates, and keto acids (18). Nucleosides can be used as precursors to essential molecules like ATP but can also be used as signaling molecules (53), yet no information on the role of these transporters in RA FLS has been described to date. Future studies should investigate the specific role of other solute carrier transporters in RA FLS to determine whether the specific transporter, a key enzyme, or a transcription factor is the most feasible option to regulate this metabolic pathway.

Other than specific transporters, one metabolic regulator, c-Myc, which plays an important role in cancer metabolism (54), appeared in our analysis, suggesting that this transcription factor has a role in metabolic reprogramming of RA FLS. Glutamine usage is promoted by c-Myc in that c-Myc up-regulates glutaminase and, in addition, up-regulates GOT-2 and glutamine synthetase, which increase glutamine dependence in cancer by turning glutamate back into glutamine (47). Lactic acid and pyruvate can also be regulated by c-Myc (55). SLC16A3, another transporter identified in our analysis, transports lactate and pyruvate. Interestingly, Ras- and c-Myc-dependent signaling events cooperate to regulate the growth and invasiveness of RA FLS (56). Further experiments are needed to understand the role of c-Myc under stress conditions, such as starvation and hypoxia, on glutamine metabolism and how c-Myc might contribute to RA pathogenesis. In addition, while specific targets of c-Myc have been challenging to identify due to its structure and location, the identification of new binding partners, such as BPTF (57), and other new strategies to inhibit c-Myc have recently been described (58).

Overall, RA FLS demonstrate changes in epigenetic marks associated with genes related to metabolism and nutrient transporters. Validation studies of 1 pathway demonstrated that the glutamine pathway, and specifically glutaminase inhibition, could regulate the aggressive phenotype of RA FLS. Additionally, our data set could potentially be used to identify other RA targets that can be used to develop novel therapeutic agents.

AUTHOR CONTRIBUTIONS

All authors were involved in drafting the article or revising it critically for important intellectual content, and all authors approved the final version to be published. Dr. Guma had full access to all of the data in the study and takes responsibility for the integrity of the data and the accuracy of the data analysis.

Study conception and design. Torres, Pedersen, Cobo, Ai, Coras, Murillo-Saich, Nygaard, Sanchez-Lopez, Murphy, Wang, Firestein, Guma.

Acquisition of data. Torres, Pedersen, Cobo, Ai, Coras, Murillo-Saich, Nygaard.




Analysis and interpretation of data. Torres, Pedersen, Cobo, Ai, Coras, Murillo-Saich, Nygaard, Sanchez-Lopez, Murphy, Wang, Firestein, Guma.

REFERENCES

- Falconer J, Murphy AN, Young SP, Clark AR, Tiziani S, Guma M, et al. Synovial cell metabolism and chronic inflammation in rheumatoid arthritis [review]. *Arthritis Rheumatol* 2018;70:984–99.
- Weyand CM, Goronzy JJ. Immunometabolism in the development of rheumatoid arthritis. *Immunol Rev* 2020;294:177–87.
- Henderson B, Bitensky L, Chayen J. Glycolytic activity in human synovial lining cells in rheumatoid arthritis. *Ann Rheum Dis* 1979;38:63–7.
- Nygaard G, Firestein GS. Restoring synovial homeostasis in rheumatoid arthritis by targeting fibroblast-like synoviocytes [review]. *Nat Rev Rheumatol* 2020;16:316–33.
- Bottini N, Firestein GS. Duality of fibroblast-like synoviocytes in RA: passive responders and imprinted aggressors. *Nat Rev Rheumatol* 2013;9:24–33.
- Bustamante MF, Garcia-Carbonell R, Whisenant KD, Guma M. Fibroblast-like synoviocyte metabolism in the pathogenesis of rheumatoid arthritis. *Arthritis Res Ther* 2017;19:110.
- De Oliveira PG, Farinon M, Sanchez-Lopez E, Miyamoto S, Guma M. Fibroblast-like synoviocytes glucose metabolism as a therapeutic target in rheumatoid arthritis. *Front Immunol* 2019;10:1743.
- Sanchez-Lopez E, Cheng A, Guma M. Can metabolic pathways be therapeutic targets in rheumatoid arthritis? [review]. *J Clin Med* 2019;8:753.
- Fearon U, Hanlon MM, Wade SM, Fletcher JM. Altered metabolic pathways regulate synovial inflammation in rheumatoid arthritis. *Clin Exp Immunol* 2019;197:170–80.
- Cairns RA, Harris IS, Mak TW. Regulation of cancer cell metabolism [review]. *Nat Rev Cancer* 2011;11:85–95.
- Zhu J, Thompson CB. Metabolic regulation of cell growth and proliferation. *Nat Rev Mol Cell Biol* 2019;20:436–50.
- Zhang Y, Zhang Y, Sun K, Meng Z, Chen L. The SLC transporter in nutrient and metabolic sensing, regulation, and drug development. *J Mol Cell Biol* 2019;11:1–13.
- Cluntun AA, Lukey MJ, Cerione RA, Locasale JW. Glutamine metabolism in cancer: understanding the heterogeneity. *Trends Cancer* 2017;3:169–80.
- Yamada D, Kawabe K, Tosa I, Tsukamoto S, Nakazato R, Kou M, et al. Inhibition of the glutamine transporter SNAT1 confers neuroprotection in mice by modulating the mTOR-autophagy system. *Commun Biol* 2019;2:346.
- Raposo B, Vaartjes D, Ahlqvist E, Nandakumar KS, Holmdahl R. System A amino acid transporters regulate glutamine uptake and attenuate antibody-mediated arthritis. *Immunology* 2015;146:607–17.
- Xu J, Jiang C, Cai Y, Guo Y, Wang X, Zhang J, et al. Intervening upregulated SLC7A5 could mitigate inflammatory mediator by mTOR-P70S6K signal in rheumatoid arthritis synoviocytes. *Arthritis Res Ther* 2020;22:200.
- Pucino V, Certo M, Bulusu V, Cucchi D, Goldmann K, Pontarini E, et al. Lactate buildup at the site of chronic inflammation promotes disease by inducing CD4(+) T cell metabolic rewiring. *Cell Metab* 2019;30:1055–74.
- Rochette L, Meloux A, Zeller M, Malka G, Cottin Y, Vergely C. Mitochondrial SLC25 carriers: novel targets for cancer therapy [review]. *Molecules* 2020;25:2417.
- Pan Z, Choi S, Ouadid-Ahidouch H, Yang JM, Beattie JH, Korichneva I. Zinc transporters and dysregulated channels in cancers. *Front Biosci (Landmark Ed)* 2017;22:623–43.

20. Gorbatenko A, Olesen CW, Boedtker E, Pedersen SF. Regulation and roles of bicarbonate transporters in cancer. *Front Physiol* 2014; 5:130.
21. Gu HF. Genetic, epigenetic and biological effects of zinc transporter (SLC30A8) in type 1 and type 2 diabetes. *Curr Diabetes Rev* 2017; 13:132–40.
22. VanWert AL, Gionfriddo MR, Sweet DH. Organic anion transporters: discovery, pharmacology, regulation and roles in pathophysiology. *Biopharm Drug Dispos* 2010;31:1–71.
23. Nemtsova MV, Zaletaev DV, Bure IV, Mikhaylenko DS, Kuznetsova EB, Alekseeva EA, et al. Epigenetic changes in the pathogenesis of rheumatoid arthritis. *Front Genet* 2019;10:570.
24. Doody KM, Bottini N, Firestein GS. Epigenetic alterations in rheumatoid arthritis fibroblast-like synoviocytes. *Epigenomics* 2017;9: 479–92.
25. Ai R, Laragione T, Hammaker D, Boyle DL, Wildberg A, Maeshima K, et al. Comprehensive epigenetic landscape of rheumatoid arthritis fibroblast-like synoviocytes. *Nat Commun* 2018;9:1921.
26. Bustamante MF, Oliveira PG, Garcia-Carbonell R, Croft AP, Smith JM, Serrano RL, et al. Hexokinase 2 as a novel selective metabolic target for rheumatoid arthritis. *Ann Rheum Dis* 2018;77:1636–43.
27. Gosselin D, Skola D, Coufal NG, Holtman IR, Schlachetzki JC, Sajti E, et al. An environment-dependent transcriptional network specifies human microglia identity. *Science* 2017;356:eaal3222.
28. Seidman JS, Troutman TD, Sakai M, Gola A, Spann NJ, Bennett H, et al. Niche-specific reprogramming of epigenetic landscapes drives myeloid cell diversity in nonalcoholic steatohepatitis. *Immunity* 2020; 52:1057–74.
29. Heinz S, Benner C, Spann N, Bertolino E, Lin YC, Laslo P, et al. Simple combinations of lineage-determining transcription factors prime cis-regulatory elements required for macrophage and B cell identities. *Mol Cell* 2010;38:576–89.
30. Liberzon A, Subramanian A, Pinchback R, Thorvaldsdottir H, Tamayo P, Mesirov JP. Molecular signatures database (MSigDB) 3.0. *Bioinformatics* 2011;27:1739–40.
31. Liberzon A, Birger C, Thorvaldsdottir H, Ghandi M, Mesirov JP, Tamayo P. The Molecular Signatures Database (MSigDB) hallmark gene set collection. *Cell Syst* 2015;1:417–25.
32. Subramanian A, Tamayo P, Mootha VK, Mukherjee S, Ebert BL, Gillette MA, et al. Gene set enrichment analysis: a knowledge-based approach for interpreting genome-wide expression profiles. *Proc Natl Acad Sci U S A* 2005;102:15545–50.
33. Beckonert O, Keun HC, Ebbels TM, Bundy J, Holmes E, Lindon JC, et al. Metabolic profiling, metabolomic and metabonomic procedures for NMR spectroscopy of urine, plasma, serum and tissue extracts. *Nat Protoc* 2007;2:2692–703.
34. Gowda GA, Raftery D. Analysis of plasma, serum, and whole blood metabolites using ¹H NMR spectroscopy. *Methods Mol Biol* 2019; 2037:17–34.
35. Tiziani S, Emwas AH, Lodi A, Ludwig C, Bunce CM, Viant MR, et al. Optimized metabolite extraction from blood serum for 1H nuclear magnetic resonance spectroscopy. *Anal Biochem* 2008;377:16–23.
36. Bartok B, Firestein GS. Fibroblast-like synoviocytes: key effector cells in rheumatoid arthritis. *Immunol Rev* 2010;233:233–55.
37. Rodriguez-Trillo A, Mosquera N, Pena C, Rivas-Tobio F, Mera-Varela A, Gonzalez A, et al. Non-canonical WNT5A signaling through RYK contributes to aggressive phenotype of the rheumatoid fibroblast-like synoviocytes. *Front Immunol* 2020;11:555245.
38. Garcia-Carbonell R, Divakaruni AS, Lodi A, Vicente-Suarez I, Saha A, Cheroutre H, et al. Critical role of glucose metabolism in rheumatoid arthritis fibroblast-like synoviocytes. *Arthritis Rheumatol* 2016;68: 1614–26.
39. Zou Y, Zeng S, Huang M, Qiu Q, Xiao Y, Shi M, et al. Inhibition of 6-phosphofructo-2-kinase suppresses fibroblast-like synoviocytes-mediated synovial inflammation and joint destruction in rheumatoid arthritis. *Br J Pharmacol* 2017;174:893–908.
40. Binięcka M, Canavan M, McGarry T, Gao W, McCormick J, Cregan S, et al. Dysregulated bioenergetics: a key regulator of joint inflammation. *Ann Rheum Dis* 2016;75:2192–200.
41. Tolboom TC, Pieterman E, van der Laan WH, Toes RE, Huidekoper AL, Nelissen RG, et al. Invasive properties of fibroblast-like synoviocytes: correlation with growth characteristics and expression of MMP-1, MMP-3, and MMP-10. *Ann Rheum Dis* 2002;61: 975–80.
42. Qadri M, Jay GD, Zhang LX, Richendrer H, Schmidt TA, Elsaid KA. Proteoglycan-4 regulates fibroblast to myofibroblast transition and expression of fibrotic genes in the synovium. *Arthritis Res Ther* 2020; 22:113.
43. You S, Yoo SA, Choi S, Kim JY, Park SJ, Ji JD, et al. Identification of key regulators for the migration and invasion of rheumatoid synoviocytes through a systems approach. *Proc Natl Acad Sci U S A* 2014; 111:550–5.
44. Molnes IB, Buckley CD, Isaacs JD. Cytokines in rheumatoid arthritis: shaping the immunological landscape. *Nat Rev Rheumatol* 2016;12:63–8.
45. Han D, Fang Y, Tan X, Jiang H, Gong X, Wang X, et al. The emerging role of fibroblast-like synoviocytes-mediated synovitis in osteoarthritis: an update. *J Cell Mol Med* 2020;24:9518–32.
46. Song G, Lu Q, Fan H, Zhang X, Ge L, Tian R, et al. Inhibition of hexokinases holds potential as treatment strategy for rheumatoid arthritis. *Arthritis Res Ther* 2019;21:87.
47. Bott AJ, Peng IC, Fan Y, Faubert B, Zhao L, Li J, et al. Oncogenic Myc induces expression of glutamine synthetase through promoter demethylation. *Cell Metab* 2015;22:1068–77.
48. Takahashi S, Saegusa J, Sendo S, Okano T, Akashi K, Irino Y, et al. Glutaminase 1 plays a key role in the cell growth of fibroblast-like synoviocytes in rheumatoid arthritis. *Arthritis Res Ther* 2017;19:76.
49. Li T, Le A. Glutamine metabolism in cancer. *Adv Exp Med Biol* 2018; 1063:13–32.
50. Altman BJ, Stine ZE, Dang CV. From Krebs to clinic: glutamine metabolism to cancer therapy. *Nat Rev Cancer* 2016;16:619–34.
51. Guma M, Sanchez-Lopez E, Lodi A, Garcia-Carbonell R, Tiziani S, Karin M, et al. Choline kinase inhibition in rheumatoid arthritis. *Ann Rheum Dis* 2015;74:1399–407.
52. Bonaventura P, Lamboux A, Albaredo F, Miossec P. A feedback loop between inflammation and Zn uptake. *PLoS One* 2016;11:e0147146.
53. Zhang J, Visser F, King KM, Baldwin SA, Young JD, Cass CE. The role of nucleoside transporters in cancer chemotherapy with nucleoside drugs. *Cancer Metastasis Rev* 2007;26:85–110.
54. Miller DM, Thomas SD, Islam A, Muench D, Sedoris K. C-Myc and cancer metabolism. *Clin Cancer Res* 2012;18:5546–53.
55. Song W, Li D, Tao L, Luo Q, Chen L. Solute carrier transporters: the metabolic gatekeepers of immune cells. *Acta Pharm Sin B* 2020;10: 61–78.
56. Pap T, Nawrath M, Heinrich J, Bosse M, Baier A, Hummel KM, et al. Cooperation of Ras- and c-Myc-dependent pathways in regulating the growth and invasiveness of synovial fibroblasts in rheumatoid arthritis. *Arthritis Rheum* 2004;50:2794–802.
57. Richart L, Pau EC, Río-Machin A, de Andrés MP, Cigudosa JC, Lobo VJ, et al. BPTF is required for c-MYC transcriptional activity and in vivo tumorigenesis. *Nat Commun* 2016;7:10153.
58. Chen H, Liu H, Qing G. Targeting oncogenic Myc as a strategy for cancer treatment. *Signal Transduct Target Ther* 2018;3:5.

Prevalence Trends of Site-Specific Osteoarthritis From 1990 to 2019: Findings From the Global Burden of Disease Study 2019

Huibin Long,¹ Qiang Liu,²  Heyong Yin,¹ Kai Wang,² Naicheng Diao,¹ Yuqing Zhang,³  Jianhao Lin,² 
and Ai Guo¹

Objective. To estimate systematic and anatomic site-specific age-standardized prevalence rates (ASRs) and analyze the secular trends of osteoarthritis (OA) at global, regional, and national levels.

Methods. Data were derived from the Global Burden of Disease Study 2019. ASRs and their estimated annual percentage changes (EAPCs) were used to describe the secular trends of OA according to age group, sex, region, country, and territory, as well as the joints involved.

Results. Globally, prevalent cases of OA increased by 113.25%, from 247.51 million in 1990 to 527.81 million in 2019. ASRs were 6,173.38 per 100,000 in 1990 and 6,348.25 per 100,000 in 2019, with an average annual increase of 0.12% (95% confidence interval [95% CI] 0.11%, 0.14%). The ASR of OA increased for the knee, hip, and other joints, but decreased for the hand, with EAPCs of 0.32 (95% CI 0.29, 0.34), 0.28 (95% CI 0.26, 0.31), 0.18 (95% CI 0.18, 0.19), and –0.36 (95% CI –0.38, –0.33), respectively. OA prevalence increased with age and revealed female preponderance, geographic diversity, and disparity with regard to anatomic site. OA of the knee contributed the most to the overall burden, while OA of the hip had the highest EAPC in most regions.

Conclusion. OA has remained a major public health concern worldwide over the past decades. The prevalence of OA has increased and diversified by geographic location and affected joint. Prevention and early treatment are pivotal to mitigating the growing burden of OA.

INTRODUCTION

Osteoarthritis (OA) is a worldwide highly prevalent chronic joint disease that causes pain, disability, and loss of function (1,2). Global trends showed a 114.5% increase in years lived with disability due to OA from 1990 to 2019 (3,4). However, there is no nonsurgical intervention that can prevent, halt, or even delay OA progression. Moreover, available medications, such as nonsteroidal antiinflammatory drugs, have been associated with a clinically relevant 50–100% increase in the risk of myocardial infarction or death from cardiovascular causes (5). Therefore, the public, health care providers, and policymakers should be aware of the heavy burden of OA.

OA prevalence varies with the joints involved. The knee is the most frequently affected joint, followed by the hand and the hip (1,6). Knee, hip, and hand OA each have a distinct effect on overall health. For instance, knee and hip OA, but not hand OA, are associated with an increased risk of cardiovascular and all-cause premature mortality (7). In addition, OA has been shown to have different pathologic mechanisms in different joints. OA of the hand has been associated with systemic inflammation, while OA of the knee and OA of the hip have been correlated with excessive joint load and injury (1,8). Taken together, these findings indicate a need for documentation regarding the burden of site-specific OA, which remains scarce in the literature.

The interpretation of the data contained herein is solely that of the authors.

Supported by the Beijing Postdoctoral Research Foundation (grant 2021-ZZ-010) and the National Natural Science Foundation of China (grant 81902247).

¹Huibin Long, MD, Heyong Yin, MD, Naicheng Diao, MD, Ai Guo, MD: Beijing Friendship Hospital, Capital Medical University, Beijing, China; ²Qiang Liu, MD, Kai Wang, MD, Jianhao Lin, MD: Peking University People's Hospital, Peking University, Beijing, China; ³Yuqing Zhang, DSc: Harvard Medical School, Boston, Massachusetts.

Author disclosures are available at <https://onlinelibrary.wiley.com/action/>

[downloadSupplement?doi=10.1002%2Fart.42089&file=art42089-sup-0001-Disclosureform.pdf](https://onlinelibrary.wiley.com/doi/10.1002/art.42089).

Address correspondence to Jianhao Lin, MD, Arthritis Clinic and Research Center, Peking University People's Hospital, Peking University, Number 11 Xizhimen South Street, Beijing, China 100044 (email: linjianhao@pkuph.edu.cn); or to Ai Guo, MD, Department of Orthopedics, Beijing Friendship Hospital, Capital Medical University, Number 95 Yong An Road, Beijing, China 100050 (email: guoaj@139.com).

Submitted for publication June 8, 2021; accepted in revised form February 4, 2022.

Although various studies have demonstrated the burden of OA in specific regions or territories, several new insights have been made. Findings on the prevalence of OA have differed between studies due to the definition used, age categories included, and sex distribution of the study population (1,9,10). For instance, Cross et al reported the age-standardized prevalence rate (ASR) of OA at the hip and knee joints but examined Global Burden of Disease (GBD) Study geographic regions only (11). Safiri et al systematically analyzed the burden of OA at the global, regional, and national levels using data derived from the GBD Study 2017; however, only the hip and knee joints were included as sites of OA (12). Therefore, we aimed to provide a systematic, comparable, and up-to-date prevalence as well as secular trend analysis of OA at 4 anatomic sites at the global, regional, and national levels, taking advantage of the new data sources, higher standardization, and improved methodology, as well as 2 new anatomic sites of OA (i.e., OA of the hand and OA of other joints except the spine), included in the GBD Study 2019 (3). In addition, we analyzed trends in countries and territories grouped according to the Socio-demographic Index (SDI).

PATIENTS AND METHODS

Overview. The GBD Study aimed to provide reliable and up-to-date global, regional, and national results on the burden of diseases, injuries, and risk factors. The study integrated all available data, including published data, grey literature data, survey data, and hospital and clinical data (13). A detailed description of the methodology for collecting and processing these data, and informing the results in the GBD Study 2019, as well as the main developments compared with earlier series, has been published elsewhere (3,14,15). Briefly, after data collection, the risk of bias was assessed for each data source and corrected for standardized estimation using a Bayesian meta-regression tool (DisMod-MR 2.1). As a result, the GBD Study 2019 provides comprehensive and systematic assessments of age- and sex-specific incidence, prevalence, mortality, years of life lost, years lived with disability, and disability-adjusted life years for 369 diseases and injuries in 204 countries and territories from 1990 to 2019. The reference definition of OA in the GBD Study 2019 was symptomatic OA that was radiologically confirmed as Kellgren/Lawrence grade 2–4 and painful for at least 1 month of the past 12 months (3,16). The details of input data and a methodologic summary for OA (including input data, age and sex splitting, data adjustment, modeling strategy, and corresponding severity and disability) are available in Supplementary Appendix 1 of the GBD Study 2019 (3).

Data source. Data on prevalent cases and ASRs of OA from 1990 to 2019, according to age group, sex, region, and country or territory, and the 4 anatomic sites (knee, hip, hand, and other joints except for the spine), were collected using the Global Health Data Exchange (GHDx) query tool (<http://ghdx.healthdata.org/gbd-results-tool>) (4). A total of 204 countries and

territories were categorized into 5 groups (i.e., low, low-middle, middle, high-middle, and high) according to the SDI, a compound indicator based on fertility, income, and educational attainment; and into 21 regions (e.g., East Asia) according to geographic location. Supplementary Tables 1–4, available on the *Arthritis & Rheumatology* website at <http://onlinelibrary.wiley.com/doi/10.1002/art.42089>, show results for knee OA, hip OA, hand OA, and OA at other sites, respectively, according to sex, SDI, and geographic region. Table 1 and Supplementary Table 5 (available on the *Arthritis & Rheumatology* website at <http://onlinelibrary.wiley.com/doi/10.1002/art.42089>) contain summary data for the 5 SDI categories, the 21 geographic regions, and 204 countries and territories. Information on SDI at the national level was obtained from GHDx (<http://ghdx.healthdata.org/record/ihme-data/gbd-2019-socio-demographic-index-sdi-1950-2019>).

Statistical analysis. We used ASRs and the corresponding estimated annual percentage changes (EAPCs) to calculate secular trends of OA (17). An age-standardized method was used when comparing OA prevalence among different populations. The ASR was generated by summing each product of the age-specific rate (β_i , where i represents the i th age group) and the corresponding number of cases (or weight; ω_i) in the same age subgroup i of the selected reference standard population (the GBD world population age standard, which is available in Supplementary Appendix 1 of the GBD Study 2019 [3]), and then dividing by the sum of the standard population weights, i.e.,

$$ASR = \frac{\sum_{i=1}^n \beta_i \omega_i}{\sum_{i=1}^n \omega_i}.$$

Trends in ASR can show the shifting patterns of OA, while EAPC is a commonly used and quantitative means of evaluating the secular trend of ASR over a specified period. Specifically, to calculate EAPCs and obtain 95% confidence intervals (95% CIs), the regression line was fitted to the natural logarithm of the ASR, i.e., $y = \alpha + \beta x + \epsilon$, where $y = \ln(ASR)$ and $x = \text{calendar year}$, and $EAPC = 100 \times (e^\beta - 1)$ (17,18). EAPC values >0 indicate an increase over time, and EAPC values <0 indicate a decrease over time. An EAPC value with a 95% CI that includes 0 indicates stability, or no change during the indicated time period.

Pearson's or Spearman's correlation coefficients were used to assess correlations between the ASR and the SDI in the corresponding years (1990 and 2019) at the national level for OA overall and for OA at each of the 4 anatomic sites to identify potentially related factors. Hierarchical cluster analysis was conducted to categorize all 204 countries and territories according to their EAPCs and 95% CIs. All data were analyzed using R software version 4.0.2 (R core team). P values less than 0.05 were considered significant.

Table 1. Number of prevalent cases and ASR of OA in 1990 and 2019*

	1990		2019		Change from 1990 to 2019	
	Prevalent cases, no. × 10 ⁶ (95% UI)	ASR, no. × 10 ³ per 100,000 (95% UI)	Prevalent cases, no. × 10 ⁶ (95% UI)	ASR, no. × 10 ³ per 100,000 (95% UI)	% change†	EAPC (95% CI)
Overall	247.51 (224.05, 275.50)	6.17 (5.61, 6.85)	527.81 (478.67, 584.79)	6.35 (5.78, 7.02)	113.25	0.12 (0.11, 0.14)
Sex						
Male	96.98 (87.37, 108.26)	5.14 (4.66, 5.71)	210.37 (190.20, 233.66)	5.32 (4.83, 5.89)	116.91	0.07 (0.05, 0.09)
Female	150.53 (136.51, 166.90)	7.08 (6.42, 7.85)	317.44 (288.48, 350.27)	7.28 (6.61, 8.04)	110.88	0.17 (0.14, 0.20)
SDI						
Low	12.56 (11.28, 14.13)	5.10 (4.61, 5.69)	29.05 (26.10, 32.63)	5.33 (4.82, 5.93)	131.27	0.16 (0.16, 0.17)
Low-middle	31.65 (28.31, 35.33)	5.07 (4.57, 5.62)	77.44 (69.56, 86.09)	5.49 (4.95, 6.08)	144.68	0.32 (0.30, 0.33)
Middle	57.29 (51.17, 63.95)	5.35 (4.81, 5.94)	149.93 (134.32, 166.72)	5.75 (5.18, 6.37)	161.69	0.30 (0.26, 0.34)
High-middle	67.38 (60.83, 74.92)	6.25 (5.66, 6.94)	130.18 (117.54, 143.95)	6.37 (5.75, 7.05)	93.19	0.01 (-0.01, 0.04)
High	78.51 (71.21, 87.00)	7.77 (7.03, 8.65)	140.97 (128.37, 155.67)	7.77 (7.03, 8.65)	79.54	0.22 (0.18, 0.26)
Site of OA						
Knee	163.91 (141.00, 187.92)	4.07 (3.52, 4.66)	364.58 (315.25, 417.40)	4.38 (3.79, 5.00)	122.42	0.32 (0.29, 0.34)
Hip	14.50 (11.17, 18.24)	0.37 (0.29, 0.46)	32.99 (25.69, 41.12)	0.40 (0.31, 0.50)	127.51	0.28 (0.26, 0.31)
Hand	74.27 (56.30, 97.42)	1.89 (1.43, 2.47)	142.48 (108.63, 186.79)	1.73 (1.32, 2.25)	91.84	-0.36 (-0.38, -0.33)
Other	27.60 (20.94, 34.93)	0.71 (0.54, 0.89)	61.42 (46.68, 77.73)	0.75 (0.57, 0.94)	122.56	0.18 (0.18, 0.19)
Region						
High-income Asia Pacific	16.23 (14.72, 17.99)	7.90 (7.17, 8.74)	32.22 (29.36, 35.37)	8.37 (7.63, 9.26)	98.55	0.48 (0.38, 0.57)
Central Asia	2.51 (2.25, 2.83)	5.34 (4.80, 6.02)	4.29 (3.83, 4.85)	5.52 (4.96, 6.18)	70.87	0.10 (0.09, 0.11)
East Asia	53.71 (47.68, 60.47)	5.88 (5.24, 6.57)	137.28 (122.01, 154.09)	6.32 (5.65, 7.08)	155.61	0.35 (0.28, 0.42)
South Asia	28.61 (25.55, 32.12)	4.79 (4.31, 5.33)	75.63 (68.06, 84.45)	5.22 (4.71, 5.79)	164.39	0.32 (0.31, 0.33)
Southeast Asia	9.96 (8.79, 11.19)	3.74 (3.31, 4.17)	26.68 (23.56, 29.92)	4.13 (3.68, 4.60)	167.81	0.37 (0.35, 0.38)
Australasia	1.76 (1.59, 1.97)	7.68 (6.92, 8.60)	3.80 (3.44, 4.23)	8.34 (7.54, 9.26)	115.73	0.18 (0.14, 0.23)
Caribbean	1.41 (1.27, 1.57)	5.41 (4.88, 6.01)	3.02 (2.73, 3.36)	5.81 (5.24, 6.44)	114.11	0.27 (0.26, 0.29)
Central Europe	7.19 (6.47, 7.97)	4.88 (4.40, 5.41)	10.44 (9.43, 11.55)	5.17 (4.66, 5.72)	45.21	0.19 (0.18, 0.19)
Eastern Europe	21.95 (19.36, 25.06)	7.87 (6.94, 8.97)	26.72 (23.73, 30.30)	7.95 (7.06, 9.03)	21.70	-0.25 (-0.36, -0.14)
Western Europe	36.93 (33.44, 40.95)	6.70 (6.06, 7.45)	57.03 (51.91, 62.91)	7.06 (6.39, 7.80)	54.45	0.21 (0.19, 0.23)
Andean Latin America	1.16 (1.05, 1.30)	5.54 (5.01, 6.14)	3.49 (3.17, 3.83)	6.13 (5.57, 6.73)	199.56	0.37 (0.35, 0.39)
Central Latin America	5.19 (4.67, 5.79)	6.03 (5.43, 6.69)	15.76 (14.24, 17.53)	6.54 (5.91, 7.24)	203.56	0.30 (0.28, 0.33)
Southern Latin America	3.45 (3.09, 3.87)	7.45 (6.69, 8.36)	6.52 (5.90, 7.28)	7.45 (6.69, 8.36)	89.24	0.24 (0.21, 0.27)
Tropical Latin America	5.08 (4.56, 5.65)	5.41 (4.87, 5.99)	14.51 (13.04, 16.10)	5.87 (5.28, 6.50)	185.43	0.30 (0.29, 0.31)
North Africa and Middle East	8.68 (7.79, 9.68)	4.89 (4.40, 5.42)	24.60 (22.08, 27.33)	5.34 (4.82, 5.91)	183.39	0.27 (0.26, 0.29)
High-income North America	31.15 (27.93, 34.89)	9.40 (8.38, 10.56)	56.67 (50.98, 63.39)	9.70 (8.75, 10.86)	81.93	0.06 (-0.07, 0.19)
Oceania	0.15 (0.13, 0.16)	4.61 (4.13, 5.13)	0.38 (0.34, 0.43)	4.91 (4.39, 5.47)	158.92	0.18 (0.14, 0.22)
Central Sub-Saharan Africa	1.30 (1.16, 1.47)	5.42 (4.88, 6.07)	3.20 (2.86, 3.61)	5.58 (5.02, 6.25)	146.28	0.07 (0.05, 0.08)
Eastern Sub-Saharan Africa	4.18 (3.75, 4.69)	5.37 (4.84, 6.01)	9.73 (8.72, 10.86)	5.61 (5.06, 6.26)	132.48	0.16 (0.15, 0.16)
Southern Sub-Saharan Africa	1.76 (1.59, 1.98)	6.25 (5.64, 6.97)	3.85 (3.46, 4.30)	6.54 (5.90, 7.28)	118.19	0.16 (0.16, 0.16)
Western Sub-Saharan Africa	5.15 (4.63, 5.76)	5.66 (5.11, 6.31)	12.00 (10.74, 13.43)	5.92 (5.35, 6.60)	132.98	0.14 (0.11, 0.18)

* ASR = age-standardized prevalence rate; OA = osteoarthritis; 95% UI = 95% uncertainty interval; EAPC = estimated annual percentage change; 95% CI = 95% confidence interval; SDI = Socio-demographic Index.

† Percentage change in absolute number.

RESULTS

Prevalent cases of OA. Globally, prevalent cases of OA increased by 113.25%, from 247.51 million in 1990 to 527.81

million in 2019 (Table 1). The highest numbers of prevalent cases in 2019 were observed in China (132.81 million), followed by India (62.36 million) and the US (51.87 million), with corresponding percentage changes from 1990 of 156.58%, 165.75%, and 79.63%,

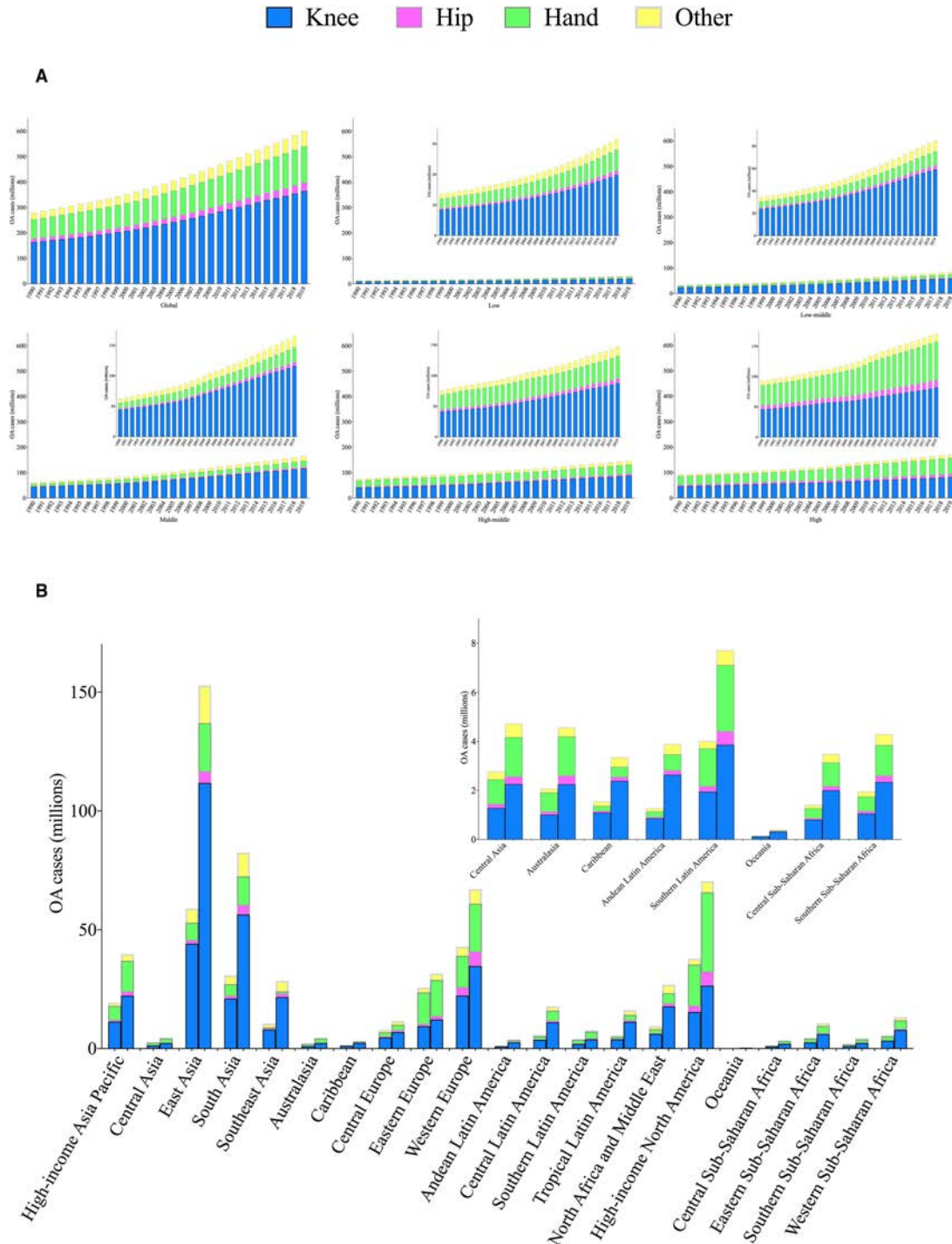


Figure 1. Total number of prevalent osteoarthritis (OA) cases and number of prevalent OA cases according to the affected joint, globally, by Socio-demographic Index (SDI) category (low, low-middle, middle, high-middle, and high) and by geographic region, for both sexes combined. **A,** Number of prevalent OA cases for each year from 1990 to 2019, globally and by SDI category. **Insets** show the same data at a magnified scale. **B,** Number of prevalent OA cases in 1990 and 2019 in the 21 indicated geographic regions. For each region, the left column shows data for 1990 and the right column shows data for 2019. **Inset** shows data for some regions at a magnified scale. Color figure can be viewed in the online issue, which is available at <http://onlinelibrary.wiley.com/doi/10.1002/art.42089/abstract>.

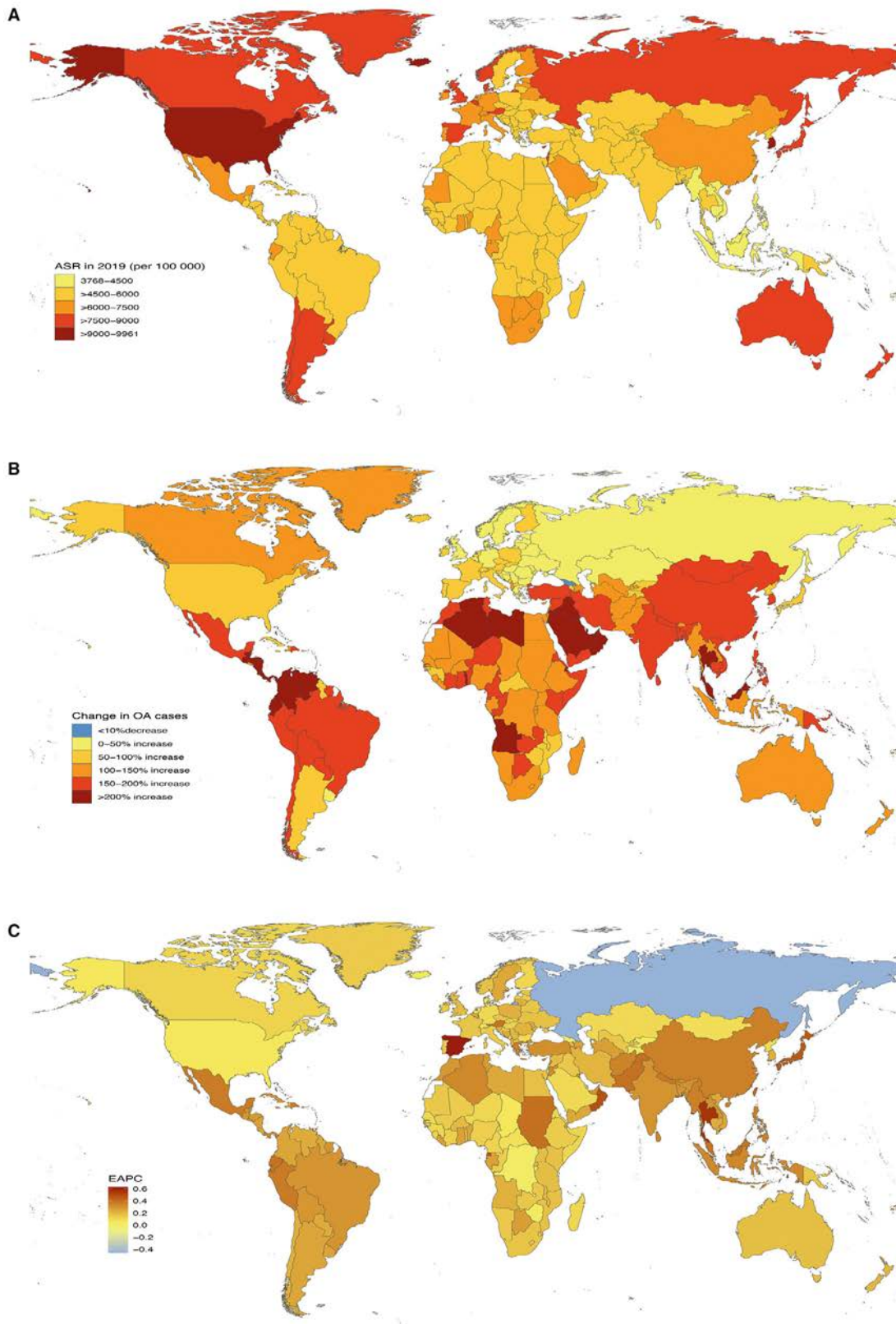


Figure 2. Prevalence of osteoarthritis (OA) for both sexes combined in 204 countries and territories. **A**, Age-standardized prevalence rate (ASR) of OA in 2019. **B**, Percentage change in prevalent cases of OA between 1990 and 2019. **C**, Estimated annual percentage change (EAPC) of OA from 1990 to 2019.

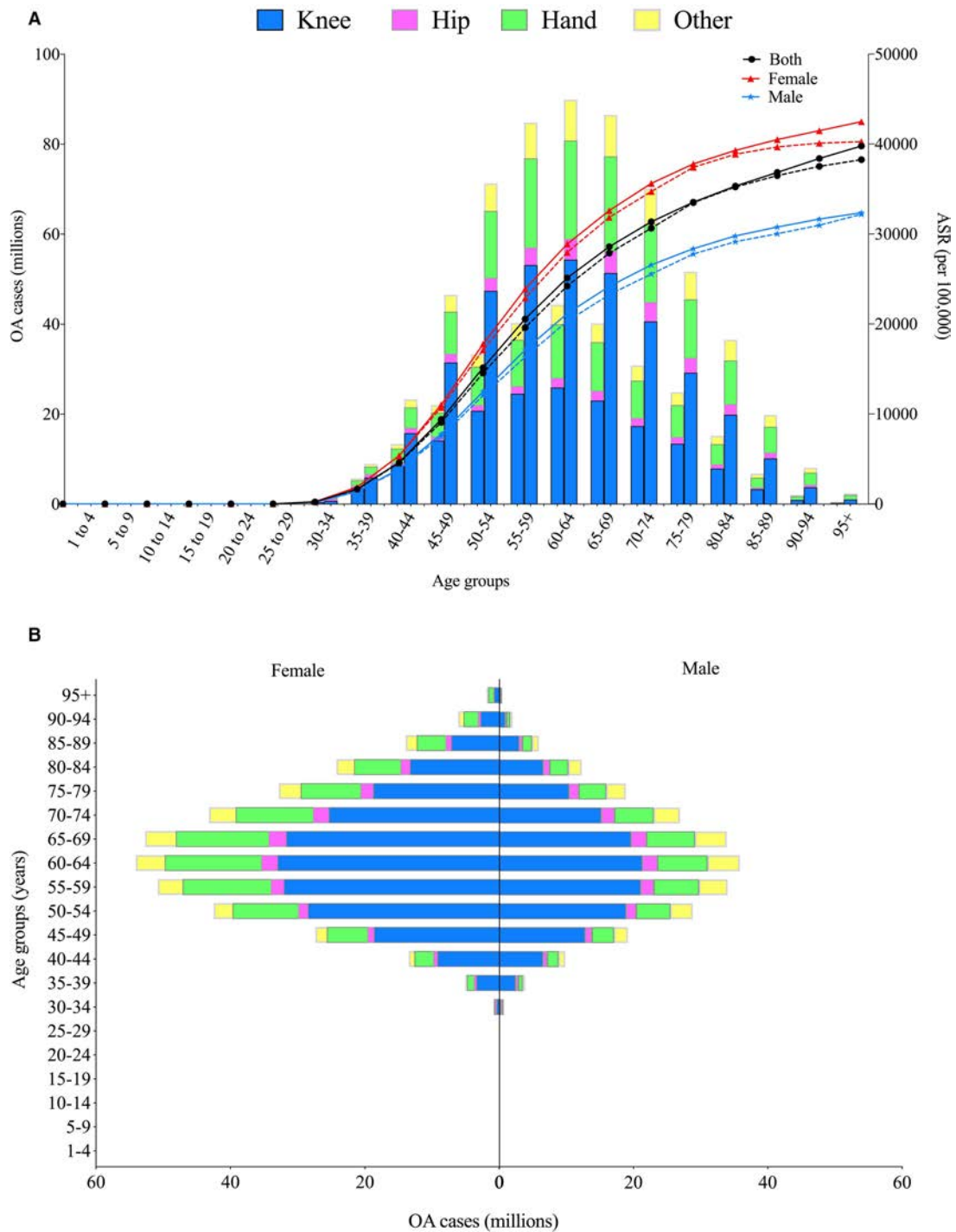


Figure 3. Global total number of prevalent osteoarthritis (OA) cases and number of prevalent OA cases according to the affected joint, by sex and age group. **A**, Global number of prevalent OA cases and age-standardized prevalence rate (ASR) by sex and age group. For each age group, the left column shows data for prevalent cases in 1990 and the right column shows data for prevalent cases in 2019. Broken lines indicate the global ASR of OA in 1990, and solid lines indicate the global ASR of OA by age group in 2019. **B**, Sex differences in global prevalent OA cases by age group in 2019. Color figure can be viewed in the online issue, which is available at <http://onlinelibrary.wiley.com/doi/10.1002/art.42089/abstract>.

respectively. Prevalent cases increased in all 5 SDI categories from 1990 to 2019, with the largest increase detected in the middle SDI category (161.69%) (Table 1 and Figure 1A). For GBD geographic regions, the most significant increase in prevalent cases was in Central Latin America (203.56%), followed by Andean Latin America

(199.56%) and Tropical Latin America (185.43%) (Table 1 and Figure 1B). At the national level, the greatest increase in OA cases was in the United Arab Emirates (1,069.81%), and the only decrease was in Georgia (-5.90%) (Supplementary Table 5 and Figure 2B). Prevalent cases of OA increased particularly in the those

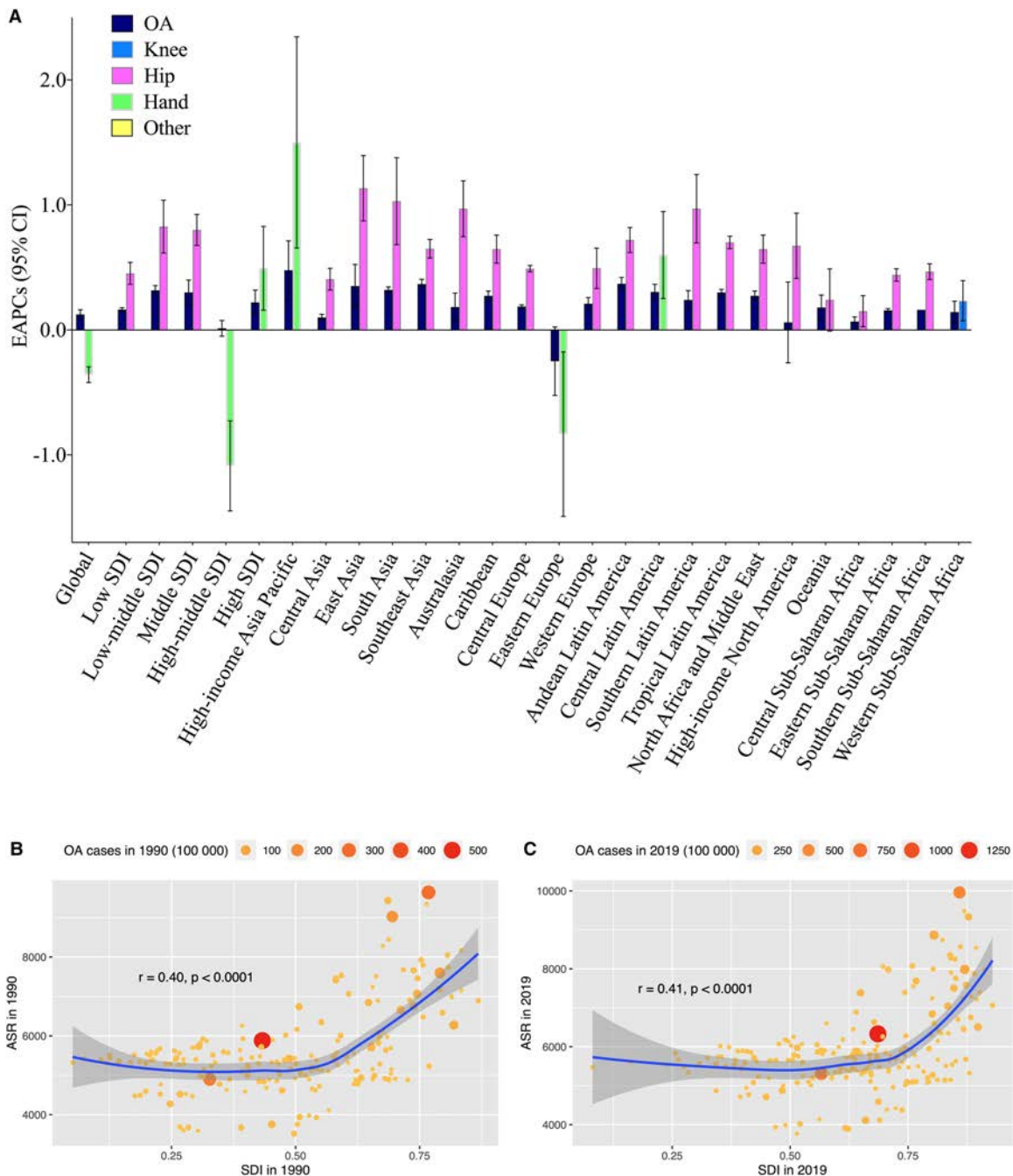


Figure 4. **A**, Estimated annual percentage change (EAPC) in total osteoarthritis (OA) and according to the affected joint from 1990 to 2019, globally, by Socio-demographic Index (SDI) category and by geographic region, for both sexes combined. Data for OA overall and for the affected sites with absolute maximum of EAPC are presented for each category. **B** and **C**, Correlation between age-standardized prevalence rate (ASR) of OA and SDI in 1990 (**B**) and 2019 (**C**). Circles represent the number of prevalent OA cases in individual countries or territories. 95% CI = 95% confidence interval. Color figure can be viewed in the online issue, which is available at <http://onlinelibrary.wiley.com/doi/10.1002/art.42089/abstract>.

ages ≥ 95 years, with the absolute number increasing almost 3.8 fold (Supplementary Table 6, available on the *Arthritis & Rheumatology* website at <http://onlinelibrary.wiley.com/doi/10.1002/art.42089>), and the peak remained stable at 60–64 years in both 1990 and 2019 (Figure 3A). There were more OA cases in women (317.44 million in 2019) than in men (210.37 million in 2019) (Table 1 and Figure 3B).

ASR of OA. The ASR of OA also varied significantly worldwide. The global ASR of OA was 6,173.38 per 100,000 in 1990, while it was 6,348.25 per 100,000 in 2019, with an average annual increase of 0.12% (95% CI 0.11%, 0.14%) (Table 1). The ASR of OA varied more than 2.64-fold across countries, with the highest level observed in the US (9,960.88 per 100,000 in 2019) and the lowest in Timor-Leste (3,768.44

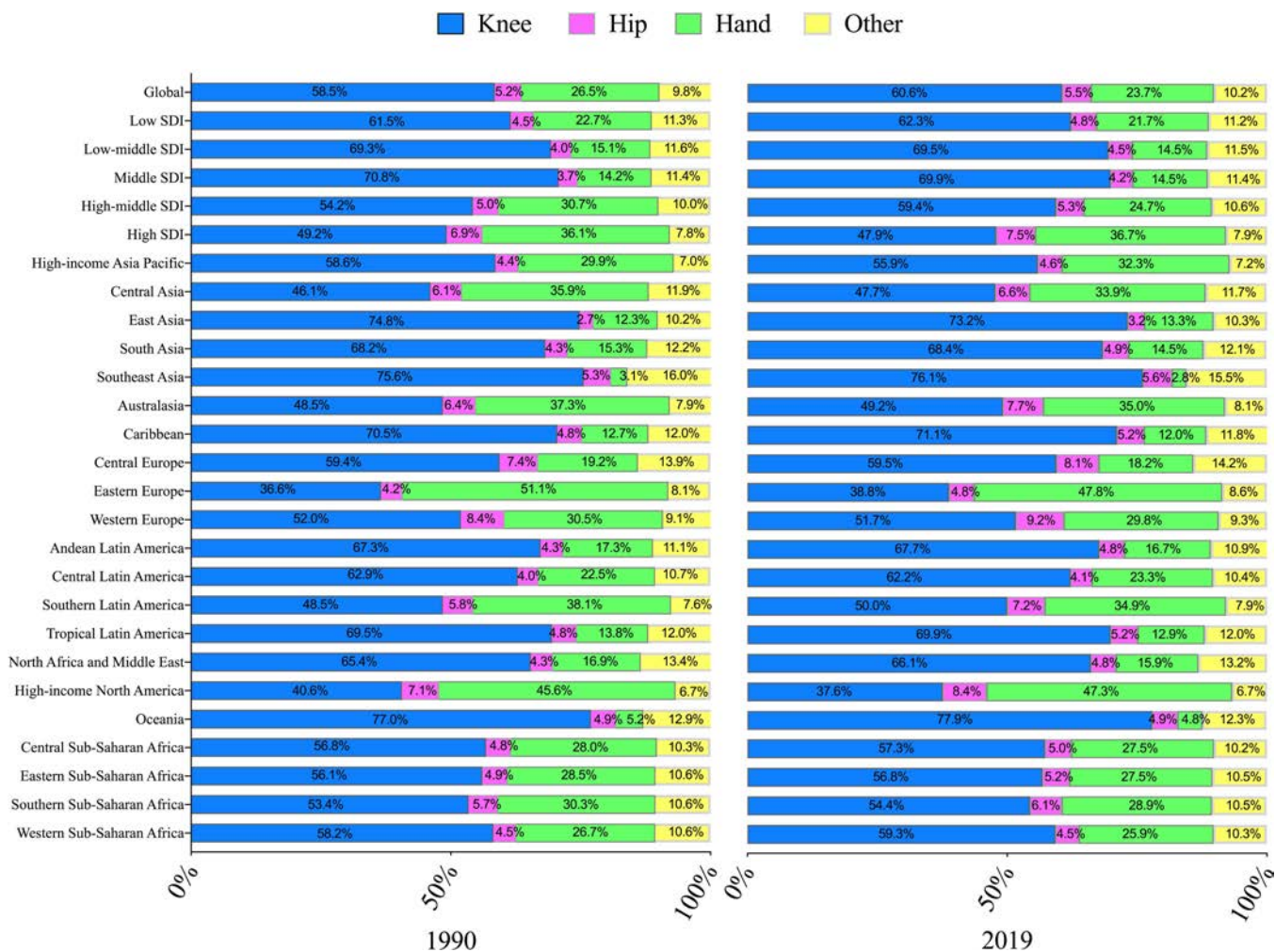


Figure 5. Percentage of total prevalent osteoarthritis (OA) cases accounted for by OA at each site (knee, hip, hand, or other) in 1990 and 2019, globally, by Socio-demographic Index (SDI) category and by geographic region, for both sexes combined. Color figure can be viewed in the online issue, which is available at <http://onlinelibrary.wiley.com/doi/10.1002/art.42089/abstract>.

per 100,000 in 2019) (Supplementary Table 5 and Figure 2A). Except for a stable trend in the high-middle SDI category (EAPC 0.01 [95% CI -0.01, 0.04]), SDI categories had increases in ASR, with the highest level observed in the low-middle category (EAPC 0.32 [95% CI 0.30, 0.33]) (Table 1 and Figure 4A).

With regard to GBD geographic regions, Eastern Europe had a decrease in ASR (EAPC -0.25 [95% CI -0.36, -0.14]), while the ASR in high-income North America remained stable (EAPC 0.06 [95% CI -0.07, 0.19]). The remaining regions had increases in ASR, which were highest in high-income Asia Pacific (EAPC 0.48 [95% CI 0.38, 0.57]) (Table 1 and Figure 4A). At the national level, the largest increase in ASR was observed in Spain (EAPC 0.63 [95% CI 0.53, 0.73]), followed by the Maldives and Thailand. Only Russia reported a decrease in the ASR of OA from 1990 to 2019 (EAPC -0.46 [95% CI -0.61, -0.30]) (Supplementary Table 5 and Figure 2C).

The global ASR of OA was higher in women and increased with age, peaking in those ages ≥95 years for both women and

men in 1990 and 2019 (Table 1 and Figure 3A). EAPCs for men and women were 0.07 (95% CI 0.05, 0.09) and 0.17 (95% CI 0.14, 0.20), respectively (Table 1). Hierarchical cluster analysis of EAPCs and their 95% CIs divided the 204 countries and territories into 5 categories, namely “high decrease,” “stable or minor increase,” “low increase,” “middle increase,” and “high increase.” Detailed results are shown in Supplementary Figure 1, available on the *Arthritis & Rheumatology* website at <http://onlinelibrary.wiley.com/doi/10.1002/art.42089>.

Prevalence of OA at different anatomic sites. Results for ASRs, change in absolute number, and EAPCs for knee, hip, and hand OA and OA at other sites are shown in Supplementary Figures 2–13, available on the *Arthritis & Rheumatology* website at <http://onlinelibrary.wiley.com/doi/10.1002/art.42089>. Figure 5 depicts the proportions of site-specific OA at the global and regional levels in 1990 and 2019. Globally, the knee was the leading OA site, followed by the hand, other sites, and the hip, accounting for ~60.6%, 23.7%, 10.2%, and 5.5%, respectively,

of the total prevalent cases in 2019. For most SDI categories and GBD geographic regions, the knee also ranked first among the 4 OA anatomic sites, while the hand superseded it in Eastern Europe and high-income North America in both 1990 and 2019. In most regions, the proportions of knee OA and hip OA increased, while the proportions of hand OA and OA at other sites decreased, between 1990 and 2019.

From 1990 to 2019, global prevalent cases of OA at all 4 anatomic sites increased, by between 91.84% for hand OA and 127.51% for hip OA (Table 1). Prevalent cases of OA at the 4 sites increased in all 5 SDI categories and 21 GBD geographic regions (Table 1 and Figure 1). At the national level, most countries and territories experienced an increase in cases, while a decrease was observed in only a few countries: in Georgia for knee OA (−3.99%), hip OA (−1.32%), hand OA (−7.59%), and OA at other sites (−1.96%); and in Niue (−2.32%) and Tokelau (−2.70%), both for hand OA (Supplementary Table 5 and Supplementary Figures 3, 6, 9, and 12). The highest ASR for knee OA was observed in the Republic of Korea (6,211.13 per 100,000 in 2019); the other 3 countries with the highest ASRs were the US for hip OA (1,031.12 per 100,000 in 2019), the US for hand OA (5,721.76 per 100,000 in 2019), and Qatar for OA at other sites (946.17 per 100,000 in 2019) (Supplementary Table 5 and Supplementary Figures 2, 5, 8, and 11).

Global ASRs for the 4 anatomic sites showed different trends, with EAPCs for knee OA, hip OA, hand OA, and OA at other sites of 0.32 (95% CI 0.29, 0.34), 0.28 (95% CI 0.26, 0.31), −0.36 (95% CI −0.38, −0.33) and 0.18 (95% CI 0.18, 0.19), respectively (Table 1). The anatomic site with the highest EAPC differed by geographic region and SDI category, with knee OA having the highest EAPC in Western Sub-Saharan Africa; hip OA having the highest EAPC in the low, low-middle, and middle SDI categories, and in 17 GBD geographic regions; and hand OA having the highest EAPC at the global level, in the high-middle and high SDI categories, and in 3 GBD geographic regions (Figure 4A and Supplementary Figure 14, available on the *Arthritis & Rheumatology* website at <http://onlinelibrary.wiley.com/doi/10.1002/art.42089>).

Factors related to OA prevalence. As illustrated in Figures 4B and C, significant positive correlations between the ASR and the SDI were observed for OA in 1990 ($r = 0.40$, $P < 0.0001$) and 2019 ($r = 0.41$, $P < 0.0001$). Site-specific correlations between the ASR and the SDI in 1990 and 2019 are depicted in Supplementary Figures 15–18, available on the *Arthritis & Rheumatology* website at <http://onlinelibrary.wiley.com/doi/10.1002/art.42089>.

DISCUSSION

Using data derived from the GBD Study 2019, we provided updated results for the prevalence of site-specific OA in 204 countries and territories from 1990 to 2019, and analyzed the secular

trends of prevalence for the first time. Prevalent cases and the ASR of OA increased over time globally and in most regions and countries. Prevalence increased with age and revealed female preponderance, geographic diversity, and anatomic site disparity. The knee was the joint most commonly affected by OA, followed by the hand. There were positive associations between the ASR and the SDI for OA overall and at each anatomic site in both 1990 and 2019.

The ASR and years lived with disability associated with hip and knee OA for GBD geographic regions were previously reported using data from the GBD Study 2010 (11). After the release of the GBD Study 2017, Safiri et al first reported the incidence, ASR, and years lived with disability due to OA at the national level (12). They also demonstrated age and sex patterns of OA and assessed the association between years lived with disability and the SDI. Due to updated data sources and the improvement of methodologies used in the GBD Study series, our study has advantages over the 2 previous studies. In addition, Safiri et al reported only the combined burden of OA and the trends in percentage change of OA in absolute number.

We found that prevalent cases and the ASR of OA increased from 1990 to 2019, consistent with the findings of previous studies (11,12). Globally, of the 369 diseases and injuries in the GBD Study 2019, OA ranked 17th highest in terms of prevalent cases and 19th in terms of ASR in 2019 (3,19), indicating a substantial disease burden. It was estimated that ~1–2.5% of national gross domestic product was attributed to the medical costs of OA, while the indirect costs, including work loss and premature retirement, were not taken into consideration (1,20).

Consistent with the findings of previous studies (11,12), our study showed that prevalence of OA increased with age and was more common in women than in men. As indicated in Supplementary Table 6, there were varying degrees of change in the numbers of OA cases in different age groups between 1990 and 2019. One possible explanation for such a result may be ascribed to the different data sources of the GBD Study. For instance, Tang et al reported that the prevalence of symptomatic knee OA peaked at ages 60–69 years and then leveled off (21); Dillon et al reported that the prevalence of symptomatic knee OA peaked at ages 70–79 years in men and then leveled off but increased monotonically with age in women (22). OA predominantly affects women, and women tend to have more severe disease (i.e., structural lesions and clinical symptoms) than men. Estrogen has been postulated to play a role in OA development; however, results from both observational studies and clinical trials have been inconclusive (23–25). Women had nearly 3-fold higher risk of developing lateral tibiofemoral radiographic OA than men; nevertheless, no such sex difference was observed for medial tibiofemoral radiographic OA (26,27). In general, women have a wider pelvis, larger Q angle, and greater knee valgus than men, which places more load on the lateral knee compartment, resulting in a higher risk of lateral disease (26).

Since higher body mass index (e.g., overweight/obesity) is a substantial risk factor for OA, geographic diversity in OA prevalence may be related to the distribution of adult obesity (1,28–30). Moreover, epidemiologic and genetic investigations have established that OA is a disease with multifactorial components based on both ecology and genetics (31–33), contributing to the geographic diversity.

Secular trends of OA prevalence differed by anatomic site. Except for a 0.36% annual decrease in hand OA, the other 3 anatomic sites all experienced increasing trends, with an annual change of 0.32% for the knee, 0.28% for the hip, and 0.18% for the other joints. OA in large joints, such as the knee and the hip, causes the most severe disability, and end-stage disease may require joint replacement if available, thus indicating that OA in large joints should comprise a significant proportion of the disease burden. However, globally as well as in most regions and countries, the joints that accounted for the main disease burden were the knee, followed by the hand and other joints except the spine, while hip OA contributed the least. Relatively low prevalence and conversely more serious severity distribution and sequelae of the hip compared to other larger joints may result in such findings (1,34).

As demonstrated here and in a previous study (12), a positive association was observed between OA prevalence and the development level of GBD regions and countries. A high prevalence of OA was observed in countries with a high SDI, such as the Republic of Korea and the US, and an increasing life expectancy is a non-negligible explanation for this result. As a complex indicator based on fertility, income, and educational attainment, the SDI represents the development level of GBD regions and countries, and indicates the quality and availability of health care. Changes in numerous risk factors for OA (20,35), including social and occupational risk factors, and epidemiologic and demographic transition, may also have contributed to the correlation.

Population expansion, aging, and the obesity epidemic have increased the number of prevalent cases and ASR of OA, thus aggravating the disease burden (1,9,30,36). According to the United Nations Department of Economic and Social Affairs, the total global population increased by 45%, from 5.32 billion in 1990 to 7.71 billion in 2019, and the proportion of people ages ≥ 60 years increased from 9.2% in 1990 to $\sim 13.5\%$ in 2019 (37). With regard to obesity, the prevalence has nearly tripled since 1975, while >1.9 billion adults and >340 million children and adolescents were overweight or obese in 2016 (28,30). Joint injuries involving ligaments, which could be responsible for joint degeneration, and better awareness and diagnosis of OA, might also have contributed to the increase in prevalence (1,33).

Considering the formidable and increasing disease burden of OA, primary and secondary prevention and early treatment might be more effective in alleviating the burden (38,39). Along with these previously emphasized aspects aimed at modifiable risk factors, such as preventing being overweight or obese, preventing knee injury, and avoiding heavy repeated joint-loading

activities, we appeal for education programs on disease progression, sequelae, early treatment methods, and rehabilitation of OA. For instance, exercise therapy effectively delays functional loss and has been recommended as core treatment for knee OA in many guidelines (2,38). In most countries and territories in the low, low-middle, and middle SDI categories, although the main causes of death are heart diseases, stroke, and chronic lung diseases (40), the burden of OA on society is likely to increase, and governments and policymakers should recognize the societal impact of OA.

Our study has several strengths. First, results from the GBD model fill a gap where actual relevant data for a given disease burden are scarce or unavailable, thus allowing comparisons across regions and over time periods. Second, we examined the site-specific secular trends of OA and the correlation between ASR and the SDI, providing policymakers data to inform disease prevention and treatment.

Several limitations of our study should be noted, including those previously acknowledged regarding the methodology of the GBD studies (3,14,15). In particular, data from individual studies included in the GBD modeling were adjusted with covariates in terms of reference definitions, implying that the quality and quantity of data included were responsible for the accuracy and validity of the results. Moreover, the definition of OA in the GBD Study 2019 excluded symptoms and disabilities associated with the spine, which were captured in the categories “low back pain” or “neck pain”, thus underestimating the burden of OA. Additionally, we considered the SDI to be an indicator of the quality and availability of health care in investigating ASR-related factors, while the effect of health systems was not assessed. This could weaken the robustness even for countries with the same SDI, as there are consequential variations in the returns of health systems (3,41).

OA is prevalent worldwide and remains a major public health concern. Although prevalent cases and the ASR of OA are increasing in most countries, especially among older people and women, trends are diverse with regard to geographic location and anatomic site. The secular trends are expected to continually increase, mainly due to population aging and the obesity epidemic. Public awareness of the modifiable risk factors, and education programs addressing disease prevention, are essential to alleviate the enormous burden of OA.

ACKNOWLEDGMENTS

We thank the staff of the Institute for Health Metrics and Evaluation and its collaborators who prepared the publicly available data.

AUTHOR CONTRIBUTIONS

All authors were involved in drafting the article or revising it critically for important intellectual content, and all authors approved the final version to be published. Dr. Guo and Dr. Lin had full access to all of the data

in the study and take responsibility for the integrity of the data and the accuracy of the data analysis.

Study conception and design. Long, Yin, Zhang, Lin, Guo.

Acquisition of data. Long, Yin.

Analysis and interpretation of data. Long, Liu, Yin, Wang, Diao, Zhang, Lin, Guo.

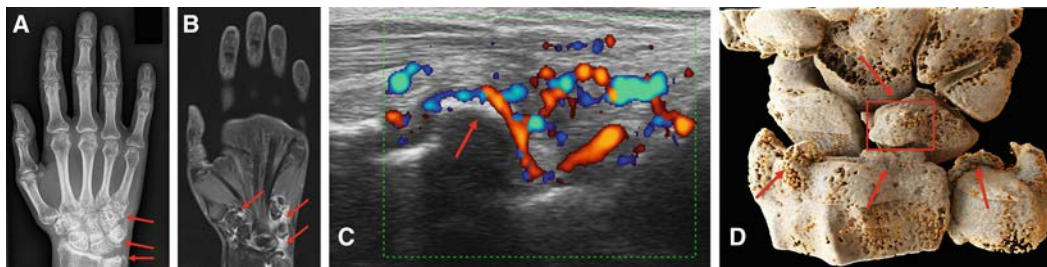
REFERENCES

- Hunter DJ, Bierma-Zeinstra S. Osteoarthritis. *Lancet* 2019;393:1745–59.
- Kolasinski SL, Neogi T, Hochberg MC, Oatis C, Guyatt G, Block J, et al. 2019 American College of Rheumatology/Arthritis Foundation guideline for the management of osteoarthritis of the hand, hip, and knee. *Arthritis Rheumatol* 2020;72:220–33.
- GBD 2019 Diseases and Injuries Collaborators. Global burden of 369 diseases and injuries in 204 countries and territories, 1990–2019: a systematic analysis for the Global Burden of Disease Study 2019. *Lancet* 2020;396:1204–22.
- Global Burden of Disease Collaborative Network. Global Burden of Disease Study 2019 (GBD 2019) Results. Seattle, United States: Institute for Health Metrics and Evaluation (IHME), 2020. URL: <http://ghdx.healthdata.org/gbd-results-tool>.
- Osteoarthritis Research Society International. Osteoarthritis Research Society International white paper: OA as a serious disease. 2016. URL: <https://oarsi.org/education/oarsi-resources/oarsi-white-paper-oa-serious-disease>.
- Andrianakos AA, Kontelis LK, Karamitsos DG, Aslanidis SI, Georgountzos AI, Kaziolas GO, et al. Prevalence of symptomatic knee, hand, and hip osteoarthritis in Greece. The ESORDIG study. *J Rheumatol* 2006;33:2507–13.
- Haugen IK, Ramachandran VS, Misra D, Neogi T, Niu J, Yang T, et al. Hand osteoarthritis in relation to mortality and incidence of cardiovascular disease: data from the Framingham heart study. *Ann Rheum Dis* 2015;74:74–81.
- Kortekaas MC, Kwok WY, Reijnen M, Kloppenburg M. Inflammatory ultrasound features show independent associations with progression of structural damage after over 2 years of follow-up in patients with hand osteoarthritis. *Ann Rheum Dis* 2015;74:1720–4.
- O'Neill TW, McCabe PS, McBeth J. Update on the epidemiology, risk factors and disease outcomes of osteoarthritis. *Best Pract Res Clin Rheum* 2018;32:312–26.
- Vina ER, Kwok CK. Epidemiology of osteoarthritis: literature update. *Curr Opin Rheumatol* 2018;30:160–7.
- Cross M, Smith E, Hoy D, Nolte S, Ackerman I, Fransen M, et al. The global burden of hip and knee osteoarthritis: estimates from the global burden of disease 2010 study. *Ann Rheum Dis* 2014;73:1323–30.
- Safiri S, Kolahi AA, Smith E, Hill C, Bettampadi D, Mansournia MA, et al. Global, regional and national burden of osteoarthritis 1990–2017: a systematic analysis of the Global Burden of Disease Study 2017. *Ann Rheum Dis* 2020;79:819–28.
- Murray CJ, Lopez AD. Measuring the global burden of disease. *N Engl J Med* 2013;369:448–57.
- GBD 2019 Demographics Collaborators. Global age-sex-specific fertility, mortality, healthy life expectancy (HALE), and population estimates in 204 countries and territories, 1950–2019: a comprehensive demographic analysis for the Global Burden of Disease Study 2019. *Lancet* 2020;396:1160–203.
- GBD 2019 Risk Factors Collaborators. Global burden of 87 risk factors in 204 countries and territories, 1990–2019: a systematic analysis for the Global Burden of Disease Study 2019. *Lancet* 2020;396:1223–49.
- Kellgren JH, Lawrence JS. Radiological assessment of osteo-arthrosis. *Ann Rheum Dis* 1957;16:494–502.
- Hankey BF, Ries LA, Kosary CL, Feuer EJ, Merrill RM, Clegg LX, et al. Partitioning linear trends in age-adjusted rates. *Cancer Causes Control* 2000;11:31–5.
- Liu Z, Jiang Y, Yuan H, Fang Q, Cai N, Suo C, et al. The trends in incidence of primary liver cancer caused by specific etiologies: results from the Global Burden of Disease Study 2016 and implications for liver cancer prevention. *J Hepatol* 2019;70:674–83.
- Global Burden of Disease Collaborative Network. GBD Compare tool: Global Burden of Disease Study 2019 (GBD 2019) Results. Seattle, United States: Institute for Health Metrics and Evaluation (IHME), 2020. URL: <https://vizhub.healthdata.org/gbd-compare/>.
- Hunter DJ, Schofield D, Callander E. The individual and socioeconomic impact of osteoarthritis. *Nat Rev Rheumatol* 2014;10:437–41.
- Tang X, Wang S, Zhan S, Niu J, Tao K, Zhang Y, et al. The prevalence of symptomatic knee osteoarthritis in China: results from the China Health and Retirement Longitudinal Study. *Arthritis Rheumatol* 2016;68:648–53.
- Dillon CF, Rasch EK, Gu Q, Hirsch R. Prevalence of knee osteoarthritis in the United States: arthritis data from the Third National Health and Nutrition Examination Survey 1991–94. *J Rheumatol* 2006;33:2271–9.
- Hanna FS, Wluka AE, Bell RJ, Davis SR, Cicuttini FM. Osteoarthritis and the postmenopausal woman: Epidemiological, magnetic resonance imaging, and radiological findings. *Semin Arthritis Rheum* 2004;34:631–6.
- Nevitt MC, Felson DT, Williams EN, Grady D, on behalf of the Heart and Estrogen/Progestin Replacement Study Research Group. The effect of estrogen plus progestin on knee symptoms and related disability in postmenopausal women: the Heart and Estrogen/Progestin Replacement Study, a randomized, double-blind, placebo-controlled trial. *Arthritis Rheum* 2001;44:811–8.
- Cirillo DJ, Wallace RB, Wu L, Yood RA. Effect of hormone therapy on risk of hip and knee joint replacement in the Women's Health Initiative. *Arthritis Rheum* 2006;54:3194–204.
- Wei J, Gross D, Lane NE, Lu N, Wang M, Zeng C, et al. Risk factor heterogeneity for medial and lateral compartment knee osteoarthritis: analysis of two prospective cohorts. *Osteoarthritis Cartilage* 2019;27:603–10.
- Wise BL, Niu J, Yang M, Lane NE, Harvey W, Felson DT, et al, on behalf of the Multicenter Osteoarthritis (MOST) Group. Patterns of compartment involvement in tibiofemoral osteoarthritis in men and women and in whites and African Americans. *Arthritis Care Res (Hoboken)* 2012;64:847–52.
- NCD Risk Factor Collaboration (NCD-RisC). Worldwide trends in body-mass index, underweight, overweight, and obesity from 1975 to 2016: a pooled analysis of 2416 population-based measurement studies in 128.9 million children, adolescents, and adults. *Lancet* 2017;390:2627–42.
- Blüher M. Obesity: global epidemiology and pathogenesis [review]. *Nat Rev Endocrinol* 2019;15:288–98.
- World Health Organization. Obesity and overweight. 2020. URL: <https://www.who.int/en/news-room/fact-sheets/detail/obesity-and-overweight>.
- Ratneswaran A, Kapoor M. Osteoarthritis year in review: genetics, genomics, epigenetics. *Osteoarthritis Cartilage* 2021;29:151–60.
- Madry H, Luyten FP, Facchini A. Biological aspects of early osteoarthritis. *Knee Surg Sports Traumatol Arthrosc* 2012;20:407–22.
- Madry H, Kon E, Condello V, Peretti GM, Steinwachs M, Seil R, et al. Early osteoarthritis of the knee. *Knee Surg Sports Traumatol Arthrosc* 2016;24:1753–62.

34. Prieto-Alhambra D, Judge A, Javaid MK, Cooper C, Diez-Perez A, Arden NK. Incidence and risk factors for clinically diagnosed knee, hip and hand osteoarthritis: influences of age, gender and osteoarthritis affecting other joints. *Ann Rheum Dis* 2014;73:1659–64.
35. Woo J, Lau E, Lau CS, Lee P, Zhang J, Kwok T, et al. Socioeconomic impact of osteoarthritis in Hong Kong: utilization of health and social services, and direct and indirect costs. *Arthritis Rheum* 2003;49:526–34.
36. Obesity: a growing threat to health in China [editorial]. *Lancet* 2014;384:716.
37. United Nations Department of Economic and Social Affairs, Population Division. World population prospects 2019. URL: <https://population.un.org/wpp/>.
38. Bannuru RR, Osani MC, Vaysbrot EE, Arden NK, Bennell K, Bierma-Zeinstra SM, et al. OARSI guidelines for the non-surgical management of knee, hip, and polyarticular osteoarthritis. *Osteoarthritis Cartilage* 2019;27:1578–89.
39. Runhaar J, Zhang Y. Can we prevent OA? *Epidemiology and public health insights and implications*. *Rheumatology (Oxford)* 2018;57 Suppl:iv3–9.
40. World Health Organization. 10 facts on ageing and health. 2017. URL: <https://www.who.int/news-room/fact-sheets/detail/10-facts-on-ageing-and-health>.
41. Frenk J. The global health system: strengthening national health systems as the next step for global progress. *PLoS Med* 2010;7:e1000089.

DOI 10.1002/art.42085

Clinical Images: Voriconazole-induced synovitis, enthesitis, and periostitis








The patient, a 30-year-old White woman, presented with de novo pain and tenderness affecting hand, elbow, shoulder, knee, and ankle joints. She had been receiving voriconazole for invasive pulmonary and cerebral aspergillosis during the 3 months before presentation. At clinical examination she had discrete synovitis. Laboratory testing revealed normal levels of acute-phase reactants and no rheumatoid factor, anti-citrullinated protein antibodies, or antinuclear antibodies. Radiography of the hands revealed marked osteoproliferation (**arrows in A**), magnetic resonance imaging showed severe carpal synovitis (**arrows in B**), and power Doppler ultrasonography detected severe synovitis and enthesitis at the elbows, wrists, and knees. The osteoproliferation zone was also visible by ultrasonography (**arrow in C**). To quantify the extent of osteoproliferation, we performed high-resolution computed tomography of the wrist, combined with cinematic rendering (a new visualization technique), and detected areas of periosteal proliferation at the distal radius, the distal ulna, and the carpal bones (**arrows and box in D**). Voriconazole is a triazole antifungal agent recommended as first-line therapy for acute invasive aspergillosis. Toxicities occur in association with supratherapeutic plasma levels of the drug; high plasma fluoride concentrations (1) and alkaline phosphatase levels (2) have also been detected. Because of the high level of inflammatory activity in our patient, we initiated prednisolone therapy, and voriconazole was switched to isavuconazole. Rapid improvement occurred after 2 weeks, prednisolone was suspended after 6 weeks, and the plasma fluoride concentration and alkaline phosphatase level gradually returned to normal. Radiologic and ultrasonography findings were unremarkable within 5 months. In summary, diagnostic images along with clinical findings showed periostitis (3,4), synovitis, and enthesitis, indicating that voriconazole can trigger the full spectrum of symptoms associated with inflammatory joint disease. In the differential diagnosis of inflammatory joint disease, voriconazole should therefore be considered a trigger of drug-induced arthritis.

We thank Dr. Klaus Engel (Siemens Healthineers) for helping to provide computed radiography images and Louis Schuster for technical assistance. Data are available on request. Open access funding enabled and organized by Projekt DEAL. Author disclosures are available at <https://onlinelibrary.wiley.com/action/downloadSupplement?doi=10.1002%2Fart.42085&file=art42085-sup-0001-Disclosureform.pdf>.

- Adwan MH. Voriconazole-induced periostitis: a new rheumatic disorder [review]. *Clin Rheumatol* 2017;36:609–15.
- Hedrick J, Droz N. Voriconazole-induced periostitis. *N Engl J Med* 2019;381:e30.
- Tan I, Lomasney L, Stacy GS, Lazarus M, Mar WA. Spectrum of voriconazole-induced periostitis with review of the differential diagnosis [review]. *AJR Am J Roentgenol* 2019;212:157–65.
- Gupta R, Kumar AN, Bandhu S, Gupta S. Skeletal fluorosis mimicking seronegative arthritis. *Scand J Rheumatol* 2007;36:154–5.

Larissa Valor-Méndez, MD 
 Jochen Wacker, MD
 Georg Schett, MD 
 Bernhard Manger, MD
 Julia Fürst, MD
 Richard Strauß, MD
 Arnd Kleyer, MD 
 Friedrich Alexander University Erlangen–Nuremberg and
 Universitätsklinikum Erlangen
 Erlangen, Germany

Association of Cardiac Biomarkers With Cardiovascular Outcomes in Patients With Psoriatic Arthritis and Psoriasis: A Longitudinal Cohort Study

Keith Colaco,¹ Ker-Ai Lee,² Shadi Akhtari,³ Raz Winer,⁴ Paul Welsh,⁵  Naveed Sattar,⁵ Iain B. McInnes,⁵ 
Vinod Chandran,⁶  Paula Harvey,³ Richard J. Cook,⁷ Dafna D. Gladman,⁶  Vincent Pigué,³ and Lihi Eder³ 

Objective. In patients with psoriatic disease (PsD), we determined whether cardiac troponin I (cTnI) and N-terminal pro–brain natriuretic peptide (NT-proBNP) were associated with carotid plaque burden and the development of cardiovascular events independent of the Framingham Risk Score (FRS).

Methods. Among 1,000 patients with PsD, carotid total plaque area (TPA) was measured in 358 participants at baseline. Cardiac troponin I and NT-proBNP were measured using automated clinical assays. The association between cardiac biomarkers and carotid atherosclerosis was assessed by multivariable regression after adjusting for cardiovascular risk factors. Improvement in the prediction of cardiovascular events beyond the FRS was tested using measures of risk discrimination and reclassification.

Results. In univariate analyses, cTnI (β coefficient 0.52 [95% confidence interval (95% CI) 0.3, 0.74], $P < 0.001$) and NT-proBNP (β coefficient 0.24 [95% CI 0.1, 0.39], $P < 0.001$) were associated with TPA. After adjusting for cardiovascular risk factors, the association remained statistically significant for cTnI (adjusted β coefficient 0.21 [95% CI 0, 0.41], $P = 0.047$) but not for NT-proBNP ($P = 0.21$). Among the 1,000 patients with PsD assessed for cardiovascular risk prediction, 64 patients had incident cardiovascular events. When comparing a base model (with the FRS alone) to expanded models (with the FRS plus cardiac biomarkers), there was no improvement in predictive performance.

Conclusion. In patients with PsD, cTnI may reflect the burden of atherosclerosis, independent of traditional cardiovascular risk factors. Cardiac troponin I and NT-proBNP are associated with incident cardiovascular events independent of the FRS, but further study of their role in cardiovascular risk stratification is warranted.

INTRODUCTION

Psoriasis and psoriatic arthritis (PsA), collectively known as psoriatic disease (PsD), are characterized by excess cardiovascular morbidity and mortality compared to the general population (1–4). While this excess risk is partly explained by high prevalence of traditional cardiovascular risk factors, chronic systemic inflammation promotes atherogenesis, thereby predisposing individuals with

PsD to an increased risk of cardiovascular events (5,6). Conventional cardiovascular risk scores, such as the Framingham Risk Score (FRS) (7), underestimate cardiovascular risk in patients with PsD and other inflammatory rheumatic diseases, because most rely only on traditional cardiovascular risk factors and fail to consider the independent risk conferred by immune disease per se (8,9).

Novel laboratory and imaging biomarkers improve cardiovascular risk prediction in the general population, and it has been

Supported by a Discovery Grant from the National Psoriasis Foundation and an operating grant from the Arthritis Society (Y10-16-394). The Psoriatic Disease Program was supported by a grant from the Krembil Foundation. Mr. Colaco's work was supported by the Enid Walker Estate, Women's College Research Institute, Arthritis Society (grant TGP-19-0446), National Psoriasis Foundation (Early Career Grant), and the Edward Dunlop Foundation. Dr. Chandran's work was supported by a Pfizer Chair Research Award, Rheumatology, University of Toronto, Canada. Dr. Eder's work was supported by a Young Investigator Award from the Arthritis Society (grant YIA-16-394) and an Early Researcher Award from the Ontario Ministry of Science and Innovation.

¹Keith Colaco, MSc: Women's College Hospital, University of Toronto, and University Health Network, Toronto, Ontario, Canada; ²Ker-Ai Lee, MMath: University of Waterloo, Waterloo, Ontario, Canada; ³Shadi Akhtari, MD, Paula Harvey, BMBS, PhD, Vincent Pigué, MD, PhD, Lihi Eder, MD, PhD: Women's

College Hospital and University of Toronto, Toronto, Ontario, Canada; ⁴Raz Winer, MD: Rambam Health Care Campus, Haifa, Israel; ⁵Paul Welsh, PhD, Naveed Sattar, MD, PhD, Iain B. McInnes, MD, PhD: University of Glasgow, Glasgow, UK; ⁶Vinod Chandran, MD, PhD, Dafna D. Gladman, MD: University of Toronto and University Health Network Toronto, Ontario, Canada; ⁷Richard J. Cook, MMath, PhD: University of Waterloo, Waterloo, Ontario, Canada.

Author disclosures are available at <https://onlinelibrary.wiley.com/action/downloadSupplement?doi=10.1002%2Fart.42079&file=art42079-sup-0001-Disclosureform.pdf>.

Address correspondence to Lihi Eder, MD, PhD, Women's College Research Institute, Room 6326, Women's College Hospital, 76 Grenville Street, Toronto, Ontario M5S 1B2, Canada. Email: lihi.eder@wchospital.ca.

Submitted for publication July 5, 2021; accepted in revised form January 25, 2022.

suggested that they could be combined with conventional scoring systems to optimize cardiovascular risk stratification (10–12).

While findings from general population cohort studies indicate that high-sensitivity troponin cardiac I (cTnI) and N-terminal pro-brain natriuretic peptide (NT-proBNP) are strong predictors of cardiovascular risk, limited information exists on patients with rheumatic diseases and particularly those with PsD (13–18). Cardiac troponin concentrations are moderately elevated in the circulation because of myocardial ischemia, and the biomarker is used in the diagnosis of myocardial infarction when levels are markedly elevated. Previous studies of patients with psoriasis (19) and systemic lupus erythematosus (20,21) demonstrated associations between elevated high-sensitivity troponin concentration and atherosclerotic plaque burden. A single small study evaluated the predictive performance of high-sensitivity troponin in patients with rheumatoid arthritis (RA) (22). Similarly, NT-proBNP, which is released by cardiac myocytes in response to volume overload and ventricular wall distension and may be elevated after myocardial ischemia, hypoxia, and fibrosis, is also increased in patients with RA. NT-proBNP has also been associated with higher all-cause mortality in patients with early inflammatory arthritis and RA; however, the predictive performance of this biomarker compared to conventional cardiovascular scores has not been tested (23–25). To date, no study has investigated the ability of cTnI and NT-proBNP to improve cardiovascular risk stratification in patients with PsD.

The data highlight the potential of these cardiac biomarkers to augment existing cardiovascular scores by considering the combined direct effect of traditional cardiovascular risk factors and systemic inflammation on the heart in patients with PsD. However, it is not clear how much incremental information is gained by using these 2 cardiac biomarkers in cardiovascular risk stratification or their association with carotid atherosclerosis in patients with PsD.

In this study, we evaluated the association between cTnI and NT-proBNP and carotid atherosclerosis presence and progression. In the context of current treatment guidelines highlighting the need to identify patients with PsD who are at high cardiovascular risk, we investigated whether these cardiac biomarkers predict clinical cardiovascular events independent of traditional cardiovascular risk factors and whether they improve cardiovascular risk stratification beyond the FRS.

PATIENTS AND METHODS

Study population. We included patients from the University of Toronto PsD cohort. The cohort comprises participants with a diagnosis of psoriasis without arthritis (PsC) who have been followed up since 2006 and those with psoriatic arthritis (PsA) who have been followed up prospectively since 1978 as part of a larger study to investigate disease-related outcomes (26,27). Among PsA patients, 98% met the Classification of Psoriatic

Arthritis (CASPAR) criteria (28). PsC patients were enrolled based on a diagnosis of psoriasis without arthritis, as confirmed by a dermatologist and rheumatologist. Participants were assessed by a rheumatologist at 6–12-month intervals, and detailed information on demographic characteristics and comorbidities, including traditional cardiovascular risk factors, medications, and disease activity, were collected according to a standard protocol. All data are stored in a web-based computerized database. Inclusion criteria included having a serum sample in the cohort biobank, no history of cardiovascular events at study entry, and being followed up for at least 1 year following study entry. The study was approved by the University Health Network Ethics Board (no. 08-0630) and all patients provided informed consent.

Biomarker measurement. Annual serum samples have been collected and stored in a biobank since 2002; thus, patients entered this study at the date they provided their first serum sample. NT-proBNP (Cobas; Roche Diagnostics) and high-sensitivity cTnI (Architect Stat; Abbott Laboratories, Abbott Diagnostics) were measured in serum samples on automated clinically validated immunoassay analyzers using the manufacturers' calibrators and quality controls. The limit of detection was 5 pg/ml for NT-proBNP and 1.1 pg/ml for cTnI.

Carotid ultrasound assessment of atherosclerosis.

Vascular imaging studies have shown increased atherosclerotic plaques and vascular inflammation in patients with PsD (29–34). As this noninvasive assessment can serve as a surrogate measure for cardiovascular risk by identifying subclinical atherosclerosis in asymptomatic patients (35), we performed a nested cohort study that included 358 patients who underwent a baseline carotid ultrasound assessment between 2009 and 2015. Each patient underwent a second carotid ultrasound 2–3 years after the baseline assessment. A single trained physician (LE) performed all ultrasound measurements in accordance with a study protocol that has previously been described in detail (29). Scans were performed with MyLab 30 and MyLab 70 XVision scanners with a linear LA523 7–13-MHz transducer (all from Esaote). The scan included detailed B-mode images of both the right and the left common carotid arteries as well as the carotid bulb, internal carotid, and external carotid arteries. All ultrasound scans were saved as video files for later reading.

The burden of atherosclerotic plaques was measured by carotid total plaque area (TPA), as previously described by Spence (36). The plane for measurement of each plaque was chosen by reviewing the video of the scan to find the largest extent of plaque as seen in the longitudinal view. The image was then frozen, and the plaque was measured by tracing around the perimeter with a cursor on the screen. The assessor then moved on to the next plaque and repeated the process until all observed plaques in the common, external, and internal carotid arteries were measured. TPA (cm²) was recorded as the sum of

areas of all plaques in the right and left carotid arteries. The outcomes of interest were TPA at baseline and the average annual progression rate of TPA that was calculated by subtracting the baseline TPA value from the follow-up TPA value, divided by the number of years between visits. Reading of the scans was performed independently of the scanning, and readers were blinded with regard to clinical data. The intraobserver intraclass correlation coefficient for TPA was 0.94.

Incident cardiovascular events. The FRS was calculated for each patient to estimate the 10-year risk of cardiovascular disease (CVD) (7). Risk factors included in the score were age, sex, current smoking status, systolic blood pressure, treatment for hypertension, diabetes mellitus, total cholesterol, and high-density lipoprotein cholesterol (HDL-c).

The primary end point was the occurrence of the first clinical cardiovascular event. A composite outcome that included the following clinical cardiovascular events was identified within 10 years of biomarker measurement: angina pectoris, myocardial infarction, transient ischemic attack (TIA), ischemic cerebrovascular accident (CVA), revascularization procedures, and cardiovascular death. Revascularization procedures included percutaneous coronary intervention, coronary artery bypass surgery, carotid endarterectomy, and vascular surgery for peripheral artery disease.

Potential cardiovascular events were first identified by searching the cohort database and linking patients' records to provincial mortality and hospitalization databases. All Ontarians are insured under a single-payer health care system, covering all hospital services. The Canadian Institute for Health Information Discharge Abstract Database and National Ambulatory Care Reporting System contain detailed information about all inpatient hospital discharges, emergency room visits, and same-day surgeries from all hospitals in Ontario, Canada. International Classification of Diseases, Tenth Revision codes were used to identify hospitalizations due to a cardiovascular event (Supplementary Table 1, available on the *Arthritis & Rheumatology* website at <https://onlinelibrary.wiley.com/doi/10.1002/art.42079>). Underlying causes of death due to CVD were verified from the Ontario Vital Statistics Death Registry. Subsequently, complete medical records describing the cardiovascular event were obtained, where available, from patients' primary care providers and specialists. Each identified potential cardiovascular event was adjudicated by reviewing data from hospital admissions, death certificates, and medical records from relevant specialists. Uncertain cases were discussed with a cardiologist (SA for cardiac events) and neurologist (RW for neurologic events) to determine whether to consider them as cardiovascular events.

Statistical analysis. Baseline characteristics were calculated as the mean \pm SD for continuous variables or frequency for categorical variables. Cardiac biomarker concentrations and

TPA were log-transformed to better approximate the normal distribution. First, we evaluated the association between cardiac biomarkers and carotid atherosclerosis.

We performed multivariable linear regression to assess the association between cardiac biomarker concentrations and TPA at baseline in patients with PsD. Adjustment was made for the following variables: age, sex, body mass index, hypertension, diabetes mellitus, current smoking, low-density lipoprotein cholesterol, HDL-c, creatinine level, and use of lipid lowering therapy. Beta coefficients and 95% confidence intervals (95% CIs) were calculated. Next, logistic regression was used to assess the association of cardiac biomarker concentrations and carotid atherosclerosis progression, defined as an annual rate of TPA progression greater than the 75th percentile.

We then evaluated the association between cardiac biomarkers and clinical cardiovascular events. This association was analyzed separately for each biomarker using a series of cause-specific Cox regression models. Subjects entered the risk set at the date of the first available serum sample and the event occurred at the date of the first cardiovascular event within 10 years. Patients who were event-free at the date at which they were last known to be alive were censored. Non-cardiovascular death was considered as a competing event. Biomarker associations were first adjusted for age and sex, followed by the FRS. The nature of the associations were tested and illustrated using penalized splines and modeled using the median value of each biomarker as the reference (37). Plots of the scaled Schoenfeld residuals against time and a statistical test of proportionality were used to assess the assumption of multiplicative covariate effects (38). We subsequently assessed the ability of cardiac biomarkers to predict cardiovascular events using cause-specific Cox regression models adjusted for the FRS. Improvement in the clinical prediction of cardiovascular events beyond the FRS was tested using the area under the receiver operating characteristic curve (AUC), net reclassification index (NRI), and integrated discrimination index (IDI). Odds ratios (ORs), hazard ratios (HRs), and 95% CIs were calculated. Analyses were performed with R (version 3.6.2) and SAS Studio 3.8.

Data availability. All data relevant to the study are included in the article or uploaded as supplementary materials (available on the *Arthritis & Rheumatology* website at <https://onlinelibrary.wiley.com/doi/10.1002/art.42079>). Requests for additional study-related data can be sent to the corresponding author.

RESULTS

Cardiac biomarkers and carotid atherosclerosis.

Characteristics of the study participants are shown in Table 1. An ultrasound assessment was performed in 358 patients with PsD. The mean \pm SD duration of follow-up was 3.69 ± 1.9 years.

Table 1. Baseline characteristics of the study population with psoriatic disease*

Variable	Carotid ultrasound assessment (n = 358)	Incident cardiovascular events (n = 1,000)
PsA, no. (%)	251 (70.1)	648 (64.8)
PsC, no. (%)	107 (29.9)	352 (35.2)
Age, years	53.8 ± 11	49 ± 12.8
Female sex, no. (%)	164 (45.8)	446 (44.6)
Psoriasis disease duration, years	23.9 ± 14.5	20 ± 14.1
PsA disease duration, years	15.1 ± 11.3	11.8 ± 10.3
Caucasian ethnicity, no. (%)	313 (87.4)	834 (83.4)
Current smoker, no. (%)	40 (11.2)	164 (16.4)
PASI score	3 ± 4.1	4.1 ± 6.3
Tender joint count†	3 ± 5.6	3.8 ± 7.3
Swollen joint count†	0.9 ± 1.9	1.5 ± 3.3
Current daily use of NSAIDs, no. (%)	135 (37.7)	265 (26.5)
Current use of DMARDs, no. (%)	137 (38.3)	362 (36.2)
Current use of biologics, no. (%)	162 (45.3)	214 (21.4)
Total cholesterol, mmol/liter	5.1 ± 1	4.2 ± 0.9
LDL-c, mmol/liter	3.0 ± 0.9	1.6 ± 0.5
HDL-c, mmol/liter	1.4 ± 0.4	1.2 ± 0.3
BMI, kg/m ²	28.4 ± 5.8	28.7 ± 5.9
Diabetes mellitus, no. (%)	19 (5.3)	77 (7.7)
Hypertension, no. (%)‡	96 (26.8)	274 (27.4)
Use of lipid-lowering medications, %	93	100
cTnl, ng/liter	3.3 ± 2.5	4.4 ± 5.1
NT-proBNP, pg/ml	73.2 ± 111	63.3 ± 115.9
Total plaque area, cm ²	0.17 ± 0.3	-
Framingham Risk Score, no. (%)		
Low-risk (<10%)	-	720 (72.0)
Medium-risk (10–19%)	-	187 (18.7)
High-risk (≥20%)	-	93 (9.3)

* Except where indicated otherwise, values are the mean ± SD. PsC = psoriasis without arthritis; PASI = Psoriasis Area Severity Index; NSAIDs = nonsteroidal antiinflammatory drugs; DMARDs = disease-modifying antirheumatic drugs; LDL-c = low-density lipoprotein cholesterol; HDL-c = high-density lipoprotein cholesterol; BMI = body mass index; cTnl = cardiac troponin I; NT-proBNP = N-terminal pro-brain natriuretic peptide.

† Only in patients with psoriatic arthritis (PsA).

‡ Systolic blood pressure >140 mm Hg or use of antihypertensive medications.

Table 2. Association of levels of cardiac biomarkers (cTnl and NT-proBNP) with carotid total plaque area in patients with PsD, using linear regression*

	Univariable analysis, β (95% CI)	P	Multivariable analysis, cTnl, β (95% CI)	P	Multivariable analysis, NT-proBNP, β (95% CI)	P
Female sex	-0.32 (-0.65, 0.02)	0.06	-0.14 (-0.47, 0.18)	0.39	-0.32 (-0.66, 0.01)	0.06
Age	0.07 (0.06, 0.09)	<0.001	0.06 (0.04, 0.07)	<0.001	0.06 (0.04, 0.07)	<0.001
BMI	0.04 (0.01, 0.06)	0.02	0.01 (-0.01, 0.04)	0.36	0.02 (0, 0.05)	0.18
Hypertension	0.77 (0.4, 1.14)	<0.001	0.09 (-0.26, 0.45)	0.60	0.06 (-0.3, 0.42)	0.75
Diabetes mellitus	0.74 (0, 1.48)	0.05	0.31 (-0.34, 0.95)	0.35	0.33 (-0.32, 0.98)	0.32
Current smoker	0.15 (-0.38, 0.69)	0.58	0.44 (-0.01, 0.89)	0.06	0.28 (-0.17, 0.73)	0.22
LDL-c	0.18 (0, 0.37)	0.05	0.26 (0.1, 0.42)	0.001	0.26 (0.1, 0.42)	0.002
HDL-c	0.07 (-0.36, 0.51)	0.74	0.01 (-0.39, 0.41)	0.96	0.02 (-0.39, 0.42)	0.92
Use of lipid-lowering therapy	1.10 (0.73, 1.46)	<0.001	0.73 (0.39, 1.07)	<0.001	0.67 (0.32, 1.01)	<0.001
Creatinine	1.48 (0.37, 2.58)	0.01	0.43 (-0.59, 1.45)	0.41	0.44 (-0.61, 1.48)	0.42
cTnl	0.52 (0.3, 0.74)	<0.001	0.21 (0, 0.41)	0.047	-	-
NT-proBNP	0.24 (0.1, 0.39)	0.002	-	-	0.09 (-0.05, 0.23)	0.21

* PsD = psoriatic disease; 95% CI = 95% confidence interval (see Table 1 for other definitions).

Using linear regression models, the association between cardiac biomarker levels and TPA at baseline was examined (Table 2). In univariate analyses, cTnI (β coefficient 0.52 [95% CI 0.3, 0.74]) and NT-proBNP (β coefficient 0.24 [95% CI 0.1, 0.39]) were associated with TPA. After adjusting for cardiovascular risk factors, lipid-lowering therapy, and creatinine level, the association remained statistically significant for cTnI (adjusted β coefficient 0.21 [95% CI 0, 0.41]) but not for NT-proBNP. We then evaluated the association between cardiac biomarker levels and atherosclerosis progression in patients with PsD using logistic regression models. Of the 358 participants, 89 had atherosclerosis progression. In the univariate analysis, cTnI was associated with atherosclerosis progression (OR 1.52 [95% CI 1.04, 2.23]) but not with NT-proBNP (OR 1.08 [95% CI 0.87, 1.34]) (Supplementary Table 2, available on the *Arthritis & Rheumatology* website at <https://onlinelibrary.wiley.com/doi/10.1002/art.42079>). In the multivariable analysis, current smoking, creatinine level, and baseline TPA predicted atherosclerosis progression. However, there was no association with either cTnI or NT-proBNP. No interaction was found between each of the biomarkers and sex.

Cardiac biomarkers and incident cardiovascular events. One thousand participants (PsA [n = 648], PsC [n = 352]) who were evaluated from 2002 to 2019 were included in this analysis. During a mean follow-up of 7.1 years (7,099 person-years), 64 patients developed an incident cardiovascular event (angina [n = 10], myocardial infarction [n = 20], TIA [n = 7], CVA [n = 11], revascularization [n = 11], cardiovascular death [n = 5]), resulting in an incidence rate of 0.9 events per 100 person-years (95% CI 0.7, 1.0).

First, we evaluated associations between cardiac biomarker levels and incident cardiovascular events. In a model

adjusted for the FRS, both cTnI (HR 3.02 [95% CI 1.12, 8.16]) and NT-proBNP (HR 2.02 [95% CI 1.28, 3.18]) were associated with cardiovascular events per 1 SD increase (Figure 1). The association was stronger in men compared to women. For cTnI, the HR in men was 3.71 (95% CI 1.10, 12.5) compared to women (HR 2.72 [95% CI 0.48, 15.5]). For NT-proBNP, the HR in men was 1.91 (95% CI 1.09, 3.36) compared to women (HR 2.11 [95% CI 0.85, 5.27]). However, the interactions between sex and either biomarker were not statistically significant.

Including both cardiac biomarkers and the FRS in a single model, NT-proBNP (HR 1.91 [95% CI 1.23, 2.97]) retained statistical significance, but cTnI only showed a trend toward an association (HR 2.60 [95% CI 0.98, 6.87]). To better understand the relationship between cardiac biomarkers and cardiovascular events, a nonlinear cardiac biomarker effect was incorporated in the Cox regression model, and this nonlinear effect was modeled using penalized splines. Figure 2 shows the splines-based HR curves using the median concentration level of each biomarker as the reference. In general, a nonlinear relationship was observed for both biomarkers and cardiovascular events. For both unadjusted and adjusted models, cTnI showed a gradual rise in cardiovascular risk up to 10 ng/liter, and then a rapid rise in increasing risk at higher levels of cTnI. NT-proBNP showed almost no increase in cardiovascular risk up to a level of 100 pg/ml and a rapid incline following this level, with almost a doubling of the HR from 100 pg/ml to 200 pg/ml (2.5 to 4.9, respectively).

Finally, we evaluated whether cardiac biomarkers could improve the performance of FRS by improving classification of patients to cardiovascular risk categories. The FRS demonstrated moderate performance (AUC 73.8) in predicting cardiovascular

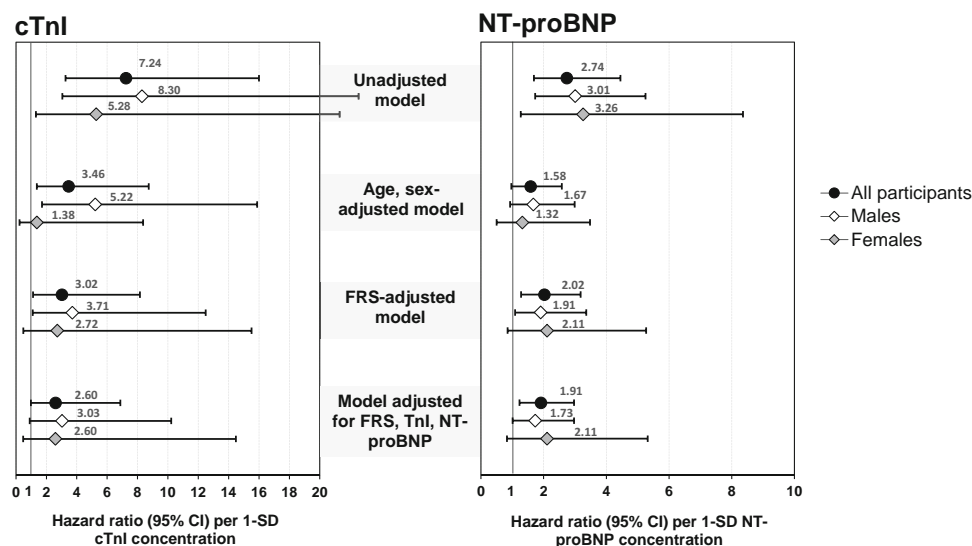


Figure 1. Hazard ratios of cardiac biomarker measures with incident cardiovascular events (n = 1,000; 64 events). Error bars show 95% confidence intervals (95% CIs). cTnI = cardiac troponin I; FRS = Framingham Risk Score; NT-proBNP = N-terminal pro-brain natriuretic peptide.

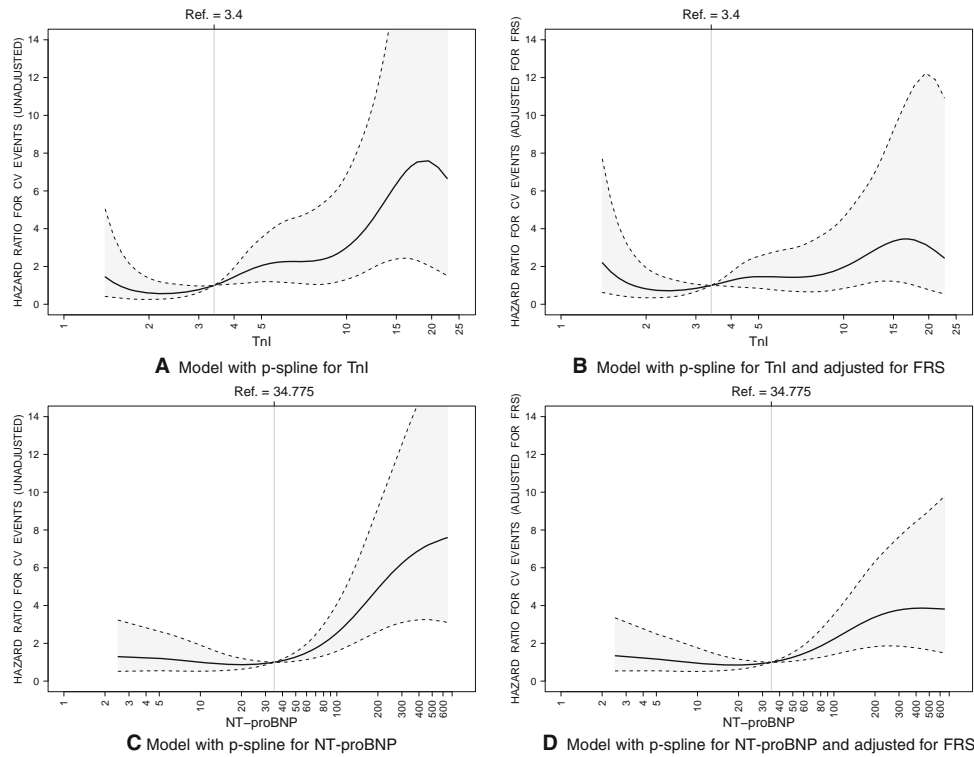


Figure 2. Splines-based hazard ratio (HR) curves to illustrate the association of cTnI and NT-proBNP with cardiovascular events, unadjusted and adjusted for the FRS. The reference (HR = 1) is the median value of each biomarker. Both penalized splines are on a log scale. Shaded areas show the lower and upper bounds of the 95% CI. CV = cardiovascular (see Figure 1 for other definitions).

risk in patients with PsD (Figure 3). When comparing a base model (with the FRS alone) to expanded models (with the FRS plus cardiac biomarkers), there was no significant improvement in predictive accuracy. The addition of cTnI, NT-proBNP, or both cTnI and NT-proBNP to the FRS did not demonstrate

improvements in any measure of risk discrimination or reclassification, including AUC, NRI, and IDI (Table 3).

DISCUSSION

In this study, we demonstrate several important findings: 1) cTnI was independently associated with the burden of atherosclerosis as measured by carotid ultrasound; 2) elevated cTnI and NT-proBNP levels were associated with a higher risk of developing future cardiovascular events independent of traditional cardiovascular risk factors, and the associations were stronger in men compared to women; and 3) the addition of cTnI or NT-proBNP did not improve the performance of the FRS for predicting cardiovascular events in patients with PsD. These findings suggest that increased atherosclerotic plaque burden is associated with subclinical cardiac injury, which is associated with elevated concentrations of cardiac biomarkers. This, in turn, may ultimately lead to clinical cardiovascular events, as observed by the strong link between cardiac biomarkers and clinical cardiovascular events. To our knowledge, this is the largest prospective study to assess the association of cardiac biomarkers with subclinical atherosclerosis, and the first study to evaluate the clinical utility of cardiac biomarkers for cardiovascular risk stratification in patients with PsD, suggesting that this noninvasive assessment offers clinical translation potential.

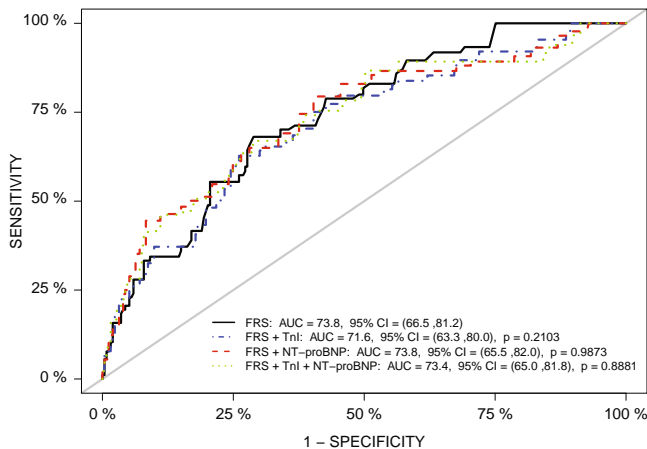


Figure 3. Comparison of the predictive performance of the base model (FRS alone) and expanded models for prediction of cardiovascular events in patients with psoriatic disease. AUC = area under the receiver operating characteristic curve (see Figure 1 for other definitions).

Table 3. Summary of predictive and reclassification indices for cardiovascular events using the FRS (base model) with and without cardiac biomarkers as model covariates, based on cause-specific Cox regression models*

	AUC			NRI			IDI		
	Estimate	95% CI	<i>P</i>	Estimate	95% CI	<i>P</i>	Estimate	95% CI	<i>P</i>
Base model	73.8	66.5, 81.2	–	–	–	–	–	–	–
Model 1 vs. base model	71.6	63.3, 80.0	0.21	0.081	–0.198, 0.20	0.67	0.005	–0.005, 0.035	0.37
Model 2 vs. base model	73.8	65.5, 82.0	0.99	0.20	–0.02, 0.38	0.06	0.017	–0.002, 0.058	0.10
Model 3 vs. base model	73.4	65.0, 81.8	0.89	0.27	0.002, 0.42	0.047	0.021	0, 0.068	0.053

* Base model = Framingham Risk Score (FRS) alone; model 1 = FRS and cTnI; model 2 = FRS and NT-proBNP; model 3 = FRS, cTnI, and NT-proBNP. AUC = area under the receiver operator characteristic curve; 95% CI = 95% confidence interval; NRI = net reclassification improvement; IDI = integrated discrimination index (see Table 1 for other definitions).

In general, studies of troponin and NT-proBNP in PsD are limited (19,39,40). Ultrasound findings in our study suggest that elevated cTnI level is associated with early vascular changes in the carotid artery and may identify patients at increased risk of future myocardial injury beyond traditional cardiovascular risk factors. Although mechanisms behind elevated cardiac biomarker levels in PsD are unclear, potential pathways include cardiomyocyte injury from inflammatory cytokines and systemic inflammation driving endothelial dysfunction or indirectly causing cardiac strain (41,42). The inflammatory hypothesis of CVD in psoriatic patients has stemmed from the observation of elevated levels of C-reactive protein (CRP) and proinflammatory cytokines, as well as studies targeting reductions in inflammatory burden among patients with inflammatory rheumatic diseases. In a prospective cohort study of patients with PsD, treatment with tumour necrosis factor inhibitors (TNFi) led to improvement in vascular inflammation, while reduced progression of carotid plaques was reported in men (43). In patients with active RA, treatment with TNFi decreased circulating levels of NT-proBNP, suggesting a potential cardiovascular risk benefit (44). Biomarkers driven by immune disease arguably might not serve to enhance prediction because they are confounded by the impact of the underlying immune disease. In our study, we assessed the role of conventional vascular biomarkers to reduce this risk.

Overall, the ability of cTnI to predict both burden and progression of carotid plaque may reflect the presence of atherosclerotic disease and/or subclinical cardiac myocyte damage, which may progress to clinical cardiovascular events. Natriuretic peptides such as NT-proBNP have a physiologically protective role, but elevated levels tend to reflect pathology in older individuals with more comorbidities (15). Therefore, in contrast to NT-proBNP, elevated cTnI level seems to be a superior marker of atherosclerotic cardiovascular risk. The utility of cTnI alone or in conjunction with carotid ultrasound to improve cardiovascular risk stratification in patients with PsD warrants further assessment. We acknowledge that we have carried out an association analysis between the cardiac biomarkers and the outcomes of interest. Causal analysis could be of interest to some, and we note that the effects of some of the

baseline variables could be affected by collider bias (45) if these baseline variables have causal effects on any intermediate biomarkers. In such cases, a more formal mediation analysis involving inverse probability weighting could be undertaken. This would require a clear specification of the causal estimates of interest.

We examined the association of cardiac biomarkers with incident cardiovascular events. One-SD increases in cTnI and NT-proBNP were strongly associated with incident cardiovascular events in the FRS-adjusted models. Interestingly, after adjusting for both cardiac biomarkers and the FRS through inclusion in the same model, NT-proBNP, but not cTnI, remained associated with cardiovascular events. These findings are consistent with those of a large European population-based cohort study, which found that both biomarkers, when included in a multimarker model, were associated with increased primary cardiovascular risk independent of traditional cardiovascular risk factors (15). Variable characteristics of the screening population, such as those of the University of Toronto PsD cohort, may influence the performance of cardiac biomarkers as risk predictors. However, a recent study of the same PsD cohort found that the burden of systemic inflammation and level of disease activity were independent risk factors of heart failure events (46).

Our study did not find an added benefit of cardiac biomarkers with regard to cardiovascular risk stratification. The addition of each biomarker individually or in combination to the FRS did not improve measures of risk discrimination or reclassification. Proving the added benefit of biomarkers to conventional scoring methods such as the FRS is challenging due to the relatively small number of events and variability in sample populations and treatment effects. The lack of improvement in performance is consistent with other studies of inflammatory rheumatic diseases that attempted to add cardiac biomarkers to the FRS to improve risk stratification (47). While the FRS was moderately predictive of subsequent cardiovascular events in our study, the addition of each biomarker resulted in similar or inferior performance. In studies of the general population, the clinical utility of cTnI and NT-proBNP in cardiovascular risk stratification also remains unclear. In a large prospective study of British women, NT-proBNP did not improve risk prediction beyond

traditional cardiovascular risk factors (48). However, in another study of older British men, inclusion of NT-proBNP in an FRS-based model yielded significant improvement in risk discrimination, and its performance was superior to an FRS-based model with CRP (49). Other approaches have included the development of multimarker scores with troponin and NT-proBNP, in combination with other emerging biomarkers of cardiovascular stress, albeit with mixed results (50). Current guidelines for the general population do not suggest using cardiac biomarkers for cardiovascular risk stratification for primary prevention in asymptomatic patients, as they are only used to assess symptoms suspected to be of cardiac origin.

Our study has notable strengths. This is the first study to investigate cTnI and NT-proBNP and their relationship with noninvasive measures of carotid atherosclerosis and clinical cardiovascular events in a large longitudinal cohort of patients with PsD. Serum samples were collected during a time when lipid-lowering therapies and disease-modifying antirheumatic drugs were widely available; therefore, the benefit of modern preventive treatments is likely reflected in the reported cardiovascular risk estimates. Further, the use of high-sensitivity assays allowed measurement of biomarker concentrations below conventional levels of detection, revealing a spectrum of low and high levels of circulating cTnI and NT-proBNP. The limitations of this study include the relatively small number of cardiovascular events, which prevented in-depth analyses of subgroups of interest (e.g., by disease group). Our study did not include a comparator group of patients without PsD, so we could not determine whether the levels of cardiac biomarkers are higher in patients with PsD. We were unable to include CRP in the analysis as we did not have measurements for all patients in the study.

In conclusion, this study established the association between elevated cardiac biomarkers, atherosclerosis, and clinical cardiovascular events in patients with PsD. Cardiac troponin I may be as effective as established measures of carotid plaque burden for identifying subclinical atherosclerosis long before cardiovascular events occur. Both cTnI and NT-proBNP are associated with incident cardiovascular events independent of traditional cardiovascular risk factors and may reflect the excess risk in patients with PsD. However, the lack of improvement in prediction metrics beyond the FRS does not support the routine use of these cardiac biomarkers for cardiovascular risk stratification in asymptomatic patients with PsD. These data encourage additional research evaluating the utility of cTnI and NT-proBNP in cardiovascular risk stratification in this patient population.

AUTHOR CONTRIBUTIONS

All authors were involved in drafting the article or revising it critically for important intellectual content, and all authors approved the final version to be published. Dr. Eder had full access to all of the data in the study and takes responsibility for the integrity of the data and the accuracy of the data analysis.

Study conception and design. Eder.

Acquisition of data. Colaco, Chandran, Gladman, Eder.

Analysis and interpretation of data. Colaco, Lee, Akhtari, Winer, Welsh, Sattar, McInnes, Harvey, Cook, Piguet, Eder.

REFERENCES

- Polachek A, Touma Z, Anderson M, Eder L. Risk of cardiovascular morbidity in patients with psoriatic arthritis: a meta-analysis of observational studies. *Arthritis Care Res (Hoboken)* 2017;69:67–74.
- Miller IM, Ellervik C, Yazdanyar S, Jemec GB. Meta-analysis of psoriasis, cardiovascular disease, and associated risk factors. *J Am Acad Dermatol* 2013;69:1014–24.
- Eder L, Wu Y, Chandran V, Cook R, Gladman DD. Incidence and predictors for cardiovascular events in patients with psoriatic arthritis. *Ann Rheum Dis* 2016;75:1680–6.
- Colaco K, Widdifield J, Luo J, Rosen CF, Alhusayen R, Paterson JM, et al. Trends in mortality and cause-specific mortality among patients with psoriasis and psoriatic arthritis in Ontario, Canada. *J Am Acad Dermatol* 2021;84:1302–9.
- Gistera A, Hansson GK. The immunology of atherosclerosis. *Nat Rev Nephrol* 2017;13:368–80.
- Szentpetery A, Haroon M, FitzGerald O. Cardiovascular comorbidities in psoriatic disease. *Rheumatol Ther* 2020;7:5–17.
- D'Agostino RB Sr, Vasan RS, Pencina MJ, Wolf PA, Cobain M, Massaro JM, et al. General cardiovascular risk profile for use in primary care: the Framingham Heart Study. *Circulation* 2008;117:743–53.
- Colaco K, Ocampo V, Ayala AP, Harvey P, Gladman DD, Piguet V, et al. Predictive utility of cardiovascular risk prediction algorithms in inflammatory rheumatic diseases: a systematic review. *J Rheumatol* 2020;47:928–38.
- Eder L, Chandran V, Gladman DD. The Framingham Risk Score underestimates the extent of subclinical atherosclerosis in patients with psoriatic disease. *Ann Rheum Dis* 2014;73:1990–6.
- Vasan RS. Biomarkers of cardiovascular disease: molecular basis and practical considerations. *Circulation* 2006;113:2335–62.
- Sillescu H, Sartori S, Sandholt B, Baber U, Mehran R, Fuster V. Carotid plaque thickness and carotid plaque burden predict future cardiovascular events in asymptomatic adult Americans. *Eur Heart J Cardiovasc Imaging* 2018;19:1042–50.
- Lorenz MW, Markus HS, Bots ML, Rosvall M, Sitzer M. Prediction of clinical cardiovascular events with carotid intima-media thickness: a systematic review and meta-analysis. *Circulation* 2007;115:459–67.
- Willeit P, Welsh P, Evans JD, Tschiderer L, Boachie C, Jukema JW, et al. High-sensitivity cardiac troponin concentration and risk of first-ever cardiovascular outcomes in 154,052 participants. *J Am Coll Cardiol* 2017;70:558–68.
- Everett BM, Zeller T, Glynn RJ, Ridker PM, Blankenberg S. High-sensitivity cardiac troponin I and B-type natriuretic Peptide as predictors of vascular events in primary prevention: impact of statin therapy. *Circulation* 2015;131:1851–60.
- Welsh P, Hart C, Papacosta O, Preiss D, McConnachie A, Murray H, et al. Prediction of cardiovascular disease risk by cardiac biomarkers in 2 United Kingdom cohort studies: does utility depend on risk thresholds for treatment? *Hypertension* 2016;67:309–15.
- Di Angelantonio E, Chowdhury R, Sarwar N, Ray KK, Gobin R, Saleheen D, et al. B-type natriuretic peptides and cardiovascular risk: systematic review and meta-analysis of 40 prospective studies. *Circulation* 2009;120:2177–87.
- Blankenberg S, Salomaa V, Makarova N, Ojeda F, Wild P, Lackner KJ, et al. Troponin I and cardiovascular risk prediction in the general population: the BiomarCaRE consortium. *Eur Heart J* 2016;37:2428–37.

18. Wang TJ, Larson MG, Levy D, Benjamin EJ, Leip EP, Omland T, et al. Plasma natriuretic peptide levels and the risk of cardiovascular events and death. *N Engl J Med* 2004;350:655–63.
19. Zhou W, Abdelrahman KM, Dey AK, Reddy A, Uceda DE, Lateef SS, et al. Association among noncalcified coronary burden, fractional flow reserve, and myocardial injury in psoriasis. *J Am Heart Assoc* 2020;9:e017417.
20. Divard G, Abbas R, Chenevier-Gobeaux C, Chanson N, Escoubet B, Chauveheid MP, et al. High-sensitivity cardiac troponin T is a biomarker for atherosclerosis in systemic lupus erythematosus patients: a cross-sectional controlled study. *Arthritis Res Ther* 2017;19:132.
21. Winau L, Baydes RH, Braner A, Drott U, Burkhardt H, Sangle S, et al. High-sensitive troponin is associated with subclinical imaging bio-signature of inflammatory cardiovascular involvement in systemic lupus erythematosus. *Ann Rheum Dis* 2018;77:1590–8.
22. Karpouzias GA, Estis J, Rezaeian P, Todd J, Budoff MJ. High-sensitivity cardiac troponin I is a biomarker for occult coronary plaque burden and cardiovascular events in patients with rheumatoid arthritis. *Rheumatology (Oxford)* 2018;57:1080–8.
23. Provan S, Angel K, Semb AG, Atar D, Kvien TK. NT-proBNP predicts mortality in patients with rheumatoid arthritis: results from 10-year follow-up of the EURIDISS study. *Ann Rheum Dis* 2010;69:1946–50.
24. Mirjafari H, Welsh P, Verstappen SM, Wilson P, Marshall T, Edlin H, et al. N-terminal pro-brain-type natriuretic peptide (NT-pro-BNP) and mortality risk in early inflammatory polyarthritis: results from the Norfolk Arthritis Registry (NOAR). *Ann Rheum Dis* 2014;73:684–90.
25. Breunig M, Kleinert S, Lehmann S, Kneitz C, Feuchtenberger M, Tony HP, et al. Simple screening tools predict death and cardiovascular events in patients with rheumatic disease. *Scand J Rheumatol* 2018;47:102–9.
26. Gladman DD, Shuckett R, Russell ML, Thorne JC, Schachter RK. Psoriatic arthritis (PSA)—an analysis of 220 patients. *Q J Med* 1987;62:127–41.
27. Eder L, Chandran V, Shen H, Cook RJ, Shanmugarajah S, Rosen CF, et al. Incidence of arthritis in a prospective cohort of psoriasis patients. *Arthritis Care Res (Hoboken)* 2011;63:619–22.
28. Taylor W, Gladman D, Helliwell P, Marchesoni A, Mease P, Mielants H, et al. Classification criteria for psoriatic arthritis: development of new criteria from a large international study. *Arthritis Rheum* 2006;54:2665–73.
29. Eder L, Jayakar J, Shanmugarajah S, Thavaneswaran A, Pereira D, Chandran V, et al. The burden of carotid artery plaques is higher in patients with psoriatic arthritis compared with those with psoriasis alone. *Ann Rheum Dis* 2013;72:715–20.
30. Eder L, Thavaneswaran A, Chandran V, Cook R, Gladman DD. Increased burden of inflammation over time is associated with the extent of atherosclerotic plaques in patients with psoriatic arthritis. *Ann Rheum Dis* 2015;74:1830–5.
31. Mehta NN, Yu Y, Saboury B, Foroughi N, Krishnamoorthy P, Raper A, et al. Systemic and vascular inflammation in patients with moderate to severe psoriasis as measured by [18F]-fluorodeoxyglucose positron emission tomography-computed tomography (FDG-PET/CT): a pilot study. *Arch Dermatol* 2011;147:1031–9.
32. Shen J, Wong KT, Cheng IT, Shang Q, Li EK, Wong P, et al. Increased prevalence of coronary plaque in patients with psoriatic arthritis without prior diagnosis of coronary artery disease. *Ann Rheum Dis* 2017;76:1237–44.
33. Sobchak C, Akhtari S, Harvey P, Gladman D, Chandran V, Cook R, et al. Value of carotid ultrasound in cardiovascular risk stratification in patients with psoriatic disease. *Arthritis Rheumatol* 2019;71:1651–9.
34. Lam SH, Cheng IT, Li EK, Wong P, Lee J, Yip RM, et al. DAPSA, carotid plaque and cardiovascular events in psoriatic arthritis: a longitudinal study. *Ann Rheum Dis* 2020;79:1320–6.
35. Johnsen SH, Mathiesen EB, Joakimsen O, Stensland E, Wilsgaard T, Lochen ML, et al. Carotid atherosclerosis is a stronger predictor of myocardial infarction in women than in men: a 6-year follow-up study of 6226 persons: the Tromso Study. *Stroke* 2007;38:2873–80.
36. Spence JD. Technology insight: ultrasound measurement of carotid plaque—patient management, genetic research, and therapy evaluation. *Nat Clin Pract Neurol* 2006;2:611–9.
37. Meira-Machado L, Cadarso-Suarez C, Gude F, Araujo A. smoothHR: an R package for pointwise nonparametric estimation of hazard ratio curves of continuous predictors. *Comput Math Methods Med* 2013;2013:745742.
38. Therneau TM, Grambsch PM. Chapter 6. In: *Modeling survival data: extending the Cox Model*. New York: Springer-Verlag New York; 2000. p. 127–52.
39. Pietrzak A, Bartosinska J, Blaszczyk R, Chodorowska G, Brzozowski W, Hercogova J, et al. Increased serum level of N-terminal Pro-B-type natriuretic peptide as a possible biomarker of cardiovascular risk in psoriatic patients. *J Eur Acad Dermatol Venereol* 2015;29:1010–4.
40. Furer V, Shenhar-Tsarfaty S, Berliner S, Arad U, Paran D, Mailis I, et al. Prevalence of high-sensitivity cardiac troponin T in real-life cohorts of psoriatic arthritis and general population: a cross-sectional study. *Rheumatol Int* 2020;40:437–44.
41. Welsh P, Tuckwell K, McInnes IB, Sattar N. Effect of IL-6 receptor blockade on high-sensitivity troponin T and NT-proBNP in rheumatoid arthritis. *Atherosclerosis* 2016;254:167–71.
42. Bradham WS, Bian A, Oeser A, Gebretsadik T, Shintani A, Solus J, et al. High-sensitivity cardiac troponin-I is elevated in patients with rheumatoid arthritis, independent of cardiovascular risk factors and inflammation. *PLoS One*. 2012;7:e38930.
43. Eder L, Joshi AA, Dey AK, Cook R, Siegel EL, Gladman DD, et al. Association of tumor necrosis factor inhibitor treatment with reduced indices of subclinical atherosclerosis in patients with psoriatic disease. *Arthritis Rheumatol* 2018;70:408–16.
44. Peters MJ, Welsh P, McInnes IB, Wolbink G, Dijkmans BA, Sattar N, et al. Tumour necrosis factor α blockade reduces circulating N-terminal pro-brain natriuretic peptide levels in patients with active rheumatoid arthritis: results from a prospective cohort study. *Ann Rheum Dis* 2010;69:1281–5.
45. Westreich D, Greenland S. The table 2 fallacy: presenting and interpreting confounder and modifier coefficients. *Am J Epidemiol* 2013;177:292–8.
46. Koppikar S, Colaco K, Harvey P, Akhtari S, Chandran V, Gladman DD, et al. Incidence of and risk factors for heart failure in patients with psoriatic disease—a cohort study. *Arthritis Care Res (Hoboken)* 2021. DOI: 0.1002/acr.24578. E-pub ahead of print.
47. Finckh A, Courvoisier DS, Pagano S, Bas S, Chevallier-Ruggeri P, Hochstrasser D, et al. Evaluation of cardiovascular risk in patients with rheumatoid arthritis: do cardiovascular biomarkers offer added predictive ability over established clinical risk scores? *Arthritis Care Res (Hoboken)* 2012;64:817–25.
48. Sattar N, Welsh P, Sarwar N, Danesh J, Di Angelantonio E, Gudnason V, et al. NT-proBNP is associated with coronary heart disease risk in healthy older women but fails to enhance prediction beyond established risk factors: results from the British Women’s Heart and Health Study. *Atherosclerosis* 2010;209:295–9.
49. Wannamethee SG, Welsh P, Lowe GD, Gudnason V, Di Angelantonio E, Lennon L, et al. N-terminal pro-brain natriuretic peptide is a more useful predictor of cardiovascular disease risk than C-reactive protein in older men with and without pre-existing cardiovascular disease. *J Am Coll Cardiol* 2011;58:56–64.
50. Wang TJ, Wollert KC, Larson MG, Coglianese E, McCabe EL, Cheng S, et al. Prognostic utility of novel biomarkers of cardiovascular stress: the Framingham Heart Study. *Circulation* 2012;126:1596–604.

Identification of Mitofusin 1 and Complement Component 1q Subcomponent Binding Protein as Mitochondrial Targets in Systemic Lupus Erythematosus

Yann L. C. Becker,¹  Jean-Philippe Gagné,² Anne-Sophie Julien,³ Tania Lévesque,¹ Isabelle Allaëys,¹ Nadine Gougéard,⁴ Vicente Rubio,⁴ François-Michel Boisvert,⁵ Dominique Jean,⁵ Eric Wagner,⁶ Guy G. Poirier,⁷ Paul R. Fortin,⁸  and Éric Boilard¹ 

Objective. Mitochondria are organelles that exhibit several bacterial features, such as a double-stranded genome with hypomethylated CpG islands, formylated proteins, and cardiolipin-containing membranes. In systemic lupus erythematosus (SLE), mitochondria and their inner components are released into the extracellular space, potentially eliciting a proinflammatory response from the immune system. While cardiolipin and mitochondrial DNA and RNA are confirmed targets of autoantibodies, other antigenic mitochondrial proteins in SLE remain to be identified. The present study was undertaken to characterize the protein repertoire recognized by antimitochondrial antibodies (AMAs) in patients with SLE.

Methods. Using shotgun proteomic profiling, we identified 1,345 proteins, 431 of which were associated with the mitochondrial proteome. Immunoreactivities to several of these candidate proteins were assessed in serum samples from a local cohort (n = 30 healthy donors and 87 patients with SLE) using enzyme-linked immunosorbent assay, and further analyzed for associations with demographic and disease characteristics.

Results. We determined that IgG antibodies to the complement component C1q binding protein were significantly elevated in the patients with SLE ($P = 0.049$) and were also associated with lupus anticoagulant positivity ($P = 0.049$). Elevated levels of IgG antibodies against mitochondrial protein mitofusin 1 (MFN-1) were promising predictors of SLE diagnosis in our cohort (adjusted odds ratio 2.99 [95% confidence interval 1.39–6.43], $P = 0.0044$). Moreover, increased levels of anti-MFN-1 were associated with the presence of antiphospholipids ($P = 0.011$) and anti-double-stranded DNA ($P = 0.0005$).

Conclusion. In this study, we characterized the mitochondrial repertoire targeted by AMAs in the setting of SLE. Our results indicate that autoantibodies can recognize secreted and/or surface proteins of mitochondrial origin. Profiling of the AMA repertoire in large prospective cohorts may improve our knowledge of mitochondrial biomarkers and their usefulness for patient stratification.

Supported by the Arthritis Society (grant 225638 to Dr. Fortin), the Canadian Institutes of Health Research (CIHR) (CIHR Foundation grant to Dr. Boilard and CIHR operating grant MOP-97916). Dr. Becker's work was supported by the Fonds de Recherche en Santé du Québec (grant 282342) and the Arthritis Society (grant TGP-18-0257). Dr. Rubio's work was supported by the Secretaría de Estado de Investigación, Desarrollo e Innovación (grant BFU2017-84264-P) and by the Fundación Ramón Areces. Dr. Poirier's work was supported by the CIHR. Dr. Boilard's work was supported by the Fonds de Recherche en Santé du Québec and the Canadian Donation and Transplantation Research Program.

¹Yann L. C. Becker, PhD, Tania Lévesque, DCS, Isabelle Allaëys, PhD, Éric Boilard, PhD: Centre de Recherche ARThrite, Axe Maladies infectieuses et immunitaires, Université Laval, Québec City, Québec, Canada; ²Jean-Philippe Gagné, PhD: Axe Maladies infectieuses et immunitaires, Laboratoire d'Immunologie et Histocompatibilité, Centre Hospitalier Universitaire (CHU) de Québec-Université Laval, Québec City, Québec, Canada; ³Anne-Sophie Julien, MSc: Université Laval, Québec City, Québec, Canada; ⁴Nadine Gougéard, BTS, Vicente Rubio, MD, PhD: Instituto de Biomedicina de Valencia of the CSIC (IBV-CSIC), Valencia, Spain, and Group 739, Centro de

Investigación Biomédica en Red para Enfermedades Raras (CIBERER-ISCI), Madrid, Spain; ⁵François-Michel Boisvert, PhD, Dominique Jean, PhD: Université de Sherbrooke, Sherbrooke, Québec, Canada; ⁶Eric Wagner, PhD: Université Laval, Laboratoire d'Immunologie et Histocompatibilité, CHU de Québec-Université Laval, Québec City, Québec, Canada; ⁷Guy G. Poirier, PhD: Axe Maladies infectieuses et immunitaires, Centre de Recherche du CHU de Québec, Faculté de Médecine, Université Laval, Québec City, Québec, Canada; ⁸Paul R. Fortin, MD, MPH, FRCPC: Centre de Recherche ARThrite, Division de Rhumatologie, CHU de Québec-Université Laval, Québec City, Québec, Canada.

Author disclosures are available at <https://onlinelibrary.wiley.com/action/downloadSupplement?doi=10.1002%2Fart.42082&file=art42082-sup-0001-Disclosureform.pdf>.

Address correspondence to Eric Boilard, PhD, Centre de Recherche du Centre Hospitalier Universitaire de Québec-Université Laval, 2705 Boulevard Laurier, Room T1-49, Québec City, Québec G1V 4G2, Canada. Email: eric.boilard@crchudequebec.ulaval.ca.

Submitted for publication June 28, 2021; accepted in revised form February 1, 2022.

INTRODUCTION

The mitochondrion, a peculiar organelle that regulates numerous cellular pathways, is derived from the endosymbiosis between an α -proteobacterium and a primitive eukaryotic cell (1). Despite their intracellular nature, whole mitochondria and/or mitochondrial components may be released into the extracellular milieu under conditions of necrosis, tissue damage (2,3), or cellular activation (4–7). The release of whole mitochondria and/or mitochondrial components (i.e., DAMPs) skews innate immunity toward a proinflammatory response (8–10). Mitochondrial antigens may also be targeted by the adaptive immune system, as indicated by the presence of a humoral response comprising various types of antimitochondrial autoantibodies (AMAs) (11–14) in various inflammatory and autoimmune conditions. However, both the pathophysiologic pathway leading to the production of AMAs and several of the antigens targeted by various AMAs remain to be characterized (11–13).

Systemic lupus erythematosus (SLE) is a complex autoimmune disease in which the immune system generates autoantibodies recognizing self epitopes. Antibodies directed against DNA and nuclear components are hallmarks of SLE (15). Autoantibodies against the mitochondrial phospholipid cardiolipin (aCL) are associated with both thrombotic and obstetric events in SLE and antiphospholipid syndrome (APS) (16). The simultaneous presence of aCL and antibodies to the 60-kd heat-shock protein (HSP60) has been associated with arterial thrombosis (17). Studies have also revealed that the lupus autoantibody repertoire comprises immunoglobulins against mitochondrial DNA (mtDNA) and mtRNA (12–14).

Despite the description of antibodies targeting mitochondrial antigens (11–13), mitochondrial epitopes expressed on the outer membrane have yet to be identified. In this study, we aimed to characterize the antigenic protein repertoire recognized by AMAs in patients with SLE.

MATERIALS AND METHODS

Serum samples. Serum samples from healthy donors and lupus patients were obtained from the Centre Hospitalier Universitaire de Quebec–Université Laval Systemic Autoimmune Rheumatic Disease Biobank and DataBase repository (SARD-BDB). Samples were collected in accordance with the Declaration of Helsinki, as previously reported (12). See the Supplementary Materials and Methods and Supplementary Tables 1, 2, and 3 for additional information, available on the *Arthritis & Rheumatology* website at <http://onlinelibrary.wiley.com/doi/10.1002/art.42082>.

Isolation and preparation of mitochondrial samples. Mitochondria were isolated according to previously published procedures (12) and subsequently lysed (Supplementary

Materials and Methods, available at <http://onlinelibrary.wiley.com/doi/10.1002/art.42082>).

Immunoprecipitation. All incubations and washings were performed using gentle rotary mixing at ambient temperatures ($\sim 21^{\circ}\text{C}$), unless otherwise indicated. In all experiments, 3 mg of protein G Dynabeads were used to isolate IgG antibodies. Before use, beads were washed 3 times with 1 ml of $1\times$ phosphate buffered saline (PBS; Wisent). A DynaMag-2 magnetic strip (ThermoFisher Scientific) was used to retain the beads in the tubes.

Total mitochondrial antigens. Protein G Dynabeads were incubated for 2 hours with 1 ml of pooled serum (Supplementary Materials and Methods, available at <http://onlinelibrary.wiley.com/doi/10.1002/art.42082>) diluted to an IgG concentration of $24\ \mu\text{g}/\text{ml}$ in lysis buffer containing protease inhibitors (Supplementary Materials and Methods). Samples containing protein G Dynabead-bound total IgG were then washed 3 times in 1.5 ml PBS and once in the same volume of lysis buffer. Samples were incubated overnight at 4°C with 1.5 ml mitochondrial lysate at a protein concentration of $3\ \text{mg}/\text{ml}$. After incubation, samples were washed 3 times in lysis buffer containing protease inhibitor cocktail and 2 times in PBS (total volume 1.5 ml). Beads were then resuspended in $100\ \mu\text{l}$ of $75\ \text{mM}$ ammonium bicarbonate (pH 8.0) and stored at -80°C until used.

Enrichment of mitochondrial outer membrane (MOM) antigens by panning. Intact mitochondria (0.5 mg as quantitated by BCA assay) were incubated overnight at 4°C with 1 ml diluted pooled serum (10%, in PBS with protease inhibitor cocktail) from pooled samples from healthy individuals or lupus patients. Unbound serum components were removed by centrifuging 3 times at $7,000g$, performed each time for 10 minutes at 4°C , with 1.5 ml PBS. Anti-whole mitochondrial antibodies (AwMA), bound to their outer membrane mitochondrial antigens, were released by incubation in 1 ml lysis buffer containing protease inhibitor cocktail overnight at 4°C to ensure the capture of IgG antibodies by protein G Dynabeads. Three washing steps in PBS containing protease inhibitor cocktail were performed, followed by 2 final washes with PBS without protease inhibitors. Samples were resuspended in $100\ \mu\text{l}$ ammonium bicarbonate buffer (pH 8.0) and stored at -80°C .

Negative controls. The same procedure used to isolate total mitochondrial antigens was performed with the use of an irrelevant monoclonal IgG (clone IV.3, targeting Fc γ receptor IIa) instead of serum-containing IgG, in order to mitigate nonspecific capture of proteins caused by either polyreactive or natural antibodies that may target mitochondrial antigens.

Identification of mitochondrial antigens recognized by AMAs through on-bead proteolysis. Isolated samples were resuspended in $200\ \mu\text{l}$ of $75\ \text{mM}$ ammonium bicarbonate (pH 8.0) and supplemented with $2\ \mu\text{g}$ trypsin/Lys-C mix (Promega). Proteins in the samples were digested overnight at

37°C on a rotating mixer. The digested products were acidified with trifluoroacetic acid, and the peptides generated from the proteolytic digestion were isolated and washed on C18 tips according to the instructions of the manufacturer (ThermoFisher Scientific). The purified peptides were then dried by vacuum centrifugation and stored at -80°C before analysis by liquid chromatography tandem mass spectrometry (Supplementary Materials and Methods, available at <http://onlinelibrary.wiley.com/doi/10.1002/art.42082>).

Detection of autoantibodies targeting selected mitochondrial antigens. Levels of autoantibodies against several mitochondrial antigens were assessed by direct enzyme-linked immunosorbent assay (ELISA), using diluted serum (1:100) from healthy individuals or patients with either primary biliary cirrhosis (PBC), SLE, or APS, as previously described (12–14).

To assess reactivity patterns in routine clinical testing, indirect immunofluorescence (IIF) tests were performed using HEp-2 cells (Bio-Rad). Serum samples from healthy individuals (n = 3), patients with PBC (n = 3), and AwMA-positive patients with SLE (n = 9) were tested at dilutions of 1:80 and 1:160, using a PhD 1x workstation (Bio-Rad). Polyclonal antibodies against complement component C1q binding protein (C1qBP)

(rabbit anti-C1qBP; Millipore) and mitofusin 1 (MFN-1) (rabbit anti-C1qBP; Proteintech) were also tested for their reactivity patterns on HEp-2 cells, at a concentration of 5 µg/ml in 1× PBS.

Samples were incubated with HEp-2 cells for 30 minutes at room temperature, washed twice in PBS for 10 minutes, and incubated for another 30 minutes in the dark with either fluorescein isothiocyanate-conjugated goat anti-human IgG (heavy and light chain) for healthy donors and patients, or Alexa Fluor 488-conjugated goat anti-rabbit IgG (heavy and light chain) for rabbit antibodies. After 2 washes, slides were assembled with antifade mounting medium and coverslips. Reactivity patterns were assessed by a trained member of the personnel (J. Côté) and validated by the laboratory director (EW), using a BX53 immunofluorescence microscope (Olympus).

Images were acquired using a Z2 confocal microscope with an LSM 800 scanning system and a 40× oil objective (ApoChomat/1.4; Carl Zeiss). ZEN 2.3 software (Carl Zeiss) was used to process images.

Statistical analysis. Sociodemographic, clinical, and laboratory values are presented as the median (interquartile range [IQR]), number (%), or mean ± SD. Healthy donor and SLE

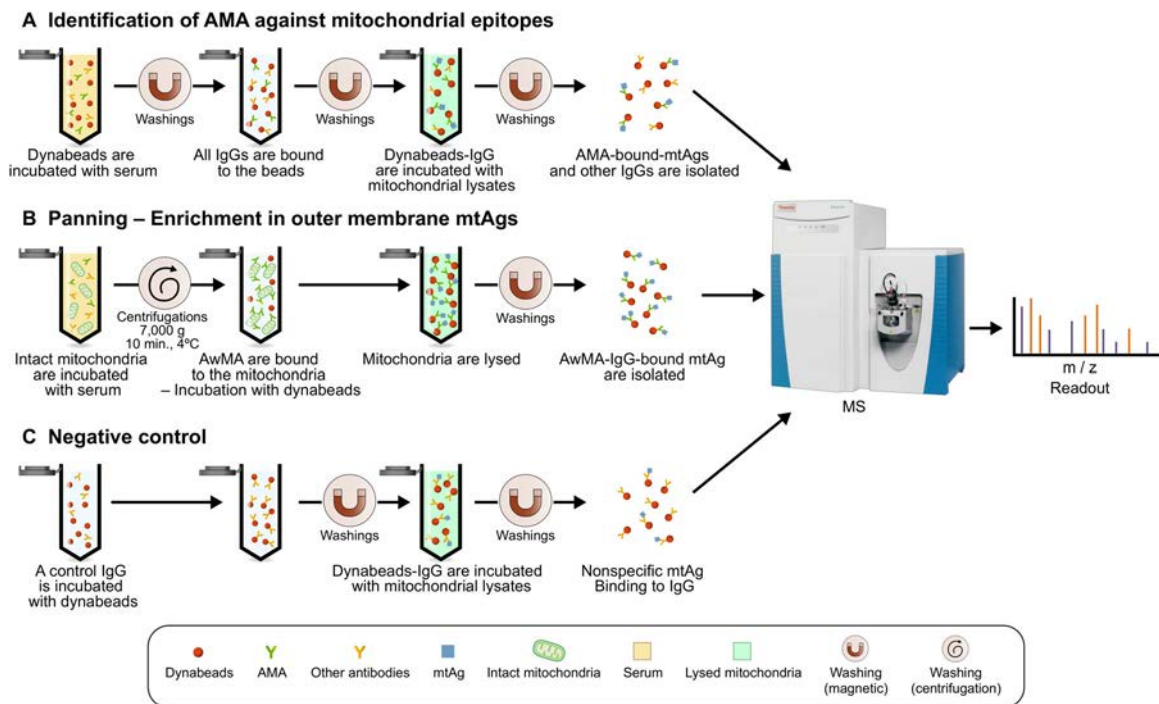


Figure 1. Workflow used for the detection of mitochondrial antigens targeted by anti-mitochondrial antibodies (AMAs) in the setting of systemic lupus erythematosus (SLE). **A**, Antibodies of the IgG subclass were isolated using protein G Dynabeads incubated in pooled serum from either 10 healthy donors or 10 SLE patients with high levels of anti-whole mitochondrial IgG (AwMA-IgG). Protein G Dynabead-bound IgG was subsequently incubated with mitochondrial lysates, allowing the affinity purification of mitochondrial antigens (mtAgs) from all sublocalizations. **B**, Freshly isolated intact mitochondria were incubated with pooled serum. Mitochondria incubated with AwMA were then lysed and AwMA-IgG were isolated with protein G Dynabeads. **C**, An irrelevant monoclonal IgG that targets Fcγ receptor IIa (a protein absent from mitochondria) was bound to Dynabeads and incubated with mitochondrial lysates in order to identify nonspecific binding of mtAgs. For each approach, samples were acquired in triplicate and mtAgs were identified by mass spectrometry (MS). Min. = minutes; m/z = mass/charge.

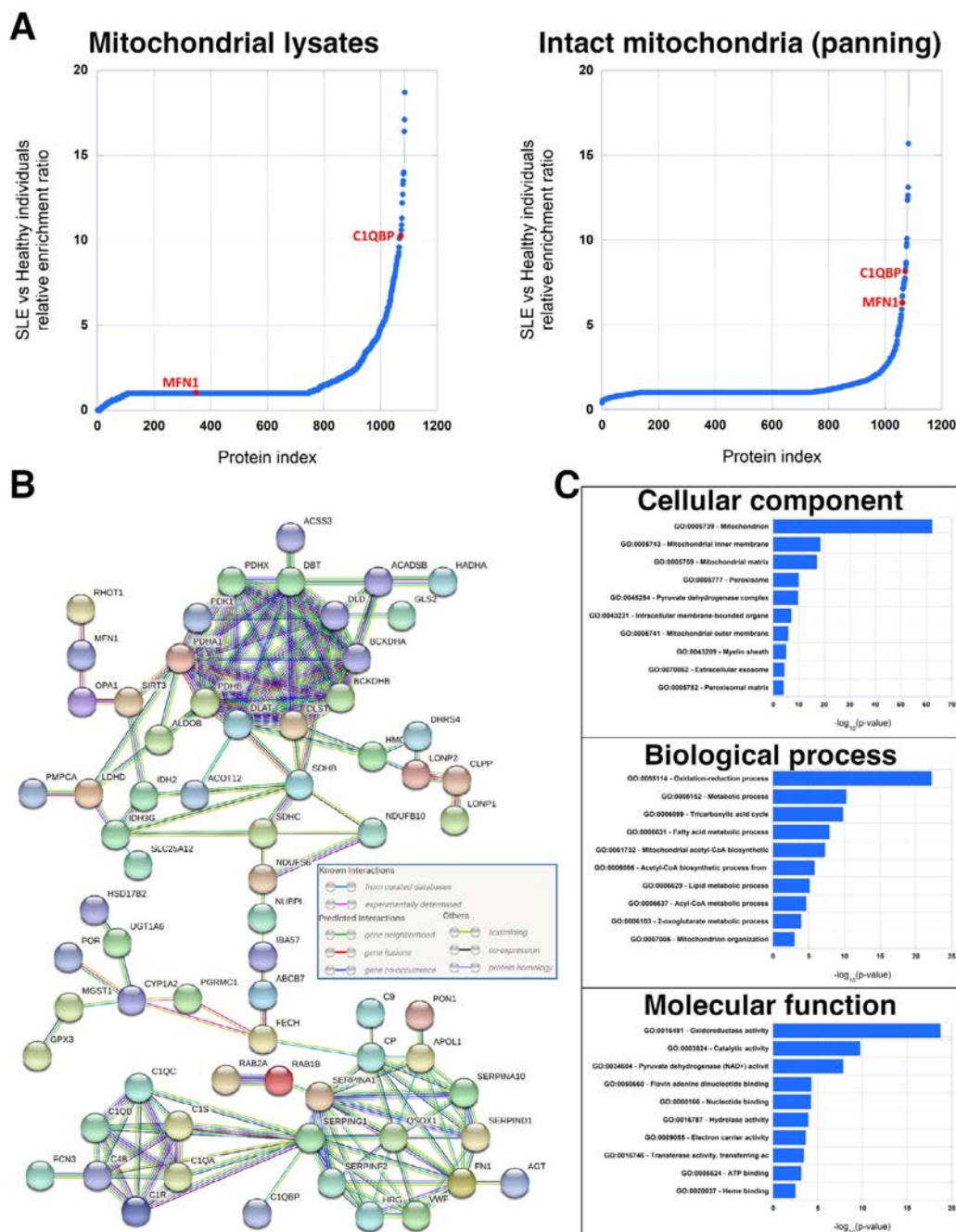


Figure 2. Mitochondrial hits identified and their mitochondrial sublocalization. **A**, Mitochondrial proteins are plotted in order of increasing ratio of enrichment (systemic lupus erythematosus [SLE] patients versus healthy controls) in samples containing mitochondrial lysates and samples containing intact mitochondria. A ratio >1 suggests enrichment in SLE patients relative to healthy individuals. For a complete list of proteins and their calculated ratios see Supplementary Table 4, available on the *Arthritis & Rheumatology* website at <http://onlinelibrary.wiley.com/doi/10.1002/art.42082>. **B**, Proteins found to be enriched in serum samples from SLE patients (ratio >2) are represented in a high-confidence protein-protein interaction network. **C**, Subcellular locations, processes, and functions of the proteins targeted by antimitochondrial antibodies in SLE were determined by gene ontology (GO) analysis. Mitochondrial metabolism processes were found to have the highest significance. MFN-1 = mitofusin 1; C1qBP = complement component C1q binding protein; acetyl-CoA = acetyl-coenzyme A.

patient groups were compared using the Wilcoxon-Mann-Whitney test, and multiple comparisons to healthy donors were performed using the Kruskal-Wallis test. Spearman's correlation coefficients were calculated to evaluate associations between

AMAs and antibodies assessed by routine clinical serologic testing. Youden index was determined to set a cutoff value for anti-C1qBP and anti-MFN-1 positivity. Separate logistic regression analyses were performed for C1qBP and MFN-1 to determine

their predictive values for SLE diagnosis (Supplementary Materials and Methods, available at <http://onlinelibrary.wiley.com/doi/10.1002/art.42082>). Statistical analyses were performed with GraphPad Prism version 9 software and SAS version 9.4 software (SAS Institute). Figures were assembled with Photoshop CC 2019 version 20.0.4. Additional information is available in the Supplementary Materials and Methods, available at <http://onlinelibrary.wiley.com/doi/10.1002/art.42082>.

Data availability. All data sets are available from the corresponding author upon reasonable request.

RESULTS

In the present study, we adopted 2 complementary approaches to identify proteins targeted by AMAs in the setting of SLE: 1) we used mitochondrial lysates to examine the complete spectrum of mitochondrial proteins targeted by AMAs and identified the proteins by immunoprecipitation, and 2) whole (i.e., intact)

mitochondria were used to capture AMA-recognizing components from the MOM. An irrelevant antibody that targets a protein absent in mitochondria was also used as a control. The latter strategy permitted identification of both nonspecific binding and potential endogenous proteins interacting with IgG (e.g., the complement pathway) (Figure 1).

A total of 1,345 proteins were identified by the combined approaches, 252 of which were withdrawn as usual contaminants (Supplementary Table 4, available at <http://onlinelibrary.wiley.com/doi/10.1002/art.42082>). When proteins were grouped by interactions, we observed an enrichment of 3 networks in SLE samples: the C1q complement component, the serpin superfamily, and members of the pyruvate dehydrogenase complex. Gene ontology analysis highlighted the mitochondrial metabolism as the function/processes with the highest significance (Figure 2C).

C1qBP, also known as p32, the receptor of the globular head of the C1q (gC1qR) or hyaluronic acid binding protein 1 (HABP1), is a protein for which RNA is encoded in the nucleus

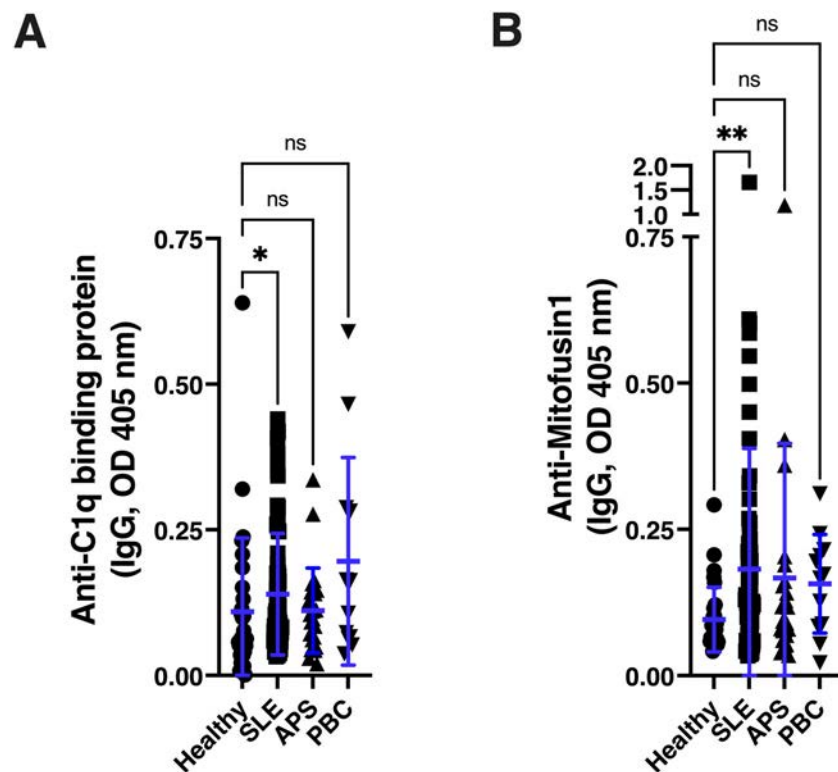


Figure 3. Increased immunoreactivity of the mitochondrial proteins complement component C1q binding protein (C1qBP) and mitofusin 1 (MFN-1) in systemic lupus erythematosus (SLE). Immunoreactivity against mitochondrial proteins was assessed by direct enzyme-linked immunosorbent assay. **A**, The receptor for C1qBP is a protein stored within the mitochondrion and subsequently dispatched to the cell surface and/or released into the extracellular space. SLE patients ($n = 87$) displayed increased levels of IgG targeting C1qBP, compared with healthy individuals ($n = 30$) ($P = 0.049$). **B**, MFN-1 is a protein expressed at the surface of the mitochondrion and is responsible for the fusion of mitochondrial outer membranes. Anti-MFN-IgG levels were significantly increased in patients with SLE, compared with healthy donors ($P = 0.0044$). Of note, levels of neither autoantibody were significantly increased in patients with antiphospholipid syndrome (APS) ($n = 27$) or primary biliary cirrhosis (PBC) ($n = 12$). Each symbol represents an individual subject. Bars show the mean \pm SD. * = $P \leq 0.05$; ** = $P < 0.01$, by Wilcoxon-Mann-Whitney test. NS = not significant.

by chromosome 17. It contains a mitochondrial targeting sequence that may be cleaved for translocating C1qBP to other compartments (e.g., to the surface of the plasma membrane, nucleus, and/or shed into the extracellular space) (18). Although C1qBP is not strictly a mitochondrial protein, its enrichment in samples from patients with SLE and its relevance to mitochondria and complement (Figure 2) stimulated further analyses. When assessed by direct ELISA, IgG against C1qBP was significantly elevated in patients with SLE ($P = 0.049$) (Figure 3A) in comparison with healthy individuals. In contrast, levels of anti-C1qBP were not significantly increased in serum samples from patients with APS or PBC (Figure 3A), 2 diseases in which AMAs have been reported (11,14).

While in the setting of PBC, antibodies target proteins from the inner mitochondrial membrane, the mitochondrial intermembrane space (IMS), or the mitochondrial matrix (MM) (11,19–21), previous studies have shown that in SLE, antibodies may also recognize components on the surface of the outer membrane (12,14,22). Thus, we assessed the localizations of the proteins to identify members of the mitochondrial proteome and found that 431 mitochondrial proteins could be assigned to the mitochondrion (168 of these proteins lacked references pertaining to their mitochondrial sublocalization). We found that 93 proteins were expressed within the MM, 6 were expressed in the mitochondrial IMS, 130 were expressed in the inner mitochondrial membrane, and 35 were expressed in the MOM. Of note, 13 proteins were

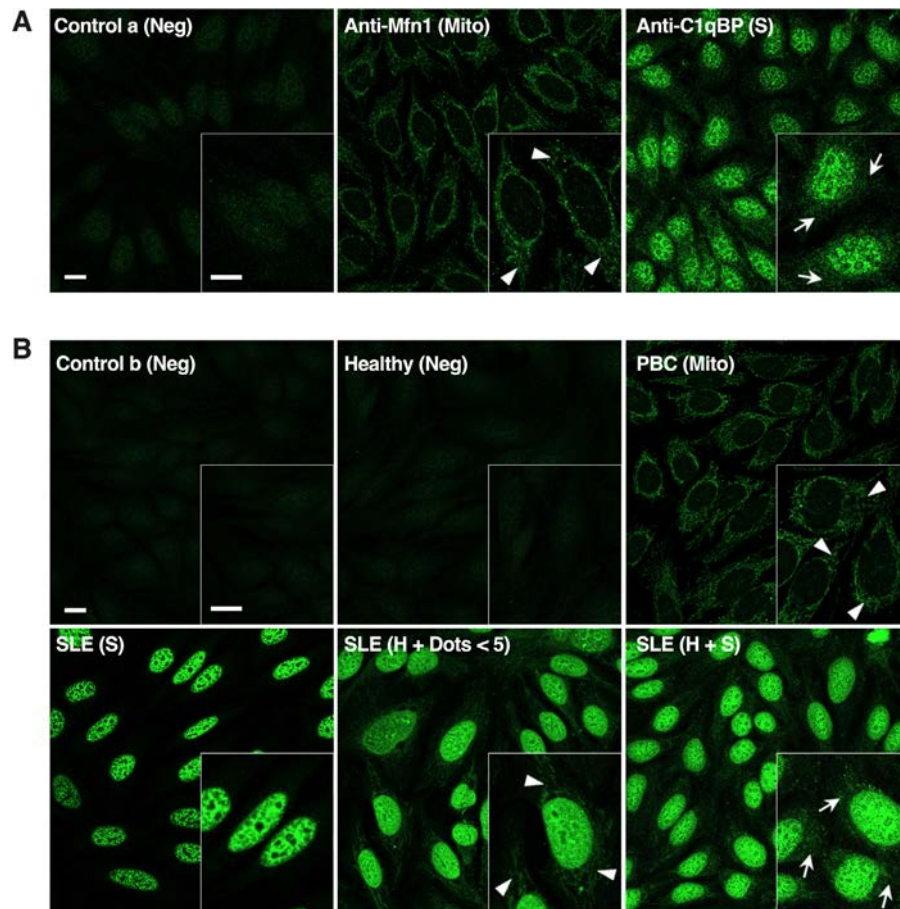


Figure 4. Indirect immunofluorescence (IIF) staining of HEp-2 cells represented by z-stack projections of 1 μm in total thickness. **A**, HEp-2 cells were stained with an isotype-matched irrelevant antibody (Control a [Neg]) or commercial antibodies (5 $\mu\text{g}/\text{ml}$ each) specific to either mitofusin 1 (anti-MFN-1) or complement component C1q binding protein (anti-C1qBP). While anti-MFN-1 displayed a reticular staining of the cytoplasm typical of antimitochondrial antibodies (Mito; **arrowheads** in anti-MFN-1 image), anti-C1qBP displayed speckled staining of the nucleus and the cytoplasm (S; **arrows** in anti-C1qBP image). **B**, Top panels show HEp-2 cells stained with fluorescein isothiocyanate-labeled anti-human IgG secondary antibody. Human serum-based negative control (Control b [Neg]) and diluted serum (1:80) from healthy donors (negative for anti-whole mitochondrial antibodies [AwMAs]) (Healthy [Neg]) displayed no signal. Serum from primary biliary cirrhosis (PBC) patients showed the typical mitochondrial-associated cytoplasmic reticular staining pattern displayed by antimitochondrial antibodies. Bottom panels show routine clinical staining of HEp-2 cells with AwMA-positive SLE serum, which allowed for the observation of various nuclear fluorescence patterns (i.e., speckled, homogeneous [H] + dots, homogeneous + speckled). No samples qualified as positive for antimitochondrial antibodies. However, confocal microscopy revealed that some samples may display cytoplasmic patterns resembling those seen in PBC. **Insets** show higher-magnification views of portions of the main images. Bars = 10 μm .

Table 1. Associations between anti-C1qBP or anti-MFN-1 antibody levels and absence versus presence of autoantibodies routinely assessed in SLE*

	Anti-C1qBP	Anti-MFN-1
Antiphospholipid		
Negative (n = 51)	0.09 (0.11)	0.12 (0.11)
Positive (n = 23)	0.12 (0.21)	0.18 (0.15)
<i>P</i>	0.097	0.011
Anticardiolipin (IgG)		
Negative (n = 60)	0.09 (0.11)	0.12 (0.10)
Positive (n = 14)	0.17 (0.27)	0.25 (0.24)
<i>P</i>	0.053	0.0004
Anti-β ₂ GPI (IgG)		
Negative (n = 64)	0.09 (0.11)	0.12 (0.13)
Positive (n = 10)	0.11 (0.24)	0.22 (0.25)
<i>P</i>	0.656	0.065
Lupus anticoagulant (IgG)		
Negative (n = 67)	0.09 (0.10)	0.12 (0.13)
Positive (n = 12)	0.13 (0.24)	0.18 (0.12)
<i>P</i>	0.049	0.068
Anti-dsDNA		
Negative (n = 62)	0.09 (0.10)	0.12 (0.08)
Positive (n = 20)	0.10 (0.18)	0.22 (0.23)
<i>P</i>	0.602	0.0005

* Positivity for antiphospholipid antibodies was defined as positivity for any, or a combination of, the various antiphospholipids assessed. Values are the median (interquartile range) optical density at 405 nm. Anti-C1qBP = anti-complement component C1q binding protein; anti-MFN-1 = anti-mitofusin 1; SLE = systemic lupus erythematosus; anti-β₂GPI = anti-β₂-glycoprotein I; anti-dsDNA = anti-double-stranded DNA.

associated with more than 1 mitochondrial compartment (Supplementary Table 4, available at <http://onlinelibrary.wiley.com/doi/10.1002/art.42082>).

We selected MFN-1, a protein from the MOM associated with the pyruvate dehydrogenase complex but distinct from the antigenic targets of AMA subtype M2, which presented an elevated score with our panning approach, for comparison among

patient groups. IgG antibodies against MFN-1 (i.e., anti-MFN1-IgG) were significantly increased in SLE patients compared to healthy individuals ($P = 0.0044$), but were not significantly increased in patients with PBC or APS (Figure 3B). For comparison, we tested the antigenicity of other mitochondrial proteins with lower prediction scores based on our panning approach. Thus, we tested enzymes from the MM involved either in the urea cycle (i.e., ornithine carbamoyltransferase, carbamoyl-phosphate synthase, and *N*-acetylglutamate synthase) or in the mitochondrial metabolism (i.e., aspartate aminotransferase and aldehyde dehydrogenase), and proteins from the inner mitochondrial membrane implicated in oxidative phosphorylation (i.e., β subunit of ATP synthase) or the electron transfer chain (i.e., α subunit of the electron transfer flavoprotein). The levels of autoantibodies against these other candidates were not significantly increased in SLE patients in comparison to healthy individuals (Supplementary Figure 1, available at <http://onlinelibrary.wiley.com/doi/10.1002/art.42082>).

Next, we determined if the autoantibodies to either of these 2 components, C1qBP and MFN-1, were associated with a definable cytoplasmic immunofluorescent staining pattern on routine HEp-2 substrates, as seen with antibodies to pyruvate dehydrogenase complex in PBC serum (11,23). IIF labelling of HEp-2 cells with a commercial antibody against C1qBP produced intense speckled staining of the nuclear region and a lower signal in the cytosol. Conversely, commercial anti-MFN-1 displayed reticular staining of the cytoplasm, typical of AMAs (Figure 4A). AwMA-positive SLE patient serum displayed a wide variety of patterns, but none qualified as positive for mitochondrial staining. In contrast, serum from PBC patients analyzed using the same approach revealed an obvious cytosolic pattern, with no nuclear staining when observed using a regular fluorescence microscope. However, when the same slides were

Table 2. Correlations between anti-C1qBP or anti-MFN-1 antibody levels and serum levels of clinically relevant antibodies and AMAs in SLE patients*

	Anti-C1qBP		Anti-MFN-1	
	<i>r_s</i>	<i>P</i>	<i>r_s</i>	<i>P</i>
Clinically relevant serum antibodies				
Anticardiolipin (n = 80)	0.25	0.02	0.45	<0.0001
Anti-IgG β ₂ GPI (n = 80)	0.12	0.28	0.26	0.02
Anti-IgG dsDNA (n = 22)	0.11	0.63	0.44	0.04
AMAs				
Anti-whole mitochondria				
IgG	0.32	0.003	0.65	<0.0001
IgM	0.08	0.46	0.31	0.003
Antimitochondrial DNA				
IgG	0.23	0.03	0.52	<0.0001
IgM	0.07	0.50	0.24	0.03
Antimitochondrial RNA				
IgG	0.03	0.75	0.27	0.01
IgM	0.03	0.82	0.27	0.01

* Correlations were determined using Spearman's correlation coefficients. AMAs = antimitochondrial antibodies (see Table 1 for other definitions).

examined using a confocal microscope, the autoantibodies from 7 out of the 9 SLE patients tested displayed various intensities of cytoplasmic staining, reminiscent of those observed in samples from patients with PBC or observed using commercial antibodies against C1qBP and MFN-1 (Figure 4 and Supplementary Table 5, available at <http://onlinelibrary.wiley.com/doi/10.1002/art.42082>).

Although we acknowledge that the number of patients examined was insufficient to draw definite conclusions on the clinical implications of these findings, exploratory biostatistical analyses were performed to determine potential associations between anti-C1qBP or anti-MFN-1 and disease characteristics in SLE patients included in our cohort. While neither anti-C1qBP nor anti-MFN-1 displayed significant associations with the various clinical manifestations assessed using univariate and multivariate logistic regression (thrombosis, carotid plaque, Systemic Lupus International Collaborating Clinics/American College of Rheumatology Damage Index score ≥ 1 [24], Systemic Lupus Erythematosus Disease Activity Index 2000 score ≥ 4 [25], arthritis, nephropathy, or dermatologic disorder) and linear regression (carotid intima-media thickness and Cutaneous Lupus Erythematosus Disease Area and Severity Index score [26]) (data not shown), we assessed the ability of these 2 AMAs to efficiently discriminate between samples from SLE patients and healthy controls using the Youden index. Calculated cutoff values were 0.064 for anti-C1qBP and 0.116 for anti-MFN-1. Antibodies to MFN-1 displayed suboptimal sensitivity, but good specificity, while anti-C1qBP had high sensitivity, but lower specificity (Supplementary Table 6, available at <http://onlinelibrary.wiley.com/doi/10.1002/art.42082>). However, both autoantibodies showed high positive predictive values. Anti-MFN-1 antibodies were also shown to be promising in the prediction of SLE diagnosis (adjusted odds ratio 2.99 [95% confidence interval 1.39–6.43], $P = 0.0044$).

Moreover, SLE patients who were positive for lupus anticoagulant (LA) displayed increased IgG anti-C1qBP levels (Table 1). IgG anti-MFN-1 levels were increased in patients who were positive for antiphospholipids (i.e., any, or a combination of, the various antiphospholipids assessed), as well as anti-double-stranded DNA autoantibodies (anti-dsDNA). When considering individual phospholipids, anti-MFN-1 were increased in patients positive for anticardiolipin (aCL) and neared significance in patients with anti- β_2 -glycoprotein I (anti- β_2 GPI). These results were further confirmed by the correlations between OD_{405 nm} measured for anti-MFN-1 and levels of aCL, anti- β_2 GPI, and anti-dsDNA measured as continuous variables (Table 2). When compared with levels of other AMAs, levels of anti-C1qBP were associated with both AwMA-IgG and anti-mtDNA-IgG. Anti-MFN-1 correlated with every AMA assessed in our cohort (Table 2). Of note, levels of anti-C1qBP also correlated with those of anti-MFN-1 (Spearman's rank correlation [r_s] = 0.49, $P < 0.0001$).

DISCUSSION

Patients with SLE display antibodies of various subclasses (e.g., IgG, IgM, IgA) against a wide array of self antigens (27). The epitopes targeted by these autoantibodies comprise, but are not limited to, phospholipids (e.g., aPL, aCL, LAC) (28,29), anti- β_2 GPI (30), nucleic acids (e.g., anti-dsDNA, anti-mtDNA, anti-mtRNA) (12,13), transcription factors, and ribonucleoproteins (i.e., antinuclear antibodies [ANAs]) (31). Furthermore, distinct autoantibodies targeting various types of mitochondrial biomolecules such as phospholipids (aCL targeting cardiolipin) (32), nucleic acids (mtDNA, mtRNA) (12–14), and antigens whose precise nature remains to be characterized (AMA subtype M5), have been reported in SLE (11,33).

While various proteins involved in the mitochondrial processing of pyruvate (e.g., periosteum-derived cell E2), sulfite oxidase, and glycogen phosphorylase are mitochondrial proteins known to be targeted by AMAs (subtypes M2, M4, and M9, respectively) in PBC (11), limited knowledge is available concerning the extent of the mitochondrial proteome targeted by AMAs in SLE. Antibodies to cardiolipin, a phospholipid uniquely synthesized in the mitochondria of humans, are known to be associated with vascular and obstetric events in SLE and APS (16,34,35). To date, the only mitochondrial protein with autoantibodies associated with disease manifestations in SLE is HSP60 (17). In the present study, we used several approaches to enrich mitochondrial antigens. We identified 1,093 different proteins, 431 (39.43%) of which were associated with the mitochondrial proteome (36). These mitochondrial proteins, targeted by circulating AMAs, reveal the extent of mitochondrial antigenicity in SLE. Of note, among all the previously known mitochondrial proteins targeted by AMAs, all of the currently known protein antigens targeted by AMAs (with the exception of glycogen phosphorylase) were detected by our mass spectrometry analyses.

Samples were treated with Benzonase nuclease in order to prevent the co-isolation of nucleic acid-interacting proteins, such as mtRNA, with bound ribonucleoproteins (mtRNP). Despite these precautions, our methods indicated the presence of non-mitochondrial proteins (e.g., complement proteins, ficolin-3, serpins). While we restricted the focus of our study to the proteins assigned to the mitochondrial proteome, such entities should be considered with caution, as they can be co-isolated in association with other biomolecules (e.g., interactors, ligands) in addition to their own potential antigenicities. Anti-RNP autoantibodies such as anti-small nuclear RNPs (snRNPs), anti-Ro/SSA, and anti-La/SSB are detected in mixed connective tissue disease as well as in SLE, Sjögren's syndrome, scleroderma, and myositis (37).

Of note, ANAs of the anti-Th/To family were reported to cross-react with mitochondrial RNA processing complex antibodies in systemic sclerosis (38). These elements suggest that, while we subtracted mtRNP given their recognition as common contaminants in proteomic analyses, further studies are needed

to appreciate their immunogenicity and the overlap between AMAs and ANAs in various systemic autoimmune rheumatic diseases. Such studies could allow improvements to patient classification in cases of difficult diagnoses or overlapping syndromes. While we tested a few different mitochondrial proteins, systematic characterization of immunoreactivities to large subsets of mitochondrial antigens would be enhanced by the use of high-throughput screening methods such as nucleic acid programmable protein arrays (39).

Two proteins with significant immunogenicities stood out among the various candidates assessed due to their increased levels in samples from patients with SLE compared to those from healthy individuals. The first protein that stood out was C1qBP, which is stored within the mitochondrion and dispatched to the MOM and/or the cell membrane, or secreted into the circulation (40,41), where it may be targeted by circulating AMAs. The second protein was MFN-1, a protein embedded in the MOM that could be recognized by AMA upon the release of whole mitochondria into the extracellular space (42). Of note, levels of autoantibodies to C1qBP or MFN-1 were not increased in PBC, another autoimmune condition characterized by the production of various AMAs (11). These autoantibodies were also not shown to be increased in APS, a disease that may be associated with the presence of pathogenic antibodies against cardiolipin in the setting of SLE (16). Complement molecules in circulation (and thus in the sera tested) may target mitochondria directly (43).

Moreover, previous studies indicate that C1qBP expressed at the surface of CD8+ T cells may bind C1q, and that translocation of the C1q–C1qBP complex to the nucleus induces a metabolic switch, leading to a reduction of inflammation and tissue damage (44–47). Therefore, we speculate that C1qBP may constitute a circulating autoantigen that enables the formation of protein complexes with C1q that may be targeted by autoantibodies in SLE, potentially contributing to the dysregulation of the biologic pathways regulated by the classical complement pathway (46–48). Autoantibodies, in association with C1q–C1qBP complexes, may also form proinflammatory protein–protein scaffolds (i.e., immune complexes, signaling through Fcγ receptors) (43), and their deposition in tissues may promote tissue damage such as lupus nephritis. However, our preliminary observations did not show associations between anti-C1qBP and kidney damage.

The strong correlation between anti-MFN-1 and AwMA suggests that MFN-1 may represent one of the main mitochondrial antigens of the MOM. Moreover, our previous work on AMAs in the setting of SLE and the correlation of AMAs with circulating mtDNA or aCL (Tables 1 and 2) implicate the mitochondrion as the source of various immunogenic biomolecules (6,12–14). When considering the preliminary performances of the 2 identified AMAs, both displayed high positive predictive values for the likelihood of an SLE diagnosis in samples from this cohort. Anti-C1qBP displayed suboptimal specificity, but high sensitivity, whereas anti-MFN-1 presented high specificity and suboptimal

sensitivity (Supplementary table 6, available at <http://onlinelibrary.wiley.com/doi/10.1002/art.42082>).

Routine detection of AMAs generally involves IIF and confirmation by ELISA (49). Of note, in several studies line immunoassays or bead-based assays were used to detect multiple autoantibodies, including various subsets of AMAs (49). We observed that commercial antibodies against MFN-1 produced classic mitochondrial staining, whereas anti-C1qBP showed staining of both nuclear and cytoplasmic regions of HEp-2 cells. These observations are concordant with the fact that MFN-1 is known to be uniquely expressed at the surface of the mitochondrion, while C1qBP may also be found in other organelles such as the nucleus or the Golgi apparatus (50).

Examination of AwMA-positive SLE serum using fluorescence microscopy, as routinely performed in clinical laboratories, indicated that none of the 9 samples assessed displayed cytoplasmic staining. However, upon further scrutiny using a confocal microscope, a proportion of these samples displayed significant cytoplasmic fluorescence resembling that observed in PBC, along with nuclear staining. Thus, the use of confocal microscopy, rather than widefield fluorescence imaging, may be better for discriminating between different subcellular stainings in conditions in which the nucleus shows dominant staining. Every patient included in our cohort was positive for ANAs, therefore we could not assess IIF patterns in AwMA-positive/ANA-negative patients. SLE is characterized by a wide repertoire of autoantibodies, and confocal microscopy may be of use in visualizing IIF patterns across cellular sublocalizations (27,28,51). The lack of specific IIF patterns in our preliminary study suggests that direct ELISA may be more informative in the detection of AMAs, as this technique would provide quantitative information on the levels of autoantibodies specific to this target.

Our study has limitations. Due to the nature of the patient recruitment, blood samples used in this study were collected at the time of inclusion in the cohort, not at first diagnosis. Thus, the levels of autoantibodies that were measured do not necessarily reflect the antibodies present at the time of diagnosis. Moreover, blood samples were not obtained at the time of occurrence of clinical events. AMA levels were thus assessed for associations with any past and/or active clinical events.

Furthermore, the sample size, ethnic distribution of the patients, and relatively low clinical activity scores at the time of phlebotomy may have influenced the various data assessed. The preliminary findings presented herein should therefore be confirmed in large inception cohorts with broader autoantibody repertoires. Such studies would allow for the recognition of fluctuations in AMA levels around the time of manifestations of active disease and for assessment of the performance of AMAs as biomarkers in SLE. Considering the dynamic range of antibody levels measured in patients with PBC and APS, replication of the results of the present study in larger cohorts of patients and evaluation of other rheumatic conditions (e.g., myositis, scleroderma) would

also provide information about the distribution of AMAs in other autoimmune diseases.

In conclusion, the autoantibody repertoire in SLE targets multiple representatives of the mitochondrial proteome, notably C1qBP and MFN-1. Further studies may reveal whether the detection of AMAs in the setting of SLE or other autoimmune conditions may improve diagnosis, prognosis, and/or patient stratification.

ACKNOWLEDGMENT

We gratefully acknowledge the contributions of Jonathan Côté (CHU de Québec-Université Laval) to the indirect immunofluorescence assays.

AUTHOR CONTRIBUTIONS

All authors were involved in drafting the article or revising it critically for important intellectual content, and all authors approved the final version to be published. Drs. Fortin and Boilard had full access to all of the data in the study and take responsibility for the integrity of the data and the accuracy of the data analysis.

Study conception and design. Becker, Gagné, Poirier, Fortin, Boilard.

Acquisition of data. Becker, Gagné, Lévesque, Allaey, Gougard, Rubio, Boisvert, Jean, Wagner, Poirier, Fortin, Boilard.

Analysis and interpretation of data. Becker, Gagné, Julien, Allaey, Wagner, Fortin, Boilard.

REFERENCES

- Andersson SG, Zomorodipour A, Andersson JO, Sicheritz-Ponten T, Alsmark UC, Podowski RM, et al. The genome sequence of *Rickettsia prowazekii* and the origin of mitochondria. *Nature* 1998;396:133–40.
- McDonald B, Pittman K, Menezes GB, Hirota SA, Slaba I, Waterhouse CC, et al. Intravascular danger signals guide neutrophils to sites of sterile inflammation. *Science* 2010;330:362–6.
- Oka T, Hikoso S, Yamaguchi O. Mitochondrial DNA that escapes from autophagy causes inflammation and heart failure. *Nature* 2012;485:251–5.
- Lood C, Blanco LP, Purmalek MM, Carmona-Rivera C, De Ravin SS, Smith CK, et al. Neutrophil extracellular traps enriched in oxidized mitochondrial DNA are interferogenic and contribute to lupus-like disease. *Nat Med* 2016;22:146–53.
- Boudreau LH, Duchez AC, Cloutier N, Soulet D, Martin N, Bollinger J, et al. Platelets release mitochondria serving as substrate for bactericidal group IIA-secreted phospholipase A2 to promote inflammation. *Blood* 2014;124:2173–83.
- Melki I, Allaey I, Tessandier N, Lévesque T, Cloutier N, Laroche A, et al. Platelets release mitochondrial antigens in systemic lupus erythematosus. *Sci Transl Med* 2021;13.
- Yousefi S, Gold JA, Andina N, Lee JJ, Kelly AM, Kozlowski E. Cata-pult-like release of mitochondrial DNA by eosinophils contributes to antibacterial defense. *Nat Med* 2008;14:949–53.
- Krysko D V, Agostinis P, Krysko O, Garg AD, Bachert C, Lambrecht BN, et al. Emerging role of damage-associated molecular patterns derived from mitochondria in inflammation. *Trends Immunol* 2011;32:157–64.
- Calfee CS, Matthay MA. Clinical immunology: culprits with evolutionary ties. *Nature* 2010;464:41–2.
- Marcoux G, Magron A, Sut C, Laroche A, Laradi S, Hamzeh-Cognasse H. Platelet-derived extracellular vesicles convey mitochondrial DAMPs in platelet concentrates and their levels are associated with adverse reactions. *Transfusion* 2019;59:2403–14.
- Berg PA, Klein R. Mitochondrial antigens and autoantibodies: from anti-M1 to anti-M9. *Klin Wochenschr* 1986;64:897–909.
- Becker Y, Loignon RC, Julien AS, Marcoux G, Allaey I, Lévesque T, et al. Anti-mitochondrial autoantibodies in systemic lupus erythematosus and their association with disease manifestations. *Sci Rep* 2019;9:4530.
- Becker Y, Marcoux G, Allaey I, Julien AS, Loignon RC, Benk-Fortin H, et al. Autoantibodies in systemic lupus erythematosus target mitochondrial RNA. *Front Immunol* 2019;10:1026.
- Becker YL, Julien AS, Godbout A, Boilard É, Fortin PR. Pilot study of anti-mitochondrial antibodies in antiphospholipid syndrome. *Lupus* 2020;29:1623–9.
- De Leeuw K, Bungener L, Roozendaal C, Bootsma H, Stegeman CA. Auto-antibodies to double-stranded DNA as biomarker in systemic lupus erythematosus: comparison of different assays during quiescent and active disease. *Rheumatology* 2017;56:698–703.
- Miyakis S, Lockshin MD, Atsumi T, Branch DW, Brey RL, Cervera R, et al. International consensus statement on an update of the classification criteria for definite antiphospholipid syndrome (APS). *J Thromb Haemost* 2006;4:295–306.
- Dieudé M, Correa JA, Neville C, Pineau C, Levine JS, Subang R, et al. Association of autoantibodies to heat-shock protein 60 with arterial vascular events in patients with antiphospholipid antibodies. *Arthritis Rheum* 2011;63:2416–24.
- Ghebrehiwet B, Geisbrecht BV, Xu X, Savitt AG, Peerschke EI. The C1q Receptors: focus on gC1qR/p33 (C1qBP, p32, HABP-1) [review]. *Semin Immunol* 2019;45:101338.
- Berg PA, Klein R. Mitochondrial antigen/antibody systems in primary biliary cirrhosis: revisited. *Liver* 1995;15:281–92.
- Tomizawa M, Shinozaki F, Fugo K, Motoyoshi Y, Sugiyama T, Yamamoto S, et al. Anti-mitochondrial M2 antibody-positive autoimmune hepatitis. *Exp Ther Med* 2015;10:1419–22.
- Klein R, Berg PA. Anti-M4 antibodies in primary biliary cirrhosis react with sulphite oxidase, an enzyme of the mitochondrial intermembrane space. *Clin Exp Immunol* 1991;84:445–8.
- Labro MT, Andrieu MC, Weber M, Homberg JC. A new pattern of non-organ- and non-species-specific anti-organelle antibody detected by immunofluorescence: the mitochondrial antibody number 5. *Clin Exp Immunol* 1978;31:357–66.
- Meek F, Khoury EL, Doniach D, Baum H. Mitochondrial antibodies in chronic liver diseases and connective tissue disorders: further characterization of the autoantigens. *Clin Exp Immunol* 1980;41:43–54.
- Petri M, Orbai AM, Alarcon GS, Gordon C, Merrill JT, Fortin PR, et al. Derivation and validation of the Systemic Lupus International Collaborating Clinics classification criteria for systemic lupus erythematosus. *Arthritis Rheum* 2012;64:2677–86.
- Gladman DD, Ibanez D, Urowitz MB. Systemic Lupus Erythematosus Disease Activity Index 2000. *J Rheumatol* 2002;29:288–91.
- Albrecht J, Taylor L, Berlin JA, Dulay S, Ang G, Fakharzadeh S, et al. The CLASI (Cutaneous Lupus Erythematosus Disease Area and Severity Index): an outcome instrument for cutaneous lupus erythematosus. *J Invest Dermatol* 2005;125:889–94.
- Dema B, Charles N. Autoantibodies in SLE: specificities, isotypes and receptors. *Antibodies (Basel)* 2016;5:2.
- Yaniv G, Twig G, Shor DB, Furer A, Sherer Y, Mozes O, et al. A volcanic explosion of autoantibodies in systemic lupus erythematosus: a diversity of 180 different antibodies found in SLE patients. *Autoimmun Rev* 2015;14:75–9.
- Ünlü O, Zülfi S, Erkan D. The clinical significance of antiphospholipid antibodies in systemic lupus erythematosus. *Eur J Rheumatol* 2016;3:75–84.

30. Price BE, Rauch J, Shia MA, Walsh MT, Lieberthal W, Gilligan HM, et al. Anti-phospholipid autoantibodies bind to apoptotic, but not viable, thymocytes in a β 2-glycoprotein I-dependent manner. *J Immunol* 1996;157:2201–8.
31. Pisetsky DS, Lipsky PE. New insights into the role of antinuclear antibodies in systemic lupus erythematosus [review]. *Nat Rev Rheumatol* 2020;16:565–79.
32. Wahl DG, Guillemin F, de Maistre E, Perret C, Lecompte T, Thibaut G. Risk for venous thrombosis related to antiphospholipid antibodies in systemic lupus erythematosus—a meta-analysis. *Lupus* 1997;6:467–73.
33. La Rosa L, Covini G, Galperin C, Catelli L, Del Papa N, Reina G, et al. Anti-mitochondrial M5 type antibody represents one of the serological markers for anti-phospholipid syndrome distinct from anti-cardiolipin and anti-b2-glycoprotein I antibodies. *Clin Exp Immunol* 1998;112:144–51.
34. Aringer M, Costenbader K, Daikh D, Brinks R, Mosca M, Ramsey-Goldman R, et al. 2019 European League Against Rheumatism/American College of Rheumatology Classification criteria for systemic lupus erythematosus. *Arthritis Rheumatol* 2019;71:1400–12.
35. Vreede AP, Bockenstedt PL, Knight JS. Antiphospholipid syndrome: an update for clinicians and scientists. *Curr Opin Rheumatol* 2017;29:458–66.
36. Palmfeldt J, Bross P. Proteomics of human mitochondria. *Mitochondrion* 2017;33:2–14.
37. Alves MR, Isenberg DA. “Mixed connective tissue disease”: a condition in search of an identity [review]. *Clin Exp Med* 2020;20:159–66.
38. Mahler M, Fritzler MJ, Satoh M. Autoantibodies to the mitochondrial RNA processing (MRP) complex also known as Th/To autoantigen [review]. *Autoimmun Rev* 2015;14:254–7.
39. Sibani S, LaBaer J. Immunoprofiling using NAPPA protein microarrays. *Methods Mol Biol* 2011;723:149–61.
40. Ghebrehiwet B, Ji Y, Valentino A, Pednekar L, Ramadass M, Habieli D, et al. Soluble gC1qR is an autocrine signal that induces B1R expression on endothelial cells. *J Immunol* 2014;192:377.
41. Xu H, Frojmovic MM, Wong T, Rauch J. p32, a platelet autoantigen recognized by an SLE-derived autoantibody that inhibits platelet aggregation. *J Autoimmun* 1995;8:97–119.
42. Chen H, Detmer SA, Ewald AJ, Griffin EE, Fraser SE, Chan DC. Mitofusins Mfn1 and Mfn2 coordinately regulate mitochondrial fusion and are essential for embryonic development. *J Cell Biol* 2003;160:189–200.
43. Pednekar L, Pathan AA, Paudyal B, Tsolaki AG, Kaur A, Abozaid SM, et al. Analysis of the interaction between globular head modules of human C1q and its candidate receptor gC1qR. *Front Immunol* 2016;7:567.
44. Brinkmann CR, Jensen L, Dagnæs-Hansen F, Holm IE, Endo Y, Fujita T, et al. Mitochondria and the lectin pathway of complement. *J Biol Chem* 2013;288:8016–27.
45. Yagi M, Uchiumi T, Takazaki S, Okuno B, Nomura M, Yoshida SI, et al. P32/gC1qR is indispensable for fetal development and mitochondrial translation: importance of its RNA-binding ability. *Nucleic Acids Res* 2012;40:9717–37.
46. Ling GS, Crawford G, Buang N, Bartok I, Tian K, Thielens NM, et al. C1q restrains autoimmunity and viral infection by regulating CD8+ T cell metabolism. *Science* 2018;360:558–63.
47. Weyand CM, Goronzy JJ. A mitochondrial checkpoint in autoimmune disease. *Cell Metabol* 2018;28:185–6.
48. Trendelenburg M. Autoantibodies against complement component C1q in systemic lupus erythematosus [review]. *Clin Transl Immunology* 2021;10:e1279.
49. Han E, Jo SJ, Lee H, Choi AR, Lim J, Jung ES, et al. Clinical relevance of combined anti-mitochondrial M2 detection assays for primary biliary cirrhosis. *Clin Chim Acta* 2017;464:113–7.
50. Choi K, Koo BH, Yoon BJ, Jung M, Yun HY, Jeon BH, et al. Overexpressed p32 localized in the endoplasmic reticulum and mitochondria negatively regulates calcium-dependent endothelial nitric oxide synthase activity. *Mol Med Rep* 2020;22:2395–403.
51. Jonkman J, Brown CM. Any way you slice it—a comparison of confocal microscopy techniques. *J Biomol Tech* 2015;26:54–65.

BRIEF REPORT

Role of Glutaminase 2 in Promoting CD4+ T Cell Production of Interleukin-2 by Supporting Antioxidant Defense in Systemic Lupus Erythematosus

Ryo Hisada, Nobuya Yoshida, Seo Yeon K. Orite,  Masataka Umeda, Catalina Burbano, Marc Scherlinger, Michihito Kono,  Suzanne Krishfield, and George C. Tsokos 

Objective. Glutaminase (GLS) isoenzymes GLS1 and GLS2 catalyze the first step of glutaminolysis. GLS1 is requisite for Th17 cell differentiation, and its inhibition suppresses autoimmune disease in animals, but the function of GLS2 is not known. The aim of this study was to investigate the role of GLS2 in CD4+ T cell function and systemic lupus erythematosus (SLE) pathogenesis.

Methods. We measured reactive oxygen species (ROS) levels, lipid peroxidation, and mitochondrial mass and polarization by flow cytometry, interleukin-2 (IL-2) production by a dual luciferase assay, and CpG DNA methylation of *IL2* by a real-time polymerase chain reaction system. The impact of the overexpression of wild-type GLS1, wild-type GLS2, or mutated GLS2 at the PDZ domain-binding motif in CD4+ T cells was examined. Furthermore, GLS2 expression in CD4+ T cells from lupus-prone mice and patients with SLE was analyzed by Western blotting.

Results. GLS2, but not GLS1, reduced ROS levels and lipid peroxidation and restored mitochondrial function in T cells. GLS2 promoted IL-2 production through the demethylation of the *IL2* promoter. Mutation of the PDZ domain-binding motif abated the ability of GLS2 to regulate IL-2 and ROS levels. In lupus-prone mice and patients with SLE, the expression of GLS2 was decreased in CD4+ T cells. Finally, GLS2 overexpression corrected ROS levels and restored IL-2 production by CD4+ T cells from lupus-prone mice and SLE patients.

Conclusion. Our findings suggest that GLS2 has a crucial role in IL-2 production by CD4+ T cells by supporting antioxidant defense, and they offer a new approach to correcting IL-2 production by T cells in SLE.

INTRODUCTION

Glutaminase (GLS) isoenzymes GLS1 and GLS2 are the first enzymes in the glutaminolysis pathway. Although both GLS1 and GLS2 convert glutamine into glutamate, these enzymes affect cell biology in distinct ways. Previous studies of various cancer cell lines have shown that the up-regulation of GLS1 promotes tumorigenesis, while the expression of GLS2 is linked to quiescent or differentiated cell states (1). Recently, we and other investigators have observed that GLS1 is essential for Th17 cell differentiation and that pharmacologic inhibition or genetic deletion of GLS1

ameliorated disease progression in lupus-prone MRL/lpr mice (2). GLS2, though, has been shown to decrease reactive oxygen species (ROS) levels through the glutathione (GSH)-dependent antioxidant system in various cancer cell lines (1). This observation is of interest because ROS have been shown to affect T cell signaling and impact T cell fate in healthy subjects and patients with systemic lupus erythematosus (SLE) (3). However, the impact of GLS2 on T cell function in SLE has not been addressed.

SLE is an autoimmune disease in which the immune system attacks its own tissues, causing widespread inflammation and tissue damage that is linked to significant morbidity and mortality (4).

Dr. Hisada's work was supported by the Uehara Memorial Foundation. Dr. Yoshida's work was supported by the 2019 Gilead Sciences Research Scholars Program in Rheumatology. Dr. Scherlinger's work was supported by the Société Française de Rhumatologie, Arthur-Sachs & Monahan fellowships, and the Philippe Foundation. Dr. Tsokos' work was supported by the NIH (grant R37-AI-49954).

Dr. Hisada, Dr. Yoshida, and Ms. Orite contributed equally to this work.

Ryo Hisada, MD, PhD, Nobuya Yoshida, MD, PhD, Seo Yeon K. Orite, Masataka Umeda, MD, PhD, Catalina Burbano, PhD, Marc Scherlinger, MD, PhD, Michihito Kono, MD, PhD, Suzanne Krishfield, BA, George C. Tsokos, MD:

Beth Israel Deaconess Medical Center and Harvard Medical School, Boston, Massachusetts.

Author disclosures are available at <https://onlinelibrary.wiley.com/action/downloadSupplement?doi=10.1002%2Fart.42112&file=art42112-sup-0001-Disclosureform.pdf>.

Address correspondence to George C. Tsokos, MD, Beth Israel Deaconess Medical Center, Harvard Medical School, 330 Brookline Avenue, CLS-937, Boston, MA 02215. E-mail: gsokos@bidmc.harvard.edu.

Submitted for publication December 14, 2021; accepted in revised form March 3, 2022.

Recent studies have shown that insufficient production of interleukin-2 (IL-2) by effector CD4+ T cells contributes to the pathogenesis of SLE (4) and that treatment with low-dose IL-2 offers clinical benefit for a wide range of autoimmune diseases, including SLE (5). However, because IL-2 has a narrow therapeutic range and a short half-life, discovery of additional molecular pathways that would enable restoration of IL-2 production is desirable.

Here we report that GLS2, but not GLS1, reduces ROS levels and promotes the ability of CD4+ T cells to produce IL-2 by demethylating *Il2*. At the translational level, we demonstrate that GLS2 protein expression is decreased in CD4+ T cells from lupus-prone mice and patients with SLE and that overexpression of GLS2 reduces ROS levels and restores IL-2 production.

MATERIALS AND METHODS

Study participants. Patients who fulfilled the American College of Rheumatology criteria for the diagnosis of SLE (6) and age-, sex-, and ethnicity-matched healthy individuals were enrolled after they provided informed consent. The Beth Israel Deaconess Medical Center (BIDMC) Institutional Review Board approved the study protocol (2006-P-0298). Demographic and clinical data and sample collection methods are described in Supplementary Table 1 and the Supplementary Methods, respectively, available on the *Arthritis & Rheumatology* website at <http://onlinelibrary.wiley.com/doi/10.1002/art.42112>.

Mice. C57BL/6J mice, MRL/MpJ-Fas^{pr}/J (MRL/*lpr*) mice, and MRL/MpJ mice were purchased from The Jackson Laboratory. For in vitro experiments, C57BL/6J mice were euthanized at 6–8 weeks of age. MRL/*lpr* and MRL/MpJ mice were euthanized at 16 weeks of age. All mice were maintained in a specific pathogen-free animal facility (BIDMC). Experiments were approved by the Institutional Animal Care and Use Committee of BIDMC.

In vitro T cell stimulation. Mouse or human naive CD4+ T cells and mouse or human CD4+ T cells were purified using specific T cell isolation kits (the mouse/human naive CD4+ T Cell Isolation Kit II and the mouse/human CD4+ T Cell Isolation Kit, respectively; Miltenyi Biotec). Purified mouse naive CD4+ T cells and mouse CD4+ T cells in RPMI 1640 medium with 10% fetal bovine serum, penicillin/streptomycin, and 2-mercaptoethanol were stimulated at 37°C with plate-bound goat anti-hamster antibodies crosslinking anti-CD3 (0.25 µg/ml; BioLegend) and anti-CD28 (0.5 µg/ml; BioXcell). Purified human naive CD4+ T cells and human CD4+ T cells in RPMI 1640 medium with 10% fetal bovine serum plus penicillin/streptomycin were stimulated with plate-bound anti-CD3 antibodies (1 µg/ml; OKT-3; BioXCell) and anti-CD28 antibodies (1 µg/ml; CD28.2; BioLegend) at 37°C.

Enzyme-linked immunosorbent assay (ELISA). The Max Deluxe Set Mouse IL-2 ELISA platform (BioLegend) was used to detect IL-2 in culture supernatants. All procedures were performed according to the manufacturer's instructions. Each assay was performed in duplicate independently.

Western blotting. Cell lysates were separated on NuPAGE 4–12% Bis-Tris gel (ThermoFisher Scientific), and proteins were transferred to a nitrocellulose membrane. The following antibodies were used for protein detection on the ECL Western blot system (Cytiva): anti-GLS2 (Abcam), anti-β-actin (Sigma-Aldrich), horseradish peroxidase (HRP)-conjugated rabbit anti-goat IgG (R&D Systems), and HRP-conjugated goat anti-mouse IgG (Abcam). Bands on blots corresponding to proteins of interest were analyzed by ImageJ software (National Institutes of Health).

Flow cytometry. The following antibodies were used for flow cytometry: CD90.2 (clone 53-2.1; BioLegend) and CD4 (clone GK1.5; ThermoFisher Scientific) for murine lymphocytes and CD3 (clone SK7; BioLegend) and CD4 (clone SK3; ThermoFisher Scientific) for human lymphocytes. Staining was performed using the Zombie UV Fixable Viability Kit (BioLegend) to eliminate dead cells. After cell surface markers were stained, CellRox Green Reagent (ThermoFisher Scientific) was used to detect ROS, Liperfluo (Dojindo) was used to detect lipid peroxidation, and staining with MitoTracker Deep Red and MitoTracker Green (Life Technologies) was performed to determine mitochondrial mass and polarization, respectively. In all transfection experiments, DsRed+CD4+ T cells were analyzed. The mean fluorescence intensity of DsRed expression in each experiment is shown in Supplementary Figure 1, available on the *Arthritis & Rheumatology* website at <http://onlinelibrary.wiley.com/doi/10.1002/art.42112>. All procedures were performed according to manufacturers' instructions. Detailed methods for cell staining are described in the Supplementary Methods.

Transfection of GLS2- and GLS2-overexpression vectors. Mouse *Gls1* and *Gls2*, human *GLS1*, or human *GLS2* sequences were subcloned into the pIRES2-DsRed-Express vector by GenScript. All constructs were verified by DNA sequencing. The plasmids were transfected by means of the Amaxa mouse/human T cell Nucleofector kit, using the X-001 program on day 1 (for murine cells) and the T-023 program on day 2 (for human cells) of culture (Lonza).

Luciferase assay. Murine *Il2* and human *IL2* promoter luciferase reporter constructs (pGL3_*ml2*_vector and pGL3_*hIL2*_vector, respectively) were purchased from GenScript. The luciferase reporter plasmids were transfected as mentioned in the previous subsection. Each reporter experiment included

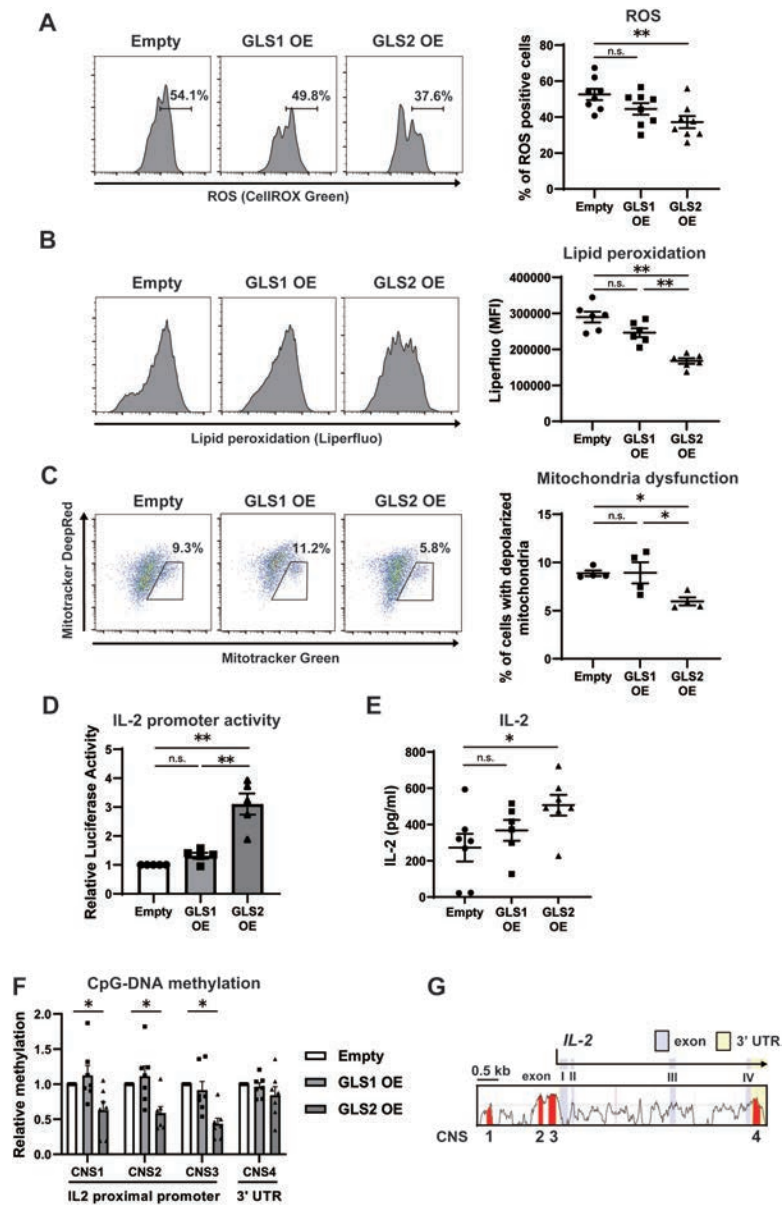


Figure 1. Epigenetic influence of glutaminase 2 (GLS2) on reactive oxygen species (ROS) levels and interleukin-2 (IL-2) production in murine CD4⁺ T cells. **A–F**, Naive CD4⁺ T cells from wild-type B6 mice were cultured with anti-CD3/anti-CD28 and transfected with empty vector (Empty), GLS1-overexpression plasmid (GLS1 OE), or GLS2-overexpression plasmid (GLS2 OE) on day 1. On day 3, CellRox Green Reagent was used to detect ROS ($n = 8$ samples per group) (**A**), Liperfluor was used to detect lipid peroxidation ($n = 6$ per group) (**B**), staining with Mitotracker Deep Red and Green was performed to assess mitochondrial polarization and mass, respectively ($n = 4$ per group) (**C**), a dual luciferase assay was used to assess IL-2 promoter activity ($n = 5$ per group) (**D**), an enzyme-linked immunosorbent assay was used to measure the IL-2 concentration in culture supernatants ($n = 7$ per group) (**E**), and an EZ DNA Methylation Kit was used to assess CpG DNA methylation ($n = 7$ per group) (**F**). In all transfection experiments, DsRed+CD4⁺ T cells were analyzed. Bars show the mean \pm SEM; symbols represent individual samples. * = $P < 0.05$; ** = $P < 0.01$, by one-way analysis of variance with Tukey's post hoc test for multiple comparisons. MFI = mean fluorescence intensity; NS = not significant. **G**, Alignment of the murine and human genes encoding IL-2 shows conserved noncoding sequences (CNS) (red) that were determined as regions of interest for further analysis of CpG DNA methylation. CNS1–CNS3 are located in the proximal promoter, which spans 2 kb, and CNS4 is located in the 3'-untranslated region (3'-UTR).

200 ng of *Renilla* luciferase construct as an internal control. Luciferase activity was quantified using a dual luciferase assay (Promega) on day 3 of culture, according to the manufacturer's instructions.

Methylated CpG (methyl-CpG) DNA immunoprecipitation. The methyl-CpG DNA immunoprecipitation assay (Zymo Research) was performed according to the manufacturer's instructions. The detailed methods for obtaining methylated DNA

are described in the Supplementary Methods, available on the *Arthritis & Rheumatology* website at <http://onlinelibrary.wiley.com/doi/10.1002/art.42112>. Methylated DNA was subjected to polymerase chain reaction (PCR) analysis on an ABI OneStepPlus real-time PCR system. Sequences of PCR primers are listed in Supplementary Table 2.

Site-directed mutagenesis. Site-directed mutagenesis for substituting the PDZ domain-binding motif in the mouse GLS2-overexpression vector with the corresponding sequence in the mouse *Gls1* gene was performed using the Q5 site-directed mutagenesis kit (New England Biolabs) with the following primers: 5'-TTGCTATAAGGATCCGCCCTCTCCCT-3' and 5'-CCCGTCGAGATTCTCTTTGGACAGGGTCTCAGC-3'.

Statistical analysis. Comparisons between 2 different groups were conducted using Student's unpaired 2-tailed *t*-tests or, if the groups were related, Student's paired *t*-tests. Comparisons between >2 groups were conducted using one-way analysis of variance with Tukey's post hoc test for multiple comparisons. Statistical analyses were performed with GraphPad Prism 7.0 software (GraphPad Software). *P* values less than 0.05 were considered statistically significant.

RESULTS

Epigenetic influence of GLS2 on ROS levels and IL-2 production in murine CD4+ T cells. GLS2 has been shown to decrease ROS levels in several cancer cell lines (1). To assess whether GLS2 reduces ROS levels in CD4+ T cells, naive CD4+ T cells from wild-type B6 mice were stimulated with anti-CD3 and anti-CD28 antibodies and transfected with either empty, GLS1-overexpression, or GLS2-overexpression plasmid vectors. As shown in Figure 1A, overexpression of GLS2, but not of GLS1, significantly reduced intracellular ROS levels. High levels of ROS cause lipid peroxidation (7) and eventually mitochondrial dysfunction (8). As expected, GLS2 overexpression decreased lipid peroxidation in CD4+ T cells (Figure 1B). A combination of MitoTracker Deep Red and MitoTracker Green staining revealed that GLS2 overexpression in CD4+ T cells was associated with a decreased percentage of CD4+ T cells with depolarized (i.e., dysfunctional) mitochondria (Figure 1C).

In a previous report, investigators showed that treatment with thiol *N*-acetylcysteine (NAC), a ROS scavenger and a precursor of GSH, reduced ROS levels and restored IL-2 production in T cells (9). Elsewhere, researchers found that thiol NAC suppressed SLE parameters when administered to patients with this disease (10). Overexpression of GLS2, but not of GLS1, significantly increased IL-2 promoter activity in CD4+ T cells and IL-2 concentrations in culture supernatants (Figures 1D and E). Because IL-2 expression is controlled by CpG DNA methylation of the *Il2* promoter (11), we assessed CpG DNA methylation in *Il2*. We focused

on 4 types of conserved noncoding sequence (CNS1–CNS4), which were identified (11) on the basis of the degree of sequence conservation and the presence of reported regulatory regions (Figure 1F). CNS1–CNS3 are located within the proximal promoter of *Il2*, whereas CNS4 localizes within the highly conserved 3'-untranslated regions. Overexpression of GLS2, but not of GLS1, resulted in significantly lower levels of CpG DNA methylation in CNS1, CNS2, and CNS3 but not in CNS4 (Figure 1G). Collectively, we have demonstrated that overexpression of GLS2, but not of GLS1, decreases ROS levels, lipid peroxidation, and mitochondrial dysfunction and results in increased IL-2 production by CD4+ T cells through demethylation of the *Il2* promoter.

PDZ domain-binding motif and GLS2-mediated modulation of ROS levels and IL-2 production. To understand how these differences between GLS1 and GLS2 occur, we focused on the structures of GLS1 and GLS2. The major amino acid sequences of GLS1 and GLS2 align closely, with most of the differences occurring in their C-termini and N-termini. In contrast to the C-terminus of GLS1, the C-terminus of GLS2 defines a PDZ domain-binding motif, which can bind to PDZ domain-containing proteins (12) (Figure 2A). Accordingly, we hypothesized that regulation of IL-2 and ROS by GLS2 depends on protein–protein interactions involving the PDZ domain. To investigate this, we generated a GLS2-overexpression vector in which the PDZ domain-binding motif was substituted with the corresponding sequence from GLS1 (Figure 2A). Intriguingly, mutation of the PDZ domain-binding motif abated the reduction in ROS levels (Figure 2B), lipid peroxidation (Figure 2C), and mitochondrial dysfunction (Figure 2D) and restored *Il2* promoter activity (Figure 2E). Together, our results indicate that the PDZ domain-binding motif at the C-terminus mediates the effect of GLS2 on cellular ROS levels, mitochondrial functions, and, ultimately, IL-2 production.

Effect of GLS2 on ROS levels and IL-2 production in CD4+ T cells from lupus-prone mice and patients with SLE. Insufficient IL-2 production and higher cytoplasmic ROS levels in CD4+ T cells are key factors in the development of SLE (3,4). As shown in Figures 3A and B, GLS2 protein expression was decreased in CD4+ T cells isolated from MRL/*lpr* mice and patients with SLE, compared with expression in those from control MRL/MpJ mice and healthy individuals, respectively. Furthermore, there was no statistically significant difference in the expression of GLS2 in murine and human CD4+ T cells with or without CD3 and CD28 antibody stimulation (Supplementary Figure 2, available on the *Arthritis & Rheumatology* website at <http://onlinelibrary.wiley.com/doi/10.1002/art.42112>), suggesting that the decreased expression of GLS2 in lupus T cells is not due to an increased frequency of activated T cells. Next, we transfected the GLS1- and GLS2-overexpression vectors into CD4+

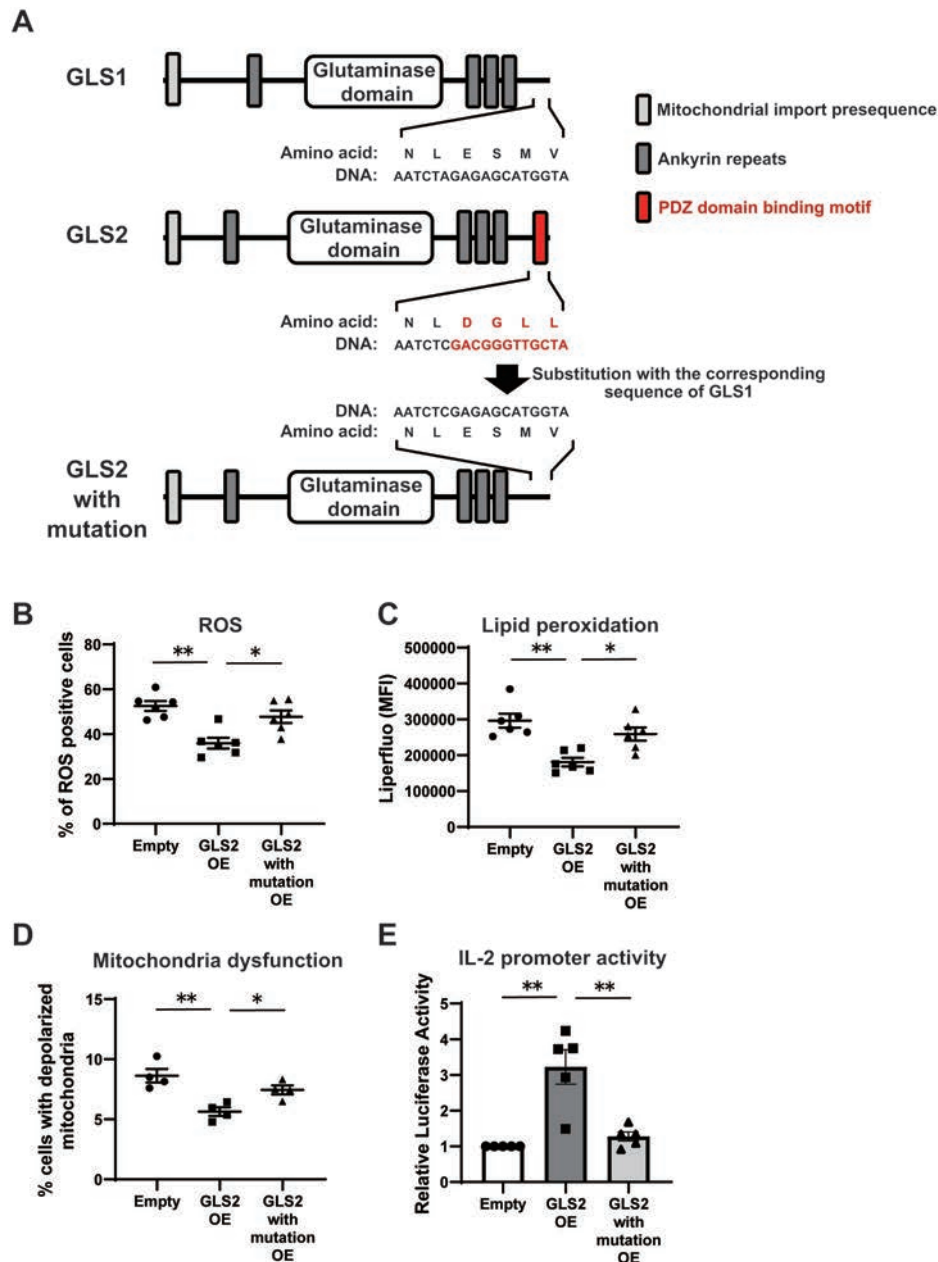


Figure 2. Role of the PDZ domain-binding motif in GLS2-mediated regulation of IL-2 and ROS levels in mice. **A**, Structures of GLS1 (isoform KGA), GLS2 (isoform GAB), and mutated GLS2, in which the PDZ domain-binding motif at the C-terminus (red) was substituted with that of GLS1, are shown. **B–E**, Naive CD4⁺ T cells from wild-type B6 mice were cultured with anti-CD3/anti-CD28 and transfected with empty vector, GLS2 OE, or mutated GLS2-overexpression plasmid (GLS2 with mutation OE) on day 1. On day 3, assessment of ROS (n = 6 samples per group) (**B**), lipid peroxidation (n = 6 per group) (**C**), mitochondrial polarization (n = 4 per group) (**D**), and *Il2* promoter activity (n = 5 per group) (**E**) was performed. In all transfection experiments, DsRed⁺ CD4⁺ T cells were analyzed. Bars show the mean \pm SEM; symbols represent individual samples. * = $P < 0.05$; ** = $P < 0.01$, by one-way analysis of variance with Tukey's post hoc test for multiple comparisons. See Figure 1 for other definitions.

T cells from MRL/*lpr* mice and patients with SLE. As expected, overexpression of GLS2, but not of GLS1, reduced ROS levels and restored IL-2 promoter activity in CD4⁺ T cells from MRL/*lpr* mice (Figures 3C and D) and patients with SLE (Figures 3E and F). These findings demonstrate that GLS2 corrects aberrant ROS levels and restores normal IL-2 production in SLE CD4⁺ T cells.

DISCUSSION

In the current study, we demonstrated that GLS2 decreases ROS levels and restores IL-2 production through demethylation of the *Il2* promoter and that the mechanism of this activity occurs at the PDZ domain-binding motif at the C-terminus of GLS2. We also observed that GLS2 corrects abnormal ROS levels and IL-2

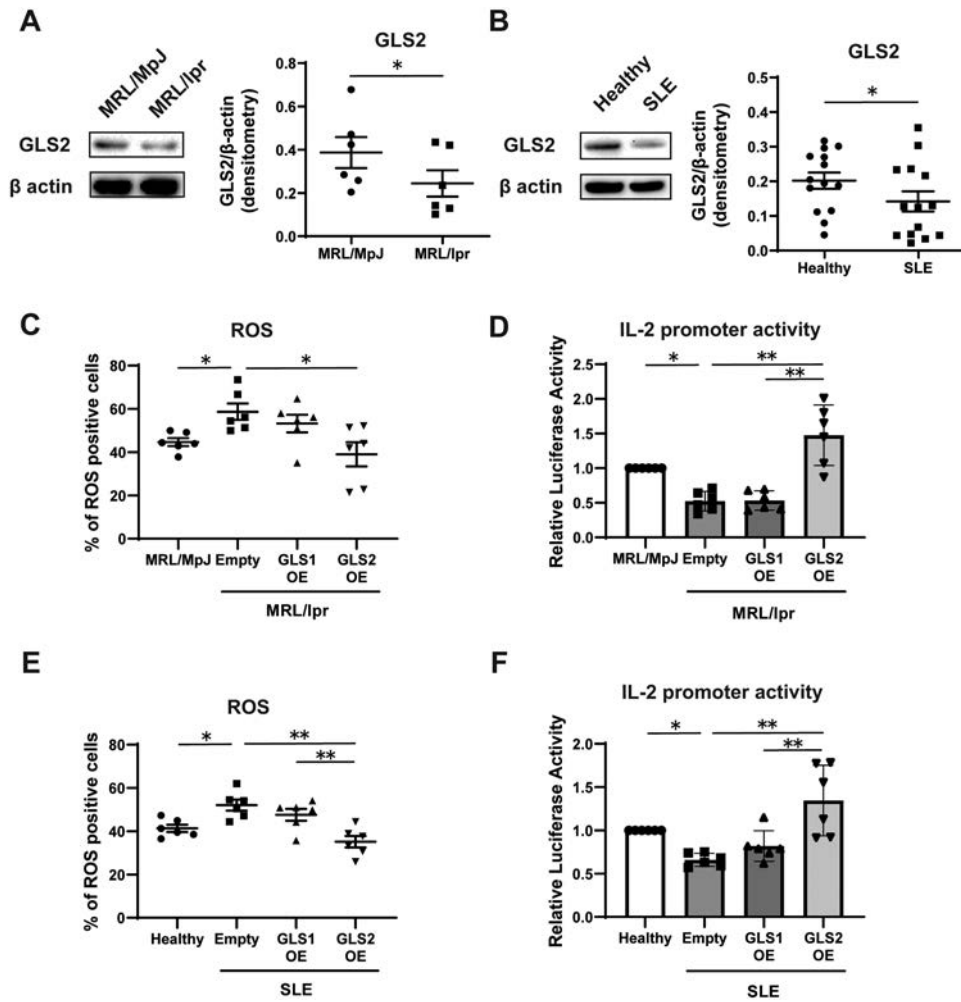


Figure 3. Effect of GLS2 on IL-2 production and ROS levels in CD4+ T cells from lupus-prone mice and patients with systemic lupus erythematosus (SLE). **A** and **B**, GLS2 and actin expression in purified CD4+ T cells from 16-week-old MRL/MpJ-Fas^{lpr}/J (MRL/lpr) and MRL.MpJ (control) mice (n = 6 samples per group) (**A**) and healthy control participants and patients with SLE (n = 14 per group) (**B**) were analyzed by Western blotting. **C–F**, Naive CD4+ T cells from 16-week-old MRL/lpr mice, MRL.MpJ mice, healthy control participants, and patients with SLE were cultured with anti-CD3/anti-CD28. Cells from MRL.MpJ mice and healthy controls were transfected with empty vector, and cells from MRL/lpr mice (**C** and **D**) and patients with SLE (**E** and **F**) were transfected with empty vector, GLS1 OE, or GLS2 OE. On day 3, assessment of ROS (n = 6 per group) and *IL2* and *IL2* promoter activity (n = 6 per group) was performed. In all transfection experiments, DsRed+CD4+ T cells were analyzed. Bars show the mean \pm SEM; symbols represent individual samples. * = $P < 0.05$; ** = $P < 0.01$, by Student’s paired *t*-test and one-way analysis of variance with Tukey’s post hoc test for multiple comparisons. See Figure 1 for other definitions.

production in CD4+ T cells from both lupus-prone MRL/lpr mice and patients with SLE.

Impaired IL-2 production and related signaling is considered a central defect in SLE because it is linked to a series of cellular abnormalities, and its restoration is expected to provide clinical benefit (3). Epigenetic events, including DNA methylation, contribute to the lineage commitment and function of helper T cells. Indeed, DNA demethylation in the *IL2* promoter is a requisite for *IL2* transcription initiation (13). Furthermore, we previously reported that CpG DNA methylation of the *IL2* promoter is significantly increased in T cells from patients with active SLE (11).

High levels of cellular ROS have been linked to the development of a variety of diseases, including cancer and SLE (3). While

moderate levels of ROS are necessary to promote T cell signaling, high levels of ROS can be detrimental to T cell survival. In fact, disruption in the GSH pathway, which causes excessive ROS levels, has been shown to reduce IL-2 production by T cells (14). In addition, cellular ROS themselves can induce specific hypermethylation by up-regulating DNA methyltransferases (DNMTs) (15). In previous studies, researchers observed that antioxidant treatment with thiol NAC reversed DNMT3a expression and DNA hypermethylation in cardiac tissues (16) and that forced expression of DNMT3a resulted in a significant increase in CpG DNA methylation of the *IL2* promoter in primary human T cells (11). Because we showed that GLS2 is associated with a greater reduction in ROS levels, it is reasonable to hypothesize that

GLS2 influences methylation of the *IL2* promoter by regulating antioxidant capacity and the expression of DNMTs. Although further analysis is needed to confirm that ROS directly regulate DNA methylation in the *IL2* promoter, we propose that GLS2 induces IL-2 production epigenetically by supporting antioxidant defense.

GLS1 and GLS2 exhibit a high degree of similarity in their amino acid sequences, particularly in the GLS enzymatic domain. However, studies of cancer cell lines have shown that GLS1 promotes tumor growth, while GLS2 suppresses tumor progression. Yet, it is unclear why GLS1 and GLS2 have contrasting roles. The main difference between GLS1 and GLS2 is the PDZ domain-binding motif at the C-terminus expressed by GLS2. We have found that the functional difference between the 2 isoforms is due to the presence of the PDZ domain-binding motif in the GLS2 isoenzyme, because its absence deprives GLS2 of its ability to suppress ROS levels and increase IL-2 production. Along this line, GLS2, but not GLS1, binds to small GTPase Rac1 and inhibits Rac1 activity, which in turn inhibits migration and metastasis of cancer cells through its C-terminus motif (17). Although both GLS isoenzymes generate glutamate, which is one of the precursors of the antioxidant GSH, we found that GLS2 is more effective than GLS1 in reducing ROS levels. This difference is linked to the presence of the PDZ domain-binding motif in the C-terminus of GLS2, which binds to still-unknown proteins that may affect ROS levels and GSH production. Furthermore, since PDZ domains often help tether receptors to cell membranes, GLS2 may alter cellular functions by interaction with tethering-related proteins.

In summary, we have presented a novel role for GLS2 in CD4+ T cell function. We showed that GLS2, through its PDZ domain-binding motif, reduces ROS levels, lipid peroxidation, and mitochondrial dysfunction and promotes IL-2 production through the demethylation of the *IL2* promoter in CD4+ T cells. At a translational level, we demonstrated that GLS2 protein expression is down-regulated in CD4+ T cells from both lupus-prone MRL/lpr mice and patients with SLE and that GLS2 overexpression reduces ROS levels and restores IL-2 production. We propose that the GLS2-initiated pathway represents a new therapeutic target in the treatment of SLE. It is important to confirm these results through further studies in vivo.

AUTHOR CONTRIBUTIONS

All authors were involved in drafting the article or revising it critically for important intellectual content, and all authors approved the final version to be published. Dr. Tsokos had full access to all of the data in the study and takes responsibility for the integrity of the data and the accuracy of the data analysis.

Study conception and design. Hisada, Yoshida, Orite, Tsokos.



Acquisition of data. Hisada, Yoshida, Orite, Umeda, Burbano, Kono, Krishfield.

Analysis and interpretation of data. Scherlinger.

REFERENCES

1. Wang Z, Liu F, Fan N, Zhou C, Li D, Macvicar T, et al. Targeting glutaminolysis: new perspectives to understand cancer development and novel strategies for potential target therapies [review]. *Front Oncol* 2020;10:589508.
2. Kono M, Yoshida N, Maeda K, Suárez-Fueyo A, Kyttaris VC, Tsokos GC. Glutaminase 1 inhibition reduces glycolysis and ameliorates lupus-like disease in MRL/lpr mice and experimental autoimmune encephalomyelitis. *Arthritis Rheumatol* 2019;71:1869–78.
3. Perl A. Oxidative stress in the pathology and treatment of systemic lupus erythematosus [review]. *Nat Rev Rheumatol* 2013;9:674–86.
4. Tsokos GC. Autoimmunity and organ damage in systemic lupus erythematosus. *Nat Immunol* 2020;21:605–14.
5. Sharabi A, Tsokos MG, Ding Y, Malek TR, Klatzmann D, Tsokos GC. Regulatory T cells in the treatment of disease. *Nat Rev Drug Discov* 2018;17:823–44.
6. Tan EM, Cohen AS, Fries JF, Masi AT, McShane DJ, Rothfield NF, et al. The 1982 revised criteria for the classification of systemic lupus erythematosus. *Arthritis Rheum* 1982;25:1271–7.
7. Su LJ, Zhang JH, Gomez H, Murugan R, Hong X, Xu D, et al. Reactive oxygen species-induced lipid peroxidation in apoptosis, autophagy, and ferroptosis. *Oxid Med Cell Longev* 2019;2019:5080843.
8. Hsu CC, Tseng LM, Lee HC. Role of mitochondrial dysfunction in cancer progression [review]. *Exp Biol Med (Maywood)* 2016;241:1281–95.
9. Hadzic T, Li L, Cheng N, Walsh SA, Spitz DR, Knudson CM. The role of low molecular weight thiols in T lymphocyte proliferation and IL-2 secretion. *J Immunol* 2005;175:7965–72.
10. Lai ZW, Hanczko R, Bonilla E, Caza TN, Clair B, Bartos A, et al. N-acetylcysteine reduces disease activity by blocking mammalian target of rapamycin in T cells from systemic lupus erythematosus patients: a randomized, double-blind, placebo-controlled trial. *Arthritis Rheum* 2012;64:2937–46.
11. Hedrich CM, Crispin JC, Rauen T, Ioannidis C, Apostolidis SA, Lo MS, et al. cAMP response element modulator α controls IL2 and IL17A expression during CD4 lineage commitment and subset distribution in lupus. *Proc Natl Acad Sci U S A* 2012;109:16606–11.
12. Marquez J, Mates JM, Campos-Sandoval JA. Glutaminases. *Adv Neurobiol* 2016;13:133–71.
13. Murayama A, Sakura K, Nakama M, Yasuzawa-Tanaka K, Fujita E, Tateishi Y, et al. A specific CpG site demethylation in the human interleukin 2 gene promoter is an epigenetic memory. *EMBO J* 2006;25:1081–92.
14. Yarosz EL, Chang CH. The role of reactive oxygen species in regulating T cell-mediated immunity and disease. *Immune Netw* 2018;18:e14.
15. Kietzmann T, Petry A, Shvetsova A, Gerhold JM, Gorkach A. The epigenetic landscape related to reactive oxygen species formation in the cardiovascular system. *Br J Pharmacol* 2017;174:1533–54.
16. Chen Z, Gong L, Zhang P, Li Y, Liu B, Zhang L, et al. Epigenetic down-regulation of Sirt 1 via DNA methylation and oxidative stress signaling contributes to the gestational diabetes mellitus-induced fetal programming of heart ischemia-sensitive phenotype in late life. *Int J Biol Sci* 2019;15:1240–51.
17. Zhang C, Liu J, Zhao Y, Yue X, Zhu Y, Wang X, et al. Glutaminase 2 is a novel negative regulator of small GTPase Rac1 and mediates p53 function in suppressing metastasis. *Elife* 2016;5:e10727.

B Cell–Specific Deletion of CR6-Interacting Factor 1 Drives Lupus-like Autoimmunity by Activation of Interleukin-17, Interleukin-6, and Pathogenic Follicular Helper T Cells in a Mouse Model

Jin-Sil Park,¹ SeungCheon Yang,¹ Sun-Hee Hwang,¹ JeongWon Choi,¹ Seung-Ki Kwok,¹ Young-Yun Kong,² Jeehee Youn,³  Mi-La Cho,¹  and Sung-Hwan Park¹

Objective. CR6-interacting factor 1 (CRIF1) is a nuclear transcriptional regulator and a mitochondrial inner membrane protein; however, its functions in B lymphocytes have been poorly defined. This study was undertaken to investigate the effects of CRIF1 on B cell metabolic regulation, cell function, and autoimmune diseases.

Methods. Using mice with B cell–specific deletion of CRIF1 (Crif1^{ΔCD19} mice), we assessed the relevance of CRIF1 function for lupus disease parameters, including anti–double-stranded DNA (anti-dsDNA), cytokines, and kidney pathology. RNA sequencing was performed on B cells from Crif1^{ΔCD19} mice. The phenotypic and metabolic changes in immune cells were evaluated in Crif1^{ΔCD19} mice. Roquin^{san/+} mice crossed with Crif1^{ΔCD19} mice were monitored to assess the functionality of CRIF1-deficient B cells in lupus development.

Results. Crif1^{ΔCD19} mice showed an autoimmune lupus-like phenotype, including high levels of autoantibodies to dsDNA and severe lupus nephritis with increased mesangial hypercellularity. While loss of CRIF1 in B cells showed impaired mitochondrial oxidative function, CRIF1-deficient B cells promoted the production of interleukin-17 (IL-17) and IL-6 and was more potent in helping T cells develop into follicular helper T cells. In a mouse model of autoimmune lupus, depletion of CRIF1 in B cells exacerbated lupus severity, and CRIF1 overexpression prevented lupus development in roquin^{san/san} mice.

Conclusion. These results demonstrated that CRIF1 negatively correlates with disease severity and that overexpression of CRIF1 ameliorates disease development. Our findings suggest that CRIF1 is essential for preventing lupus development by maintaining B cell self tolerance.

INTRODUCTION

Systemic lupus erythematosus (SLE) is a complex autoimmune disease characterized by the production of pathogenic autoantibodies and cytokines in multiple organs (1,2). In SLE, autoantibodies recognize various nuclear self antigens, including DNA, histones, and ribonucleoproteins. Among these, anti–double-stranded DNA (anti-dsDNA) antibodies have emerged as a

significant SLE indicator (3). Autoantibodies cause chronic inflammation, leading to tissue damage in the skin, joints, central nervous system, and kidneys (1,2).

High-affinity autoantibodies are generated upon interaction between self-reactive B cells and overactive follicular helper T (T_{fh}) cells within the germinal center (GC) (4). Dysregulation of GC B cells and T_{fh} cells is critical for lupus development. In lupus-prone roquin^{san/san} mice, excessive interferon-γ (IFN_γ)

Supported by a grant of the Korea Health Technology R&D Project through the Korea Health Industry Development Institute, funded by the Ministry of Health & Welfare, Republic of Korea (grant no. HI20C1496) and by Basic Science Research Program through the National Research Foundation of Korea grant funded by the Korean government (grant no. 2020R1A2C2099615) and by the Ministry of Education (grant no. 2021R111A1A01050939).

Drs. Cho and S-H. Park contributed equally to this work.

¹Jin-Sil Park, PhD, SeungCheon Yang, MS, Sun-Hee Hwang, MS, JeongWon Choi, MS, Seung-Ki Kwok, MD, PhD, Mi-La Cho, PhD, Sung-Hwan Park, MD, PhD: The Catholic University of Korea, Seoul, Republic of Korea; ²Young-Yun Kong, PhD: Seoul National University, Seoul, Republic of Korea; ³Jeehee Youn, PhD: Hanyang University, Seoul, Republic of Korea.

Address correspondence to Sung-Hwan Park, MD, PhD, Division of Rheumatology, Department of Internal Medicine, Seoul St. Mary's Hospital, College of Medicine, The Catholic University of Korea, 222 Banpo-Daero, Seocho-gu, Seoul 06591, Republic of Korea; or to Mi-La Cho, PhD, Rheumatism Research Center, Catholic Institutes of Medical Science, The Catholic University of Korea, 222 Banpo-Daero, Seocho-gu, Seoul 06591, Republic of Korea. Email: rapark@catholic.ac.kr or iammila@catholic.ac.kr.

Author disclosures are available at <https://onlinelibrary.wiley.com/action/downloadSupplement?doi=10.1002%2Fart.42091&file=art42091-sup-0001-Disclosureform.pdf>.

Submitted for publication December 7, 2020; accepted in revised form February 9, 2022.

signaling promotes the accumulation of Tfh cells and GC B cells, triggering lupus development (5), whereas CD28 deficiency reduces the numbers of spontaneous Tfh cells and GC B cells, preventing lupus development (6). In lupus patients, an increase in circulating Tfh cells correlates with multiple high-titer autoantibodies and severe end-organ inflammation (7); furthermore, circulating Tfh cells exhibit characteristics of GC Tfh cells in the lymphoid follicles and are associated with autoantibody-producing plasmablasts (8). Accumulating evidence shows that Tfh cells promote autoimmune lupus by activating B cells, but the role of B cells in the development of Tfh cells remains unclear.

B cell differentiation is associated with high cellular metabolic demands. Dynamic metabolic reprogramming induces B cell growth, activation, and effector functions; nevertheless, metabolic disorders result in sustained B cell hyperactivation that causes autoimmunity or malignant transformation (9). A recent study indicated that generation of distinct B cell subsets requires initial slight changes in mitochondrial reactive oxygen species (mROS) within mitochondria^{high} B cells (10). B cells are antigen-presenting cells, undergoing mitochondrial depolarization during antigen uptake and presentation. Consequently, metabolic rewiring is pivotal for B cell activation and function (11). Upon antigen encounter, B cells increase their glycolysis rate, mitochondrial function, and cell surface expression of glucose transporter 1 through phosphatidylinositol 3-kinase (PI3K) and c-Myc (12,13). In the absence of costimulation, B cell receptor (BCR)-activated B cells undergo apoptosis due to the accumulation of dysfunctional mitochondria and increased intracellular calcium levels (14). Although several studies have shown that cellular metabolism contributes to determining B cell fates and functions, the importance of metabolism in T cells and macrophages has been demonstrated. However, little is known about the intracellular signaling and metabolic pathways involved in B cell differentiation and function.

The transcription factor CR6-interacting factor 1 (CRIF1) regulates the cell cycle and growth (15) by modulating the expression of nerve growth factor 1B, androgen receptor, NF-E2-related factor 2, and STAT3 (16–19). Recently, CRIF1 has also been identified as a mitochondrial protein associated with large mitochondrial subunits and is essential for mitochondrial function (20). Loss of CRIF1 results in increased levels of ROS in mitochondria (21). Furthermore, there is evidence that CRIF1 activity may affect inflammatory responses. CRIF1 deficiency promotes endothelial inflammation and insulin resistance (22,23). In addition, CRIF1 is down-regulated by β -amyloid-induced ROS, and CRIF1 overexpression restores the mitochondrial dysfunction, alleviating the pathogenesis of Alzheimer's disease (24). However, little is known about the role of CRIF1 in autoimmune disease, particularly its function in B lymphocytes.

In the present study, we investigated the role of CRIF1 in B cell characteristics and the effect of B cell-specific CRIF1

depletion in the pathogenesis of lupus in a mouse model. Crif1^{ΔCD19} mice exhibited high levels of IgG, IgG2c, and IgG3 autoantibodies against dsDNA and developed severe lupus nephritis with increased mesangial hypercellularity. The loss of CRIF1 in B cells impaired mitochondrial function and increased the frequency of B cells producing interleukin-17 (IL-17) and IL-6, as well as Tfh cells. Importantly, CRIF1 overexpression ameliorated disease development in a murine model of severe lupus. Our findings suggest that CRIF1 is critical for B cell function and prevention of autoimmune diseases.

MATERIALS AND METHODS

Mice. This study received ethics approval from the Animal Research Ethics Committee of The Catholic University of Korea; the procedure conformed to all National Institutes of Health guidelines (permit nos. CUMC-2017-0063-01, CUMC-2017-0122-02, and CUMC-2019-0190-01).

Patients. Blood specimens were obtained from patients with SLE (n = 6; age range 23–54 years). The diagnosis of SLE was established in accordance with the 2019 European Alliance of Associations for Rheumatology/American College of Rheumatology classification criteria (25), and disease activity was evaluated using the SLE Disease Activity Index score (26). Informed consent was obtained from all patients in accordance with the Declaration of Helsinki. Approval by the ethics committee of Seoul St. Mary's Hospital (Seoul, Republic of Korea) was obtained for all procedures (permit no. KC20TISI0012).

Statistical analysis. Statistical analyses were performed using GraphPad Prism, version 8 for Windows. *P* values were calculated using a 2-tailed paired *t*-test and two-way analysis of variance (grouped). *P* values less than 0.05 were considered statistically significant.

RESULTS

Autoimmune lupus-like phenotype exhibited by Crif1^{ΔCD19} mice. We generated a CD19-specific CRIF1-deficient mouse model (Crif1^{ΔCD19}). B cells from Crif1^{ΔCD19} mice exhibited significantly lower CRIF1 levels than B cells from wild-type (WT) mice (Supplementary Figure 1A, available on the *Arthritis & Rheumatology* website at <https://onlinelibrary.wiley.com/doi/10.1002/art.42091>). To evaluate CRIF1 function in B cells, we monitored the phenotypic changes in 7- and 20-week-old Crif1^{ΔCD19} mice. Compared to WT mice, Crif1^{ΔCD19} mice displayed a higher ratio of spleen weight:body weight as age increased (Supplementary Figure 1B). However, Crif1^{ΔCD19} mice showed no significant differences in the absolute number of splenocytes, despite significant cell viability impairments (Supplementary Figures 1C and D). Interestingly, increased

percentages of dendritic cells, neutrophils, and macrophages were observed in the spleens of both 7- and 20-week-old *Crif1*^{ΔCD19} mice (Supplementary Figure 1E).

Next, we assessed whether B cell-specific CRIF1 deletion affected B cell development. The frequencies of mature and transitional type 1 and 2 B cells were similar in 7-week-old *Crif1*^{ΔCD19} mice, 20-week-old *Crif1*^{ΔCD19} mice, and WT mice (Supplementary Figure 1F). Compared to WT mice, *Crif1*^{ΔCD19} mice had a higher frequency of splenic IgG-secreting B220+ cells (Figure 1A). Furthermore, a higher concentration of IgG was detected in the supernatants of splenocytes from *Crif1*^{ΔCD19} mice than in the supernatants of splenocytes from WT mice (Figure 1B). The concentrations of total IgG, IgG2c, and IgG3 were significantly higher in the serum from 20-week-old *Crif1*^{ΔCD19} mice than in serum from WT mice; however, these

differences were not evident in the 7-week-old mice (Figure 1C). Similarly, serum from 20-week-old *Crif1*^{ΔCD19} mice had significantly higher concentrations of dsDNA-specific IgG2c and IgG3 autoantibodies compared to the serum from WT mice (Figure 1D). These results suggest that the loss of CRIF1 in B cells drives autoimmune lupus development.

To determine the effect of B cell-specific CRIF1 depletion on humoral autoimmune responses in vivo, we performed histologic analysis of kidney sections from 20-week-old *Crif1*^{ΔCD19} and WT mice. The numbers of IL-6, IL-17, or chemokine monocyte chemoattractant protein 1 (MCP-1)-positive cells were significantly higher in the kidneys of *Crif1*^{ΔCD19} mice than in the kidneys of WT mice. Moreover, *Crif1*^{ΔCD19} mice exhibited severe lupus nephritis with increased mesangial hypercellularity (Figure 1E). These findings suggest that CRIF1

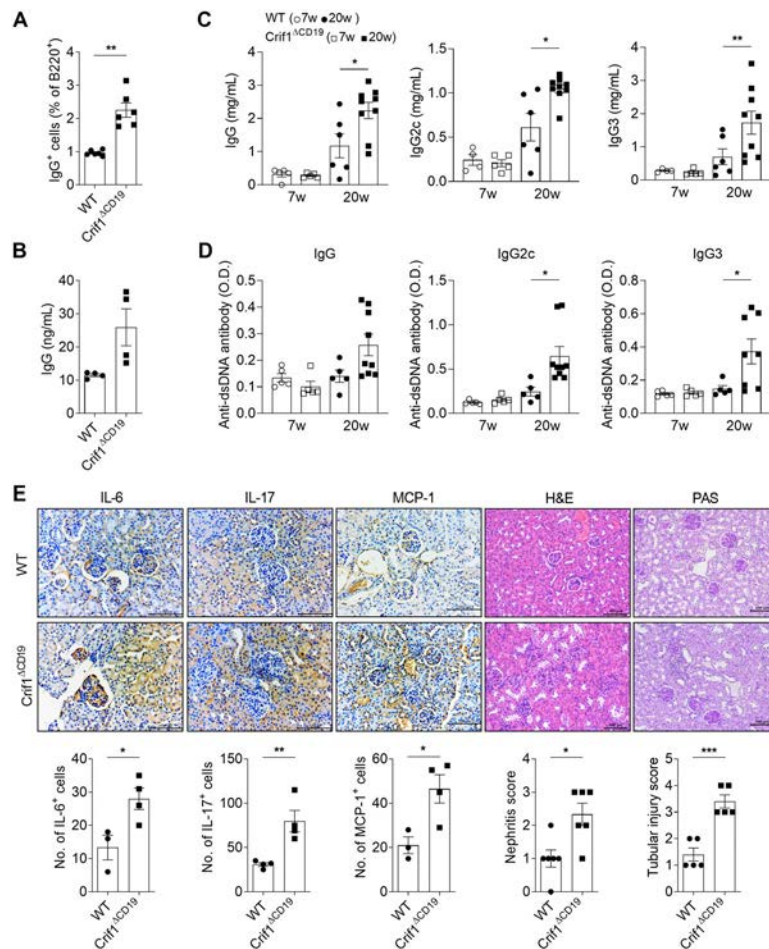


Figure 1. CR6-interacting factor 1 (CRIF1) depletion in B cells aggravates autoimmune lupus in mice. **A**, Frequencies of B220+IgG+ splenocytes in wild-type (WT) and *Crif1*^{ΔCD19} mice (n = 6 mice per group), as assessed by flow cytometry. **B**, Concentrations of IgG in the supernatants of splenocytes obtained from WT and *Crif1*^{ΔCD19} mice and cultured without stimulation for 72 hours (n = 4 mice per group). **C** and **D**, Amounts of IgG, IgG2c, and IgG3 (**C**) and anti-double-stranded DNA (anti-dsDNA) IgG, IgG2c, and IgG3 autoantibodies (**D**) in serum collected from 7-week-old (7w) or 20-week-old (20w) WT or *Crif1*^{ΔCD19} mice, as measured by enzyme-linked immunosorbent assay. Data were pooled from 2 independent experiments with a total of 4–9 mice per group. **E**, Kidney sections from 20-week-old WT and *Crif1*^{ΔCD19} mice stained for interleukin-6 (IL-6), IL-17, monocyte chemoattractant protein 1 (MCP-1), hematoxylin and eosin (H&E), and periodic acid–Schiff (PAS). Representative histologic features are shown. Original magnification × 200. Bars = 100 μm. Symbols represent individual mice; bars show the mean ± SEM. * = *P* < 0.05; ** = *P* < 0.01; *** = *P* < 0.001, by Student’s unpaired *t*-test.

deficiency in B cells is sufficient to promote lupus nephritis in vivo.

Distinct gene expression and function exhibited by CRIF1-deficient B cells. To identify the genes and pathways involved in the abnormal features of CRIF1-deficient B cells, we performed global gene expression analysis by RNA-based next-generation sequencing (RNA-Seq) of B cells. At a threshold change in expression of >2-fold, $P < 0.05$, and false discovery rate of <0.1, 520 differentially expressed genes (DEGs) were up-regulated and 400 DEGs were down-regulated in B cells from $Crif1^{\Delta CD19}$ mice

relative to WT mice (Figures 2A and B and Supplementary Figure 2A, available on the *Arthritis & Rheumatology* website at <https://onlinelibrary.wiley.com/doi/10.1002/art.42091>). Analysis of gene ontology terms revealed the significant enrichment of genes associated with immune receptor activity, cytokine receptor activity, transmembrane receptor protein kinase activity, and complement receptor activity in CRIF1-deficient B cells relative to WT B cells (Figure 2C and Supplementary Figure 2B). KEGG pathway analysis showed that the up-regulated genes were enriched in inflammation and disease-related signals and cell death, whereas reduced genes encoding molecules were associated with antiinflammatory signals and metabolic

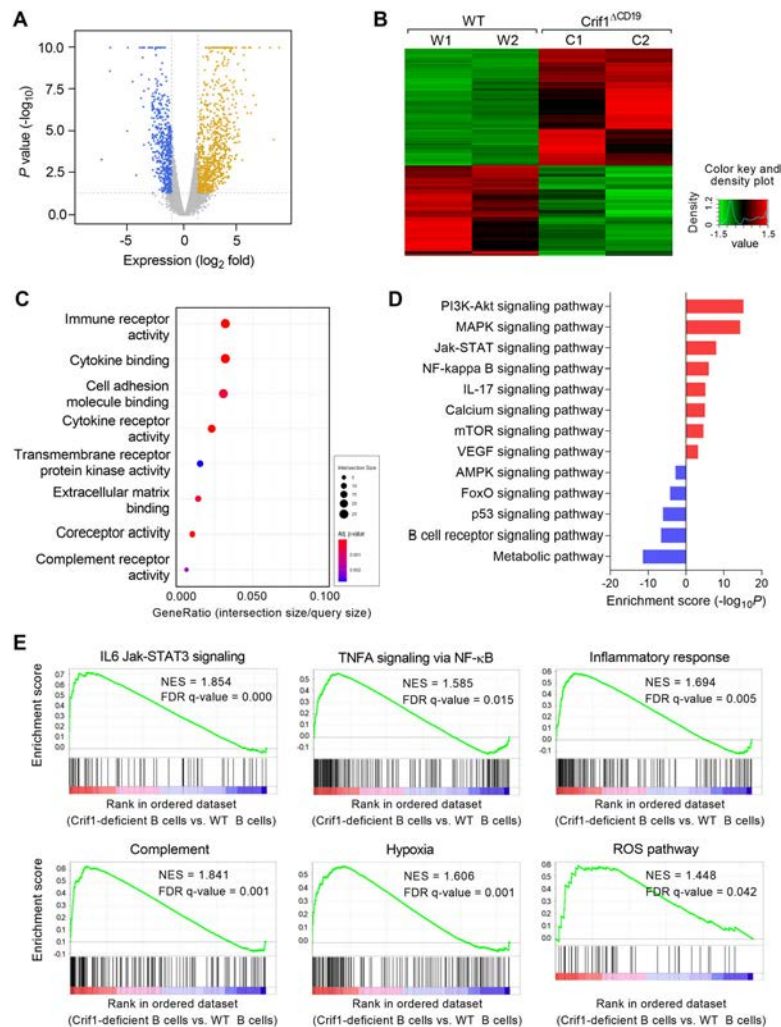


Figure 2. CRIF1-deficient B cells exhibit distinct gene expression and function. **A**, Volcano plots showing gene expression levels determined by RNA-sequencing analysis (\log_2 values and associated P values) in splenic B cells from 16-week-old $Crif1^{\Delta CD19}$ mice, compared to splenic B cells from WT mice. Yellow dots indicate up-regulated genes, and blue dots indicate down-regulated genes in $Crif1^{\Delta CD19}$ mice, compared to WT mice. **B**, Heatmap showing differentially expressed genes (DEGs) between splenic $Crif1^{\Delta CD19}$ mouse B cells and WT mouse B cells. **C**, Bubble plots showing up-regulated pathways and enriched gene ontology molecular functions in CRIF1-deficient mouse B cells. The y-axis represents biologic processes, and the x-axis represents adjusted P values. The sizes and colors of bubbles indicate the fold-enrichment per category and enrichment significance, respectively. **D**, KEGG pathway analysis of up-regulated (red) and down-regulated (blue) genes. **E**, Gene set enrichment analysis of gene signatures associated with JAK/STAT, tumor necrosis factor (TNF)/NF- κ B, inflammatory response, complement, hypoxia, and reactive oxygen species (ROS) pathways. PI3K = phosphatidylinositol 3-kinase; mTOR = mammalian target of rapamycin; VEGF = vascular endothelial growth factor; NES = normalized enrichment score; FDR = false discovery rate (see Figure 1 for other definitions).

pathways in CRIF1-deficient B cells, relative to their expression in WT B cells (Figures 2D and E and Supplementary Figures 2C and D). These results indicate that CRIF1-deficient B cells exhibit amplified inflammatory responses and cell death signals.

Altered metabolic profiles exhibited by CRIF1-deficient B cells. We investigated the role of CRIF1 in B cell development and function. To examine the effect of B cell-specific CRIF1 depletion on mitochondrial function and mitochondrial membrane potential ($\Delta\Psi_m$), we stained splenocytes ex vivo with MitoTracker Green ($\Delta\Psi_m$ independent; total mitochondria) and MitoTracker Red ($\Delta\Psi_m$ dependent; respiring mitochondria) (27). Dysfunctional nonrespiring mitochondria (MitoTracker Green^{high}, MitoTracker Red^{low}) accumulated in CRIF1-deficient B cells (Figure 3A). Decreases in $\Delta\Psi_m$ are associated with increases in mROS levels (28). An increase in mROS was

observed in CRIF1-deficient B cells with low $\Delta\Psi_m$ (Figure 3B), and mROS induction correlated with total mitochondrial mass indicated by MitoTracker Green staining (Figure 3C). These data suggest that CRIF1 deficiency in B cells leads to the accumulation of dysfunctional mitochondria and mROS.

To assess mitochondrial energetic capacity, we measured oxygen consumption rate (OCR), an oxidative phosphorylation indicator, in splenic B cells isolated from WT and Crif1^{ΔCD19} mice. CRIF1-deficient B cells stimulated with lipopolysaccharide (LPS) had significantly decreased oxidative phosphorylation activity with reduced levels of basal respiration, maximal respiration, and ATP-coupled OCR (Figures 3D and E). We also analyzed splenocytes by flow cytometry after staining with annexin V and propidium iodide (PI). The percentages of late apoptotic (annexin V+PI+) B cells and necrotic (annexin V-PI+) B cells were significantly higher in Crif1^{ΔCD19} mice than in WT mice (Figure 3F). Crif1^{ΔCD19} mice had a profoundly

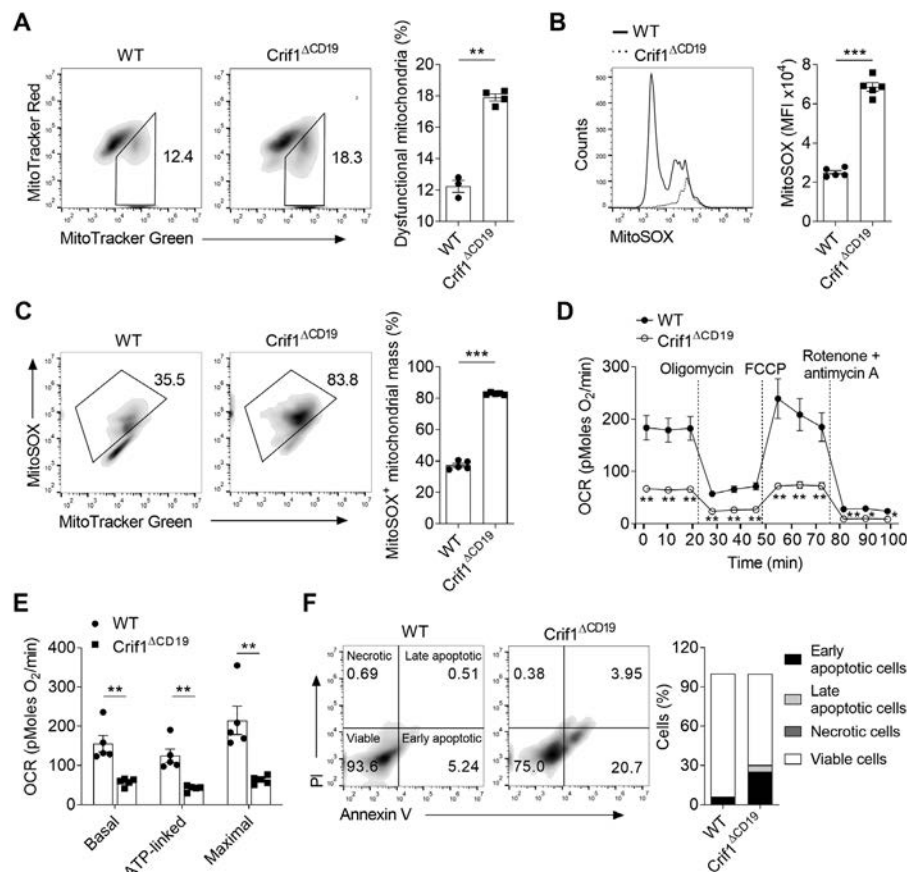


Figure 3. CRIF1 regulates mitochondria function in B cells. **A**, Splenocytes from 18-week-old WT mice ($n = 3$) and Crif1^{ΔCD19} mice ($n = 4$) were stained with MitoTracker Green and MitoTracker Red and then analyzed by flow cytometry. **B** and **C**, Splenocytes from WT and Crif1^{ΔCD19} mice ($n = 5$ per group) were stained with MitoSOX (**B**) or MitoTracker Green and MitoSOX (**C**) and then analyzed by flow cytometry. **D** and **E**, B220+ cells from WT and Crif1^{ΔCD19} mice ($n = 5$ group) were cultured with lipopolysaccharide (LPS) for 12 hours. Oxygen consumption rate (OCR) changes during treatment with oligomycin ($10 \mu\text{M}$), carbonyl cyanide-*p*-trifluoromethoxyphenylhydrazone (FCCP) ($3 \mu\text{M}$), and rotenone plus antimycin A ($10 \mu\text{M}$) were assessed by extracellular flux analysis (**D**), and oxidative phosphorylation activity during basal or maximal respiration and the ATP-coupled OCR were assessed (**E**). **F**, Splenocytes from WT mice ($n = 5$) and Crif1^{ΔCD19} mice ($n = 4$) were analyzed by flow cytometry after staining with annexin V and propidium iodide (PI). Data are representative of 2 independent experiments. In **A–E**, symbols represent individual mice; bars show the mean \pm SEM. * = $P < 0.05$; ** = $P < 0.01$; *** = $P < 0.001$, by Student's unpaired *t*-test. See Figure 1 for other definitions.

lower number of Ki-67–positive cells and a higher number of TUNEL-positive cells than WT mice (Supplementary Figure 3, available on the *Arthritis & Rheumatology* website at <https://onlinelibrary.wiley.com/doi/10.1002/art.42091>). These results indicate that CRIF1 deficiency in B cells results in the accumulation of dysfunctional mitochondria, metabolic alterations, and cell death.

Promotion of IL-17 and IL-6 production by B cell-specific CRIF1 deficiency. Splenic B cell subsets in $Crif1^{\Delta CD19}$ mice showed overt abnormalities. Notably, the percentages of GC B cells and plasma cells were significantly increased in 20-week-old $Crif1^{\Delta CD19}$ mice, compared with those in WT mice (Figure 4A).

Next, we addressed whether CRIF1 deficiency affected B cell–derived IL-17 (29) and IL-6 (30) and exacerbated autoimmune diseases. Compared to control mice, $Crif1^{\Delta CD19}$ mice had a significantly greater number of B cells producing IL-17, whereas the number of IL-10–producing B cells (B10 cells) was similar in the 2 groups (Figure 4B). Immunofluorescence analysis of spleen sections showed an exacerbated number of IL-17– and IL-6–producing B cells in $Crif1^{\Delta CD19}$ mice (Supplementary Figure 4A, available on the *Arthritis & Rheumatology* website at <https://onlinelibrary.wiley.com/doi/10.1002/art.42091>).

Next, we examined whether CRIF1 deficiency regulates the expression of surface molecules. Compared to WT mice,

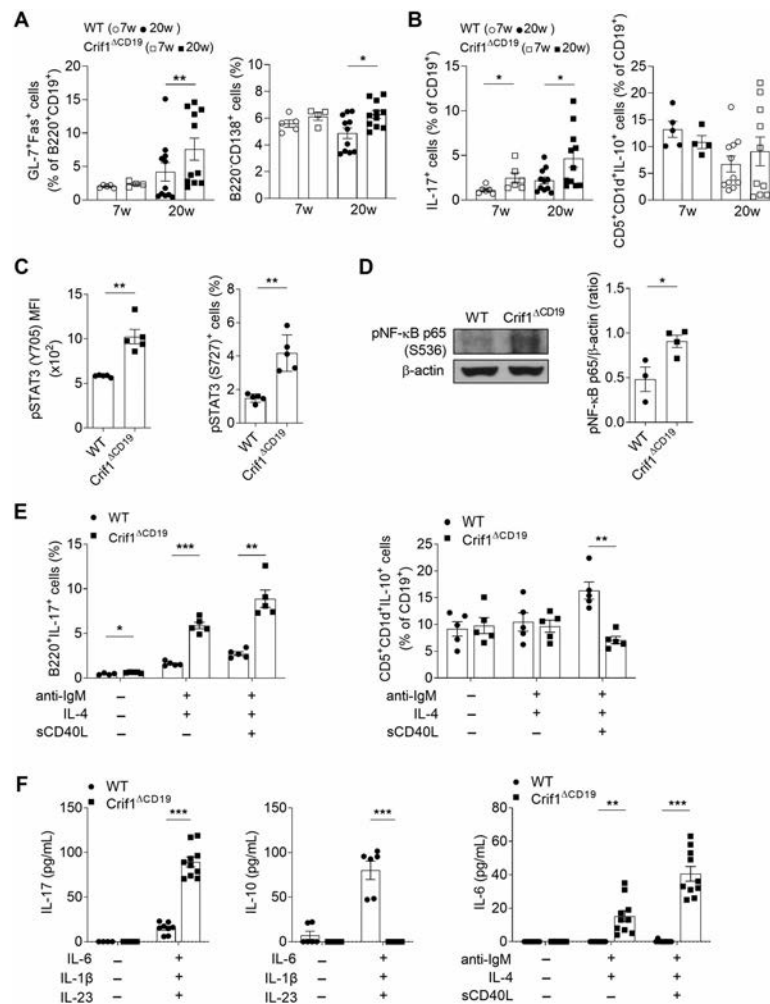


Figure 4. CRIF1 depletion enhances IL-17 and IL-6 production in B cells by activating STAT3 and NF-κB. **A** and **B**, The frequencies of germinal center B cells (B220+GL7+Fas+cells) and plasma cells (B220–CD138+) (**A**) and B220+IL-17+ and B10 cells (CD19+CD5+CD1d+IL-10+) (**B**) in splenocytes from 7-week-old and 20-week-old WT and $Crif1^{\Delta CD19}$ mice were assessed by flow cytometry. **C**, Phosphorylated STAT3 in splenic B cells was assessed by flow cytometry. **D**, Phosphorylated NF-κB p65 in splenic B cells was assessed by immunoblotting. **E**, Splenic B cells from 20-week-old WT and $Crif1^{\Delta CD19}$ mice were cultured with medium alone (control), IgM antibody (10 μg/ml), IL-4 (20 ng/ml), and/or soluble CD40L (sCD40L) (1 μg/ml) for 72 hours. The frequencies of B220+IL-17+ cells and B10 cells were analyzed by flow cytometry. **F**, Splenic B cells from 20-week-old WT and $Crif1^{\Delta CD19}$ mice were cultured with medium alone (control), IL-6 (10 ng/ml), IL-1β (10 ng/ml), and/or IL-23 (10 ng/ml) for 6 days. Concentrations of IL-17 and IL-10 in **E** and IL-6 in **F** were determined by enzyme-linked immunosorbent assay. Data are representative of 2 independent experiments. Symbols represent individual mice; bars show the mean ± SEM. * = $P < 0.05$; ** = $P < 0.01$; *** = $P < 0.001$, by Student's unpaired *t*-test. See Figure 1 for other definitions.

Crif1^{ΔCD19} mice exhibited higher expression of inducible costimulator ligand (ICOSL), CXCR5, CCR7, intercellular adhesion molecule 1 (ICAM-1), and ICAM-2 in B cells (Supplementary Figure 4B). Considering that STAT3 is responsible for the production of IL-17, IL-6, and IL-10 in human B cells, we examined phosphorylated STAT3 in B cells from WT and Crif1^{ΔCD19} mice. B cells from Crif1^{ΔCD19} mice had higher frequencies of phosphorylated STAT3 (Tyr705 and Ser727) as compared to their WT counterparts (Figure 4C). Furthermore, the levels of phosphorylated NF-κB p65 (Ser536) were higher in CRIF1-deficient B cells than in WT B cells (Figure 4D).

We then evaluated the effects of CRIF1 depletion on B cell development and function in vitro. To this end, we cultured purified splenic B cells alone, in the presence of anti-IgM and IL-4, or in the presence of anti-IgM, IL-4, and soluble CD40 ligand (sCD40L) for 72 hours. Consistent with our ex vivo findings, the percentage of IL-17-producing B cells was higher in stimulated CRIF1-deficient B cells than in stimulated WT B cells (Figure 4E). Anti-IgM, IL-4, and sCD40L stimulation resulted in a lower

frequency of B10 cells in CRIF1-deficient B cells than in WT B cells (Figure 4E). To determine the production of IL-17 in CRIF1-deficient B cells, splenic B cells from WT and Crif1^{ΔCD19} mice were cultured with IL-6, IL-1β, and IL-23 for 6 days (31). Increased IL-17 levels were detected in the supernatants of stimulated CRIF1-deficient B cells, whereas IL-10 production was decreased. Furthermore, increased IL-6 levels were detected in the supernatants of anti-IgM-, IL-4-, and sCD40L-stimulated CRIF1-deficient B cells than in WT B cells (Figure 4F). Taken together, these results suggest that the absence of CRIF1 in B cells accelerates the production of the inflammatory cytokines IL-17 and IL-6 and affects the expression of surface molecules.

Enhanced Tfh cell responses affected by B cell-specific CRIF1 deficiency. Recent studies have demonstrated that B cells are essential for the generation of Tfh cells. Expression of ICOSL on B cells regulates the generation of Tfh cells dependent on IL-6 and STAT3 (32). In addition, ICAM-1 and ICAM-2 on B cells are critical molecular factors in the cognate T cell–B cell interaction

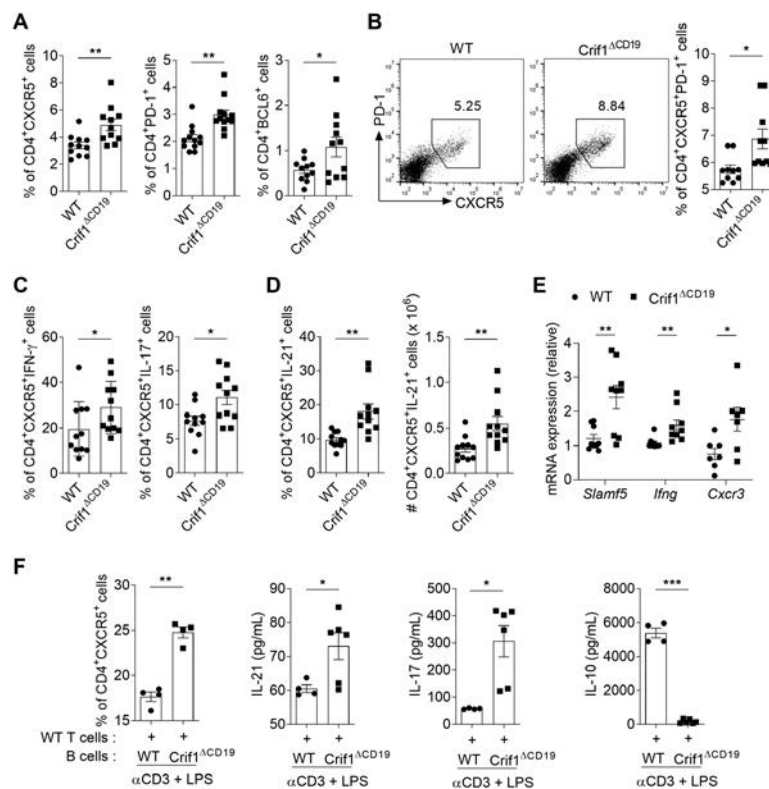


Figure 5. B cell-specific CRIF1 depletion promotes follicular helper T (Tfh) cell development. **A** and **B**, The frequencies of CXCR5+, programmed death 1 (PD-1)-positive, and Bcl-6+ splenic CD4+ cells (**A**) or CXCR5+PD-1+ splenic CD4+ cells (**B**) in 20-week-old WT and Crif1^{ΔCD19} mice were assessed by flow cytometry. **C**, Frequencies of interferon-γ (IFNγ)-positive or IL-17+ cells in CD4+CXCR5+ cells among ex vivo splenocytes from WT and Crif1^{ΔCD19} mice were assessed by flow cytometry. **D**, Frequencies and absolute numbers of IL-21+ cells in CD4+CXCR5+ cells among ex vivo splenocytes from WT and Crif1^{ΔCD19} mice were assessed by flow cytometry. **E**, Quantitative polymerase chain reaction analysis was performed for Tfh cell-related genes in splenic CD4+ cells from WT and Crif1^{ΔCD19} mice. **F**, Splenic T cells from WT mice were cocultured with B cells from Crif1^{ΔCD19} mice (n = 6) and WT mice (n = 4) in the presence of anti-CD3 and lipopolysaccharide (LPS) for 7 days. The frequencies of CD4+CXCR5+ cells and concentrations of IL-21, IL-17, and IL-10 in the culture supernatants were determined by flow cytometry and enzyme-linked immunosorbent assay, respectively. Symbols represent individual mice; bars show the mean ± SEM. * = P < 0.05; ** = P < 0.01; *** = P < 0.001, by Student's unpaired t-test. See Figure 1 for other definitions.

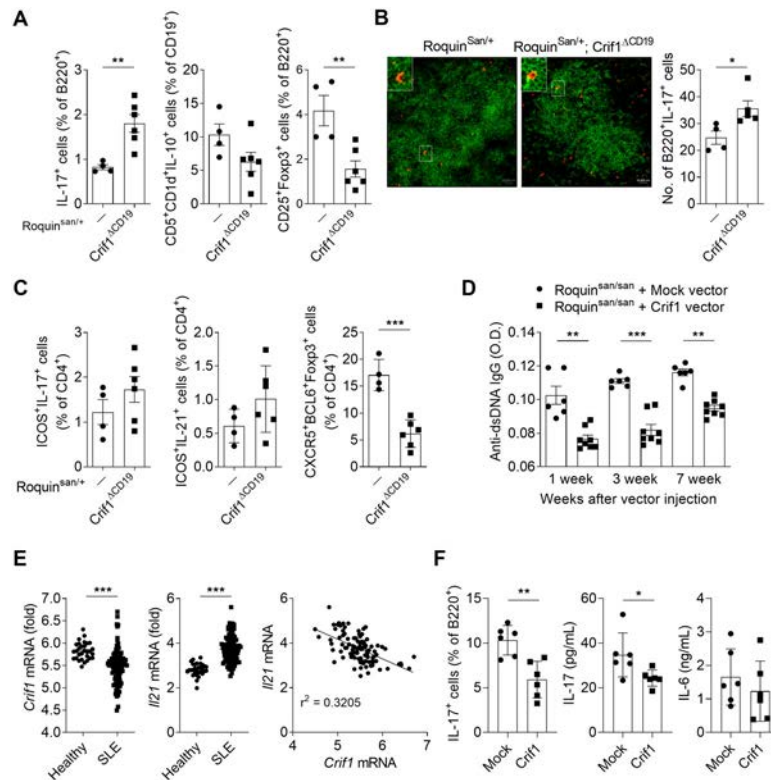


Figure 6. CRIF1 protects against autoimmune lupus. **A–C**, In 12-week-old *roquin*^{san/+} mice ($n = 4$) and *roquin*^{san/+}/*Crif1*^{ΔCD19} mice ($n = 6$), frequencies of B220+IL-17+ splenocytes, CD19+CD5+CD14+IL-10+ splenocytes, and B220+CD25+FoxP3+ splenocytes (**A**) and frequencies of CD4+ inducible costimulator (ICOS)-positive IL-17+ splenocytes, CD4+ICOS+IL-21+ splenocytes, and CD4+CXCR5+Bcl-6+FoxP3+ splenocytes were assessed by flow cytometry (**C**), and spleen sections were stained with anti-B220 (green) and anti-IL-17 (red) and examined using immunofluorescence, with findings quantified as the number of B220+IL-17+ cells (**B**). Original magnification $\times 200$. Bars = 20 μm . **Inset**, Higher-magnification views of the outlined areas. **D**, Five-month-old *roquin*^{san/san} mice were injected with 100 μg p3XFLAG-CMV-10-CRIF1 ($n = 8$) or mock vector ($n = 6$) every 7 days for 7 weeks. The concentration of anti-dsDNA IgG autoantibodies in the serum was measured by enzyme-linked immunosorbent assay (ELISA). **E**, Association of *CRIF1* and *IL21* expression levels in blood from patients with systemic lupus erythematosus (SLE) patients and healthy controls (GEO accession no. GSE61635). **F**, Peripheral blood mononuclear cells from SLE patients ($n = 6$) were transfected with control or CRIF1 overexpression vector and incubated with lipopolysaccharide (1 $\mu\text{g}/\text{ml}$) for 3 days. The frequency of B220+IL-17+ cells and concentrations of IL-17 and IL-6 in the culture supernatants were determined by flow cytometry and ELISA, respectively. Symbols represent individual mice; bars show the mean \pm SEM. * = $P < 0.05$; ** = $P < 0.01$; *** = $P < 0.001$, by Student's unpaired *t*-test. See Figure 1 for other definitions.

(33). Since CRIF1-deficient B cells produce higher levels of IL-17 and IL-6 and express increased percentages of surface molecules such as ICOSL and ICAM, we next determined whether loss of CRIF1 in B cells influenced the response of T cells. *Crif1*^{ΔCD19} mice had similar percentages of annexin V+PI+ late apoptotic T cells and annexin V-PI+ necrotic T cells as compared to WT mice (Supplementary Figure 5A, available on the *Arthritis & Rheumatology* website at <https://onlinelibrary.wiley.com/doi/10.1002/art.42091>). *Crif1*^{ΔCD19} mice showed a reduced proportion of IFN γ -producing Th1 or IL-4-producing Th2 cells (Supplementary Figures 5B and C), whereas no differences were detected in the frequency of Th17 cells, IL-10-producing T cells, and regulatory T cells, compared with WT mice (Supplementary Figures 5D–F). Additionally, there was a greater abundance of T cells in the splenic white pulp area of *Crif1*^{ΔCD19} mice as compared to WT mice (Supplementary Figure 5G).

To determine whether the development of Tfh cells was affected by CRIF1-deficient B cells in vivo, we analyzed the markers for Tfh cells, including CXCR5 (34), programmed death 1 (PD-1) (35), and transcription repressor Bcl-6 (36), in T cells from WT and *Crif1*^{ΔCD19} mice. The percentages of CXCR5+, PD-1+, and Bcl-6+ cells were significantly higher in *Crif1*^{ΔCD19} mice than in WT mice (Figure 5A). Moreover, the subset of CD4+ T cells expressing CXCR5 and PD-1 was increased in *Crif1*^{ΔCD19} mice compared with that in WT mice (Figure 5B). In parallel with the increased frequency in ex vivo splenocytes, immunofluorescence analysis of spleen sections revealed a significantly increased number of CD4+CXCR5+PD-1+ cells and CD4+ICOS+Bcl-6+ cells in *Crif1*^{ΔCD19} mice (Supplementary Figure 6A, available on the *Arthritis & Rheumatology* website at <https://onlinelibrary.wiley.com/doi/10.1002/art.42091>). *Crif1*^{ΔCD19} mice had an increased percentage of IFN γ in CD4+CXCR5+, CD4+ICOS+, or CD4+Bcl-6+ cells and

of IL-17 in CD4+CXCR5+ or CD4+ICOS+ cells, compared to WT mice (Figure 5C and Supplementary Figures 6B and C). Notably, the percentage and the absolute number of IL-21-producing CXCR5+, ICOS+, or Bcl-6+ CD4+ T cells were significantly increased in the spleens of *Crif1*^{ΔCD19} mice (Figure 5D and Supplementary Figures 6D and E). However, the numbers of CD4+CXCR5+Bcl-6+FoxP3+ T follicular regulatory (Tfr) cells were similar in both groups of mice (Supplementary Figure 6F).

Tfh cell signature genes, including *Slamf5*, *Irfng*, and *Cxcr3*, were up-regulated in T cells from *Crif1*^{ΔCD19} mice relative to those in WT mice (Figure 5E). Next, we determined whether CRIF1-deficient B cells promoted the development of T cells toward Tfh cells in vitro. CRIF1-deficient B cells were more potent in inducing CXCR5 expression in T cells than those from WT mice. Increased levels of IL-21 and IL-17 were detected in the supernatants, while IL-10 was reduced in the supernatants (Figure 5F). Collectively, these results indicated that CRIF1-deficient B cells strongly helped T cells develop into Tfh cells.

Autoimmunity prevented by CRIF1 overexpression.

Sanroque mice (roquin^{san/san} mice), which have an M199R mutation in the roquin protein, exhibit a lupus-like phenotype consisting of lymphadenopathy, high-affinity anti-dsDNA antibodies, splenomegaly, higher expression of ICOS in T cells, and increased Tfh cells (37). To assess the effect of CRIF1 deficiency in B cells on lupus development, we crossed roquin^{san/+} mice with *Crif1*^{ΔCD19} mice. Notably, roquin^{san/+}/*Crif1*^{ΔCD19} mice exhibited an increased frequency of splenic IL-17-producing B cells, compared to roquin^{san/+} mice, whereas the frequency of B10 cells and B220+ CD25+ FoxP3+ regulatory B cells was more reduced in these mice than in roquin^{san/+} mice (Figure 6A). The spleen sections of roquin^{san/+}/*Crif1*^{ΔCD19} mice also showed a higher distribution of IL-17-producing B cells as compared to roquin^{san/+} mice (Figure 6B). In addition, the frequencies of CD4+ICOS+IL-17+ cells and CD4+ICOS+IL-21+ cells were slightly increased, while the frequency of CD4+CXCR5+Bcl-6+FoxP3+ Tfr cells was significantly decreased in these mice, compared to roquin^{san/+} mice (Figure 6C), indicating that the loss of CRIF1 in B cells may play a role in the development of lupus.

To determine the therapeutic effects of CRIF1 overexpression in lupus, 5-month-old female roquin^{san/san} mice were injected with p3XFLAG-CMV-10-CRIF1 every 7 days for 7 weeks. The serum from p3XFLAG-CMV-10-CRIF1-treated roquin^{san/san} mice had a significantly lower concentration of IgG autoantibodies to dsDNA with disease progression compared to control vector-treated mice (Figure 6D). To determine the clinical relevance of CRIF1 in SLE, we analyzed publicly available microarray data (GEO accession no. GSE61635). Blood from SLE patients contained lower *CRIF1* messenger RNA (mRNA) levels and higher *IL21* mRNA levels than blood from healthy controls. In SLE blood, *CRIF1* mRNA levels negatively correlated with *IL21* mRNA levels (Figure 6E). To determine whether CRIF1 exhibits therapeutic

effects in the B cells of SLE patients, peripheral blood mononuclear cells were transfected with control or CRIF1-overexpressing vector and stimulated with LPS for 3 days. Overexpression of CRIF1 reduced the frequency of B220+IL-17+ cells and the amount of IL-17 and IL-6 in the supernatants, compared to control vector-treated cells (Figure 6F). These results suggest that CRIF1 in B cells plays an important role in maintaining immune homeostasis and preventing the development of autoimmune diseases (Supplementary Figure 7, available on the *Arthritis & Rheumatology* website at <https://onlinelibrary.wiley.com/doi/10.1002/art.42091>).

DISCUSSION

In this study, we report a novel function of CRIF1 as a negative regulator in B cells via linking metabolic homeostasis and inflammation, thereby regulating the development of autoimmune diseases, including lupus. *Crif1*^{ΔCD19} mice showed higher levels of autoantibodies against dsDNA and developed severe lupus nephritis with mesangial hypercellularity. While CRIF1 deficiency in B cells resulted in altered metabolic profiles, CRIF1-deficient B cells exhibited significant enrichment of molecules associated with B cell activation, the inflammatory response, and cytokine-mediated signaling. Importantly, loss of CRIF1 in B cells accelerated the production of inflammatory cytokines, including IL-17 and IL-6 in vivo and in vitro, and was more potent in helping T cells develop into Tfh cells. Using in vivo animal models of autoimmune lupus, we demonstrated that depletion of CRIF1 in B cells aggravated lupus severity, whereas CRIF1 overexpression ameliorated disease signs. Our findings identify a previously unknown mechanism by which CRIF1 acts as a critical checkpoint to maintain immune homeostasis and prevent the development of autoimmune diseases.

Several studies have indicated that B cell fates are strongly associated with cellular metabolism. Here, we demonstrated that CRIF1 deficiency drives the accumulation of dysfunctional mitochondria and mROS. At the same time, B cells have decreased glycolysis capacity and show eventual cell death. It has been reported that the production of mROS is involved in the inhibition of B cell antigen receptor signaling in B cells (38). We speculate that these changes via CRIF1 deficiency affect the downstream first signal for B cells because the second signal for B cells through binding of CD40L had no effect on cell viability in WT and *Crif1*^{ΔCD19} mice. Our results suggest that mitochondrial dysfunction due to CRIF1 deficiency leads to inflammatory cell death, such as necroptosis. Inflammatory cell death induction may explain the prevalent inflammation status of CRIF1-deficient B cells. Indeed, ex vivo CRIF1-deficient B cells showed an increased frequency of necrotic B cells and enrichment of genes involved in cell death and calcium signaling, as well as in PI3K/Akt, JAK/STAT, NF-κB, and mammalian target of rapamycin (mTOR) pathways. These data are consistent with those from a previous study showing that programmed necroptosis is

accompanied by mitochondrial ROS production (39), ATP depletion (40), and mitochondrial dysfunction (41).

Furthermore, isolated B cells from patients with active SLE had necroptosis, and Toll-like receptor- and BCR-activated necroptotic SLE B cells exhibited mitochondrial dysfunction and hypoxia (42). Because these dead cells have the potential to act as autoantigens, a defect in the clearance of dead cells may also play a role in exacerbating chronic inflammatory diseases such as SLE (43,44). Based on our findings, we suggest that CRIF1-deficient B cells cause problems in the clearance process to increase autoantigen; the resulting autoreactive B cells create a vicious cycle that promotes the activation of Tfh cells, thereby exacerbating lupus. Further studies are needed to determine the detailed molecular mechanisms by which CRIF1 functions in mitochondria-mediated programmed cell death and clearance of dead cells among B cells.

B cells are traditionally known for their effector function, involving the induction and regulation of T cell immune responses through antigen presentation to T cells and optimal T cell activation (45,46). There is growing evidence suggesting that B cells participate in immune response-mediated antibody-independent functions, mainly by producing different cytokines (45). For example, inducible CD11a^{high}FcγRIII^{high} B cells produce high amounts of IFN γ in mice challenged with *Listeria monocytogenes* and increase the resistance of macrophages to this infection through IFN γ production (47). Tumor necrosis factor production by B cells drives the generation of IFN γ -producing Th1 cell development in *Toxoplasma gondii*-infected mice (48), and IL-2 production by B cells promotes Th2 cell expansion and differentiation in *Heligmosomoides polygyrus*-infected mice (46).

Here, we showed that, without purposeful immunization or infection, CRIF1-deficient B cells produced significantly higher amounts of IL-6 and IL-17 and that the frequency of IFN γ -, IL-17-, and IL-21-producing Tfh cells increased in Crif1 ^{Δ CD19} mice. IL-6-secreting B cells are induced during experimental autoimmune encephalomyelitis (EAE) development, and IL-6 accelerates the pathogenesis of EAE by promoting the Th17 response (49). B cell-derived IL-6 is critical for the transcription of *IL21* in T cells and differentiation into Tfh cells (50). In addition, IL-6 production in B cells is enhanced by IFN γ synergizing with the B cell activation signal, and B cell-derived IL-6 promotes autoimmune GC formation and, thereby, systemic inflammation in mouse lupus (30). It was recently reported that B cells are relevant sources of IL-17A and IL-17F in response to infection with *Trypanosoma cruzi* via triggering intracellular signaling dependent on the Btk/Tec family (29). However, the molecular regulation of IL-17 production in B cells has been incompletely defined to date. The up-regulated inflammation-related signaling pathways (PI3K/Akt, JAK/STAT3, NF- κ B, and mTOR) observed in CRIF1-deficient B cells might be involved in enhanced inflammatory cytokine production. In the present study, our findings showed that CRIF1 deficiency caused more IL-17 production from some B cells. Further studies are needed to determine whether this is the

result of direct or indirect competition between these inflammation-related transcription factors and CRIF1 in B cells and, furthermore, whether the interaction between CRIF1-deficient B cells and T cells acts on IL-17 production in B cells.

B10 cells can act directly on effector T cells and repress T cell cytokine production, thereby suppressing several T cell-mediated inflammatory diseases, including SLE, EAE, and collagen-induced arthritis (51–53). Hypoxia-inducible factor 1 α (HIF-1 α)-dependent glycolysis is required for B10 cell expansion. HIF-1 α -deficient B cells accelerate collagen-induced arthritis (54), and B cell-specific aryl hydrocarbon receptor deficiency reduces IL-10 expression while promoting inflammatory gene expression and exacerbating antigen-induced arthritis (55). Our results demonstrated that CRIF1 was crucial in producing IL-10 by B cells. Lack of CRIF1 in B cells caused the reduced frequency of B10 cells and IL-10 production via stimulation with anti-IgM, IL-4, and sCD40L. In accordance with findings from other studies (13,54), CRIF1-deficient B cells with a lower glycolytic activity showed reduced IL-10 production; thus, it is likely that CRIF1 can act as a regulator in B10 cells, either directly or indirectly.

Therapeutically, overexpression of CRIF1 may provide a treatment option to modulate the balance between the levels of inflammatory and regulatory cells and inhibit the development of autoimmune lupus. Indeed, we observed that the expression of *CRIF1* was down-regulated in tissues and blood from SLE patients and in animal models, and loss of CRIF1 in B cells accelerated the development of lupus in roquin^{san/+} mice. Moreover, CRIF1 overexpression improved the symptoms of SLE, which is consistent with our previous findings (56). However, little is known about the therapeutic effects of fostering CRIF1 in autoimmune diseases. Although not studied in autoimmune disease, it has been revealed that β -amyloid-induced ROS reduces the level of CRIF1 by facilitating Sp-1 and promoting CRIF1-induced improvement of β -amyloid-mediated mitochondrial dysfunction and cell death (24). Endothelial cell-specific loss of CRIF1 inhibits sirtuin 1 expression in a ROS-dependent manner and causes vascular dysfunction in mice (21). In particular, it has been reported that myeloid-specific loss of CRIF1 leads to M1-like macrophages and the development of systemic insulin resistance associated with adipose inflammation (57). Indeed, we recently reported that CRIF1 controls the differentiation of Th17 cells by suppressing STAT3 (56), indicating that CRIF1 is likely to play a role in immune cells. Our findings suggest a role for CRIF1 in autoimmune disease by which CRIF1 controls the production of inflammatory cytokines, provides potent help for T cell development into Tfh cells, and prevents autoimmune disease.

In summary, the results of this study reveal a previously unknown role for CRIF1 in the maintenance of metabolic and immune homeostasis in B cells, which might explain its role in inhibiting autoimmune diseases. CRIF1 depletion in B cells drives the accumulation of dysfunctional mitochondria and metabolic disorders, activating inflammation-related signaling pathways. Skewing toward a more inflammatory status in CRIF1-deficient B cells facilitates the development of pathogenic Tfh cells, which

aggravates autoimmune diseases. Therefore, restoring CRIF1 expression might be a promising strategy to treat B cell-mediated autoimmune diseases, including SLE.

ACKNOWLEDGMENTS

We thank Si-Young Choi, MS, for providing technical support.

AUTHOR CONTRIBUTIONS

All authors were involved in drafting the article or revising it critically for important intellectual content, and all authors approved the final version to be published. Drs. Cho and S-H. Park had full access to all of the data in the study and take responsibility for the integrity of the data and the accuracy of the data analysis.

Study conception and design. J-S. Park, Cho, S-H. Park.

Acquisition of data. J-S. Park, Yang, Hwang, Choi.




Analysis and interpretation of data. J-S. Park, Kwok, Kong, Youn, Cho, S-H. Park.

REFERENCES

- Kaul A, Gordon C, Crow MK, Touma Z, Urowitz MB, van Vollenhoven R, et al. Systemic lupus erythematosus. *Nat Rev Dis Primers* 2016;2:16039.
- Bernatsky S, Ramsey-Goldman R, Labrecque J, Joseph L, Boivin JF, Petri M, et al. Cancer risk in systemic lupus: an updated international multi-centre cohort study. *J Autoimmun* 2013;42:130–5.
- Isenberg DA, Manson JJ, Ehrenstein MR, Rahman A. Fifty years of anti-ds DNA antibodies: are we approaching journey's end? *Rheumatology (Oxford)* 2007;46:1052–6.
- Kim CH, Rott LS, Clark-Lewis I, Campbell DJ, Wu L, Butcher EC. Subspecialization of CXCR5+ T cells: B helper activity is focused in a germinal center-localized subset of CXCR5+ T cells. *J Exp Med* 2001;193:1373–81.
- Lee SK, Silva DG, Martin JL, Pratama A, Hu X, Chang PP, et al. Interferon- γ excess leads to pathogenic accumulation of follicular helper T cells and germinal centers. *Immunity* 2012;37:880–92.
- Linterman MA, Rigby RJ, Wong RK, Yu D, Brink R, Cannons JL, et al. Follicular helper T cells are required for systemic autoimmunity. *J Exp Med* 2009;206:561–76.
- Simpson N, Gatenby PA, Wilson A, Malik S, Fulcher DA, Tangye SG, et al. Expansion of circulating T cells resembling follicular helper T cells is a fixed phenotype that identifies a subset of severe systemic lupus erythematosus. *Arthritis Rheum* 2010;62:234–44.
- Zhang X, Lindwall E, Gauthier C, Lyman J, Spencer N, Alarakhia A, et al. Circulating CXCR5+CD4+ helper T cells in systemic lupus erythematosus patients share phenotypic properties with germinal center follicular helper T cells and promote antibody production. *Lupus* 2015;24:909–17.
- Muschen M. Metabolic gatekeepers to safeguard against autoimmunity and oncogenic B cell transformation. *Nat Rev Immunol* 2019;19:337–48.
- Jang KJ, Mano H, Aoki K, Hayashi T, Muto A, Nambu Y, et al. Mitochondrial function provides instructive signals for activation-induced B-cell fates. *Nat Commun* 2015;6:6750.
- Bonifaz L, Cervantes-Silva M, Ontiveros-Dotor E, Lopez-Villegas E, Sanchez-Garcia F. A role for mitochondria in antigen processing and presentation. *Immunology* 2014;144:461–71.
- Doughty CA, Bleiman BF, Wagner DJ, Dufort FJ, Mataraza JM, Roberts MF, et al. Antigen receptor-mediated changes in glucose metabolism in B lymphocytes: role of phosphatidylinositol 3-kinase signaling in the glycolytic control of growth. *Blood* 2006;107:4458–65.
- Caro-Maldonado A, Wang R, Nichols AG, Kuraoka M, Milasta S, Sun LD, et al. Metabolic reprogramming is required for antibody production that is suppressed in anergic but exaggerated in chronically BAFF-exposed B cells. *J Immunol* 2014;192:3626–36.
- Akkaya M, Traba J, Roesler AS, Miozzo P, Akkaya B, Theall BP, et al. Second signals rescue B cells from activation-induced mitochondrial dysfunction and death. *Nat Immunol* 2018;19:871–84.
- Oh NS, Yoon SH, Lee WK, Choi JY, Min DS, Bae YS. Phosphorylation of CKBBP2/CRIF1 by protein kinase CKII promotes cell proliferation. *Gene* 2007;386:147–53.
- Park KC, Song KH, Chung HK, Kim H, Kim DW, Song JH, et al. CR6-interacting factor 1 interacts with orphan nuclear receptor Nur77 and inhibits its transactivation. *Mol Endocrinol* 2005;19:12–24.
- Suh JH, Shong M, Choi HS, Lee K. CR6-interacting factor 1 represses the transactivation of androgen receptor by direct interaction. *Mol Endocrinol* 2008;22:33–46.
- Kang HJ, Hong YB, Kim HJ, Bae I. CR6-interacting factor 1 (CRIF1) regulates NF-E2-related factor 2 (NRF2) protein stability by proteasome-mediated degradation. *J Biol Chem* 2010;285:21258–68.
- Kwon MC, Koo BK, Moon JS, Kim YY, Park KC, Kim NS, et al. Crif1 is a novel transcriptional coactivator of STAT3. *EMBO J* 2008;27:642–53.
- Kim SJ, Kwon MC, Ryu MJ, Chung HK, Tadi S, Kim YK, et al. CRIF1 is essential for the synthesis and insertion of oxidative phosphorylation polypeptides in the mammalian mitochondrial membrane. *Cell Metab* 2012;16:274–83.
- Nagar H, Jung SB, Ryu MJ, Choi SJ, Piao S, Song HJ, et al. CR6-interacting factor 1 deficiency impairs vascular function by inhibiting the Sirt1-endothelial nitric oxide synthase pathway. *Antioxid Redox Signal* 2017;27:234–49.
- Piao S, Lee JW, Nagar H, Jung SB, Choi S, Kim S, et al. CR6 interacting factor 1 deficiency promotes endothelial inflammation by SIRT1 downregulation. *PLoS One* 2018;13:e0192693.
- Ryu MJ, Kim SJ, Kim YK, Choi MJ, Tadi S, Lee MH, et al. Crif1 deficiency reduces adipose OXPHOS capacity and triggers inflammation and insulin resistance in mice. *PLoS Genet* 2013;9:e1003356.
- Byun J, Son SM, Cha MY, Shong M, Hwang YJ, Kim Y, et al. CR6-interacting factor 1 is a key regulator in A β -induced mitochondrial disruption and pathogenesis of Alzheimer's disease. *Cell Death Differ* 2015;22:959–70.
- Aringer M, Costenbader K, Daikh D, Brinks R, Mosca M, Ramsey-Goldman R, et al. 2019 European League Against Rheumatism/American College of Rheumatology classification criteria for systemic lupus erythematosus. *Arthritis Rheumatol* 2019;71:1400–12.
- Bombardier C, Gladman DD, Urowitz MB, Caron D, Chang DH, and the Committee on Prognosis Studies in SLE. Derivation of the SLE-DAI: a disease activity index for lupus patients. *Arthritis Rheum* 1992;35:630–40.
- Tal MC, Sasai M, Lee HK, Yordy B, Shadel GS, Iwasaki A. Absence of autophagy results in reactive oxygen species-dependent amplification of RLR signaling. *Proc Natl Acad Sci U S A* 2009;106:2770–5.
- Weinberg SE, Sena LA, Chandel NS. Mitochondria in the regulation of innate and adaptive immunity. *Immunity* 2015;42:406–17.
- Bermejo DA, Jackson SW, Gorosito-Serran M, Acosta-Rodriguez EV, Amezcua-Vesely MC, Sather BD, et al. Trypanosoma cruzi transsialidase initiates a program independent of the transcription factors ROR γ and Ahr that leads to IL-17 production by activated B cells. *Nat Immunol* 2013;14:514–22.

30. Arkatkar T, Du SW, Jacobs HM, Dam EM, Hou B, Buckner JH, et al. B cell-derived IL-6 initiates spontaneous germinal center formation during systemic autoimmunity. *J Exp Med* 2017;214:3207–17.
31. Oliveira-Brito PK, Roque-Barreira MC, da Silva TA. The response of IL-17-producing B cells to ArtinM is independent of its interaction with TLR2 and CD14. *Molecules* 2018;23.
32. Nurieva RI, Chung Y, Hwang D, Yang XO, Kang HS, Ma L, et al. Generation of T follicular helper cells is mediated by interleukin-21 but independent of T helper 1, 2, or 17 cell lineages. *Immunity* 2008;29:138–49.
33. Zaretsky I, Atrakchi O, Mazor RD, Stoler-Barak L, Biram A, Feigelson SW, et al. ICAMs support B cell interactions with T follicular helper cells and promote clonal selection. *J Exp Med* 2017;214:3435–48.
34. Vinuesa CG, Tangye SG, Moser B, Mackay CR. Follicular B helper T cells in antibody responses and autoimmunity. *Nat Rev Immunol* 2005;5:853–65.
35. Haynes NM, Allen CD, Lesley R, Ansel KM, Killeen N, Cyster JG. Role of CXCR5 and CCR7 in follicular Th cell positioning and appearance of a programmed cell death gene-1^{high} germinal center-associated subpopulation. *J Immunol* 2007;179:5099–108.
36. Yu D, Rao S, Tsai LM, Lee SK, He Y, Sutcliffe EL, et al. The transcriptional repressor Bcl-6 directs T follicular helper cell lineage commitment. *Immunity* 2009;31:457–68.
37. Vinuesa CG, Cook MC, Angelucci C, Athanasopoulos V, Rui L, Hill KM, et al. A RING-type ubiquitin ligase family member required to repress follicular helper T cells and autoimmunity. *Nature* 2005;435:452–8.
38. Ogura M, Inoue T, Yamaki J, Homma MK, Kurosaki T, Homma Y. Mitochondrial reactive oxygen species suppress humoral immune response through reduction of CD19 expression in B cells in mice. *Eur J Immunol* 2017;47:406–18.
39. Tait SW, Oberst A, Quarato G, Milasta S, Haller M, Wang R, et al. Widespread mitochondrial depletion via mitophagy does not compromise necroptosis. *Cell Rep* 2013;5:878–85.
40. Dashzeveg N, Taira N, Lu ZG, Kimura J, Yoshida K. Palmdelphin, a novel target of p53 with Ser46 phosphorylation, controls cell death in response to DNA damage. *Cell Death Dis* 2014;5:e1221.
41. Golstein P, Kroemer G. Cell death by necrosis: towards a molecular definition. *Trends Biochem Sci* 2007;32:37–43.
42. Fan H, Liu F, Dong G, Ren D, Xu Y, Dou J, et al. Activation-induced necroptosis contributes to B-cell lymphopenia in active systemic lupus erythematosus. *Cell Death Dis* 2014;5:e1416.
43. Mahajan A, Herrmann M, Munoz LE. Clearance deficiency and cell death pathways: a model for the pathogenesis of SLE. *Front Immunol* 2016;7:35.
44. Baumann I, Kolowos W, Voll RE, Manger B, Gaipl U, Neuhuber WL, et al. Impaired uptake of apoptotic cells into tingible body macrophages in germinal centers of patients with systemic lupus erythematosus. *Arthritis Rheum* 2002;46:191–201.
45. Lund FE, Randall TD. Effector and regulatory B cells: modulators of CD4⁺ T cell immunity. *Nat Rev Immunol* 2010;10:236–47.
46. Wojciechowski W, Harris DP, Sprague F, Mousseau B, Makris M, Kusser K, et al. Cytokine-producing effector B cells regulate type 2 immunity to *H. polygyrus*. *Immunity* 2009;30:421–33.
47. Bao Y, Liu X, Han C, Xu S, Xie B, Zhang Q, et al. Identification of IFN- γ -producing innate B cells. *Cell Res* 2014;24:161–76.
48. Menard LC, Minns LA, Darche S, Mielcarz DW, Foureau DM, Roos D, et al. B cells amplify IFN- γ production by T cells via a TNF- α -mediated mechanism. *J Immunol* 2007;179:4857–66.
49. Barr TA, Shen P, Brown S, Lampropoulou V, Roch T, Lawrie S, et al. B cell depletion therapy ameliorates autoimmune disease through ablation of IL-6-producing B cells. *J Exp Med* 2012;209:1001–10.
50. Karnowski A, Chevrier S, Belz GT, Mount A, Emslie D, D'Costa K, et al. B and T cells collaborate in antiviral responses via IL-6, IL-21, and transcriptional activator and coactivator, Oct2 and OBF-1. *J Exp Med* 2012;209:2049–64.
51. Evans JG, Chavez-Rueda KA, Eddaoudi A, Meyer-Bahlburg A, Rawlings DJ, Ehrenstein MR, et al. Novel suppressive function of transitional 2 B cells in experimental arthritis. *J Immunol* 2007;178:7868–78.
52. Matsushita T, Yanaba K, Bouaziz JD, Fujimoto M, Tedder TF. Regulatory B cells inhibit EAE initiation in mice while other B cells promote disease progression. *J Clin Invest* 2008;118:3420–30.
53. Matsumoto M, Baba A, Yokota T, Nishikawa H, Ohkawa Y, Kayama H, et al. Interleukin-10-producing plasmablasts exert regulatory function in autoimmune inflammation. *Immunity* 2014;41:1040–51.
54. Meng X, Grottsch B, Luo Y, Knaup KX, Wiesener MS, Chen XX, et al. Hypoxia-inducible factor-1 α is a critical transcription factor for IL-10-producing B cells in autoimmune disease. *Nat Commun* 2018;9:251.
55. Piper CJ, Rosser EC, Oleinika K, Nistala K, Krausgruber T, Rendeiro AF, et al. Aryl hydrocarbon receptor contributes to the transcriptional program of IL-10-producing regulatory B cells. *Cell Rep* 2019;29:1878–92.
56. Park JS, Choi SY, Hwang SH, Kim SM, Choi J, Jung KA, et al. CR6-interacting factor 1 controls autoimmune arthritis by regulation of signal transducer and activator of transcription 3 pathway and T helper type 17 cells. *Immunology* 2019;156:413–21.
57. Jung SB, Choi MJ, Ryu D, Yi HS, Lee SE, Chang JY, et al. Reduced oxidative capacity in macrophages results in systemic insulin resistance. *Nat Commun* 2018;9:1551.

Aptamer-Based Screen of Neuropsychiatric Lupus Cerebrospinal Fluid Reveals Potential Biomarkers That Overlap With the Choroid Plexus Transcriptome

Kamala Vanarsa,¹ Prashanth Sasidharan,¹ Valeria Duran,¹ Sirisha Gokaraju,¹ Malavika Nidhi,¹ 
Anto Sam Crosslee Louis Sam Titus,¹ Sanam Soomro,¹ Ariel D. Stock,² Evan Der,² Chaim Putterman,²
Benjamin Greenberg,³ Chi Chiu Mok,⁴  John G. Hanly,⁵  and Chandra Mohan¹

Objective. As no gold-standard diagnostic test exists for neuropsychiatric systemic lupus erythematosus (NPSLE), we undertook this study to execute a broad screen of NPSLE cerebrospinal fluid (CSF) using an aptamer-based platform.

Methods. CSF was obtained from NPSLE patients and subjected to proteomic assay using the aptamer-based screen. Potential biomarkers were identified and validated in independent NPSLE cohorts in comparison to other neurologic diseases.

Results. Forty proteins out of the 1,129 screened were found to be elevated in NPSLE CSF. Based on enzyme-linked immunosorbent assay validation, CSF levels of angiostatin, α 2-macroglobulin, DAN, fibronectin, hepatocellular carcinoma clone 1, IgM, lipocalin 2, macrophage colony-stimulating factor (M-CSF), and serine protease inhibitor G1 were significantly elevated in a predominantly White NPSLE cohort ($n = 24$), compared to patients with other neurologic diseases ($n = 54$), with CSF IgM (area under the curve [AUC] 0.95) and M-CSF (AUC 0.91) being the most discriminatory proteins. In a second Hong Kong–based NPSLE cohort, CSF IgM (AUC 0.78) and lipocalin 2 (AUC 0.85) were the most discriminatory proteins. Several CSF proteins exhibited high diagnostic specificity for NPSLE in both cohorts. Elevated CSF complement C3 was associated with an acute confusional state. Eleven molecules elevated in NPSLE CSF exhibited concordant elevation in the choroid plexus, suggesting shared origins.

Conclusion. Lipocalin 2, M-CSF, IgM, and complement C3 emerge as promising CSF biomarkers of NPSLE with diagnostic potential.

INTRODUCTION

Systemic lupus erythematosus (SLE) can present with a wide variety of central nervous system (CNS) and peripheral nervous system (PNS) manifestations, collectively termed neuropsychiatric SLE (NPSLE) (1). The prevalence of NPSLE among SLE patients varies from 40.3% to 91% (1,2). Manifestations of CNS involvement in NPSLE include seizures, aseptic meningitis, acute confusional states, cerebrovascular disease, psychosis, and mood disorders. Peripheral nervous system manifestations include autonomic neuropathy, cranial neuropathy, mononeuropathy,

polyneuropathy, and demyelinating syndrome, among others. Neuropsychiatric events occur most frequently early during the disease course in most cases, either as a presenting symptom or within the first 5 years of disease onset (3). The pathogenesis of NPSLE is not fully understood. Various mechanisms have been shown to be involved, including the formation of autoantibodies, vasculopathy, immune cell infiltrates, breach of the blood–brain barrier, and effects of various cytokines and other soluble mediators. These cytokines are believed to alter blood–brain barrier function, increase antibody production, and recruit immune cells (4–7).

Supported in part by the NIH (grant R01 AR074096) and the Lupus Research Alliance.

¹Kamala Vanarsa, MS, Prashanth Sasidharan, MBBS, Valeria Duran, MS, Sirisha Gokaraju, MD, Malavika Nidhi, BS, Anto Sam Crosslee Louis Sam Titus, PhD, Sanam Soomro, PhD, Chandra Mohan, MD, PhD: University of Houston, Houston, Texas; ²Ariel D. Stock, MD, Evan Der, PhD, Chaim Putterman, MD: Albert Einstein College of Medicine, New York, New York; ³Benjamin Greenberg, MD: University of Texas Southwestern Medical Center, Dallas; ⁴Chi Chiu Mok, MD, FRCP: Tuen Mun Hospital, Hong Kong, China; ⁵John G. Hanly, MD, FRCP: Queen Elizabeth

II Health Sciences Center and Dalhousie University Halifax, Nova Scotia, Canada.

Author disclosures are available at <https://onlinelibrary.wiley.com/action/downloadSupplement?doi=10.1002%2Fart.42080&file=art42080-sup-0001-Disclosureform.pdf>.

Address correspondence to Chandra Mohan, MD, PhD, Department Biomedical Engineering, University of Houston, 3605 Cullen Boulevard, Houston, TX 77204. Email: cmohan@central.uh.edu.

Submitted for publication February 9, 2021; accepted in revised form January 27, 2022.

Currently, we do not have reliable biomarkers that can help establish a definitive diagnosis of NPSLE. Antibodies with biomarker potential in NPSLE include serum antiphospholipid antibodies, anti-ribosomal P antibodies, anti-*N*-methyl-D-aspartate antibodies, and antiganglioside antibodies (8–10). Among cerebrospinal fluid (CSF) markers, CSF IgG index, the presence of oligoclonal bands, and antineuronal antibodies are deemed promising (8). However, as no gold-standard diagnostic test exists, we elected to carry out a broad screening of CSF from NPSLE patients, using a platform that has proven effective in screening lupus nephritis (LN) patients for urinary biomarkers (11), based on a library of aptamers.

Aptamers are short sequences of nucleic acids that can be further selected based on their binding specificities. Commercially available libraries of aptamers allow comprehensive screening of >1,000 human protein targets, representing some of the largest screening platforms currently available in targeted proteomics (12). Given that a similar screen has been useful in uncovering urine markers elevated in LN (11), we reasoned that this approach might be effective in other end-organ manifestations of SLE. Specifically, we hypothesized that NPSLE-specific biomarkers might be present in patient CSF. Therefore, we screened CSF from NPSLE patients and other neurologic disease controls in order to identify potential protein biomarkers that might have specificity for NPSLE. This represents the first broad screen of NPSLE CSF for protein biomarkers, using the aptamer-based platform.

PATIENTS AND METHODS

Patients, sample collection, and sample preparation. CSF samples used in this study were obtained with informed consent from 2 NPSLE patient cohorts, referred to as the Halifax cohort and the Hong Kong cohort. CSF samples for the Halifax NPSLE cohort were obtained from the Dalhousie Lupus Clinic Cohort, Division of Rheumatology, Queen Elizabeth II Health Sciences Center in Halifax, Nova Scotia, Canada (13), with informed consent. This cohort included 24 NPSLE patients and 54 neurologic disease controls. The NPSLE patients (mean age 37 years old) were predominantly White women with a wide range of neuropsychiatric manifestations (Supplementary Tables 1 and 2, available on the *Arthritis & Rheumatology* website at <https://onlinelibrary.wiley.com/doi/10.1002/art.42080>). The 54 neurologic disease controls comprised 31 patients with confirmed or suspected multiple sclerosis (MS), 3 patients with amyotrophic lateral sclerosis, and 1 patient each with the following: cerebellar disease, chronic inflammatory demyelinating polyneuropathy, fibromyalgia, Charcot-Marie-Tooth disease, Horner's syndrome, intercranial hypertension, large artery vasculopathy, leukodystrophy, progressive multifocal leukoencephalopathy, polyneuropathy, diabetic neuropathy, progressive muscular atrophy, progressive myelopathy, Parkinson's disease, primary demyelination, radiculopathy, transverse myelitis, vascular cognitive

impairment, and essential tremor. This cohort was used for both the initial aptamer-based proteomic screen and for the primary enzyme-linked immunosorbent assay (ELISA) validation study.

The Hong Kong cohort included patients seen at the Tuen Mun Hospital in Hong Kong, China, comprising 17 NPSLE patients and 15 control subjects. The NPSLE patients were all Chinese women (mean age 47 years old) presenting mostly with psychosis, seizures, or confusion (Supplementary Table 2, available on the *Arthritis & Rheumatology* website at <https://onlinelibrary.wiley.com/doi/10.1002/art.42080>). CSF was obtained from the control subjects who were being evaluated for seizures ($n = 2$), sepsis/infection ($n = 5$), temporal lobe epilepsy ($n = 1$), headaches ($n = 4$), dizziness ($n = 1$), cranial nerve palsies ($n = 1$), or neuropathy ($n = 1$). This cohort was used for the secondary ELISA validation study.

CSF was also obtained from an additional cohort of patients with MS and miscellaneous neurologic ailments, as well as healthy subjects, from the University of Texas Southwestern Medical Center (UTSW) in Dallas, with informed consent. This cohort was used for the initial aptamer-based proteomic screen. Demographic data on these cohorts are summarized in Supplementary Table 1 (available on the *Arthritis & Rheumatology* website at <https://onlinelibrary.wiley.com/doi/10.1002/art.42080>).

For NPSLE patients, CSF samples were collected as part of the diagnostic evaluation when patients presented with an NP event. CSF samples were collected between 1988 and 2017. Sequentially collected CSF samples were archived and used for this study. The study was approved by the research ethics board of the Nova Scotia Health Authority (central zone) and the institutional review boards of UTSW, Tuen Mun Hospital, and the University of Houston. All CSF samples were obtained following clinical indications for a lumbar puncture and were aliquoted and stored at -80°C . Patients were not involved in the design, conduct, reporting, or dissemination of this research.

Aptamer-based screening for 1,129 proteins. A discovery cohort comprised of 23 subjects (8 healthy controls, 7 controls with other neurologic conditions, and 8 NPSLE patients) was used for the initial screening of 1,129 unique proteins, using a pre-fabricated aptamer-based targeted proteomic assay (12) (Supplementary Table 1, available on the *Arthritis & Rheumatology* website at <https://onlinelibrary.wiley.com/doi/10.1002/art.42080>). In this targeted proteomic screening, streptavidin-coated beads labeled with 1,129 unique aptamers were added to each CSF sample to allow them to bind to their corresponding protein targets. After incubation, the beads were removed from the sample, the proteins attached to the aptamers were biotinylated, and all aptamer-protein complexes were cleaved from the initial streptavidin beads and recoupled to a new bead, with the biotinylated protein attached to the bead. The aptamers were then removed from the beads and quantitated using a

DNA microarray. The levels of various protein biomarkers were then analyzed using a variety of statistical tools, as described below. Biomarker studies and data analyses were performed at the Houston Omics Collaborative (<https://hoc.bme.uh.edu/>).

Validation study using ELISA. For the primary validation study using the Halifax cohort, CSF was obtained from 78 subjects: 24 NPSLE patients and 54 neurologic disease controls.

Clinical and demographic features are described in Supplementary Table 2 (available on the *Arthritis & Rheumatology* website at <https://onlinelibrary.wiley.com/doi/10.1002/art.42080>). Identified biomarkers were validated using ELISA assays, following manufacturer instructions. For each biomarker ELISA assay, a CSF dilution curve was set up, and the optimal CSF dilution to use for each ELISA was established, as detailed in Supplementary Table 3 (available on the *Arthritis & Rheumatology* website at

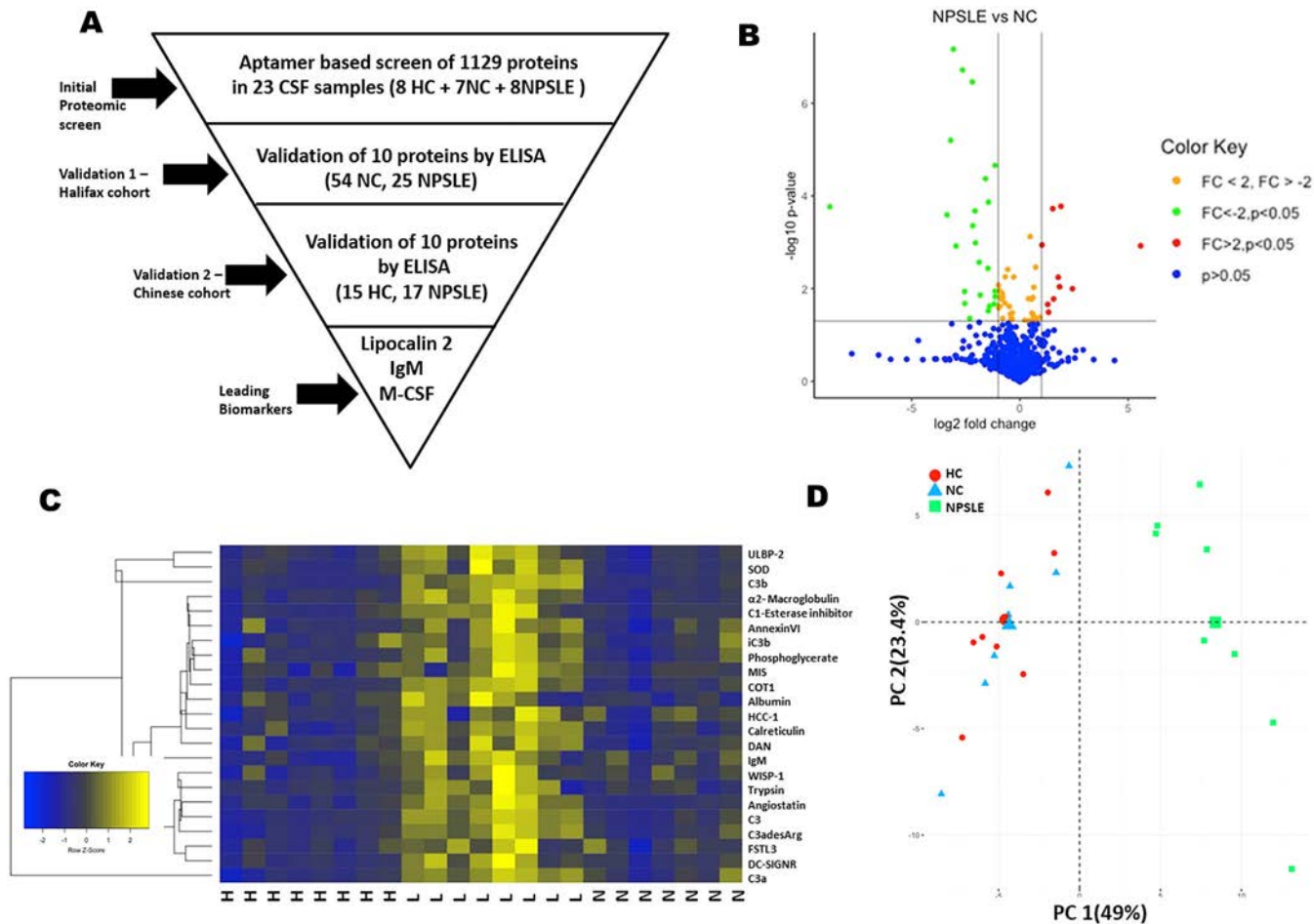


Figure 1. Aptamer-based screening of neuropsychiatric systemic lupus erythematosus (NPSLE) cerebrospinal fluid (CSF) samples for 1,129 proteins. Results were obtained from the discovery cohort (Halifax cohort), as detailed in Supplementary Table 1 (available on the *Arthritis & Rheumatology* website at <https://onlinelibrary.wiley.com/doi/10.1002/art.42080>). **A**, Consolidated Standards of Reporting Trials flow chart displaying the cohorts and protein screening methods used in this study. This diagram illustrates the steps of selecting proteins at each stage, beginning with a comprehensive proteomic screening and concluding with enzyme-linked immunosorbent assay (ELISA) validation in 2 independent cohorts. **B**, Volcano plot showing results of the aptamer-based screening of 1,129 proteins analyzed in 23 CSF samples, drawn from 8 NPSLE patients, 7 patients with other neurologic diseases (NCs), and 8 healthy controls (HCs). Ninety-five proteins were found to be elevated in CSF from NPSLE patients compared to CSF from healthy controls ($P < 0.05$) and neurologic disease controls ($P < 0.1$) (both by Mann-Whitney U test). Each dot represents the fold change (FC) in levels of 1 of the 1,129 proteins. **C**, Heatmap showing results of the aptamer-based screening, displaying the expression profiles of 23 proteins elevated at a fold change >2 in NPSLE CSF, compared to that of healthy controls ($P < 0.05$) and neurologic disease controls ($P < 0.1$) (both by Mann-Whitney U test). The heatmap shows the relative concentrations of these proteins in NPSLE patients (L), neurologic disease controls (N), and healthy controls (H). Protein levels above the median value (for each biomarker) are yellow, while those below the median are blue, and those comparable to the median value are shown in black. **D**, Two-dimensional principal components analysis (PC) plot displaying the ability of the 23-protein marker panel to distinguish between NPSLE patients, healthy controls, and neurologic disease controls. Each symbol represents an individual sample. The first 2 principal components explain 72.4% of the variance. M-CSF = macrophage colony-stimulating factor; ULBP-2 = UL-16 binding protein 2; SOD = superoxide dismutase; MIS = müllerian inhibiting substance; HCC-1 = hepatocellular carcinoma clone 1; WISP-1 = Wnt-1-inducible signaling pathway protein 1; FSTL-3 = follistatin-related protein 3.

<https://onlinelibrary.wiley.com/doi/10.1002/art.42080>). Briefly, for each assay protein, CSF samples were added to a microplate precoated with capture antibody, and then incubated, washed, and followed by addition of capture antibody, horseradish peroxidase, and substrate. The absolute levels of CSF protein biomarkers were assessed using standard curves run on each ELISA plate. Secondary ELISA validation was performed using 32 CSF samples from the Hong Kong cohort, comprising 15 NPSLE patients and 17 healthy controls. Demographic features of the Hong Kong cohort are detailed in Supplementary Table 2.

Heatmap analysis, cluster analysis, volcano plot, random forest classification, and Bayesian network analysis. Data from the protein array screening assay were used to generate a heatmap that clustered proteins with similar expression patterns together. The data from each group were imported into R for clustering analysis and heatmap generation. Proteins were clustered in an unsupervised manner based on Euclidean distance. R was then used to generate a volcano plot of \log_2 fold change of expression versus the $-\log_{10} P$ value, as determined by Mann-Whitney U test. Random forest classification analysis, a machine learning algorithm for dimensionality reduction, was executed using R, with 1,000 bootstrap sampling iterations, to identify the relative importance of each biomarker in disease classification using the Gini index. Ingenuity Pathway Analysis was used to determine enriched pathway networks by ranking the proteins based on fold change and P values that were significantly overexpressed in NPSLE CSF compared to the controls. The ranked genes were searched using the Qiagen Knowledge Base to find pathways that included these proteins. Canonical pathways were ranked by P values of overlap, calculated using right-tailed Fisher's exact test. The top transcription factors and signaling molecules that regulated the up-regulated proteins in NPSLE were deciphered using iRegulon and Cytoscape (<http://iregulon.aertslab.org/>). Bayesian network analysis was performed using the BayesiaLab software, Bayesia version 7.0.1. Continuous data were discretized into 3 bins using the R2-GenOpt algorithm, and the maximum weight spanning tree algorithm ($\alpha = 0.45$) was used for unsupervised learning of the network.

Statistical analysis. All data were plotted and analyzed using GraphPad Prism 7, Microsoft Excel, or R. Several packages such as ggplot2, dplyr, and heatmap.2 were used to generate figures. All data in this study were analyzed using the Mann-Whitney U test, as several data sets were not normally distributed. P values and q values (P values adjusted for false discovery rate for multiple testing correction) were computed for each biomarker. Spearman's correlation coefficient was used for the correlation analysis, and the Kruskal-Wallis test was used for multiple comparisons. Sensitivity, specificity, area under the receiver operating curve (AUC) analysis, positive predictive values

(PPVs), and negative predictive values (NPVs) were calculated using easyROC software. Cutoff values were calculated so as to maximize the Youden index. PPVs and NPVs were adjusted for prevalence, assuming the prevalence of NPSLE among SLE patients to be ~50% (1,2).

RESULTS

Aptamer-based interrogation of 1,129 proteins. The overall flow plan for this study is outlined in the Consolidated Standards of Reporting Trials diagram in Figure 1A. An aptamer-based screening for the presence of 1,129 proteins was first carried out using CSF samples from NPSLE patients, neurologic disease controls, and healthy controls evaluated for neurologic diseases but found to be negative. In this initial screening of 1,129 proteins, 95 proteins showed significant differences in NPSLE CSF compared to healthy control CSF ($P < 0.05$) and also compared to neurologic disease control CSF ($P < 0.1$) (Figure 1B and Supplementary Figure 1, available on the *Arthritis & Rheumatology* website at <https://onlinelibrary.wiley.com/doi/10.1002/art.42080>).

Of the 95 differentially expressed proteins, 40 proteins were elevated in NPSLE CSF compared to both healthy controls and neurologic disease controls at a fold change of ≥ 1.3 ; of these, 23 proteins were elevated in NPSLE CSF at a fold change of ≥ 2 compared to healthy controls ($P < 0.05$ by Mann-Whitney U test) and neurologic disease controls ($P < 0.1$ by Mann-Whitney U test). Eleven of these proteins exhibited q values less than 0.05, adjusted for false discovery rate, for multiple testing correction. The levels of the 23 most discriminatory CSF proteins are plotted as a heatmap in Figure 1C. Principal component analysis using these 23 CSF proteins (Figure 1D) successfully differentiated NPSLE patients from patients with other neurologic diseases or healthy individuals, with the first 2 principal components explaining 72.4% of the variance.

This panel of 23 CSF proteins with discriminatory potential in NPSLE included many proteins of immunologic importance (including complement C3, C3a, C3b, C3-des-arg, C1 esterase inhibitor, IgM, DC-SIGNR) interconnected via several functional networks, including cell-cell signaling, hematologic system development and function, cardiovascular disease, cell death and survival, and cellular development, based on Ingenuity Pathway Analysis (Supplementary Figure 2, available on the *Arthritis & Rheumatology* website at <https://onlinelibrary.wiley.com/doi/10.1002/art.42080>). The top transcription factor and signaling molecule regulating these up-regulated proteins in NPSLE were ETV6 and ETS1, respectively (Figures 2A and B). Correlation analysis of these 23 proteins revealed discrete clusters with similar expression profiles, with the largest cluster encompassing 5 complement proteins, as well as IgM and angiostatin (Figure 2C). We also carried out an orthogonal analysis using a machine learning algorithm, random forest analysis, to identify additional proteins that discriminate NPSLE CSF from that of controls. Random forest

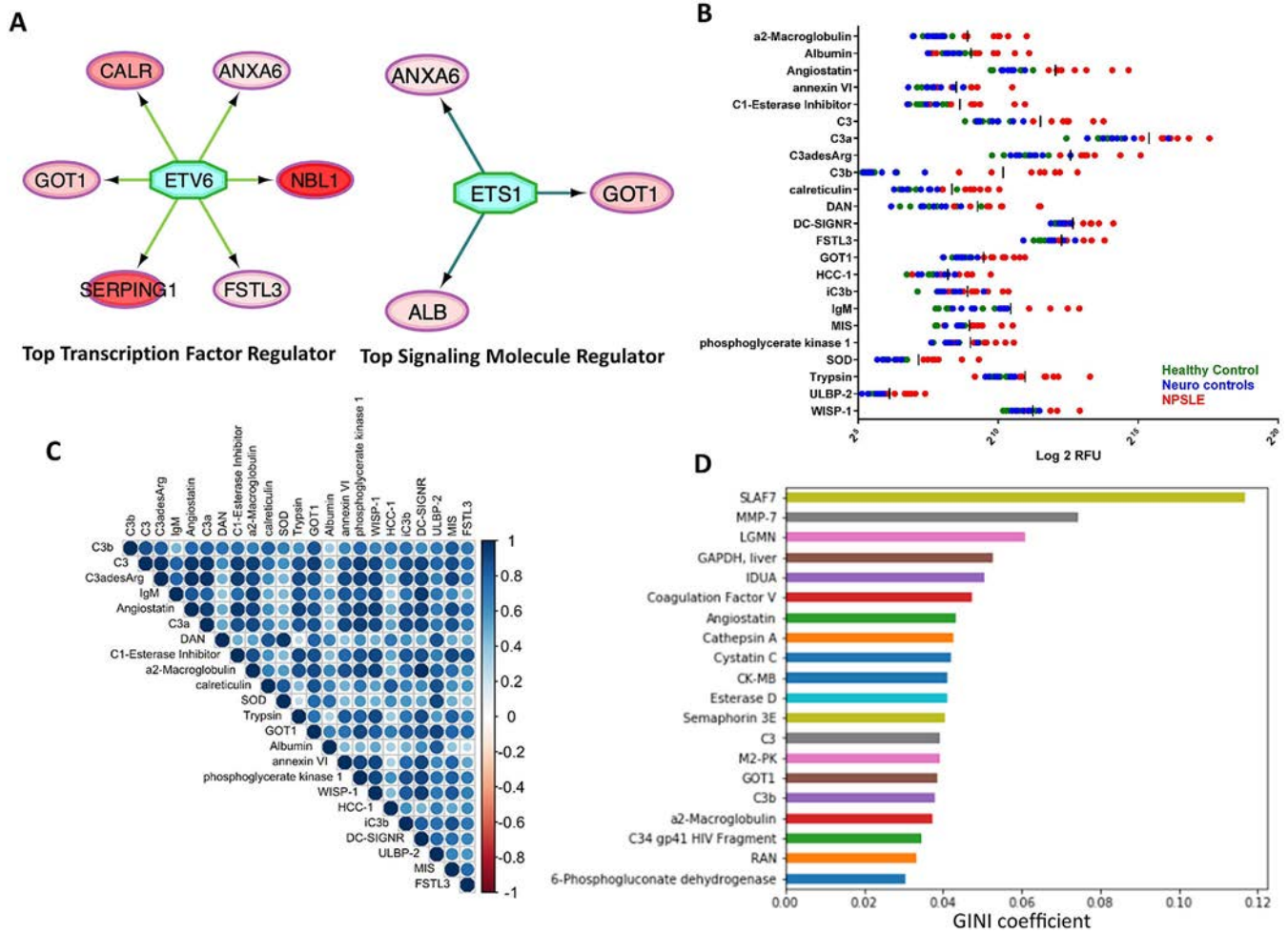


Figure 2. Functional grouping and discriminatory potential of 23 CSF proteins in NPSLE. Results were obtained from the discovery cohort (Halifax cohort), comprising 23 subjects (8 healthy controls, 7 neurologic disease controls, 8 NPSLE patients), as detailed in Supplementary Table 1 (available on the *Arthritis & Rheumatology* website at <https://onlinelibrary.wiley.com/doi/10.1002/art.42080>). **A**, Top transcription factor regulator (turquoise) (left) and top signaling molecule regulator (turquoise) (right) were identified for the top 23 proteins elevated in NPSLE patients ($P < 0.05$) via the iRegulon plugin for Cytoscape. Nodes with a fold change of ≥ 2 range in color from pink to red. **B**, Dot plot shows the expression levels of the most discriminatory 23 CSF proteins in healthy controls, neurologic disease controls, and NPSLE patients, according to aptamer-based screening. **C**, Based on their expression profiles in CSF from NPSLE patients, healthy controls, and neurologic disease controls, the most discriminatory 23 CSF proteins clustered into several subgroups, according to correlation analysis. **D**, Random forest analysis was performed using all differentially expressed CSF proteins (when comparing NPSLE patients to healthy controls/neurologic disease controls) as input. The 20 CSF proteins with the largest impact on classification, ordered by their Gini coefficient, are plotted. SLAF7 = SLAM family member 7; MMP-7 = matrix metalloproteinase 7; LGMN = legumain; IDUA = α -L-iduronidase; CK-MB = creatine kinase-MB; M2-PK = M2 pyruvate kinase; RAN = Ras-related nuclear protein (see Figure 1 for other definitions).

analysis revealed SLAM family member 7 and matrix metalloproteinase 7 as additional discriminatory molecules in CSF with a significant impact on NPSLE versus healthy control discrimination (Figure 2D).

These 23 proteins, as well as 3 additional proteins implicated in the murine NPSLE literature, lipocalin 2, M-CSF, and fibronectin 1 (FN1) (14,15,16) were evaluated for ELISA validation, as outlined in Supplementary Table 3 (available on the *Arthritis & Rheumatology* website at <https://onlinelibrary.wiley.com/doi/10.1002/art.42080>). Of these 26 proteins, 16 proteins were not pursued further, either because they exhibited similar expression profiles

with high correlation coefficients to other selected candidates or because their expression levels were very low on the aptamer screen, suggesting that they may fall below the detection limits of ELISA. The remaining 10 proteins were pursued with ELISA testing, including α 2-macroglobulin, angiostatin, complement C3, DAN, FN, hepatocellular carcinoma clone 1 (HCC-1), IgM, lipocalin 2, M-CSF, and serine protease inhibitor G1 (SERPING1).

Primary ELISA validation of CSF proteins in the Halifax NPSLE cohort. The 10 selected molecules were validated by ELISA in 79 CSF samples drawn from 24 NPSLE patients (Halifax

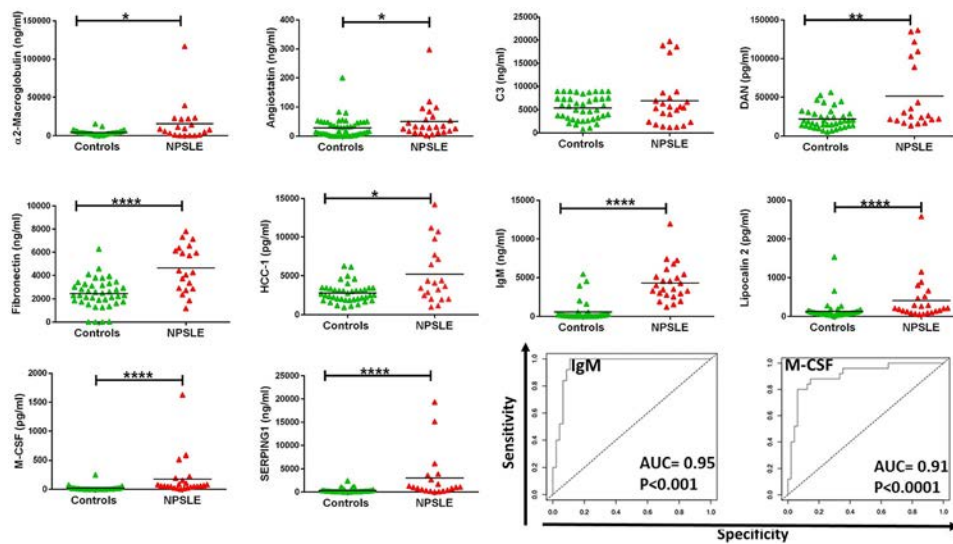


Figure 3. ELISA validation of CSF proteins in the Halifax cohort. Ten proteins were assessed by ELISA in CSF from 25 NPSLE patients and 54 neurologic disease controls. The control group included 31 patients with definite or probable multiple sclerosis or a wide array of other neurologic diseases, as detailed in Supplementary Table 2 (available on the *Arthritis & Rheumatology* website at <https://onlinelibrary.wiley.com/doi/10.1002/art.42080>). Symbols represent individual subjects; bars show the mean. * = $P < 0.05$; ** = $P < 0.01$; *** = $P < 0.001$; **** = $P < 0.0001$. In the bottom right panels, receiver operating characteristic curve analyses of CSF IgM and M-CSF are shown, displaying their ability to distinguish NPSLE patients from other neurologic disease patients. Data on the CSF protein lipocalin 2 have previously been reported (ref. 16). SERPING1 = serine protease inhibitor G1; AUC = area under the receiver operating characteristic curve (see Figure 1 for other definitions).

cohort, predominantly White) and 54 neurologic disease controls, as tabulated in Supplementary Table 2 (available on the *Arthritis & Rheumatology* website at <https://onlinelibrary.wiley.com/doi/10.1002/art.42080>). The 54 neurologic disease controls included 31 patients with definite or probable MS and patients with a wide array of neurologic diseases. Information on the kit manufacturer, CSF dilution, and selection criteria for these 10 molecules is listed in Supplementary Table 3. Angiostatin, DAN, HCC-1, IgM, lipocalin 2, M-CSF, α 2-macroglobulin, FN, and SERPING1 were validated to be significantly elevated in the CSF of NPSLE patients from the Halifax cohort ($P < 0.05$) (Figure 3). Whereas some CSF proteins exhibited a bimodal distribution in NPSLE patients (e.g., C3, FN1, HCC-1), others such as IgM exhibited a bell-shaped distribution.

Next, receiver operating curve (ROC) analysis was performed to ascertain which CSF proteins best distinguished NPSLE from other neurologic diseases. IgM (AUC 0.95), M-CSF (AUC 0.91), lipocalin 2 (AUC 0.82), FN (AUC 0.81), SERPING1 (AUC 0.78), DAN (AUC 0.75), HCC-1 (AUC 0.69), and angiostatin (AUC 0.65) best distinguished NPSLE patients from those with other neurologic diseases in the Halifax cohort, in order of diminishing discriminatory capacity (Table 1 and Figure 3). CSF IgM, angiostatin, and M-CSF were the most sensitive biomarkers (sensitivity range 80–100%), with IgM being the most sensitive (100%). In terms of specificity, CSF levels of complement C3, M-CSF, α 2-macroglobulin, IgM, FN, and HCC-1 were the most specific at distinguishing NPSLE patients from the neurologic disease controls, with CSF C3 having the highest specificity (100%) (Table 1). Most of the interrogated CSF proteins exhibited high

PPVs after adjustment for NPSLE prevalence; however, the NPVs of these proteins were modest. Of the 4 NPSLE patients with elevated C3 CSF levels, 3 presented with acute confusion; in contrast, only 2 of the 19 NPSLE patients with normal CSF C3 exhibited acute confusion ($P = 0.02$ by Fisher's exact test).

Bayesian network analysis was then performed using the expression levels of these 10 CSF proteins in the Halifax cohort. CSF IgM, DAN, HCC-1, and lipocalin 2 were revealed to have the strongest impact on this network, as reflected by their node size (Supplementary Figure 3, available on the *Arthritis & Rheumatology* website at <https://onlinelibrary.wiley.com/doi/10.1002/art.42080>). CSF IgM, FN, and M-CSF showed the highest association with disease classification status, with CSF IgM being the most dominant node force.

Secondary ELISA validation of CSF protein biomarkers in the Hong Kong NPSLE cohort. To ascertain whether the CSF proteins validated to be discriminatory of NPSLE in the Halifax cohort might also be predictive in other ethnicities, ELISA validation was performed using 32 CSF samples from the Hong Kong cohort, comprising 15 NPSLE patients and 17 healthy controls who had been evaluated for neurologic ailments using lumbar puncture but were otherwise found to be disease-free after neurologic examination and evaluation of routine CSF analysis. CSF levels of IgM, lipocalin 2, M-CSF, and SERPING1 were validated to be significantly elevated in NPSLE patients from the Hong Kong cohort compared to the healthy controls ($P < 0.05$) (Figure 4). ROC analysis revealed that CSF lipocalin 2 (AUC

Table 1. CSF proteins that best distinguish NPSLE from controls in the Halifax and Hong Kong NPSLE cohorts, based on ELISA*

Protein	CSF protein level, mean (median)		NPSLE patients vs. controls						
	NPSLE patients	Controls	Fold change	Cutoff level	AUC	Sensitivity, %	Specificity, %	PPV, %†	NPV, %‡
Halifax cohort (NPSLE patients, n = 24; controls, n = 54)									
α2-macroglobulin, pg/ml	149,961 (7,683) 49	3,805 (3,656) 28	3.9	7,683	0.63	52	93	93.2	59.4
Angiostatin, ng/ml	6,801 (5,497)	5,243 (4,994)	1.8	12	0.65‡	88	44	53.5	51.8
C3, ng/ml	52,113 (26,632)	22,074 (18,790)	1.3	17,392	0.51	16	100	45.1	46.7
DAN, pg/ml	4,577 (4,255)	2,440 (2,313)	2.4	21,457	0.75§	76	63	87.2	58.8
Fibronectin, pg/ml	5,080 (3,665)	2,804 (2,538)	1.9	3,539	0.81§	67	85	89.8	62.5
HCC-1, pg/ml	4,331 (4,030)	477	1.8	3,665	0.69‡	52	85	87.2	58.8
IgM, ng/ml	397 (206)	123	9.1	1,220	0.95§	100	89	87.6	62.6
Lipocalin 2, pg/ml	171	16	3.2	126	0.82§	76	80	88.3	57.2
M-CSF, pg/ml	2,861 (1,009)	304 (154)	10.4	41	0.91§	80	94	92.0	56.3
SERPING1, pg/ml			9.4	415	0.78¶	71	80	92.1	57.7
Hong Kong cohort (NPSLE patients, n = 17; controls, n = 15)									
α2-macroglobulin, pg/ml	27,104 (6,048) 25	4,595 (5,223) 38	5.9	10,530	0.60	35	100	100.0	54.8
Angiostatin, ng/ml	10,295 (2,617) 1,746 (879)	5,633 (6,536) 1,351 (1,434)	0.7	2	0.57	100	33	46.9	47.6
C3, ng/ml	3,257 (1,732) 884 (838)	4,584 (3,718) 973 (1,195)	1.8	10,115	0.37	18	100	100.0	54.8
DAN, pg/ml	9,204 (7,320) 313 (273)	4,239 (4,175) 193	1.3	2,546	0.45	30	100	43.1	45.2
Fibronectin, pg/ml			0.7	10,045	0.34	6	100	30.6	23.6
HCC-1, pg/ml			0.9	2,119	0.43	12	100	49.5	49.3
IgM, ng/ml			2.2	5,586	0.78#	70	100	100.0	65.4
Lipocalin 2, pg/ml			1.6	122	0.85§	94	80	75.5	59.6
M-CSF, pg/ml			2.0	95	0.71‡	47	100	87.6	63.8
SERPING1, ng/ml			4.5	558	0.68	59	93	100.0	58.6

* CSF = cerebrospinal fluid; ELISA = enzyme-linked immunosorbent assay; AUC = area under the receiver operating characteristic curve; PPV = positive predictive value; NPV = negative predictive value; HCC-1 = hepatocellular carcinoma clone 1; M-CSF = macrophage colony-stimulating factor; SERPING1 = serine protease inhibitor G1.

† Adjusted for prevalence of neuropsychiatric systemic lupus erythematosus (NPSLE) among SLE patients, set at 50%.

‡ P < 0.05 by Mann-Whitney U test.

§ P < 0.0001 by Mann-Whitney U test.

¶ P < 0.001 by Mann-Whitney U test.

P < 0.01 by Mann-Whitney U test.

0.85), IgM (AUC 0.78), and M-CSF (AUC 0.71) best distinguished NPSLE patients from healthy controls in the Hong Kong cohort (Table 1 and Figure 4). CSF angiostatin and lipocalin 2 were among the most sensitive biomarkers (sensitivity 100% and 94%, respectively), while CSF M-CSF, IgM, complement C3, HCC-1, FN, DAN, and α 2-macroglobulin were all equally specific (100%) in distinguishing NPSLE patients from healthy controls. Of note, CSF α 2-macroglobulin, IgM, C3, and SERPING1 exhibited high PPVs of 100%.

Overlap of NPSLE CSF proteome with choroid plexus transcriptome. We next explored the potential origins of the proteins found to be elevated in NPSLE CSF. Although transcriptomic data from the brain of a human NPSLE patient are not currently available, the transcriptome of the choroid plexus from the MRL/lpr murine model of lupus (in which NPSLE-like disease develops) has recently been reported, based on RNA-Seq analysis (17,18). We searched this database for the expression levels of the 40 CSF proteins significantly elevated in NPSLE CSF, based on the initial aptamer-based proteomic screening, as well as the 3 additional proteins selected for ELISA testing: M-CSF, lipocalin 2, and FN1. These 43 proteins represented 38 unique molecules. The corresponding genes for 32 of these 38 molecules were identified in the murine NPSLE choroid plexus transcriptome database (17). Interestingly, 11 of these 32 molecules were also significantly elevated in the murine NPSLE choroid plexus, with the rest being comparable in expression to the levels in the

healthy choroid plexus. When the fold ratios of these 11 molecules were found to be significantly elevated in NPSLE CSF and choroid plexus were plotted, a strong correlation was noted ($R = 0.63$, $P = 0.037$) (Figure 5), indicating that the higher the elevation of a marker in the choroid plexus, the higher its elevation is in the CSF. These results are consistent with the choroid plexus being an important source of the identified CSF biomarkers.

DISCUSSION

The diagnosis of NPSLE is clinically challenging, and the currently available tools are less than optimal. For example, no good and accurate way exists to distinguish primary NPSLE from secondary NPSLE. Indeed, neuropsychiatric manifestations are sometimes treated empirically, and if they respond to immunosuppression, NPSLE is inferred. We believe that proteomic investigations of blood and CSF will eventually lead to the fabrication of a serum- or CSF-based diagnostic panel that permits accurate diagnosis of NPSLE, with significantly higher specificity for this disease compared to other neuroinflammatory diseases or infections. This will become feasible when the entire (serum or CSF) proteome can be comprehensively interrogated, which is not currently possible. Such a panel will be clinically useful to diagnose NPSLE with high confidence. As alluded to below, the implicated proteins may also pave the way toward more effective therapeutics for NPSLE. Finally, these insights may also shed light on the

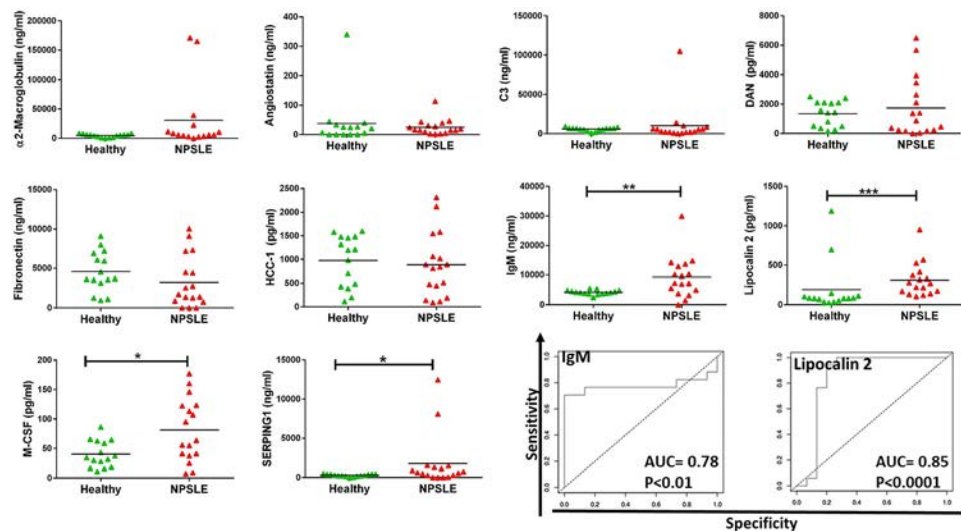


Figure 4. ELISA validation of CSF proteins in the Hong Kong cohort. Ten proteins were assessed by ELISA in CSF from 15 NPSLE patients and 17 healthy controls. The control group included individuals tested for neurologic ailments using lumbar puncture but who were otherwise found to be disease-free after neurologic evaluation and CSF analysis, as detailed in Supplementary Table 2 (available on the *Arthritis & Rheumatology* website at <https://onlinelibrary.wiley.com/doi/10.1002/art.42080>). Symbols represent individual subjects; bars show the mean. * = $P < 0.05$; ** = $P < 0.01$; *** = $P < 0.001$; **** = $P < 0.0001$. In the bottom right panels, receiver operating characteristic curve analyses of CSF IgM and lipocalin 2 are shown, displaying their ability to distinguish NPSLE patients from healthy controls. Data on the CSF protein lipocalin 2 have previously been reported (ref. 16). SERPING1 = serine protease inhibitor G1; AUC = area under the receiver operating characteristic curve (see Figure 1 for other definitions).

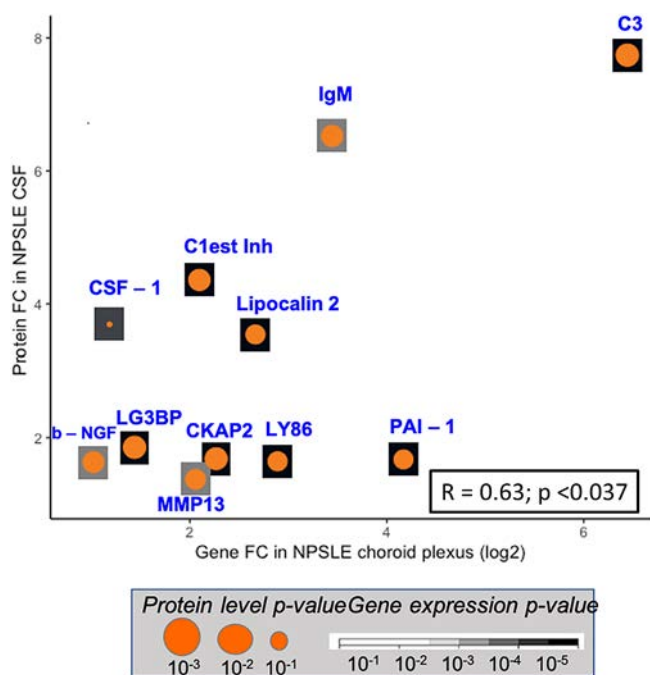


Figure 5. Fold change in CSF protein levels in NPSLE patients versus fold change in gene levels assessed in the choroid plexus murine lupus model. The choroid plexus transcriptome from a murine lupus model of NPSLE-like disease was searched for the expression levels of all 40 CSF proteins significantly elevated in the CSF of NPSLE patients, according to the initial aptamer-based proteomic screening, as well as 3 additional proteins selected for ELISA testing: M-CSF, lipocalin 2, and fibronectin 1. These 43 proteins represented 38 unique molecules. Of these 38 molecules, 32 could also be identified in the NPSLE choroid plexus mouse transcriptome. Eleven molecules were significantly elevated both in the CSF proteome (from this study) and the choroid plexus transcriptome. The respective fold ratios in the 2 omics data sets, shown plotted against each other, correlated with each other ($R = 0.63$, $P = 0.037$). The gene expression P value is indicated by the white to black color scale of each square, while the protein level P value is indicated by the size of the orange circle. See Figure 1 for definitions.

pathophysiology underlying NPSLE. The current CSF proteomic study is an initial step in that direction.

In the current study, we describe the largest ever targeted proteomic analysis of NPSLE CSF, using an aptamer-based platform that has the capacity to interrogate >1,000 protein targets. Several general themes emerge from this proteomic analysis. First, as previously reported for urine biomarkers in LN (11), this aptamer-based targeted proteomic approach has proven to be effective in identifying protein biomarker candidates that can successfully be validated by an orthogonal platform, ELISA. Second, as we have reported in LN (11), how well a biomarker performs can be significantly influenced by patient ethnicity, suggesting the importance of tailoring the biomarker to patient race and ethnicity.

Third, molecules that are hyperexpressed in diseased end-organs in SLE may become enriched in the body fluid draining or

bathing that tissue. Therefore, while urine may be the optimal fluid for identifying biomarkers for LN (11), CSF may be the preferred fluid for mining biomarkers for NPSLE, given the observation that 11 biomarker candidates were significantly enriched in the CSF and also the choroid plexus (albeit in different species), with a quantitative correlation. The fact that a correlation was even observed despite the species difference (humans versus mice) makes this all the more significant. The choroid plexus in both murine and human NPSLE has been shown to be enriched with tertiary lymphoid structures (17), which could easily serve as a source for CSF enriched biomarkers. Other proteins that are elevated in NPSLE CSF but not expressed or elevated in the NPSLE choroid plexus could have arisen from other parts of the brain, or simply filtered from the blood, especially in the case of blood-brain barrier disruption. The latter may explain the elevation of high abundance serum proteins such as albumin and α 2-macroglobulin in the CSF of these patients.

Fourth, the same proteins that are hyperexpressed in different tissues appear to be associated with different end-organ diseases. For example, several biomarker candidates reported here have been observed in a proteomic screening of LN, except that they were identified in different tissues. Thus, molecules such as complement proteins cystatin, DC-SIGNR, lipocalin 2, M-CSF, and superoxide dismutase may be generic biomarkers of SLE and reflect disease activity or organ damage. When the kidneys are targeted, these markers may be elevated in the urine (in part, due to leakage) while brain involvement may manifest with CSF elevations of these same molecules, although we have not established causality yet.

Finally, each of the identified molecules has interesting pathogenic and potential diagnostic ramifications, as discussed below. Several of the assayed CSF proteins, including α 2-macroglobulin, IgM, complement C3, M-CSF, and SERPING1 exhibited high specificity and PPVs for NPSLE diagnosis (Table 1). The diagnostic metrics calculated in Table 1 used a cutoff value to maximize sensitivity and specificity (i.e., the Youden index). Alternatively, setting a more stringent cutoff value (to maximize specificity/PPV) for these 5 CSF proteins enables attainment of 100% PPV in both NPSLE cohorts. Therefore, these 5 proteins have the potential to serve as diagnostic markers for NPSLE when the appropriate test cutoffs are used.

CSF IgM levels were significantly elevated in NPSLE patients compared to all controls in both the Halifax and Hong Kong cohorts ($P < 0.001$ and $P < 0.01$, respectively), with high ROC AUC values in both cohorts. Indeed, its ability to distinguish NPSLE from other neurologic diseases was 0.95 in the Halifax cohort. CSF IgM exhibited a sensitivity of 100% in both cohorts and a specificity of 100% in the Halifax cohort, bolstering its diagnostic potential in NPSLE, but further validation is warranted. Increased intrathecal IgM has been demonstrated in patients with MS, correlating with the subsequent development of pathologic magnetic resonance imaging (MRI) findings (19,20). Another

study showed a negative correlation between elevated intrathecal IgM levels and disease progression in MS, alluding to a possible protective role of IgM in patients with inflammatory CNS disease (21). Besides an elevated IgG index, an early study also suggested that the CSF IgM index might also be elevated in NPSLE (22). Various IgG autoantibodies have been described in NPSLE CSF, but IgM autoantibodies have not received similar attention (23–25). Plasma cells have been observed in CSF and brain tissue in MS (26,27). Given that activated B cells, germinal center B cells, and plasma cells are enriched in the NPSLE choroid plexus (17), with a parallel increase in IgM in the choroid plexus (Figure 5), this could potentially explain the elevated CSF IgM in NPSLE. Further studies are needed to ascertain the relative diagnostic utility of different immunoglobulin isotypes and specificities in NPSLE CSF.

The elevation in CSF lipocalin 2 in both NPSLE cohorts has recently been reported (16). Interestingly, this inflammatory mediator has been implicated in various disease processes, including renal disease (28,29), cerebral ischemia (30), cardiovascular diseases (31), chronic obstructive pulmonary disease (32), cancers (33–35), and retinal inflammation (36). Lipocalin 2 has been shown to be hyperexpressed within the brain in murine NPSLE, associated with glial cell apoptosis (16). This may be explained by either local production of lipocalin 2 in the brain (16) or from elevated serum lipocalin 2 levels associated with SLE (37). In the current study, relative to the other biomarker candidates, CSF lipocalin 2 ranked among the top few markers, in terms of the ROC AUC value, to distinguish NPSLE patients from controls. Indeed, in Chinese patients with NPSLE, CSF lipocalin 2 emerged as the most discriminatory marker.

M-CSF is a cytokine responsible for the growth and differentiation of monocyte–macrophage cell lineages. It is produced by a variety of cells, including endothelial cells, fibroblasts, osteoblasts, smooth muscle cells, and macrophages (38), and is a key factor that increases macrophage numbers and function in a variety of tissues (39). In this study, we found increased CSF levels of M-CSF in NPSLE patients compared to neurologic disease controls in the Halifax cohort ($P < 0.0001$; AUC 0.91) as well as in the Hong Kong cohort ($P < 0.05$). While previous studies have demonstrated elevated serum M-CSF levels in NPSLE, the current study is the first to demonstrate elevated levels in CSF. Importantly, the pathogenic relevance of M-CSF in murine NPSLE has recently been reported (15). M-CSF has been shown to play a role in other CNS pathologies, including MS and Alzheimer's disease (40–45). The choroid plexus could be one potential source for this cytokine in the CSF of NPSLE patients (Figure 5). Given its superior biomarker potential in NPSLE and its potential pathogenic and therapeutic relevance (17), future studies are warranted to further explore this in human NPSLE.

Interestingly, several complement proteins were elevated in NPSLE CSF (Figure 2), with complement C3 exhibiting the highest

fold increase in murine NPSLE choroid plexus of all molecules that overlapped between the CSF proteomic and choroid plexus transcriptomic data sets (Figure 5). Circulating complement consumption, which has been well documented in NPSLE (46), could readily be explained by the increased complement deposition within the damaged tissue in NPSLE (47), as demonstrated in LN. A previous study showed increased C3 in NPSLE, particularly in NPSLE patients presenting with acute confusional state (48), corroborating our own observation that 75% of the NPSLE patients with elevated CSF C3 had acute confusion. Given its high specificity and its unique association with acute confusional state, this diagnostic potential of CSF C3 warrants prospective trials in NPSLE patients. However, this may not be unique to NPSLE, as increased CSF complement and immune complexes have also been documented in MS, Alzheimer's disease, and depression (49–51).

Other CSF proteins elevated in NPSLE are suggestive of a breach in the blood–brain barrier, including FN and $\alpha 2$ -macroglobulin (48,52,53). We have recently reported that blood–brain barrier leakage in NPSLE is associated with gray matter loss and cognitive impairment (54). Collectively, the observed biomarker profiles suggest that the CSF proteome likely mirrors the underlying inflammation in the choroid plexus and other parts of the brain afflicted in NPSLE. Shortcomings of this study include the limited sample size for screening and validation and failure to include patients with other disease manifestations (e.g., aseptic meningitis). It would also be important to test the performance of these biomarkers in a cohort with paired serum/CSF and MRI data (indicating blood–brain barrier breach). A larger sample size is needed to validate the apparent association of CSF complement C3 with acute confusion. It is also important to expand the fraction of the human proteome interrogated so as to encompass other neurologic targets implicated in the NPSLE literature but not captured in this study, including microtubule-associated protein 2B, triosephosphate isomerase, and septin 7, among others (55,56).

ACKNOWLEDGMENT

We acknowledge the critical feedback received from Dr. Ioannis Parodis (Karolinska Institute, Sweden).

AUTHOR CONTRIBUTIONS

All authors were involved in drafting the article or revising it critically for important intellectual content, and all authors approved the final version to be published. Dr. Mohan had full access to all of the data in the study and takes responsibility for the integrity of the data and the accuracy of the data analysis.

Study conception and design. Mohan.

Acquisition of data. Vanarsa, Nidhi, Titus.


Analysis and interpretation of data. Vanarsa, Sasidharan, Duran, Gokaraju, Soomro, Stock, Der, Putterman, Greenberg, Mok, Hanly, Mohan.

REFERENCES

1. Hanly JG, Kozora E, Beyea SD, Birnbaum J. Nervous system disease in systemic lupus erythematosus: current status and future directions [review]. *Arthritis Rheumatol* 2019;71:33–42.
2. Ainiala H, Loukkola J, Peltola J, Korpela M, Hietaharju A. The prevalence of neuropsychiatric syndromes in systemic lupus erythematosus. *Neurology* 2001;57:496–500.
3. Hanly JG, Urowitz MB, Su L, Bae SC, Gordon C, Wallace DJ, et al. Prospective analysis of neuropsychiatric events in an international disease inception cohort of patients with systemic lupus erythematosus. *Ann Rheum Dis* 2010;69:529–35.
4. Schwartz N, Stock AD, Putterman C. Neuropsychiatric lupus: new mechanistic insights and future treatment directions [review]. *Nat Rev Rheumatol* 2019;15:137–52.
5. Afeltra A, Garzia P, Mitterhofer AP, Vadacca M, Galluzzo S, Del Porto F, et al. Neuropsychiatric lupus syndromes: relationship with antiphospholipid antibodies. *Neurology* 2003;61:108–10.
6. Syuto T, Shimizu A, Takeuchi Y, Tanaka S, Hasegawa M, Nagai Y, et al. Association of antiphosphatidylserine/prothrombin antibodies with neuropsychiatric systemic lupus erythematosus. *Clin Rheumatol* 2009;28:841–5.
7. Mackay M, Vo A, Tang CC, Small M, Anderson EW, Ploran EJ, et al. Metabolic and microstructural alterations in the SLE brain correlate with cognitive impairment. *JCI Insight* 2019;4:e124002.
8. West SG, Emlen W, Wener MH, Kotzin BL. Neuropsychiatric lupus erythematosus: a 10-year prospective study on the value of diagnostic tests. *Am J Med* 1995;99:153–63.
9. Bonfa E, Golombek SJ, Kaufman LD, Skelly S, Weissbach H, Brot N, et al. Association between lupus psychosis and anti-ribosomal P protein antibodies. *N Engl J Med* 1987;317:265–71.
10. Senécal J, Raymond Y. The pathogenesis of neuropsychiatric manifestations in systemic lupus erythematosus: a disease in search of autoantibodies, or autoantibodies in search of a disease? *J Rheumatol* 2004;31:2093–8.
11. Stanley S, Vanarsa K, Soliman S, Habazi D, Pedroza C, Gidley G, et al. Comprehensive aptamer-based screening identifies a spectrum of urinary biomarkers of lupus nephritis across ethnicities. *Nat Commun* 2020;11:2197.
12. SomaLogic. SOMAscan proteomic assay technical white paper. 2015, p. 1–14.
13. Hanly JG, Robichaud J, Fisk JD. Anti-NR2 glutamate receptor antibodies and cognitive function in systemic lupus erythematosus. *J Rheumatol* 2006;33:1553–8.
14. Stock AD, Wen J, Doerner J, Herlitz LC, Gulino M, Putterman C. Neuropsychiatric systemic lupus erythematosus persists despite attenuation of systemic disease in MRL/lpr mice. *J Neuroinflammation* 2015;12:205.
15. Chalmers SA, Wen J, Shum J, Doerner J, Herlitz L, Putterman C. CSF-1R inhibition attenuates renal and neuropsychiatric disease in murine lupus. *Clin Immunol* 2017;185:100–8.
16. Mike EV, Makinde HM, Gulino M, Vanarsa K, Herlitz L, Gadhi G, et al. Lipocalin-2 is a pathogenic determinant and biomarker of neuropsychiatric lupus. *J Autoimmun* 2019;96:59–73.
17. Stock AD, Der E, Gelb S, Huang M, Weidenheim K, Ben-Zvi A, et al. Tertiary lymphoid structures in the choroid plexus in neuropsychiatric lupus. *JCI Insight* 2019;4:e124203.
18. Jeltsch-David H, Muller S. Neuropsychiatric systemic lupus erythematosus and cognitive dysfunction: the MRL-lpr mouse strain as a model. *Autoimmun Rev* 2014;13:963–73.
19. Klein A, Selter RC, Hapfelmeier A, Berthele A, Müller-Myhsok B, Pongratz V, et al. CSF parameters associated with early MRI activity in patients with MS. *Neurol Neuroimmunol Neuroinflamm* 2019;6:e573.
20. Abdelhak A, Hottenrott T, Mayer C, Hintereder G, Zettl UK, Stich O, et al. CSF profile in primary progressive multiple sclerosis: re-exploring the basics. *PLoS One* 2017;12:e0182647.
21. Wen J, Stock AD, Chalmers SA, Putterman C. The role of B cells and autoantibodies in neuropsychiatric lupus. *Autoimmun Rev* 2016;15:890–5.
22. Emerudh J, Olsson T, Lindström F, Skogh T. Cerebrospinal fluid immunoglobulin abnormalities in systemic lupus erythematosus. *J Neurol Neurosurg Psychiatry* 1985;48:807–13.
23. Hirohata S, Arinuma Y, Takayama M, Yoshio T. Association of cerebrospinal fluid anti-ribosomal P protein antibodies with diffuse psychiatric/neuropsychological syndromes in systemic lupus erythematosus. *Arthritis Res Ther* 2007;9:R44.
24. Arinuma Y, Yanagida T, Hirohata S. Association of cerebrospinal fluid anti-NR2 glutamate receptor antibodies with diffuse neuropsychiatric systemic lupus erythematosus. *Arthritis Rheum* 2008;58:1130–5.
25. Yamada Y, Nozawa K, Nakano S, Mitsuo Y, Hiruma K, Doe K, et al. Antibodies to microtubule-associated protein-2 in the cerebrospinal fluid are a useful diagnostic biomarker for neuropsychiatric systemic lupus erythematosus. *Mod Rheumatol* 2016;26:562–8.
26. Pollok K, Mothes R, Ulbricht C, Liebheit A, Gerken JD, Uhlmann S, et al. The chronically inflamed central nervous system provides niches for long-lived plasma cells. *Acta Neuropathol Commun* 2017;5:88.
27. Confavreux C, Caudie C, Touraine F, Ventre JJ, Aimard G, Devic M. Plasma cells in cerebrospinal fluid and multiple sclerosis: diagnostic yield and clinicobiological correlations. *Acta Neurol Scand* 1986;74:432–8.
28. Sun WY, Bai B, Luo C, Yang K, Li D, Wu D, et al. Lipocalin-2 derived from adipose tissue mediates aldosterone-induced renal injury. *JCI Insight* 2018;3:e120196.
29. Gan J, Zhou X. Comparison of urine neutrophil gelatinase-associated lipocalin and interleukin-18 in prediction of acute kidney injury in adults. *Medicine* 2018;97:e12570.
30. Zhao N, Xu X, Jiang Y, Gao J, Wang F, Xu X, et al. Lipocalin-2 may produce damaging effect after cerebral ischemia by inducing astrocytes classical activation. *J Neuroinflammation* 2019;16:168.
31. Sivalingam Z, Larsen SB, Grove EL, Hvas A, Kristensen SD, Magnusson NE. Neutrophil gelatinase-associated lipocalin as a risk marker in cardiovascular disease. *Clin Chem Lab Med* 2017;56:5–18.
32. Wang Y, Jia M, Yan X, Cao L, Barnes PJ, Adcock IM, et al. Increased neutrophil gelatinase-associated lipocalin (NGAL) promotes airway remodelling in chronic obstructive pulmonary disease. *Clin Sci (Lond)* 2017;131:1147–59.
33. Gomez-Chou SB, Swidnicka-Siergiejko AK, Badi N, Chavez-Tomar M, Lesinski GB, Bekaii-Saab T, et al. Lipocalin-2 promotes pancreatic ductal adenocarcinoma by regulating inflammation in the tumor microenvironment. *Cancer Res* 2017;77:2647–60.
34. Cymbaluk-Płoska A, Chudecka-Głaz A, Pius-Sadowska E, Machaliński B, Sompolska-Rzechuła A, Kwiatkowski S, et al. The role of lipocalin-2 serum levels in the diagnostics of endometrial cancer. *Cancer Biomark* 2019;24:315–24.
35. Hu C, Yang K, Li M, Huang W, Zhang F, Wang H. Lipocalin 2: a potential therapeutic target for breast cancer metastasis. *Oncotargets Ther* 2018;11:8099–106.
36. Parmar T, Parmar VM, Perusek L, Georges A, Takahashi M, Crabb JW, et al. Lipocalin 2 plays an important role in regulating inflammation in retinal degeneration. *J Immunol* 2018;200:3128–41.
37. Abella V, Scotece M, Conde J, Gómez R, Lois A, Pino J, et al. The potential of lipocalin-2/NGAL as biomarker for inflammatory and metabolic diseases [review]. *Biomarkers* 2015;20:565–71.
38. Ushach I, Zlotnik A. Biological role of granulocyte macrophage colony-stimulating factor (GM-CSF) and macrophage colony-stimulating factor

- (M-CSF) on cells of the myeloid lineage. *J Leukoc Biol* 2016;99:481–9.
39. Rojo R, Raper A, Ozdemir DD, Lefevre L, Grabert K, Wollscheid-Lengeling E, et al. Deletion of a *Csf1r* enhancer selectively impacts CSF1R expression and development of tissue macrophage populations. *Nat Commun* 2019;10:3215.
 40. Jin W, Shi SX, Li Z, Li M, Wood K, Gonzales RJ, et al. Depletion of microglia exacerbates postischemic inflammation and brain injury. *J Cereb Blood Flow Metab*;37:2224–36.
 41. Konno T, Kasanuki K, Ikeuchi T, Dickson DW, Wszolek ZK. CSF1R-related leukoencephalopathy: a major player in primary microgliopathies [review]. *Neurology* 2018;91:1092–104.
 42. Pons V, Rivest S. New therapeutic avenues of mCSF for brain diseases and injuries. *Front Cell Neurosci* 2018;12:499.
 43. Du Yan S, Zhu H, Fu J, Yan SF, Roher A, Tourtellotte WW, et al. Amyloid- β peptide–receptor for advanced glycation endproduct interaction elicits neuronal expression of macrophage-colony stimulating factor: a proinflammatory pathway in Alzheimer disease. *Proc Natl Acad Sci* 1997;94:5296–301.
 44. Laske C, Stransky E, Hoffmann N, Maetzler W, Straten G, Eschweiler GW, et al. Macrophage colony-stimulating factor (M-CSF) in plasma and CSF of patients with mild cognitive impairment and Alzheimer's disease. *Curr Alzheimer Res* 2010;7:409–14.
 45. Xu C, Fu F, Li X, Zhang S. Mesenchymal stem cells maintain the microenvironment of central nervous system by regulating the polarization of macrophages/microglia after traumatic brain injury. *Int J Neurosci* 2017;127:1124–35.
 46. Magro-Checa C, Schaarenburg RA, Beart HJ, Huizinga TW, Steup-Beekman GM, Trouw LA. Complement levels and anti-C1q autoantibodies in patients with neuropsychiatric systemic lupus erythematosus. *Lupus* 2016;25:878–88.
 47. Cohen D, Rijnink EC, Nabuurs RJA, Steup-Beekman GM, Versluis MJ, Emmer BJ, et al. Brain histopathology in patients with systemic lupus erythematosus: identification of lesions associated with clinical neuropsychiatric lupus syndromes and the role of complement. *Rheumatology (Oxford, England)* 2017;56:77–86.
 48. Asano T, Ito H, Kariya Y, Hoshi K, Yoshihara A, Ugawa Y, et al. Evaluation of blood-brain barrier function by quotient $\alpha 2$ macroglobulin and its relationship with interleukin-6 and complement component 3 levels in neuropsychiatric systemic lupus erythematosus. *PLoS One* 2017;12:e0186414.
 49. Daborg J, Andreasson U, Pekna M, Lautner R, Hanse E, Minthon L, et al. Cerebrospinal fluid levels of complement proteins C3, C4 and CR1 in Alzheimer's disease. *J Neural Transm (Vienna)* 2012;119:789–97.
 50. Jans H, Heltberg A, Zeeberg I, Kristensen JH, Fog T, Raun NE. Immune complexes and the complement factors C4 and C3 in cerebrospinal fluid and serum from patients with chronic progressive multiple sclerosis. *Acta Neurol Scand* 1984;69:34–8.
 51. Pillai A, Bruno D, Nierenberg J, Pandya C, Feng T, Reichert C, et al. Complement component 3 levels in the cerebrospinal fluid of cognitively intact elderly individuals with major depressive disorder. *Biomark Neuropsychiatry* 2019;1:100007.
 52. Suzuki Y, Hashimoto K, Hoshi K, Ito H, Kariya Y, Miyazaki K, et al. Ratio of $\alpha 2$ -macroglobulin levels in cerebrospinal fluid and serum: an expression of neuroinflammation in acute disseminated encephalomyelitis. *Pediatr Neurol* 2019;98:61–7.
 53. Stock AD, Gelb S, Pasternak O, Ben-Zvi A, Putterman C. The blood brain barrier and neuropsychiatric lupus: new perspectives in light of advances in understanding the neuroimmune interface. *Autoimmun Rev* 2017;16:612–19.
 54. Kamintsky L, Beyea SD, Fisk JD, Hashmi JA, Omisade A, Calkin C, et al. Blood-brain barrier leakage in systemic lupus erythematosus is associated with gray matter loss and cognitive impairment. *Ann Rheum Dis* 2020;79:1580–87.
 55. Lefranc D, Launay D, Dubucquoi S, de Seze J, Dussart P, Vermersch M, et al. Characterization of discriminant human brain antigenic targets in neuropsychiatric systemic lupus erythematosus using an immunoproteomic approach. *Arthritis Rheum* 2007;56:3420–32.
 56. Sato S, Yashiro M, Asano T, Kobayashi H, Watanabe H, Migita K. Association of anti-triosephosphate isomerase antibodies with aseptic meningitis in patients with neuropsychiatric systemic lupus erythematosus. *Clin Rheumatol* 2017;36:1655–9.

Critical Role of Notch-1 in Mechanistic Target of Rapamycin Hyperactivity and Vascular Inflammation in Patients With Takayasu Arteritis

Wanwan Jiang,¹ Mengyao Sun,² Ying Wang,¹ Ming Zheng,¹ Zixin Yuan,¹ Shixiong Mai,³ Xin Zhang,³ Longhai Tang,⁴ Xiyu Liu,³ Chunhong Wang,¹ and Zhenke Wen¹ 

Objective. Takayasu arteritis (TA) is a major type of large vessel vasculitis characterized by progressive inflammation in vascular layers. In our recent study we identified a central role of mechanistic target of rapamycin (mTOR) hyperactivity in proinflammatory T cell differentiation in TA. This study was undertaken to explore potential mechanisms underpinning T cell–intrinsic mTOR hyperactivity and vascular inflammation in TA, with a focus on Notch-1.

Methods. Notch-1 expression and activity was determined according to Notch-1, activated Notch-1, and HES-1 levels. We detected mTOR activity with intracellular expression of phosphorylated ribosomal protein S6. Differentiation of proinflammatory T cells was analyzed by detecting Th1 and Th17 lineage-determining transcription factors. The function of Notch-1 was evaluated using γ -secretase inhibitor DAPT and gene knockdown using a short hairpin RNA (shRNA) strategy. We performed our translational study using humanized NSG mouse chimeras in which human vasculitis was induced using immune cells from TA patients.

Results. CD4⁺ T cells from TA patients exerted Notch-1^{high}, leading to mTOR hyperactivity and spontaneous maldifferentiation of Th1 cells and Th17 cells. Blockade of Notch-1 using DAPT and Notch-1 shRNA efficiently abrogated mTOR complex 1 (mTORC1) activation and proinflammatory T cell differentiation. Mechanistically, Notch-1 promoted mTOR expression, interacted with mTOR, and was associated with lysosomal localization of mTOR. Accordingly, systemic administration of DAPT and CD4⁺ T cell–specific gene knockdown of Notch-1 could alleviate vascular inflammation in humanized TA chimeras.

Conclusion. Expression of Notch-1 is elevated in CD4⁺ T cells from TA patients, resulting in mTORC1 hyperactivity and proinflammatory T cell differentiation. Targeting Notch-1 is a promising therapeutic strategy for the clinical management of TA.

INTRODUCTION

Takayasu arteritis (TA), a chronic and progressive autoimmune large vessel vasculitis (LVV) that mainly affects the aorta and major branches, is seen in all ethnicities around the world with increasing prevalence rates (1). While the mainstay of TA treatment is limited to

nonspecific glucocorticoids, a number of studies have shown that CD4⁺ T cells play a critical role in driving vascular inflammation in TA (1–4). Specifically, Th1 cells and Th17 cells are the dominant proinflammatory T cell subsets that infiltrate the adventitia layer, leading to vascular inflammation in TA (1,5–7). Thus, investigations regarding the maldifferentiation of proinflammatory T cells are

Supported by the National Natural Science Foundation of China (grants 82071826 and 82000445), National Natural Science Foundation of Jiangsu Province (grants BK20211542 and BK20201407), Priority Academic Program Development of Jiangsu Higher Education Institutions, Jiangsu Specially-Appointed Professor Program, Suzhou Municipal Science and Technology Bureau (grant ZXL2022460), Suzhou Municipal Health Commission (grant GWZX202004), National Natural Science Foundation of Jilin Province (grant YDZJ202101ZYTS116), and Education Department of Jilin Province (grant JJKH20211122KJ).

¹Wanwan Jiang, BS, Ying Wang, BS, Ming Zheng, MS, Zixin Yuan, BS, Chunhong Wang, MD, Zhenke Wen, MD, PhD: Soochow University, Suzhou, China; ²Mengyao Sun, MD: First Hospital of Jilin University, Changchun, China; ³Shixiong Mai, MD, Xin Zhang, MD, Xiyu Liu, MD, PhD: China–Japan Union Hospital of Jilin University, Changchun, China; ⁴Longhai Tang, MD: Suzhou Blood Center, Suzhou, China.

Ms. Jiang, Dr. Sun, Ms. Y. Wang, and Ms. Zheng contributed equally to this work.

Author disclosures are available at <https://onlinelibrary.wiley.com/action/downloadSupplement?doi=10.1002%2Fart.42103&file=art42103-sup-0001-Disclosureform.pdf>.

Address correspondence to Xiyu Liu, MD, PhD, Department of Thoracic Surgery, China–Japan Union Hospital of Jilin University, Changchun 130033, China (email: xiyuliu2020@jlu.edu.cn); or to Chunhong Wang, MD, Cyrus Tang Hematology Center, State Key Laboratory of Radiation Medicine and Protection, Soochow University, Suzhou 215123, China (email: wangch@suda.edu.cn); or to Zhenke Wen, MD, PhD, Jiangsu Key Laboratory of Infection and Immunity, Institutes of Biology and Medical Sciences, Soochow University, Suzhou, Jiangsu 215123, China (email: zkwen@suda.edu.cn).

Submitted for publication September 27, 2021; accepted in revised form February 17, 2022.

relevant in elucidating TA pathogenesis and exploring therapeutic strategies.

Mechanistic target of rapamycin (mTOR) coordinates eukaryotic cell growth and metabolism with environmental nutrients and growth factors, playing a central role in regulating many fundamental cell processes, from protein synthesis to autophagy (8–10). Mechanistic target of rapamycin complex 1 (mTORC1), which contains the specific subunit regulatory-associated protein of mechanistic target of rapamycin (RAPTOR) and is sensitive to rapamycin, is well known for controlling the differentiation of Th1 cells and Th17 cells (11–14). In contrast, mTORC2 is believed to be essential for Th2 cell differentiation (12,13). In our recent study, we identified mTORC1 hyperactivity as a critical signature in CD4+ T cells in TA patients driving spontaneous maldifferentiation of proinflammatory T cells (1). Inhibiting mTORC1 using rapamycin or RAPTOR short hairpin RNA (shRNA) abrogates maldifferentiation of proinflammatory T cells from TA patients (1). Blocking mTORC1 can alleviate vascular inflammation in humanized TA chimeras (1). However, the mechanisms underpinning mTORC1 hyperactivity in TA T cells are not fully understood; therefore, a greater understanding of these mechanisms might expand the therapeutic targets in TA.

Notch-1 is a conserved receptor that controls the differentiation and function of multiple cell types, including immune cells (12,15–17). A significant amount of evidence has indicated that Notch-1 signaling plays an important role in CD4+ T cell differentiation and function (12,18–21). Of note, CD4+ T cells from patients with giant cell arteritis (GCA), another type of LVV, have increased Notch-1 activity that results in proinflammatory T cell differentiation (12). Upon stimulation by high levels of circulating vascular endothelial growth factor (VEGF), microendothelial cells in the adventitia of GCA-affected arteries express Jagged-1, forming a structural niche to induce Notch-1 activity in contacted CD4+ T cells (12). Such Notch-1^{high} activity in GCA T cells results in Akt/mTORC1 activation, which promotes the differentiation of Th1 cells and Th17 cells (12). Collectively, Notch-1 signaling could be a master regulator of mTORC1 activity in T cells. These findings allow us to explore whether Notch-1 is involved in mTORC1^{high} in T cells in TA patients.

In this study, we aimed to elucidate the potential function of Notch-1 in regulating mTORC1 activity and proinflammatory T cell differentiation in TA patients. We identified Notch-1^{high} as a cell-intrinsic signature of TA T cells leading to mTORC1^{high} and proinflammatory T cell differentiation. Of importance, we learned that Notch-1 physically interacts with mTOR and is associated with lysosomal mTOR localization. Targeting Notch-1 may be a promising therapeutic strategy in TA.

PATIENTS AND METHODS

All data included in current study are available upon reasonable request from the corresponding authors.

Patients. In total, 69 TA patients and 38 age-matched healthy individuals were enrolled in this study. A total of 20 patients with small vessel vasculitis granulomatosis with polyangiitis (GPA) were recruited as the control. Clinical characteristics of TA and GPA patients are summarized in Supplementary Table 1 (available on the *Arthritis & Rheumatology* website at <http://onlinelibrary.wiley.com/doi/10.1002/art.42103>). Human aortic arteries were collected from surgery tissue, and informed consent was obtained from all participants. All experiments were performed in compliance with the Declaration of Helsinki and approved by the Soochow University Institutional Review Board.

Cell isolation and culture. Cell isolation and culture were performed as previously described (1,11). Specifically, peripheral blood mononuclear cells (PBMCs) were isolated by gradient centrifugation using lymphocyte separation medium (Corning). CD4+ T cells were purified from PBMCs using a human CD4+ T cell enrichment kit (StemCell Technologies), with a cell purity consistently >95%. Cells were cultured in RPMI 1640 medium supplemented with 10% fetal bovine serum (ThermoFisher Scientific) and penicillin/streptomycin/glutamine (ThermoFisher Scientific).

Reagents. The Notch-1 inhibitor DAPT and mTORC1 inhibitor rapamycin were purchased from Sigma-Aldrich. Human Notch-1 shRNA, RAPTOR shRNA, and the control shRNA were from Santa Cruz Biotechnology. Nucleofector kits from Lonza were used for T cell transfections. All reagents were used according to the manufacturers' instructions.

T cell differentiation. Proinflammatory Th1 and Th17 cells were identified as previously described (1,11,12). Briefly, CD4+ T cells were stimulated with anti-CD3/CD28 beads (cell: bead ratio 2:1) (ThermoFisher Scientific) for 4 days, followed by analyses of lineage-determining transcription factors, including T-bet and retinoic acid receptor-related orphan nuclear receptor γ (ROR γ), using flow cytometry.

Flow cytometry. T cells were treated with Fix buffer I (BD Biosciences) and Perm buffer III (BD Biosciences) and stained with antibodies as follows: fluorescein isothiocyanate/allophycocyanin (APC)–Cy7 anti-CD4 (clone OKT4; BioLegend), phycoerythrin (PE)–anti-T-bet (clone eBio4B10; ThermoFisher Scientific), APC–anti-ROR γ (clone AFKJS-9; ThermoFisher Scientific), PE–anti-phosphorylated S6RP (Ser^{235/236}) (clone D57.2.2E; Cell Signaling Technology), PE–anti-Notch-1 (12-5785-82; ThermoFisher Scientific), mouse anti-Notch-1 (sc-373891; Santa Cruz Biotechnology) with Alexa Fluor 647 anti-mouse IgG (A-21235; ThermoFisher Scientific), Alexa Fluor 488 Anti-HES-1 antibody (ab196328; Abcam), rabbit anti-activated Notch-1 (ab52301; Abcam), rabbit anti-RAPTOR (42-4000; ThermoFisher Scientific), and rabbit anti-phosphorylated Akt (9271S; Nucleofector) with Alexa Fluor 488 anti-rabbit IgG (A-11034; ThermoFisher Scientific).

Scientific). Cells were stained for 45 minutes at 4°C. Flow cytometry was performed on an LSR II flow cytometer (BD Biosciences). Data were analyzed using FlowJo software (Tree Star).

Immunofluorescence. Protein expression of human CD3 and interferon- γ (IFN γ) in arterial tissue sections were detected by immunostaining as previously described (1,11,12). Briefly, frozen sections of arterial tissue were stained with mouse anti-human CD3 antibody (1:100) (clone SPV-T3b; ThermoFisher Scientific) and visualized using Alexa Fluor 594 anti-mouse IgG (1:200) (A-11032; ThermoFisher Scientific). Rabbit anti-human IFN γ antibody (1:50) (ab9657; Abcam) and Alexa Fluor 488 anti-rabbit IgG (1:200) (A-11034; ThermoFisher Scientific) were used to stain

human IFN γ . Images of the stained sections were acquired using a LSM710 confocal microscope (Carl Zeiss) with a Plan neofluar 40 \times /1.3na oil objective lens.

Immunoblotting and immunoprecipitation.

Immunoblotting and coimmunoprecipitation were performed as previously described (11,22). The antibodies used were anti-mTOR (sc-517464; Santa Cruz Biotechnology), anti-phosphorylated S6 ribosomal protein (sc-293144; Santa Cruz Biotechnology), anti-S6 ribosomal protein (sc-74459; Santa Cruz Biotechnology), anti-Notch-1 (sc-373891; Santa Cruz Biotechnology), anti-phosphorylated Akt (Ser⁴⁷³) (9271; Cell Signaling Technology), anti-Akt (9272; Cell Signaling Technology), and anti-lysosome-associated

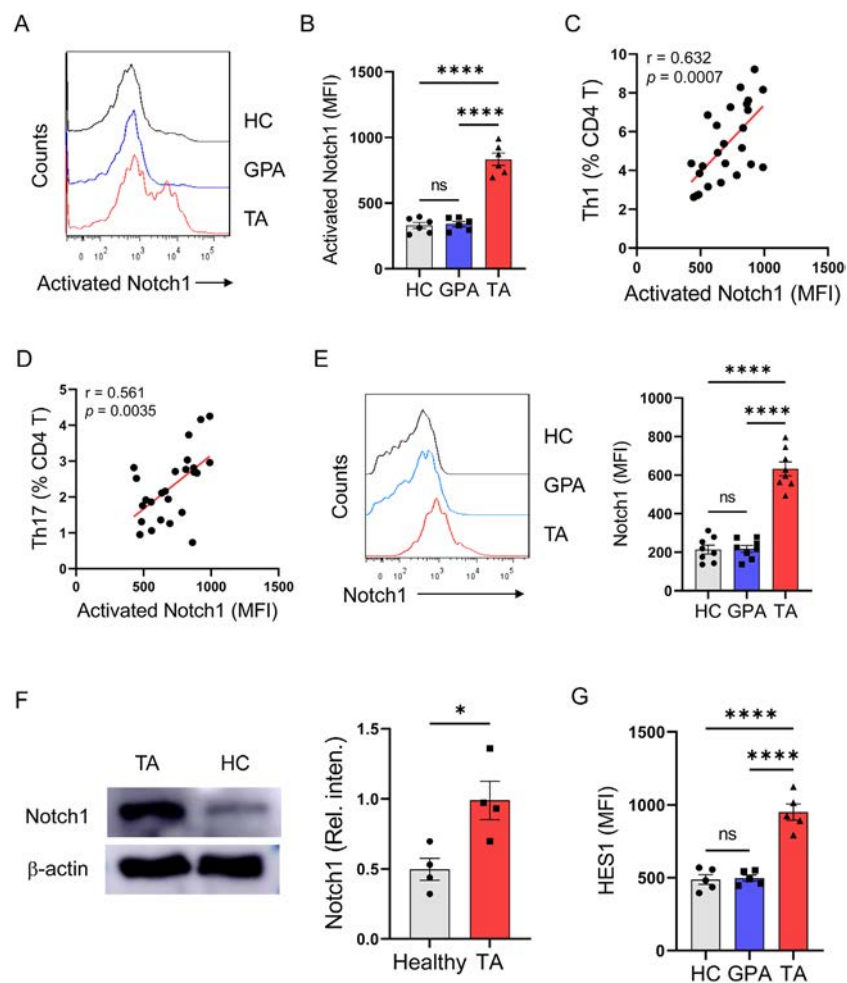


Figure 1. Notch-1 hyperactivity and maldifferentiation of CD4⁺ T cells in patients with Takayasu arteritis (TA). **A** and **B**, CD4⁺ T cells gated from fresh peripheral blood mononuclear cells from 6 TA patients (2 untreated; 4 women) were analyzed for intracellular levels of activated Notch-1. Six age-matched healthy control subjects (HCs, 3 women) and 6 patients with granulomatosis with polyangiitis (GPA) (2 untreated; 3 women) were included as control groups. Representative histograms (**A**) and quantification of the values (**B**) are shown. **C** and **D**, Intracellular levels of activated Notch-1 in CD4⁺ T cells correlated with frequencies of T-bet-expressing Th1 cells (**C**) and retinoic acid receptor-related orphan nuclear receptor γ -expressing Th17 cells (**D**) in 25 TA patients (3 untreated; 19 women) as analyzed with Pearson's correlation coefficient. **E–G**, CD4⁺ T cells from 17 age-matched TA patients receiving treatment (13 women), 12 GPA patients receiving treatment (9 women), and healthy controls were stimulated with anti-CD3/CD28 beads for 3 days, after which we investigated for the expression of Notch-1 (**E** and **F**) and HES-1 (**G**). In **B** and **E–G**, bars show the mean \pm SEM; symbols represent individual samples. * = $P < 0.05$ by unpaired t -test; **** = $P < 0.0001$ by analysis of variance and Tukey's multiple comparisons test. MFI = mean fluorescence intensity; NS = not significant; Rel. inten. = relative intensity. Color figure can be viewed in the online issue, which is available at <http://onlinelibrary.wiley.com/doi/10.1002/art.42103/abstract>.

membrane protein 1 (sc-20011; Santa Cruz Biotechnology). As an internal control, we used β -actin, detected with anti- β -actin (sc-81178; Santa Cruz Biotechnology).

Humanized TA chimeras. Human artery–NSG mouse chimeras representing human TA were generated as previously described (1). Briefly, 8-week-old NSG mice (Biocytogen) were housed in institutional pathogen-free animal facilities and subcutaneously engrafted with human arterial tissue fragments. Buprenorphine (0.125 mg/kg body weight) was used to control the postsurgical pain. The human artery–NSG mouse chimeras were intraperitoneally injected with lipopolysaccharide (10 μ g/mouse) (Sigma) on day 9 and were reconstituted with PBMCs (15×10^6 cells/mouse) from patients with active TA on day 10. Chimeras implanted with arterial pieces from the same donor were randomly assigned to control and treatment groups. DAPT treatment (100 mg/kg) was achieved by intraperitoneal injection after immune reconstitution (23,24). For some experiments, CD4+ T cells were isolated from the TA PBMCs, transfected with Notch-1 shRNA or control shRNA, and injected into the chimeras together with the CD4-T–depleted TA PBMCs for immune reconstitution. Human arterial graft explants were collected on day 25 for the detection of vasculitis. Experiments were conducted in accordance with the Animals in Research: Reporting In Vivo Experiments guidelines and approved by Animal Care and Use Committee of Soochow University.

Statistical analysis. Data are presented as the mean \pm SEM. Student's *t*-test was used for 2-group comparisons with Bonferroni correction for multiple comparisons. Analysis of variance with Tukey's multiple comparisons test was used for comparisons of >2 groups. We used Pearson's correlation coefficient for testing correlations. All statistics were performed using GraphPad Prism 9.0, and *P* values less than 0.05 were considered significant.

RESULTS

Exertion of Notch-1^{high} and spontaneous proinflammatory T cell differentiation in CD4+ T cells from TA patients. To detect the possible involvement of Notch-1 signaling in proinflammatory T cell differentiation in TA patients, CD4+ T cells were gated from freshly isolated PBMCs from TA patients, GPA patients, and healthy controls, to analyze protein expression of activated Notch-1. We observed higher expression of activated Notch-1 in CD4+ T cells from TA patients, associated with circulating frequencies of Th1 cells and Th17 cells in TA patients (Figures 1A–D).

To understand whether Notch-1^{high} is a cell-intrinsic signature for TA CD4+ T cells, CD4+ T cells were isolated from TA PBMCs and stimulated with anti-CD3/CD28 beads to detect Notch-1 expression and activity. As expected, TA CD4+ T cells exerted higher Notch-1 expression and activity compared to CD4+ T cells from GPA patients and healthy individuals

(Figures 1E–G and Supplementary Figure 1, <http://onlinelibrary.wiley.com/doi/10.1002/art.42103>), accompanied by elevated maldifferentiation of Th1 cells and Th17 cells (1) (Supplementary Figure 1B). Notch-1^{high} expression was not exclusive to CD4+ T cells and was also observed in CD8+ T cells and B cells from TA patients (Supplementary Figure 2, <http://onlinelibrary.wiley.com/doi/10.1002/art.42103>). Essentially, T cells from TA patients express cell-intrinsic Notch-1^{high}, reflecting proinflammatory T cell differentiation.

Critical role of Notch-1 signaling in proinflammatory T cell differentiation in TA patients. To determine the function of Notch-1 signaling in the maldifferentiation of proinflammatory T cells in TA patients, CD4+ T cells were isolated from TA PBMCs and stimulated with anti-CD3/CD28 beads in the presence or absence of DAPT. Inhibition of Notch-1 with DAPT efficiently abrogated Th1/Th17 cell differentiation in TA T cells (Figures 2A and B). Gene knockdown of Notch-1 using shRNA also impaired proinflammatory T cell differentiation of TA T cells (Figures 2C and D and Supplementary Figure 3, <http://onlinelibrary.wiley.com/doi/10.1002/art.42103>). Vice versa, transfection of Notch-1 intracellular domain (NICD) in healthy CD4+ T cells resulted in enhanced differentiation of proinflammatory T cells, mimicking the TA CD4+ T cells (Figure 2E). Transfection of NICD further promoted the differentiation of proinflammatory TA T cells (Supplementary Figure 4, <http://onlinelibrary.wiley.com/doi/10.1002/art.42103>).

To verify the function of Notch-1 signaling in proinflammatory T cell differentiation of TA T cells in vivo, immune-deficient NSG mice were immune-reconstituted with PBMCs from TA patients and were treated with or without DAPT. Compared to chimeras reconstituted with healthy PBMCs, higher frequencies of splenic Th1 cells and Th17 cells were detected in those reconstituted with TA PBMCs (Figures 2F and G). Treatment with DAPT significantly reduced the frequencies of splenic Th1 cells and Th17 cells in these chimeras reconstituted with TA PBMCs (Figures 2H and I). Taken together, Notch-1^{high} is critical for the maldifferentiation of proinflammatory T cells in TA patients.

Dependency of Notch-1^{high}-induced proinflammatory T cell differentiation on mTORC1. We identified mTORC1 hyperactivity as a cell-intrinsic mechanism for proinflammatory T cell differentiation in TA patients (1). To determine whether Notch-1^{high}-induced proinflammatory T cell differentiation was dependent on mTORC1, CD4+ T cells from healthy donors were transfected with NICD, stimulated with anti-CD3/CD28 beads in the presence or absence of rapamycin, and Th1 cells and Th17 cells were measured. We found that Notch-1^{high}-driven proinflammatory T cell differentiation was blocked by the mTORC1 inhibitor rapamycin (Figures 3A and B), and RAPTOR shRNA gene knockdown of mTORC1 also impeded Notch-1^{high}-induced proinflammatory T cell differentiation (Figures 3C

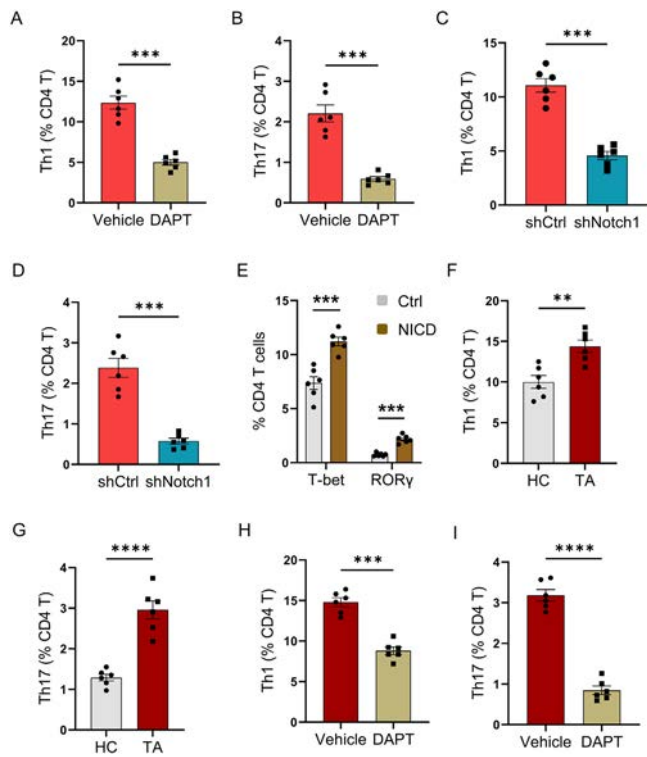


Figure 2. Notch-1 plays a critical role in proinflammatory T cell differentiation in TA. **A** and **B**, CD4⁺ T cells from TA patients were stimulated with anti-CD3/CD28 beads in the presence or absence of DAPT (10 mM) for 4 days and were analyzed for frequencies of T-bet-expressing Th1 cells (**A**) and retinoic acid receptor-related orphan nuclear receptor γ (ROR γ)-expressing Th17 cells (**B**). **C–E**, CD4⁺ T cells from TA patients were transfected with Notch-1 short hairpin RNA (shRNA) (shNotch-1) or control shRNA (shCtrl) (**C** and **D**) and CD4⁺ T cells from healthy donors were transfected with or without Notch-1 intracellular domain (NICD) (**E**), and cells were then stimulated with anti-CD3/CD28 beads for 4 days. **F** and **G**, NSG mice were reconstituted with peripheral blood mononuclear cells (PBMCs) from healthy donors or TA patients, and after 7 days, splenic Th1 cells (**F**) and Th17 cells (**G**) were measured. **H** and **I**, NSG mice reconstituted with TA PBMCs were treated with DAPT for 7 days, followed by measurement of splenic Th1 cells (**H**) and Th17 cells (**I**). Bars show the mean \pm SEM; symbols represent individual samples. ** = $P < 0.01$; *** = $P < 0.001$; **** = $P < 0.0001$, by paired t -test with Bonferroni correction in **E** or by paired t -test alone. See Figure 1 for other definitions. Color figure can be viewed in the online issue, which is available at <http://onlinelibrary.wiley.com/doi/10.1002/art.42103/abstract>.

and **D** and Supplementary Figure 5, <http://onlinelibrary.wiley.com/doi/10.1002/art.42103>). Additionally, findings from an independent replication of our previous study showed that rapamycin and gene knockdown of RAPTOR significantly blocked maldifferentiation of proinflammatory CD4⁺ T cells in TA patients (Supplementary Figure 6, <http://onlinelibrary.wiley.com/doi/10.1002/art.42103>), rendering them similar to healthy CD4⁺ T cells (1).

To verify the crucial role of mTORC1 in Notch-1-mediated Th1 and Th17 cell differentiation, we investigated the possible effect of Notch-1 on microRNA-29 (miR-29), which can be repressed by Notch-1 in murine T cells and thus facilitate Th1

differentiation (25). However, the effect of Notch-1 on miR-29 expression was highly cell-context dependent (25), and Notch-1 increased expression of miR-29 in CD4⁺ T cells from healthy donors (Supplementary Figure 7A, <http://onlinelibrary.wiley.com/doi/10.1002/art.42103>). Similarly, levels of miR-29 were elevated in CD4⁺ T cells from TA patients (Supplementary Figure 7B). Further, miR-29 blockade did not have a significant effect on Notch-1-mediated Th1/Th17 differentiation (Supplementary Figure 7C). Such findings further support the notion that Notch-1^{high} drives the maldifferentiation of Th1 cells and Th17 cells through an mTOR-dependent mechanism.

Role of Notch-1 in the expression and activity of mTORC1 in T cells. To understand the mechanisms underpinning mTOR-dependent proinflammatory T cell differentiation by Notch-1^{high}, CD4⁺ T cells from healthy donors were transfected with NICD, stimulated with anti-CD3/CD28 beads, and assayed

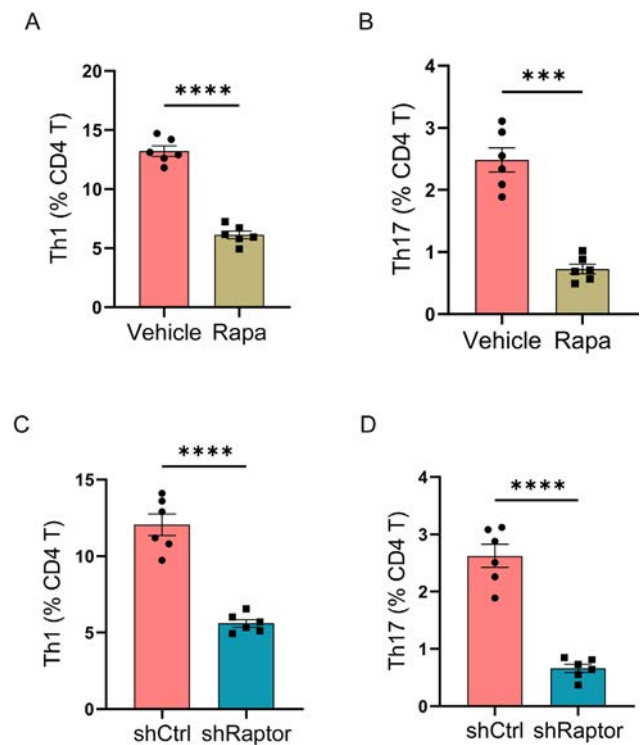


Figure 3. Notch-1 initiates proinflammatory T cell differentiation via mechanistic target of rapamycin (Rapa) complex 1. **A** and **B**, CD4⁺ T cells from healthy donors were transfected with Notch-1 intracellular domain (NICD) and stimulated with anti-CD3/CD28 beads in the presence or absence of rapamycin (50 nM) for 4 days, followed by measurement of Th1 cells (**A**) and Th17 cells (**B**). **C** and **D**, CD4⁺ T cells from healthy donors were cotransfected with NICD plus regulatory-associated protein of mechanistic target of rapamycin short hairpin RNA (shRNA) (shRaptor) or control shRNA (shCtrl) and stimulated with anti-CD3/CD28 beads for 4 days, followed by measurement of Th1 cells (**A**) and Th17 cells (**B**). Bars show the mean \pm SEM; symbols represent individual samples. *** = $P < 0.001$; **** = $P < 0.0001$, by paired t -test. Color figure can be viewed in the online issue, which is available at <http://onlinelibrary.wiley.com/doi/10.1002/art.42103/abstract>.

for mTORC1 expression. We found an ~2–3-fold increase in mTOR protein expression in response to Notch-1^{high} in CD4+ T cells (Figures 4A and B). This increase of mTOR was induced at the transcriptional level, as transfection of NICD promoted higher levels of messenger RNA mTOR in CD4+ T cells (Supplementary Figure 8A, <http://onlinelibrary.wiley.com/doi/10.1002/art.42103>). Of note, Notch-1^{high} also enhanced the expression of RAPTOR, a mTORC1-specific subunit, leaving rapamycin-insensitive companion of mTOR unaffected (Supplementary Figure 8B). Further, Notch-1^{high} promoted mTORC1 activity in CD4+ T cells (Figures 4C and D). Intracellular levels of phosphorylated S6RP were significantly elevated by NICD transfection in healthy CD4+ T cells. Vice versa, transfection of TA CD4+ T cells with Notch-1 shRNA efficiently decreased protein levels of phosphorylated S6RP (Figure 4E). Consistent with these findings, DAPT treatment also blocked the activity of mTORC1 in TA CD4+ T cells, resulting in reduced levels of intracellular phosphorylated S6RP (Figures 4F and G). Additionally, Notch-1^{high} did not significantly affect mTORC2 activity in CD4+ T cells, leaving phosphorylated Akt levels unaffected (Figures 4D and E and Supplementary Figure 9, <http://onlinelibrary.wiley.com/doi/10.1002/art.42103>).

In CD4+ T cells from TA patients, intracellularly activated Notch-1 also positively correlated with levels of phosphorylated S6RP (Figure 4H). Thus, Notch-1 signaling drives expression and activation of mTORC1 in CD4+ T cells, resulting in proinflammatory T cell differentiation in TA patients.

Association between Notch-1 and lysosome localization of mTOR in T cells. The correlation between mTORC1 activation and the translocation of mTOR to the organelle lysosome is well known (11,26). Consistent with mTORC1 hyperactivity in TA CD4+ T cells, mTOR lysosomal load was increased in these CD4+ T cells compared to healthy control cells (Figure 5A). Of note, transfection of healthy CD4+ T cells with NICD was associated with increased localization of mTOR onto the lysosome upon activation (Figure 5B). Vice versa, inhibition of Notch-1 signaling with DAPT decreased the lysosomal load of mTOR in activated CD4+ T cells (Figure 5C).

To understand how Notch-1 may correlate with lysosomal localization of mTOR, Notch-1 was immunoprecipitated and immunoblotted for mTOR protein. T cell stimulation with anti-CD3/CD28 beads promoted expression of mTOR and Notch-1,

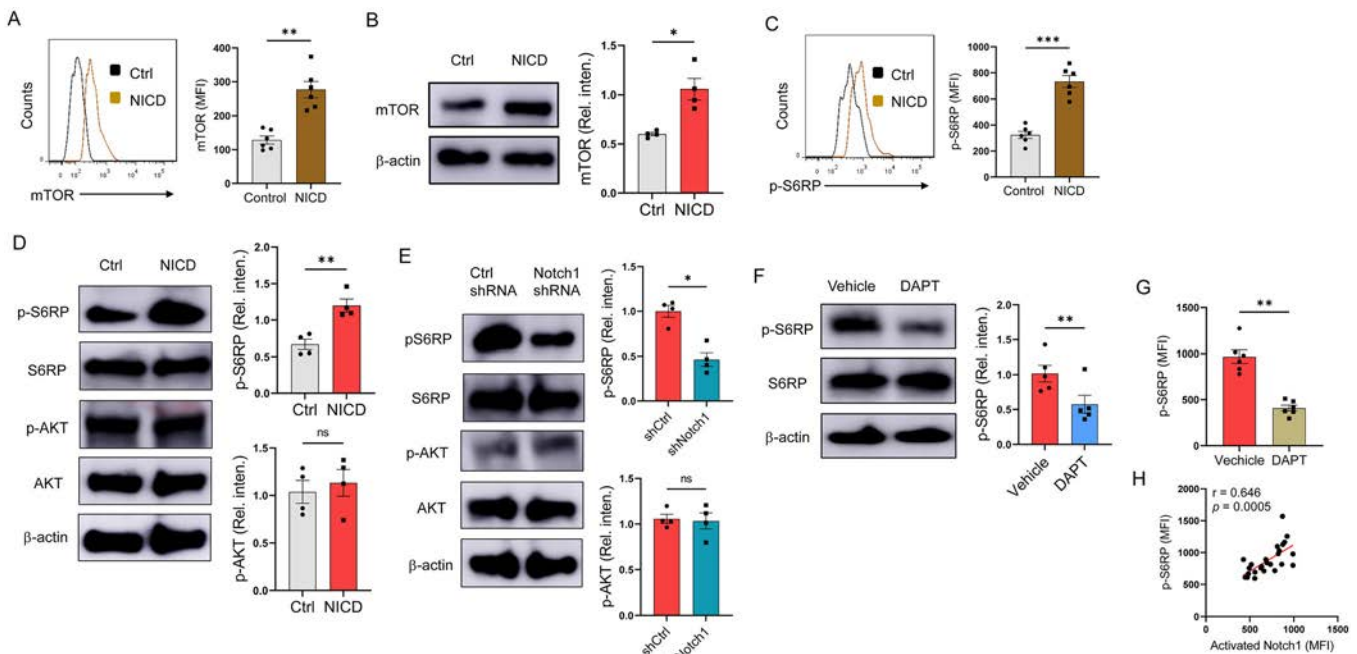


Figure 4. Notch-1 promotes expression and activity of mechanistic target of rapamycin complex 1 (mTORC1) in T cells. **A** and **B**, CD4+ T cells from healthy donors were transfected with or without Notch-1 intracellular domain (NICD), stimulated with anti-CD3/CD28 beads for 3 days, and analyzed for intracellular mTOR expression (MFI [**A**] and relative intensity [**B**]). **C** and **D**, CD4+ T cells from healthy donors were transfected with or without NICD, stimulated with anti-CD3/CD28 beads for 3 days, and analyzed for intracellular expression of phosphorylated S6RP (**C**), S6RP, phosphorylated Akt, and Akt (**D**). We used β -actin from the same membrane as the loading control. **E**, CD4+ T cells from TA patients were transfected with Notch-1 short hairpin RNA (shRNA) or control (Ctrl) shRNA, stimulated with anti-CD3/CD28 beads for 3 days, and analyzed for intracellular expression of phosphorylated S6RP, S6RP, phosphorylated Akt, and Akt. **F** and **G**, CD4+ T cells from TA patients were stimulated with anti-CD3/CD28 beads in the presence or absence of DAPT (10 mM) for 3 days and analyzed for intracellular levels of phosphorylated S6RP and S6RP (MFI [**G**] or relative intensity [**F**]). In **E–G**, β -actin from the same membrane was used as loading control. **H**, Intracellular levels of activated Notch-1 correlated with phosphorylated S6RP expression in CD4+ T cells from 25 TA patients as analyzed with Pearson's correlation coefficient. In **A–G**, bars show the mean \pm SEM; symbols represent individual samples. * = $P < 0.05$, ** = $P < 0.01$, *** = $P < 0.001$, by paired t -test. See Figure 1 for other definitions. Color figure can be viewed in the online issue, which is available at <http://onlinelibrary.wiley.com/doi/10.1002/art.42103/abstract>.

and we observed that Notch-1 physically interacts with mTOR in these T cells (Figure 5D). Therefore, Notch-1 might interact with mTOR and thus be involved in lysosomal localization of mTOR, leading to mTORC1^{high} expression in CD4⁺ T cells from TA patients.

Efficient alleviation of vascular inflammation in humanized TA mouse chimeras by targeting of Notch-1.

To evaluate the Notch-1-based therapeutic strategy for TA treatment, humanized TA chimeras were generated using immune-deficient NSG mice, which were engrafted with human

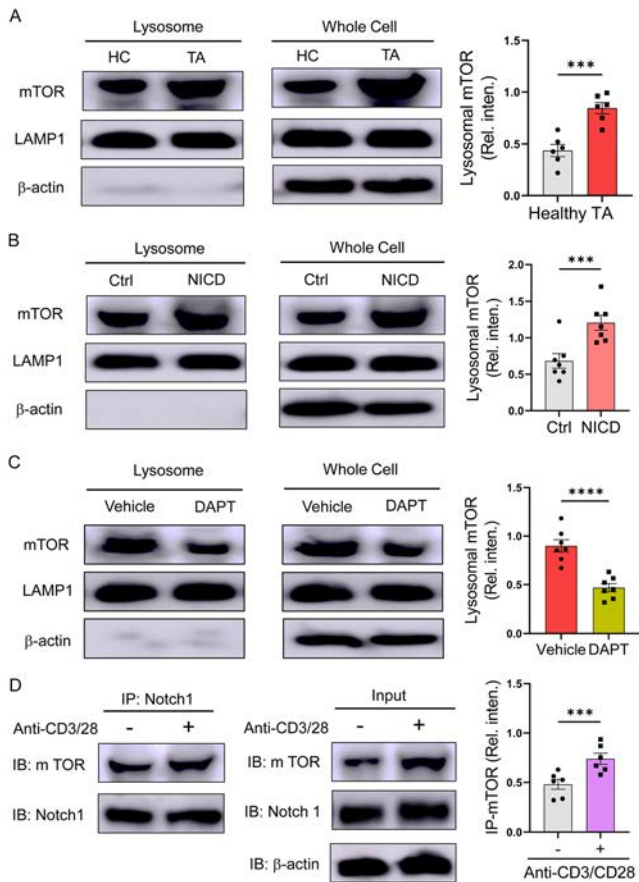


Figure 5. Notch-1 is associated with lysosomal localization of mechanistic target of rapamycin (mTOR) in T cells. **A–C**, CD4⁺ T cells from TA patients or healthy donors were stimulated with anti-CD3/CD28 beads for 3 days (**A**), healthy control cells were transfected with or without (Ctrl) Notch-1 intracellular domain (NICD) and stimulated with anti-CD3/CD28 beads for 3 days (**B**), and CD4⁺ T cells were stimulated with anti-CD3/CD28 beads in the presence or absence of DAPT (10 mM) for 3 days (**C**), and lysosomal mTOR was detected by immunoblotting (IB). Lysosome-associated membrane protein 1 (LAMP-1) was used as the lysosomal loading control. **D**, After Jurkat T cells were left unstimulated or stimulated with anti-CD3/CD28 beads for 3 days, we investigated the interaction between Notch-1 and mTOR. Notch-1 was used as the immunoprecipitated (IP) loading control, and β -actin as the whole cell loading control. Bars show the mean \pm SEM; symbols represent individual samples. *** = $P < 0.001$; **** = $P < 0.0001$, by unpaired t -test in **A** or by paired t -test. See Figure 1 for other definitions.

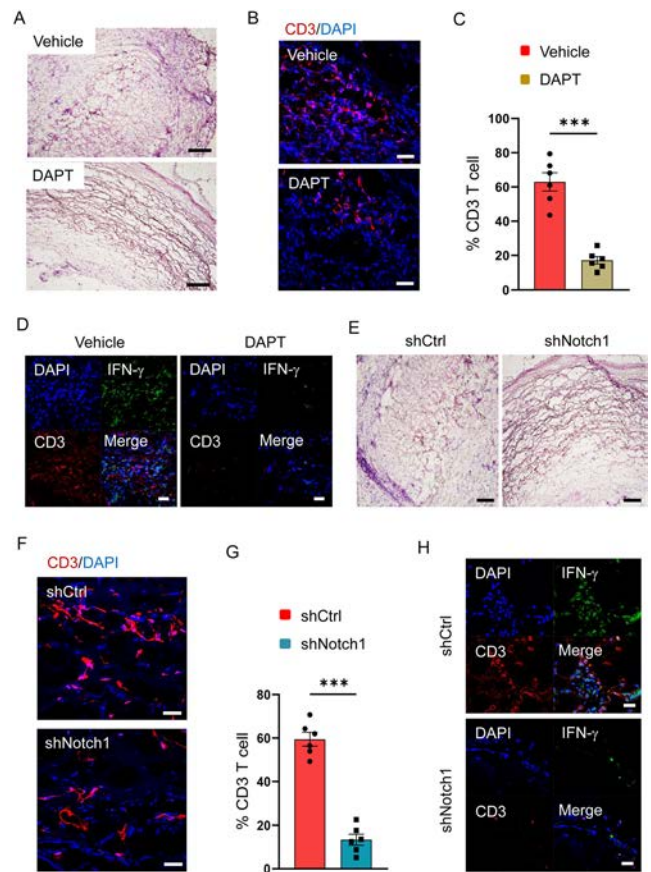


Figure 6. Targeting Notch-1 impedes vascular inflammation in humanized Takayasu arthritis (TA) chimeras. Human artery–NSG chimeras were reconstituted with TA peripheral blood mononuclear cells (PBMCs) and treated with DAPT. **A–D**, Hematoxylin and eosin (H&E) staining of human arterial tissue (**A**) and immunostaining of human CD3 protein in the adventitia of arterial grafts (**B** and **C**) and human CD3 protein with interferon- γ (IFN γ) proteins in human arterial tissue (**D**), each from the indicated chimeras. CD4⁺ T cells from TA PBMCs were transfected with Notch-1 short hairpin RNA (shRNA) (shNotch-1) or control shRNA (shCtrl) prior to immune reconstitution of human artery–NSG chimeras. **E–H**, H&E staining of human arterial tissue (**E**) and immunostaining of human CD3 protein (**F** and **G**) and human CD3 protein with IFN γ proteins (**H**) in arterial grafts, each from the indicated chimeras. In the quantification results presented in **C** and **G**, bars show the mean \pm SEM; symbols represent individual samples. In the photomicrographs, bars = 200 μ m in **A** and **E**; 20 μ m in **B–D** and **H–G**. *** = $P < 0.001$.

arterial tissue fragments and reconstituted with PBMCs from TA patients (1). These humanized TA chimeras were characterized by proinflammatory CD4⁺ T cell–dominant vascular inflammation (1). DAPT treatment in chimeras ameliorated vascular inflammation in engrafted human tissue (Figure 6A). Furthermore, DAPT treatment reduced infiltration of CD3⁺ T cells (Figures 6B and C) and inhibited the differentiation of IFN γ -expressing T cells in engrafted human arterial tissue (Figure 6D).

To test whether targeting Notch-1 within CD4⁺ T cells affects vascular inflammation in humanized TA chimeras, CD4⁺ T cells

were isolated from TA PBMCs, transfected with Notch-1 shRNA, and rejoined the TA PBMCs for immune reconstitution of NSG mouse chimeras. Knockdown of Notch-1 in CD4+ T cells prior to immune-reconstitution resulted in compromised vascular inflammation in engrafted human tissue (Figure 6E). Targeting Notch-1 in TA CD4+ T cells efficiently abrogated CD3+ T cell infiltration and IFN γ production in engrafted human arterial tissue (Figures 6F–H). Our results strongly indicate that targeting Notch-1 is a promising therapeutic strategy for the treatment of TA.

DISCUSSION

In TA patients, CD4+ T cells spontaneously maldifferentiate proinflammatory Th1 cells and Th17 cells, driving vascular inflammation in the aorta and its major branches (1,5). Mechanistically, TA CD4+ T cells demonstrate cell-intrinsic mTORC1 hyperactivity, resulting in proinflammatory T cell differentiation (1). In the current study, we extend on previous studies by pinpointing that Notch-1 critically regulates mTORC1 in CD4+ T cells. Specifically, CD4+ T cells in TA patients exert Notch-1^{high}, promoting the expression of mTOR and leading to mTORC1 hyperactivity. Targeting Notch-1 signaling efficiently alleviates vascular inflammation in humanized TA chimeras, indicating that Notch-1–based therapeutic strategies are promising for TA treatment.

Notch-1 plays a critical function in several stages of lymphocyte development, including T cell and B cell lineage choices (27). Notch-1 regulates the maturation of CD4 cells and CD8 cells by modulating T cell receptor signal strength (28), and it also primes CD4+ T cells for Th1 cell differentiation through repressing miR-29 (25). Noncanonical Notch-1 signaling drives the activation and differentiation of peripheral CD4+ T cells (29). Notch-1 also controls the magnitude of the CD4+ T cell responses by promoting cellular longevity (30). Of note, mechanisms underlying the function of Notch-1 could be distinct in different diseases. As such, CSL/RNA binding protein–J κ –independent Notch-1 signaling is crucial for the differentiation of functional Th1 cell responses following leishmaniasis infection (31). A study showed that, due to activating mutations in the *NOTCH1* gene, Notch signaling was highly activated in >65% of patients with T cell–acute lymphoblastic leukemia (32). Notch-1^{high} in T cell–ALL promotes the phosphorylation of mTOR, leading to robust leukemia cell growth (33,34). In the current study, we identified that Notch-1^{high} is a signature of TA CD4+ T cells, promoting maldifferentiation of Th1 cells and Th17 cells in TA patients. These findings indicate that Notch-1^{high} is the cell-intrinsic mechanism underlying proinflammatory T cell differentiation in TA patients.

The critical function of Notch-1 signaling in regulating mTOR pathway has long been an active area of investigation (12,35–37). Notch-1 signaling is known to activate the phosphatidylinositol 3-kinase/Akt–mTOR1 pathway via the transcriptional and posttranslational repression of the phosphatase and tensin

homolog deleted on chromosome 10 (38). In the current study, we identified a previously unknown interaction between Notch-1 and mTOR in CD4+ T cells. Notch-1^{high} not only induces expression of mTOR but also interacts with mTOR. Notch-1^{high} is associated with the lysosomal localization of mTOR and results in mTORC1 hyperactivity. Additionally, activated Notch-1 correlates with elevated levels of phosphorylated S6RP in circulating CD4+ T cells from TA patients, reflecting the magnitude of proinflammatory T cells. This phenomenon in TA patients is similar in GCA patients, in which Notch-1^{high} in CD4+ T cells also correlated with increased proinflammatory T cells (12,23).

Our findings indicate that Notch-1^{high} and mTORC1^{high} are cell-intrinsic signals for the maldifferentiation of proinflammatory T cells in TA patients and GCA patients (1,12), which might mechanistically indicate that TA and GCA are early-stage and late-stage variations of the same disorder. In support of this idea, although TA and GCA present at different frequencies and in different ages, both disorders share similar clinical symptoms, signs, and imaging abnormalities, indicating strong similarities and subtle differences in the distribution of arterial disease (1,39–42). In patients in clinical practice and in humanized chimeras representing human LVs including GCA and TA, CD4+ T cells are the predominant infiltrating T cells in vascular layers (1,4,12). In line with predominant CD4+ T cell infiltration in vascular layers, >80% of IFN γ -producing T cells in humanized TA chimeras were CD4+ T cells (Supplementary Figure 10, <http://onlinelibrary.wiley.com/doi/10.1002/art.42103>), indicating the crucial involvement of these proinflammatory CD4+ T cells in disease pathogenesis. While Th1 cells and Th17 cells are the major vascular drivers of TA and GCA, glucocorticoids efficiently reduce tissue Th1 cells, but not Th17 cells, in both patient groups (1,40,43). Additionally, in the current study, we demonstrated that Notch-1–based therapies using DAPT and Notch-1 shRNA can be used to treat vascular inflammation in humanized TA chimeras. Administration of DAPT also effectively inhibits vascular inflammation in humanized GCA chimeras (23) in which human vasculitis was induced using immune cells from GCA patients.

In patients with GCA, circulating VEGF could induce Jagged-1 expression in adventitial microendothelial cells, inducing Notch-1 activation in endothelial cell (EC)–interacting T cells (12). Meanwhile, how Notch-1^{high} is programmed in TA patients still warrants future study. Serum from TA patients could promote HES-1 protein expression in human microendothelial cells (Supplementary Figure 11, <http://onlinelibrary.wiley.com/doi/10.1002/art.42103>), which might reflect mTOR hyperactivity in ECs from those patients and indicates the existence of circulating Notch-1–driven components (44).

In essence, CD4+ T cells from TA patients exerted cell-intrinsic Notch-1^{high}, which interacts with mTOR, which is associated with lysosomal mTOR localization, promoting mTOR activity and driving the maldifferentiation of TA T cells in vascular inflammation. Accordingly, aside from mTORC1, targeting Notch-1 is

a novel and promising strategy for TA treatment. These results shed new light on TA immune pathogenesis and are relevant to the clinical management of LVV.

AUTHOR CONTRIBUTIONS

All authors were involved in drafting the article or revising it critically for important intellectual content, and all authors approved the final version to be published. Dr. Zhenke had full access to all of the data in the study and takes responsibility for the integrity of the data and the accuracy of the data analysis.

Study conception and design. C. Wang, Wen.

Acquisition of data. Jiang, Y. Wang, Zheng, Wen.



Analysis and interpretation of data. Jiang, Sun, Yuan, Mai, Zhang, Tang, Liu, Wen.

REFERENCES

- Zhang J, Zhao L, Wang J, Cheng Z, Sun M, Zhao J, et al. Targeting mechanistic target of rapamycin complex 1 restricts proinflammatory T cell differentiation and ameliorates Takayasu arteritis. *Arthritis Rheumatol* 2020;72:303–15.
- Torp CK, Br uner M, Keller KK, Brouwer E, Hauge EM, McGonagle D, et al. Vasculitis therapy refines vasculitis mechanistic classification [review]. *Autoimmun Rev* 2021;20:102829.
- Erdogan M. Aortitis: an update [review]. *Curr Opin Rheumatol* 2021;33:34–40.
- Weyand CM, Goronzy JJ. Immune mechanisms in medium and large-vessel vasculitis [review]. *Nat Rev Rheumatol* 2013;9:731–40.
- Saadoun D, Garrido M, Comarmond C, Desbois AC, Domont F, Savey L, et al. Th1 and Th17 cytokines drive inflammation in Takayasu arteritis. *Arthritis Rheumatol* 2015;67:1353–60.
- Misra DP, Chaurasia S, Misra R. Increased circulating Th17 cells, serum IL-17A, and IL-23 in Takayasu arteritis. *Autoimmune Dis* 2016;2016:7841718.
- Savioli B, Abdulhad WH, Brouwer E, Kallenberg CG, de Souza AW. Are cytokines and chemokines suitable biomarkers for Takayasu arteritis [review]? *Autoimmun Rev* 2017;16:1071–8.
- Saxton RA, Sabatini DM. mTOR signaling in growth, metabolism, and disease [review]. *Cell* 2017;169:361–71.
- Waickman AT, Powell JD. mTOR, metabolism, and the regulation of T-cell differentiation and function [review]. *Immunol Rev* 2012;249:43–58.
- Chi H. Regulation and function of mTOR signalling in T cell fate decisions [review]. *Nat Rev Immunol* 2012;12:325–38.
- Wen Z, Jin K, Shen Y, Yang Z, Li Y, Wu B, et al. *N*-myristoyltransferase deficiency impairs activation of kinase AMPK and promotes synovial tissue inflammation. *Nat Immunol* 2019;20:313–25.
- Wen Z, Shen Y, Berry G, Shahram F, Li Y, Watanabe R, et al. The microvascular niche instructs T cells in large vessel vasculitis via the VEGF-Jagged1-Notch pathway. *Sci Transl Med* 2017;9:eaal3322.
- Delgoffe GM, Pollizzi KN, Waickman AT, Heikamp E, Meyers DJ, Horton MR, et al. The kinase mTOR regulates the differentiation of helper T cells through the selective activation of signaling by mTORC1 and mTORC2. *Nat Immunol* 2011;12:295–303.
- Kennedy BK, Lamming DW. The mechanistic target of rapamycin: the grand conductor of metabolism and aging [review]. *Cell Metab* 2016;23:990–1003.
- Jin K, Wen Z, Wu B, Zhang H, Qiu J, Wang Y, et al. NOTCH-induced rerouting of endosomal trafficking disables regulatory T cells in vasculitis. *J Clin Invest* 2021;131:e136042.
- Meurette O, Mehlen P. Notch signaling in the tumor microenvironment [review]. *Cancer Cell* 2018;34:536–48.
- Jackstadt R, van Hooff SR, Leach JD, Cortes-Lavaud X, Lohuis JO, Ridgway RA, et al. Epithelial NOTCH signaling rewires the tumor microenvironment of colorectal cancer to drive poor-prognosis subtypes and metastasis. *Cancer Cell* 2019;36:319–36.e7.
- Akiyama M, Ohtsuki S, Berry GJ, Liang DH, Goronzy JJ, Weyand CM. Innate and adaptive immunity in giant cell arteritis [review]. *Front Immunol* 2021;11:621098.
- Umar D, Das A, Gupta S, Chattopadhyay S, Sarkar D, Mirji G, et al. Febrile temperature change modulates CD4 T cell differentiation via a TRPV channel-regulated Notch-dependent pathway. *Proc Natl Acad Sci U S A* 2020;117:22357–66.
- Laky K, Fowlkes BJ. Notch signaling in CD4 and CD8 T cell development [review]. *Curr Opin Immunol* 2008;20:197–202.
- Laky K, Fleischacker C, Fowlkes BJ. TCR and Notch signaling in CD4 and CD8 T-cell development [review]. *Immunol Rev* 2006;209:274–83.
- Zhang HG, Guo J, Yuan Y, Zuo Y, Liu J, Zhu L, et al. Ubiquitin E3 ligase c-Cbl is a host negative regulator of Nef protein of HIV-1. *Front Microbiol* 2020;11:597972.
- Piggott K, Deng J, Warrington K, Younge B, Kubo JT, Desai M, et al. Blocking the NOTCH pathway inhibits vascular inflammation in large-vessel vasculitis. *Circulation* 2011;123:309–18.
- Long J, Yang C, Zheng Y, Loughran P, Guang F, Li Y, et al. Notch signaling protects CD4+ T cells from STING-mediated apoptosis during acute systemic inflammation. *Sci Adv* 2020;6:eabc5447.
- Chandiran K, Lawlor R, Pannuti A, Perez GG, Srinivasan J, Golde TE, et al. Notch-1 primes CD4+ T cells for T helper type 1 differentiation through its early effects on miR-29. *Mol Immunol* 2018;99:191–8.
- Zhang CS, Jiang B, Li M, Zhu M, Peng Y, Zhang YL, et al. The lysosomal v-ATPase-Ragulator complex is a common activator for AMPK and mTORC1, acting as a switch between catabolism and anabolism. *Cell Metab* 2014;20:526–40.
- MacDonald HR, Wilson A, Radtke F. Notch-1 and T-cell development: insights from conditional knockout mice [review]. *Trends Immunol* 2001;22:155–60.
- Izon DJ, Punt JA, Xu L, Karnell FG, Allman D, Myung PS, et al. Notch-1 regulates maturation of CD4+ and CD8+ thymocytes by modulating TCR signal strength. *Immunity* 2001;14:253–64.
- Dongre A, Surampudi L, Lawlor RG, Fauq AH, Miele L, Golde TE, et al. Non-canonical Notch signaling drives activation and differentiation of peripheral CD4+ T cells. *Front Immunol* 2014;5:54.
- Helbig C, Gentek R, Backer RA, de Souza Y, Derks IA, Eldering E, et al. Notch controls the magnitude of T helper cell responses by promoting cellular longevity. *Proc Natl Acad Sci U S A* 2012;109:9041–6.
- Auderset F, Schuster S, Coutaz M, Koch U, Desgranges F, Merck E, et al. Redundant Notch-1 and Notch2 signaling is necessary for IFN γ secretion by T helper 1 cells during infection with *Leishmania major*. *PLoS Pathog* 2012;8:e1002560.
- Sanchez-Martin M, Ferrando A. The NOTCH-1-MYC highway toward T-cell acute lymphoblastic leukemia [review]. *Blood* 2017;129:1124–33.
- Chan SM, Weng AP, Tibshirani R, Aster JC, Utz PJ. Notch signals positively regulate activity of the mTOR pathway in T-cell acute lymphoblastic leukemia. *Blood* 2007;110:278–86.
- Kishton RJ, Barnes CE, Nichols AG, Cohen S, Gerriets VA, Siska PJ, et al. AMPK is essential to balance glycolysis and mitochondrial metabolism to control T-ALL cell stress and survival. *Cell Metab* 2016;23:649–62.
- Hibdon ES, Razumilava N, Keeley TM, Wong G, Solanki S, Shah YM, et al. Notch and mTOR signaling pathways promote human gastric cancer cell proliferation. *Neoplasia* 2019;21:702–12.

36. Demitrack ES, Gifford GB, Keeley TM, Carulli AJ, VanDussen KL, Thomas D, et al. Notch signaling regulates gastric antral LGR5 stem cell function. *EMBO J* 2015;34:2522–36.
37. Lee K, Nam KT, Cho SH, Gudapati P, Hwang Y, Park DS, et al. Vital roles of mTOR complex 2 in Notch-driven thymocyte differentiation and leukemia. *J Exp Med* 2012;209:713–28.
38. Hales EC, Taub JW, Matherly LH. New insights into Notch-1 regulation of the PI3K-AKT-mTOR1 signaling axis: targeted therapy of γ -secretase inhibitor resistant T-cell acute lymphoblastic leukemia [review]. *Cell Signal* 2014;26:149–61.
39. Kernani TA. Takayasu arteritis and giant cell arteritis: are they a spectrum of the same disease [review]? *Int J Rheum Dis* 2019;22 Suppl 1:41–8.
40. Watanabe R, Berry GJ, Liang DH, Goronzy JJ, Weyand CM. Pathogenesis of giant cell arteritis and Takayasu arteritis—similarities and differences. *Curr Rheumatol Rep* 2020;22:68.
41. Seko Y. Giant cell and Takayasu arteritis [review]. *Curr Opin Rheumatol* 2007;19:39–43.
42. Furuta S, Cousins C, Chaudhry A, Jayne D. Clinical features and radiological findings in large vessel vasculitis: are Takayasu arteritis and giant cell arteritis 2 different diseases or a single entity? *J Rheumatol* 2015;42:300–8.
43. Nakaoka Y, Isobe M, Takei S, Tanaka Y, Ishii T, Yokota S, et al. Efficacy and safety of tocilizumab in patients with refractory Takayasu arteritis: results from a randomised, double-blind, placebo-controlled, phase 3 trial in Japan (the TAKT study). *Ann Rheum Dis* 2018;77:348–54.
44. Hadjadj J, Canaud G, Mirault T, Samson M, Bruneval P, Régent A, et al. mTOR pathway is activated in endothelial cells from patients with Takayasu arteritis and is modulated by serum immunoglobulin G. *Rheumatology (Oxford)* 2018;57:1011–20.

Self-Assembled Human Skin Equivalents Model Macrophage Activation of Cutaneous Fibrogenesis in Systemic Sclerosis

Mengqi Huang,¹  Avi Smith,² Matthew Watson,³ Rajan Bhandari,⁴ Lauren M. Baugh,³ Irena Ivanovska,⁵ Trishawna Watkins,² Irene Lang,² Maria Trojanowska,⁶  Lauren D. Black III,² Patricia A. Pioli,⁴ Jonathan Garlick,² and Michael L. Whitfield⁴

Objective. The development of precision therapeutics for systemic sclerosis (SSc) has been hindered by the lack of models that accurately mimic the disease in vitro. This study was undertaken to design and test a self-assembled skin equivalent (saSE) system that recapitulates the cross-talk between macrophages and fibroblasts in cutaneous fibrosis.

Methods. SSc-derived dermal fibroblasts (SScDFs) and normal dermal fibroblasts (NDFs) were cultured with CD14+ monocytes from SSc patients or healthy controls to allow de novo stroma formation. Monocyte donor-matched plasma was introduced at week 3 prior to seeding keratinocytes to produce saSE with a stratified epithelium. Tissue was characterized by immunohistochemical staining, atomic force microscopy, enzyme-linked immunosorbent assay, and quantitative reverse transcriptase–polymerase chain reaction.

Results. Stroma synthesized de novo from NDFs and SScDFs supported a fully stratified epithelium to form saSE. A thicker and stiffer dermis was generated by saSE with SScDFs, and more interleukin-6 and transforming growth factor β (TGF β) was secreted by saSE with SScDFs compared to saSE with NDFs, regardless of the inclusion of monocytes. Tissue with SSc monocytes and plasma had amplified dermal thickness and stiffness relative to control tissue. Viable CD163+ macrophages were found within the stroma of saSE 5 weeks after seeding. Additionally, SSc saSE contained greater numbers of CD163+ and CD206+ macrophages compared to control saSE. TGF β blockade inhibited stromal stiffness to a greater extent in SSc saSE compared to control saSE.

Conclusion. These data suggest reciprocal activation between macrophages and fibroblasts that increases tissue thickness and stiffness, which is dependent in part on TGF β activation. The saSE system may serve as a platform for preclinical therapeutic testing and for molecular characterization of SSc skin pathology through recapitulation of the interactions between macrophages and fibroblasts.

INTRODUCTION

Systemic sclerosis (SSc) is a heterogeneous disease of unknown etiology that is characterized by vascular dysfunction, inflammation, and fibrosis (1). The lack of adequate model systems for studying SSc has been a limiting factor for both basic science and preclinical trials. Animal models of SSc include the tight skin (TSK1/+, TSK2/+), sclerodermatous graft-versus-host disease (sclGVHD), and bleomycin-induced dermal fibrosis mouse

models, and have been used to make important advances in understanding the underlying physiopathology of fibrotic disease (2). However, a limitation of these animal models is that they fail to recapitulate the full spectrum of pathologic progression of disease in humans (3,4). Alternatively, conventional 2-dimensional in vitro culture systems that use simple monolayers, in which cells derived from SSc patient biopsy samples are grown on a plastic surface, do not provide the cell–cell interactions that exist in systemic biologic models. Moreover, cells cultured in vitro lose their

Supported in part by the National Institute of Arthritis and Musculoskeletal and Skin Diseases, NIH (Small Business Innovative Research grants 1R43-AR-072170-01 and 2R-44-AR-072170-02). Dr. Pioli's work was supported by the National Scleroderma Foundation. Dr. Whitfield's work was supported by the Scleroderma Research Foundation.

¹Mengqi Huang, PhD: Dartmouth Geisel School of Medicine, Hanover, New Hampshire, and University of Pittsburgh, Pittsburgh, Pennsylvania; ²Avi Smith, MS, Trishawna Watkins, BS, Irene Lang, DDS, Lauren D. Black III, PhD, Jonathan Garlick, DDS, PhD: Tufts University, Boston, Massachusetts; ³Matthew Watson, PhD, Lauren M. Baugh, PhD: Tufts University, Medford, Massachusetts; ⁴Rajan Bhandari, PhD, Patricia A. Pioli, PhD, Michael

L. Whitfield, PhD: Dartmouth Geisel School of Medicine, Hanover, New Hampshire; ⁵Irena Ivanovska, PhD: Celdara Medical, LLC, Lebanon, New Hampshire; ⁶Maria Trojanowska, PhD: Boston University School of Medicine, Boston, Massachusetts.

Author disclosures are available at <https://onlinelibrary.wiley.com/action/downloadSupplement?doi=10.1002%2Fart.42097&file=art42097-sup-0001-Disclosureform.pdf>.

Address correspondence to Michael L. Whitfield, PhD, 7400 Remsen, Hanover, NH 03755. Email: michael.l.whitfield@dartmouth.edu.

Submitted for publication November 19, 2020; accepted in revised form February 15, 2022.

in vivo genetic features over time, leading to challenges in the interpretation of results that fail to represent patient tissue (5–8).

Recent advances demonstrate the value of using in vitro 3-dimensional (3-D) models to mimic the pathogenesis of SSc in humans. These models have been used to construct complex, multicellular tissue with cell–cell and cell–matrix interactions by using patient-derived tissue-resident cells to induce fibrotic characteristics (9–12). Three-dimensional culture platforms compensate for genetic differences between animal models and humans and eliminate nonbiologically relevant cellular responses induced by direct contact with plastic culture dishes. Moreover, 3-D tissue models have become increasingly complex through the incorporation of relevant cell types, such as vascular endothelial cells, fibroblasts, alveolar epithelial cells, and adipocytes (13–16). The addition of these cell types to the extracellular matrix (ECM) scaffold provides a useful tool for the study of differential cell activation and the dysregulation of specific signaling pathways that underlie fibrosis in SSc (9,13,15). Although it is known that immune cells mediate fibrosis, currently available 3-D tissue models of SSc have failed to account for immune dysregulation in the disease pathology (2).

To address this, we have developed an all-human self-assembled skin equivalent (saSE) that is fabricated with de novo stroma deposited by dermal fibroblasts embedded with peripheral monocytes. The stroma is in direct contact with a full stratified epithelium differentiated from keratinocytes. The saSE model has been adapted from our 2 previous skin-like tissue models (self-assembled stroma [SAS] and human skin equivalent [HSE] models), and is characterized by the de novo matrix deposition of SAS and the physiologic structure of the epithelial-mesenchymal layers of HSE (10,17). More importantly, by seeding tissue with patients' fibroblasts and plasma, we have demonstrated that not only can primary human monocytes survive within saSE, but also that these cells polarize into activated macrophages, a pivotal immune cell type associated with profibrotic activation (18). Therefore, this novel skin equivalent may serve as a preclinical platform for screening candidate drugs in the personalized medical treatment of SSc.

MATERIALS AND METHODS

Patient and public involvement. SSc patients participated in the study through the donation of skin biopsy samples, peripheral blood mononuclear cells, and plasma samples for cell isolation and subsequent tissue construction.

Isolation of human-derived cells and plasma.

Demographic and clinical characteristics of the SSc patients who donated primary cells and plasma for this study were obtained at the time of consent and are listed in Table 1. All participants provided written informed consent as approved by the Tufts Medical Center, the Dartmouth-Hitchcock Medical Center/

Geisel School of Medicine Institutional Review Board, or the Northwestern University Institutional Review Board. Plasma and peripheral blood monocytes were obtained from whole blood from SSc patients and age- and sex-matched healthy controls using established methods (19).

Whole blood samples were treated with heparin, and cellular components were separated from the plasma supernatant by centrifugation at 400g for 35 minutes at 20°C. Peripheral blood mononuclear cells were isolated from heparinized whole blood using Ficoll-Paque Premium (density 1.077 g/ml; GE Healthcare). Monocytes were purified from mononuclear cells using CD14 MicroBeads (Miltenyi Biotec). This method of cell isolation routinely generates monocytes that are >95% pure (20). Monocytes and plasma were stored at –80°C and thawed once prior to use, with the exception of monocyte CM00 (Table 1), which was pre-differentiated in vitro or used to seed 3-D tissue immediately after isolation.

SSc-derived and normal dermal fibroblasts (SScDFs and NDFs) were isolated from 3-mm skin biopsy samples collected in our previous studies (10). Fibroblast strains were expanded for use at passages 6 through 8 in all experiments (7). Keratinocytes previously isolated from the foreskin of an anonymous neonatal donor were used in all experiments at passage 6.

Cell culture. Fibroblasts were cultured in medium containing low-glucose Dulbecco's modified Eagle's medium (DMEM; Invitrogen) with 10% fetal bovine serum (FBS; HyClone), 1% penicillin/streptomycin (ThermoFisher Scientific), and 8 mM HEPES (Sigma-Aldrich). Keratinocytes were cultured on an irradiated 3T3 feeder cell layer in medium containing a 3:1 mixture of DMEM/F-12 (ThermoFisher Scientific), 5% FBS, 0.18 mM adenine, 8 mM HEPES, 0.5 µg/ml hydrocortisone (Sigma), 10^{–10}M cholera toxin (all from Sigma), 10 ng/ml epidermal growth factor (EGF; PeproTech), and 5 µg/ml insulin (ThermoFisher Scientific). CD14+ monocytes used to construct saSE were cultured in RPMI 1640 with 2.05 mM L-glutamine (Invitrogen) supplemented with 10% FBS at 37°C upon thawing from liquid nitrogen. To induce macrophage differentiation in vitro, healthy monocytes were seeded in 12-well plates at 5 × 10⁵ cells/well for 7 days with complete RPMI medium supplemented with 50 ng/ml macrophage colony-stimulating factor (M-CSF) or 10 ng/ml granulocyte–macrophage colony-stimulating factor (GM-CSF) before being added to saSE. All human cells were stored for long-term use in basal culture medium supplemented with 20% FBS and 10% DMSO (Sigma) in liquid nitrogen.

Generation of coculture and triculture skin equivalents. For cocultured tissue, fibroblasts were harvested at 90% confluence and seeded onto 24-well Millicell Hanging Cell Culture inserts of 1.0 µm pore size (Millipore) with 16,000 cells per insert. For tricultured tissue, monocytes in suspension were combined

Table 1. Demographic and clinical characteristics of participants who donated the human primary cells and plasma used in the production of self-assembled skin equivalents*

Participant ID	Cell line	Plasma	Age/sex	Disease duration, years	Race, health status
Monocytes and plasma					
JR001	-	SP01	51/F	NA	White, dcSSc
DL002	-	SP02	62/M	13	White, dcSSc
JC004	SM03	SP03	71/F	27	White, dcSSc
JK06	SM04	SP04	73/F	34	White, dcSSc
BC006	-	SP05	65/F	NA	White, dcSSc
CR012	-	SP06	50/F	NA	White, dcSSc
PaPi	CM00	NA	46/F	-	White, healthy
VC008	-	CP01	53/F	-	African American, healthy
BT009	-	CP02	63/M	-	Hispanic, healthy
JP003	CM03	CP03	71/F	-	African American, healthy
IL005	CM04	CP04	75/F	-	White, healthy
JR011	-	CP05	64/F	-	Asian, healthy
SW10	-	CP06	54/F	-	White, healthy
Dermal fibroblasts					
SD16-26	SScDF01	-	45/F	NA	White, dcSSc
SSc1909	SScDF02	-	63/F	NA	White, dcSSc
SSc1900	SScDF03	-	50/M	NA	White, dcSSc
SD15-13	SScDF04	-	64/M	NA	White, dcSSc
BIIB4	SScDF05	-	72/F	17	White, dcSSc
N15-4	NDF01	-	23/F	-	White, healthy
N14-6	NDF02	-	28/F	-	White, healthy
N15-1	NDF03	-	60/M	-	White, healthy
N16-1	NDF04	-	34/M	-	White, healthy
BIIB5	NDF05	-	53/F	-	White, healthy
BIIB6	NDF06	-	62/F	-	White, healthy
Keratinocytes					
No ID	NHK	-	Neonatal/M	NA	NA, healthy

* SP = systemic sclerosis-derived plasma; NA = not available; dcSSc = diffuse cutaneous systemic sclerosis; SM = systemic sclerosis-derived monocyte; CM = control monocyte; CP = control plasma; SScDF = systemic sclerosis-derived dermal fibroblast; NDF = normal dermal fibroblast; NHK = normal human keratinocyte.

with fibroblasts at 24×10^4 , 16×10^3 , 8×10^3 , and 4×10^3 cells per insert to generate model 1, or seeded 2 weeks later to generate model 2. Fibroblasts with or without monocytes were fed medium containing a 3:1 mixture of DMEM/F-12, 5% FetalClone II serum (FCII; HyClone), 0.18 mM adenine, 8 mM HEPES, 0.5 $\mu\text{g/ml}$ hydrocortisone, 10^{-10}M cholera toxin, 10 ng/ml EGF, 5 $\mu\text{g/ml}$ insulin, and 10 $\mu\text{g/ml}$ L-ascorbic acid-2-phosphate (Sigma). Culture medium was changed every 4 days for 3 weeks to form the stromal layer in the 3-D tissue. In experiments with plasma-treated tissue, 5% SSc or healthy control plasma replaced FCII in the culture medium during the third week.

In experiments with transforming growth factor β (TGF β) with or without Smad3 inhibitor (SIS3)-treated constructs, culture medium was supplemented with 2 ng/ml TGF β 1 (R&D Systems) and 3 μM SIS3 (Tocris) in the third week. At the 3-week time point, keratinocytes were seeded at 7×10^4 keratinocytes/well onto the stromal tissue surface and fed epidermal growth medium (patented by Organogenesis) from both insert (200 μl) and bottom chambers (1 ml) for 5 days. Tissue was then raised to an air-liquid interface and fed from the bottom chamber with 700 μl cornification medium (patented by Organogenesis) to enable epithelial differentiation for 1 week.

Immunohistochemistry. The saSE was fixed in 10% formalin overnight at 4°C, embedded in paraffin, and sectioned at a thickness of 6 μm . For anti-bromodeoxyuridine (anti-BrdU) staining, saSE was pulsed with 10 μM BrdU (Invitrogen) for 6 hours before fixation. Antigen retrieval was performed by submerging the deparaffinized sections in citric buffer at 95°C for 15 minutes followed by 0.2% bovine serum albumin/phosphate buffered saline (BSA/PBS) blocking buffer containing 1% horse serum for 1 hour. Immunohistochemical staining was performed using primary antibody against BrdU (product no. 1170376; Roche) at a dilution of 1:40 and primary antibodies against Ki-67 (product no. ab16667), keratin 10 (K-10; product no. ab9026), α -smooth muscle actin (α -SMA; product no. ab7818), and CD163 (product no. ab156769) (all from Abcam) at a density of 1:100 in 0.2% BSA/PBS at 4°C overnight, followed by biotinylated anti-mouse/rabbit IgG secondary antibody (Vector) in 0.2% BSA/PBS for 1 hour at room temperature.

Biotinylated antibody-bound proteins were detected by incubating the sections with avidin-biotin complex for 30 minutes and visualized by staining with 3, 3'-diaminobenzidine peroxidase substrates (Vector). Tissue sections were counterstained with hematoxylin to identify nuclei. Hematoxylin and eosin staining

was performed to assess tissue morphology. Tissue sections were deparaffinized in xylene, rehydrated in gradient ethanol, and washed with distilled water for hematoxylin staining, then rinsed in acid alcohol and counterstained with eosin. All images were taken using a Nikon Eclipse 80i microscope and SPOT Advanced software (Diagnostic Instruments).

Atomic force microscopy (AFM). Intact saSE was sent to the Bioengineering Department at Tufts University at week 5 for measurement by AFM, as previously described by our group (10,17). Briefly, a 5- μm -diameter borosilicate spherical tip (Novascan) with a spring constant of 0.06 N/m was used to detect the elastic modulus on the stromal side surface of saSE. Results were analyzed by averaging the measurements across the detected area under force-contact mode. The number of tissue samples in each AFM experiment is indicated in the figure legends.

Enzyme-linked immunosorbent assay. Coculture supernatants from saSE constructed from NDFs (NDFs-saSE; $n = 4$) or from SScDFs (SScDFs-saSE; $n = 4$) were collected after 5 weeks of culture and analyzed using Quantikine enzyme-linked immunosorbent assay kits (R&D Systems) for human interleukin-6 (IL-6; product no. D6050) and active TGF β 1 (product no. SB100B) according to the manufacturer's protocol. The concentrations of IL-6 and active TGF β 1 were normalized to levels detected in the cornification medium containing 2% bovine calf serum (HyClone).

Real-time quantitative polymerase chain reaction (qPCR). The saSE was homogenized by TissueLyser II with stainless beads (5 mm; Qiagen). Total RNA was isolated from saSE using the QIAshredder and QIAcube (Qiagen) according to the manufacturer's protocol. RNA integrity and concentration were assessed using the Agilent 4200 TapeStation, and all samples met quality control criteria using Agilent RNA ScreenTape. From each sample, 0.7 μg RNA was used to synthesize complementary DNA using the iScript cDNA Synthesis kit (Bio-Rad). Real-time qPCR was performed using TaqMan probe single tube assays (Life Technologies) for measurement of *CD163*, *CD206*, *ITGAM*, and *CD14* expression. A StepOnePlus Real-Time PCR System (Applied Biosystems) was used for amplification and detection. Threshold cycle number was determined using Opticon software. Thermal cycling conditions consisted of an initial incubation at 50°C for 2 minutes and 95°C for 10 minutes, followed by 40 cycles of 95°C for 15 seconds and 60°C for 1 minute. Product accumulation was measured during the extension phase, and all samples were run in triplicate. The relative levels of *CD163*, *CD206*, and *ITGAM* messenger RNA (mRNA) expression were normalized to the levels of *CD14* and represented as relative mRNA expression determined by the $\Delta\Delta C_t$ method.

Cytokine array. Triculture supernatants were collected after re-epithelization of SSc saSE ($n = 6$) and control saSE ($n = 6$) on day 25, and cytokine content was analyzed using a Human 41-Plex kit (Millipore) according to the manufacturer's protocol. The cytokine panel consisted of EGF, fibroblast growth factor 2, eotaxin, TGF α , granulocyte colony-stimulating factor, Flt-3L, GM-CSF, CX $_3$ CL1, interferon- α 2, interferon- γ , CXCL1, IL-10, CCL7, IL-12p40, CCL22, IL-12p70, platelet-derived growth factor AA, IL-13, platelet-derived growth factor BB, IL-15, soluble CD40L, IL-17A, IL-1 receptor antagonist, IL-1 α , IL-9, IL-1 β , IL-2, IL-3, IL-4, IL-5, IL-6, IL-7, IL-8, CXCL10, CCL2, CCL3, CCL4, CCL5, tumor necrosis factor, tumor necrosis factor β (lymphotoxin), and vascular endothelial growth factor (VEGF). Values were normalized to basal levels in epidermal growth medium (patented by Organogenesis) containing 0.3% chelated FBS (HyClone).

Statistical analysis. All results are shown as the mean \pm SD. Statistical analyses were performed using GraphPad Prism and analyzed by Mann-Whitney test to compare the differences between 2 groups. One-way analysis of variance was used to compare the differences among ≥ 3 groups, followed by Tukey's multiple comparison test to perform pairwise comparisons between groups. *P* values less than 0.05 were considered significant.

RESULTS

Recapitulation of fibrotic features of SSc patient skin by coculture skin equivalents. To generate an all-human skin equivalent, we combined the characteristics of 2 previously described skin-like models to maintain the complexity of the full stratified epithelium and its cross-talk with de novo stroma synthesized by dermal fibroblasts (Figure 1). Our initial studies used 2 essential cell types (keratinocytes and fibroblasts) to create skin-equivalent tissue. Foreskin keratinocytes were seeded directly onto the SAS-like tissue deposited by primary fibroblasts

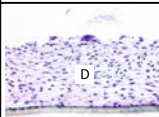
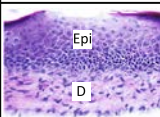
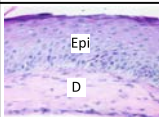
	Self-assembled stroma (SAS)	Self-assembled skin equivalent (saSE)	Human skin equivalent (HSE)
Complexity			
Throughput	24-well	24-well	6-well
Extracellular matrix	<i>de novo</i>	<i>de novo</i>	Mostly bovine Type I collagen

Figure 1. Characteristics of self-assembled stroma, human skin equivalent, and self-assembled skin equivalent including tissue complexity, throughput, and type of extracellular matrix deposited by dermal fibroblasts. D = dermis; Epi = epidermis.

that had been isolated from forearm skin biopsy samples (Figure 2A). Both NDF- and SScDF-derived cellular stroma supported the formation of fully stratified epithelium (Figure 2B). SScDF-saSE demonstrated notable increases in both stromal thickness and rigidity compared to NDF-saSE (Figure 2C), consistent with differences we previously observed between NDFs and SScDFs in SAS without the presence of epithelium (10).

Next, we assessed expression of IL-6 and TGF β in the supernatants of saSE, as these cytokines have been shown to mediate skin thickening in SSc patients (21–24). Soluble levels of both IL-6 and active TGF β 1 were significantly higher in SScDF-saSE than in NDF-saSE (Figure 2D). Notably, the magnitude of the increased IL-6 expression in SScDFs versus NDFs was lower in SAS tissue that lacked the epidermal layer compared to saSE (see Supplementary Figure 1A, available on the *Arthritis & Rheumatology* website at <http://onlinelibrary.wiley.com/doi/10.1002/art.42097>). Interestingly, the increased level of active TGF β 1 in

SScDF-saSE compared to NDF-saSE was abrogated in SAS (Supplementary Figure 1A). These results suggest that cross-talk between fibroblasts and keratinocytes significantly contributes to the increased levels of circulating IL-6 and TGF β 1 (21–24) observed in SSc patients.

To further determine the effect of circulating factors on profibrotic phenotypes, NDFs and SScDFs were treated with either healthy control plasma or SSc patient plasma for 1 week (Figure 2A). Strikingly, the addition of SSc patient plasma to SScDF-saSE resulted in increased stromal thickness and stiffness when compared to SScDF-saSE treated with control plasma (Figure 2E). In contrast, treatment of NDFs with SSc patient plasma did not result in significant changes in either stiffness or thickness relative to that observed with control plasma (Figure 2E). In prior studies, we observed a similarly enhanced level of ECM accumulation in SScDFs induced by TGF β 1 (10), which was elevated in SSc patient plasma compared to control

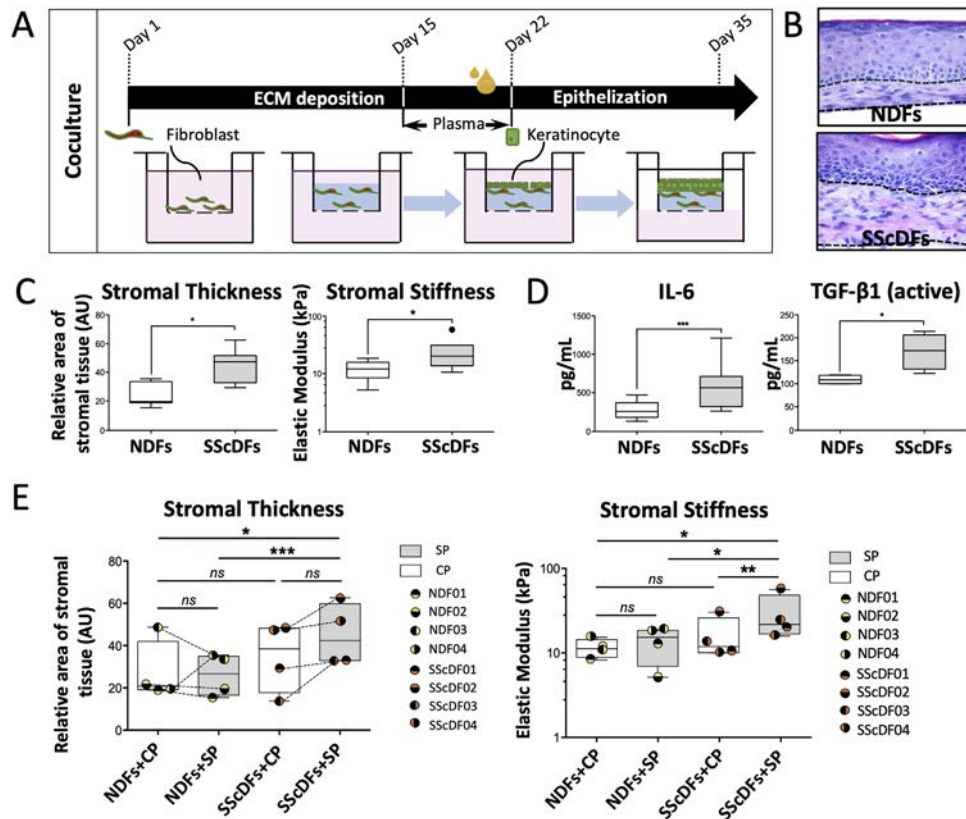


Figure 2. Characterization of self-assembled skin equivalent (saSE) constituted with normal dermal fibroblasts (NDFs) or systemic sclerosis (SSc)-derived dermal fibroblasts (SScDFs) and keratinocytes. **A**, Schematic overview of the generation of saSE by seeding keratinocytes onto de novo stromal layer deposited by fibroblasts. **B**, Representative images of hematoxylin and eosin-stained sections of saSE constructed with NDFs or SScDFs, with the stromal layer outlined by dashed lines. **C**, Stromal layer thickness assessed by determination of relative tissue surface area, and stromal layer rigidity measured by elastic modulus. **D**, Levels of soluble interleukin 6 (IL-6) and transforming growth factor β (TGF β) secreted into medium cultured with NDF- or SScDF-saSE on day 35. **E**, Stromal layer thickness assessed by determination of relative tissue surface area, and stromal layer rigidity measured by elastic modulus. NDF- and SScDF-saSE was cultured with healthy control plasma or SSc plasma ($n = 4$ NDFs and 4 SScDFs). In **C–E**, data are presented as box plots, where the boxes represent the interquartile range (IQR), the lines within the boxes represent the median, and the lines outside the boxes represent 1.5 \times the IQR; symbols in **E** represent individual samples. * = $P < 0.05$; ** = $P < 0.01$; *** = $P < 0.001$. ECM = extracellular matrix; CP = control plasma; SP = SSc plasma; NS = not significant.

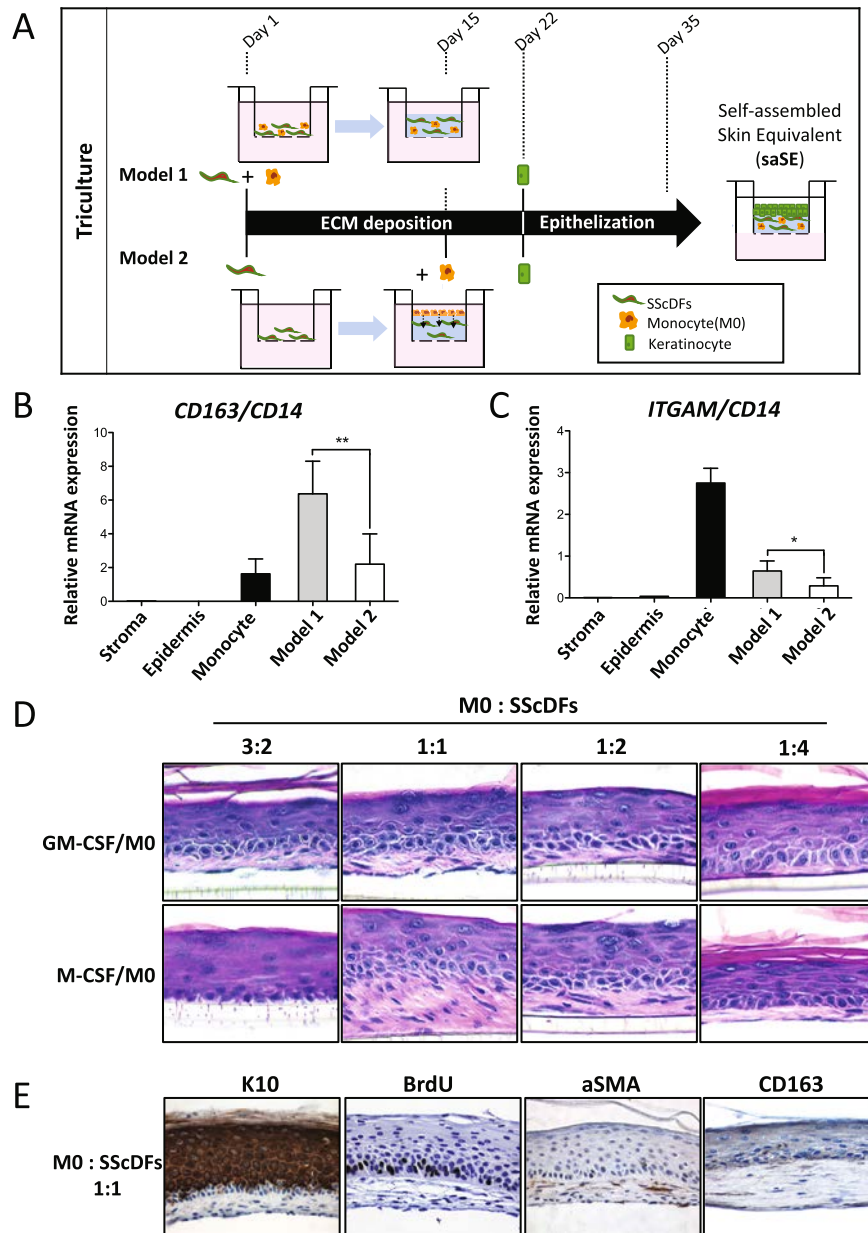


Figure 3. Incorporation of monocytes into saSE tissue. **A**, Schematic overview of 2 approaches to introducing monocytes into saSE. In model 1, dermal fibroblasts from patients with SSc were seeded with monocytes on day 1 and cultured for 5 weeks; in model 2, monocytes were seeded 2 weeks after SScDFs and cultured for an additional 3 weeks. **B** and **C**, Relative levels of *CD163* and *ITGAM* mRNA expression normalized to the expression of *CD14* in stromal tissue generated by seeding SScDFs for 5 weeks, in epidermal layers dissociated from saSE, and in fresh monocytes isolated from peripheral blood from a control donor. Relative mRNA expression was determined by the $\Delta\Delta C_t$ method. Bars show the mean \pm SD. * = $P < 0.05$; ** = $P < 0.01$, by Mann-Whitney test. **D**, Representative images of hematoxylin and eosin–stained saSE constructed with various ratios of SScDFs and monocytes pretreated with granulocyte–macrophage colony-stimulating factor (GM-CSF) or macrophage colony-stimulating factor (M-CSF). **E**, Representative images of saSE constructed using a 1:1 ratio of SScDFs and monocytes immunohistochemically stained with keratin 10 (K10), bromodeoxyuridine (BrdU), and α -smooth muscle actin (α -SMA). See Figure 2 for other definitions.

plasma (Supplementary Figure 1B). The differential response of SScDFs and NDFs to SSc patient plasma implies aberrant signaling pathway activation in SSc patient fibroblasts. Taken together, these findings demonstrate that saSE constructed with patient fibroblasts and plasma, along with control keratinocytes, recapitulates the dermal pathology of SSc.

Addition of monocytes to mimic immune responses in SSc patient skin. To provide a platform to study the immune response in SSc skin using saSE, we used 2 different approaches to incorporate human control CD14+ monocytes from peripheral blood into the stromal layer with the existing cell types, SScDFs and keratinocytes (Figure 3A). In model 1, monocytes were

seeded with fibroblasts on day 1 and cultured for 5 weeks; in model 2, fibroblasts were seeded for the first 2 weeks to form ECM, and then monocytes were added onto ECM for the subsequent 3 weeks. We hypothesized that monocytes would differentiate into macrophages and migrate into the underlying stromal tissue (Figure 3A).

We measured the enrichment of genes expressed by macrophages in these models at week 5 to compare the abundance and viability of the myeloid cells cultured in saSE. As shown in Figures 3B and C, expression of *CD163*, which is up-regulated on activated macrophages, and *ITGAM*, which encodes CD11b (a monocyte/macrophage marker), were significantly higher in model 1 and were nearly absent in fibroblast-synthesized SAS and in tissue in which the epidermal layer was separated from saSE. Notably, expression of *CD163* in model 1 was higher than in fresh monocytes, whereas *ITGAM* expression was lower in saSE (models 1 and 2) than in fresh monocytes, suggesting that the monocytes not only survived but may have differentiated into *CD163*+ polarized macrophages embedded within the SScDF-derived stromal layer. A time course study of *CD163* and *ITGAM* mRNA expression in model 1 suggested that macrophage differentiation occurred within the first 2 weeks of stromal deposition, and was not impeded by the addition of keratinocytes (Supplementary Figure 2A, <http://onlinelibrary.wiley.com/doi/10.1002/art.42097>).

To determine the optimal monocyte:fibroblast ratio to observe macrophage-induced fibrotic activation, monocytes were differentiated into macrophages with GM-CSF (to induce classical pathway activation) or M-CSF (to induce alternative pathway activation) and mixed with SScDFs at 3:2, 1:1, 1:2, and 1:4 macrophage:fibroblast ratios to generate saSE (Figure 3D). Deposition of a stromal layer was noted at 1:1 and 1:2 cell ratios in saSE regardless of whether monocytes were differentiated with GM-CSF or M-CSF. A 1:1 ratio of SScDFs and M-CSF-differentiated macrophages yielded the thickest stromal layer among all conditions tested (Figure 3D and Supplementary Figure 2B, <http://onlinelibrary.wiley.com/doi/10.1002/art.42097>). This is consistent with the results of previous studies that suggest alternative pathway-activated macrophages contribute to the pathogenesis of fibrosis in SSc (25).

We also assessed the impact of monocyte addition on keratinocyte proliferation and myofibroblast differentiation. As noted in Supplementary Figures 2C and D, slightly more proliferating basal keratinocytes stained with Ki-67 in tissue that included GM-CSF-treated monocytes compared to tissue that included M-CSF-treated monocytes. In contrast, a higher percentage of α -SMA-positive cells was detected in tissue constructed with M-CSF-treated monocytes mixed at varying ratios with SSc fibroblasts, implicating a role of alternative pathway-activated monocytes in myofibroblast activation. Accordingly, the 1:1 ratio of fibroblasts and monocytes in the model 1 triculture saSE was used in subsequent experiments to generate individualized tissue,

in order to more completely model the dermal pathology observed in SSc. We confirmed the presence of stratified epithelium, proliferating basal keratinocytes, myofibroblasts, and macrophages by immunohistochemical staining using keratin 10 and BrdU (keratinocytes), α -SMA (myofibroblasts), and CD163 (macrophages) (Figure 3E).

Recapitulation of hallmarks of cutaneous fibrosis in SSc by individualized all-human skin equivalents.

To mimic SSc patient skin using saSE, we incorporated SSc patient-derived monocytes into saSE constructed with SScDFs and replaced the serum in the culture medium with monocyte donor-matched plasma (Figure 4A). Control saSE was constructed using NDFs and healthy donor monocytes and autologous plasma to mimic normal skin (Figure 4A). SSc saSE contracted more and consistently showed increased stromal thickness and stiffness compared to control saSE (Figures 4B and C). Notably, stromal rigidity was increased almost 3-fold in SSc saSE fabricated with monocytes versus control saSE, compared to a <2-fold increase in saSE constructed with SScDFs and NDFs in the absence of monocytes (Figure 2C and Figure 4C). This result implicates a pathophysiological role for macrophages in the induction of fibrosis in SSc.

To elucidate the polarized status of macrophages in saSE, expression of mRNA for *CD163* and *CD206* was measured by real-time qPCR. SSc saSE showed increased levels of both *CD163* and *CD206* mRNA, which are up-regulated in alternative pathway-activated macrophages, compared to control saSE (Figure 4D). Consistent with this result, increased numbers of CD163+ cells were detected in SSc saSE compared to control saSE by immunohistochemical staining (average 45.1% versus 21.8% [Figure 4E and Supplementary Figure 3A, available at <http://onlinelibrary.wiley.com/doi/10.1002/art.42097>]). The potential impact of macrophages on epidermal proliferation was assessed by quantifying the percentage of Ki-67+ keratinocytes in the tissue stroma; no significant differences were observed between SSc saSE and control saSE (Supplementary Figure 3B).

Elevated levels of IL-6, CCL22, and VEGF have previously been detected in SSc patient serum (26,27). Consistent with this, we found that these cytokines were also present at higher levels in SSc saSE supernatants compared to supernatants from control saSE (Figure 4F), which suggests that multiple cell types contribute collectively to systemic dysregulation of cytokines. Conversely, soluble G-CSF, CCL3, and CCL4 were down-regulated in SSc saSE (Figure 4F), and other cytokines within the 42-plex array panel showed either no difference between SSc saSE and control saSE, or were below detection limits (Supplementary Figure 4, <http://onlinelibrary.wiley.com/doi/10.1002/art.42097>). Among the up-regulated cytokines in the tissue supernatants, CCL22 is produced by dermal macrophages and dendritic cells (28,29), and CD163+ macrophages have been identified as a major source of CCL22 (30). Taken together, these results

suggest niche-dependent differentiation of CD14⁺ SSc monocytes into SSc macrophages that express CD163, CD206, and CCL22 in saSE constructed with SScDFs and SSc plasma.

Amelioration of the TGF β -induced fibrotic phenotype in SSc saSE by suppression of Smad3. To validate the potential use of saSE as a screening platform for antifibrotic

therapies, we evaluated tissue responses to TGF β , one of the best-characterized fibrogenic mediators in SSc, and tested whether modulation of TGF β signaling via Smad3 inhibition resulted in attenuation of fibrosis. We treated control and SSc saSE constitutively with TGF β 1 and SIS3, which is a small molecular inhibitor of Smad3 (31), at week 3 for 7 days after full epithelial establishment in saSE (Figure 5A).

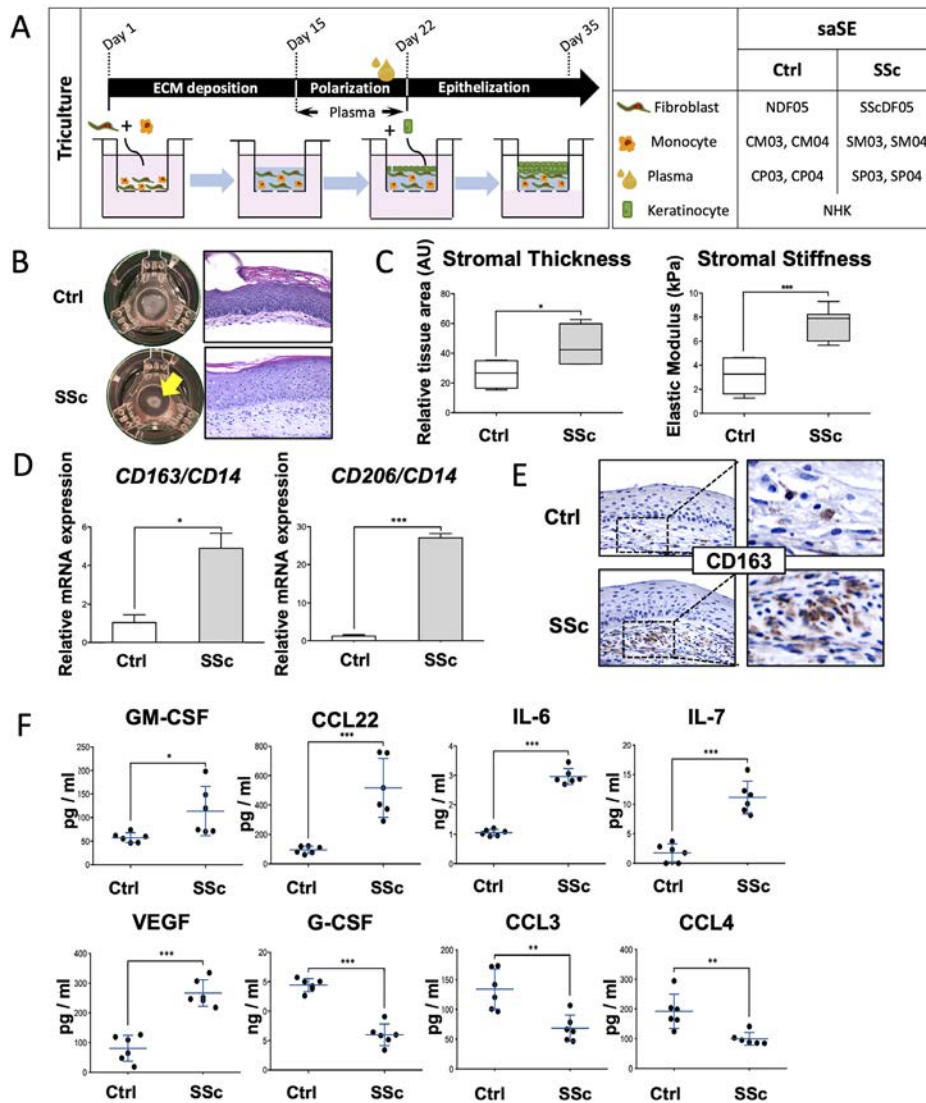


Figure 4. Construction and analysis of all-human SSc saSE and control saSE. **A**, Schematic overview of control (Ctrl) and SSc saSE generation. NDFs and healthy donor monocytes and plasma were used to construct control saSE. SScDFs and monocytes and plasma from SSc patients were used to construct SSc saSE. Keratinocytes were isolated from donated neonatal foreskin. **B**, Overhead pictures of control and SSc saSE samples growing in air–liquid interface and representative morphology of hematoxylin and eosin–stained control ($n = 4$) and SSc saSE ($n = 4$) tissue sections. **Yellow arrow** indicates contracted tissue. **C**, Stromal layer thickness assessed by determination of relative tissue surface area using ImageJ software and stromal layer rigidity measured by elastic modulus. Data are presented as box plots, where the boxes represent the IQR, the lines within the boxes represent the median, and the lines outside the boxes represent $1.5\times$ the IQR. **D**, Relative levels of *CD163* and *CD206* mRNA expression normalized to the expression of *CD14*, determined by the $\Delta\Delta C_t$ method. **E**, Immunohistochemical staining of CD163⁺ cells in control and SSc saSE. Right panels show higher-magnification views of the boxed areas in the left panels. **F**, Soluble levels of granulocyte–macrophage colony-stimulating factor (GM-CSF), G-CSF, IL-6, IL-7, vascular endothelial growth factor (VEGF), CCL3, CCL4, and CCL22 in control and SSc saSE supernatants on day 25. In **D** and **F**, Bars show the mean \pm SD; symbols in **F** represent individual samples. * = $P < 0.05$; ** $P < 0.01$; *** = $P < 0.001$. CM = control monocyte; SM = SSc monocyte; NHK = normal human keratinocyte. (see Figure 2 for other definitions).

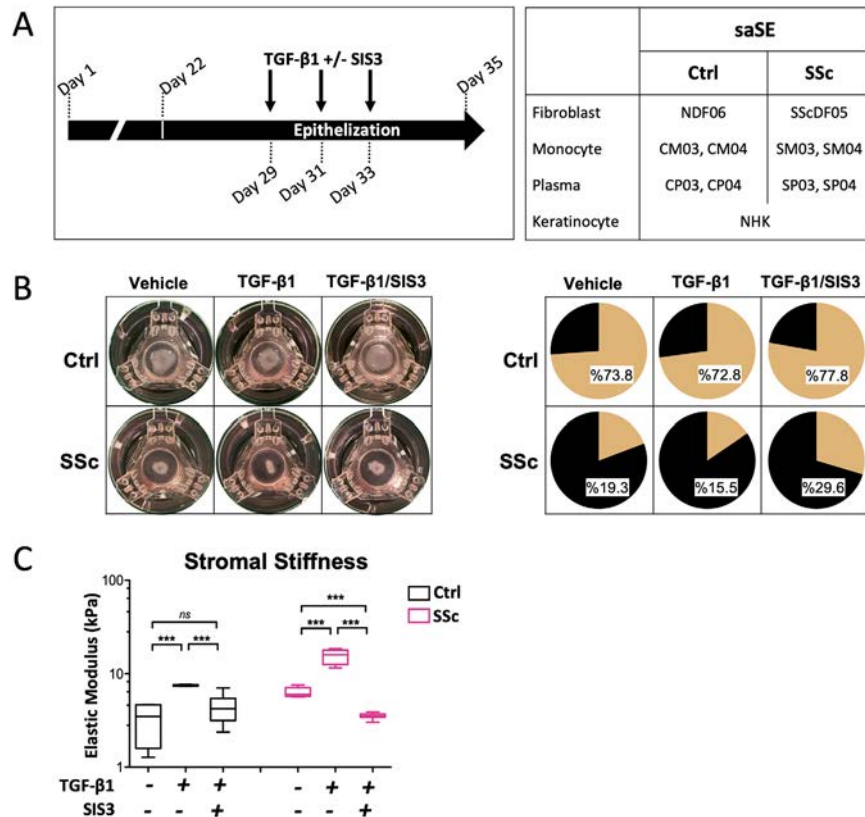


Figure 5. TGF β -induced profibrotic responses in all-human control (Ctrl) and SSc saSE. **A**, Overview of treatment of control ($n = 4$) and SSc saSE ($n = 4$) with 2 ng/ml TGF β 1 and/or 3 μ M Smad3 inhibitor (SIS3) for 6 days. Medium was refreshed with TGF β 1 with or without SIS3 every 2 days after establishment of epithelization (arrows). **B**, Overhead pictures of control and SSc saSE on day 35, and pie graphs representing the ratio of average tissue surface area (in tan) to total culture area. **C**, Rigidity of stromal layer of control and SSc saSE measured by elastic modulus. Data are presented as box plots, where the boxes represent the IQR, the lines within the boxes represent the median, and the lines outside the boxes represent 1.5 \times the IQR. *** = $P < 0.001$. CM = control monocyte; SM = SSc monocyte; NHK = normal human keratinocyte. (see Figure 2 for other definitions).

As demonstrated in Figure 5B, TGF β 1-induced contraction, which was inversely associated with tissue surface area in cultures, was observed in both control and SSc saSE. SSc saSE was more susceptible than control saSE to the effects of TGF β on fibrosis, as TGF β 1 treatment resulted in increased contractility (as indicated by decreased surface area from 19.3% to 15.5% in SSc SaSE compared to 73.8% to 72.8% in control saSE) (Figure 2B). Interestingly, when tissue was cultured concurrently with SIS3 and TGF β 1, contractility was inhibited in both control and SSc saSE, as suggested by the increased surface area of saSE from 73.8% to 77.8% in SSc saSE and from 19.3% to 29.6% in control saSE (Figure 5B). This may be attributable to SIS3 inhibition of endogenous Smad3-mediated TGF β signaling in saSE. In support of this, we found that SAS tissue constructed with SScDFs formed nodules in response to TGF β treatment, and this effect was abrogated by the addition of SIS3 (Supplementary Figure 5, <http://onlinelibrary.wiley.com/doi/10.1002/art.42097>). This was consistent with our previous finding in HSE tissue (i.e., keratinocytes + bovine collagen [Figure 1]), in which TGF β 1-induced stromal tissue contraction was enhanced by the inclusion of the epidermal layer (17).

The rigidity of the stroma in saSE was measured to determine if TGF β -induced stiffness could be suppressed by SIS3 (Figure 5C). Surprisingly, TGF β /SIS3-treated SSc saSE demonstrated a less stiff stroma than vehicle-treated SSc saSE, whereas no significant differences were observed between TGF β /SIS3-treated control saSE and vehicle-treated control saSE (Figure 5C). This result is consistent with decreased contractility observed in TGF β /SIS3-treated SSc saSE (Figure 5B), and may be explained by higher levels of endogenous TGF β in SSc saSE (Figure 2D). In summary, these results suggest the utility of saSE systems as in vitro models to mimic individualized responses to profibrogenic mediators and to evaluate the therapeutic efficacy of treatments that inhibit profibrotic regulators.

DISCUSSION

There is an unmet need for in vitro model systems that better represent the complexity and heterogeneity of disease in SSc patients, which is attributable to interpatient genetic and molecular variability (2,3,32–34). While animal models are a useful tool

for elucidating mechanisms of fibrosis, they do not recapitulate the full range of clinical features associated with SSc (2,3,32,35). Although bleomycin-induced, TSK1+, TSK2+, and sclGVHD mouse models of fibrosis are well characterized, they incompletely recapitulate all aspects of SSc. In recent years, several new model systems have emerged to fill this translational gap. The use of humanized mice, which carry human tissue transplants, enable direct studies of patient cells in a complex in vivo environment (36). In addition, human organ equivalents, which allow human cells to differentiate and form organ-like structures in vitro, have shown great potential as patient-derived platforms for therapeutic discovery (9).

Similar to human organ equivalents, ex vivo human tissue culture preserves the integrity of tissue architecture and the interplay of multiple resident cells within a naive tissue environment (37–40). However, access to human discarded surgical tissue is limited, especially as SSc is a rare disease. The use of human organ equivalents can overcome this limitation, as the fabrication process requires little beyond tissue culture supplies, and facilitates reproducibility of experimental results among multiple research institutes.

In this study, we focused on the development of in vitro skin models in which the fibroblasts produce their own ECM to produce a dermal-like tissue. Our initial work established 2 complimentary skin-like tissue models (HSE and SAS [Figure 1]) in which human patient-derived cells are used to study the cross-talk and interaction of human keratinocytes and fibroblasts (17). Our current study expands these models to include immune cells and SSc patient-derived circulating factors. The goal of this work was to create a realistic SSc 3-D tissue microenvironment, in which epithelial–dermal-immune cell cross-talk fostered the types of cell differentiation phenotypes observed in vivo.

Bioengineered in vitro models of SSc skin must be capable of recapitulating at least 1 (if not all) of the 3 clinical hallmarks of cutaneous fibrosis: altered matrix deposition, inflammatory cell infiltration, and increased dermal rigidity. The saSE characterized in this study closely resembles the physiology of human skin, with a fully stratified epithelium differentiated from neonatal foreskin fibroblasts and a dermal layer made from de novo matrix deposited by skin fibroblasts, where fibrosis occurs in SSc skin (41). Thus, we refer to saSE as an all-human skin equivalent to emphasize that it is composed entirely of primary human cell components, which distinguishes it from previous skin models, in which bovine collagen served as the matrix layer, or models fabricated with scaffold to support cellular distribution and tissue organization (9,10,42). Rather, saSE serves as a novel model, with de novo matrix derived from primary human SSc fibroblasts that support the differentiation of keratinocytes to form polarized epithelium of the skin. Furthermore, SSc saSE is characterized by markedly increased stromal deposition and stiffness compared to control saSE.

One challenge of creating in vitro models that resemble human cutaneous SSc is the need for incorporation of myeloid cells to mimic infiltration of inflammatory cells into SSc skin. Circulating monocytes differentiate into macrophages during active fibrosis and resolution phases of the disease (18). Subsets of profibrotic macrophages persist in tissue in SSc and induce prolonged fibroblast activation and chronic tissue inflammation, culminating in fibrosis (24,43). It has been reported that SSc patients have a higher percentage and elevated numbers of peripheral blood monocytes compared to healthy controls (44,45). Moreover, monocytes from SSc patients have an increased potential to trans-differentiate upon stimulation to myofibroblasts that express type I collagen and α -SMA (46). Furthermore, recent studies suggest that macrophages derived from the peripheral blood and skin of SSc patients have a profibrotic phenotype (CD163 + CD206+) (10,45,47). Thus, establishing pathophysiologically relevant in vitro models of SSc with monocytes and macrophages is crucial to recapitulate human SSc pathology.

In this regard, we have now shown that SSc saSE constructed with patient-derived fibroblasts and CD14+ peripheral blood monocytes results in macrophages with increased expression of CD206 and CD163 compared to control saSE constructed with healthy control cells. Consistent with this, cytokine profiling of saSE supernatant suggested a predominant underlying inflammatory activation of SSc monocytes and fibroblasts embedded in SSc saSE, as indicated by up-regulated secretion of IL-6, which is a well-characterized profibrogenic mediator in SSc (21,48). Our 3-D skin equivalent provides a novel tool to investigate the process of monocyte to profibrotic macrophage differentiation in vitro and to determine how the interplay of macrophages with resident fibroblasts leads to the progression of fibrosis in SSc.

Despite the improvement of increasing cellular complexity by adding immunocytes in saSE, other cell types implicated as important in SSc have not been addressed. For instance, incorporating endothelial cells into de novo stromal tissue may help the study of disease-associated vasculopathy (9,49). Also, in ongoing studies to investigate the role of each cell type in fibrosis, our group is using saSE to study cell–cell interactions at the systemic level to provide more mechanistic insight into the pathology of SSc (50). Since the fibroblasts and monocytes could be from patients with different genetic subsets and thus have different activation states, our future studies will utilize donor-matched cells to generate fully individualized skin models in vitro. We have also recently described a higher-throughput culture platform by increasing the current scale format of 24 wells to 96 wells for drug screening purposes (51).

Collectively, our findings demonstrate that saSE provides an opportunity to achieve greater precision in testing personalized responses of potential candidate drugs for SSc. Use of saSE may also contribute to the elucidation of basic mechanisms of SSc, ultimately generating additional therapeutic targets.

ACKNOWLEDGMENTS

We would like to thank Paula Dabenigno and Catherine Murphy (Tufts Clinical and Translational Research Center) and Dr. Gary Rogers (Tufts Medical Center) for their assistance in sample collection, and Dr. Monique Hinchcliff (Yale University) for providing essential material for tissue construction. We are grateful to Nicolette Kafasis and James Kirchmeyer for institutional review board and research coordination, and Jack Armitage and the New England Chapter of the Scleroderma Foundation for their assistance, advocacy, and support. We also thank Drs. Yolanda Nesbeth and Jake Reder (Celdara Medical, LLC) for providing perspectives on the translational aspects of this work, and for their collaboration and partial funding.

AUTHOR CONTRIBUTIONS

All authors were involved in drafting the article or revising it critically for important intellectual content, and all authors approved the final version to be published. Dr. Whitfield had full access to all of the data in the study and takes responsibility for the integrity of the data and the accuracy of the data analysis.

Study conception and design. Huang, Smith, Ivanovska, Pioli, Garlick, Whitfield.

Acquisition of data. Huang, Smith, Watson, Bhandari, Baugh, Watkins, Lang, Trojanowska, Black.

Analysis and interpretation of data. Huang, Smith, Watson, Baugh, Black, Pioli, Garlick, Whitfield.

ADDITIONAL DISCLOSURES


Author Ivanovska is an employee of Celdara Medical, LLC.

REFERENCES

- Smeets RL, Kersten BE, Joosten I, Kaffa C, Alkema W, Koenen H, et al. Diagnostic profiles for precision medicine in systemic sclerosis; stepping forward from single biomarkers towards pathophysiological panels. *Autoimmun Rev* 2020;102515.
- Yue X, Yu X, Petersen F, Riemekasten G. Recent advances in mouse models for systemic sclerosis. *Autoimmun Rev* 2018;17:1225–34.
- Sargent JL, Li Z, Aliprantis AO, Greenblatt M, Lemaire R, Wu MH, et al. Identification of optimal mouse models of systemic sclerosis by interspecies comparative genomics. *Arthritis Rheumatol* 2016;68:2003–15.
- Beyer C, Schett G, Distler O, Distler JH. Animal models of systemic sclerosis: prospects and limitations [review]. *Arthritis Rheum* 2010; 62:2831–44.
- Whitfield ML, Finlay DR, Murray JI, Troyanskaya OG, Chi JT, Pergamenschikov A, et al. Systemic and cell type-specific gene expression patterns in scleroderma skin. *Proc Natl Acad Sci U S A* 2003;100:12319–24.
- Gardner H, Shearstone JR, Bandaru R, Crowell T, Lynes M, Trojanowska M, et al. Gene profiling of scleroderma skin reveals robust signatures of disease that are imperfectly reflected in the transcript profiles of explanted fibroblasts. *Arthritis Rheum* 2006;54:1961–73.
- Lang I, Huang M, Smith A, Finkelman M, Whitfield ML, Garlick J. Effect of scleroderma-derived fibroblast passage number on 3D Self-assembled tissues [poster]. Presented at the International Association for Dental Research/American Association for Dental Research/Canadian Association for Dental Research General Session; 2019 June 19–22; Vancouver, British Columbia, Canada.
- Chadli L, Sotthwes B, Li K, Andersen SN, Cahir-McFarland E, Cheung M, et al. Identification of regulators of the myofibroblast phenotype of primary dermal fibroblasts from early diffuse systemic sclerosis patients. *Sci Rep* 2019;9:4521.
- Matei AE, Chen CW, Kiesewetter L, Gyorfı AH, Li YN, Trinh-Minh T, et al. Vascularised human skin equivalents as a novel in vitro model of skin fibrosis and platform for testing of antifibrotic drugs. *Ann Rheum Dis* 2019;78:1686–92.
- Huang M, Cai G, Baugh LM, Liu Z, Smith A, Watson M, et al. Systemic sclerosis dermal fibroblasts induce cutaneous fibrosis through lysyl oxidase-like 4: new evidence from three-dimensional skin-like tissues. *Arthritis Rheumatol* 2019;72:791–801.
- Kim JW, Kim Y, Kim J, Park MJ, Kwon E, Lee J, et al. AB0189 3d skin organoid mimicking systemic sclerosis generated by patient-derived induced pluripotent stem cells: ‘disease in a dish’ and development of animal model. *Ann Rheum Dis* 2018;77 Suppl:1281.
- Watanabe T, Nishimoto T, Mlakar L, Heywood J, Malaab M, Hoffman S, et al. Optimization of a murine and human tissue model to recapitulate dermal and pulmonary features of systemic sclerosis. *PLoS One* 2017;12:e0179917.
- Bellas E, Seiberg M, Garlick J, Kaplan DL. In vitro 3D full-thickness skin-equivalent tissue model using silk and collagen biomaterials. *Macromol Biosci* 2012;12:1627–36.
- Bourland J, Fradette J, Auger FA. Tissue-engineered 3D melanoma model with blood and lymphatic capillaries for drug development. *Sci Rep* 2018;8:13191.
- Cores J, Hensley MT, Kinlaw K, Rikard SM, Dinh PU, Paudel D, et al. Safety and efficacy of allogeneic lung spheroid cells in a mismatched rat model of pulmonary fibrosis. *Stem Cells Transl Med* 2017;6:1905–16.
- Smith A, Huang M, Watkins T, Burguin F, Baskin J, Garlick JA. De novo production of human extracellular matrix supports increased throughput and cellular complexity in 3D skin equivalent model. *J Tissue Eng Regen Med* 2020;14:1019–27.
- Huang M, Liu Z, Baugh L, DeFuria J, Maione A, Smith A, et al. Lysyl oxidase enzymes mediate TGF- β 1-induced fibrotic phenotypes in human skin-like tissues. *Lab Invest* 2018;99:514–527.
- Wynn TA, Vannella KM. Macrophages in tissue repair, regeneration, and fibrosis. *Immunity* 2016;44:450–62.
- Bhandari R, Ball MS, Martyanov V, Popovich D, Schaafsma E, Han S, et al. Profibrotic activation of human macrophages in systemic sclerosis. *Arthritis Rheumatol* 2020;72:1160–9.
- Yeager MP, Pioli PA, Collins J, Barr F, Metzler S, Sites BD, et al. Glucocorticoids enhance the in vivo migratory response of human monocytes. *Brain Behav Immun* 2016;54:86–94.
- Denton CP, Ong VH, Xu S, Chen-Harris H, Modrusan Z, Lafyatis R, et al. Therapeutic interleukin-6 blockade reverses transforming growth factor-beta pathway activation in dermal fibroblasts: insights from the faSScinate clinical trial in systemic sclerosis. *Ann Rheum Dis* 2018;77:1362–71.
- O’Reilly S, Cant R, Ciechomska M, van Laar JM. Interleukin-6: a new therapeutic target in systemic sclerosis? *Clin Transl Immunology* 2013;2:e4.
- Ghosh AK, Yuan W, Mori Y, Varga J. Smad-dependent stimulation of type I collagen gene expression in human skin fibroblasts by TGF- β involves functional cooperation with p300/CBP transcriptional coactivators. *Oncogene* 2000;19:3546–55.
- Hinz B. Tissue stiffness, latent TGF- β 1 activation, and mechanical signal transduction: implications for the pathogenesis and treatment of fibrosis. *Curr Rheumatol Rep* 2009;11:120–6.
- Kania G, Rudnik M, Distler O. Involvement of the myeloid cell compartment in fibrogenesis and systemic sclerosis [review]. *Nat Rev Rheumatol* 2019;15:288–302.
- Scala E, Pallotta S, Frezzolini A, Abeni D, Barbieri C, Sampogna F, et al. Cytokine and chemokine levels in systemic sclerosis: relationship

- with cutaneous and internal organ involvement. *Clin Exp Immunol* 2004;138:540–6.
27. Choi JJ, Min DJ, Cho ML, Min SY, Kim SJ, Lee SS, et al. Elevated vascular endothelial growth factor in systemic sclerosis. *J Rheumatol* 2003;30:1529–33.
 28. Copyright. In: Rich RR, Fleisher TA, Shearer WT, Schroeder HW, Frew AJ, Weyand CM, editors. *Clinical Immunology (Third Edition)*. Edinburgh: Mosby; 2008. p. iv.
 29. Rapp M, Wintergerst MW, Kunz WG, Vetter VK, Knott MM, Lisowski D, et al. CCL22 controls immunity by promoting regulatory T cell communication with dendritic cells in lymph nodes. *J Exp Med* 2019;216:1170–81.
 30. Tanita K, Fujimura T, Sato Y, Lyu C, Kambayashi Y, Ogata D, et al. Bexarotene reduces production of CCL22 from tumor-associated macrophages in cutaneous T-cell lymphoma. *Front Oncol* 2019;9:907.
 31. Jinnin M, Ihn H, Tamaki K. Characterization of SIS3, a novel specific inhibitor of Smad3, and its effect on transforming growth factor- β 1-induced extracellular matrix expression. *Mol Pharmacol* 2006;69:597–607.
 32. Marangoni RG, Varga J, Tourtellotte WG. Animal models of scleroderma: recent progress. *Curr Opin Rheumatol* 2016;28:561–70.
 33. Volkmann ER, Varga J. Emerging targets of disease-modifying therapy for systemic sclerosis. *Nat Rev Rheumatol* 2019;15:208–24.
 34. Distler JH, Györfi AH, Ramanujam M, Whitfield ML, Königshoff M, Lafyatis R. Shared and distinct mechanisms of fibrosis [review]. *Nat Rev Rheumatol* 2019;15:705–30.
 35. Storkanova H, Tomcik M. Animal models of systemic sclerosis. In: Radic M, editor. *Systemic Sclerosis*. London: IntechOpen; 2017.
 36. Shultz LD, Keck J, Burzenski L, Jangalwe S, Vaidya S, Greiner DL, et al. Humanized mouse models of immunological diseases and precision medicine. *Mamm Genome* 2019;30:123–42.
 37. Xu W, Hong SJ, Jia S, Zhao Y, Galiano RD, Mustoe TA. Application of a partial-thickness human ex vivo skin culture model in cutaneous wound healing study. *Lab Invest* 2012;92:584–99.
 38. Rakita A, Nikolic N, Mildner M, Matiasek J, Elbe-Burger A. Re-epithelialization and immune cell behaviour in an ex vivo human skin model. *Sci Rep* 2020;10:1.
 39. Lehmann M, Buhl L, Alsafadi HN, Klee S, Hermann S, Mutze K, et al. Differential effects of Nintedanib and Pirfenidone on lung alveolar epithelial cell function in ex vivo murine and human lung tissue cultures of pulmonary fibrosis. *Respir Res* 2018;19:175.
 40. Alsafadi HN, Staab-Weijnitz CA, Lehmann M, Lindner M, Peschel B, Königshoff M, et al. An ex vivo model to induce early fibrosis-like changes in human precision-cut lung slices. *Am J Physiol Lung Cell Mol Physiol* 2017;312:L896–902.
 41. Do NN, Eming SA. Skin fibrosis: models and mechanisms. *Curr Res Transl Med* 2016;64:185–93.
 42. Huang M, Liu Z, Baugh L, DeFuria J, Maione A, Smith A, et al. Lysyl oxidase enzymes mediate TGF- β 1-induced fibrotic phenotypes in human skin-like tissues. *Lab Invest* 2019;99:514–27.
 43. Misharin AV, Morales-Nebreda L, Reyfman PA, Cuda CM, Walter JM, McQuattie-Pimentel AC, et al. Monocyte-derived alveolar macrophages drive lung fibrosis and persist in the lung over the life span. *J Exp Med* 2017;214:2387–404.
 44. Lescoat A, Lecureur V, Roussel M, Sunnaram BL, Ballerie A, Coiffier G, et al. CD16-positive circulating monocytes and fibrotic manifestations of systemic sclerosis. *Clin Rheumatol* 2017;36:1649–54.
 45. Higashi-Kuwata N, Jinnin M, Makino T, Fukushima S, Inoue Y, Muchemwa FC, et al. Characterization of monocyte/macrophage subsets in the skin and peripheral blood derived from patients with systemic sclerosis. *Arthritis Res Ther* 2010;12:R128.
 46. Binai N, O'Reilly S, Griffiths B, van Laar JM, Hugel T. Differentiation potential of CD14+ monocytes into myofibroblasts in patients with systemic sclerosis. *PLoS One* 2012;7:e33508.
 47. Higashi-Kuwata N, Makino T, Inoue Y, Takeya M, Ihn H. Alternatively activated macrophages (M2 macrophages) in the skin of patient with localized scleroderma. *Exp Dermatol* 2009;18:727–9.
 48. Choy EH, De Benedetti F, Takeuchi T, Hashizume M, John MR, Kishimoto T. Translating IL-6 biology into effective treatments [review]. *Nat Rev Rheumatol* 2020;16:335–45.
 49. Magdeldin T, López-Dávila V, Pape J, Cameron GW, Emberton M, Loizidou M, et al. Engineering a vascularised 3D in vitro model of cancer progression. *Sci Rep* 2017;7:44045.
 50. Toledo DM, Huang M, Wang Y, Mehta BK, Wood TA, Smith A, et al. Multi-omic characterization of engineered skin equivalent tissues from patients with systemic sclerosis molecularly resembles patient skin. Unpublished observations. 2020.
 51. Popovich D, Whitfield M, Wang Y, Cai G, Huang M. Computational methods for drug repositioning of systemic sclerosis using gene fold-change and network analyses [abstract]. *Arthritis Rheumatol* 2019;71 Suppl 10.

Role for Granulocyte Colony-Stimulating Factor in Neutrophilic Extramedullary Myelopoiesis in a Murine Model of Systemic Juvenile Idiopathic Arthritis

Bert Malengier-Devlies,¹  Eline Bernaerts,¹ Kourosh Ahmadzadeh,¹ Jessica Filtjens,¹ Jessica Vandenhaute,¹ 
Bram Boeckx,² Oliver Burton,³ Amber De Visscher,¹  Tania Mitera,¹ Nele Berghmans,¹ Geert Verbeke,¹
Adrian Liston,³ Diether Lambrechts,² Paul Proost,¹  Carine Wouters,⁴ and Patrick Matthys¹

Objective. Systemic juvenile idiopathic arthritis (JIA) is a systemic inflammatory disease with childhood onset. Systemic JIA is associated with neutrophilia, including immature granulocytes, potentially driven by the growth factor granulocyte-colony stimulating factor (G-CSF). This study was undertaken to investigate the role of G-CSF in the pathology of systemic JIA.

Methods. Injection of Freund's complete adjuvant (CFA) in BALB/c mice induces mild inflammation and neutrophilia in wild-type (WT) mice and a more pronounced disease, reminiscent to that of JIA patients, in interferon- γ -knockout (IFN γ -KO) mice. Extramedullary myelopoiesis was studied in CFA-immunized mice by single-cell RNA sequencing, and the effect of G-CSF receptor (G-CSFR) blockage on neutrophil development and systemic JIA pathology was evaluated. Additionally, plasma G-CSF levels were measured in patients.

Results. Both in systemic JIA patients and in a corresponding mouse model, plasma G-CSF levels were increased. In the mouse model, we demonstrated that G-CSF is responsible for the observed neutrophilia and extramedullary myelopoiesis and the induction of immature neutrophils and myeloid-derived suppressor-like cells. Administration of a G-CSFR antagonizing antibody blocked the maturation and differentiation of neutrophils in CFA-immunized mice. In IFN γ -KO mice, treatment was associated with almost complete inhibition of arthritis due to reduced neutrophilia and osteoclast formation. Disease symptoms were ameliorated, but slight increases in interleukin-6 (IL-6), tumor necrosis factor, and IL-17 were detected upon G-CSFR inhibition in the IFN γ -KO mice, and were associated with mild increases in weight loss, tail damage, and immature red blood cells.

Conclusion. We describe the role of G-CSF in a mouse model of systemic JIA and suggest an important role for G-CSF-induced myelopoiesis and neutrophilia in regulating the development of arthritis.

INTRODUCTION

Systemic juvenile idiopathic arthritis (JIA) is a childhood disorder characterized by arthritis and systemic inflammation, such as quotidian fever, skin rash, weight loss, polyserositis, hepatosplenomegaly, and lymphadenopathy. Hematologic

features include neutrophilia, lymphocytopenia, anemia, thrombocytosis and increased levels of interleukin-6 (IL-6), IL-18, and S100 proteins (1–4). Systemic JIA is considered as a systemic inflammatory disease with a pathogenic role for IL-1 β and IL-6 as evident by successful treatment with IL-1 or IL-6 antagonists (5).

Supported by FWO grant G0A3218N and Katholieke Universiteit Leuven C1 grant C16/17/010. Mr. Ahmadzadeh, Dr. Vandenhaute, and Ms. De Visscher are FWO Fellows (awards 1S75320N, 1S10618N, and 11K0722N, respectively). Dr. Wouters' work was supported by unrestricted grants to KU Leuven from Novartis, Roche, GSK Immuno-inflammation, and Pfizer.

¹Bert Malengier-Devlies, PhD, Eline Bernaerts, MS, Kourosh Ahmadzadeh, MS, Jessica Filtjens, PhD, Jessica Vandenhaute, PhD, Amber De Visscher, MS, Tania Mitera, BS, Nele Berghmans, PhD, Geert Verbeke, PhD, Paul Proost, PhD, Patrick Matthys, PhD: Katholieke Universiteit (KU) Leuven, Leuven, Belgium; ²Bram Boeckx, PhD, Diether Lambrechts, PhD: KU Leuven and Vlaams Instituut voor Biotechnologie-KU Leuven, Leuven, Belgium; ³Oliver Burton, PhD, Adrian Liston, PhD: KU Leuven and Vlaams Instituut voor

Biotechnologie-KU Leuven, Leuven, Belgium, and the Babraham Institute, Cambridge, UK; ⁴Carine Wouters, MD, PhD: KU Leuven, University Hospitals Leuven, and European Reference Network for Rare Immunodeficiency, Auto-inflammatory and Autoimmune Diseases at University Hospital Leuven, Leuven, Belgium.

Author disclosures are available at <https://onlinelibrary.wiley.com/action/downloadSupplement?doi=10.1002%2Fart.42104&file=art42104-sup-0001-Disclosureform.pdf>.

Address correspondence to Patrick Matthys, PhD, Laboratory of Immunobiology, Rega Institute, Katholieke Universiteit Leuven, Herestraat 49, Box 1044, 3000 Leuven, Belgium. Email: patrick.matthys@kuleuven.be.

Submitted for publication March 27, 2021; accepted in revised form February 27, 2022.

Neutrophils are the most abundant innate immune effectors in the human circulation. Neutrophils kill pathogens through overlapping oxidative and nonoxidative mechanisms including phagocytosis and degranulation (6). Inappropriate activation of neutrophils in a sterile inflammatory setting can result in host tissue damage, as described in several autoimmune and autoinflammatory disorders (7). Increasing evidence has emerged for neutrophils with immunomodulatory properties (known as myeloid-derived suppressor cells [MDSCs]) (8). In systemic JIA, the role of neutrophils remains largely unknown. Recently, increased numbers of immature and hypermature neutrophils were described in patients with systemic JIA, which correlated with inflammatory disease parameters and which were reduced upon IL-1 β blockage (9–11). Neutrophils are a key source of S100 proteins, amplifying the innate immune response. Furthermore, patient neutrophils showed an inflammatory gene expression and primed phenotype (9–11). The presence of immature granulocytes in patient blood is indicative of extensive myelopoiesis.

Our group developed a mouse model of systemic JIA that mimicked the disease in its clinical, hematologic, and histologic features (12). The model relies on administration of Freund's complete adjuvant (CFA) containing heat-killed *Mycobacterium butyricum* in BALB/c mice and requires the use of interferon- γ -knockout (IFN γ -KO) mice, since wild-type (WT) mice only develop a transient inflammatory disease reaction (12). While systemic JIA patients do not have mutations in the IFN γ gene or its receptor, the clinical relevance of the model is related to the fact that natural killer (NK) cells from these patients display profound defects in IL-18-induced IFN γ production (13,14). Within 2 weeks post-CFA challenge, IFN γ -KO mice developed arthritis, lymphadenopathy, anemia, thrombocytosis, and increased levels of IL-6. Moreover, the mice developed splenomegaly and extensive and poorly understood myelopoiesis and neutrophilia, characterized by the presence of immature neutrophils (12).

Granulocyte colony-stimulating factor (G-CSF) is the major regulator of granulocyte production. G-CSF signals through the G-CSF receptor (G-CSFR) expressed on myeloid progenitors, neutrophils, monocytes, macrophages, as well as endothelial cells (15). Administration of G-CSF increases peripheral blood neutrophil numbers and enhances their migration into tissues by promoting adhesion molecules expressed on neutrophils and endothelial cells (16). In a clinical setting, G-CSF is used to treat neutropenia or to mobilize hematopoietic stem cells for transplantation purposes (17).

Neutrophils may be a major contributor to the inflammatory cascade of systemic JIA, but studies in animal models are lacking. In an attempt to study the role of neutrophils in our systemic JIA-like mouse model, we previously used anti-Ly-6G-depleting antibodies, but unfortunately, this approach only partially depleted immature neutrophils, and the treatment was followed by a rebound of new neutrophils (18). In the current study, we

hypothesized that G-CSF might be involved in driving myelopoiesis and the pathogenesis of systemic JIA. To this end, we treated systemic JIA mice with a G-CSFR-blocking monoclonal antibody and studied the extramedullary development of neutrophils and its effect on the development of disease. In a cohort of systemic JIA patients, we also measured G-CSF and granulocyte-macrophage CSF (GM-CSF).

SUBJECTS AND METHODS

Patients. In this study, 7 macrophage activation syndrome (MAS) patients, 10 systemic JIA patients, and 15 age and sex-balanced healthy controls were recruited. Matched systemic JIA samples were collected during the active disease state ($n = 10$) and during the inactive disease state ($n = 8$). This study was performed at the University Hospital of Leuven, conducted according to the Declaration of Helsinki, and approved by the Katholieke Universiteit Leuven Ethics Committee (S58814). Patient classification was based on the criteria of the International League of Associations for Rheumatology. A detailed list of patient characteristics can be found in Supplementary Table 1, available on the *Arthritis & Rheumatology* website at <https://onlinelibrary.wiley.com/doi/10.1002/art.42104>. Samples were collected before any therapeutic intervention or at disease flares. Healthy controls were recruited via collaboration with the Department of Pediatrics of the University Hospital of Leuven and comprised patients admitted to the hospital for elective surgical procedures without systemic inflammation or those who were siblings of pediatric patients.

Mouse model of systemic JIA. Systemic JIA-like disease was induced in 6–9-week-old WT and IFN γ -KO BALB/c mice, as previously described (12) and as extensively detailed in the Supplementary Methods, available on the *Arthritis & Rheumatology* website at <https://onlinelibrary.wiley.com/doi/10.1002/art.42104>.

Anti-G-CSF antibody treatment. Mice were injected intraperitoneally, twice a week, with 200 μ g anti-G-CSFR (α G-CSFR) (Ch5E2-VR81-mIgG1k) (19), starting 1 day prior to immunization. CFA-immunized WT and IFN γ -KO mice injected intraperitoneally with phosphate buffered saline (PBS) were included as controls. To reduce any cage effect, all conditions were manually divided among the different cages, and all cages with either WT or IFN γ -KO mice contained mice from all 3 different groups (treatment-naive mice, CFA-immunized and PBS-treated mice, and CFA-immunized and α G-CSFR-treated mice). Mice were euthanized between days 16 and 25. No mice were excluded in this study.

Blood analysis. Murine blood samples were obtained by heart puncture with heparin (Leo Pharma). Blood cell analysis was performed on a Cell-Dyn 3700 Hematology Analyzer (Abbott Diagnostics). Plasma was stored at -80° C. Human peripheral blood mononuclear cells were obtained by

Lymphoprep density centrifugation. Cells were stored in liquid nitrogen in cryopreservation medium (90% fetal calf serum, 10% dimethyl sulfoxide). Human plasma was isolated, centrifuged for 10 minutes at 1,000g, and stored at -80°C .

Histologic and cytospin analysis. For cytospin analysis, single-cell suspensions were spun on a slide, fixed with methanol, hematoxylin and eosin (H&E)-stained, and microscopically counted. For histologic examination, fore limbs and hind limbs were fixed in 10% formalin and decalcified with formic acid. Paraffin sections were stained with H&E and scored under blinded conditions for the following: infiltration of mono- and polymorphonuclear cells, hyperplasia of the synovium, and pannus formation. Severity was scored as 0 (absent), 1 (mild), 2 (average), 3 (severe), or 4 (extensive).

In vitro osteoclast formation. Splenocytes were cultured in α -minimum essential medium REGA-3 and stimulated with RANKL (100 ng/ml) and M-CSF (20 ng/ml) (both from R&D Systems). After 3 days, cells were restimulated for 3–4 days, and stained for tartrate-resistant acid phosphatase (TRAP), as previously described (20). TRAP+ multinucleated cells (≥ 3 nuclei) were defined as osteoclasts.

Protein quantification. G-CSF, IL-1 β , IL-6, IL-17, IL-22, and tumor necrosis factor (TNF) were measured by the ProcartaPlex mouse multiplex enzyme-linked immunosorbent assay (ThermoFisher). Meso Scale Discovery's multiplex assay was used to measure human plasma C-reactive protein (CRP) and inflammatory cytokines. All were conducted according to the manufacturer's protocols.

Flow cytometry. Spleens and inguinal lymph nodes (LNs) were passed through a cell strainer (70 μm) to obtain single-cell suspensions. Red blood cells (RBCs) were lysed using ACK lysing buffer (Gibco). Cells were incubated with Fc receptor blocking reagent (Miltenyi Biotec) and extracellularly stained. Dead cells were excluded using Zombie Aqua 516 (BioLegend). Intracellular staining of cytokines was performed using a Fixation and Permeabilization kit, according to protocols of the manufacturer (BD Biosciences). Transcription factors were stained with a FoxP3/transcription factor staining set (ThermoFisher Scientific). A list of the antibodies used is presented in Supplementary Table 2, available on the *Arthritis & Rheumatology* website at <https://onlinelibrary.wiley.com/doi/10.1002/art.42104>. Flow cytometry was performed using the BD LSR Fortessa X20, and data were analyzed with FlowJo, version 10.

Chemotaxis assay. The in vivo chemotactic response of murine neutrophils toward CXCL8 (amino acid 6-77) was assessed as previously described (21).

Single-cell RNA-sequencing. Single-cell RNA-sequencing (RNA-seq) was applied to sorted CD3–CD19–Gr-1+ splenocytes from WT and IFN γ -KO mice immunized with CFA. Cells were barcoded by the 10X Genomics system and sequenced on an Illumina HiSeq4000. All details about single-cell RNA-seq procedures and analyses are described in the Supplementary Methods, available on the *Arthritis & Rheumatology* website at <https://onlinelibrary.wiley.com/doi/10.1002/art.42104>.

Statistical analysis. Graphs were created using GraphPad Prism software version 8.0. Statistics were assessed in R or GraphPad Prism. Statistics are extensively described in the Supplementary Methods. Statistics and sample size for each analysis are included in the figure legends. All statistical analyses were performed at the 5% significance level.

Data availability. All data are available upon request.

RESULTS

Increased levels of G-CSF that correlate with proinflammatory cytokines and absolute number of neutrophils in patients with active systemic JIA. In our study, 3 groups of patients were included: MAS patients ($n = 7$), patients with active systemic JIA ($n = 10$), and disease-matched patients with inactive systemic JIA (missing 2 measurements; $n = 8$). Those were compared to age- and sex-matched healthy controls ($n = 15$). Disease activity parameters are shown in Supplementary Table 1, available on the *Arthritis & Rheumatology* website at <https://onlinelibrary.wiley.com/doi/10.1002/art.42104>. Clinical features and laboratory parameters were determined, and the levels of 10 inflammatory cytokines were analyzed in the plasma. Increased plasma levels of IL-6, IL-18, and CRP were assessed (Supplementary Table 1). G-CSF levels were significantly increased in patients with active systemic JIA (mean 58.2 pg/ml [range 9–228.0]) compared to healthy controls (mean 12.3 pg/ml [range 8.1–27.6]). In patients in an inactive disease state, G-CSF levels were within the normal range (mean 19.0 pg/ml [range 8.4–41.5]) (Supplementary Figure 1A, available on the *Arthritis & Rheumatology* website at <https://onlinelibrary.wiley.com/doi/10.1002/art.42104>). Increased G-CSF levels were also detected in MAS patients (mean 43.2 pg/ml [range 17.7–123.4]) (Supplementary Figure 1A).

Levels of GM-CSF were normal across all patient groups (Supplementary Figure 1B). Correlation studies within the active systemic JIA group revealed a positive correlation between G-CSF level and the absolute number of white blood cells, monocytes, neutrophils, and plasma levels of both IL-6 and IL-1 β . Furthermore, a negative correlation between G-CSF level and the absolute number of lymphocytes was observed (Supplementary Figure 1C).

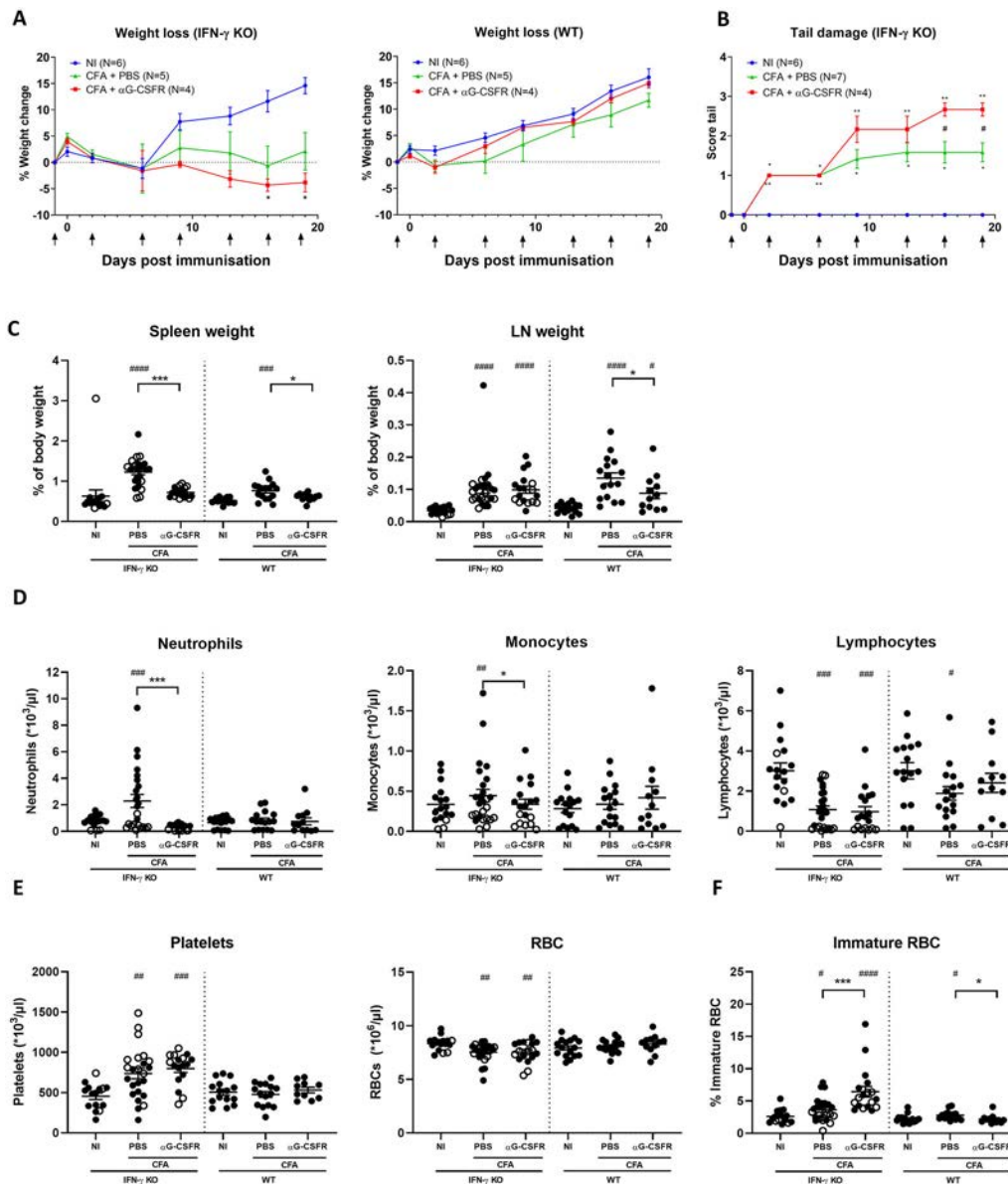


Figure 1. Effects of anti-granulocyte colony-stimulating factor receptor (α G-CSFR) antibody on Freund's complete adjuvant (CFA)-induced inflammation. CFA-immunized interferon- γ -knockout (IFN γ -KO) mice ($n = 18$) and wild-type mice (WT) ($n = 12$) were injected intraperitoneally twice a week with α G-CSFR (200 μ g) (arrows). Mice were euthanized between days 16 and 25 postimmunization. Phosphate buffered saline (PBS)-injected CFA-immunized IFN γ -KO mice ($n = 26$) and WT mice ($n = 16$) were included as controls and compared to treatment-naïve (NI) mice ($n = 15$ – 17). **A**, Percentage change in body weight ($n = 1$ experiment). **B**, Tail damage ($n = 1$ experiment) (for more details, see Supplementary Table 7B at <https://onlinelibrary.wiley.com/doi/10.1002/art.42104>). **C**, Spleen weight and inguinal lymph node (LN) weight expressed as percentage of total body weight. **D** and **E**, Neutrophil, monocyte, and lymphocyte counts (**D**) and platelet and red blood cell (RBC) counts (**E**) in blood samples, as measured with a blood cell analyzer. **F**, Percentage immature RBCs (TER119+CD71+) as measured by flow cytometry. Graphs show results from 3 pooled experiments. Each circle represents a single mouse; bars show the median and interquartile range for each group. Solid circles represent specific pathogen-free (SPF) conditions; open circles represent non-SPF conditions. * = $P < 0.05$; *** = $P < 0.001$ between indicated groups. # = $P < 0.05$; ## = $P < 0.01$; ### = $P < 0.001$; #### = $P < 0.0001$ versus IFN γ -KO treatment-naïve mice or WT treatment-naïve mice. All statistics were obtained using a linear mixed-effects model.

In mice, CFA immunization has been shown to induce in IFN γ -KO mice a systemic JIA-like disease (12). Similar to systemic JIA patients with active disease, increased levels of G-CSF were measured in the plasma upon immunization. A significantly

increased level was observed in immunized IFN γ -KO mice when compared to WT mice (Supplementary Figure 1D). In conclusion, plasma G-CSF levels were increased in both human systemic JIA and in the mouse model.

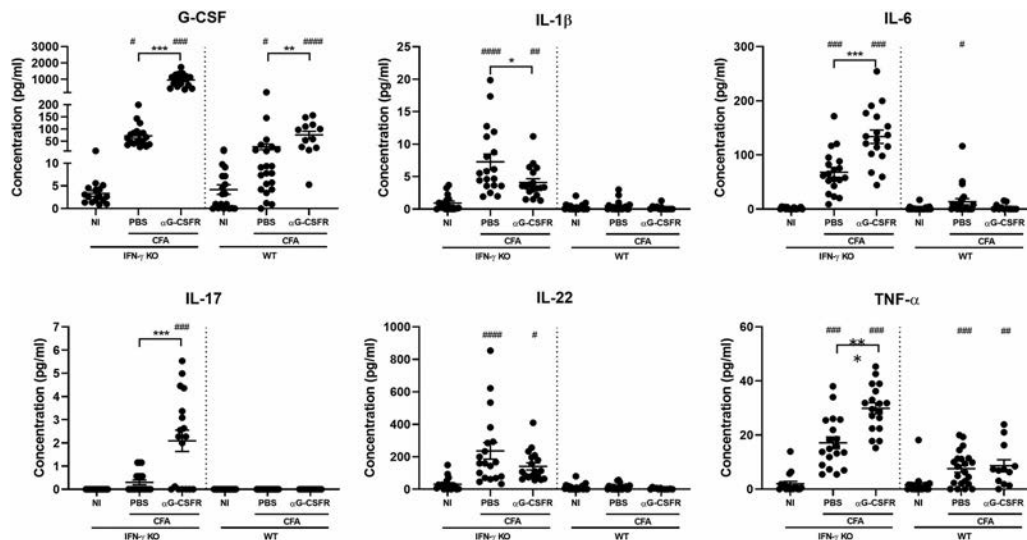


Figure 2. Altered plasma cytokine levels in α G-CSFR-treated CFA-immunized IFN γ -KO mice. CFA-immunized IFN γ -KO mice ($n = 18$) and WT mice ($n = 12$) were injected intraperitoneally twice a week with α G-CSFR (200 μ g). Mice were euthanized between days 16 and 25 postimmunization. PBS-injected CFA-immunized IFN γ -KO mice ($n = 19$) and WT mice ($n = 22$) were included as controls and compared to treatment-naive mice ($n = 17$ –21). Plasma levels of G-CSF, interleukin-1 β (IL-1 β), IL-6, IL-17, IL-22, and tumor necrosis factor (TNF) were measured with a ProcartaPlex multiplex system. Graphs show results from 3 pooled experiments. Each circle represents a single mouse; bars show the median and interquartile range for each group. * = $P < 0.05$; ** = $P < 0.01$; *** = $P < 0.001$ between indicated groups. # = $P < 0.05$; ## = $P < 0.01$; ### = $P < 0.001$; #### = $P < 0.0001$ versus IFN γ -KO treatment-naive mice or WT treatment-naive mice. All statistics were obtained using a linear mixed-effects model. See Figure 1 for other definitions.

Effects of α G-CSFR antibody on CFA-induced inflammation in IFN γ -KO and WT mice.

Next, we examined whether endogenous G-CSF causes CFA-induced inflammation by using a monoclonal antibody that blocks the G-CSF receptor (α G-CSFR). In sham-treated animals, we confirmed our previously reported findings that a single injection of CFA in the tail elicits local and systemic inflammation, with symptoms including tail damage, weight loss, splenomegaly, lymphadenopathy, neutrophilia, lymphopenia, thrombocytosis, and anemia. All of these symptoms were either more pronounced or exclusively present in IFN γ -KO mice compared to WT counterparts (Figure 1 and Supplementary Table 3, available on the *Arthritis & Rheumatology* website at <https://onlinelibrary.wiley.com/doi/10.1002/art.42104>) (12). When CFA-challenged IFN γ -KO mice were treated with α G-CSFR antibody, tail damage was found to be increased and mild weight loss occurred (Figures 1A and B). In WT mice, α G-CSFR antibody injection had no effect on body weight changes (Figure 1A) and did not increase tail damage (data not shown).

To investigate the effects of α G-CSFR injection on other systemic JIA-like symptoms, mice were euthanized between days 16 and 25. Anti-G-CSFR administration inhibited splenomegaly in both IFN γ -KO and WT mice. While enlargement of LNs was not affected by α G-CSFR antibody treatment in IFN γ -KO mice, those in WT animals were significantly reduced (Figure 1C). Hematologic analysis of CFA-challenged IFN γ -KO mice revealed that α G-CSFR administration completely inhibited neutrophilia and,

in part, monocytosis, while lymphopenia and thrombocytosis were not affected. In WT mice, lymphopenia was partially restored upon treatment (Figures 1D and E). Anemia, evaluated by the drop in number of RBCs, was not affected by α G-CSFR antibody treatment (Figure 1E). CFA-immunized IFN γ -KO mice showed a significant increase in percentage of immature TER119+CD71+ RBCs, which was further increased upon antibody injection. In contrast, in WT mice, the immature RBCs were significantly reduced by α G-CSFR treatment (Figure 1F).

When cytokines were analyzed in plasma from mice, significantly increased levels of G-CSF, IL-1 β , IL-6, IL-17, IL-22, and TNF were measured in IFN γ -KO mice upon CFA administration. In contrast to levels in human patients, levels of IL-18 remained unchanged (mean 214.2 pg/ml [range 0–647] and mean 124.4 pg/ml [range 0–734] in treatment-naive and CFA-immunized IFN γ -KO mice, respectively). In WT mice, CFA induced increased levels of G-CSF, IL-6, and TNF (Figure 2). An increased G-CSF level was seen upon α G-CSFR administration in both IFN γ -KO and WT mice, which is most likely a direct consequence of blocking cytokine internalization. In CFA-challenged IFN γ -KO mice, α G-CSFR antibody injection slightly reduced plasma levels of IL-1 β and IL-22. In contrast, IL-6, IL-17, and TNF levels were slightly elevated in α G-CSFR-injected CFA-immunized IFN γ -KO mice, which may explain their increased weight loss, tail damage, and hematologic alterations when compared to PBS-treated mice. No elevated cytokine levels were seen in WT counterparts when treated with α G-CSFR antibody.

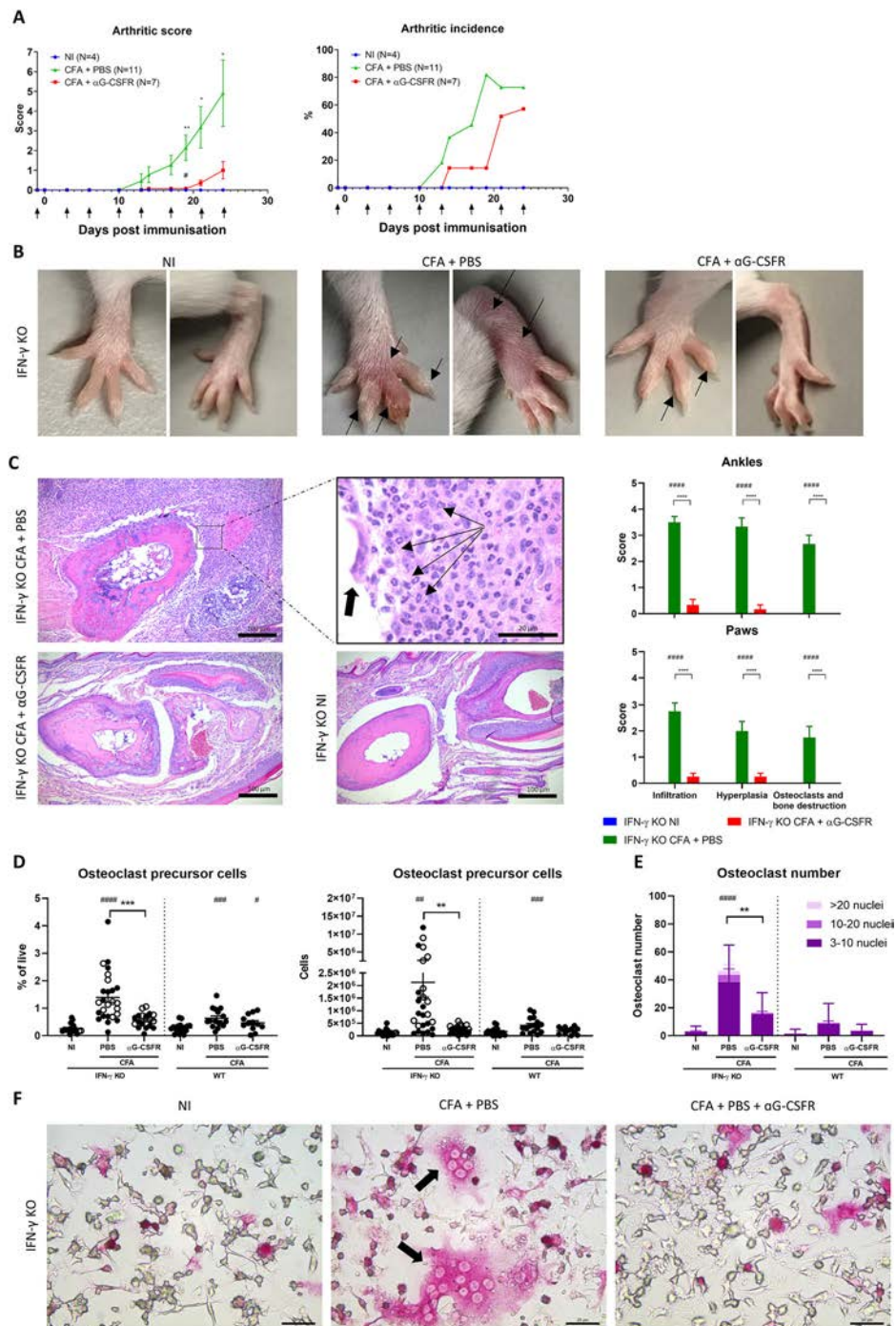


Figure 3. Reduced arthritis severity and incidence and osteoclasts upon α G-CSFR treatment. CFA-immunized IFN γ -KO mice ($n = 18$) and WT mice ($n = 12$) were injected intraperitoneally twice a week with α G-CSFR (200 μ g) (arrows). Mice were euthanized between days 16 and 25 post-immunization. PBS-injected CFA-immunized IFN γ -KO mice ($n = 26$) and WT mice ($n = 16$) were included as controls and compared to treatment-naive mice ($n = 15$ –17). **A**, Arthritis score and incidence ($n = 1$ experiment). Bars show the mean \pm SD. **B**, Photographs of front paw (left panels) and hind paw (right panels). Arrows show redness and/or swelling. **C**, Representative photomicrographs of hematoxylin and eosin-stained ankle sections. Magnified view of the boxed area shows synovial tissue infiltrated with neutrophils (arrows) and multinucleated osteoclast (large arrow). Histology scores, determined as described in Subjects and Methods, are also shown. **D**, Number of osteoclast precursors in the spleen. Each circle represents a single mouse; bars show the median and interquartile range for each group. Solid circles represent SPF conditions; open circles represent non-SPF conditions. **E** and **F**, Number of in vitro-generated tartrate-resistant acid phosphatase-positive multinucleated osteoclasts (**E**) with representative photographs (**F**) ($n = 8$ –14). Osteoclasts are marked with arrows. Graphs show results from 3 pooled experiments. * = $P < 0.05$; ** = $P < 0.01$; *** = $P < 0.001$; **** = $P < 0.0001$ between indicated groups. # = $P < 0.05$; ## = $P < 0.01$; ### = $P < 0.001$; #### = $P < 0.0001$ versus IFN γ -KO treatment-naive mice or WT treatment-naive mice. All statistics were obtained using a linear mixed-effects model. See Figure 1 for definitions.

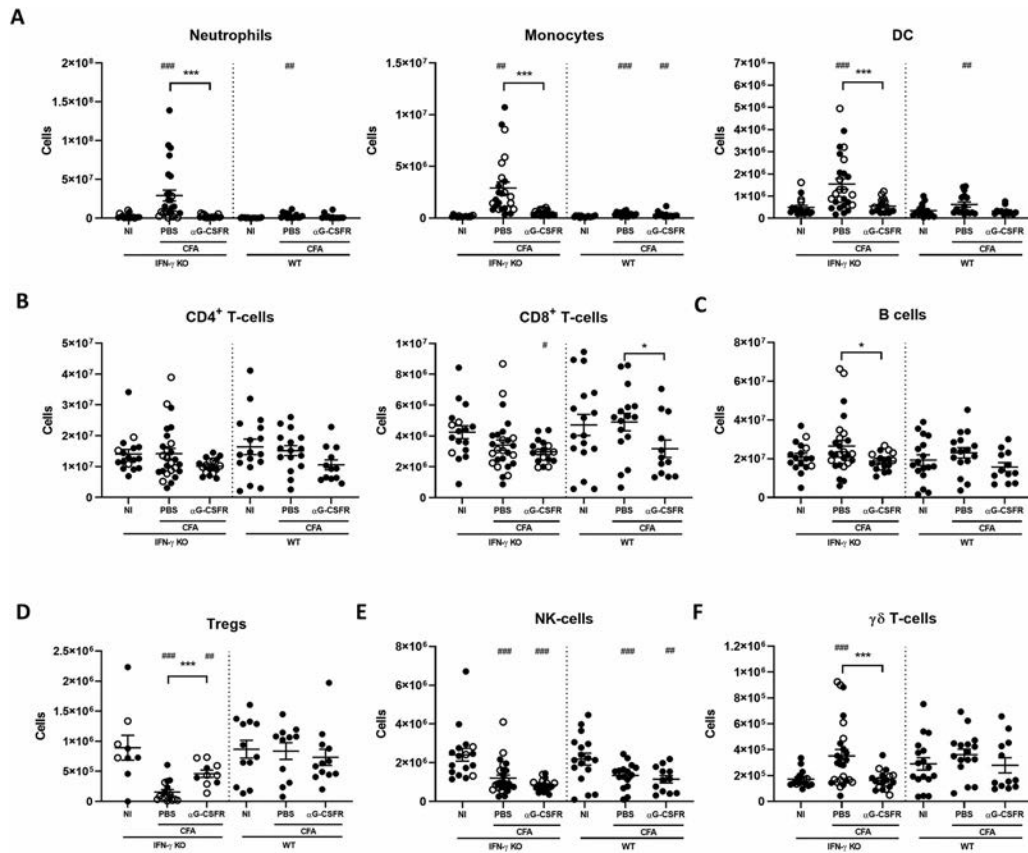


Figure 4. Anti-G-CSFR treatment induces a reduced splenic myelopoiesis in CFA-immunized mice. CFA-immunized IFN γ -KO mice ($n = 18$) and WT mice ($n = 12$) were injected intraperitoneally twice a week with α G-CSFR (200 μ g). Mice were euthanized between days 16 and 25 postimmunization. PBS-injected CFA-immunized IFN γ -KO mice ($n = 26$) and WT mice ($n = 16$) were included as controls and compared to treatment-naive mice ($n = 15$ –17). Absolute number of different immune cells in the spleen, including myeloid neutrophils (CD11b+Ly6G+), monocytes (CD11b+Ly6C+), and dendritic cells (DCs) (CD11b+CD11c+) (A), lymphoid CD4 $^{+}$ T cells (CD3+CD4+) and CD8 $^{+}$ T cells (CD3+CD8+) (B), B cells (C), Treg cells (CD3+CD25+) (D), natural killer (NK) cells (CD3–CD122+DX5+) (E), and $\gamma\delta$ T cells (CD3+CD4+ $\gamma\delta$ TCR+) (F) were assessed by flow cytometry. Graphs show results from 3 pooled experiments. Each circle represents a single mouse; bars show the median and interquartile range for each group. Solid circles represent SPF conditions; open circles represent non-SPF conditions. * = $P < 0.05$; *** = $P < 0.001$ between indicated groups. # = $P < 0.05$; ## = $P < 0.01$; ### = $P < 0.001$ versus IFN γ -KO treatment-naive mice or WT treatment-naive mice. All statistics were obtained using a linear mixed-effects model. See Figure 1 for other definitions.

In conclusion, these results demonstrate that G-CSF is associated with neutrophilia in CFA-immunized mice. Anti-G-CSFR treatment caused an improvement of clinical and hematologic features in IFN γ -KO mice, even though a modest increase of some systemic inflammatory features was observed.

Counteracting effects of G-CSFR blockage on the development of arthritis. As we previously reported, ~40% of IFN γ -KO mice develop arthritis 3 weeks post-CFA challenge (12). Conventional animal housing is known to accelerate the onset and incidence of arthritis (22). In one of our experimental set-ups, mice were housed in a conventional animal facility. As shown in Figure 3A, joint inflammation was seen in CFA-immunized IFN γ -KO mice from day 13 onward and reached an incidence of >80% during the course of the experiment. On day 24, 9 of 11 mice had developed redness and swelling of the joints, with a mean \pm SD arthritis score of 4.9 ± 1.7 . In contrast,

α G-CSFR antibody-treated mice developed less arthritis as indicated by a lower incidence and lower arthritis score (mean \pm SD 1.0 ± 0.4 in 4 of 7 mice). Representative images of the joint inflammation in the front and hind paws of IFN γ -KO mice are also shown (Figure 3B). Representative histologic sections of joints from IFN γ -KO mice show hyperplasia of synovial tissue, infiltration of the synovium with mononuclear and polymorphonuclear cells, and pannus formation with osteoclasts and bone destruction (Figure 3C). Reduced severity of arthritis in the α G-CSFR antibody-treated mice was associated with an inhibition of cell infiltration, hyperplasia, and pannus formation.

To predict the possible development of arthritis, numbers of osteoclast precursor cells (CD3–B220–CD11b+CD115+ cells) in the spleen were assessed, as previously described (23). In IFN γ -KO mice, CFA immunization was associated with an increased number of osteoclast precursor cells, which was significantly reduced by α G-CSFR antibody injection. Likewise, in WT mice,

CFA immunization induced the generation of osteoclast precursor cells, but to a lower extent when mice were treated with α G-CSFR antibody (Figure 3D). In addition, when osteoclasts were generated in vitro, high numbers of multinucleated osteoclasts were generated from CFA-immunized IFN γ -KO mice, while those from mice treated with α G-CSFR antibody were found to be significantly lower (Figures 3E and F).

To assess the direct effect of α G-CSFR binding on neutrophil migration, CFA-immunized IFN γ -KO mice were intraperitoneally injected with α G-CSFR or isotype control. After 4 hours, the in vivo chemotactic capacity to CXCL8 was measured in the flushed peritoneal cavity, 2 hours postinjection of the chemokine. Injection of CXCL8 induced the migration of neutrophils with an activated phenotype defined by a low CD62L expression. However, we observed no differences between the α G-CSFR-injected mice and isotype control-injected mice (Supplementary Figures 2A and B, available on the *Arthritis & Rheumatology* website at <https://onlinelibrary.wiley.com/doi/10.1002/art.42104>). Therefore, in our experimental set-up and model, we concluded that neutrophils retain their capacity to migrate toward CXCL8 upon G-CSFR blockage.

In conclusion, α G-CSFR antibody treatment inhibited development of arthritis in CFA-immunized mice. The reduced arthritis upon α G-CSFR treatment may be explained by the reduced number of neutrophils or the reduced formation of osteoclasts.

Major role for G-CSF-induced extramedullary myelopoiesis. The presence of extramedullary myelopoiesis has previously been described in CFA-immunized mice (24). To determine the effect of α G-CSFR treatment on CFA-induced hematopoiesis and myelopoiesis, flow cytometric analysis was performed on LNs and the spleen. In LNs, no aberrant differences were found in T cells, B cells, $\gamma\delta$ T cells, or NK cells (data not shown). In spleens from CFA-immunized mice, both neutrophils (Ly6G+CD11b+) and monocytes (Ly6C+CD11b+) were significantly increased compared to nonimmunized controls. A marked reduction of this myeloid compartment was seen upon treatment with α G-CSFR, reaching significance in the IFN γ -KO mice only. The increased number of CD11c+ dendritic cells (DCs) (largely CD11b+ myeloid DCs) was also reverted upon α G-CSFR treatment (Figure 4A). Associated with the decreased myeloid compartment, mice showed a relative increased number of lymphocytes (data not shown). However, no differences were found in the absolute numbers of CD4+ T cells (CD3+CD4+), CD8+ T cells (CD3+CD8+), and B cells (CD19+), or they were slightly reduced upon treatment in the WT mice (CD8+ T cells only) or the IFN γ -KO mice (B cells only) (Figures 4B and C).

In CFA-challenged IFN γ -KO mice, Treg cells (CD3+CD4+FoxP3+CD25+) were significantly decreased compared to nonimmunized controls. Unexpectedly, a restored number of Treg cells were found in the α G-CSFR-treated group. In WT mice, the number of Treg cells remained unaltered (Figure 4D). In both IFN γ -KO and

WT animals, the absolute number of NK cells (CD3–CD122+DX5+) were decreased after immunization although were not altered in the antibody-injected mice (Figure 4E). Interestingly, both in CFA-immunized WT and IFN γ -KO mice, α G-CSFR treatment induced a reduced number of $\gamma\delta$ T cells (Figure 4F). In conclusion, G-CSF stimulates myelopoiesis in the spleens of CFA-immunized mice, either directly or indirectly i.e., via mobilization of myeloid progenitor cells from the bone marrow (BM).

Five neutrophil clusters identified during extramedullary myelopoiesis by single-cell sequencing.

CFA immunization is associated with an important de novo generation of neutrophils outside the BM (12,24,25). To characterize the cellular landscape of the different neutrophils, single-cell RNA-seq was applied to Gr-1–sorted splenocytes (depicting both Ly6G+ and Ly6C+ cells) from CFA-challenged WT and IFN γ -KO mice (Figure 5A). Unbiased clustering identified 8 clusters (Figure 5B), and Supplementary Figure 3A shows a heat map of the top marker genes (available on the *Arthritis & Rheumatology* website at <https://onlinelibrary.wiley.com/doi/10.1002/art.42104>). Based on the key neutrophil markers Ly6G and CXCR2, clusters 0, 1, 2, 3, and 5 were annotated as neutrophils. Cluster 4 represented monocytes, expressing high levels of CCR2 and Ly6C. Since *Irf8* was found to be a main transcription factor in conventional and plasmacytoid DCs, cluster 6 was annotated as DCs. Finally, a negligible cluster 7 (<1% of sorted cells) was found to represent NK cells (Supplementary Figure 3A).

Within neutrophils, 5 clusters could be found. Based on the expression of transcription factors (Figure 5C), granule proteins (Figure 5D), and cell cycle genes (data not shown), neutrophils were divided into pre-neutrophils (cluster 5), immature neutrophils (clusters 1 and 3), and mature neutrophils (clusters 0 and 2). Within the immature neutrophils, 2 clusters were found. The top 50 differentially expressed genes (DEGs) are shown in Supplementary Table 4, available on the *Arthritis & Rheumatology* website at <https://onlinelibrary.wiley.com/doi/10.1002/art.42104>. It mainly demonstrates an enhanced maturation in cluster 1 compared to cluster 3. Mature neutrophils might also be divided into 2 clusters (clusters 0 and 2), in which cluster 0 represents the inflammatory neutrophils, showing an increased expression of IL-1 β , G-CSFR (*Csf3r*), and CD101 (Figure 5E). Assessment of the different neutrophilic functions exposed that pre-neutrophils were highly proliferative cells, whereas mature neutrophils had the highest antimicrobial and proinflammatory capacity (as seen in chemotaxis, phagocytosis, reactive oxygen species, and activation scores) (Figure 1F and Supplementary Figure 3B).

Using Slingshot, we reconstructed a one-branch neutrophil differentiation pathway (Figure 5G). Gene expression of proliferation, primary granules, and early transcription factors decreased along the trajectory (e.g., *Cdk1*), proinflammatory marker gene expression increased (e.g., *Il1b*), while specific and gelatinase granule marker genes were expressed in between the

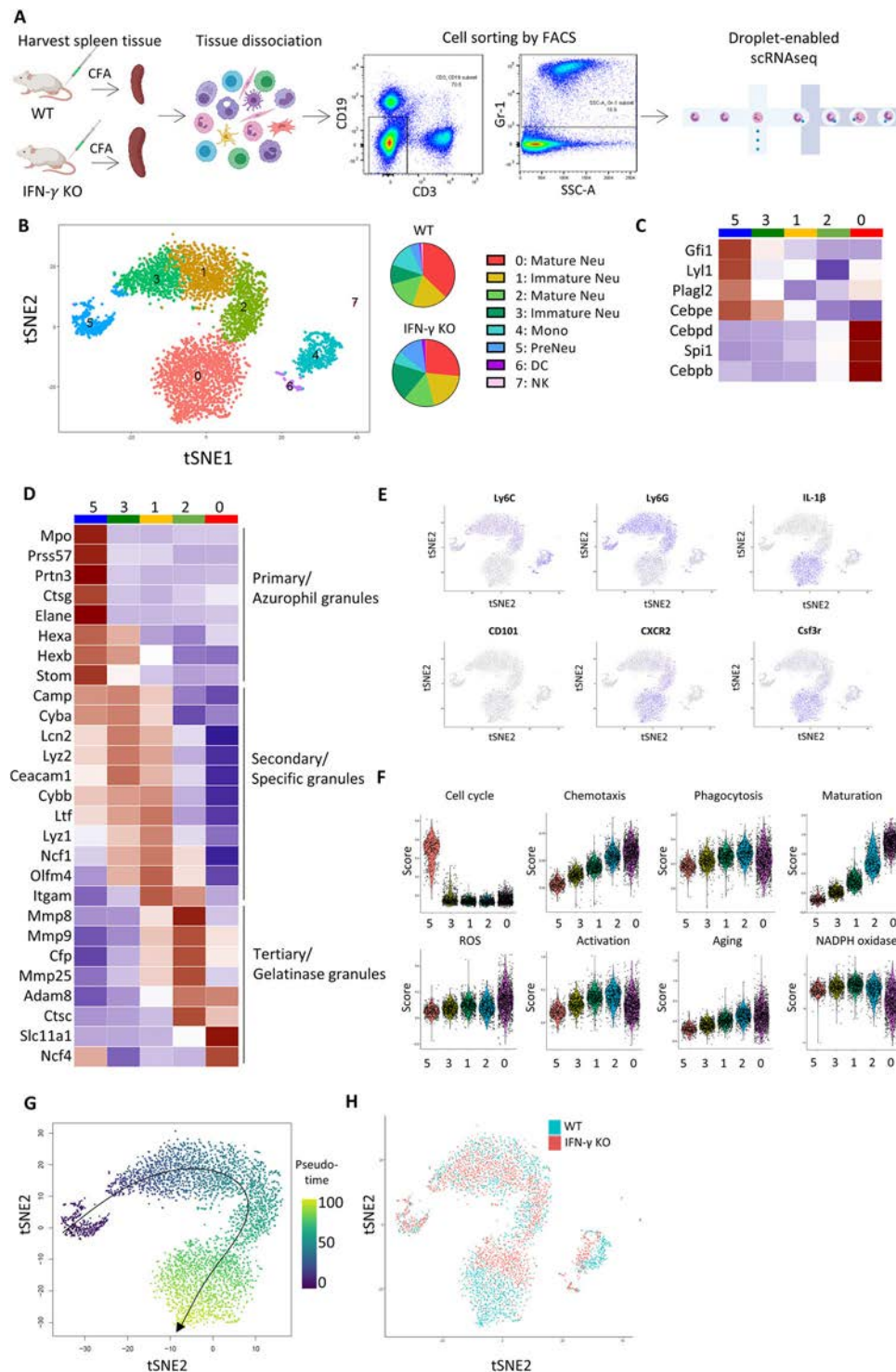


Figure 5. Single-cell RNA sequencing (scRNA-seq) reveals 5 distinct neutrophil (Neu) clusters in CFA-immunized IFN γ -KO and WT mice. **A**, Approach overview for single-cell RNA sequencing where CD3–CD19–Gr-1⁺ splenocytes were sorted from CFA-immunized IFN γ -KO and WT mice by fluorescence-activated cell sorting (FACS), followed by droplet-enabled single-cell RNA-seq. **B**, Seurat analysis of 4,702 cells from CFA-immunized WT mice (2,138 cells) and IFN γ -KO mice (2,564 cells), in which 18,177 genes analyzed are shown in a t-distributed stochastic neighbor embedding (t-SNE) projection. Colors indicate the distinct clusters of Gr-1⁺ splenocytes. Pie charts show the relative contribution of each cell type (in %) in CFA-immunized WT and IFN γ -KO mice. **C** and **D**, Heatmaps showing the expression of genes encoding myeloid development-related transcription factors (**C**) and granule production (**D**) assessed in each neutrophil subcluster. **E**, Dot plots showing the main cell type markers. **F**, Violin plots showing scores of cell cycle, chemotaxis, phagocytosis, maturation, reactive oxygen species (ROS), activation, aging, and NADPH oxidase in each neutrophil cell subcluster. **G**, Pseudo-time trajectory for neutrophils based on Slingshot. **H**, Projection of t-SNE stratifying CFA-immunized WT and IFN γ -KO mice. DC = dendritic cell; NK = natural killer; IL-1 β = interleukin-1 β (see Figure 1 for definitions).

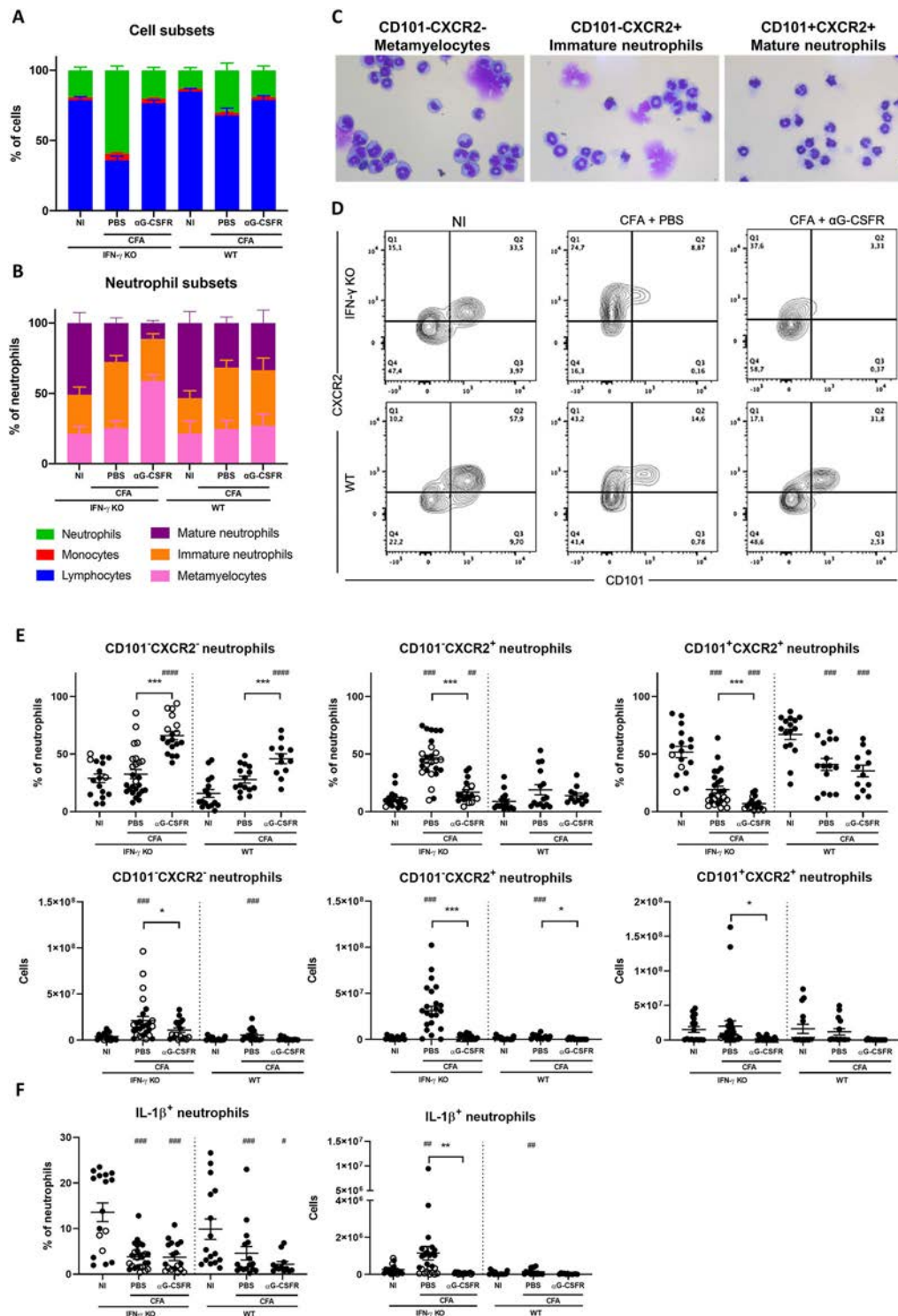


Figure 6. Left shift in neutrophils upon α G-CSFR treatment. CFA-immunized IFN γ -KO mice ($n = 18$) and WT mice ($n = 12$) were injected intraperitoneally twice a week with α G-CSFR (200 μ g). Mice were euthanized between days 16 and 25 postimmunization. PBS-injected CFA-immunized IFN γ -KO mice ($n = 26$) and WT mice ($n = 16$) were included as controls and compared to treatment-naive mice ($n = 15$ –17). **A** and **B**, Spleen cytopsin preparations were counted. **C**, Splenocytes were sorted by fluorescence-activated cell sorting based on CXCR2 and CD101. Cytopsin preparations represent sorted metamyelocytes (CD101–CXCR2–), immature neutrophils (CD101–CXCR2+), and mature neutrophils (CD101+CXCR2+). **D**, Representative flow cytometric plots show different neutrophil clusters based on the markers CD101 and CXCR2 in all experimental groups. **E**, The number of different clusters was assessed by flow cytometry. **F**, The number of interleukin-1 β (IL-1 β)–expressing neutrophils in the spleen was calculated. Graphs show results from 3 pooled experiments. Each circle represents a single mouse; bars show the median and interquartile range for each group. Solid circles represent SPF conditions; open circles represent non-SPF conditions. * = $P < 0.05$; ** = $P < 0.01$; *** = $P < 0.001$ between indicated groups. # = $P < 0.05$; ## = $P < 0.01$; ### = $P < 0.001$; #### = $P < 0.0001$ versus IFN γ -KO treatment-naive mice or WT treatment-naive mice. All statistics were obtained using a linear mixed-effects model. See Figure 1 for other definitions.

differentiation path (e.g., *Ltf*) (Figures 1C and D and Supplementary Figure 4, available on the *Arthritis & Rheumatology* website at <https://onlinelibrary.wiley.com/doi/10.1002/art.42104>). Interestingly, we noticed a reduction in the number of unique molecular identifiers along the differentiation path, corresponding to the gene silencing reported (data not shown). When we compared WT and IFN γ -KO mice, we confirmed a reduced number of mature neutrophils in the spleens of CFA-immunized IFN γ -KO mice (Figure 5B). Notably, both cluster 0 and cluster 4 showed a remarkable polarized distribution of WT and IFN γ -KO cells (Figure 5H).

More in-depth comparisons between IFN γ -KO and WT mice in cluster 0 identified 198 DEGs (73 up, 125 down) (Supplementary Table 5, available on the *Arthritis & Rheumatology* website at <https://onlinelibrary.wiley.com/doi/10.1002/art.42104>). Twenty-six of these genes were associated with MDSCs, e.g., *Wfdc17*, *Ifitm1*, and *Igfbbp6*, as described by Alshetaiwi et al (26), and they were increasingly expressed in IFN γ -KO mice only. Furthermore, *Cebpb*, a transcription factor induced by G-CSF, was highly up-regulated in the IFN γ -KO mice (27). Supplementary Table 6 (available on the *Arthritis & Rheumatology* website at <https://onlinelibrary.wiley.com/doi/10.1002/art.42104>) shows genes that are differentially expressed along the maturation trajectory between IFN γ -KO mice and WT mice. It includes IFN-regulated genes, generally up-regulated in mature neutrophils and tempered in the IFN γ -KO mice (Supplementary Figure 5A, available on the *Arthritis & Rheumatology* website at <https://onlinelibrary.wiley.com/doi/10.1002/art.42104>). The granulocyte differentiation regulating genes *Cebpb* and *Lrg1* and the proinflammatory genes *Tlr1*, *Alox5ap*, and *Nfkbia* were all increasingly expressed along with neutrophil maturation in the IFN γ -KO mice (Supplementary Figure 5B).

Using single-cell RNA-seq, Xie et al and Grieshaber-Bouyer et al studied mouse neutrophils in the BM, peripheral blood, and spleens of treatment-naïve mice, describing 8 (G0–G4, G5a, G5b, and G5c) and 4 (P1–4) neutrophil clusters, respectively (28,29). When merging our data set with the data set of Xie et al, only G2 overlapped with our C5 subset. This subset has a hallmark feature of active proliferation and represents the pre-neutrophils (Supplementary Figure 6A, available on the *Arthritis & Rheumatology* website at <https://onlinelibrary.wiley.com/doi/10.1002/art.42104>). Incomplete merging might be attributed to batch effects that could not be normalized using Harmony. Nevertheless, when mapping the top genes only, G3 (CXCR2^{low} immature neutrophils) genes were expressed by both C5, C3, and C1. Top genes in G4 (CXCR2^{high} mature neutrophils) overlapped with C2. Interestingly, C0 showed high expression of genes described to be expressed by G5a, G5b, and G5c (peripheral mature neutrophils) (Supplementary Figure 6B). In contrast, when merging the data set of Grieshaber-Bouyer et al, all subsets were overlapping (Supplementary Figure 6A). In analogy to the presented neutrotime (showing gradual neutrophil maturation from P1 toward

P4, from pre-neutrophils to mature neutrophils via immature neutrophils), we observed a similar differentiation path with overlapping phenotypes (Supplementary Figure 6B). Based on these results, we may conclude that neutrophils in the spleen of CFA-immunized mice follow a similar differentiation path as described in the BM. Importantly, in the published splenic data sets on treatment-naïve mice, pre-neutrophils and immature neutrophils were absent and only presented in the spleens of our immunized mice (28,29).

In conclusion, in homeostatic conditions, pre-neutrophils and immature neutrophils are absent in the spleen but emerge upon CFA immunization, showing a similar G-CSF-driven differentiation path as described in the BM (28–30). Compared to WT mice, CFA-immunized IFN γ -KO mice exposed an increased number of immature neutrophils and MDSC-polarized mature neutrophils.

Altered relative distribution of neutrophil subclusters via G-CSFR blockage. Spleen cytospin preparations confirmed the increased neutrophil-to-lymphocyte ratio measured by flow cytometry in CFA-immunized mice (Figure 6A). Morphologically, neutrophils were divided into mature neutrophils, immature neutrophils, and metamyelocytes (representing the pre-neutrophils). Mature neutrophils have a lobbed nucleus, whereas immature and metamyelocytes have a thin- and thick-banded nucleus, respectively (31) (Supplementary Figure 7, available on the *Arthritis & Rheumatology* website at <https://onlinelibrary.wiley.com/doi/10.1002/art.42104>). Quantification in the spleen revealed a relative increase in immature neutrophils. Interestingly, these emerged on day 10 postimmunization, the day mice started to develop overt signs of inflammation (data not shown). Anti-G-CSFR treatment restored the neutrophil-to-lymphocyte ratio but also induced a relatively increased percentage of metamyelocytes in CFA-immunized IFN γ -KO mice. In WT mice, no major differences were observed (Figure 6B).

In addition, we performed a more in-depth analysis by flow cytometry. Based on 2 maturation markers, CD101 and CXCR2, mature neutrophils (CD101+CXCR2+), immature neutrophils (CD101–CXCR2+), and metamyelocytes (CD101–CXCR2–) may be distinguished (30), which we confirmed (Figure 6C). Compared to treatment-naïve mice, CFA immunization did not affect the percentage of CD101–CXCR2– neutrophils, whereas it induced a relative increase in CD101–CXCR2+ neutrophils, in IFN γ -KO mice only (Figures 6D and E). Consequently, this resulted in a reduced percentage of CD101+CXCR2+ neutrophils in CFA-immunized mice. Upon antibody treatment, the percentage of CD101–CXCR2– neutrophils was increased in both IFN γ -KO and WT mice compared to treatment-naïve mice, or compared to sham-treated CFA-immunized mice in the IFN γ -KO mice group only. When comparing the PBS- and α G-CSFR-treated groups, the percentage of immature and mature neutrophils were both significantly decreased in the treated IFN γ -KO mice (Figure 6E). Interestingly, the reduced percentage of mature

neutrophils was associated with a decreased percentage of IL-1 β + neutrophils (Figure 6F). Note that the absolute number of each neutrophil subtype was decreased upon treatment (Figures 6E and F). Supplementary Figure 8 shows the mean fluorescence intensity of Ly6G, CD11b, CD101, CXCR2, and CXCR4 on neutrophils in the spleen (available on the *Arthritis & Rheumatology* website at <https://onlinelibrary.wiley.com/doi/10.1002/art.42104>). Taken together, these findings indicate α G-CSFR-mediated neutrophil maturation and differentiation deficiency in the spleen of CFA-immunized IFN γ -KO mice but not in CFA-immunized WT mice.

DISCUSSION

Systemic JIA patients are characterized by massive neutrophilia and develop splenomegaly (1,2), possibly due to extramedullary myelopoiesis. Recently, 2 studies described the phenotypical and functional characteristics of these neutrophils in systemic JIA (9,10). Despite these studies, the neutrophil developmental path during extramedullary myelopoiesis remains largely unknown. Here, we used a mouse model of systemic JIA, relying on injection of CFA in IFN γ -KO mice (12) to study the etiology of CFA-induced myelopoiesis and neutrophilia, as well as its functional importance in the development of systemic JIA.

Our study highlights an important direct or indirect role for G-CSF in the pathophysiology of systemic JIA. The main findings are summarized in Supplementary Figure 9 and Supplementary Table 4, available on the *Arthritis & Rheumatology* website at <https://onlinelibrary.wiley.com/doi/10.1002/art.42104>. Both in systemic JIA patients and in our mouse model, increased plasma levels of G-CSF were detected, correlating with the absolute number of neutrophils. In mice, α G-CSFR administration blocked splenomegaly, neutrophilia, and plasma IL-1 β levels and reduced incidence, clinical severity, and histologic abnormalities of arthritis in IFN γ -KO mice. These observations are consistent with previous studies that used these G-CSFR-blocking antibodies in the treatment of arthritis (19,32). In contrast, α GM-CSF treatment in CFA-immunized IFN γ -KO mice had no effect on the systemic JIA-like symptoms (data not shown). Our results fit the “remnant epitopes generate autoimmunity” model, which states that cells and molecules of the innate immune system can start autoimmune reactions by cytokine-regulated proteolysis yielding remnant epitopes (33). In this regard, it is worth mentioning that systemic JIA follows a biphasic clinical course, in which the innate immune system is mainly involved in the onset of the disease, whereas the adaptive immune system contributes to the later chronic arthritic phenotype (34).

Single-cell RNA-seq identified 5 neutrophilic clusters associated with extramedullary myelopoiesis, which were identical to those found in BM (30). Interestingly, we confirmed that these clusters could be separated in the spleen based on the expression of CD101 and CXCR2 (30). Single-cell RNA-seq also

showed that mature neutrophils from IFN γ -KO mice had an increased expression of MDSC-related genes and CCAAT/enhancer binding protein β , a transcription factor associated with emergency granulopoiesis, induced by G-CSF (26,27). MDSCs are often described in cancer but also expand during chronic and acute inflammatory conditions, including sepsis (35). Neutrophil transcriptome analysis in systemic JIA patients showed an inflammatory gene expression profile, overlapping with the transcriptome of sepsis (9,10,36). Studying the effect of G-CSF on neutrophil clusters, we showed that α G-CSFR treatment caused a maturation deficiency and “left shift” in the spleen from mature toward more immature neutrophils and pre-neutrophils in CFA-treated IFN γ -KO mice.

Generally, G-CSF is considered one of the main regulators involved in the expansion and maturation of neutrophils (17,37). In inflammatory conditions, G-CSF is regulated by the IL-23/IL-17/G-CSF axis (38,39). In this pathway, IL-1 β and IL-6 are released by early activation of neutrophils and monocytes and, along with IL-23, stimulate IL-17 expression in lymphocytes, subsequently regulating the systemic induction of G-CSF and eventually driving massive neutrophil release (40,41). Innate immune cells including $\gamma\delta$ T cells are an additional important source of IL-17 (42–44). Moreover, a positive feedback loop between neutrophil-derived IL-1 β or S100 proteins and $\gamma\delta$ T cells was demonstrated in patients with active systemic JIA (44). In accordance with this auto-amplification mechanism, systemic JIA patients have been successfully treated with IL-1 β - and IL-6-targeting agents (9). Considering the upstream effects of IL-1 β on G-CSF, future research is needed to understand their mutual regulation. As neutrophils are an important cellular source of IL-1 β , it is tempting to speculate that they might in part be responsible for the observed inflammation—including the development of arthritis—by its production of IL-1 β .

In addition, by regulating the IL-17 cytokine expression, IFN γ is linked to the IL-23/IL-17/G-CSF axis, and its absence may partially explain the enhanced phenotype observed in the IFN γ -KO mice. This was reflected by enhanced levels of both IL-17 and G-CSF in the model. Previously, using our systemic JIA-like mouse model, we identified that both IL-17 and IL-23 play a pivotal role in the pathogenesis of the disease, and blockage of both cytokines almost completely abolished splenomegaly and granulocytosis. Together with CD4+ T cells, $\gamma\delta$ T cells were shown to be the main source of IL-17 (12). The reduced number of $\gamma\delta$ T cells upon α G-CSFR treatment may in part explain the observed ameliorated phenotype but requires additional research.

Unexpectedly, slight increases in IL-6, TNF, and IL-17 were detected upon G-CSFR inhibition. This appears to be specific to IFN γ -KO mice only and is associated with a mild increase in weight loss, tail damage, and number of immature RBCs. TNF and IL-6 are 2 cytokines known to have cachexic properties (45,46). Since neutrophils have both pro- and antiinflammatory properties, the reduced number of neutrophils and, more specifically, MDSC-like

cells in CFA-immunized IFN γ -KO mice, may explain the aggravated phenotype observed after α G-CSFR blocking. Recently, Rybakin et al showed that neutrophil-derived matrix metalloproteinase 9 (MMP-9) reduces the abundance of signaling-competent IL-2. Therefore, it may be that the reduced levels of neutrophils (and MMP-9) upon α G-CSFR treatment increase the levels of active IL-2, leading to enhanced T cell activation and numbers of Treg cells (47). However, we postulate that the aggravated local inflammation around the tail injection site is directly linked to the inherent function of neutrophils, since they are major phagocytic cells that rapidly infiltrate sites of inflammation and clear foreign particles, in this case the killed mycobacteria that are present in CFA. Therefore, due to insufficient numbers of neutrophils, the killed mycobacteria might not be properly resolved and continuously stimulate the innate immune cells.

Our study has some limitations. First, G-CSF may indirectly be responsible for the observed inflammatory pathology via its regulatory effects on neutrophil numbers and functions. Therefore, we cannot rule out a reduced joint migration upon G-CSFR-blockage. While we observed no reduced CXCL8-mediated peritoneal migration in our CFA-immunized IFN γ -KO mice, effects upon antibody ligation might be site- or stimulus-specific, as previously shown (48). We are not able to study the direct role of neutrophils, because neutrophil depletion was incomplete in the model and was followed by a fast rebound of new neutrophils, as previously described (18). In addition, neutrophil-deficient mice are not available in the BALB/c strain. Second, when studying extramedullary granulopoiesis in the spleen, we cannot exclude the potential contribution of medullary granulopoiesis. Ballesteros et al showed that neutrophils may be retained in the tissues (49), but by comparing CFA-immunized mice to treatment-naïve mice, we demonstrated infiltration of pre-neutrophils and immature neutrophils in the immunized mice only. Notably, in patients with active systemic JIA, a peripheral expansion of immature CD34+CD33+ myelomonocytic precursor cells was reported. These may home in the spleen and subsequently mature (2,11). Thus, additional research is needed to exclude infiltration of BM-derived pre-neutrophils and immature neutrophils.

Third, our study did not include the use of an isotype antibody control. However, we previously showed in the collagen-induced arthritis model, which also requires CFA immunization, that the use of an isotype antibody did not affect the development of arthritis nor neutrophilia in the spleen (50). Finally, the sample size of our patient cohort was small and requires validation in an independent larger cohort of systemic JIA patients. In conclusion, G-CSFR blockade is suitable to inhibit excessive extramedullary myelopoiesis and arthritis development. Future research is needed to clarify the exact role of G-CSF in systemic JIA in a clinical setting.

ACKNOWLEDGMENTS

We sincerely thank Prof. Ghislain Opendakker for critically reviewing the manuscript. We thank Prof. Jeroen Vanoirbeek for the use of his

conventional animal housing facility. Anti-granulocyte colony-stimulating factor receptor antibody (Ch5E2-VR81-mIgG1k) was kindly provided by CSL Limited Australia. We thank Dr. Lisa Lindqvist, Dr. Helen Cao, and Dr. Judith Field from CSL Limited Australia for their help and critical review. We thank Dr. Mieke Metzemaekers and Dr. Mieke Gouwy for their assistance in the chemotaxis experiments.

AUTHOR CONTRIBUTIONS

All authors were involved in drafting the article or revising it critically for important intellectual content, and all authors approved the final version to be published. Dr. Malengier-Devlies had full access to all of the data in the study and takes responsibility for the integrity of the data and the accuracy of the data analysis.

Study conception and design. Malengier-Devlies, Bernaerts, Proost, Wouters, Matthys.

Acquisition of data. Malengier-Devlies, Bernaerts, Ahmadzadeh, Filtjens, Vandenhoute, Broeckx, Burton, De Visscher, Mitera, Berghmans.



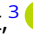








Analysis and interpretation of data. Ahmadzadeh, Filtjens, Vandenhoute, Broeckx, Burton, Verbeke, Liston, Lambrechts, Proost, Wouters, Matthys.

REFERENCES

1. Woo P. Systemic juvenile idiopathic arthritis: diagnosis, management, and outcome [review]. *Nat Clin Pract Rheumatol* 2006;2:28–34.
2. Mellins ED, Macaubas C, Grom AA. Pathogenesis of systemic juvenile idiopathic arthritis: some answers, more questions [review]. *Nat Rev Rheumatol* 2011;7:416–26.
3. Prakken B, Albani S, Martini A. Juvenile idiopathic arthritis [review]. *Lancet* 2011;377:2138–49.
4. Avau A, Put K, Wouters CH, Matthys P. Cytokine balance and cytokine-driven natural killer cell dysfunction in systemic juvenile idiopathic arthritis [review]. *Cytokine Growth Factor Rev* 2015;26:35–45.
5. Canny S, Mellins E. New frontiers in the treatment of systemic juvenile idiopathic arthritis [review]. *F1000Res* 2017;6:971.
6. Nauseef WM, Borregaard N. Neutrophils at work [review]. *Nat Immunol* 2014;15:602–11.
7. Liew PX, Kubes P. The neutrophil's role during health and disease [review]. *Physiol Rev* 2019;99:1223–48.
8. Silvestre-Roig C, Hidalgo A, Soehnlein O. Neutrophil heterogeneity: implications for homeostasis and pathogenesis [review]. *Blood* 2016;127:2173–81.
9. Ter Haar NM, Tak T, Mokry M, Scholman RC, Meerding JM, de Jager W, et al. Reversal of sepsis-like features of neutrophils by interleukin-1 blockade in patients with systemic-onset juvenile idiopathic arthritis. *Arthritis Rheumatol* 2018;70:943–56.
10. Brown RA, Henderlight M, Do T, Yasin S, Grom AA, DeLay M, et al. Neutrophils from children with systemic juvenile idiopathic arthritis exhibit persistent proinflammatory activation despite long-standing clinically inactive disease. *Front Immunol* 2018;9:2995.
11. Fall N, Barnes M, Thornton S, Luyrink L, Olson J, Ilowite NT, et al. Gene expression profiling of peripheral blood from patients with untreated new-onset systemic juvenile idiopathic arthritis reveals molecular heterogeneity that may predict macrophage activation syndrome. *Arthritis Rheum* 2007;56:3793–804.
12. Avau A, Mitera T, Put K, Brisse E, Filtjens J, Uyttenhove C, et al. Systemic juvenile idiopathic arthritis-like syndrome in mice following stimulation of the immune system with Freund's complete adjuvant: regulation by interferon- γ . *Arthritis Rheumatol* 2014;66:1340–51.
13. Put K, Vandenhoute J, Avau A, van Nieuwenhuijze A, Brisse E, Dierckx T, et al. Inflammatory gene expression profile and defective

- interferon- γ and granzyme K in natural killer cells from systemic juvenile idiopathic arthritis patients. *Arthritis Rheumatol* 2017;69:213–24.
14. De Jager W, Vastert SJ, Beekman JM, Wulffraat NM, Kuis W, Coffey PJ, et al. Defective phosphorylation of interleukin-18 receptor β causes impaired natural killer cell function in systemic-onset juvenile idiopathic arthritis. *Arthritis Rheum* 2009;60:2782–93.
 15. Demetri GD, Griffin JD. Granulocyte colony-stimulating factor and its receptor [review]. *Blood* 1991;78:2791–808.
 16. Liu F, Wu HY, Wesselschmidt R, Komaga T, Link DC. Impaired production and increased apoptosis of neutrophils in granulocyte colony-stimulating factor receptor-deficient mice. *Immunity* 1996;5:491–501.
 17. Roberts AW. G-CSF: a key regulator of neutrophil production, but that's not all [review]. *Growth Factors* 2005;23:33–41.
 18. Pollenus E, Malengier-Devlies B, Vandermosten L, Pham TT, Mitera T, Possemiers H, et al. Limitations of neutrophil depletion by anti-Ly6G antibodies in two heterogenic immunological models. *Immunol Lett* 2019;212:30–6.
 19. Campbell IK, Leong D, Edwards KM, Rayzman V, Ng M, Goldberg GL, et al. Therapeutic targeting of the G-CSF receptor reduces neutrophil trafficking and joint inflammation in antibody-mediated inflammatory arthritis. *J Immunol* 2016;197:4392–402.
 20. De Klerck B, Carpentier I, Lories RJ, Habraken Y, Piette J, Carmeliet G, et al. Enhanced osteoclast development in collagen-induced arthritis in interferon- γ receptor knock-out mice as related to increased splenic CD11b⁺ myelopoiesis. *Arthritis Res Ther* 2004;6:R220–31.
 21. Metzemaekers M, Vandendriessche S, Berghmans N, Gouwy M, Proost P. Truncation of CXCL8 to CXCL8(9–77) enhances actin polymerization and in vivo migration of neutrophils. *J Leukoc Biol* 2020;107:1167–73.
 22. Liu X, Zeng B, Zhang J, Li W, Mou F, Wang H, et al. Role of the gut microbiome in modulating arthritis progression in mice. *Sci Rep* 2016;6:30594.
 23. Imbrechts M, Avau A, Vandehaute J, Malengier-Devlies B, Put K, Mitera T, et al. Insufficient IL-10 production as a mechanism underlying the pathogenesis of systemic juvenile idiopathic arthritis. *J Immunol* 2018;201:2654–63.
 24. Matthys P, Vermeire K, Mitera T, Huang S, Schols D, Wolf-Peters C De, et al. Enhanced autoimmune arthritis in IFN- γ receptor-deficient mice is conditioned by mycobacteria in Freund's adjuvant and by increased expansion of Mac-11⁺ myeloid cells. *J Immunol* 1999;163:3505–10.
 25. Billiau A, Matthys P. Modes of action of Freund's adjuvants in experimental models of autoimmune diseases. *J Leukoc Biol* 2001;70:849–60.
 26. Alshetaiwi H, Pervolarakis N, McIntyre LL, Ma D, Nguyen Q, Rath JA, et al. Defining the emergence of myeloid-derived suppressor cells in breast cancer using single-cell transcriptomics. *Sci Immunol* 2020;5:eaay6017.
 27. Manz MG, Boettcher S. Emergency granulopoiesis [review]. *Nat Rev Immunol* 2014;14:302–14.
 28. Grieshaber-Bouyer R, Radtke FA, Cunin P, Stifano G, Levescot A, Vijaykumar B, et al. The neutrotime transcriptional signature defines a single continuum of neutrophils across biological compartments. *Nat Commun* 2021;12:2856.
 29. Xie X, Shi Q, Wu P, Zhang X, Kambara H, Su J, et al. Single-cell transcriptome profiling reveals neutrophil heterogeneity and orchestrated maturation during homeostasis and bacterial infection. *Nat Immunol* 2020;21:1119–33.
 30. Evrard M, Kwok IW, Chong SZ, Teng KW, Becht E, Chen J, et al. Developmental analysis of bone marrow neutrophils reveals populations specialized in expansion, trafficking, and effector functions. *Immunity* 2018;48:364–79.
 31. Pillay J, Tak T, Kamp VM, Koenderman L. Immune suppression by neutrophils and granulocytic myeloid-derived suppressor cells: similarities and differences. *Cell Mol Life Sci* 2013;70:3813–27.
 32. Scalzo-Inguanti K, Monaghan K, Edwards K, Herzog E, Miroso D, Hardy M, et al. A neutralizing anti-G-CSFR antibody blocks G-CSF-induced neutrophilia without inducing neutropenia in nonhuman primates. *J Leukoc Biol* 2017;102:537–49.
 33. Opendakker G, El-Asrar AA, Van Damme J. Remnant epitopes generating autoimmunity: from model to useful paradigm [review]. *Trends Immunol* 2020;41:367–78.
 34. Nigrovic PA. Is there a window of opportunity for treatment of systemic juvenile idiopathic arthritis [review]? *Arthritis Rheumatol* 2014;66:1405–13.
 35. Schrijver IT, Théroude C, Roger T. Myeloid-derived suppressor cells in sepsis [review]. *Front Immunol* 2019;10:327.
 36. Ramanathan K, Glaser A, Lythgoe H, Ong J, Beresford MW, Midgley A, et al. Neutrophil activation signature in juvenile idiopathic arthritis indicates the presence of low-density granulocytes. *Rheumatology* 2018;57:488–98.
 37. Hamilton JA, Achuthan A. Colony stimulating factors and myeloid cell biology in health and disease [review]. *Trends Immunol* 2013;34:81–9.
 38. Coffelt SB, Kersten K, Doornebal CW, Weiden J, Vrijland K, Hau C-S, et al. IL-17-producing $\gamma\delta$ T cells and neutrophils conspire to promote breast cancer metastasis. *Nature* 2015;522:345–8.
 39. Schwarzenberger P, Huang W, Ye P, Manuel M, Zhang Z, Bagby G, et al. Requirement of endogenous stem cell factor and granulocyte-colony-stimulating factor for IL-17-mediated granulopoiesis. *J Immunol* 2000;164:4783–9.
 40. Chung Y, Chang SH, Martinez GJ, Yang XO, Nurieva R, Kang HS, et al. Critical regulation of early Th17 cell differentiation by interleukin-1 signaling. *Immunity* 2009;30:576–87.
 41. Sutton CE, Lalor SJ, Sweeney CM, Breton CF, Lavelle EC, Mills KH. Interleukin-1 and IL-23 induce innate IL-17 production from $\gamma\delta$ T cells, amplifying Th17 responses and autoimmunity. *Immunity* 2009;31:331–41.
 42. Papotto PH, Ribot JC, Silva-Santos B. IL-17+ $\gamma\delta$ T cells as kick-starters of inflammation [review]. *Nat Rev Immunol* 2017;18:604–11.
 43. Eyles JL, Hickey MJ, Norman MU, Croker BA, Roberts AW, Drake SF, et al. A key role for G-CSF-induced neutrophil production and trafficking during inflammatory arthritis. *Blood* 2008;112:5193–202.
 44. Kessel C, Lippitz K, Weinlage T, Hinze C, Wittkowski H, Holzinger D, et al. Proinflammatory cytokine environments can drive interleukin-17 overexpression by $\gamma\delta$ T cells in systemic juvenile idiopathic arthritis. *Arthritis Rheumatol* 2017;69:1480–94.
 45. Matthys P, Billiau A. Cytokines and cachexia [review]. *Nutrition* 1997;13:763–70.
 46. De Benedetti F, Meazza C, Martini A. Role of interleukin-6 in growth failure: an animal model [review]. *Horm Res* 2002;58:24–7.
 47. Rybakina V, Stas M, Ugarte-Berzal E, Noppen S, Vandoooren J, Van Aelst I, et al. Gelatinase B/matrix metalloproteinase-9 and other neutrophil proteases switch off interleukin-2 activity. *Biochem J* 2019;476:2191–208.
 48. Cunin P, Lee PY, Kim E, Schmider AB, Cloutier N, Pare A, et al. Differential attenuation of β 2 integrin-dependent and -independent neutrophil migration by Ly6G ligation. *Blood Adv* 2019;3:256–67.
 49. Ballesteros I, Rubio-Ponce A, Genua M, Lusito E, Kwok I, Fernández-Calvo G, et al. Co-option of neutrophil fates by tissue environments. *Cell* 2020;183:1282–97.
 50. Kelchtermans H, Schurgers E, Geboes L, Mitera T, Van Damme J, Van Snick J, et al. Effector mechanisms of interleukin-17 in collagen-induced arthritis in the absence of interferon- γ and counteraction by interferon- γ . *Arthritis Res Ther* 2009;11:R122.

Identification of Distinct Inflammatory Programs and Biomarkers in Systemic Juvenile Idiopathic Arthritis and Related Lung Disease by Serum Proteome Analysis

Guangbo Chen,¹  Gail H. Deutsch,²  Grant S. Schulert,³  Hong Zheng,¹ SoRi Jang,¹ Bruce Trapnell,³ 
Pui Y. Lee,⁴  Claudia Macaubas,¹  Katherine Ho,¹ Corinne Schneider,⁵ Vivian E. Saper,¹ 
Adriana Almeida de Jesus,⁶ Mark A. Krasnow,⁷ Alexei Grom,³ Raphaela Goldbach-Mansky,⁶  Purvesh Khatri,¹ 
Elizabeth D. Mellins,¹  and Scott W. Canna⁸ 

Objective. Recent observations in systemic juvenile idiopathic arthritis (JIA) suggest an increasing incidence of high-mortality interstitial lung disease often characterized by a variant of pulmonary alveolar proteinosis (PAP). Co-occurrence of macrophage activation syndrome (MAS) and PAP in systemic JIA suggests a shared pathology, but patients with lung disease associated with systemic JIA (designated SJIA-LD) also commonly experience features of drug reaction such as atypical rashes and eosinophilia. This study was undertaken to investigate immunopathology and identify biomarkers in systemic JIA, MAS, and SJIA-LD.

Methods. We used SOMAscan to measure ~1,300 analytes in sera from healthy controls and patients with systemic JIA, MAS, SJIA-LD, or other related diseases. We verified selected findings by enzyme-linked immunosorbent assay and lung immunostaining. Because the proteome of a sample may reflect multiple states (systemic JIA, MAS, or SJIA-LD), we used regression modeling to identify subsets of altered proteins associated with each state. We tested key findings in a validation cohort.

Results. Proteome alterations in active systemic JIA and MAS overlapped substantially, including known systemic JIA biomarkers such as serum amyloid A and S100A9, and novel elevations in the levels of heat-shock proteins and glycolytic enzymes. Interleukin-18 levels were elevated in all systemic JIA groups, particularly MAS and SJIA-LD. We also identified an MAS-independent SJIA-LD signature notable for elevated levels of intercellular adhesion molecule 5 (ICAM-5), matrix metalloproteinase 7 (MMP-7), and allergic/eosinophilic chemokines, which have been previously associated with lung damage. Immunohistochemistry localized ICAM-5 and MMP-7 in the lungs of patients with SJIA-LD. The ability of ICAM-5 to distinguish SJIA-LD from systemic JIA/MAS was independently validated.

Conclusion. Serum proteins support a systemic JIA-to-MAS continuum; help distinguish systemic JIA, systemic JIA/MAS, and SJIA-LD; and suggest etiologic hypotheses. Select biomarkers, such as ICAM-5, could aid in early detection and management of SJIA-LD.

The SOMAscan assay was supported by a grant to the Intramural Research Program of the National Institute of Allergy and Infectious Diseases from the Systemic JIA Foundation. Dr. Chen is an Eli Lilly Fellow of the Life Science Research Foundation. Dr. Jang's work was supported by a Dean's Postdoctoral Fellowship, School of Medicine, Stanford. Drs. Macaubas and Mellins' work was supported by the National Institute of Arthritis and Musculoskeletal and Skin Diseases, NIH (grants R01-AR-066551 and AR-061297) and the Arthritis Foundation Great West Region Arthritis Center of Excellence. Drs. Schneider and Canna's work was supported by the RK Mellon Institute for Pediatric Research and the National Institute of Allergy and Infectious Diseases, NIH (grants K22-AI-123366, NICHD-R01, and HD-098428). Drs. Saper and Mellins' work was supported by the Lucille Packard Foundation for Children's Health and the Childhood Arthritis and Rheumatology Research Alliance/Arthritis Foundation. Drs. de Jesus and Goldbach-Mansky's work was supported by the

National Institute of Allergy and Infectious Diseases intramural research program. Dr. Khatri's work was supported by the Bill and Melinda Gates Foundation (grant OPP1113682), the National Institute of Allergy and Infectious Diseases, NIH (grants 1U19-AI-109662, U19-AI-057229, and 5R01-AI-125197), the Department of Defense (contracts W81XWH-18-1-0253 and W81XWH1910235), and the Ralph and Marian Falk Medical Research Trust.

Drs. Khatri, Mellins, and Canna contributed equally to this work.

¹Guangbo Chen, PhD, Hong Zheng, PhD, SoRi Jang, PhD, Claudia Macaubas, PhD, Katherine Ho, Vivian E. Saper, MD, Purvesh Khatri, PhD, Elizabeth D. Mellins, MD: Stanford University, Stanford, California; ²Gail H. Deutsch, MD: University of Washington Medical Center, Seattle; ³Grant S. Schulert, MD, PhD, Bruce Trapnell, MS, MD, Alexei Grom, MD: University of Cincinnati College of Medicine, Cincinnati, Ohio; ⁴Pui Y. Lee, MD, PhD: Boston Children's Hospital, Boston, Massachusetts; ⁵Corinne Schneider,

INTRODUCTION

Systemic juvenile idiopathic arthritis (JIA) is a chronic inflammatory disease of childhood characterized by a combination of systemic inflammation, quotidian fever, evanescent rash, adenopathy/organomegaly, serositis, and arthritis (1). Its adult equivalent is adult-onset Still's disease (2). Macrophage activation syndrome (MAS) is a life-threatening form of secondary hemophagocytic lymphohistiocytosis that complicates the course in ~10% of patients with systemic JIA (3). It is characterized by cytokine storm, very high serum ferritin levels, progression to organ failure, and a mortality rate of up to 17%. Active systemic JIA and MAS may share a common etiology, representing a spectrum of disease severity (4).

For decades, pleuritis and pleural effusions were the lung manifestations described in systemic JIA (1,5). Recent observations suggested an increasing incidence of high-mortality interstitial lung disease (ILD) (6–8), concurrent with the increased use of anti-interleukin-1 (anti-IL-1) and anti-IL-6 therapies (8). Though several systemic JIA-related lung disease subtypes were described, a striking and novel clinical presentation (and the focus of the present study, hereafter referred to as “SJIA-LD”) included acute digital clubbing, characteristic radiologic patterns, and pathology consistent with a variant of pulmonary alveolar proteinosis (PAP)/endogenous lipid pneumonia (ELP), with more lymphocyttoplasmic infiltration and vascular changes than primary PAP (6,8). This phenotype was highly enriched in patients with prior exposure to IL-1- or IL-6-blocking therapies (odds ratio [OR] 13, $P = 0.001$) (9), and such patients often had histories of eosinophilia, anaphylaxis to tocilizumab, and/or rashes atypical for systemic JIA (6,8). Though lung transcriptional studies and findings in bronchoalveolar lavage fluid suggested interferon- γ (IFN γ) activity (6), these clinical features combined with the recent discovery of a strong association with HLA-DRB1*15 (OR 15.5) were consistent with severe delayed hypersensitivity reactions to IL-1 and IL-6 inhibitors.

Initial descriptions of SJIA-LD were associated with severe disease (MAS in 80% of patients) (7), but larger follow-up series suggested that MAS at systemic JIA onset was not associated with the unusual clinical features seen in the SJIA-LD group, and some patients with treatment-responsive systemic JIA nevertheless developed lung disease. However, 71% had overt or subclinical MAS at the detection of or during lung disease. MAS is commonly triggered by environmental stimuli like infection (10), and this high MAS rate during SJIA-LD suggested that the inflammation associated with SJIA-LD may stimulate or help maintain MAS (9).

To better understand the underlying pathology and relationships between systemic JIA and its complications MAS and SJIA-LD, we assembled serum proteomes from a multicenter cohort of patients with systemic JIA with or without these complications and relevant comparator patients (with monogenic auto-inflammatory diseases or PAP from other causes). We also sought to identify biomarkers that might aid in detecting or monitoring lung disease in systemic JIA.

PATIENTS AND METHODS

Cohort and disease definitions. Several names have been used for the syndrome of digital clubbing, characteristic radiographic findings, and PAP-variant parenchymal lung disease observed in systemic JIA (6,7,8,11). Herein, we use the term “SJIA-LD” to identify patients known to have or strongly suspected of having this constellation of features (Supplementary Table 1, available on the *Arthritis & Rheumatology* website at <http://onlinelibrary.wiley.com/doi/10.1002/art.42099>). Clinical data and serum from patients with SJIA-LD, healthy controls, patients with inactive systemic JIA, active systemic JIA, MAS, hereditary/autoimmune PAP, STING-associated vasculopathy of infancy (SAVI; all with ILD, prior to JAK inhibitor therapy), neonatal-onset multisystem inflammatory disease (NOMID; prior to IL-1 blockade), or NLRC4-related MAS (NLRC4-MAS) were collected under ongoing protocols using established diagnostic, classification, or genetic criteria. Notably, arthritis was not required for classification as systemic JIA. The study included a discovery cohort composed of all groups listed above, as well as a validation cohort consisting of only samples from controls and systemic JIA patients (see Table 1; and Supplementary Table 1 and Supplementary Methods, available on the *Arthritis & Rheumatology* website at <http://onlinelibrary.wiley.com/doi/10.1002/art.42099>).

Serum protein analysis. For the discovery cohort, we profiled serum samples by SOMAscan assay (SOMALogic), an aptamer-based proteomics platform (12), in collaboration with the National Institutes of Health Center for Human Immunology. A total of 1,271 analytes were evaluated, with most being mapped to a single protein (exceptions are listed in Supplementary Tables 2–4, available on the *Arthritis & Rheumatology* website at <http://onlinelibrary.wiley.com/doi/10.1002/art.42099>). IL-18 was assessed by Luminex. CXCL9 and IL-18 binding protein were measured by both SOMAscan and Luminex to verify reproducibility (Supplementary Figure 1, available on the *Arthritis &*

BAS: University of Pittsburgh Medical Center, Pittsburgh, Pennsylvania; ⁶Adriana Almeida de Jesus, MD, PhD, Raphaela Goldbach-Mansky, MD, MHS: National Institute of Allergy and Infectious Diseases, Bethesda, Maryland; ⁷Mark A. Krasnow, MD, PhD: Howard Hughes Medical Institute, Stanford University, Stanford, California; ⁸Scott W. Canna, MD: University of Pittsburgh Medical Center, Pittsburgh, Pennsylvania, and The Children's Hospital of Philadelphia, Philadelphia, Pennsylvania.

Author disclosures are available at <https://onlinelibrary.wiley.com/action/downloadSupplement?doi=10.1002%2Fart.42099&file=art42099-sup-0001-Disclosureform.pdf>.

Address correspondence to Scott W. Canna, MD, 1110A Abramson Building, 3615 Civic Center Boulevard, Philadelphia, PA 19104. Email: cannas@chop.edu.

Submitted for publication February 3, 2021; accepted in revised form February 15, 2022.

Table 1. Group definitions and demographic characteristics of the discovery cohort*

Group	Clinical definition	No. of patients	No. of samples†	Age, median (IQR) years	Sex, no. (% female)	Center (no. of patients)
Healthy controls‡	No known pulmonary or rheumatic/autoinflammatory disease	21	21	8.9 (1.4–17)	7 (37)§	Cincinnati (6); NIAID (8); Chile (7)
Inactive systemic JIA‡	Inactive at time of sampling per submitting investigator	28	30	12 (7–16)	18 (64)	Stanford (3); Cincinnati (21); NIAID (4)
Active systemic JIA‡	Active per submitting investigator but did not meet MAS criteria at time of sampling	24	25	12 (8–14)	14 (58)	Stanford (2); Cincinnati (20); NIAID (2)
MAS‡	Met MAS criteria at time of sampling	10	12	9.4 (4.1–16)	7 (70)	Cincinnati (5); NIAID (5)
SJIA-LD‡¶	Had radiologic evidence of lung disease#	10	30	5.2 (4.3–8.1)	6 (60)	Stanford (1); Cincinnati (3); NIAID (10)
SJIA-LD FC ^{low} ‡	Ferritin or CRP not elevated	8	18	4.4 (3.8–6.4)	5 (63)	Cincinnati (1); NIAID (7)
SJIA-LD FC ^{high} ‡	Ferritin and CRP elevated	6	12	6.5 (5–8.6)	3 (50)	Stanford (1); Cincinnati (2); NIAID (3)
PAP	PAP due to anti-GM-CSF autoantibodies (n = 10) or genetic causes (n = 4) without systemic JIA or known rheumatic/autoinflammatory disease	14	14	34 (17–47)	8 (57)	Cincinnati (14)
SAVI	All patients had radiologic ILD, prior to treatment with JAK inhibitors	4	4	15 (10–18)	4 (100)	NIAID (4)
NOMID	NOMID prior to treatment with IL-1 inhibitors	5	5	9.2 (8.6–18)	4 (80)	NIAID (5)
Inactive NLRC4-related MAS	Inactive per submitting investigator	2	5	5.3 (3.2–7.4)	2 (100)	NIAID (2)
NLRC4-related MAS	Active MAS per submitting investigator	2	5	4.8 (2.5–7.2)	2 (100)	NIAID (2)
Total	–	120	151	–	–	–

* All patients with systemic juvenile idiopathic arthritis (JIA) met the modified International League of Associations for Rheumatology criteria (51). IQR = interquartile range; NIAID = National Institute of Allergy and Infectious Diseases; PAP = pulmonary alveolar proteinosis; anti-GM-CSF = anti-granulocyte-macrophage colony-stimulating factor; SAVI = STING-associated vasculopathy with onset in infancy; NOMID = neonatal-onset multisystem inflammatory disease; IL-1 = interleukin-1.

† When multiple samples were obtained from the same patient within one clinical group, the SOMAscan data were merged by averaging.

‡ Patient groups included in Linear Models for Microarray Data analysis.

§ Two healthy controls were missing data on sex.

¶ The systemic JIA-associated lung disease (SJIA-LD) group was subdivided into those with high levels of both ferritin and C-reactive protein (CRP; SJIA-LD FC^{high}) and those with low levels of either ferritin or CRP (SJIA-LD FC^{low}), based on their values relative to active macrophage activation syndrome (MAS) (for thresholds, see Supplementary Figures 3A and B, available on the *Arthritis & Rheumatology* website at <http://onlinelibrary.wiley.com/doi/10.1002/art.42099>). Four patients overlapped between the FC^{low} and FC^{high} subgroups.

See Supplementary Table 1 for details.

Rheumatology website at <http://onlinelibrary.wiley.com/doi/10.1002/art.42099>). We performed intercellular adhesion molecule 5 (ICAM-5) enzyme-linked immunosorbent assay (ELISA) on remnant sera from the discovery cohort as a technical verification. Serum and plasma samples from an independent validation cohort were assayed for IL-18 and CXCL9 by Luminex and for ICAM-5 and MMP-7 by ELISA. Table 1, Supplementary Table 1, and the Supplementary Methods contain further details.

Linear regression-based modeling analysis. A schematic overview of the study is shown in Supplementary Figure 2A, available on the *Arthritis & Rheumatology* website at <http://onlinelibrary.wiley.com/doi/10.1002/art.42099>. Patients' disease, and therefore their proteomes, may reflect multiple disease components (e.g., patients with SJIA-LD may have an active systemic JIA disease component). Thus, our analysis required distinguishing patient groups from disease components, with some overlap of disease and component names (e.g., the active systemic JIA group versus the systemic JIA disease component). Likewise, components can contribute to the proteomes of multiple disease groups (e.g., MAS

disease component in both MAS and SJIA-LD patient samples). To capture the serum proteome alterations attributed to a specific disease component, we used Linear Models for Microarray Data (LIMMA), in which the overall proteome alteration was regressed against the disease component(s) present in each individual patient (Supplementary Figures 2B and C, available on the *Arthritis & Rheumatology* website at <http://onlinelibrary.wiley.com/doi/10.1002/art.42099>). We used these disease components to assign disease activity scores (for systemic JIA, MAS, SJIA-LD) to individual samples. For details on LIMMA, disease component construction, and calculating disease activity scores, see the Supplementary Methods.

RESULTS

Characteristics of the discovery cohort including patients with systemic JIA, MAS, SJIA-LD, or related inflammatory conditions. We included 151 serum samples from 120 patients for proteomic profiling using SOMAscan. These represented 10 patient groups based on clinical characterizations (Table 1 and Supplementary Table 1). Most

samples and patients were from 5 main groups that we analyzed by linear regression: healthy controls ($n = 21$), patients with inactive systemic JIA ($n = 28$), patients with active systemic JIA ($n = 24$), patients with MAS ($n = 10$), and patients with SJIA-LD ($n = 10$) (Supplementary Methods). The SJIA-LD samples were divided into those with high levels of both ferritin and C-reactive protein (CRP; SJIA-LD FC^{high}) and those with low levels of either ferritin or CRP (SJIA-LD FC^{low}) (Supplementary Figures 3A and B, available on the *Arthritis & Rheumatology* website at <http://onlinelibrary.wiley.com/doi/10.1002/art.42099>). Samples were selected based on clinical diagnosis. Postselection data showed that all SJIA-LD patient samples were collected during or following exposure to IL-1 or IL-6 inhibitors, and 87% of genotyped patients in the SJIA-LD group carried the HLA-DRB1*15 risk allele (Supplementary Table 1).

In all sera studied, the proteome in a single sample may reflect contributions of multiple concurrent pathologic processes

(Supplementary Figure 2). A central goal of this study was to capture the serum proteome alterations attributed to a specific disease component (systemic JIA, MAS, or SJIA-LD), as distinguished from the disease groups (see above and Supplementary Methods). We used LIMMA to determine the statistically significant differences associated with each disease component (Figures 1A–C; and Supplementary Figures 2B and C, available on the *Arthritis & Rheumatology* website at <http://onlinelibrary.wiley.com/doi/10.1002/art.42099>).

Further exaggeration of many molecular changes present in systemic JIA by MAS.

We first characterized the systemic JIA and MAS components. For the systemic JIA component (patients with active systemic JIA versus healthy controls), we found 86 significantly altered proteins, with most (85%) elevated in the systemic JIA group (Figure 1A; and Supplementary Table 2, available on the *Arthritis & Rheumatology* website at <http://onlinelibrary.wiley.com/doi/10.1002/art.42099>). Many of these proteins, including

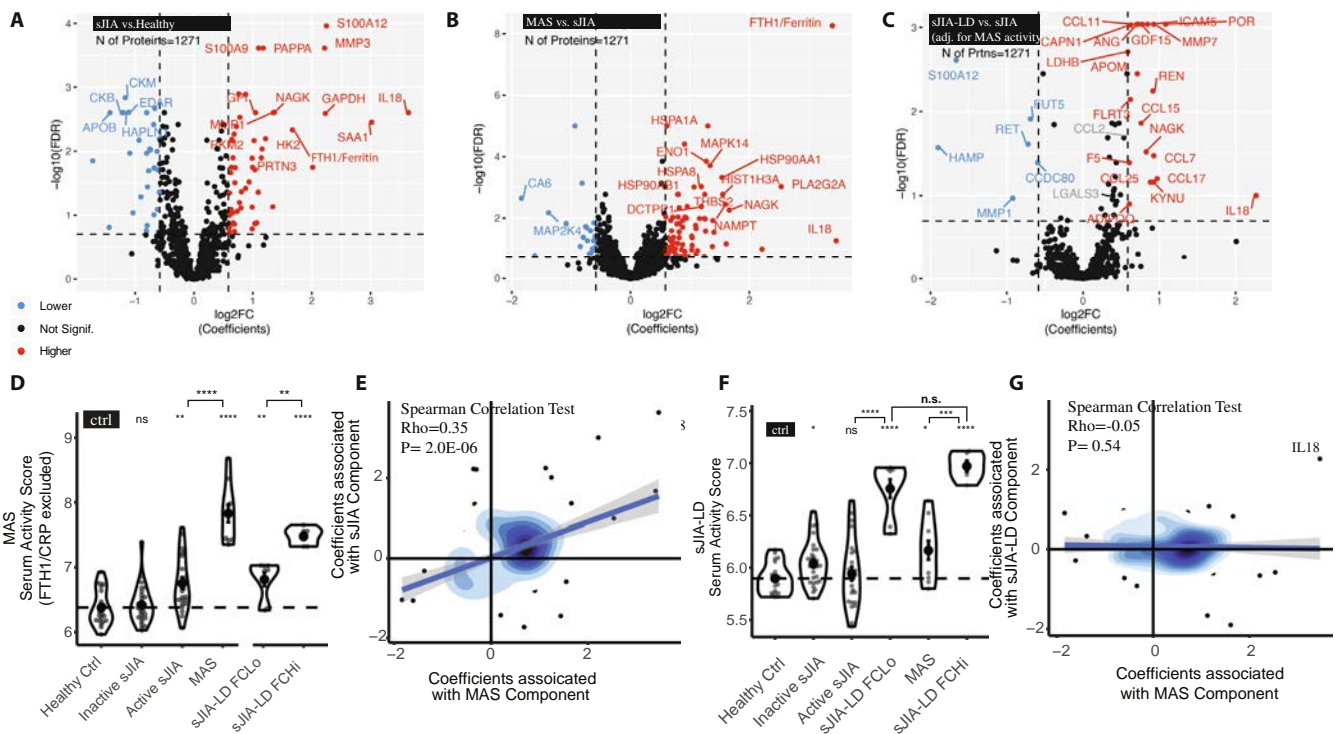


Figure 1. Serum proteome profiles associated with active systemic juvenile idiopathic arthritis (sJIA), macrophage activation syndrome (MAS), and systemic JIA-associated lung disease (SJIA-LD). **A–C**, Volcano plots showing the proteins (indicated by gene names) with significantly changed abundance in the systemic JIA (**A**), MAS (**B**), and SJIA-LD (**C**) disease components. Broken lines indicate significance thresholds [false discovery rate [FDR]–adjusted $P < 20\%$ and fold change [FC] > 1.5]. **D** and **F**, Violin plots showing the MAS serum activity score (calculated without ferritin [FTH1] or C-reactive protein [CRP] values, as described in Patients and Methods) (**D**) and the SJIA-LD serum activity score (**F**) in the indicated groups. The SJIA-LD group was subdivided into those with low levels of either ferritin or CRP (SJIA-LD FC^{Lo}) and those with high levels of both ferritin and CRP (SJIA-LD FC^{Hi}) (see Table 1). Black circles and error bars show the median and interquartile range. Gray circles represent individual samples. Broken lines indicate the median value in healthy controls. * = $P < 0.05$; ** = $P < 0.01$; *** = $P < 0.001$; **** = $P < 0.0001$ versus controls except where indicated otherwise, by Wilcoxon’s signed rank test without the assumption of normal distribution. P values were adjusted using the Benjamini-Hochberg procedure. NS = not significant. **E** and **G**, Correlation between the coefficients (\log_2 FC) assigned by Linear Models for Microarray Data to the systemic JIA and MAS disease components (**E**) and the SJIA-LD and MAS disease components (**G**) (see Supplementary Methods, available on the *Arthritis & Rheumatology* website at <http://onlinelibrary.wiley.com/doi/10.1002/art.42099>) for the 174 proteins identified as significantly altered in at least 1 of the 3 disease components (systemic JIA, MAS, or SJIA-LD). Color figure can be viewed in the online issue, which is available at <http://onlinelibrary.wiley.com/doi/10.1002/art.42099/abstract>.

ferritin, IL-18, CRP, and S100A12 (Supplementary Figures 3C–F), have been previously associated with systemic JIA using other techniques, supporting the validity of SOMAscan measurements. We also identified several proteins not typically associated with systemic JIA, such as MMP-3 (a protease induced by IL-6 [13]), and various metabolic enzymes, including GAPDH, *N*-acetyl-D-glucosamine kinase, hexokinase, and glucose-6-phosphate isomerase.

We also compared profiles of patients with inactive systemic JIA to those of healthy controls. The levels of 7 proteins were significantly different (Supplementary Figure 4, available on the *Arthritis & Rheumatology* website at <http://onlinelibrary.wiley.com/doi/10.1002/art.42099>), including the IL-10-induced monokine CCL16, consistent with a state of compensated inflammation in inactive systemic JIA (14).

The analysis of the MAS component compared patients with active systemic JIA to those with MAS and identified 105 significantly different proteins (Figure 1B and Supplementary Table 3). These included many glycolytic enzymes (e.g., GAPDH and lactate dehydrogenase [LDH]) and several chaperone proteins (e.g., Hsp70, Hsp90). When calculating the MAS serum activity score, we excluded CRP and ferritin, since these are used to help define MAS (see the Supplementary Methods). As expected, the MAS score (even without CRP and ferritin) was significantly greater in MAS than in systemic JIA (Figure 1D) and was significantly correlated with ferritin level (Spearman's $\rho = 0.57$, $P < 2.2 \times 10^{-16}$) and CRP ($\rho = 0.5$, $P = 1.5 \times 10^{-9}$) (Supplementary Figures 5A and B, available on the *Arthritis & Rheumatology* website at <http://onlinelibrary.wiley.com/doi/10.1002/art.42099>). The MAS serum activity score was also higher in samples from patients with active NLRC4-MAS versus those with inactive NLRC4-MAS (Supplementary Figure 5C). In the linear regression model, each protein received a coefficient reflecting its contribution to the component (Supplementary Methods). We observed a strong correlation between the protein coefficients associated with systemic JIA and MAS disease components (Figure 1E and Supplementary Figure 5D), suggesting that MAS further exaggerated a serum proteome already altered in systemic JIA.

Elevation of proteins involved in leukocyte-mediated immunity and cellular metabolism in the systemic JIA and MAS serum proteomes. Examining the top altered proteins in the systemic JIA and MAS disease components (Supplementary Tables 2–4), we found a few proteins whose functional relationship to disease was novel or unclear. Specifically, heat shock proteins Hsp70 (HSPA1A, HSPA8) and Hsp90 (HSP90AA1, HSP90AB1) were up-regulated in many patients, particularly in those with MAS (Supplementary Table 3 and Figure 2A). These proteins function as intracellular molecular chaperones, but they may also be extracellular DAMPs (15). Additionally, many glycolytic enzymes, like enolase 1 and GAPDH, were strongly elevated in MAS and systemic JIA (Figure 2B). We performed Gene Ontology (GO) term enrichment analysis on the proteins significantly changed for each disease

component (Supplementary Table 5, available on the *Arthritis & Rheumatology* website at <http://onlinelibrary.wiley.com/doi/10.1002/art.42099>). Consistent with systemic immune activation, proteins involved in the GO term “leukocyte mediated immunity” (Figure 2C) were elevated in both the systemic JIA and MAS disease components. In addition, we found that the systemic JIA and MAS disease components were enriched for proteins involved in the GO term “monocarboxylic acid metabolic process;” only the systemic JIA component met statistical significance (Figure 2D and Supplementary Table 5).

Identification of serum alterations associated with lung disease independent of MAS activity in patients with SJIA-LD.

Clinical data showing that SJIA-LD could arise in the absence of MAS (8), as well as our observation that many SJIA-LD samples had low MAS scores (Figure 1D), suggested that active systemic JIA or MAS did not sufficiently explain SJIA-LD disease activity. Therefore, we sought to identify the proteins driving an SJIA-LD disease component. To track whether SJIA-LD samples with strong MAS features biased or confounded identification of the SJIA-LD component, the SJIA-LD samples were divided into those with high levels of both ferritin and CRP (SJIA-LD FC^{high}) and those without (SJIA-LD FC^{low}). The SJIA-LD FC^{low} group had a comparable MAS serum activity score to the active systemic JIA group. The SJIA-LD FC^{high} group had a significantly higher MAS serum activity score than the active systemic JIA or SJIA-LD FC^{low} groups but it trended toward a lower MAS serum activity score than the MAS group (Figure 1D). This suggests significant smoldering MAS activity in some SJIA-LD samples even though none were obtained during periods meeting clinical MAS criteria.

Comparing SJIA-LD patients to systemic JIA patients and MAS patients identified 26 proteins (20 up-regulated and 6 down-regulated) significantly associated with the SJIA-LD disease component, including ICAM-5, MMP-7, and CCL11/eotaxin-1 (Figure 1C). Using these proteins, we calculated the SJIA-LD serum activity score and, as expected, found it was higher in SJIA-LD samples than in either active systemic JIA or MAS (Figure 1F) (see the Supplementary Methods for details on adjustment for MAS activity). Unlike the MAS serum activity score, the SJIA-LD serum activity score did not differ between the SJIA-LD FC^{low} and SJIA-LD FC^{high} groups, and both groups had substantially higher SJIA-LD serum activity than the MAS group (Figure 1F). The small elevation of the SJIA-LD activity score in the MAS group was entirely attributable to IL-18 (Supplementary Figures 6A and B, available on the *Arthritis & Rheumatology* website at <http://onlinelibrary.wiley.com/doi/10.1002/art.42099>).

As expected according to the model design, there was no correlation between the protein abundance coefficients of the SJIA-LD component and those of the MAS component (Figure 1G and Supplementary Figure 6C). The SJIA-LD serum activity score was not elevated in primary PAP (caused by granulocyte-macrophage

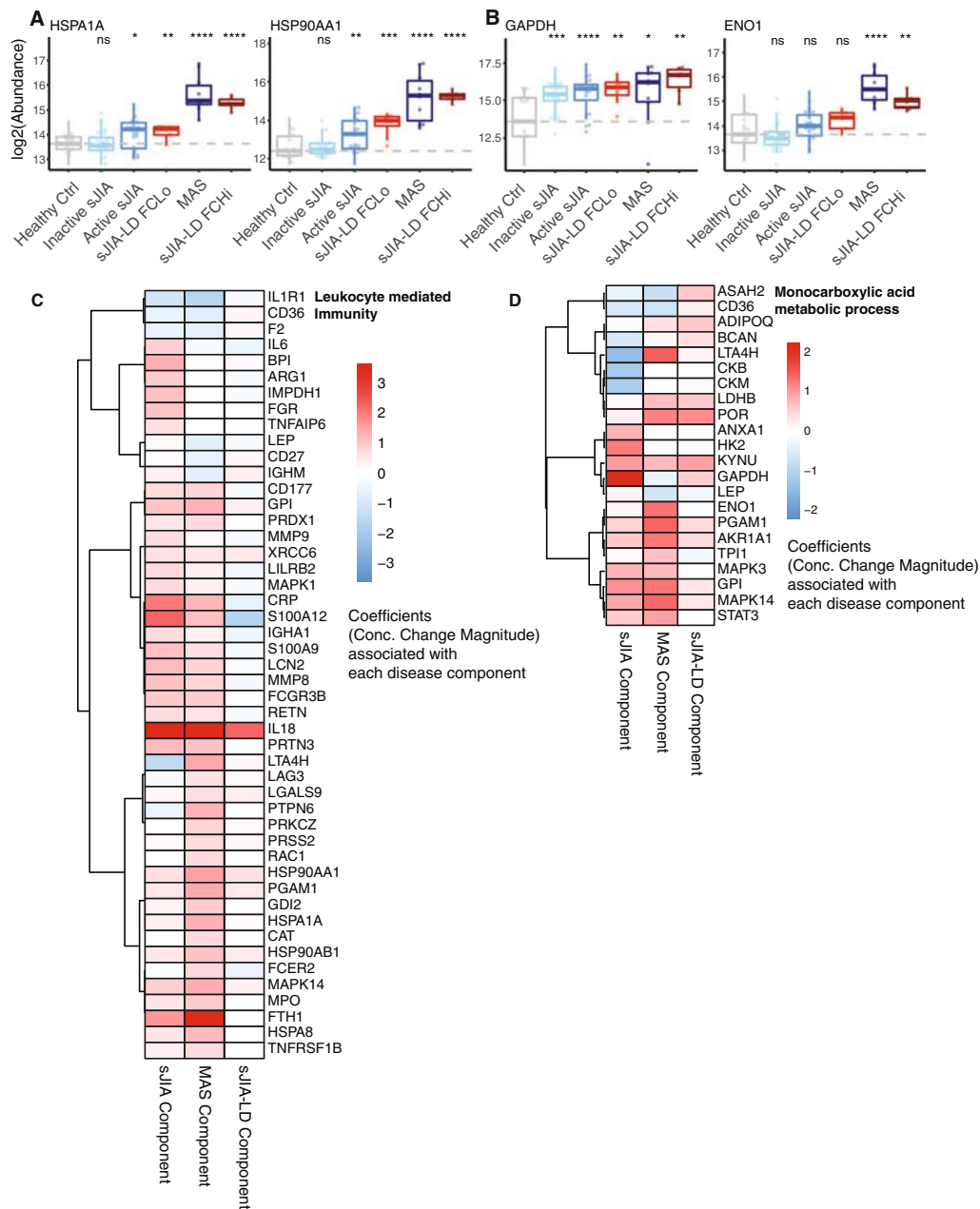


Figure 2. Protein functional groups for different disease components. **A** and **B**, Examples of significantly elevated heat-shock proteins (HSP1A and HSP90AA1) (**A**) and proteins involved in glycolytic process (GAPDH and enolase 1 [ENO1]) (**B**) in the indicated groups. Data are shown as box plots. Each box represents the 25th to 75th percentiles. Lines inside the boxes represent the median. Lines outside the boxes represent the 10th and 90th percentiles. Circles represent individual subjects. Broken lines indicate the median value in healthy controls. * = $P < 0.05$; ** = $P < 0.01$; *** = $P < 0.001$; **** = $P < 0.0001$ versus healthy controls, by Wilcoxon's signed rank test. P values were adjusted using the Benjamini-Hochberg procedure. **C** and **D**, Proteins present in SOMAscan for 2 different functional groups defined by the Gene Ontology (GO) terms "leukocyte mediated immunity" (**C**) and "monocarboxylic acid metabolic process" (**D**). GO term enrichment results are provided in Supplementary Table 5, available on the *Arthritis & Rheumatology* website at <http://onlinelibrary.wiley.com/doi/10.1002/art.42099>. Heatmaps show the coefficient of concentration (conc.) change for each protein associated with each disease component, as determined by Linear Models for Microarray Data, with disease components and genes clustered by Euclidean distances. To facilitate analysis, gene names are presented but represent protein targets (see the Supplementary Methods, available on the *Arthritis & Rheumatology* website at <http://onlinelibrary.wiley.com/doi/10.1002/art.42099>). See Figure 1 for other definitions. Color figure can be viewed in the online issue, which is available at <http://onlinelibrary.wiley.com/doi/10.1002/art.42099/abstract>.

colony-stimulating factor–neutralizing autoantibodies or surfactant-related mutations), suggesting different causes (Supplementary Figures 6A and B). Several patients with SJIA-LD had samples from

multiple time points analyzed by SOMAscan. Following the disease component-specific serum activity scores longitudinally, we found no correlation between the SJIA-LD serum activity score and the

systemic JIA or MAS serum activity scores (Supplementary Figure 7, available on the *Arthritis & Rheumatology* website at <http://onlinelibrary.wiley.com/doi/10.1002/art.42099>). Overall, these

findings corroborate clinical observations suggesting that SJIA-LD may be triggered by a mechanism distinct from systemic JIA, MAS, and other well-characterized PAP conditions.

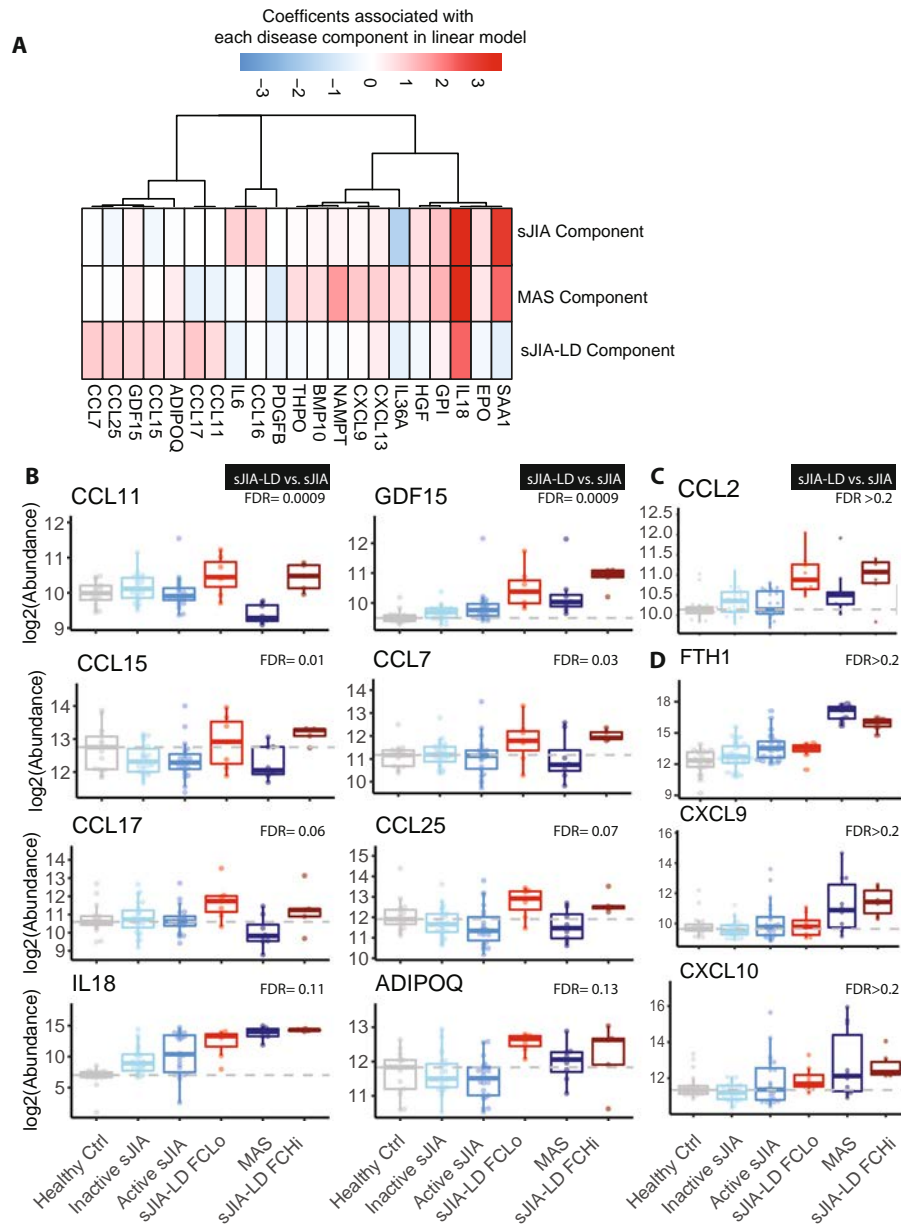


Figure 3. Differences in cytokine/chemokine serum abundance in SJIA-LD versus systemic JIA and MAS. **A**, Heatmap showing the coefficient of concentration change from the Linear Models for Microarray Data analysis for cytokines/chemokines associated with each disease component in the linear regression model. Cytokines/chemokines shown are those that reached significance in at least 1 disease component and were associated with the respective Gene Ontology term (see the Supplementary Methods, available on the *Arthritis & Rheumatology* website at <http://onlinelibrary.wiley.com/doi/10.1002/art.42099>). **B**, Eight cytokines/chemokines with significantly altered abundance in the SJIA-LD disease component. The abundance of each cytokine/chemokine in the indicated groups is shown (see Supplementary Figure 9, available on the *Arthritis & Rheumatology* website at <http://onlinelibrary.wiley.com/doi/10.1002/art.42099>, for data on additional disease groups). **C**, Abundance of CCL2, which approached significance for the SJIA-LD disease component. **D**, Abundance of ferritin and of CXCL9 and CXCL10, 2 interferon-inducible chemokines. In **B–D**, data are shown as box plots. Each box represents the 25th to 75th percentiles. Lines inside the boxes represent the median. Lines outside the boxes represent the 10th and 90th percentiles. Circles represent individual subjects. Broken lines indicate the median value in healthy controls. The FDR for the comparison between SJIA-LD and active systemic JIA or MAS patients, controlled for MAS activity scores, is shown (see Patients and Methods and Supplementary Table 4). To facilitate analysis, gene names are presented but represent protein targets (see the Supplementary Methods). See Figure 1 for definitions. Color figure can be viewed in the online issue, which is available at <http://onlinelibrary.wiley.com/doi/10.1002/art.42099/abstract>.

Elevations in IL-18 and type II chemokines in the SJIA-LD serum proteome profile. Different types of inflammation are characterized by distinct serum cytokine and chemokine profiles. Consistent with our proteome-wide analysis, the changes in cytokine and chemokine levels associated with

active systemic JIA and MAS components appeared similar (Figure 3A). Only IL-18 significantly contributed to all 3 components (systemic JIA, MAS, and SJIA-LD), confirming its association with systemic JIA/MAS and suggesting an independent role in SJIA-LD (Supplementary Figure 8, available on the *Arthritis &*

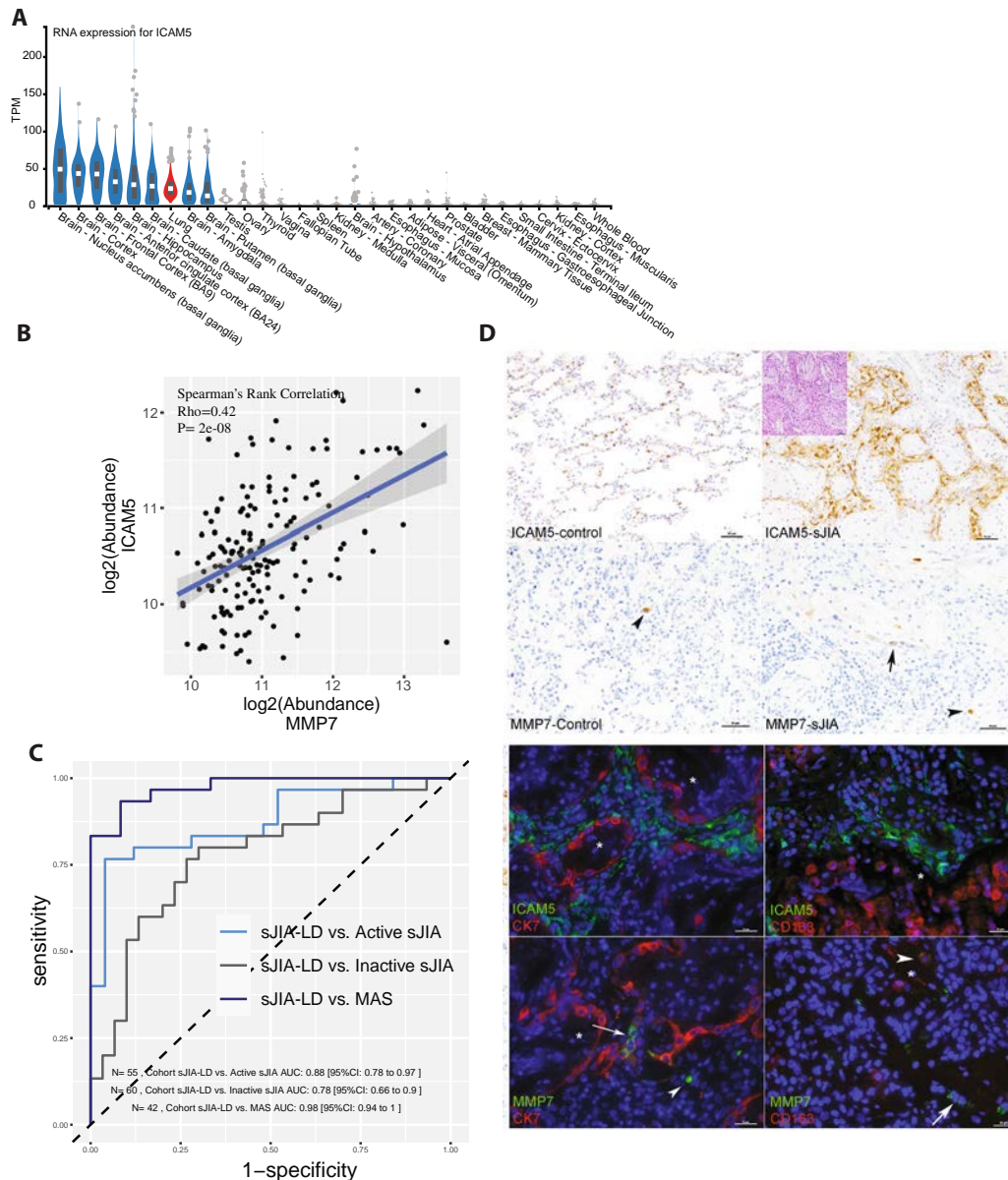


Figure 4. Pulmonary localization of intercellular adhesion molecule 5 (ICAM-5) and matrix metalloproteinase 7 (MMP-7) and their performance in the discovery cohort. **A**, Violin plots of *ICAM5* mRNA expression in the 30 organs with the highest expression in an autopsy cohort (Genotype-Tissue Expression); red indicates expression in lung samples. Gray boxes represent the 25th to 75th percentiles. White boxes indicate the median. Circles indicate outliers. TPM = transcripts per million. **B**, Correlation of MMP-7 and ICAM-5 protein levels among all systemic JIA serum samples. **C**, Receiver operating characteristic curves using ICAM-5 to classify different comparisons in the discovery cohort. AUC = area under the curve; 95% CI = 95% confidence interval. **D**, Top, Staining for ICAM-5 and MMP-7 in lung samples from healthy controls and patients with systemic JIA. Inset shows characteristic histologic features of pulmonary alveolar proteinosis/endogenous lipoid pneumonia in a patient with SJIA-LD. Bottom, ICAM-5 protein expression in lung interstitial fibroblast cells in contrast with epithelial cells (indicated by cytokeratin 7 [CK-7]) and macrophages (CD163) in lung samples from patients with SJIA-LD. **Arrows** indicate MMP-7-expressing epithelial cells. **Arrowheads** indicate MMP-7-expressing macrophages and hematopoietic cells. **Asterisks** denote alveolar lumen. Nuclei are counterstained with DAPI (blue). Bars = 50 μm in top panels; 25 μm in bottom panels. See also Supplementary Figures 12 and 13, available on the *Arthritis & Rheumatology* website at <http://online.library.wiley.com/doi/10.1002/art.42099>. See Figure 1 for other definitions.

Rheumatology website at <http://onlinelibrary.wiley.com/doi/10.1002/art.42099>.

Among the cytokines/chemokines associated with the SJIA-LD disease activity component, most strongly associated were CCL11 (eotaxin 1) and CCL17 (thymus and activation-regulated chemokine [TARC]), which did not contribute significantly to the systemic JIA or MAS components (Figure 3B; and Supplementary Figure 9, available on the *Arthritis & Rheumatology* website at <http://onlinelibrary.wiley.com/doi/10.1002/art.42099>). CCL17/TARC, CCL11/eotaxin 1, and CCL2/monocyte chemoattractant protein 1 (MCP-1) are potent chemoattractants for Th2 cells, eosinophils, and myeloid cells, respectively. They were similarly increased in both the SJIA-LD FC^{high} and SJIA-LD FC^{low} groups, although CCL2 (a chemokine associated with other lung diseases [16]) did not meet the predefined significance threshold in LIMMA analysis (Figures 3B and C; and Supplementary Figure 9 and Supplementary Table 4, available on the *Arthritis & Rheumatology* website at <http://onlinelibrary.wiley.com/doi/10.1002/art.42099>). The MAS-associated, IFN-inducible chemokines CXCL9 and CXCL10 showed similar trends as ferritin and were not routinely elevated in SJIA-LD (Figure 3D). Most of the cytokines/chemokines significantly contributing to the SJIA-LD activity score (including CCL11 and CCL17) were not elevated in autoimmune/hereditary PAP (Supplementary Figures 6A and 9).

ICAM-5 as a potential biomarker for SJIA-LD independent of systemic JIA or MAS. ICAM-5 was one of the proteins most significantly associated with SJIA-LD in the discovery cohort (Figure 1C; and Supplementary Figure 10, available on the *Arthritis & Rheumatology* website at <http://onlinelibrary.wiley.com/doi/10.1002/art.42099>). To verify the SOMAscan ICAM-5 findings, we measured ICAM-5 by ELISA in 80 remnant samples previously profiled with SOMAscan. With regard to CXCL9 and IL-18 binding protein (Supplementary Figure 1), we found a strong correlation between ELISA and SOMAscan results (Supplementary Figure 11, available on the *Arthritis & Rheumatology* website at <http://onlinelibrary.wiley.com/doi/10.1002/art.42099>). Accordingly, only SJIA-LD samples showed ICAM-5 elevation by ELISA, although ELISA showed poorer sensitivity than SOMAscan at low ICAM-5 concentrations.

ICAM-5 function has been best characterized in the nervous system due to high expression in the brain (17). However, autopsy data from healthy adults (Genotype-Tissue Expression) (18) showed ICAM-5 expression in the lung comparable to that seen in the central nervous system (Figure 4A). Levels of MMP-7, a matrix metalloproteinase that efficiently cleaves ICAM-5 *in vitro* (19), were also significantly elevated in SJIA-LD sera (Figure 1C and Supplementary Figure 10) and correlated with serum concentrations of ICAM-5 (Figure 4B). In the SOMAscan cohort, the serum ICAM-5 concentration alone was capable of distinguishing SJIA-LD from inactive systemic JIA, active systemic JIA, or MAS cases (Figure 4C).

To determine whether proteins identified by serum SOMAscan profiling were also expressed in lung tissue, we used

immunostaining to evaluate lung biopsy specimens from 8 patients with SJIA-LD, 3 patients with genetic disorders in surfactant metabolism (*SFTPC*, *NKX2.1*, and *GATA2*), 1 patient with idiopathic ILD, and 3 controls (with asthma/aspiration, bronchopneumonia, and normal lung adjacent to tumor). Consistent with our prior evaluation of SJIA-LD histology (8), the lungs of SJIA-LD patients exhibited the characteristic pattern of PAP and/or ELP (8) with mixed acute and chronic inflammatory cells and rare interstitial fibrosis (Supplementary Table 6, available on the *Arthritis & Rheumatology* website at <http://onlinelibrary.wiley.com/doi/10.1002/art.42099> and Figure 4D). Lung pathology from the patients with genetic disorders in surfactant metabolism showed a similar spectrum of PAP/ELP with more prominent fibrosis.

All samples showed membrane-associated ICAM-5 that was largely restricted to interstitial fibroblasts, confirmed by double-labeling with the epithelial marker cytokeratin 7 (Figure 4D; and Supplementary Figure 12, available on the *Arthritis & Rheumatology* website at <http://onlinelibrary.wiley.com/doi/10.1002/art.42099>). ICAM-5 expression was especially prominent in case 1 (SJIA-LD) and case 9 (*GATA2*) (Supplementary Table 6), and overall proportional to the number of interstitial fibroblasts (data not shown). MMP-7 was expressed rarely in some macrophages (marked by CD163) and epithelial cells (Figure 4D; and Supplementary Table 6 and Supplementary Figure 13, available on the *Arthritis & Rheumatology* website at <http://onlinelibrary.wiley.com/doi/10.1002/art.42099>).

We also immunostained for several other proteins identified by SOMAscan. IL-18 staining was limited in non-ILD controls but increased within macrophages, inflammatory cells, and epithelial cells in both systemic JIA and other ILD cases. In most biopsy specimens, galectin-3 was expressed strongly in alveolar macrophages and more mildly in bronchial and alveolar epithelial cells. Robust expression of CCL2 was observed in the presence of neutrophilic and monocytic inflammation. Rare monocytes and macrophages expressed CCL17 in systemic JIA cases (Supplementary Table 6 and data not shown).

Validation of ICAM-5 as a biomarker for lung disease in systemic JIA.

We next organized an independent multicenter validation cohort consisting of 49 serum samples and 29 plasma samples from healthy controls, patients with inactive systemic JIA, patients with active systemic JIA, patients with MAS, and patients with SJIA-LD (Supplementary Table 7, available on the *Arthritis & Rheumatology* website at <http://onlinelibrary.wiley.com/doi/10.1002/art.42099>). Reviewing the validation cohort for intercurrent lung disease identified a few systemic JIA patients with transient, non-PAP lung ailments (e.g., lobar pneumonia). These we classified as systemic JIA patients with “other lung disease” and included due to the association of ICAM-5 with lung disease in contexts beyond SJIA-LD (Supplementary Table 1). The validation cohort samples were assayed for IL-18, CXCL9, ICAM-5, and MMP-7 by antibody-based methods.

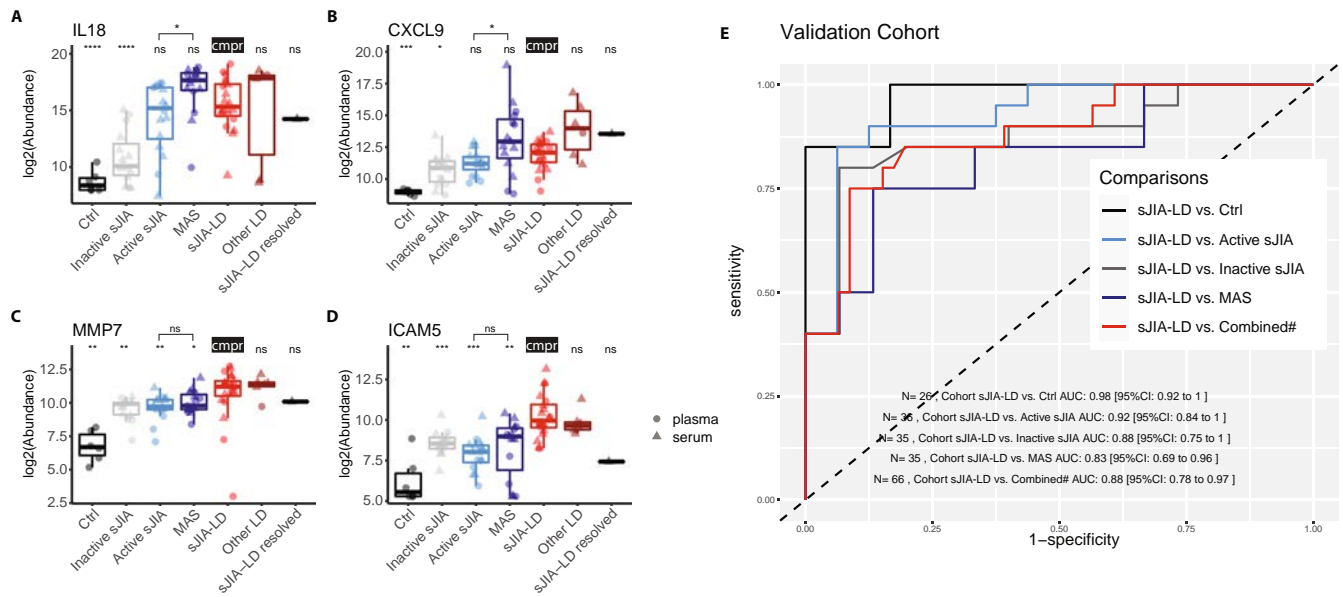


Figure 5. Validation of intercellular adhesion molecule 5 (ICAM-5) as an MAS-independent marker of lung disease in systemic JIA. **A–D**, Serum samples and plasma samples from an independent cohort were assayed for interleukin-18 (IL-18) (**A**) and CXCL9 (**B**) by Luminex and for matrix metalloproteinase 7 (MMP-7) (**C**) and ICAM-5 (**D**) by enzyme-linked immunosorbent assay. “Other LD” indicates systemic JIA patients with intercurrent non-pulmonary alveolar proteinosis lung disease (lobar pneumonia or pulmonary hypertension), whereas “SJIA-LD resolved” indicates a patient with a distant history of radiographic abnormalities resolved at the time of sampling. Further details are provided in Supplementary Tables 1 and 7, available on the *Arthritis & Rheumatology* website at <http://onlinelibrary.wiley.com/doi/10.1002/art.42099>. In each patient group, data from a given patient were included only once, except for in the “other LD” group, in which samples from the same patient in different disease stages were used to represent variability (such as pneumonia with inactive systemic JIA versus MAS, noting the large variation in systemic JIA/MAS markers [**A** and **B**]) but small variations for the lung disease markers MMP-7 [**C**] and ICAM-5 [**D**]). Data are shown as box plots. Each box represents the 25th to 75th percentiles. Lines inside the boxes represent the median. Lines outside the boxes represent the 10th and 90th percentiles. * = $P < 0.05$; ** = $P < 0.01$; *** = $P < 0.001$; **** = $P < 0.0001$, versus the SJIA-LD group except where indicated otherwise, by Wilcoxon’s signed rank test without the assumption of normal distribution. **E**, Receiver operating characteristic analyses of ICAM-5 distinguishing SJIA-LD from other forms of systemic JIA. The combined group included inactive systemic JIA, active systemic JIA, and MAS. AUC = area under the curve; 95% CI = 95% confidence interval (see Figure 1 for other definitions). Color figure can be viewed in the online issue, which is available at <http://onlinelibrary.wiley.com/doi/10.1002/art.42099/abstract>.

Compared with healthy controls and patients with inactive systemic JIA, IL-18 levels were elevated in active systemic JIA, MAS, and SJIA-LD (Figure 5A), and CXCL9 levels were elevated in many MAS patients (Figure 5B). In contrast, MMP-7 and ICAM-5 were more specifically and significantly increased in the SJIA-LD group (Figures 5C and D). These findings were similar in both serum and plasma (Supplementary Figures 14 and 15, available on the *Arthritis & Rheumatology* website at <http://onlinelibrary.wiley.com/doi/10.1002/art.42099>). Of note, ICAM-5 was elevated in a few systemic JIA patients with lobar pneumonia or pulmonary hypertension, but it was normal in a patient with SJIA-LD with a distant history of lung disease that had resolved at sampling (Figure 5D and Supplementary Table 1). These findings support the notion that ICAM-5 is a potential biomarker for lung disease in systemic JIA distinct from the inflammatory changes associated with systemic JIA/MAS (Figure 5E), but ICAM-5 elevation is not specific for PAP/ELP.

DISCUSSION

Serum proteome profiles can provide clues to pathogenesis as well as clinically actionable biomarkers, and they can be particularly

useful in investigating novel complications such as PAP/ELP arising in patients with systemic JIA. To approach both biological and clinical questions concerning systemic JIA and its serious complications, MAS and PAP, we measured serum levels of 1,271 proteins using SOMAscan, verified selected data from this platform using an antibody-based approach, and validated key results in an independent cohort. Our analyses yielded several insights. First, they provided an unbiased confirmation of known biomarkers of systemic JIA (S100 proteins, SAA, CRP, and IL-6) and MAS (ferritin and IL-18) and also corroborated the more recent finding of elevated IL-18 levels in SJIA-LD (6,11,20,21). Second, they identified new proteins/pathways of potential utility in understanding systemic JIA and MAS, including glycolytic enzymes and heat-shock proteins that can act as extracellular DAMPs. Correlation analyses suggested that the systemic JIA and MAS serum proteomes were related. Finally, the proteins associated with SJIA-LD reflected inflammation programs distinct from systemic JIA/MAS. Immunostaining identified cells in the lungs that may be important sources of serum proteins associated with SJIA-LD. We validated ICAM-5 as a biomarker of lung disease in an independent set of systemic JIA samples, most usefully in association with SJIA-LD.

Among the novel proteins identified in the MAS profile, the HSPs may reflect an unfolded protein response, such as that reported to sustain macrophage survival in atherosclerotic lesions (22). However, these chaperone proteins also play extracellular roles in wound healing, tissue regeneration, and immune responses (23). Their elevated serum concentration may reflect stress-induced secretion or cell death (24). Inflammatory forms of cell death (pyroptosis, necroptosis, etc.) are capable of releasing alarmins and DAMPs, such as HSPs, S100 proteins, and IL-33.

Glycolysis-associated proteins (Figures 2B and D) were associated with the systemic JIA and MAS components. Increasingly, aerobic glycolysis is recognized as a necessary metabolic state to execute inflammatory programs in many immune cell types. Many glycolytic enzymes “moonlight” as regulators of inflammatory responses (25–27), and animal studies suggest that inhibiting glycolysis may be therapeutic in cytokine storms (28). The systemic JIA and MAS serum programs also included many neutrophil/monocyte proteins (e.g., S100 proteins, proteinase 3, myeloperoxidase, lipocalin 2, CD163, and CD177) (Supplementary Tables 2 and 3), possibly reflecting their secretion and/or release during cell death.

A high frequency of MAS in SJIA-LD (6,8) suggested a connection between SJIA-LD and the IL-18/IFN γ axis underlying MAS. Indeed, SJIA-LD patients' peripheral blood often carries an IFN transcriptional signature (11). In our study, a portion of SJIA-LD serum samples (SJIA-LD FC^{high}) showed elevated CXCL9 and CXCL10 levels, similar to those in the MAS group, although CXCL9 and CXCL10 levels were not consistently elevated in a previous analysis of bronchoalveolar lavage fluid from 6 patients with SJIA-LD (6). Taken together, these data could be consistent with a role for MAS upstream or downstream of SJIA-LD (Supplementary Figure 16, available on the *Arthritis & Rheumatology* website at <http://onlinelibrary.wiley.com/doi/10.1002/art.42099>). Consistent with SJIA-LD reported in some patients without preceding MAS (8), we found that the SJIA-LD signature did not correlate with MAS serum activity across patients (Figures 1D and F) or time points (Supplementary Figure 7), and many cytokines/chemokines had similar abundance in both the SJIA-LD FC^{low} and SJIA-LD FC^{high} groups (Figure 3B). Our data demonstrate that the SJIA-LD proteome can be present without high MAS activity, supporting the independent origin model (Supplementary Figure 16B). The implication of this model is that treatments targeting the parallel systemic JIA and MAS proteome patterns (anti-IL-1, anti-IL-6, and anti-IFN γ) may be insufficient to manage SJIA-LD. However, it is also possible that MAS activity is necessary for SJIA-LD (at initiation and/or progression), and that the SJIA-LD component indicates lung-specific damage/healing responses rather than a primary pathologic process. Understanding the interaction between the IL-18/IFN γ axis and SJIA-LD development will be crucial as therapies targeting this axis become available (29).

A more practical clinical concern is the need for diagnostic and monitoring biomarkers for SJIA-LD. LDH, surfactant proteins, and

mucin 1 (the source of the KL-6 antigen) are biomarkers commonly associated with lung disease (30–34). Of these, we observed elevation of LDH levels only in SJIA-LD (Supplementary Figure 10), and LDH levels were also elevated in systemic JIA and MAS. Our findings in 2 independent cohorts suggest that ICAM-5 and MMP-7 may serve better to identify lung disease distinct from systemic JIA/MAS activity. However, it is unlikely that they are specific to SJIA-LD. We found elevated MMP-7 levels in patients with autoimmune/hereditary PAP, and elevation of both ICAM-5 and MMP-7 in a few patients with SAVI-related ILD (Supplementary Figure 10). In our validation cohort, using more available antibody-based methods, ICAM-5 consistently and specifically increased in SJIA-LD, compared to systemic JIA and MAS. Consistent with our hypothesis, ICAM-5 appeared also to be elevated in cases with pneumonia or pulmonary hypertension, but normal in a systemic JIA patient with a distant history of lung disease that had resolved at sampling (Figure 5D and Supplementary Table 1). Elevation of ICAM-5 levels were observed in idiopathic pulmonary fibrosis (35,36), rheumatoid arthritis-associated ILD (37), and bronchoalveolar lavage fluid from patients with neuroendocrine hyperplasia of infancy (38) (Supplementary Table 8, available on the *Arthritis & Rheumatology* website at <http://onlinelibrary.wiley.com/doi/10.1002/art.42099>).

In previous studies, the tissue or cell of origin for these biomarkers was not investigated. We found ICAM-5 predominantly in interstitial fibroblasts by immunostaining (Figure 4D), and in fibroblasts, type II alveolar cells, and ciliated cells by RNA sequencing (39) (Supplementary Figure 17, available on the *Arthritis & Rheumatology* website at <http://onlinelibrary.wiley.com/doi/10.1002/art.42099>). MMP-7 has been shown to efficiently cleave ICAM-5 and is also elevated in various other ILDs (35,37,40). We hypothesize that ICAM-5 elevation in blood may be traced back to lung-specific activity of proteases like MMP-7 in SJIA-LD, and the marker pair may be elevated in a variety of lung diseases.

Cytokines/chemokines contributing to the SJIA-LD component (particularly CCL17/TARC, CCL7/MCP3, CCL25, growth differentiation factor 15/macrophage inhibitory cytokine 1 [41] and CCL11/eotaxin 1) (Supplementary Table 8) could be part of profibrotic and/or type 2 immune responses. Supporting the notion of a reactive/profibrotic role, the levels of these chemokines (along with MMP-7) were also elevated in the proteomic profiles of other ILDs (35–38). In a mouse model, expression of a PAP-causing surfactant mutant led to overproduction of CCL17, CCL7, and MMP-7 proteins in type II alveolar cells (42). CCL11 has a profibrotic effect in the lung (43–45). Notably, lung biopsy specimens from patients with SJIA-LD, even from children with longstanding disease, showed remarkably little fibrosis (6,7,8,11), possibly due to the young age of the subjects.

However, these same SJIA-LD-associated chemokines are also induced during type 2 immune responses (46). Accumulating epidemiologic, clinical, and HLA findings in PAP variant SJIA-LD suggest a causal drug hypersensitivity reaction (7–9). Of the HLA-typed

subjects in this study, 87% carried the HLA-DRB1*15 allele (Supplementary Table 1). In particular, CCL11 and CCL17 elevations have been observed in drug hypersensitivity reactions (47). However, these chemokine results are preliminary, and elevations of these chemokines are observed in other lung diseases (35–38). Thus, these serum chemokine elevations could be consistent with both wound-healing responses in the lung and hypersensitivity reactions. This distinction is critical and further prospective studies are essential.

This exploratory study has several limitations. First, though the largest to date, our limited SJIA-LD sample size may not reflect the between-patient heterogeneity or capture the temporal spectrum of this syndrome. Secondly, because all systemic JIA/MAS/SJIA-LD patients were being treated at sampling (sometimes with 2 or more agents), we cannot exclude confounding by disease activity and treatment. However, we previously observed little treatment variation between SJIA-LD and systemic JIA without LD of comparable disease severity (8), suggesting small between-group differences in treatment. Nonetheless, clinical/treatment heterogeneity could contribute to biomarker heterogeneity, such as the variability we observed in levels of CXCL9 and CXCL10, 2 chemokines rapidly responsive to treatment (48), in the MAS group (Figure 3D and Figure 5B). However, recent population biomarker studies highlight the practical value of validated findings in clinically heterogeneous cohorts, leading to successful translation into point-of-care diagnostics (49,50).

Overall, we have leveraged a novel, high-dimensional proteomics platform to identify serum proteins relevant to systemic JIA, MAS, and the life-threatening development of lung immunopathology, and we have used complementary techniques to localize and validate the results. Unbiased analyses reinforced the primacy of known biomarkers for systemic JIA and MAS and highlighted novel markers and pathways. Analysis of SJIA-LD revealed features of smoldering MAS in many, but also a distinct serum proteome with features of lung-specific inflammation, damage repair, and/or hypersensitivity responses. Further, we identified a biomarker (ICAM-5) that may be useful as a first-line screening or monitoring tool for lung disease in children for whom functional or radiologic testing may be impractical or high-risk. A positive result may help identify patients in need of further pulmonary testing. Prospective, longitudinal studies of biomarkers like ICAM-5 in patients with systemic JIA are warranted to directly test their diagnostic and/or prognostic value. Finally, our data can serve as a resource to investigators, clinicians, and families grappling with the management of systemic JIA, MAS, and SJIA-LD.

ACKNOWLEDGMENTS

We are grateful for the assistance of Angelique Biancotto, Katie Stagliano, and Jessica Mann at the NIH Center for Human Immunology. We also thank Bhupinder Nahal and the Division of Pediatric Rheumatology at the University of California San Francisco, led by Dr. Emily von Scheven, as well as Dr. Sergio Vargas of the Program in Microbiology, Instituto de Ciencias Biomédicas, Universidad de Chile, for collection of several serum samples and associated clinical data.

AUTHOR CONTRIBUTIONS

All authors were involved in drafting the article or revising it critically for important intellectual content, and all authors approved the final version to be published. Dr. Canna had full access to all of the data in the study and takes responsibility for the integrity of the data and the accuracy of the data analysis.

Study conception and design. Mellins, Canna.

Acquisition of data. Deutsch, Schulert, Trapnell, Lee, Macaubas, Schneider, Saper, de Jesus, Grom, Goldbach-Mansky, Mellins, Canna.




Analysis and interpretation of data. Chen, Zheng, Jang, Ho, Krasnow, Khatri, Mellins, Canna.

REFERENCES

- Gurion R, Lehman TJ, Moorthy LN. Systemic arthritis in children: a review of clinical presentation and treatment. *Int J Inflam* 2012;2012: 271569.
- Gerfaud-Valentin M, Cottin V, Jamilloux Y, Hot A, Gaillard-Coadon A, Durieu I, et al. Parenchymal lung involvement in adult-onset Still disease: a STROBE-compliant case series and literature review. *Medicine* 2016;95:e4258.
- Schulert GS, Grom AA. Pathogenesis of macrophage activation syndrome and potential for cytokine-directed therapies. *Annu Rev Med* 2015;66:145–59.
- Behrens EM, Beukelman T, Paessler M, Cron RQ. Occult macrophage activation syndrome in patients with systemic juvenile idiopathic arthritis. *J Rheumatol* 2007;34:1133.
- García-Peña P, Boixadera H, Barber I, Toran N, Lucaya J, Enríquez G. Thoracic findings of systemic diseases at high-resolution CT in children. *Radiographics* 2011;31:465–82.
- Schulert GS, Yasin S, Carey B, Chalk C, Do T, Schapiro AH, et al. Systemic juvenile idiopathic arthritis-associated lung disease: characterization and risk factors. *Arthritis Rheumatol* 2019;71:1943–54.
- Kimura Y, Weiss JE, Haroldson KL, Lee T, Punaro M, Oliveira S, et al. Pulmonary hypertension and other potentially fatal pulmonary complications in systemic juvenile idiopathic arthritis. *Arthritis Care Res (Hoboken)* 2013;65:745–52.
- Saper VE, Chen G, Deutsch GH, Guillerman RP, Birgmeier J, Jagadeesh K, et al. Emergent high fatality lung disease in systemic juvenile arthritis. *Ann Rheum Dis* 2019;78:1722.
- Saper VE, Ombrello MJ, Tremoulet AH, Montero-Martin G, Prahalad S, Canna S, et al. Severe delayed hypersensitivity reactions to IL-1 and IL-6 inhibitors link to common HLA-DRB1*15 alleles. *Ann Rheum Dis* 2021;81:406–15.
- Minoia F, Davi S, Horne A, Demirkaya E, Bovis F, Li C, et al. Clinical features, treatment, and outcome of macrophage activation syndrome complicating systemic juvenile idiopathic arthritis: a multinational, multicenter study of 362 patients. *Arthritis Rheumatol* 2014; 66:3160–9.
- De Jesus AA, Hou Y, Brooks S, Malle L, Biancotto A, Huang Y, et al. Distinct interferon signatures and cytokine patterns define additional systemic autoinflammatory diseases. *J Clin Invest* 2020;130:1669–82.
- Hensley P. SOMAmers and SOMAscan: a protein biomarker discovery platform for rapid analysis of sample collections from bench top to the clinic. *J Biomol Tech* 2013;24 Suppl:S5.
- Yang S, Kim J, Ryu JH, Oh H, Chun CH, Kim BJ, et al. Hypoxia-inducible factor-2 α is a catabolic regulator of osteoarthritic cartilage destruction. *Nat Med* 2010;16:687–93.
- Macaubas C, Nguyen KD, Peck A, Buckingham J, Deshpande C, Wong E, et al. Alternative activation in systemic juvenile idiopathic arthritis monocytes. *Clin Immunol* 2012;142:362–72.

15. Sangiuliano B, Perez NM, Moreira DF, Belizario JE. Cell death-associated molecular-pattern molecules: inflammatory signaling and control. *Mediators Inflamm* 2014;2014:821043.
16. Rose CE Jr, Sung SS, Fu SM. Significant involvement of CCL2 (MCP-1) in inflammatory disorders of the lung. *Microcirculation* 2003;10:273–88.
17. Yang H. Structure, expression, and function of ICAM-5. *Comp Funct Genomics* 2012;2012:368938.
18. GTEx Consortium. Human Genomics. The Genotype–Tissue Expression (GTEx) pilot analysis: multitissue gene regulation in humans. *Science* 2015;348:648.
19. Conant K, Wang Y, Szklarczyk A, Dudak A, Mattson MP, Lim ST. Matrix metalloproteinase-dependent shedding of intercellular adhesion molecule-5 occurs with long-term potentiation. *Neuroscience* 2010;166:508–21.
20. Shimizu M, Yokoyama T, Yamada K, Kaneda H, Wada H, Wada T, et al. Distinct cytokine profiles of systemic-onset juvenile idiopathic arthritis-associated macrophage activation syndrome with particular emphasis on the role of interleukin-18 in its pathogenesis. *Rheumatology (Oxford)* 2010;49:1645–53.
21. Weiss ES, Girard-Guyonvarc'h C, Holzinger D, de Jesus AA, Tariq Z, Picarsic J, et al. Interleukin-18 diagnostically distinguishes and pathogenically promotes human and murine macrophage activation syndrome. *Blood* 2018;131:1442–55.
22. Dickhout JG, Lhoták Š, Hilditch BA, Basseri S, Colgan SM, Lynn EG, et al. Induction of the unfolded protein response after monocyte to macrophage differentiation augments cell survival in early atherosclerotic lesions. *FASEB J* 2011;25:576–89.
23. Pockley AG, Henderson B. Extracellular cell stress (heat shock) proteins-immune responses and disease: an overview. *Philos Trans R Soc Lond B Biol Sci* 2018;373:20160522.
24. Lancaster GI, Febbraio MA. Exosome-dependent trafficking of HSP70: a novel secretory pathway for cellular stress proteins. *J Biol Chem* 2005;280:23349–55.
25. Takaoka Y, Goto S, Nakano T, Tseng HP, Yang SM, Kawamoto S, et al. Glyceraldehyde-3-phosphate dehydrogenase (GAPDH) prevents lipopolysaccharide (LPS)-induced, sepsis-related severe acute lung injury in mice. *Sci Rep* 2014;4:5204.
26. Chang CH, Curtis JD, Maggi LB Jr, Faubert B, Villarino AV, O'Sullivan D, et al. Posttranscriptional control of T cell effector function by aerobic glycolysis. *Cell* 2013;153:1239–51.
27. Kornberg MD, Bhargava P, Kim PM, Putluri V, Snowman AM, Putluri N, et al. Dimethyl fumarate targets GAPDH and aerobic glycolysis to modulate immunity. *Science* 2018;360:449–53.
28. Wang A, Pope SD, Weinstein JS, Yu S, Zhang C, Booth CJ, et al. Specific sequences of infectious challenge lead to secondary hemophagocytic lymphohistiocytosis-like disease in mice. *Proc Natl Acad Sci U S A* 2019;116:2200–9.
29. Yasin S, Solomon K, Canna SW, Girard-Guyonvarc'h C, Gabay C, Schiffrin E, et al. IL-18 as therapeutic target in a patient with resistant systemic juvenile idiopathic arthritis and recurrent macrophage activation syndrome. *Rheumatology (Oxford)* 2020;59:442–5.
30. Tzouveleki A, Kouliatsis G, Anevlavis S, Bouros D. Serum biomarkers in interstitial lung diseases. *Respir Res* 2005;6:78.
31. Bonella F, Ohshimo S, Miaotian C, Griese M, Guzman J, Costabel U. Serum KL-6 is a predictor of outcome in pulmonary alveolar proteinosis. *Orphanet J Rare Dis* 2013;8:53.
32. Oguz EO, Kucuksahin O, Turgay M, Yildizgoren MT, Ates A, Demir N, et al. Association of serum KL-6 levels with interstitial lung disease in patients with connective tissue disease: a cross-sectional study. *Clin Rheumatol* 2016;35:663–6.
33. Ishikawa N, Hattori N, Yokoyama A, Kohno N. Utility of KL-6/MUC1 in the clinical management of interstitial lung diseases. *Respir Investig* 2012;50:3–13.
34. Lee JS, Lee EY, Ha YJ, Kang EH, Lee YJ, Song YW. Serum KL-6 levels reflect the severity of interstitial lung disease associated with connective tissue disease. *Arthritis Res Ther* 2019;21:58.
35. O'Dwyer DN, Norman KC, Xia M, Huang Y, Gurczynski SJ, Ashley SL, et al. The peripheral blood proteome signature of idiopathic pulmonary fibrosis is distinct from normal and is associated with novel immunological processes. *Sci Rep* 2017;7:46560.
36. Todd JL, Neely ML, Overton R, Durham K, Gulati M, Huang H, et al. Peripheral blood proteomic profiling of idiopathic pulmonary fibrosis biomarkers in the multicentre IPF-PRO Registry. *Respir Res* 2019;20:227.
37. Wu X, De Frias SP, Taheri S, Hoffman K, Easthausen I, Esposito AJ, et al. Differential protein expression in rheumatoid arthritis interstitial lung disease. *Am J Respir Crit Care Med* 2020;201:A 7796.
38. Deterding RR, Wagner BD, Harris JK, DeBoer EM. Pulmonary aptamer signatures in children's interstitial and diffuse lung disease. *Am J Respir Crit Care Med* 2019;200:1496–504.
39. Travaglini KJ, Nabhan AN, Penland L, Sinha R, Gillich A, Sit RV, et al. A molecular cell atlas of the human lung from single-cell RNA sequencing. *Nature* 2020;587:619–25.
40. Kennedy B, Branagan P, Moloney F, Haroon M, O'Connell OJ, O'Connor TM, et al. Biomarkers to identify ILD and predict lung function decline in scleroderma lung disease or idiopathic pulmonary fibrosis. *Sarcoidosis Vasc Diffuse Lung Dis* 2015;32:228–36.
41. Zimmers TA, Jin X, Hsiao EC, McGrath SA, Esqueda AF, Koniaris LG. Growth differentiation factor-15/macrophage inhibitory cytokine-1 induction after kidney and lung injury. *Shock* 2005;23:543–8.
42. Katzen J, Wagner BD, Venosa A, Kopp M, Tomer Y, Russo SJ, et al. An SFTPC BRICHOS mutant links epithelial ER stress and spontaneous lung fibrosis. *JCI Insight* 2019;4:e126125.
43. Wynn TA. Fibrotic disease and the T (H)1/T (H)2 paradigm. *Nat Rev Immunol* 2004;4:583–94.
44. Puxeddu I, Bader R, Piliiponsky AM, Reich R, Levi-Schaffer F, Berkman N. The CC chemokine eotaxin/CCL11 has a selective profibrogenic effect on human lung fibroblasts. *J Allergy Clin Immunol* 2006;117:103–10.
45. Kass DJ, Nouriaie M, Glassberg MK, Ramreddy N, Fernandez K, Harlow L, et al. Comparative profiling of serum protein biomarkers in rheumatoid arthritis-associated interstitial lung disease and idiopathic pulmonary fibrosis. *Arthritis Rheumatol* 2020;72:409–19.
46. Pease JE, Williams TJ. Chemokines and their receptors in allergic disease. *J Allergy Clin Immunol* 2006;118:305–18.
47. Musette P, Janela B. New insights into drug reaction with eosinophilia and systemic symptoms pathophysiology. *Front Med* 2017;4:179.
48. Lounder DT, Bin Q, de Min C, Jordan MB. Treatment of refractory hemophagocytic lymphohistiocytosis with emapalumab despite severe concurrent infections. *Blood Adv* 2019;3:47–50.
49. Sutherland JS, van der Spuy G, Gindeh A, Thuong NT, Namuganga AR, Owolabi O, et al. Diagnostic accuracy of the Cepheid 3-gene host response fingerstick blood test in a prospective, multi-site study: interim results. *Clin Infect Dis* 2021;22:ciab839.
50. Sweeney TE, Braviak L, Tato CM, Khatri P. Genome-wide expression for diagnosis of pulmonary tuberculosis: a multicohort analysis. *Lancet Respir Med* 2016;4:213–24.
51. DeWitt EM, Kimura Y, Beukelman T, Nigrovic PA, Onel K, Prahalad S, et al. Consensus treatment plans for new-onset systemic juvenile idiopathic arthritis. *Arthritis Care Res (Hoboken)* 2012;64:1001–10.

Brain Structural Changes During Juvenile Fibromyalgia: Relationships With Pain, Fatigue, and Functional Disability

Maria Suñol,¹  Michael F. Payne,² Han Tong,³ Thomas C. Maloney,⁴ Tracy V. Ting,³ Susmita Kashikar-Zuck,³ 
Robert C. Coghill,³ and Marina López-Solà¹ 

Objective. Juvenile fibromyalgia (FM) is a prevalent chronic pain condition affecting children and adolescents worldwide during a critical period of brain development. To date, no published studies have addressed the pathophysiology of juvenile FM. This study was undertaken to characterize gray matter volume (GMV) alterations in juvenile FM patients for the first time, and to investigate their functional and clinical relevance.

Methods. Thirty-four female adolescents with juvenile FM and 38 healthy adolescents underwent a structural magnetic resonance imaging examination and completed questionnaires assessing core juvenile FM symptoms. Using voxel-based morphometry, we assessed between-group GMV differences and associations between GMV and functional disability, fatigue, and pain interference in juvenile FM. We also studied whether validated brain patterns predicting pain, cognitive control, or negative emotion were amplified/attenuated in juvenile FM patients and whether structural alterations reported in adult FM were replicated in adolescents with juvenile FM.

Results. Compared to controls, juvenile FM patients showed GMV reductions in the anterior midcingulate cortex (aMCC) region (family-wise error corrected P [$P_{FWE-corr}$] = 0.04; estimated with threshold-free cluster enhancement [TFCE]; $n = 72$) associated with pain. Within the juvenile FM group, patients reporting higher functional disability had larger GMV in inferior frontal regions ($P_{FWE-corr} = 0.006$; TFCE estimated; $n = 34$) linked to affective, self-referential, and language-related processes. Last, GMV reductions in juvenile FM showed partial overlap with findings in adult FM, specifically for the anterior/posterior cingulate cortices ($P = 0.02$ and $P = 0.03$, respectively; $n = 72$).

Conclusion. Pain-related aMCC reductions may be a structural hallmark of juvenile FM, whereas alterations in regions involved in emotional, self-referential, and language-related processes may predict disease impact on patients' well-being. The partial overlap between juvenile and adult FM findings strengthens the importance of early symptom identification and intervention to prevent the transition to adult forms of the disease.

INTRODUCTION

Juvenile fibromyalgia (FM) affects 2–6% of children and adolescents, mostly females, and is characterized by widespread musculoskeletal pain and other debilitating symptoms, such as functional disability and fatigue. Juvenile FM symptoms often persist into adulthood, highlighting the importance of early recognition and intervention (1,2). Research has provided insight into the clinical characteristics of juvenile FM (2,3), but there is a research gap regarding disease pathophysiology. A recent review provided the first robust evidence of central hyperexcitability in

children with chronic pain and preliminarily suggested altered cortical nociceptive processing (4). Additionally, a functional magnetic resonance imaging (fMRI) study showed that adolescents with idiopathic pain had decreased activation in the thalamus and precentral and middle frontal gyri during pain processing (5).

Conversely, neuroimaging research in adult FM has flourished over the past 2 decades, suggesting that chronic pain symptoms are associated with brain alterations involving multiple circuits and functional domains (6–11). At the structural level, meta-analyses in adult FM have consistently found gray matter volume (GMV) reductions in regions involved in affective and

Supported by the National Institute of Arthritis and Musculoskeletal and Skin Diseases, NIH (grants R01-AR-074795 and P30-AR-076316). Dr. Lopez-Sola's work was supported by the Serra Hunter Programme of the Generalitat de Catalunya.

¹Maria Suñol, PhD, Marina López-Solà, PhD: University of Barcelona, Barcelona, Spain; ²Michael F. Payne, MA: Cincinnati Children's Hospital Medical Center, Cincinnati, Ohio; ³Han Tong, MBBS, MSc, Tracy V. Ting, MD, MSc, Susmita Kashikar-Zuck, PhD, Robert C. Coghill, PhD: Cincinnati Children's Hospital Medical Center and University of Cincinnati, Cincinnati, Ohio; ⁴Thomas C. Maloney, MSc: University of Cincinnati, Cincinnati, Ohio.

Author disclosures are available at <https://onlinelibrary.wiley.com/action/downloadSupplement?doi=10.1002%2Fart.42073&file=art42073-sup-0001-Disclosureform.pdf>.

Address correspondence to Maria Suñol, PhD, or Marina López-Solà, PhD, Department of Medicine, School of Medicine and Health Sciences, University of Barcelona, Casanova, 143, Ala Nord, 5a planta, Barcelona 08036, Spain. Email: msunol@ub.edu or mlopezsola@ub.edu.

Submitted for publication August 5, 2021; accepted in revised form January 21, 2022.

cognitive dimensions of pain, such as the anterior midcingulate cortex (aMCC), the medial prefrontal cortex (mPFC), and the default mode network (6,7). Such reductions have been in part correlated with age, leading researchers to suggest that atrophy in older patients with FM may result from long-term exposure to nociceptive input (7,12,13). The opposite was hypothesized for younger patients, for whom recurrent overengagement of pain modulatory circuits could result in hypertrophy earlier in the disease course followed by atrophy later in life (12,13). Importantly, GMV loss in adult FM has been identified beyond pain-processing regions in brain circuits involved in self-referential processing, executive function, and emotion regulation (14), highlighting the importance of studying whole-brain structural alterations. Moreover, studies have shown a strong correspondence between structural and functional brain abnormalities, specifically in cingulate and dorsal mPFC regions (15,16). Therefore, studies combining structural findings with functional meta-analytic decoding, or validated brain patterns predicting relevant functional domains, may help identify a link between structural abnormalities and their functional relevance in patients with chronic pain.

Pathophysiologic findings at an early disease stage could inform interventions that may more effectively target the multidimensional symptom constellation in juvenile FM. Along these lines, fMRI research in adult FM has linked pain catastrophizing with increased primary somatosensory cortex–anterior insula functional connectivity, which normalized after cognitive behavioral therapy (17). Likewise, it has shown that alterations in the descending pain inhibition pathway improved with regular exercise (18). Therefore, we hypothesize that, if replicated in youth with juvenile FM, such alterations could be modulated with similar treatment strategies as in adults. New insights regarding whether distinct pathophysiologic findings predict different treatment response trajectories may help tailor first treatment actions and most appropriate treatment combinations in a personalized manner. Such knowledge might also contribute to the development of new psychobiologically informed treatments, which could potentially alter the trajectory of juvenile FM symptoms and foster a healthier transition into adulthood (19).

In this study, we investigated GMV abnormalities in adolescent girls with juvenile FM and associations with disease-related functional interference. We combined voxel-based morphometry and functional meta-analytic decoding of structural data to provide insight into potential functional roles of structural alterations in juvenile FM. Based on findings in adult FM (6,7), we hypothesized that 1) compared to healthy adolescents, juvenile FM patients would show alterations in the cingulate and medial prefrontal cortices and the parahippocampal gyrus, and 2) within the juvenile FM group, individual differences in functional disability, fatigue, and pain interference would be associated with structural abnormalities in circuits involved in emotional processing and cognitive modulation of pain and emotion (anterior insula, prefrontal cortices, limbic, and striatal regions) (20,21). We also investigated whether 3 validated brain patterns involving

medial prefrontal regions and predicting pain, cognitive control, or negative emotion (22) were amplified or attenuated in juvenile FM. Given that amplified pain is a core juvenile FM symptom, we anticipated between-group differences specifically for the pain-predictive pattern. Finally, we tested whether structural alterations reported in adult FM were replicated in adolescents with juvenile FM to potentially identify a link between structural abnormalities in juvenile and adult forms of the disease.

PATIENTS AND METHODS

Participants. This study included 34 adolescent girls diagnosed as having juvenile FM (mean \pm SD age 16.37 ± 1.07 years [range 13–18 years]) and 38 healthy adolescent girls (mean \pm SD age 15.89 ± 1.32 years [range 13–18 years]). The sample size was decided assuming similar power as previous studies that assessed structural differences between adults with FM and healthy controls using voxel-based morphometry (studies included in meta-analyses [6,7]). We enrolled female participants exclusively because most chronic pain conditions occurring in adolescence predominantly affect girls (23) and because boys with juvenile FM are sufficiently rare as to raise questions about the potential for a distinct mechanism (24). Inclusion and exclusion criteria are detailed in the Supplementary Methods, available on the *Arthritis & Rheumatology* website at <http://onlinelibrary.wiley.com/doi/10.1002/art.42073>. Participants provided informed assent, and their parents or legal guardians provided written informed consent. The study protocol and consent forms were approved by the Institutional Review Board of the Cincinnati Children's Hospital Medical Center (study ID: 2017-7771) in compliance with the Declaration of Helsinki.

Clinical measures. Developmentally appropriate and validated self-report measures were used to assess disability, fatigue, and pain interference. Participants self-reported their functional disability (physical difficulty experienced when doing their daily activities) using the 15-item Functional Disability Inventory (FDI) (25) and their fatigue symptoms over the past week using the 10-item Patient-Reported Outcomes Measurement Information System (PROMIS) Pediatric Fatigue-Short Form (26). Additionally, juvenile FM patients completed the Brief Pain Inventory (BPI) (27), from which we extracted mean pain intensity and pain interference scores. Healthy adolescents did not complete the BPI because they were selected based on having no pain.

Imaging data acquisition. MRI data acquisition is detailed in the Supplementary Methods, available on the *Arthritis & Rheumatology* website at <http://onlinelibrary.wiley.com/doi/10.1002/art.42073>.

Data analysis. Statistical analyses of demographic and clinical variables. Differences between juvenile FM patients and

healthy adolescents with regard to sociodemographic and clinical variables were analyzed by chi-square and 2-sample *t*-tests, using SPSS software version 26 (IBM).

Voxel-based morphometry protocol. Voxel-based morphometry quantifies gray matter at a voxelwise, whole-brain level (28), allowing for a comprehensive measurement of gray matter throughout the brain. In this study, structural data were preprocessed using MatLab-R2021a (MathWorks) and SPM12 (UCL). First, a trained researcher (MS) reviewed all images to ensure they were free from acquisition artifacts and magnetic field inhomogeneities. Then, images were preprocessed using a standard pipeline combining voxel-based morphometry with Diffeomorphic Anatomical Registration Through Exponentiated Lie Algebra algorithm (DARTEL) (29) and including 4 main steps: tissue segmentation, normalization, modulation, and Gaussian smoothing. After segmentation, the resulting rigidly transformed versions of gray matter were normalized using DARTEL. Specifically, images were iteratively matched to a template generated from their own mean to generate a series of templates with increasing resolution. Native space gray matter images were then registered to the highest resolution template within a high-dimensional diffeomorphic framework. Since the DARTEL method creates a study-specific template and then spatially normalizes individual images to this template, it provides better registration, specifically in the boundaries of gray and white matter, than previous voxel-based morphometry methods (29).

Spatially normalized tissue maps were modulated by the Jacobian determinants from the corresponding flow fields to restore the volumetric information lost during the high-dimensional spatial registration. This modulation step multiplies each voxel by the relative change in volume, which allows for a comparison of absolute GMV corrected for individual brain size (30). Only normalized and modulated images were transformed to a standard Montreal Neurological Institute (MNI) template and resliced to 1.5 mm. Therefore, volume computations were not affected by this final transformation to MNI space. Similarly, multiple neuroimaging studies have used this template in adolescents (for example, ref. 31). Moreover, using a standard MNI template enables us to compare our findings with the results of previous studies that used this template (for example, ref. 12). Finally, images were smoothed with an 8-mm full-width at half-maximum isotropic Gaussian kernel. A trained researcher (MS) reviewed all processed images to ensure image quality.

Statistical analyses of brain structural data. To assess regional GMV differences between juvenile FM patients and controls, we estimated a *t*-test model with SPM12. As a standard procedure in voxel-based morphometry analyses (32), we added age and total GMV as nuisance variables, and excluded all voxels with a gray matter value of <0.2 (maximum value 1).

To test associations between regional GMV and clinical variables in juvenile FM patients, we performed multiple regression

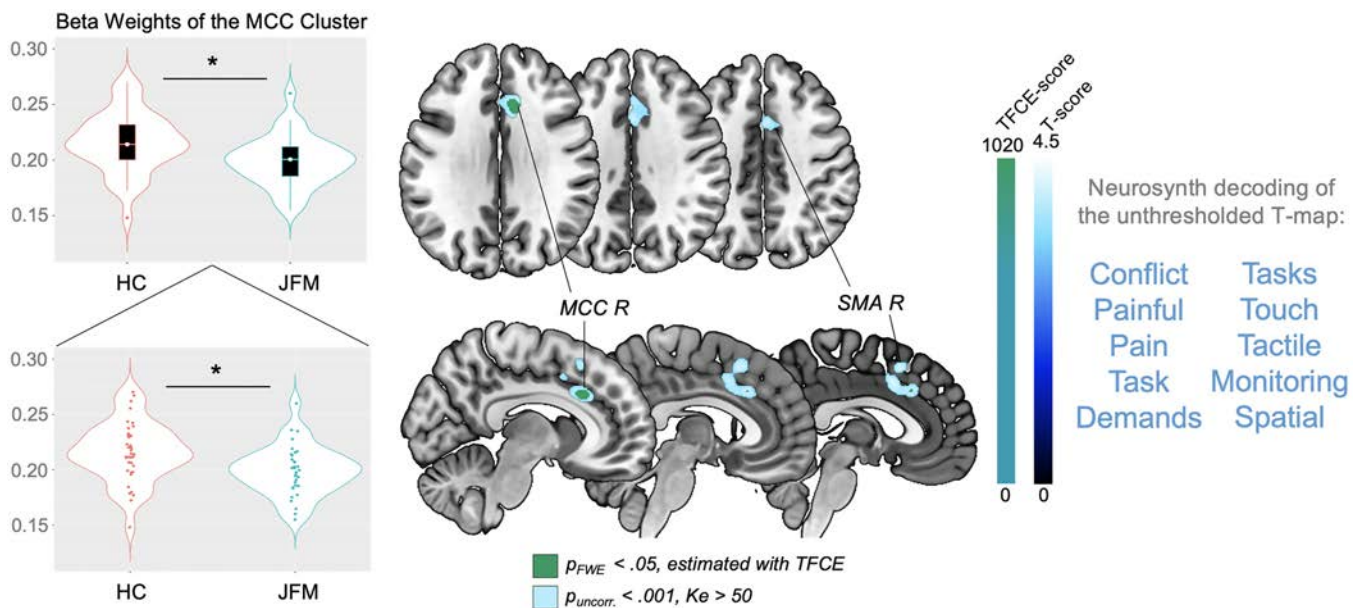


Figure 1. Regions of significantly reduced gray matter volume (GMV) in adolescents with juvenile fibromyalgia (JFM) compared to healthy controls (HCs). Left, Violin plots of the beta weights of the anterior midcingulate cortex (aMCC) cluster in healthy controls and patients with juvenile FM. In the top panel, each box represents the 25th to 75th percentiles. Lines inside the boxes represent the median. Lines outside the boxes represent the 10th and 90th percentiles. Circles indicate outliers. In the bottom panel, circles indicate individual subjects. * = $P < 0.01$. Middle, Brain maps showing significant between-group GMV differences (contrast: juvenile FM patients < healthy controls). Results are presented at a significance level of family-wise error corrected P ($P_{FWE-corr}$) < 0.05, estimated using the threshold-free cluster enhancement (TFCE) approach, and uncorrected P (P_{uncorr}) < 0.001 with a cluster extent (K_e) > 50 voxels. Right, The 10 functional annotations most associated with the unthresholded t-map, obtained by meta-analytic decoding using Neurosynth. R = right; SMA = supplementary motor area.

models in SPM12 with the following independent variables of interest in each separate model: 1) functional disability score from the FDI, 2) fatigue symptoms, measured with the PROMIS form, and 3) pain interference score from the BPI. Each model included age and total GMV as nuisance covariates and GMV as the dependent variable. We excluded voxels with a gray matter value of <0.2.

To correct for multiple comparisons, we performed, for each analysis, a voxelwise nonparametric permutation test with 5,000 random permutations using the threshold-free cluster enhancement (TFCE) approach (33) implemented in the SPM-TFCEr214 toolbox (dbm.neuro.uni-jena.de/tfce), and the whole-

brain significance threshold was set at a family-wise error corrected P value ($P_{FWE-corr}$) of less than 0.05. The TFCE approach was introduced to increase the sensitivity of voxel-based analysis (33) and is currently recommended and widely used in voxel-based morphometry studies (34). Compared to voxelwise or clusterwise inferences, TFCE inference improves power and validity and relies on minimal assumptions about data distribution (33). For completion, imaging results were also explored at an uncorrected threshold of $P < 0.001$ and a cluster extent (Ke) >50 voxels.

Neurosynth meta-analytic decoding. To interpret the functional role of structural regions differing in GMV between juvenile

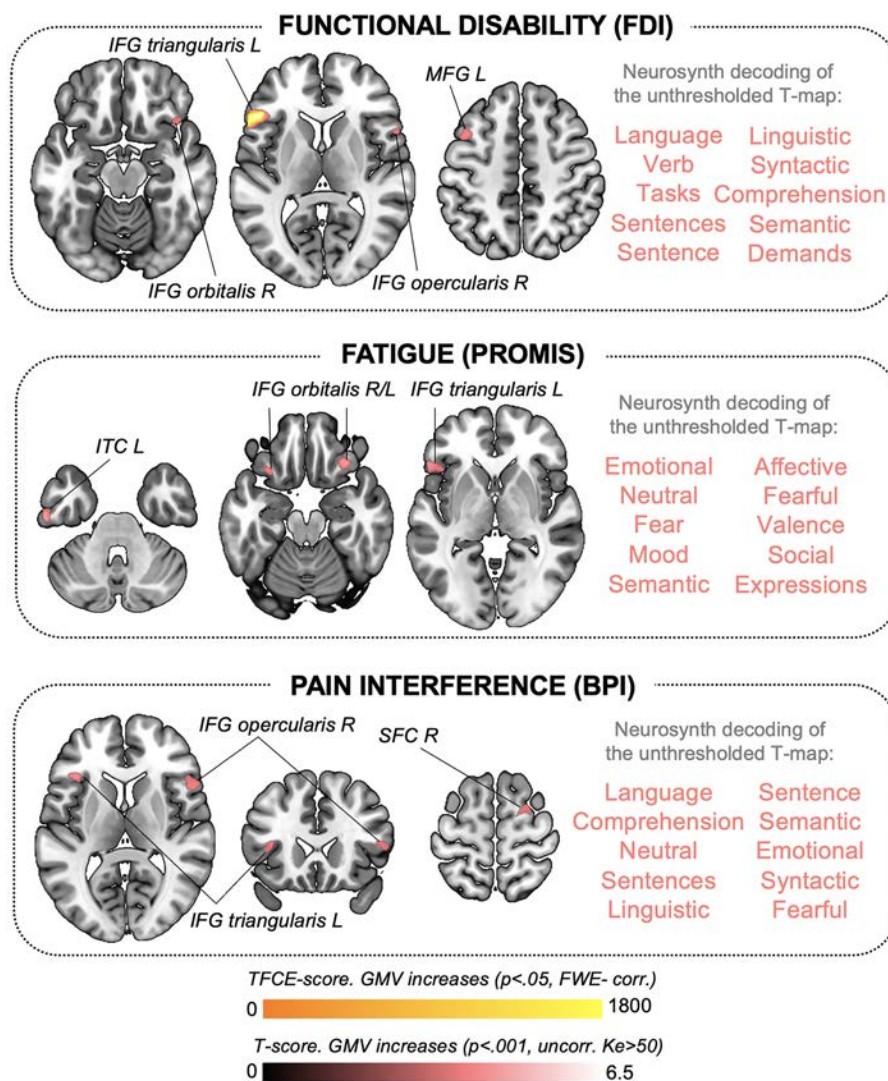


Figure 2. GMV changes associated with clinical symptoms in adolescents with juvenile FM. Brain maps show significant correlations between GMV and clinical symptoms reflecting disease-related functional interference in adolescents with juvenile FM, including functional disability as measured by the Functional Disability Inventory (FDI), fatigue as measured by Patient-Reported Outcomes Measurement Information System (PROMIS), and pain interference as measured by the Brief Pain Inventory (BPI). Results are presented at a significance level of $P_{FWE-corr} < 0.05$ (GMV increases shown in yellow) and $P_{uncorr} < 0.001$ with $Ke > 50$ voxels (GMV increases shown in red). We did not observe negative correlations at the $P_{FWE-corr}$ or P_{uncorr} level. The 10 functional annotations most associated with the corresponding unthresholded t-map, obtained by meta-analytic decoding using Neurosynth, are shown to the right of each brain map. L = left; IFG = inferior frontal gyrus; MFG = middle frontal gyrus; ITC = inferior temporal cortex; SFC = superior frontal cortex (see Figure 1 for other definitions).

FM patients and controls, or associated with clinical symptoms in the juvenile FM group, we performed meta-analytic decoding using the Neurosynth database (35) (neurosynth.org). This meta-analytic strategy leverages the power of large data sets to compute whole-brain distributions for psychological terms. Thus, it allows performing unbiased reverse-inferences to identify terms consistently associated with a particular brain coordinate across neuroimaging studies (35). We uploaded the unthresholded t-maps produced in our study onto the Neurosynth database and decoded them, which returned psychological and anatomic terms associated with the spatial pattern of each analysis (Supplementary Table 1, available on the *Arthritis & Rheumatology* website at <http://onlinelibrary.wiley.com/doi/10.1002/art.42073>, shows a list of the 50 Neurosynth terms most correlated with each t-map and their Pearson's correlation coefficients.) For interpretation purposes, we selected the 10 psychological terms (i.e., referring to psychological functions) most correlated with each map and displayed them in Figures 1 and 2 (36).

Evaluation of patterns predicting pain, cognitive control, and negative emotion in juvenile FM. Our voxel-based morphometry analysis showed that juvenile FM patients had reduced GMV in the right aMCC. To study the functional organization of the medial frontal cortex (MFC) surrounding this region, we tested whether the similarity between our structural maps and previously validated brain patterns predicting either pain, cognitive control, or negative emotion across 18 studies and specifically involving the aMCC–dorsal MFC (22) differed between juvenile FM patients and healthy adolescents. The maps developed by Kragel et al (22) corresponding to the partial least squares regression coefficients for the different functional domains being predicted are available at the Canlab repository (github.com/canlab/Neuroimaging_Pattern_Masks/tree/master/Multivariate_signature_patterns/2018_Kragel_MFC_Generalizability). We extracted the weighted maps corresponding to pain, cognitive control, and negative emotion in the dorsomedial aspect of the frontal cortex including anterior and posterior MCC and dorsal

Table 1. Demographic and clinical characteristics of the patients with juvenile FM and healthy controls*

	Controls (n = 38)	Patients with juvenile FM (n = 34)	t/LRV
Demographic characteristic			
Age, years	15.89 ± 1.32	16.37 ± 1.07	-1.67
Race, no. Caucasian/non-Caucasian	35/3	32/2	0.11†
Annual household income (scale 1–6)‡	5.13 ± 2.07	5.09 ± 2.02	0.09
Education level of caregiver 1 (scale 1–5)§	3.97 ± 0.88	3.88 ± 0.91	0.43
Education level of caregiver 2 (scale 1–5)§	3.74 ± 0.78	3.63 ± 0.98	0.55
Brain			
Total GMV volume	787.70 ± 59.87	785.50 ± 53.17	0.16
Total WMV	384.27 ± 40.42	399.49 ± 36.89	-1.66
Clinical variables			
Functional disability (FDI)	0.5 ± 1.25	22.74 ± 9.26	-13.89¶
Fatigue (PROMIS)	14.28 ± 6.64	35.23 ± 6.87	-12.30¶
Pain interference (BPI)	-	4.29 ± 1.55	-
Average pain intensity	-	5.43 ± 1.42	-
Medication, no. (%)			
Pain-related drugs#	-	12 (35.29)	-
Psychiatric drugs**	-	15 (44.12)	-
Gastrointestinal drugs††	-	7 (20.59)	-
Melatonin	-	3 (8.82)	-
Antihistamines	-	3 (8.82)	-
Vitamins/iron supplements	-	3 (8.82)	-
Birth control	2 (5.26)	2 (5.88)	-
Hypertension treatment	1 (2.63)	-	-
Statins	1 (2.63)	-	-

* Except where indicated otherwise, values are the mean ± SD. FM = fibromyalgia; GMV = gray matter volume; WMV = white matter volume; FDI = Functional Disability Inventory; PROMIS = Patient-Reported Outcomes Measurement Information System; BPI = Brief Pain Inventory.

† Likelihood ratio value (LRV).

‡ Annual household income is shown using a scale of 1–6, where 1 = <\$24,999; 2 = \$25,000 to \$49,999; 3 = \$50,000 to \$74,999; 4 = \$75,000 to \$99,000; 5 = \$100,000 to \$124,999; and 6 = >\$125,000.

§ Caregiver education level is shown using a scale of 1–5, where 1 = less than high school; 2 = high school/GED; 3 = partial college or trade school; 4 = college graduate; 5 = postgraduate degree.

¶ Significant values ($P < 0.001$).

Pain-related drugs included antiepileptic drugs, nonsteroidal antiinflammatory drugs, muscle relaxants, acetaminophen, and/or acetylsalicylic acid.

** Psychiatric drugs included antidepressants, anxiolytics, and attention deficit hyperactivity disorder drugs.

†† Gastrointestinal drugs included antacids, antireflux drugs, and constipation drugs.

MFC. For each subject, we computed the dot product between our preprocessed structural images, regressed by age and total GMV, and pain, cognitive control, and negative emotion-weighted maps. Dot product was calculated using publicly available code at the Canlab repository ([canlab.github.io](https://github.com/canlab)) running on MatLab. We then ran 2-sample *t*-tests using SPSS to assess between-group differences in pattern similarity for each weighted map.

Evaluation of GMV differences in regions found altered in adults with FM. To identify potentially overlapping alterations between adult and juvenile forms of FM, we assessed GMV alterations in regions of interest (ROIs) identified based on previous meta-analytic evidence in adult FM patients. The selection and construction of ROIs is detailed in the Supplementary Methods, available on the *Arthritis & Rheumatology* website at <http://onlinelibrary.wiley.com/doi/10.1002/art.42073>. For each subject, we computed the mean parameter estimates (beta values representing GMV for each subject after removing age and total GMV effects) within each of the 6 final ROIs. Finally, we assessed between-group differences in mean parameter estimates for each ROI using 2-sample *t*-tests in SPSS.

RESULTS

Demographic and clinical variables. Adolescents with juvenile FM and healthy controls did not differ in terms of sex (all female), age, race, household income, or caregiver education level (all $P > 0.1$) (Table 1). As anticipated, juvenile FM patients reported significantly higher functional disability ($t = 13.89$, $P < 0.001$) and fatigue symptoms ($t = 12.30$, $P < 0.001$) (Table 1). Since controls were selected based on having no pain (numerical rating scales for pain of 0), mean pain intensity and pain interference were only assessed in juvenile FM participants (mean \pm SD intensity 5.43 ± 1.42 ; mean \pm SD interference 4.29 ± 1.55), indicating moderate intensity and mild-to-moderate interference. Medication details are presented in Table 1.

Whole-brain voxel-based morphometry analyses.
Reductions in GMV in juvenile FM. The groups did not differ in total GMV ($P = 0.87$). Compared to controls, juvenile FM patients had significantly less regional GMV in a cluster of the right aMCC ($P_{\text{FWE-corr}} = 0.04$; TFCE estimated). At the uncorrected threshold ($P < 0.001$; $K_e > 50$ voxels), this cluster extended to the left aMCC and bilateral supplementary motor area. Neurosynth meta-analytic decoding revealed that the unthresholded *t*-map for this contrast was related to, among others, the functional terms “pain,” “painful,” and “conflict” (Figure 1 and Table 2). However, correlations between the beta weights of the FWE-corrected aMCC cluster and clinical variables (functional disability, fatigue, pain interference, and pain intensity) did not reveal any significant association (all $P > 0.3$) (Supplementary Table 2, available on the *Arthritis & Rheumatology* website at <http://onlinelibrary.wiley.com/doi/10.1002/art.42073>), which suggests that, in our sample,

GMV reductions in this area do not track clinical severity but instead identify the category of juvenile FM patients as compared with healthy adolescents. Similarly, beta weights of the aMCC cluster did not correlate with symptom duration ($r = 0.078$; $P = 0.677$), which indicates that this alteration does not depend on how long patients have been experiencing juvenile FM symptoms.

Correlations between GMV and clinical juvenile FM symptoms. Functional disability correlated with increased GMV in the left inferior frontal gyrus (IFG) ($P_{\text{FWE-corr}} = 0.006$; TFCE estimated). At the uncorrected level ($P < 0.001$; $K_e > 50$ voxels), functional disability was linked to larger volumes in the bilateral IFG and the left middle frontal gyrus. Additionally, fatigue correlated with increased GMV in the bilateral IFG and the left inferior temporal cortex. Pain interference was associated with larger GMV in the left and right IFG and the right superior frontal cortex. These findings are detailed in Table 2. Figure 2 shows the anatomy of the findings and the associated meta-analytic terms based on Neurosynth decoding of each unthresholded, symptom-predicting *t*-map. Notably, *t*-maps reflecting GMV increases associated with functional disability, fatigue, and pain interference in juvenile FM patients were strongly linked to emotional and/or language production processes.

Importantly, the symptom-GMV associations described above remained significant after including symptom duration as an additional nuisance variable, along with age and total GMV, in the multiple regression models. Thus, these associations are independent of symptom duration. As a post hoc analysis, we built an additional model with symptom duration as a predictor variable, GMV as the dependent variable, and age and total GMV as nuisance covariates. We found no significant associations at the corrected level ($P_{\text{FWE-corr}} < 0.05$; TFCE estimated). At the uncorrected threshold ($P < 0.001$, $K_e > 50$ voxels), symptom duration correlated with GMV decreases in right-lateralized clusters in temporoparietal areas (Supplementary Table 3, available on the *Arthritis & Rheumatology* website at <http://onlinelibrary.wiley.com/doi/10.1002/art.42073>). According to Neurosynth decoding, the corresponding *t*-map was most associated with theory of mind and language-related processes (Supplementary Figure 1, available on the *Arthritis & Rheumatology* website at <http://onlinelibrary.wiley.com/doi/10.1002/art.42073>).

Reduced similarity between brain structure and a validated pain-predictive pattern involving the aMCC-dorsal MFC in juvenile FM. We tested whether validated brain patterns predicting either pain, cognitive control, or negative emotion, specifically in the aMCC-dorsal MFC region (22), differed between juvenile FM patients and controls. We found between-group differences only in the pain pattern, which is consistent with the location of GMV between-group differences and the fact that pain is a core complaint in juvenile FM. Specifically,

Table 2. Results of the whole-brain voxel-based morphometry analyses*

	Brain region	x, y, z†	T	Cluster size, voxels‡
Structural results at $P_{\text{FWE-corr}} < 0.05$, estimated with TFCE				
GMV differences between adolescents with juvenile FM and controls				
Contrast: juvenile FM < controls	aMCC R	9, 22, 30	1018.43§	113
Correlations between GMV and clinical symptoms in adolescents with juvenile FM				
Functional disability (FDI)				
↑GMV	IFG pars triangularis L	-54, 22, 4	1784.78§	340
Structural results at $P_{\text{uncorr}} < 0.001$, $K_e > 50$ voxels				
GMV differences between adolescents with juvenile FM and controls				
Contrast: juvenile FM < controls	aMCC R	9, 22, 30	4.14	983
Correlations between GMV and clinical symptoms in adolescents with juvenile FM				
Functional disability (FDI)				
↑GMV	IFG pars triangularis L	-54, 22, 4	6.47	805
↑GMV	IFG pars opercularis R	57, 14, 15	4.35	242
↑GMV	MFG L	-42, 12, 48	4.13	191
↑GMV	IFG pars orbitalis R	42, 21, -14	3.81	117
Fatigue (PROMIS)				
↑GMV	Inferior temporal cortex L	-60, -16, -33	5.03	115
↑GMV	IFG pars triangularis L	-54, 26, -3	4.83	317
↑GMV	IFG pars orbitalis R	32, 27, -21	4.63	366
↑GMV	IFG pars triangularis L	-50, 28, 9	4.54	82
↑GMV	IFG pars orbitalis L	-30, 21, -20	4.18	76
Pain interference (BPI)				
↑GMV	IFG pars triangularis L	-38, 26, 10	4.97	157
↑GMV	IFG pars opercularis R	52, 16, 12	4.21	264
↑GMV	Superior frontal cortex R	28, -3, 66	4.11	154

* $P_{\text{FWE-corr}}$ = family wise error rate-corrected P value; GMV = gray matter volume; FM = fibromyalgia; aMCC = anterior midcingulate cortex; R = right; FDI = Functional Disability Inventory; IFG = inferior frontal gyrus; L = left; P_{uncorr} = uncorrected P value; MFG = middle frontal gyrus; PROMIS = Patient-Reported Outcomes Measurement Information System; BPI = Brief Pain Inventory.

† Anatomic coordinates (x, y, z) are given in Montreal Neurological Institute space.

‡ Voxel size $1.5 \times 1.5 \times 1.5$ mm.

§ Threshold-free cluster enhancement (TFCE) values.

the dot product between structural data and the pain-weighted map was significantly lower in juvenile FM patients compared to controls within the aMCC-dorsal MFC mask ($t = 2.47$, $P = 0.016$) (Figure 3). Thus, the anatomic aMCC pattern resembled the functional pain pattern significantly less in juvenile FM patients than in controls. We found no differences for the patterns predicting cognitive control or negative emotion (all $P > 0.4$).

GMV differences between adolescents with juvenile FM and healthy adolescents within meta-analytic regions altered in adults with FM. Consistent with meta-analytic findings in adults (6,7), GMV reductions in 2 ROIs, located in the left anterior cingulate cortex (ACC) and the right posterior cingulate cortex (PCC), were replicated in adolescents with juvenile FM ($P = 0.02$ and $P = 0.03$, respectively) (Figure 4A). Neurosynth meta-analytic decoding showed that the left ACC ROI was associated with functional terms such as “pain,” “autobiographical,” and “mentalizing” (the ability to understand the mental state of oneself or others), whereas the right PCC ROI was associated with “suppressed,” “declines,” and “resting state.” The remaining ROIs extracted from the meta-analyses (6,7), located in the cerebellum,

the dorsal ACC, and the fusiform and parahippocampal gyri, did not show evidence of alteration in juvenile FM patients (all $P > 0.4$), as opposed to what has been reported in adults with FM (see Figure 4B). Notably, among our sample, 2 juvenile FM participants had Chiari malformations, which is no higher than might be expected based on population prevalence (37).

DISCUSSION

To our knowledge, this is the first study assessing brain structural alterations in juvenile FM. Results indicate that decreased GMV in the aMCC may be a key feature of juvenile FM. This region is a core element of central acute pain processing (9,10,38–40), involved in affective encoding, cognitive interpretation, anticipation, and response selection (41). Consistent with these findings, meta-analytic decoding revealed that among all t-maps generated in our study, the one for aMCC was the only one associated with the terms “pain” and “painful.” Moreover, results showed that the anatomic aMCC pattern resembled the validated aMCC-dorsal MFC pain predictive pattern—and not the negative emotion or cognitive control ones—significantly less in juvenile FM patients than in healthy adolescents.

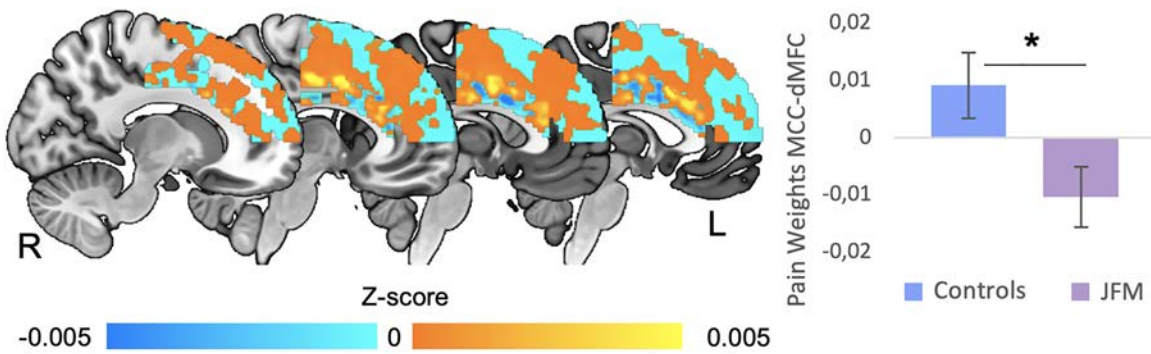


Figure 3. Differences in the similarity between brain structure and a validated pain-predictive pattern in anterior midcingulate cortex (aMCC)–dorsal medial frontal cortex (dMFC) circuits in patients with juvenile fibromyalgia (JFM) compared to healthy adolescents. The anatomic aMCC–dMFC pattern resembled the functional pain pattern significantly less in juvenile FM patients than in healthy adolescents ($t = 2.47$, $P = 0.016$). We found no between-group differences in the patterns predicting cognitive control and negative emotion within the aMCC–dMFC (all $P > 0.05$). Bars show the mean \pm SEM. * = $P < 0.02$.

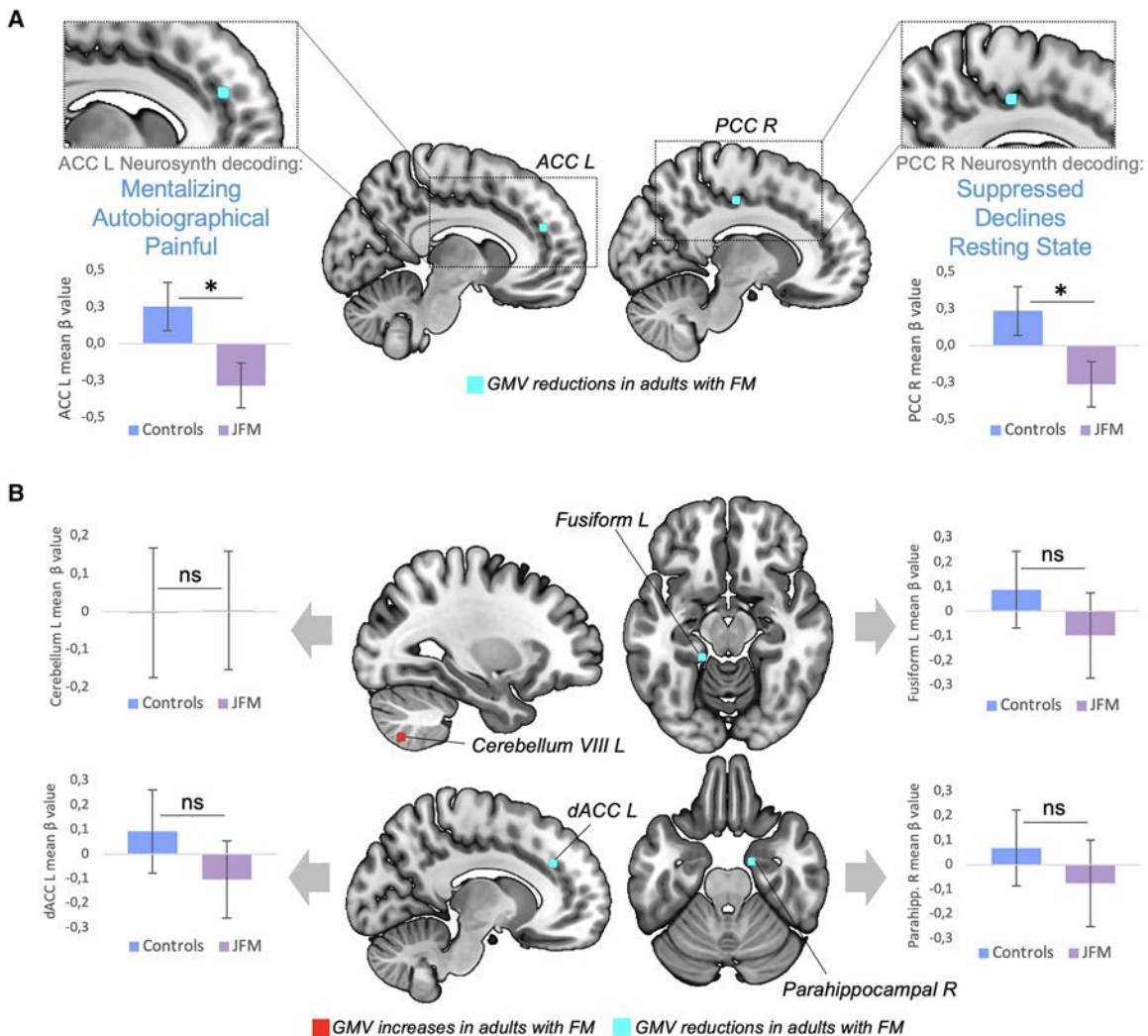


Figure 4. Replication in juvenile fibromyalgia (JFM) of meta-analytic gray matter volume (GMV) alterations observed in adults with FM. **A**, Peaks of GMV altered in both adults with FM and adolescents with juvenile FM (all $P < 0.03$). Notably, the GMV at these peaks was decreased in both adult and juvenile forms of FM. Three associated functional annotations, obtained by meta-analytic decoding using Neurosynth, are shown for each region. **B**, Peaks of GMV altered in adults with FM but not in adolescents with juvenile FM (all $P > 0.4$). Bars show the mean \pm SEM. * = $P < 0.03$. L = left; R = right; dACC = dorsal anterior cingulate cortex; PCC = posterior cingulate cortex; NS = not significant ($P > 0.05$).

We also found that adolescents with juvenile FM exhibited GMV reductions in 2 of the 3 cingulate regions (i.e., ACC, PCC) that meta-analyses reported to be decreased in adult FM patients. Previous studies have shown that repetitive painful stimulation leads to aMCC gray matter increases in healthy subjects (42), whereas patients with chronic pain display GMV reductions in this region (6,7). Our findings do not support the hypothesis that younger patients may show increased GMV as a consequence of overengaging pain modulatory systems (12,13). Instead, results suggest that reductions in the cingulate cortex, mainly in the aMCC, may be a structural hallmark of both adult and juvenile forms of FM, independent of symptom duration. Longitudinal studies are warranted to determine whether such alterations predate chronic pain onset or reflect an early pain-driven alteration. Notably, other GMV alterations reported in adults were not replicated in juvenile FM patients, which may be due to the limited power of the present investigation or may suggest that they appear later in life as a result of progression of chronic pain or medication exposure.

The aMCC is not selective for pain (43,44). Research has linked activity in this area with multiple functions, including attention, cognitive control, reward-based learning, decision-making, and emotional and social processing (for review, see refs. 41 and 43). To deepen our understanding of the functional contributions of the MFC surrounding the region where we found GMV reductions in juvenile FM patients, we assessed how this structural pattern resembled functional patterns predicting pain, cognitive control, and negative emotion within the aMCC–dorsal MFC (22), and how this similarity differed between groups. In adolescents with juvenile FM, the anatomic aMCC pattern resembled the pain pattern significantly less than in controls, which may suggest that the anatomic hallmark of nociceptive pain processing has been attenuated to some degree in juvenile FM patients.

Whether such findings reflect the effects of excessive engagement of the pain-specific functional pattern or a reorganization of acute nociceptive processing brain circuits in patients remains to be elucidated. This finding indicates that pattern similarity reductions in patients occur beyond the cluster showing GMV reductions and reflects an overall reduction of the normal pain predictive pattern in patients. Moreover, it supports the idea of altered organization of aMCC–dorsal MFC circuits. Future functional studies using experimental pain tasks are warranted to test the extent to which this alteration replicates during pain processing to further interpret this novel finding. Taken together, alterations of the pain pattern in juvenile FM patients, along with meta-analytic decoding findings specifically mentioning the terms “pain” and “painful,” suggest that this abnormality may be related to pain processing and decision-making/evaluative aspects in the context of pain and less with other emotional/affective/cognitive processes.

Regarding regions associated with individual differences in patients’ clinical symptoms reflecting pain-related suffering and

diminished functional ability, we found a significant association between functional disability and the left ventrolateral prefrontal cortex (vlPFC). Meta-analyses have linked the left vlPFC with language processes during emotion regulation, suggesting that it might support active reinterpretation of the meaning of emotional stimuli and facilitate the selection of appropriate reappraisals (45). Likewise, the vlPFC has been associated with retrieval of semantic autobiographical memories and self-related judgments (46). Consistent with these findings, at the uncorrected level, we found that other symptoms reflecting the impact that juvenile FM has on patients’ functional ability (i.e., functional disability, fatigue, and pain interference) all correlated with GMV increases in the vlPFC. Taken together, these findings suggest that juvenile FM patients with higher levels of pain-related suffering and impairment show augmented GMV in brain circuits involved in instantiating representations of the *self* and the *world* through language.

Adding further support to this interpretation, at the uncorrected level, fatigue correlated with increased volumes in the left inferior temporal cortex, linked to visual and mnemonic processing (47), and functional disability and pain interference correlated with larger volumes in the right superior frontal cortex, involved in self-focused reappraisal (48), and in the left middle frontal gyrus, associated with attention reorienting (49). Notably, these associations were independent of symptom duration. Neurosynth decoding confirmed that these variables were associated with a brain pattern related to emotional, self-related judgment, and language-related processes. Future studies should test whether alterations in the nature, recurrence, and valence of patients’ narratives about themselves and the world may predict greater levels of suffering and disability in juvenile FM and to which extent vlPFC circuits mediate such associations.

From a neurodevelopmental perspective, frontal GMV decreases after age 11 years in healthy girls because of synaptic pruning (50). This maturation occurs earlier in ventral than in dorsal regions (50). Thus, vlPFC volume increases associated with juvenile FM impairment may reflect a link between these symptoms and developmental immaturity in frontal circuits specializing in emotional appraisal and regulation, which reinforces the need to consider therapeutic strategies that target these circuits, which may have the potential to reverse alterations before they become hard-wired and to mitigate the functional and psychosocial impact of pain-related symptoms on the life of adolescents with juvenile FM.

Finally, symptom duration was associated with reduced GMV in temporoparietal areas—at an uncorrected level—including theory of mind– and language-related regions. The findings suggest that not only disease-related disability, but also juvenile FM duration may be linked to alterations in regions mediating mentalizing and emotional awareness through language. Last, our between-group and symptom duration–related findings taken together do not support the hypothesis of hypertrophy in young FM patients as a group (12,13). However, juvenile FM patients with greater symptom severity showed GMV increases; thus,

future studies with larger samples are warranted to assess whether different structural correlates underlie distinct patient clusters identified based on symptom severity.

This study has some notable limitations. First, we enrolled only females; thus, our findings cannot be generalized to male patients—although they are quite rare. Future studies are warranted to examine between-sex differences in juvenile FM-related structural alterations and the ages at which these changes occur. Second, since this is the first study assessing the structural abnormalities of juvenile FM, replication of our findings in independent samples is crucial to determine their robustness and translational utility. Likewise, the brain–symptom severity correlations presented here, although providing a cohesive picture of the alterations and opening venues for future research, are still preliminary, based on exploratory thresholds, and need replication. Nevertheless, such correlational findings highlight the importance of studying individual differences to characterize different patient profiles. Although medication regimen was stable for at least 3 weeks before the MRI assessment (no modifications in type, dose, or intake regimen), medication could have acted as a confounding factor. Last, despite the efforts to recruit diverse patient profiles, our sample had a low representation of subjects of different races and ethnicities and those with low socioeconomic status. Future community-oriented clinical research is needed to overcome the systematically high proportion of White participants with medium-high socioeconomic status in research samples.

In conclusion, this study provides the first evidence of structural alterations in adolescents with juvenile FM. Our findings suggest that pain-related GMV reductions in the aMCC are common to juvenile FM patients as a group, whereas alterations in regions involved in affective, self-relevant memory, and language processes predict disease impact on clinical variables related to patients' well-being. Taken together, the findings reinforce the need to combine pain-specific, sensory therapies with therapies aimed at promoting cognitive regulation of pain, negative affect, and potentially pervasive self-related narratives patients may hold of themselves. Also, the findings indicate partial overlap in the structural circuitry compromised in both juvenile and adult FM, potentially establishing a link between juvenile and adult forms of the disease and strengthening the need for early, neurobiologically oriented interventions to prevent the transition from juvenile to adult FM.

ACKNOWLEDGMENTS

The authors gratefully thank Matt Lanier, Kaley Bridgewater, Kelsey Murphy, Brynne Williams, and Lacey Haas (Imaging Research Center, Department of Radiology, Cincinnati Children's Hospital Medical Center) for their contributions to MRI data collection.

AUTHOR CONTRIBUTIONS

All authors were involved in drafting the article or revising it critically for important intellectual content, and all authors approved the final version to be published. Dr. Suñol had full access to all of the data in the

study and takes responsibility for the integrity of the data and the accuracy of the data analysis.

Study conception and design. Suñol, Maloney, Ting, Kashikar-Zuck, Coghill, López-Solà.

Acquisition of data. Payne, Tong.

Analysis and interpretation of data. Suñol, Coghill, López-Solà.

REFERENCES

1. Ting TV, Barnett K, Lynch-Jordan A, Whitacre C, Henrickson M, Kashikar-Zuck S. 2010 American College of Rheumatology adult fibromyalgia criteria for use in an adolescent female population with juvenile fibromyalgia. *J Pediatr* 2016;169:181–7.
2. Kashikar-Zuck S, Ting TV, Arnold LM, Bean J, Powers SW, Graham TB, et al. Cognitive behavioral therapy for the treatment of juvenile fibromyalgia: a multisite, single-blind, randomized, controlled clinical trial. *Arthritis Rheum* 2012;64:297–305.
3. Kashikar-Zuck S, Lynch AM, Slater S, Graham TB, Swain NF, Noll RB. Family factors, emotional functioning, and functional impairment in juvenile fibromyalgia syndrome. *Arthritis Rheum* 2008;59:1392–98.
4. Pas R, Ickmans K, Van Oosterwijck S, Van der Cruyssen K, Foubert A, Leysen L, et al. Hyperexcitability of the central nervous system in children with chronic pain: a systematic review. *Pain Med* 2018;19:2504–14.
5. Molina J, Amaro E Jr, da Rocha LG, Jorge L, Santos FH, Len CA. Functional resonance magnetic imaging (fMRI) in adolescents with idiopathic musculoskeletal pain: a paradigm of experimental pain. *Pediatr Rheumatol Online J* 2017;15:81.
6. Lin C, Lee SH, Weng HH. Gray matter atrophy within the default mode network of fibromyalgia: a meta-analysis of voxel-based morphometry studies. *Biomed Res Int* 2016;7:296125.
7. Shi H, Yuan C, Dai Z, Ma H, Sheng L. Gray matter abnormalities associated with fibromyalgia: a meta-analysis of voxel-based morphometric studies. *Semin Arthritis Rheum* 2016;46:330–7.
8. Napadow V, Kim J, Clauw DJ, Harris RE. Decreased intrinsic brain connectivity is associated with reduced clinical pain in fibromyalgia. *Arthritis Rheum* 2012;64:2398–403.
9. López-Solà M, Pujol J, Wager TD, Garcia-Fontanals A, Blanco-Hinojo L, Garcia-Blanco S, et al. Altered functional magnetic resonance imaging responses to nonpainful sensory stimulation in fibromyalgia patients. *Arthritis Rheumatol* 2014;66:3200–9.
10. López-Solà M, Woo CW, Pujol J, Deus J, Harrison BJ, Monfort J, et al. Towards a neurophysiological signature for fibromyalgia. *Pain* 2017;158:34–47.
11. Pujol J, Macià D, Garcia-Fontanals A, Blanco-Hinojo L, López-Solà M, Garcia-Blanco S, et al. The contribution of sensory system functional connectivity reduction to clinical pain in fibromyalgia. *Pain* 2014;155:1492–503.
12. Ceko M, Bushnell MC, Fitzcharles MA, Schweinhardt P. Fibromyalgia interacts with age to change the brain. *Neuroimage Clin* 2013;3:249–60.
13. Moayed M, Weissman-Fogel I, Salomons TV, Crawley AP, Goldberg MB, Freeman BV, et al. Abnormal gray matter aging in chronic pain patients. *Brain Res* 2012;1456:82–93.
14. Bushnell MC, Ceko M, Low LA. Cognitive and emotional control of pain and its disruption in chronic pain. *Nat Rev Neurosci* 2013;14:502–11.
15. Jin F, Zheng P, Liu H, Guo H, Sun Z. Functional and anatomical connectivity-based parcellation of human cingulate cortex. *Brain Behav* 2018;8:e01070.
16. Tovar DT, Chavez RS. Large-scale functional coactivation patterns reflect the structural connectivity of the medial prefrontal cortex. *Soc Cogn Affect Neurosci* 2021;16:875–82.

17. Lazaridou A, Kim J, Cahalan CM, Loggia ML, Franceschelli O, Berna C, et al. Effects of cognitive-behavioral therapy (CBT) on brain connectivity supporting catastrophizing in fibromyalgia. *Clin J Pain* 2017; 33:215–21.
18. Ellingson LD, Stegner AJ, Schwabacher IJ, Koltyn KF, Cook DB. Exercise strengthens central nervous system modulation of pain in fibromyalgia. *Brain Sci* 2016;6:8.
19. Kashikar-Zuck S, King C, Ting TV, Arnold LM. Juvenile fibromyalgia: different from the adult chronic pain syndrome? *Curr Rheumatol Rep* 2016;18:19.
20. Lutz J, Jäger L, de Quervain D, Krauseneck T, Padberg F, Wichnalek M, et al. White and gray matter abnormalities in the brain of patients with fibromyalgia: a diffusion-tensor and volumetric imaging study. *Arthritis Rheum* 2008;58:3960–69.
21. Martucci KT, Mackey SC. Neuroimaging of pain: human evidence and clinical relevance of central nervous system processes and modulation. *Anesthesiology* 2018;128:1241–54.
22. Kragel PA, Kano M, Van Oudenhove L, Ly HG, Dupont P, Rubio A, et al. Generalizable representations of pain, cognitive control, and negative emotion in medial frontal cortex. *Nat Neurosci* 2018;21: 283–89.
23. Fillingim RB, King CD, Ribeiro-Dasilva MC, Rahim-Williams B, Riley JL III. Sex, gender, and pain: a review of recent clinical and experimental findings. *J Pain* 2009;10:447–85.
24. Mogil JS. Qualitative sex differences in pain processing: emerging evidence of a biased literature. *Nat Rev Neurosci* 2020;21:353–65.
25. Walker LS, Greene JW. The functional disability inventory: measuring a neglected dimension of child health status. *J Pediatr Psychol* 1991;16:39–58.
26. PROMIS. PROMIS Instrument Development and Psychometric Evaluation Scientific Standards Version 2.0. 2013.
27. Daut RL, Cleeland CS, Flanery RC. Development of the Wisconsin brief pain questionnaire to assess pain in cancer and other diseases. *Pain* 1983;17:197–210.
28. Ashburner J, Friston KJ. Voxel-based morphometry—the methods. *Neuroimage* 2000;11:805–21.
29. Ashburner J. A fast diffeomorphic image registration algorithm. *Neuroimage* 2007;38:95–113.
30. Yaxu Y, Ren Z, Ward J, Jiang Q. Atypical brain structures as a function of gray matter volume (GMV) and gray matter density (GMD) in young adults relating to autism spectrum traits. *Front Psychol* 2020;11:523.
31. Kennedy JT, Astafiev SV, Golosheykin S, Korucuoglu O, Anokhin AP. Shared genetic influences on adolescent body mass index and brain structure: a voxel-based morphometry study in twins. *Neuroimage* 2019;199:261–72.
32. Barnes J, Ridgway GR, Bartlett J, Henley SM, Lehmann M, Hobbs N, et al. Head size, age and gender adjustment in MRI studies: a necessary nuisance? *Neuroimage* 2010;53:1244–55.
33. Smith SM, Nichols TE. Threshold-free cluster enhancement: addressing problems of smoothing, threshold dependence and localisation in cluster inference. *Neuroimage* 2009;44:83–98.
34. Li H, Nickerson LD, Nichols TE, Gao JH. Comparison of a non-stationary voxelation-corrected cluster-size test with TFCE for group-Level MRI inference. *Hum Brain Mapp* 2017;38:1269–80.
35. Yarkoni T, Poldrack RA, Nichols TE, Van Essen DC, Wager TD. Large-scale automated synthesis of human functional neuroimaging data. *Nat Methods* 2011;8:665–70.
36. Koban L, Jepma M, López-Solà M, Wager TD. Different brain networks mediate the effects of social and conditioned expectations on pain. *Nat Commun* 2019;10:4096.
37. Kahn EN, Muraszko KM, Maher CO. Prevalence of Chiari I malformation and syringomyelia. *Neurosurg Clin N Am* 2015;26:501–7.
38. Coghill RC, Talbot JD, Evans AC, Meyer E, Gjedde A, Bushnell MC, et al. Distributed processing of pain and vibration by the human brain. *J Neurosci* 1994;14:4095–108.
39. Coghill RC, Sang CN, Maisog JM, Iadarola MJ. Pain intensity processing within the human brain: a bilateral, distributed mechanism. *J Neurophysiol* 1999;82:1934–43.
40. Wager TD, Atlas LY, Lindquist MA, Roy M, Woo CW, Kross E. An fMRI-based neurologic signature of physical pain. *N Engl J Med* 2013;368:1388–97.
41. Vogt BA. Midcingulate cortex: structure, connections, homologies, functions and diseases. *J Chem Neuroanat* 2016;74:28–46.
42. Teutsch S, Herken W, Bingel U, Schoell E, May A. Changes in brain gray matter due to repetitive painful stimulation. *Neuroimage* 2008;15:42: 845–9.
43. Shackman AJ, Salomons TV, Slagter HA, Fox AS, Winter JJ, Davidson RJ. The integration of negative affect, pain and cognitive control in the cingulate cortex. *Nat Rev Neurosci* 2011;12: 154–67.
44. Silvestrini N, Chen JI, Piché M, Roy M, Vachon-Preseu E, Woo CW, et al. Distinct fMRI patterns colocalized in the cingulate cortex underlie the after-effects of cognitive control on pain. *Neuroimage* 2020;217: 116898.
45. Buhle JT, Silvers JA, Wager TD, Lopez R, Onyemekwu C, Kober H, et al. Cognitive reappraisal of emotion: a meta-analysis of human neuroimaging studies. *Cereb Cortex* 2014;24:2981–90.
46. Denny BT, Kober H, Wager TD, Ochsner KN. A meta-analysis of functional neuroimaging studies of self- and other judgments reveals a spatial gradient for mentalizing in medial prefrontal cortex. *J Cogn Neurosci* 2012;24:1742–52.
47. Ranganath C. Working memory for visual objects: complementary roles of inferior temporal, medial temporal, and prefrontal cortex. *Neuroscience* 2006;139:277–89.
48. Falquez R, Couto B, Ibanez A, Freitag MT, Berger M, Arens EA, et al. Detaching from the negative by reappraisal: the role of right superior frontal gyrus (BA9/32). *Front Behav Neurosci* 2014;8:165.
49. Japee S, Holiday K, Satyshur MD, Mukai I, Ungerleider LG. A role of right middle frontal gyrus in reorienting of attention: a case study. *Front Syst Neurosci* 2015;9:23.
50. Lenroot RK, Giedd JN. Brain development in children and adolescents: insights from anatomical magnetic resonance imaging. *Neurosci Biobehav Rev* 2006;30:718–29.

LETTERS

DOI 10.1002/art.42066

Vascular deposition of monosodium urate crystals in gout: analysis of cadaveric tissue by dual-energy computed tomography and compensated polarizing light microscopy

To the Editor:

Cardiovascular disease is common among people with gout (1). A hypothesized link between cardiovascular disease and gout is deposition of monosodium urate (MSU) crystals in atherosclerotic plaque (2). Dual-energy computed tomography (DECT) is a sensitive and specific imaging technique for detecting and characterizing MSU crystal deposits in peripheral joint tissues, in both gout (3,4) and asymptomatic hyperuricemia (5). Recent studies using DECT have shown that color-coded images consistent with MSU crystals are present in calcified vessels of most people with gout (6–8). However, it remains highly controversial whether these findings represent true MSU crystal deposition or artifacts due to live imaging (9–11). This study examined the use of DECT and compensated polarizing light microscopy to detect MSU crystal deposition in the large vessels of cadaveric donors with gout.

Six male cadaveric donors (mean age at death 78 years) with a documented history of gout, including 2 with visible tophi, were studied. Collection and use of cadaveric tissue specimens accorded with the New Zealand Human Tissue Act 2008. Vascular tissue specimens were dissected from the arch of the aorta through the descending aorta at the level of the diaphragm and included the proximal few centimeters of the brachiocephalic,

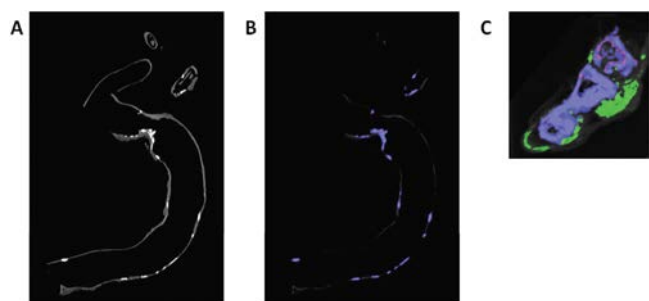


Figure 1. Dual-energy computed tomography (DECT). **A**, Representative conventional CT image of cadaveric vascular tissue. **B**, Representative DECT image of cadaveric vascular tissue from the same donor, demonstrating areas of vascular calcification in blue, but no urate deposition (color-coded green). **C**, Representative DECT image of a positive control cadaveric tophaceous peripheral joint demonstrating urate deposition (color-coded green) within tophaceous deposits. Nail artifact in the toenail is also visible.

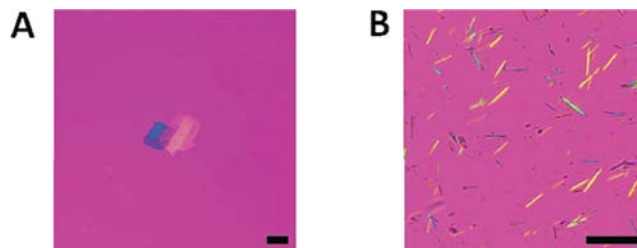




Figure 2. Compensated polarizing light microscopy. **A**, Representative polarizing microscopy image from an aspirate of cadaveric vascular tissue demonstrating plate-like cholesterol crystals, but no needle-shaped negatively birefringent crystals. **B**, Representative polarizing microscopy image from an aspirate of a positive control cadaveric tophaceous joint demonstrating numerous needle-shaped negatively birefringent crystals. Bars = 10 μm .

common carotid, and subclavian arteries. A dissected vascular tissue sample from each donor was laid on a CT table and scanned by DECT (Somatom Definition Flash, Siemens Healthineers), and a rheumatologist (ND) and radiologist (AD) analyzed the findings on a Siemens workstation, using gout-specific proprietary software (syngo MMWP VE 36A 2009; Siemens Healthineers). After scanning, 100 μl of phosphate buffered saline was injected into the vessel wall at 10 standardized sites across each sample, and aspirated fluid was analyzed with polarizing light microscopy by a rheumatologist (ND) and laboratory scientist (M. Alhilali). Positive controls included tissue specimens from peripheral joints of different cadaveric donors with tophaceous gout that were processed using the same protocols, as well as synthesized MSU crystals. The Supplementary Materials, available on the *Arthritis & Rheumatology* website at <https://onlinelibrary.wiley.com/doi/10.1002/art.42066>, include the imaging protocol, workstation settings, and microscopy sites.

DECT scanning of cadaveric vascular tissue samples detected calcification in all specimens but no evidence of MSU deposition (Figure 1A). In contrast, in positive control tophaceous joint specimens, color-coded DECT images provided clear evidence of MSU crystal deposition (Figure 1B). Microscopic analysis demonstrated plate-like cholesterol crystals in vascular tissue samples from 5 donors (mean \pm SD 3.2 ± 1.9 sites/donor) (Figure 2A). A single negatively birefringent needle-shaped crystal was visualized by microscopy from one of the 60 sampled vascular tissue sites, with no MSU crystals evident at the other 59 sites. In contrast, microscopy revealed numerous MSU crystals in aspirates from positive control tophaceous joint specimens (Figure 2B).

This analysis has not demonstrated MSU crystal deposition in the resected vascular tissue of cadaveric donors with gout by DECT (when using default postprocessing settings) or polarizing light microscopy, in contrast to positive control cadaveric tophaceous peripheral joints. Study limitations include the absence of antemortem imaging studies and the lack of an analysis of the entire vascular system. However, this study raises the possibility that DECT-based MSU-coded plaques in peripheral arteries on live imaging do not reflect true MSU crystal deposition.

Author disclosures are available at <https://onlinelibrary.wiley.com/action/downloadSupplement?doi=10.1002%2Fart.42066&file=art42066-sup-0001-Disclosureform.pdf>.

Nicola Dalbeth, MD, FRACP 
 Mariam Alhilali, BSc (Hons)
 Peter Riordan, MSc
 Ravi Narang, MBChB
 Ashika Chhana, PhD 
 Sue McGlashan, PhD
 Anthony Doyle, MBChB, FRANZCR
 University of Auckland
 Auckland, New Zealand
 Mariano Andres, PhD
 Hospital General Universitario de Alicante
 Universidad Miguel Hernández
 Alicante, Spain

- Zhu Y, Pandya BJ, Choi HK. Comorbidities of gout and hyperuricemia in the US general population: NHANES 2007–2008. *Am J Med* 2012; 125:679–87.e1.
- Park JJ, Roudier MP, Soman D, Mokadam NA, Simkin PA. Prevalence of birefringent crystals in cardiac and prostatic tissues, an observational study. *BMJ Open* 2014;4:e005308.
- Richette P, Doherty M, Pascual E, Barskova V, Becce F, Castaneda J, et al. 2018 updated European League Against Rheumatism evidence-based recommendations for the diagnosis of gout. *Ann Rheum Dis* 2020;79:31–8.
- Choi HK, Al-Arfaj AM, Eftekhari A, Munk PL, Shojania K, Reid G, et al. Dual energy computed tomography in tophaceous gout. *Ann Rheum Dis* 2009;68:1609–12.
- Dalbeth N, House ME, Aati O, Tan P, Franklin C, Home A, et al. Urate crystal deposition in asymptomatic hyperuricaemia and symptomatic gout: a dual energy CT study. *Ann Rheum Dis* 2015;74:908–11.
- Feuchtner GM, Plank F, Beyer C, Schwabl C, Held J, Bellmann-Weiler R, et al. Monosodium urate crystal deposition in coronary artery plaque by 128-slice dual-energy computed tomography: an ex vivo phantom and in vivo study. *J Comput Assist Tomogr* 2021;45: 856–62.
- Klauser AS, Halpern EJ, Strobl S, Gruber J, Feuchtner G, Bellmann-Weiler R, et al. Dual-energy computed tomography detection of cardiovascular monosodium urate deposits in patients with gout. *JAMA Cardiol* 2019;4:1019–28.
- Barazani SH, Chi WW, Pyzik R, Chang H, Jacobi A, O'Donnell T, et al. Quantification of uric acid in vasculature of patients with gout using dual-energy computed tomography. *World J Radiol* 2020;12: 184–94.
- Becce F, Ghoshhajra B, Choi HK. Identification of cardiovascular monosodium urate crystal deposition in patients with gout using dual-energy computed tomography. *JAMA Cardiol* 2020;5:486.
- Pascart T, Carpentier P, Choi HK, Norberciak L, Ducoulombier V, Luraschi H, et al. Identification and characterization of peripheral

vascular color-coded DECT lesions in gout and non-gout patients: the VASCURATE study. *Semin Arthritis Rheum* 2021;51:895–902.

- Mallinson PI, Coupal T, Reisinger C, Chou H, Munk PL, Nicolaou S, et al. Artifacts in dual-energy CT gout protocol: a review of 50 suspected cases with an artifact identification guide. *AJR Am J Roentgenol* 2014;203:W103–9.

DOI 10.1002/art.42106

Sequencing of the 16S ribosomal DNA gene and virulence of the oral microbiome in patients with rheumatoid arthritis: comment on the article by Kroese et al

To the Editor:

We read with great interest the article by Dr. Kroese et al (1) on the association between the oral microbiome and rheumatoid arthritis (RA). The authors reported new insights into early indicators of autoimmune disease through comparisons of oral microbiota in patients with early RA, patients at risk of developing RA, and healthy individuals.

Kroese and colleagues used next-generation sequencing and polymerase chain reaction to identify the 16S ribosomal DNA (rDNA) of oral microorganisms. Although next-generation sequencing of the 16S V3–V5 variable region, as used by Kroese and colleagues, undoubtedly can detect a wide spectrum of bacteria, it can neglect species of small colonies (2). Specifically, next-generation 16S rDNA gene sequencing cannot achieve taxonomic resolution of scarce bacterial communities at the species and strain level due to the potential limitations of this method, particularly with regard to identification of bacteria of unknown etiology or microbial species of low abundance (2). For example, *Porphyromonas gingivalis*, an RA-inducing bacterium (3,4) that was shown by Kroese and colleagues to have very low abundance in their 3 patient populations, may be subject to a limited taxonomic resolution. Thus, we propose that sequencing analyses assessing correlations between oral microbiota and the development of RA should utilize full-length 16S intragenomic copy variants based on the V1–V9 sequence of rDNA (2). This approach can allow for clearer pictures of oral dysbiosis in populations with early RA or at risk of RA. Moreover, because *P gingivalis* has been suggested to trigger RA through induction of anti-citrullinated protein antibody (ACPA)–dependent pathogenesis (3,4), further studies on the interactions between *P gingivalis* and the disease-enriched species observed by Kroese and colleagues, such as survival symbiosis and secreted toxicities that may induce ACPA production through augmentation of the virulence of these bacteria (5), may help to clarify the etiology of RA.

In addition, although Kroese and colleagues demonstrated proportional and quantitative differences between oral microorganisms, the virulence of microorganisms might be inconsistent with their population sizes. In particular, the virulence of

microorganisms varies depending on signals in their microenvironments and cross-microorganism interactions that affect their virulent gene expression (6). Because these determinants may reshape our knowledge with regard to the importance of RA-associated oral microorganisms, mechanistic studies illustrating relationships between these microorganisms and RA could provide further evidence to support the notion that bacterial species are involved in the pathogenesis of the disease.

Finally, although Kroese and colleagues asked study participants about their oral hygiene practices, scaling during dental visits was not considered. Importantly, scaling can alter the oral microbiome and can resolve oral dysbiosis, as evidenced by ecologic drift and community turnovers in plaque biofilms and saliva (7,8). These changes involve significant decreases in disease-associated taxa, such as *Veillonella*, *Prevotella*, and *Porphyromonas* species (7–10), which were also identified in the participants in the study by Kroese et al. Thus, we recommend that, in future studies, scaling should be considered as a modifiable factor for bacteria-associated RA.

The pathogenesis of RA is not yet fully comprehended (1). RA is known to have a negative effect on a patient's quality of life, and we appreciate the contributions of Kroese et al in probing deeper into the severity of this illness.

Drs. Luan and Chen contributed equally to this work. Author disclosures are available at <https://onlinelibrary.wiley.com/action/downloadSupplement?doi=10.1002%2Fart.42106&file=art42106-sup-0001-Disclosureform.pdf>.

Yu-Ze Luan, MD 
 Brian Shiiian Chen, MD
 School of Medicine
 Chung Shan Medical University
 Taichung, Taiwan
 Kevin Sheng-Kai Ma, DDS 
 University of Pennsylvania
 Philadelphia, PA
 and Harvard T. H. Chan School of
 Public Health
 Boston, MA
 and National Taiwan University
 Taipei, Taiwan

- Kroese JM, Brandt BW, Buijs MJ, Crielaard W, Lobbezoo F, Loos BG, et al. Differences in the oral microbiome in patients with early rheumatoid arthritis and individuals at risk of rheumatoid arthritis compared to healthy individuals. *Arthritis Rheumatol* 2021;73:1986–93.
- Johnson JS, Spakowicz DJ, Hong BY, Petersen LM, Demkowicz P, Chen L, et al. Evaluation of 16S rRNA gene sequencing for species and strain-level microbiome analysis. *Nat Commun* 2019;10:5029.
- Ma KS, Chiang CH, Chen YW, Wang LT. Correspondence to ‘Bacterial citrullinated epitopes generated by *Porphyromonas gingivalis* infection—a missing link for ACPA production’. *Ann Rheum Dis* 2021. E-pub ahead of print. doi:10.1136/annrheumdis-2020-219255
- Wu KJ, Tu CC, Hu JX, Chu PH, Ma KS, Chiu HY. Severity of periodontitis and salivary interleukin-1 β are associated with psoriasis involvement. *J Formos Med Assoc* 2022. E-pub ahead of print. doi:10.1016/j.jfma.2022.01.017
- Sakkas LI, Daoussis D, Liossis SN, Bogdanos DP. The infectious basis of ACPA-positive rheumatoid arthritis. *Front Microbiol* 2017;8:1853.
- Hajishengallis G, Lamont RJ. Dancing with the stars: how choreographed bacterial interactions dictate nosymbiocity and give rise to keystone pathogens, accessory pathogens, and pathobionts. *Trends Microbiol* 2016;24:477–89.
- Chen C, Hemme C, Beleno J, Shi ZJ, Ning D, Qin Y, et al. Oral microbiota of periodontal health and disease and their changes after non-surgical periodontal therapy. *ISME J* 2018;12:1210–24.
- Ma KS, Lai JN, Veeravalli JJ, Chiu LT, Van Dyke TE, Wei JC. Fibromyalgia and periodontitis: Bidirectional associations in population-based 15-year retrospective cohorts. *J Periodontol* 2021. E-pub ahead of print. doi:10.1002/JPER.21-0256
- Ma KS, Wu MC, Thota E, Wang YH, Alqaderi HE, Wei JC. Tonsillectomy as a risk factor of periodontitis: a population-based cohort study. *J Periodontol* 2021. E-pub ahead of print. doi:10.1002/JPER.21-0215
- Ma KS, Hasturk H, Carreras I, Dedeoglu A, Veeravalli JJ, Huang JY, et al. Dementia and the risk of periodontitis: a population-based cohort study. *J Dent Res* 2022;101:270–7.

DOI 10.1002/art.42107

Reply

To the Editor:

We thank Dr. Luan et al for their interest in our study. We appreciate the opportunity to respond.

It is argued that studies should use full-length 16S ribosomal RNA (rRNA) gene variants instead of next-generation sequencing of the 16S rRNA V3–V5 variable region (note that we studied the V4 region) to identify bacteria of potentially unknown etiology and species of low abundance. As mentioned in a study by Johnson et al (as cited by Luan et al), full-length 16S rRNA sequences indeed enable accurate classification of organisms at a very high taxonomic resolution (1). However, this method is not yet available for high-throughput analyses. Although we appreciate the desire to explore the microbiome in full depth, other factors (e.g., research questions, possible disadvantages of maximum detail, costs) should also be considered. In the cited report it was also concluded that most variable regions are sufficient to identify genera (1), which we argue to be sufficient to detect possible dysbiosis and compare groups on overall microbiome composition.

Luan et al referred to *Porphyromonas gingivalis* as “an RA-inducing bacterium,” and the articles cited by Luan et al to support their statement do suggest a role for *P gingivalis* in RA, as described in a study by Mankia et al (2) and in a study by Ma et al describing its possible mechanism of action (3). We would like to suggest that some caution be applied in interpreting these potentially insufficiently substantiated conclusions. There is also evidence disproving an independent role of *P gingivalis*, with a study showing, for example, no value of anti-*P gingivalis* antibody levels for the prediction of RA development (4). Reviews on the topic emphasize the lack of conclusive evidence for a causal role and suggest a focus on microbiome dysbiosis in a broader sense (5–7). The pitfall of being highly interested in a possible role of

Table 1. Dentist and dental hygienist visits among patients with early RA, at-risk individuals, and healthy controls*

	Patients with early RA†	At-risk individuals†	Healthy controls†	P
Dentist visits				
No. (%) with at least 1 visit/year	43 (86)	45 (90)	47 (9)	0.41‡
Months since last visit, median (IQR)	4 (2–11.3)	4 (1.8–8)	2 (0.8–6)	0.11§
Dental hygienist visits				
No. (%) with at least 1 visit/year	26 (52)	25 (50)	25 (50)	0.97‡
Months since last visit, median (IQR)	4 (2–17.5)	5 (1.4–9.8)	4 (1–12)	0.74§

* IQR = interquartile range.

† Group size was n = 50 for evaluation of dentist visits. Group sizes for the last visit to a dental hygienist were as follows: n = 36 for patients with early rheumatoid arthritis (RA), n = 34 for the at-risk group, and n = 40 for the healthy control group.

‡ By chi-square test.

§ By Kruskal-Wallis test.

P. gingivalis in RA is that belief will lead the research. While our data showed a low abundance of *P. gingivalis* in our study participants and Luan et al suggested that this may be due to a limited sequencing method, it should also be considered that *P. gingivalis* simply was not present in sufficient numbers, consistent with earlier findings in RA patients (8). Furthermore, another study on RA patients that used an identical sequencing approach, as well as *P. gingivalis*-specific quantitative polymerase chain reaction, showed a significant correlation between the findings produced by the 2 different methods in terms of *P. gingivalis* identification and proportion (9), thereby supporting our sequencing results. We do acknowledge the extensive literature on a possible role of *P. gingivalis* in RA induction, but we would also like to encourage openness to other hypotheses and mechanisms.

With regard to the comment on the effects of scaling, we can only agree that scaling can indeed alter the oral microbiome. Although not mentioned in our article, we did ask participants about their dentist and/or dental hygienist visits and recent periodontitis treatment. For clarification, we include Table 1, which presents the specifics on dentist and dental hygienist visits in our participants and which shows no significant differences between the groups. Only 2 participants (1 in the early RA group and 1 in the at-risk group) reported having received treatment for periodontitis during the preceding year. Considering these data, we do not expect recent scaling to have significantly influenced our results.

Again, we would like to thank Luan and colleagues for their time and consideration of our article. We hope our comments will help to clarify their concerns.

Johanna M. Kroese, DDS, PhD 
 Bernd W. Brandt, PhD
 Mark J. Buijs
 Wim Crielaard, PhD
 Frank Lobbezoo, DDS, PhD
 Bruno G. Loos, DDS, MSc, PhD
 Egija Zaura, DDS, PhD
 Academic Centre for Dentistry of Amsterdam
 University of Amsterdam
 and Vrije Universiteit Amsterdam

Laurette van Boheemen, MD, PhD 
 Dirkjan van Schaardenburg, MD, PhD
 Amsterdam Rheumatology and Immunology Center
 Reade and Amsterdam University Medical Center
 Catherine M. C. Volgenant, DDS, PhD
 Academic Centre for Dentistry of Amsterdam
 University of Amsterdam
 and Vrije Universiteit Amsterdam
 Amsterdam, The Netherlands

- Johnson JS, Spakowicz DJ, Hong BY, Petersen LM, Demkowicz P, Chen L, et al. Evaluation of 16S rRNA gene sequencing for species and strain-level microbiome analysis. *Nat Commun* 2019;10:5029.
- Mankia K, Cheng Z, Do T, Hunt L, Meade J, Kang J, et al. Prevalence of periodontal disease and periodontopathic bacteria in anti-cyclic citrullinated protein antibody-positive at-risk adults without arthritis. *JAMA Netw Open* 2019;2:e195394.
- Ma KS, Chiang CH, Chen YW, Wang LT. Correspondence to 'Bacterial citrullinated epitopes generated by *Porphyromonas gingivalis* infection—a missing link for ACPA production'. *Ann Rheum Dis* 2021. doi:10.1136/annrheumdis-2020-219255. E-pub ahead of print.
- De Smit M, van de Stadt LA, Janssen KM, Doornbos-van der Meer B, Vissink A, van Winkelhoff AJ, et al. Antibodies against *Porphyromonas gingivalis* in seropositive arthralgia patients do not predict development of rheumatoid arthritis. *Ann Rheum Dis* 2014; 73:1277–9.
- Lorenzo D, GianVincenzo Z, Carlo Luca R, Karan G, Jorge V, Roberto M, et al. Oral-gut microbiota and arthritis: is there an evidence-based axis? *J Clin Med* 2019;8:1753.
- Wells PM, Williams FM, Matey-Hernandez ML, Menni C, Steves CJ. 'RA and the microbiome: do host genetic factors provide the link? *J Autoimmun* 2019;99:104–15.
- Moller B, Kollert F, Sculean A, Villiger PM. Infectious triggers in periodontitis and the gut in rheumatoid arthritis (RA): a complex story about association and causality. *Front Immunol* 2020;11:1108.
- Lopez-Oliva I, Paropkari AD, Saraswat S, Serban S, Yonel Z, Sharma P, et al. Dysbiotic subgingival microbial communities in periodontally healthy patients with rheumatoid arthritis. *Arthritis Rheumatol* 2018;70:1008–13.
- Beyer K, Zaura E, Brandt BW, Buijs MJ, Brun JG, Crielaard W, et al. Subgingival microbiome of rheumatoid arthritis patients in relation to their disease status and periodontal health. *PLoS One* 2018;13:e0202278.

DOI 10.1002/art.42116

Increased cadmium inhalation as a possible explanation for an increased risk of rheumatoid arthritis development: comment on the article by Okamoto et al

To the Editor:

This letter is to comment on the recently reported study by Dr. Okamoto and colleagues, in which higher levels of spontaneous citrullinated histone H3-expressing neutrophil extracellular trap (NET) formation in sputum neutrophils were demonstrated in individuals with rheumatoid arthritis (RA) and those at risk of RA development compared to healthy controls (1). Furthermore, in at-risk subjects, levels of IgA anti-citrullinated protein antibodies (ACPAs) in the sputum correlated significantly with the percentage of neutrophils that underwent citrullinated histone H3 NET formation. In addition, compared to healthy controls, analyses of the sputum of patients with RA and at-risk subjects revealed a reduction in endocytosis in macrophages and showed correlations between sputum-induced citrullinated histone H3 formation and sputum levels of the inflammatory cytokines interleukin-1 β (IL-1 β), IL-6, and tumor necrosis factor (TNF) in at-risk subjects.

Okamoto et al clearly identified that citrullinated histone H3-expressing NET formation is of potential importance in both the generation of an RA-related mucosal antibody response and inflammatory cytokines relevant to RA in RA at-risk subjects. Given that an ACPA response greatly increases the risk of developing RA (2), it is conceivable that citrullinated histone NET formation is of importance in RA pathogenesis.


Smoking has been identified as an important risk factor for the development of RA (2). Cigarette smoke contains thousands of constituents, and the exact compound within cigarette smoke that triggers RA has not been established. Specifically, cadmium is an important component of cigarette smoke, air pollution, and other occupational and industrial substances and has been shown to be associated with RA pathogenesis (3). Two large epidemiologic studies have recently linked cadmium exposure to RA (4,5).

Cadmium can trigger NET formation (6) and has been observed to be a citrullinating agent in 2 independent studies (7,8). Furthermore, cadmium decreases macrophage efferocytosis and is associated with peptidylarginine deiminase type 4 up-regulation (9) and has also been found to induce the formation of the inflammatory cytokines IL-1 β , IL-6, and TNF from various lung cell lines (10). Essentially, cadmium has been observed to trigger most of the features of inflammation described in the study by Okamoto et al. It is therefore imperative that cadmium is studied further in RA patients and RA at-risk populations.

Okamoto et al are in a unique position to investigate the role of cadmium and other metals by measuring their concentrations

in the sputum of participants in their previously studied cohorts by sector field inductively coupled plasma mass spectrometry. I suspect the results will be noteworthy.

Funding for work related to cadmium and rheumatoid arthritis was received from the Cornwall Arthritis Trust. Author disclosures are available at <https://onlinelibrary.wiley.com/action/downloadSupplement?doi=10.1002%2Fart.42116&file=art42116-sup-0001-Disclosureform.pdf>.

David G. Hutchinson, MRCP, MD 
Royal Cornwall Hospital Trust
Truro UK

- Okamoto Y, Devoe S, Seto N, Minarchick V, Wilson T, Rothfuss HM, et al. Association of sputum neutrophil extracellular trap subsets with IgA anti-citrullinated protein antibodies in subjects at risk for rheumatoid arthritis. *Arthritis Rheumatol* 2022;74:38–48.
- Scherer HU, Häupl T, Burmester GR. The etiology of rheumatoid arthritis. *J Autoimmun* 2020;110:102400.
- Hutchinson D. Cadmium, one of the villains behind the curtain: has exposure to cadmium helped to pull the strings of seropositive rheumatoid arthritis pathogenesis all along? *Int J Clin Rheumatol* 2015;18:570–3.
- Joo SH, Lee J, Hutchinson D, Song YW. Prevalence of rheumatoid arthritis in relation to serum cadmium concentrations: cross-sectional study using Korean National Health and Nutrition Examination Survey (KNHANES) data. *BMJ Open* 2019;9:e023233.
- Chen L, Sun Q, Peng S, Tan T, Mei G, Chen H, et al. Associations of blood and urinary heavy metals with rheumatoid arthritis risk among adults in NHANES, 1999–2018. *Chemosphere* 2022;289:133147.
- Wang C, Wei Z, Han Z, Wang J, Zhang X, Wang Y, et al. Neutrophil extracellular traps promote cadmium chloride-induced lung injury in mice. *Environ Pollut* 2019;254:113021.
- Hutchinson D, Müller J, McCarthy JE, Gun'ko YK, Verma NK, Bi X, et al. Cadmium nanoparticles citrullinate cytokeratins within lung epithelial cells: cadmium as a potential cause of citrullination in chronic obstructive pulmonary disease. *Int J Chron Obstruct Pulmon Dis* 2018;13:441–9.
- Li FJ, Surolia R, Li H, Wang Z, Liu G, Kulkarni T, et al. Citrullinated vimentin mediates development and progression of lung fibrosis. *Sci Transl Med* 2021;13:eaba2927.
- Surolia R, Li FJ, Singh P, Dsouza KG, Stephens CT, Antony VB. Cadmium decreases macrophage efferocytosis and induces emphysema via PAD4 upregulation [abstract]. *Am J Respir Crit Care Med* 2021;203:A3134.
- Låg M, Rodionov D, Ovrevik J, Bakke O, Schwarze PE, Refsnes M. Cadmium-induced inflammatory responses in cells relevant for lung toxicity: expression and release of cytokines in fibroblasts, epithelial cells and macrophages. *Toxicol Lett* 2010;193:252–60.

DOI 10.1002/art.42115

Reply

To the Editor:

We thank Dr. Hutchinson for his thoughtful comments on our article and for describing his interesting hypothesis that increased cadmium inhalation could be a trigger of the increased NETosis and decreased efferocytosis identified in our study subjects'

sputum neutrophils and macrophages, respectively. We agree that the relationship between cadmium-induced NETosis in the lung, ACPA generation, and RA development is an area that needs further exploration. However, inhalation of cadmium in the US occurs most commonly from cigarette smoking, and most of those at risk of RA development in our study (67%) had never smoked, suggesting that other factors likely contributed to our findings.

We suspect that the role of cadmium in RA development is in accordance with the “mucosal origins hypothesis” that environmental factors, which may include cadmium, have effects on immune cells in the lung or at other mucosal sites, and these mucosal immune responses, which can include citrullinated protein-expressing NET formation and mucosal ACPA generation, are initially a protective response but can lead to RA in some individuals after a period of uncontrolled immune dysregulation (1). It is also important to consider the effects of cadmium on other immune cells (2). In RA at-risk individuals, we previously demonstrated enhanced peptidylarginine deiminase 4–driven peripheral monocyte extracellular trap formation expressing citrullinated histone H3 following ex vivo Toll-like receptor stimulation (3). An understanding of the responses of different immune cells to environmental factors, including cadmium, is necessary to understand the influence of these factors in the complex disease development model of RA.

In our study, we focused on airway-derived neutrophils and NETosis, but we have also been intrigued by the recent finding that cadmium-induced citrullination of vimentin was associated with pulmonary fibrosis in a mouse model (4). A proportion of RA patients will develop RA-associated interstitial lung disease (ILD). Although smoking is an established risk factor, an improved understanding of the exact mechanisms by which ILD develops in RA is needed to improve clinical care, and the investigation of smoking-associated cadmium-induced citrullination of profibrotic proteins in the lung or cadmium-induced NETosis may be informative. Chronic obstructive pulmonary disease (COPD) also disproportionately impacts RA patients. Cadmium is found to partially mediate the well-established association between smoking and COPD (5), suggesting that cadmium inhalation could impact multiple aspects of RA-associated lung disease.

We agree with Dr. Hutchinson that future research in this area is needed. More studies with human cells and investigations to understand the temporal relationships among cadmium inhalation, immune cell effects, and RA are especially needed. In addition, understanding the phenotype of NETs induced by cadmium or other inhaled factors will be important as the protein content of NETs, which is key to NET-associated ACPA generation, can differ based on the NET-triggering stimulus, local cytokine environment, and other factors (e.g., sex, genetics, diet, medications). Understanding these aspects will be necessary to

better understand how cadmium-induced NETs may contribute to RA pathogenesis.

Yuko Okamoto, MD
Tokyo Women's Medical University
Tokyo, Japan
 M. Kristen Demoruelle, MD, PhD 
University of Colorado School of Medicine
Aurora, CO

1. Holers VM, Demoruelle MK, Kuhn KA, Buckner JH, Robinson WH, Okamoto Y, et al. Rheumatoid arthritis and the mucosal origins hypothesis: protection turns to destruction. *Nat Rev Rheumatol* 2018;14:542–57.
2. Wang Z, Sun Y, Yao W, Ba Q, Wang H. Effects of cadmium exposure on the immune system and immunoregulation. *Front Immunol* 2021;12:695484.
3. Okamoto Y, Ghosh T, Okamoto T, Schuyler RP, Seifert J, Chary LL, et al. Subjects at-risk for future development of rheumatoid arthritis demonstrate a PAD4- and TLR-dependent enhanced histone H3 citrullination and proinflammatory cytokine production in CD14(hi) monocytes. *J Autoimmun* 2021;117:102581.
4. Li FJ, Surolia R, Li H, Wang Z, Liu G, Kulkarni T, et al. Citrullinated vimentin mediates development and progression of lung fibrosis. *Sci Transl Med* 2021;13:eaba2927.
5. Rokadia HK, Agarwal S. Serum heavy metals and obstructive lung disease: results from the National Health and Nutrition Examination Survey. *Chest* 2013;143:388–97.

DOI 10.1002/art.42100

Suggested additions to future directions: comment on the ACR white paper on antimalarials and cardiac toxicity by Desmarais et al

To the Editor:

I read with interest the American College of Rheumatology white paper on antimalarial-associated cardiac toxicity in patients with rheumatic or dermatologic diseases (1). While I agree with all that was written, the Future Studies section of the white paper includes the following omissions, which, if addressed, could enhance our understanding of the issue.

First, hydroxychloroquine (HCQ) is broken down into at least 5 different metabolites, and no two individuals receiving the same dose will have the same HCQ level. Hence, any future studies should correlate symptoms with HCQ levels, which can be easily measured (2,3).

Second, digital electrocardiographic devices that can assess corrected QT (QTc) intervals in real time are inexpensive and readily available, and they can be worn by patients who might be at risk for arrhythmias (4). Patients with such a device can maintain a diary, and the timing of dizziness symptoms or heart palpitations can be compared to the cardiac rhythm.


Third, all too many COVID-19–related studies and pre-COVID-19 cardiomyopathy studies reviewed by Dr. Desmarais and colleagues included patients who were

prescribed chloroquine (at daily doses of up to 1.2 gm), rather than HCQ. In the rheumatology community, chloroquine accounts for <1% of all prescriptions, and many conclusions drawn by Desmarais et al are disproportionate to real-world experience.

Finally, anti-SSA (anti-Ro 52) antibodies are associated with heart block in patients with systemic lupus erythematosus, including asymptomatic adults (5). Future studies of antimalarial therapy in patients with rheumatic and dermatologic diseases should assess whether HCQ treatment is harmful in those who test positive for anti-SSA and, if so, should evaluate the association between adverse events and HCQ levels.

In light of these considerations, the ideal study of antimalarial use for rheumatic and dermatologic diseases would include prospective evaluation of HCQ levels, QTc intervals, and anti-SSA levels in patients who have and those who have not started HCQ therapy. Our group is in the process of initiating a study that will address these considerations. I believe that the white paper's conclusions should be amended to include these suggestions.

Author disclosures are available at <https://onlinelibrary.wiley.com/action/downloadSupplement?doi=10.1002%2Fart.42100&file=art42100-sup-0001-Disclosureform.pdf>.

Daniel J. Wallace, MD, FACP, MACR 
Cedars-Sinai Medical Center
and David Geffen School of Medicine at
the University of California, Los Angeles
Los Angeles, CA

1. Desmarais J, Rosenbaum JT, Costenbader KH, Ginzler EM, Fett N, Goodman S, et al. American College of Rheumatology white paper on antimalarial cardiac toxicity. *Arthritis Rheumatol* 2021;73:2151–60.
2. Wallace DJ, Gudsoorkar VS, Weisman MH, Venuturupalli SR. New insights into mechanisms of therapeutic effects of antimalarial agents in SLE [review]. *Nat Rev Rheumatol* 2012;8:522–33.
3. Durcan L, Clarke WA, Magder LS, Petri M. Hydroxychloroquine blood levels in systemic lupus erythematosus: clarifying dosing controversies and improving adherence. *J Rheumatol* 2015;42:2092–7.
4. Chung EH, Guise KD. QTC intervals can be assessed with the AliveCor heart monitor in patients on dofetilide for atrial fibrillation. *J Electrocardiol* 2015;48:8–9.
5. Bourré-Tessier J, Clarke AE, Huynh T, Bernatsky S, Joseph L, Belisle P, et al. Prolonged corrected QT interval in anti-Ro/SSA-positive adults in systemic lupus erythematosus. *Arthritis Care Res (Hoboken)* 2011;63:1031–7.








DOI 10.1002/art.42102

Reply

To the Editor:

We are grateful to Dr. Wallace for his careful reading of our white paper. His points are well made, and we are delighted that the white paper has prompted these constructive ideas

for further study. The portable electrocardiographic devices available for monitoring the QT interval, such as the KardiaMobile device (AliveCor) (1,2) cited by Dr. Wallace, hold promise but need further investigation in robust trials focusing on the QTc interval in patients receiving antimalarial medications. While space constraints limited what we could state about future studies in our white paper, and because our article could not be amended after publication, we hope that Dr. Wallace's letter will serve in the same capacity that an addendum might.

Julianna Desmarais, MD 
Nicole Fett, MD
Oregon Health & Science University
Portland, OR
James T. Rosenbaum, MD 
Oregon Health & Science University
and Legacy Devers Eye Institute
Portland, OR
Karen H. Costenbader, MD, MPH 
Brigham and Women's Hospital
Boston, MA
Ellen M. Ginzler, MD, MPH
State University of New York
Downstate Health Sciences University
Brooklyn, NY
Susan Goodman, MD 
Hospital for Special Surgery at New York-
Presbyterian Weill Cornell Medicine
New York, NY
James O'Dell, MD
University of Nebraska Medical Center
and Omaha VA Hospital
Omaha, NE
Christian A. Pineau, MD
McGill University
Montreal, Quebec, Canada
Gabriela Schmajuk, MD 
University of California San Francisco
San Francisco VA Medical Center
and Philip R. Lee Institute for Health Policy
San Francisco, CA
Victoria P. Werth, MD 
University of Pennsylvania
and Corporal Michael J. Crescenz VAMC
Philadelphia, PA
Mark S. Link, MD 
University of Texas Southwestern Medical Center
Dallas, TX
Richard Kovacs, MD
Indiana University School of Medicine
Indianapolis, IN

1. Al-Alusi MA, Ding E, McManus DD, Lubitz SA. Wearing your heart on your sleeve: the future of cardiac rhythm monitoring [review]. *Curr Cardiol Rep* 2019;21:158.
2. Chung EH, Guise KD. QTC intervals can be assessed with the AliveCor heart monitor in patients on dofetilide for atrial fibrillation. *J Electrocardiol* 2015;48:8–9.

DOI 10.1002/art.42101

Successful use of cyclosporin A and interleukin-1 blocker combination therapy in VEXAS syndrome: a single-center case series

To the Editor:

VEXAS (vacuoles, E1 enzyme, X-linked, autoinflammatory, somatic syndrome) is a recently recognized autoinflammatory disease that is induced by somatic mutations of the *UBA1* gene and mostly affects older men (1). Since its first description in 2020, the number of patients diagnosed as having VEXAS has rapidly increased, thus expanding the spectrum of clinical manifestations known to be associated with this newly recognized condition (2,3). Common features of VEXAS patients are a high degree of refractoriness to most immunosuppressive treatments and a marked dependence on treatment with medium-to-high doses of glucocorticoids (4). Recently, investigators in a multicenter French retrospective study (5) reported the use of azacytidine in 11 VEXAS patients with a concomitant myelodysplastic syndrome. In this series, the authors observed a clinical response in 5 patients (46%), with a major response in 3 and a minor response in 2. Of interest, most patients with a clinical response had received several types of therapy, including biologic and conventional synthetic disease-modifying antirheumatic drugs, none of which were effective. Here we report our successful use of combination therapy including cyclosporin A and interleukin-1 blockers for the treatment of VEXAS.

Three men with VEXAS (median age 69 years [interquartile range {IQR} 68–70]) were identified among patients followed up in the autoinflammatory diseases clinic at San Raffaele Hospital (Segrate, Italy). Genomic DNA from peripheral blood mononuclear

cells was analyzed by Sanger sequencing for the presence of *UBA1* mutations involving methionine-41 (p.Met41). The p.Met41Val variant was identified in 2 patients, and the p.Met41Thr variant was detected in 1 patient. An unspecified autoinflammatory disease was originally diagnosed in 2 patients, and relapsing polychondritis was originally diagnosed in the other patient. The median time to VEXAS diagnosis was 30 months (IQR 29–57) after initial presentation to the clinic.

All patients were initially treated with prednisone (dosage range 50–62.5 mg/day); however, relapse of adverse inflammatory events occurred after reducing the prednisone dosage to <20 mg/day. For this reason, different steroid-sparing agents were introduced over time; unfortunately, treatment with these drugs had to be stopped because of side effects or ineffectiveness (Table 1). Before starting combination therapy, 2 patients had been treated with anakinra, which was stopped because of extensive adverse cutaneous reactions. Of note, in 1 of these patients, anakinra was safely reintroduced, together with cyclosporin A, without the appearance of adverse reactions, even when steroid therapy was tapered. In the 2 remaining patients, cyclosporin A was added to anakinra or to canakinumab, owing to persistent systemic inflammation upon reduction of the steroid dosage (Table 1).

After the start of combination therapy, a marked improvement was observed in all patients, thus allowing safe tapering of steroid treatment. Six months after initiation of combination therapy, all patients were receiving a low dosage of prednisone (5 mg/day), and no relapse of systemic manifestations was observed. This was paralleled by optimal control of systemic markers of inflammation (Table 1). Combination therapy was well tolerated by all patients. Two patients experienced clinically

Table 1. Clinical characteristics, laboratory findings, and treatments for 3 men with VEXAS syndrome*



	Age, years	Clinical characteristics at presentation	Markers of inflammation at presentation	Previous therapy, reason for stopping	Combination therapy, agent (dosage)	Markers of inflammation	
						At start of combination therapy	At last evaluation
Patient 1	70	Fever, skin lesions, lung involvement, arthritis	ESR 120 mm/hour, CRP 120 mg/liter, ferritin 1,638 ng/ml	ANK, adverse event; CNK, ineffectiveness	ANK (100 mg/day), CsA (200 mg/day), pred. (30 mg/day)	ESR 59 mm/hour, CRP 92 mg/liter, ferritin 623 ng/ml	ESR 20 mm/hour, CRP 1.3 mg/liter, ferritin 445 ng/ml
Patient 2	69	Fever, skin lesions, lung involvement, polychondritis, arthritis, aphthosis	ESR 117 mm/hour, CRP 161 mg/liter, ferritin 1,484 ng/ml	ANK, adverse event; TCZ, neutropenia	CNK (300 mg every 5 weeks), CsA (300 mg/day), pred. (15 mg/day)	ESR 99 mm/hour, CRP 26 mg/liter, ferritin 526 ng/ml	ESR 51 mm/hour, CRP 2.8 mg/liter, ferritin 430 ng/ml
Patient 3	68	Fever, arthritis, skin lesions, polychondritis, lung involvement, orbital pseudotumor	ESR 120 mm/hour, CRP 202 mg/liter, ferritin 1,680 ng/ml	MTX, ineffectiveness; TCZ, neutropenia; TOFA, ineffectiveness	ANK (100 mg/day), CsA (200 mg/day), pred. (20 mg/day)	ESR 42 mm/hour, CRP 31 mg/liter, ferritin 980 ng/ml	ESR 29 mm/hour, CRP 0.8 mg/liter, ferritin 380 ng/ml

* VEXAS = vacuoles, E1 enzyme, X-linked, autoinflammatory, somatic syndrome; ESR = erythrocyte sedimentation rate; CRP = C-reactive protein; ANK = anakinra; CNK = canakinumab; CsA = cyclosporin A; pred. = prednisone; TCZ = tocilizumab; MTX = methotrexate; TOFA = tofacitinib.

significant neutropenia (800 and 900/mm³), which was not thought to be associated with infection. Only 1 case of mild upper respiratory tract infection was observed, in the patient without neutropenia.

This is the first report of successful immunomodulatory combination therapy for VEXAS syndrome. In our cohort, we observed that cyclosporin A combined with an interleukin-1 blocker can be effective in dampening systemic inflammation and controlling systemic manifestations of the disease. Moreover, combination treatment showed a strong steroid-sparing effect. The only concern associated with this therapeutic scheme was neutropenia; however, it was not associated with an increased risk of infection. Longer follow-up and replication of these preliminary results in larger cohorts are required.

Drs. Campochiaro and Tomelleri contributed equally to this work. Author disclosures are available at <https://onlinelibrary.wiley.com/action/downloadSupplement?doi=10.1002%2Fart.42101&file=art42101-sup-0001-Disclosureform.pdf>.

Corrado Campochiaro, MD 
Alessandro Tomelleri, MD 
Giulio Cavalli, MD, PhD
Giacomo De Luca, MD
San Raffaele Hospital, IRCCS
and Vita-Salute San Raffaele University
Greta Grassini, PhD

Maria G. Cangi, PhD
San Raffaele Hospital, IRCCS
Lorenzo Dagna, MD
San Raffaele Hospital, IRCCS
and Vita-Salute San Raffaele University
Milan, Italy

1. Beck DB, Ferrada MA, Sikora KA, Ombrello AK, Collins JC, Pei W, et al. Somatic mutations in UBA1 and severe adult-onset autoinflammatory disease. *N Engl J Med* 2020;383:2628–38.
2. Muratore F, Marvisi C, Castrignanò P, Nicoli D, Farnetti E, Bonanno O, et al. VEXAS syndrome: a case series from a single-center cohort of Italian patients with vasculitis. *Arthritis Rheumatol* 2022;74:665–70.
3. Koster MJ, Warrington KJ. VEXAS within the spectrum of rheumatologic disease. *Semin Hematol* 2021;58:218–25.
4. Georgin-Lavialle S, Terrier B, Guedon AF, Heibling M, Comont T, Lazaro E, et al. Further characterization of clinical and laboratory features occurring in VEXAS syndrome: large-scale analysis of a multicenter case series of 116 French patients. *Br J Dermatol* 2022;186:564–74.
5. Comont T, Heiblig M, Rivière E, Terriou L, Rossignol J, Bouscary D, et al. Azacitidine for patients with vacuoles, E1 enzyme, X-linked, autoinflammatory, somatic syndrome (VEXAS) and myelodysplastic syndrome: data from the French VEXAS registry. *Br J Haematol* 2022;196:969–74.